frontiers | Research Topics

In celebration of women in molecular and cellular reproduction

Edited by
Dolores Busso, Vanina Gabriela Da Ros and Patricia S. Cuasnicu

Published in
Frontiers in Cell and Developmental Biology

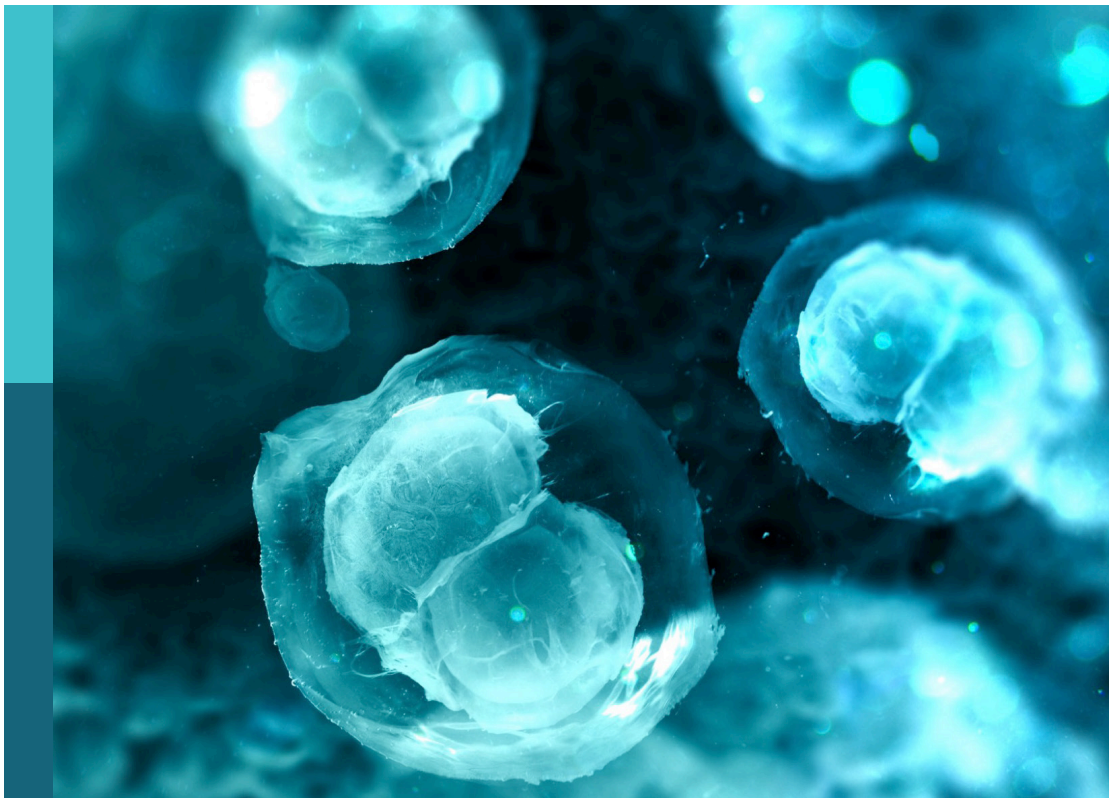

ISSN 1664-8714
ISBN 978-2-8325-4893-6
DOI 10.3389/978-2-8325-4893-6

About Frontiers

Frontiers is more than just an open access publisher of scholarly articles: it is a pioneering approach to the world of academia, radically improving the way scholarly research is managed. The grand vision of Frontiers is a world where all people have an equal opportunity to seek, share and generate knowledge. Frontiers provides immediate and permanent online open access to all its publications, but this alone is not enough to realize our grand goals.

Frontiers journal series

The Frontiers journal series is a multi-tier and interdisciplinary set of open-access, online journals, promising a paradigm shift from the current review, selection and dissemination processes in academic publishing. All Frontiers journals are driven by researchers for researchers; therefore, they constitute a service to the scholarly community. At the same time, the *Frontiers journal series* operates on a revolutionary invention, the tiered publishing system, initially addressing specific communities of scholars, and gradually climbing up to broader public understanding, thus serving the interests of the lay society, too.

Dedication to quality

Each Frontiers article is a landmark of the highest quality, thanks to genuinely collaborative interactions between authors and review editors, who include some of the world's best academicians. Research must be certified by peers before entering a stream of knowledge that may eventually reach the public - and shape society; therefore, Frontiers only applies the most rigorous and unbiased reviews. Frontiers revolutionizes research publishing by freely delivering the most outstanding research, evaluated with no bias from both the academic and social point of view. By applying the most advanced information technologies, Frontiers is catapulting scholarly publishing into a new generation.

What are Frontiers Research Topics?

Frontiers Research Topics are very popular trademarks of the *Frontiers journals series*: they are collections of at least ten articles, all centered on a particular subject. With their unique mix of varied contributions from Original Research to Review Articles, Frontiers Research Topics unify the most influential researchers, the latest key findings and historical advances in a hot research area.

Find out more on how to host your own Frontiers Research Topic or contribute to one as an author by contacting the Frontiers editorial office: frontiersin.org/about/contact

In celebration of women in molecular and cellular reproduction

Topic editors

Dolores Busso — Universidad de los Andes, Chile

Vanina Gabriela Da Ros — CONICET Institute of Biology and Experimental Medicine (IBYME), Argentina

Patricia S. Cuasnicu — CONICET Institute of Biology and Experimental Medicine (IBYME), Argentina

Citation

Busso, D., Da Ros, V. G., Cuasnicu, P. S., eds. (2024). *In celebration of women in molecular and cellular reproduction*. Lausanne: Frontiers Media SA.

doi: 10.3389/978-2-8325-4893-6

Table of contents

frontiers | Frontiers in Cell and Developmental Biology

TYPE Mini Review
PUBLISHED 15 February 2023
DOI 10.3389/fcell.2023.1090997

OPEN ACCESS

EDITED BY
Dolores Busso,
Universidad de los Andes, Chile

REVIEWED BY
Jinxiang Wu,
The Second Affiliated Hospital of Fujian Medical University, China
Susana B. Rulli,
Universidad Maimónides, Argentina
Hang-Soo Park,
The University of Chicago, United States

*CORRESPONDENCE
Zixiang Geng,
gengzx@foxmail.com
Ying Liu,
liuying19@mail.jlu.edu.cn
Yongfang Zhao,
zhao_dingding@126.com

SPECIALTY SECTION
This article was submitted to Molecular and Cellular Reproduction, a section of the journal Frontiers in Cell and Developmental Biology

RECEIVED 06 November 2022
ACCEPTED 06 February 2023
PUBLISHED 15 February 2023

CITATION
Geng Z, Guo H, Li Y, Liu Y and Zhao Y (2023), Stem cell-derived extracellular vesicles: A novel and potential remedy for primary ovarian insufficiency.
Front. Cell Dev. Biol. 11:1090997.
doi: 10.3389/fcell.2023.1090997

Stem cell-derived extracellular vesicles: A novel and potential remedy for primary ovarian insufficiency

Zixiang Geng[1,2]*, Hailing Guo[1,2], Yifei Li[3], Ying Liu[4]* and Yongfang Zhao[1,2]*

[1]Shi's Center of Orthopedics and Traumatology, Shuguang Hospital Affiliated to Shanghai University of Traditional Chinese Medicine, Shanghai, China, [2]Institute of Traumatology and Orthopedics, Shanghai Academy of Traditional Chinese Medicine, Shanghai, China, [3]Shanghai University of Traditional Chinese Medicine, Shanghai, China , [4]Department of Dermatology, Shanghai Songjiang District Central Hospital, Shanghai, China

Primary ovarian insufficiency (POI) is an essential cause of young female fertility loss. At present, there are many treatments for primary ovarian insufficiency, but due to the complexity of the pathogenesis of primary ovarian insufficiency, the efficacy still could not be satisfactory. Stem cell transplantation is a feasible intervention protocol for primary ovarian insufficiency. However, its wide application in the clinic is limited by some defects such as tumorigenic and controversial ethical issues. Stem cell-derived extracellular vesicles (EVs) represent an important mode of intercellular communication attracting increasing interest. It is well documented that stem cell-derived extracellular vesicles for primary ovarian insufficiency with exciting therapeutic effects. Studies have found that stem cell-derived extracellular vesicles could improve ovarian reserve, increase the growth of follicles, reduce follicle atresia, and restore hormone levels of FSH and E2. Its mechanisms include inhibiting ovarian granulosa cells (GCs) apoptosis, reactive oxygen species, and inflammatory response and promoting granulosa cells proliferation and angiogenesis. Thus, stem cell-derived extracellular vesicles are a promising and potential method for primary ovarian insufficiency patients. However, stem cell-derived extracellular vesicles are still a long way from clinical translation. This review will provide an overview of the role and the mechanisms of stem cell-derived extracellular vesicles in primary ovarian insufficiency, and further elaborate on the current challenges. It may suggest new directions for future research.

KEYWORDS

primary ovarian insufficiency, premature ovarian failure, stem cells, extracellular vesicles, exosomes

Introduction

Primary ovarian insufficiency (POI), also known as premature ovarian failure (POF) or premature menopause, is defined as cessation of menstruation before the expected age of menopause (Qin et al., 2015). In recent years, according to epidemiological surveys, POI is becoming a common disease in women's reproductive systems, with an incidence rate of 1% (Szeliga et al., 2021). Studies have shown that 1 in 1,000 women between the ages of 15 and 29 and 1 in 100 women between the ages of 30 and 39 experience POI (Nippita and Baber,

TABLE 1 Preclinical studies of stem cells-derived EVs in POI.

EVs cellular origin	Model	Treatment	Functions	Pathways	Ref
rBMSCs	CTX-rat	150 μg EVs (100 μL PBS)/every other day for 2 weeks by intraperitoneal injection	inhibit GCs apoptosis	miR-144-5p *via* PTEN-PI3K/AKT	Yang et al. (2020)
mBMSCs	Cisplatin-mouse	125 μg EVs (100 μL PBS)/after model establishment 1st, 5th, and 10th day by tail vein injection	inhibit GCs apoptosis	miR-644-5p *via* P53	Sun et al. (2019)
hUCMSCs	CTX-mouse	1×10^6 cells- EVs (200 μL PBS)/model establishment 8th, 9th day by intraperitoneal injection	Inhibit GCs apoptosis and inflammation	phosphorylation of AKT and P38	Deng et al. (2021)
		150 μg EVs/two times (Once every 7 days) by intraperitoneal injection	promote GCs proliferation	Hippo Pathway	Li et al. (2021a)
		10^{11}, 5×10^{11}, and 10^{12} cells- EVs particles/mL by intra-ovarian injection	promote GCs proliferation; alleviate ROS accumulation	miR-17-5P *via* SIRT7-PARP1/γH2AX/XRCC6	Ding et al. (2020)
	Cisplatin-rat	400 μg EVs (200 μL PBS)/after model establishment by tail vein injection	promote angiogenesis and attenuate GCs apoptosis	miR-126-3p *via* PIK3R2-AKT/mTOR	Qu et al. (2022)
	Cisplatin-rat GCs	30 μg/ml EVs	inhibit GCs apoptosis	Caspase-3; Bcl-2/Bax; StAR	Zhang et al. (2020)
	GCs (KGN and SVOG cells)	30 μg/ml EVs	promote GCs estrogen secretion	miR-21 *via* LATS1-LOXL2/YAP	Cai et al. (2022)
	Cisplatin-mouse	125 μg EVs (100 μL PBS)/after model establishment by tail vein injection	promote GCs proliferation; inhibit GCs apoptosis	miR-29a *via* HBP1-Wnt/β-catenin	Gao et al. (2022)
	Cisplatin-rat GCs	100 μg/ml EVs	inhibit GCs apoptosis	Caspase-3; Bcl-2/Bax; cleaved PARP	Sun et al. (2017)
	CTX/BUS-mouse	150 μg EVs (100 μL PBS)/once a week for 4 weeks by tail vein injection	induce angiogenesis	PI3K/AKT	Yang et al. (2019)
hESCs	CTX/BUS-mouse	1×10^8 cells- EVs (200 μL)/once every 2 days for three times by tail vein injection	promote GCs proliferation; inhibit GCs apoptosis	PI3K/AKT	Liu et al. (2020)
CD44+/CD105+ hAFSCs	CTX-mouse	1×10^6 cells- EVs/every 2 days for 4 weeks by tail vein injection	inhibit GCs apoptosis	miR-369-3p *via* YAF2-PDCD5/p53	Geng et al. (2022b)
mAFSCs	CTX/BUS-mouse	125 μg EVs by intra-ovarian injection	inhibit GCs apoptosis	miR-10a	Xiao et al. (2016)
hADSC	CTX-rat	intra-ovarian injection	inhibit GCs apoptosis; induce angiogenesis	VEGF; Bcl-2/Bax	Ling et al. (2019)
	CTX-mouse	1×10^6 cells- EVs by intra-ovarian injection	inhibit GCs apoptosis; promote GCs proliferation;	SMAD pathway	Huang et al. (2018)
MenSCs	VCD-rat	25 μg EVs (50 μL) by intra-ovarian injection	promote GCs proliferation; regulate the composition of the ovarian extracellular matrix; accelerate the recruitment of dormant follicles	DAZL; FOXL2	Zhang et al. (2021)

EVs: extracellular vesicles; POI: primary ovarian insufficiency; rBMSCs: rat bone marrow mesenchymal stem cells; mBMSCs: mouse bone marrow mesenchymal stem cells; hUCMSCs: human umbilical cord mesenchymal stem cells; hESCs: human embryonic stem cells; hAFSCs: human amniotic fluid stem cells; mAFSCs: mouse amniotic fluid stem cells; hADSC: human adipose stem cells; MenSCs: menstrual blood-stem cells; ROS: reactive oxygen species; CTX: cyclophosphamide; VCD: 4-vinylcyclohexene diepoxide; BUS: busulfan; GCs: granulosa cells.

2007; Panay and Fenton, 2008). There is a close relationship between ovarian granulosa cells (GCs) quality and the occurrence of POI (Zhu et al., 2021; Geng et al., 2022a) because senescence and cell cycle disorders in GCs result in a significant reduction of ovarian reserve (Fu et al., 2017; Liu et al., 2021). In clinics, hormone replacement therapy is the most commonly used management for POI patients but has a higher risk of various complications such as breast and ovarian cancer (Shelling, 2010; Kovanci and Schutt, 2015; Szeliga et al., 2021). Therefore, it is essential to find a safer and more effective way to treat POI.

Not surprisingly, stem cell-based therapies hold tremendous potential for treating POI in both preclinical and clinical trials (Ding et al., 2018; Yin et al., 2020; Fu et al., 2021; Mashayekhi et al., 2021; Wang et al., 2022a). Recent research suggests stem cells may provide therapeutic effects by paracrine means, specifically using extracellular vesicles (EVs) that include exosomes (Zhang et al.,

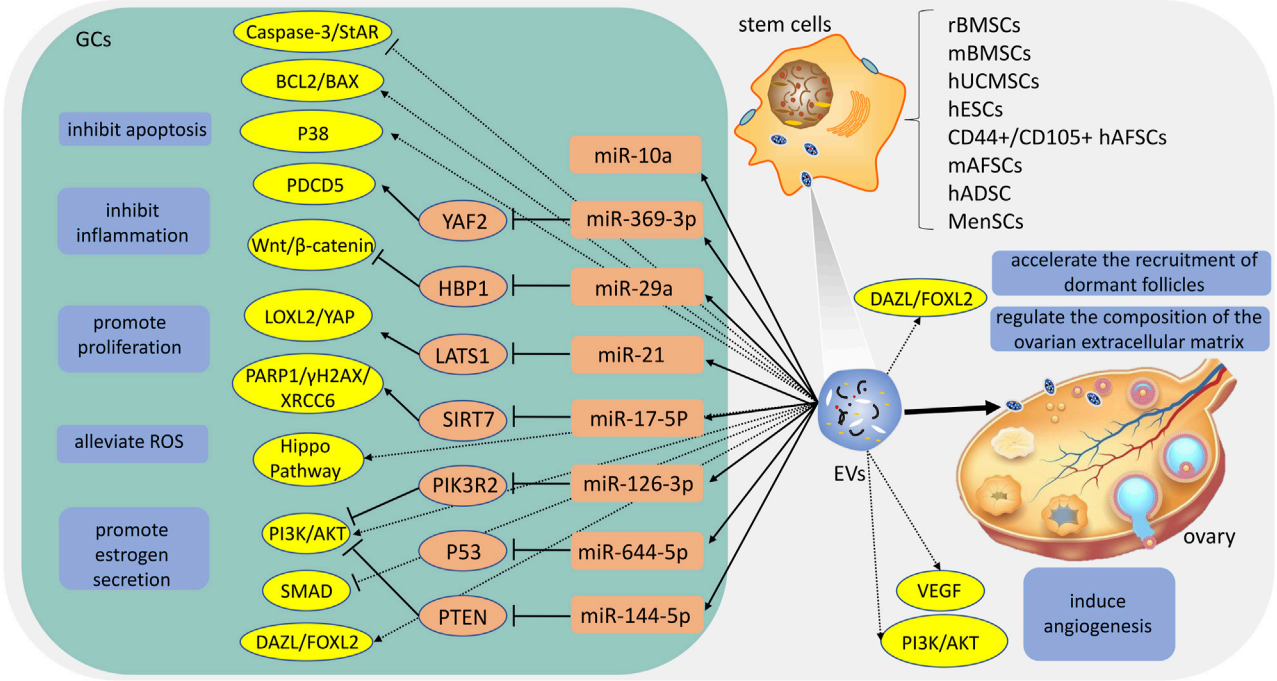

FIGURE 1
The potential mechanisms of different extracellular vesicles (EVs). rBMSCs: rat bone marrow mesenchymal stem cells; mBMSCs: mouse bone marrow mesenchymal stem cells; hUCMSCs: human umbilical cord mesenchymal stem cells; hESCs: human embryonic stem cells; hAFSCs: human amniotic fluid stem cells; mAFSCs: mouse amniotic fluid stem cells; hADSC: human adipose stem cells; MenSCs: menstrual blood-stem cells; ROS: reactive oxygen species; GCs: granulosa cells.

2019a; Liu et al., 2021; Qu et al., 2022). The diameters of EVs range from approximately 30 nm–3,000 nm, and their biomolecular composition determines their functions, as well as their source and conditions (Riazifar et al., 2017). EVs are initially considered to be cellular debris or a way to remove toxic or unneeded by-products from the cell. Although EVs have ancient evolutionary origins and conserved mechanisms of generation, they play crucial physiological roles in cell-to-cell communication (Zhang et al., 2015; Xu et al., 2018). It is common for cells to secrete EVs, and these EVs can also be found in body fluids (Villarroya-Beltri et al., 2014; Xu et al., 2021). Substantial evidence has implicated that stem cell-derived EVs play an obvious role in the treatment of various diseases (Gnecchi et al., 2005; Clevers et al., 2014; Doeppner et al., 2015). It is worth noting that stem cell-derived EVs have shown promising results in treating POI. In this review, we summarize the applications of stem cells-derived EVs in POI and expound on the underlying cellular and molecular mechanisms. We also discuss the expectations for the future of stem cells-derived EVs.

The difference between stem cells and stem cell-derived EVs

Stem cells have the potential for self-renewal and multidirectional differentiation, such as adipose stem cells (ADSCs), bone marrow mesenchymal stem cells (BMSCs), umbilical cord mesenchymal stem cells (UCMSCs) (Williams et al., 2008; Liao and Chen, 2014; Huang et al., 2021). Stem cells play vital roles in maintaining cellular homeostasis and restoring it upon tissue injury (Riazifar et al., 2017). Extensive research has shown that stem cells hold significant therapeutic potential in a variety of human diseases (Yamanaka, 2020). However, stem cells treatment carries an increased risk of conditions including organ failure and neurodegenerative disease (Poulos, 2018). Another potential safety risk for stem cell transplantation is increased immunogenicity (Nguyen et al., 2016). By far, the biggest concern is the tumorigenicity of stem cells due to their long-term culture, which may result in the accumulation of karyotypic abnormalities, copy number variation, and loss of heterozygosity (Lund et al., 2012). Hence, an increasing interest has been shifted toward stem cells-derived EVs. It is now clear from stem cell research that EVs are essential for cells to protect or regenerate injured cells, possibly through a paracrine effect mediated by the EVs (Han et al., 2021). In general, EVs, including exosomes and microvesicles (MVs), are membrane-enclosed vesicles containing proteins and nucleic acids (van Niel et al., 2018; Andaluz Aguilar et al., 2020). Exosomes are EVs with a size range of 40–160 nm (average 100 nm) in diameter with an endosomal origin (Kalluri and LeBleu, 2020). MVs, which vary from 50 to 1,000 nm in diameter, appear to have multiple points of origin, ranging from the selective outward pinching of the plasma membrane to membrane shedding and/or vesicles resulting from cell death (Stahl and Raposo, 2019). EVs comprise complex contents, such as nucleic acids including DNA, mRNAs, non-coding RNAs (ncRNAs), lipids, and various

proteins (Mathivanan et al., 2010; Mashouri et al., 2019). Compared to stem cells, stem cell-derived EVs possess multiple advantages including ethical access, abundant source, and low immunogenicity (Fang et al., 2020; Watanabe et al., 2021; Hade et al., 2022; Xia et al., 2022). Hence, stem cell-derived EVs are considered to be a safer regenerative medicine approach for treating many otherwise untreatable diseases such as POI (Ding et al., 2020). But it should not be ignored that stem cells have the capacity for self-renewal, unlimited proliferation, and differentiation but not EVs.

The pathogenesis of POI and the application of stem cell-derived EVs

The pathogenesis of POI has not been fully elucidated as it involves multiple factors including genetic, immunological, and environmental factors. A wide range of genetic defects is associated with POI, including X chromosome defects, which collectively account for 10%–25% of cases (Chen et al., 2018). More than 80 genes concern gonadal development, DNA replication/meiosis, DNA repair, and hormone synthesis (Franca and Mendonca, 2020). Furthermore, some POI patients suffer from autoimmune diseases, mainly thyroid autoimmune diseases (Dragojevic-Dikic et al., 2010). Common methods of anticancer treatment such as chemotherapy and radiotherapy could also cause female reproductive dysfunction (Meirow and Nugent, 2001). Cyclophosphamide and cisplatin are commonly used in clinical practice, and becoming the most common method of establishing an animal model of POI. In addition, other recognized causes of POI include metabolism disorders, infections, toxins, and environmental factors (Naleway et al., 2018; Moslehi et al., 2019; Rostami Dovom et al., 2019; El Bakly et al., 2020).

At present, there have been numerous researches on the treatment of stem cell-derived EVs for POI and has received considerable clinical attention. Among these studies, sources of EVs include umbilical cord mesenchymal stem cells, bone marrow mesenchymal stem cells, embryonic stem cells, amniotic fluid stem cells, adipose stem cells, and menstrual blood stem cells (Ling et al., 2019; Tracy et al., 2019; Liu et al., 2020; Yang et al., 2020; Li et al., 2021a; Zhang et al., 2021) (Table 1). Studies have found that stem cell-derived EVs could improve ovarian reserve, increase the growth of follicles, reduce follicle atresia, and restore hormone levels of FSH and E2 (Fu et al., 2021). EVs contain a variety of lipids, nucleic acids, and proteins, and play an important role in cell-cell communication by transporting several molecules from donors to recipients (Mittelbrunn and Sanchez-Madrid, 2012). In particular, miRNA. miRNA is a distinct class of small (approximately 22 nucleotides), single-stranded, and non-coding RNAs, and play critical functions in the regulation of cellular gene expression by binding to complementary sequences in the target mRNAs, leading to either translational repression or target degradation of the specific mRNAs (Ha and Kim, 2014). Several studies indicate that miRNA carried by EVs plays a key role in the treatment of POI (Xiao et al., 2016; Ding et al., 2020; Geng et al., 2022b; Cai et al., 2022). In the following section, we explore the potential mechanisms and application value of different EVs (Figure 1).

Human umbilical cord mesenchymal stem cells-derived EVs (hUCMSCs-EVs)

It is the placenta that supplies foetal nutrition and connects the mother and the foetus during pregnancy (Tang et al., 2021). hUCMSCs-EVs can be isolated from various hUCMSCs compartments or the complete hUCMSCs. There are round or oval membranous vesicles, which can be aggregated and distributed, and their membrane structure is clearly defined (Vohra et al., 2020). hUCMSCs-EVs express the EVs-specific four-transmembrane protein markers CD9, CD63, CD81 and tumor susceptibility gene 101 protein (TSG101), heat shock protein70 (HSP70), and the multivesicular biosynthesis-related protein ALIX (Sun et al., 2017; Yang et al., 2019; Zhang et al., 2020; Deng et al., 2021; Cai et al., 2022; Gao et al., 2022; Qu et al., 2022). In 2017, hUCMSCs- EVs were first described for application to POI by Sun et al. (2017). Studies show that hUCMSCs-EVs ameliorate GCs stress and apoptosis *in vitro*, and the underlying mechanism may be related to the upregulation of BCL2 and the downregulation of BAX, cleaved caspase-3, and PARP (Sun et al., 2017; Deng et al., 2021). In addition, Sun et al. (2017) suggest that microRNA-24, microRNA-106a, microRNA-19b, and microRNA-25 may be closely related to apoptosis. After then, multiple studies show that hUCMSCs-EVs could restore serum FSH and estrogen levels, preserve the ovarian reserve and avoid antral follicle atresia. The mechanism involves the Hippo pathway and PI3K-AKT pathway (Yang et al., 2019; Li et al., 2021a). Li et al. (2021a) propose that when the key Hippo molecule (YAP) is blocked, hUCMSCs-EVs suppress the proliferation and function of ovarian cells by regulating the Hippo pathway. Moreover, complex ovarian vascular systems are critical for ovarian function and follicle development, which make the follicle and/or corpus luteum receive nutrients, oxygen, and hormone support, as well as synthesize and release steroids (Kamat et al., 1995; Robinson et al., 2009; Ezoe et al., 2014). Yang et al. (2019) consider that angiogenesis also plays a critical role in the application of hUCMSCs-derived EVs. Furthermore, the EVs-mediated transfer of miRNA is an important way by which stem cell function. Some miRNA including miR-126-3p, miR-21, miR-29a, and miR-17-5P carried by hUCMSCs-EVs could play a role at the post-transcriptional level (Ding et al., 2020; Cai et al., 2022; Gao et al., 2022; Qu et al., 2022). By binding to the 3′UTR of target genes, these miRNAs inhibit the expression of particular molecules to inhibit reactive oxygen species (ROS) production and apoptosis and promote cell survival, proliferation, and angiogenesis in GCs. It is worth mentioning that the protective effect of EVs on cisplatin-damaged GCs showed a dose-dependent effect. GCs are significantly more viable when 15 μg/mL of hUCMSC-EVs are added to their culture for 24 h; 25 g/mL is even more effective when administered for 48 h (Zhang et al., 2020).

Bone marrow mesenchymal stem cells-derived EVs (BMSCs-EVs)

BMSCs is the first stem cell used to evaluate the efficacy in the treatment of POI (Fu et al., 2017). Studies have revealed that BMSCs or EVs infusion could decrease the expression of pro-inflammatory cytokines and oxidised biomolecules (He et al., 2018). BMSCs-EVs are cup-shaped or spherical in shape, with a clear model structure around them, and the diameters of EVs distribution ranged between 30 and 2,000 nm (Li et al., 2021b; Yu et al., 2021). BMSCs-EVs express the EVs-specific four-transmembrane protein markers CD9, CD63, CD81 and TSG101, HSP70, and the multivesicular biosynthesis-related protein ALIX (Tang et al., 2021). Moreover, BMSCs-EVs are negative for CD14, CD34, and CD45 (Li et al., 2019; Tang et al., 2021). BMSCs-EVs appear to have a significant anti-apoptotic effect *in vitro* and *in vivo* (Su et al., 2021; Wen et al., 2021; Xiong et al., 2021; Wang et al., 2022b). Sun et al. (2019) and Yang et al. (2020) also suggest that BMSCs-EVs inhibit GCs apoptosis by carrying miR-144-5p and miR-644-5p to inhibit PTEN and p53.

Embryonic stem cells-derived EVs (ESCs-EVs)

Embryonic stem cells, derived from the blastocyst stage embryos, are distinguished by their ability to self-renew and differentiate into all cell types (Ohtsuka and Dalton, 2008; Martello and Smith, 2014). Thus, ESCs-EVs are extensively studied. Many studies have shown that ESCs-EVs can suppress senescence, facilitate cell proliferation, and inhibit cell apoptosis and oxidation (Khan et al., 2015; Bae et al., 2019; Zhang et al., 2019b; Tavakoli Dargani and Singla, 2019; Abbaszadeh et al., 2020). But ESCs-EVs are poorly studied in POI. Only one study suggests that ESCs-EVs could improve ovarian function by regulating the PI3K/AKT signaling pathway (Liu et al., 2020). Due to ESCs exhibiting strong self-renewal capability and pluripotency, ESCs-EVs are worth further exploration in POI.

Amniotic fluid stem cell-derived EVs (AFSCs-EVs)

Amniotic fluid is a rich source of stem cells that can be easily obtained through amniocentesis during standard prenatal care procedures (Di Trapani et al., 2015). The procedure to obtain AFSCs is non-invasive, safe, and without social controversy (Soncini et al., 2007; Parolini et al., 2008; Diaz-Prado et al., 2010). Hence, amniotic fluid stem cells seem to be the optimal source of EVs. Xiao et al. (2016) reveal that mouse AFSC-EVs contained two microRNAs (miRNAs), miR-146a and miR-10a, which inhibited apoptosis in damaged GCs and prevented ovarian follicles from atresia in mice following cyclophosphamide (CTX). Liu et al. (2012) find that CD44+/CD105+ human AFCs possess the characteristics of mesenchymal stem cells (Zou et al., 2011) and it can survive and proliferate over the long term in the ovarian tissues of a mouse model of chemotherapy-induced POI . Subsequently, AFSCs-EVs are isolated and used in POI. Geng et al. (2022b) indicate that CD44+/CD105+ human AFSC-EVs carrying miR-369-3p could specifically downregulate the expression of YAF2, inhibit the stability of PDCD5/p53, and reduce the apoptosis of OGCs, thereby exerting therapeutic effects on POI. In addition, compared with BMSCs, AFSCs secreted higher levels of EVs (Tracy et al., 2019). Therefore, AFSCs-EVs may be more valuable than other EVs.

Human adipose stem cells-derived EVs (hADSC-EVs)

It is widely accepted that adult stem cells can be found in abundance, readily accessible, and replenishable in adipose tissue. ADSCs are obtained from the subcutaneous adipose tissue removed during liposuction surgeries or abdominoplasties (Fu et al., 2021). Nowadays, ADSCs are widely used to treat various ailments of the skin. However, few studies have been reported on POI. Huang et al. (2018) reveal that the hADSC-EVs recover the ovarian function of POI by downregulating SMAD2, SMAD3, and SMAD5 expression. HADSC-conditioned media containing various cytokines and microvesicles secreted by HADSCs is concentrated and injected into the bilateral ovaries of POI rats in one study. The results show that hADSC-conditioned media injection partially reduces ovarian injury and improved ovarian function in rats with POI (Ling et al., 2019). We have reasons to believe that hADSC-EVs play an indispensable role. Certainly, more evidence is needed to demonstrate these linkages.

Menstrual blood stem cells-derived EVs (MenSCs-EVs)

MenSC-derived small EVs were first reported in 2016 (Lopez-Verrilli et al., 2016), and the authors revealed that MenSC-derived small EVs promote axonal regeneration after nerve injury in the central and peripheral nervous systems. MenSCs-EVs are still in the early stages of study, unlike some common MSC sources such as bone marrow, umbilical cord, and adipose tissue (Chen et al., 2021). Until now the only evidence suggests that GCs were proliferated in primordial and primary follicles by MenSCs-EVs, and apoptosis was inhibited. MenSCs-EVs also increased the expression of early follicle markers, for example, DAZL and FOXL2 (Zhang et al., 2021). *In vivo*, transplantation of MenSCs-EVs in the rat model of POI promoted follicle development and restored estrous cyclicity and serum sex hormone levels. In addition, by transplanting MenSCs-EVs, the extracellular matrix of the ovary was regulated and dormant follicles were recruited sooner. As a result, MenSCs-EVs significantly promoted follicle development *in vitro* and *in vivo* and restored fertility in POI rats.

Future challenges of stem cell-derived EVs

In the last few years, stem cell-derived EVs have emerged as a new therapeutic strategy for many diseases. Although multiple preclinical studies have shown that stem cell-derived EVs have positive effects in treating POI, it is far from being sufficient.

Therefore, in order to benefit POI patients as quickly as possible, further pre-clinical and clinical studies are warranted. But the optimal source of EVs should be found before this time. Regrettably, there are no studies to compare the therapeutic effects of different EVs for POI. Moreover, due to the ultra-short duration of the development of EVs, their safety and consistent regulatory issue are not conclusive (Hu et al., 2022).

To isolate EVs from various cell types, tremendous effort has been devoted in the past. Currently, there is numerous separative technique of EVs including precipitation, membrane affinity, size-exclusion chromatography, iodixanol gradient, and phosphatidylserine affinity (Lee et al., 2021). But no method is perfect. Furthermore, many studies have reported the Effect of storage temperature and frozen/thawed cycles on EVs size and biological activity, and 80°C was chosen as the optimum temperature to ensure both treatment outcomes and transport capacity (Kusuma et al., 2018; Le Saux et al., 2020). It is also one of the main challenges for EVs to mass culture. The strategies for mass-production of EVs include modulating the components or secretary machinery proteins of EVs, increasing the intracellular Ca ions, adjusting biochemical cues such as extracellular DNA, liposomes, and proton concentration, and applying physicomechanical cues such as forces and other stimuli (e.g., electricity, thermal, photodynamic, and radiative stress) (Lee et al., 2021). It is worth mentioning that the development of nanotechnology and biomaterials provide a viable means with which to tackle the previously mentioned problems (Lee et al., 2021). However, related studies were not available in POI.

In conclusion, although stem cell-derived EVs hold great prospects in treating POI, the following questions also need to be addressed: 1) the optimal source of EVs; 2) the safety of stem cell-derived EVs; 3) the mass cultivation and preservation of stem cell-derived EVs; 4) the clinical evaluation of stem cell-derived EVs; 5) the mechanism of stem cell-derived EVs.

Conclusion

It is evident that stem cell-derived EVs have the potential in treating POI. However, more research was needed to investigate the mechanism of stem cell-derived EVs in POI and more efficient means for obtaining and preserving EVs to make benefit patients safer and faster.

Author contributions

ZXG: Draft the manuscript. YL: Data collection. HLG: Revise the manuscript. YFL: Revise the manuscript. YFZ: Quality control.

Funding

This work was supported by the Shanghai Chronic Osteopathy Clinical Medical Research Center (20MC1920600), Three-year Clinical Action Plan of Shanghai Shenkang Hospital Development Center (SHDC2020CR3090B), and Major Project of "Medical Innovation Research Project" of Shanghai Municipal Commission of Science and Technology (21Y3192020).

Conflict of interest

The authors declare that the research was conducted in the absence of any commercial or financial relationships that could be construed as a potential conflict of interest.

Publisher's note

References

Abbaszadeh, H., Ghorbani, F., Derakhshani, M., Movassaghpour, A., and Yousefi, M. (2020). Human umbilical cord mesenchymal stem cell-derived extracellular vesicles: A novel therapeutic paradigm. *J. Cell Physiol.* 235 (2), 706–717. doi:10.1002/jcp.29004

Andaluz Aguilar, H., Iliuk, A. B., Chen, I. H., and Tao, W. A. (2020). Sequential phosphoproteomics and N-glycoproteomics of plasma-derived extracellular vesicles. *Nat. Protoc.* 15 (1), 161–180. doi:10.1038/s41596-019-0260-5

Bae, Y. U., Son, Y., Kim, C. H., Kim, K. S., Hyun, S. H., Woo, H. G., et al. (2019). Embryonic stem cell-derived mmu-miR-291a-3p inhibits cellular senescence in human dermal fibroblasts through the TGF-beta receptor 2 pathway. *J. Gerontol. A Biol. Sci. Med. Sci.* 74 (9), 1359–1367. doi:10.1093/gerona/gly208

Cai, J. H., Sun, Y. T., and Bao, S. (2022). HucMSCs-exosomes containing miR-21 promoted estrogen production in ovarian granulosa cells via LATS1-mediated phosphorylation of LOXL2 and YAP. *Gen. Comp. Endocrinol.* 321-322, 114015. doi:10.1016/j.ygcen.2022.114015

Chen, A., Tiosano, D., Guran, T., Baris, H. N., Bayram, Y., Mory, A., et al. (2018). Mutations in the mitochondrial ribosomal protein MRPS22 lead to primary ovarian insufficiency. *Hum. Mol. Genet.* 27 (11), 1913–1926. doi:10.1093/hmg/ddy098

Chen, L., Qu, J., Mei, Q., Chen, X., Fang, Y., Chen, L., et al. (2021). Small extracellular vesicles from menstrual blood-derived mesenchymal stem cells (MenSCs) as a novel therapeutic impetus in regenerative medicine. *Stem Cell Res. Ther.* 12 (1), 433. doi:10.1186/s13287-021-02511-6

Clevers, H., Loh, K. M., and Nusse, R. (2014). Stem cell signaling. An integral program for tissue renewal and regeneration: Wnt signaling and stem cell control. *Science* 346 (6205), 1248012. doi:10.1126/science.1248012

Deng, T., He, J., Yao, Q., Wu, L., Xue, L., Wu, M., et al. (2021). Human umbilical cord mesenchymal stem cells improve ovarian function in chemotherapy-induced premature ovarian failure mice through inhibiting apoptosis and inflammation via a paracrine mechanism. *Reprod. Sci.* 28 (6), 1718–1732. doi:10.1007/s43032-021-00499-1

Di Trapani, M., Bassi, G., Fontana, E., Giacomello, L., Pozzobon, M., Guillot, P. V., et al. (2015). Immune regulatory properties of CD117(pos) amniotic fluid stem cells vary according to gestational age. *Stem Cells Dev.* 24 (1), 132–143. doi:10.1089/scd.2014.0234

Diaz-Prado, S., Muinos-Lopez, E., Hermida-Gomez, T., Rendal-Vazquez, M. E., Fuentes-Boquete, I., de Toro, F. J., et al. (2010). Multilineage differentiation potential of cells isolated from the human amniotic membrane. *J. Cell. Biochem.* 111 (4), 846–857. doi:10.1002/jcb.22769

Ding, C., Zhu, L., Shen, H., Lu, J., Zou, Q., Huang, C., et al. (2020). Exosomal miRNA-17-5p derived from human umbilical cord mesenchymal stem cells improves ovarian function in premature ovarian insufficiency by regulating SIRT7. *Stem Cells* 38 (9), 1137–1148. doi:10.1002/stem.3204

Ding, L., Yan, G., Wang, B., Xu, L., Gu, Y., Ru, T., et al. (2018). Transplantation of UC-MSCs on collagen scaffold activates follicles in dormant ovaries of POF patients with

long history of infertility. *Sci. China Life Sci.* 61 (12), 1554–1565. doi:10.1007/s11427-017-9272-2

Doeppner, T. R., Herz, J., Gorgens, A., Schlechter, J., Ludwig, A. K., Radtke, S., et al. (2015). Extracellular vesicles improve post-stroke neuroregeneration and prevent postischemic immunosuppression. *Stem Cells Transl. Med.* 4 (10), 1131–1143. doi:10.5966/sctm.2015-0078

Dragojevic-Dikic, S., Marisavljevic, D., Mitrovic, A., Dikic, S., Jovanovic, T., and Jankovic-Raznatovic, S. (2010). An immunological insight into premature ovarian failure (POF). *Autoimmun. Rev.* 9 (11), 771–774. doi:10.1016/j.autrev.2010.06.008

El Bakly, W., Medhat, M., Shafei, M., Tash, R., Elrefai, M., Shoukry, Y., et al. (2020). Optimized platelet rich plasma releasate (O-rPRP) repairs galactosemia-induced ovarian follicular loss in rats by activating mTOR signaling and inhibiting apoptosis. *Heliyon* 6 (9), e05006. doi:10.1016/j.heliyon.2020.e05006

Ezoe, K., Murata, N., Yabuuchi, A., Okuno, T., Kobayashi, T., Kato, O., et al. (2014). Long-term adverse effects of cyclophosphamide on follicular growth and angiogenesis in mouse ovaries. *Reprod. Biol.* 14 (3), 238–242. doi:10.1016/j.repbio.2014.04.007

Fang, S. B., Zhang, H. Y., Wang, C., He, B. X., Liu, X. Q., Meng, X. C., et al. (2020). Small extracellular vesicles derived from human mesenchymal stromal cells prevent group 2 innate lymphoid cell-dominant allergic airway inflammation through delivery of miR-146a-5p. *J. Extracell. Vesicles* 9 (1), 1723260. doi:10.1080/20013078.2020.1723260

Franca, M. M., and Mendonca, B. B. (2020). Genetics of primary ovarian insufficiency in the next-generation sequencing era. *J. Endocr. Soc.* 4 (2), bvz037. doi:10.1210/jendso/bvz037

Fu, X., He, Y., Wang, X., Peng, D., Chen, X., Li, X., et al. (2017). Overexpression of miR-21 in stem cells improves ovarian structure and function in rats with chemotherapy-induced ovarian damage by targeting PDCD4 and PTEN to inhibit granulosa cell apoptosis. *Stem Cell Res. Ther.* 8 (1), 187. doi:10.1186/s13287-017-0641-z

Fu, Y. X., Ji, J., Shan, F., Li, J., and Hu, R. (2021). Human mesenchymal stem cell treatment of premature ovarian failure: New challenges and opportunities. *Stem Cell Res. Ther.* 12 (1), 161. doi:10.1186/s13287-021-02212-0

Gao, T., Cao, Y., Hu, M., and Du, Y. (2022). Human umbilical cord mesenchymal stem cell-derived extracellular vesicles carrying MicroRNA-29a improves ovarian function of mice with primary ovarian insufficiency by targeting HMG-box transcription factor/wnt/β-catenin signaling. *Dis. Markers* 2022, 5045873. doi:10.1155/2022/5045873

Geng, Z., Chen, H., Zou, G., Yuan, L., Liu, P., Li, B., et al. (2022). Human amniotic fluid mesenchymal stem cell-derived exosomes inhibit apoptosis in ovarian granulosa cell via miR-369-3p/YAF2/PDCD5/p53 pathway. *Oxid. Med. Cell Longev.* 2022, 3695848. doi:10.1155/2022/3695848

Geng, Z., Liu, P., Yuan, L., Zhang, K., Lin, J., Nie, X., et al. (2022). Electroacupuncture attenuates ac4C modification of P16 mRNA in the ovarian granulosa cells of a mouse model premature ovarian failure. *Acupunct. Med. J. Br. Med. Acupunct. Soc.* 41, 27–37. doi:10.1177/09645284221085284

Gnecchi, M., He, H., Liang, O. D., Melo, L. G., Morello, F., Mu, H., et al. (2005). Paracrine action accounts for marked protection of ischemic heart by Akt-modified mesenchymal stem cells. *Nat. Med.* 11 (4), 367–368. doi:10.1038/nm0405-367

Ha, M., and Kim, V. N. (2014). Regulation of microRNA biogenesis. *Nat. Rev. Mol. Cell Biol.* 15 (8), 509–524. doi:10.1038/nrm3838

Hade, M. D., Suire, C. N., Mossell, J., and Suo, Z. (2022). Extracellular vesicles: Emerging frontiers in wound healing. *Med. Res. Rev.* 42 (6), 2102–2125. doi:10.1002/med.21918

Han, Z., Liu, S., Pei, Y., Ding, Z., Li, Y., Wang, X., et al. (2021). Highly efficient magnetic labelling allows MRI tracking of the homing of stem cell-derived extracellular vesicles following systemic delivery. *J. Extracell. Vesicles* 10 (3), e12054. doi:10.1002/jev2.12054

He, Y., Chen, D., Yang, L., Hou, Q., Ma, H., and Xu, X. (2018). The therapeutic potential of bone marrow mesenchymal stem cells in premature ovarian failure. *Stem Cell Res. Ther.* 9 (1), 263. doi:10.1186/s13287-018-1008-9

Hu, J. C., Zheng, C. X., Sui, B. D., Liu, W. J., and Jin, Y. (2022). Mesenchymal stem cell-derived exosomes: A novel and potential remedy for cutaneous wound healing and regeneration. *World J. Stem Cells* 14 (5), 318–329. doi:10.4252/wjsc.v14.i5.318

Huang, B., Lu, J., Ding, C., Zou, Q., Wang, W., and Li, H. (2018). Exosomes derived from human adipose mesenchymal stem cells improve ovary function of premature ovarian insufficiency by targeting SMAD. *Stem Cell Res. Ther.* 9 (1), 216. doi:10.1186/s13287-018-0953-7

Huang, L. H., Rau, C. S., Wu, S. C., Wu, Y. C., Wu, C. J., Tsai, C. W., et al. (2021). Identification and characterization of hADSC-derived exosome proteins from different isolation methods. *J. Cell Mol. Med.* 25 (15), 7436–7450. doi:10.1111/jcmm.16775

Kalluri, R., and LeBleu, V. S. (2020). The biology, function, and biomedical applications of exosomes. *Science* 2020367 (6478). doi:10.1126/science.aau6977

Kamat, B. R., Brown, L. F., Manseau, E. J., Senger, D. R., and Dvorak, H. F. (1995). Expression of vascular permeability factor/vascular endothelial growth factor by human granulosa and theca lutein cells. Role in corpus luteum development. *Am. J. Pathol.* 146 (1), 157–165.

Khan, M., Nickoloff, E., Abramova, T., Johnson, J., Verma, S. K., Krishnamurthy, P., et al. (2015). Embryonic stem cell-derived exosomes promote endogenous repair mechanisms and enhance cardiac function following myocardial infarction. *Circ. Res.* 117 (1), 52–64. doi:10.1161/CIRCRESAHA.117.305990

Kovanci, E., and Schutt, A. K. (2015). Premature ovarian failure: Clinical presentation and treatment. *Obstet. Gynecol. Clin. North Am.* 42 (1), 153–161. doi:10.1016/j.ogc.2014.10.004

Kusuma, G. D., Barabadi, M., Tan, J. L., Morton, D. A. V., Frith, J. E., and Lim, R. (2018). To protect and to preserve: Novel preservation strategies for extracellular vesicles. *Front. Pharmacol.* 9, 1199. doi:10.3389/fphar.2018.01199

Le Saux, S., Aarrass, H., Lai-Kee-Him, J., Bron, P., Armengaud, J., Miotello, G., et al. (2020). Post-production modifications of murine mesenchymal stem cell (mMSC) derived extracellular vesicles (EVs) and impact on their cellular interaction. *Biomaterials* 231, 119675. doi:10.1016/j.biomaterials.2019.119675

Lee, J. H., Yoon, J. Y., Lee, J. H., Lee, H. H., Knowles, J. C., and Kim, H. W. (2021). Emerging biogenesis technologies of extracellular vesicles for tissue regenerative therapeutics. *J. Tissue Eng.* 12, 20417314211019015. doi:10.1177/20417314211019015

Li, G. Q., Fang, Y. X., Liu, Y., Meng, F. R., Wu, X., Zhang, C. W., et al. (2021). MicroRNA-21 from bone marrow mesenchymal stem cell-derived extracellular vesicles targets TET1 to suppress KLF4 and alleviate rheumatoid arthritis. *Ther. Adv. Chronic Dis.* 12, 20406223211007369. doi:10.1177/20406223211007369

Li, Z., Liu, F., He, X., Yang, X., Shan, F., and Feng, J. (2019). Exosomes derived from mesenchymal stem cells attenuate inflammation and demyelination of the central nervous system in EAE rats by regulating the polarization of microglia. *Int. Immunopharmacol.* 67, 268–280. doi:10.1016/j.intimp.2018.12.001

Li, Z., Zhang, M., Zheng, J., Tian, Y., Zhang, H., Tan, Y., et al. (2021). Human umbilical cord mesenchymal stem cell-derived exosomes improve ovarian function and proliferation of premature ovarian insufficiency by regulating the Hippo signaling pathway. *Front. Endocrinol. (Lausanne)* 12, 711902. doi:10.3389/fendo.2021.711902

Liao, H. T., and Chen, C. T. (2014). Osteogenic potential: Comparison between bone marrow and adipose-derived mesenchymal stem cells. *World J. Stem Cells* 6 (3), 288–295. doi:10.4252/wjsc.v6.i3.288

Ling, L., Feng, X., Wei, T., Wang, Y., Wang, Y., Wang, Z., et al. (2019). Human amnion-derived mesenchymal stem cell (hAD-MSC) transplantation improves ovarian function in rats with premature ovarian insufficiency (POI) at least partly through a paracrine mechanism. *Stem Cell Res. Ther.* 10 (1), 46. doi:10.1186/s13287-019-1136-x

Liu, M., Qiu, Y., Xue, Z., Wu, R., Li, J., Niu, X., et al. (2020). Small extracellular vesicles derived from embryonic stem cells restore ovarian function of premature ovarian failure through PI3K/AKT signaling pathway. *Stem Cell Res. Ther.* 11 (1), 3. doi:10.1186/s13287-019-1508-2

Liu, T., Huang, Y., Guo, L., Cheng, W., and Zou, G. (2012). CD44+/CD105+ human amniotic fluid mesenchymal stem cells survive and proliferate in the ovary long-term in a mouse model of chemotherapy-induced premature ovarian failure. *Int. J. Med. Sci.* 9 (7), 592–602. doi:10.7150/ijms.4841

Liu, T., Jing, F., Huang, P., Geng, Z., Xu, J., Li, J., et al. (2021). Thymopentin alleviates premature ovarian failure in mice by activating YY2/Lin28A and inhibiting the expression of let-7 family microRNAs. *Cell Prolif.* 54 (8), e13089. doi:10.1111/cpr.13089

Lopez-Verrilli, M. A., Caviedes, A., Cabrera, A., Sandoval, S., Wyneken, U., and Khoury, M. (2016). Mesenchymal stem cell-derived exosomes from different sources selectively promote neuritic outgrowth. *Neuroscience* 320, 129–139. doi:10.1016/j.neuroscience.2016.01.061

Lund, R. J., Narva, E., and Lahesmaa, R. (2012). Genetic and epigenetic stability of human pluripotent stem cells. *Nat. Rev. Genet.* 13 (10), 732–744. doi:10.1038/nrg3271

Martello, G., and Smith, A. (2014). The nature of embryonic stem cells. *Annu. Rev. Cell Dev. Biol.* 30, 647–675. doi:10.1146/annurev-cellbio-100913-013116

Mashayekhi, M., Mirzadeh, E., Chekini, Z., Ahmadi, F., Eftekhari-Yazdi, P., Vesali, S., et al. (2021). Evaluation of safety, feasibility and efficacy of intra-ovarian transplantation of autologous adipose derived mesenchymal stromal cells in idiopathic premature ovarian failure patients: Non-randomized clinical trial, phase I, first in human. *J. Ovarian Res.* 14 (1), 5. doi:10.1186/s13048-020-00743-3

Mashouri, L., Yousefi, H., Aref, A. R., Ahadi, A. M., Molaei, F., and Alahari, S. K. (2019). Exosomes: Composition, biogenesis, and mechanisms in cancer metastasis and drug resistance. *Mol. Cancer* 18 (1), 75. doi:10.1186/s12943-019-0991-5

Mathivanan, S., Ji, H., and Simpson, R. J. (2010). Exosomes: Extracellular organelles important in intercellular communication. *J. Proteomics* 73 (10), 1907–1920. doi:10.1016/j.jprot.2010.06.006

Meirow, D., and Nugent, D. (2001). The effects of radiotherapy and chemotherapy on female reproduction. *Hum. Reprod. Update* 7 (6), 535–543. doi:10.1093/humupd/7.6.535

Mittelbrunn, M., and Sanchez-Madrid, F. (2012). Intercellular communication: Diverse structures for exchange of genetic information. *Nat. Rev. Mol. Cell Biol.* 13 (5), 328–335. doi:10.1038/nrm3335

Moslehi, N., Mirmiran, P., Azizi, F., and Tehrani, F. R. (2019). Do dietary intakes influence the rate of decline in anti-mullerian hormone among eumenorrheic women? A population-based prospective investigation. *Nutr. J.* 18 (1), 83. doi:10.1186/s12937-019-0508-5

Naleway, A. L., Mittendorf, K. F., Irving, S. A., Henninger, M. L., Crane, B., Smith, N., et al. (2018). Primary ovarian insufficiency and adolescent vaccination. *Pediatrics* 142 (3), e20180943. doi:10.1542/peds.2018-0943

Nguyen, P. K., Neofytou, E., Rhee, J. W., and Wu, J. C. (2016). Potential strategies to address the major clinical barriers facing stem cell regenerative therapy for cardiovascular disease: A review. *JAMA Cardiol.* 1 (8), 953–962. doi:10.1001/jamacardio.2016.2750

Nippita, T. A., and Baber, R. J. (2007). Premature ovarian failure: A review. *Climacteric* 10 (1), 11–22. doi:10.1080/13697130601135672

Ohtsuka, S., and Dalton, S. (2008). Molecular and biological properties of pluripotent embryonic stem cells. *Gene Ther.* 15 (2), 74–81. doi:10.1038/sj.gt.3303065

Panay, N., and Fenton, A. (2008). Premature ovarian failure: A growing concern. *Climacteric* 11 (1), 1–3. doi:10.1080/13697130701878635

Parolini, O., Alviano, F., Bagnara, G. P., Bilic, G., Buhring, H. J., Evangelista, M., et al. (2008). Concise review: Isolation and characterization of cells from human term placenta: Outcome of the first international workshop on placenta derived stem cells. *Stem Cells* 26 (2), 300–311. doi:10.1634/stemcells.2007-0594

Poulos, J. (2018). The limited application of stem cells in medicine: A review. *Stem Cell Res. Ther.* 9 (1), 1. doi:10.1186/s13287-017-0735-7

Qin, Y., Jiao, X., Simpson, J. L., and Chen, Z. J. (2015). Genetics of primary ovarian insufficiency: New developments and opportunities. *Hum. Reprod. Update* 21 (6), 787–808. doi:10.1093/humupd/dmv036

Qu, Q., Liu, L., Cui, Y., Liu, H., Yi, J., Bing, W., et al. (2022). miR-126-3p containing exosomes derived from human umbilical cord mesenchymal stem cells promote angiogenesis and attenuate ovarian granulosa cell apoptosis in a preclinical rat model of premature ovarian failure. *Stem Cell Res. Ther.* 13 (1), 352. doi:10.1186/s13287-022-03056-y

Riazifar, M., Pone, E. J., Lotvall, J., and Zhao, W. (2017). Stem cell extracellular vesicles: Extended messages of regeneration. *Annu. Rev. Pharmacol. Toxicol.* 57, 125–154. doi:10.1146/annurev-pharmtox-061616-030146

Robinson, R. S., Woad, K. J., Hammond, A. J., Laird, M., Hunter, M. G., and Mann, G. E. (2009). Angiogenesis and vascular function in the ovary. *Reproduction* 138 (6), 869–881. doi:10.1530/REP-09-0283

Rostami Dovom, M., Noroozzadeh, M., Mosaffa, N., Zadeh-Vakili, A., Piryaei, A., and Ramezani Tehrani, F. (2019). Induced premature ovarian insufficiency by using D galactose and its effects on reproductive profiles in small laboratory animals: A systematic review. *J. Ovarian Res.* 12 (1), 96. doi:10.1186/s13048-019-0565-6

Shelling, A. N. (2010). Premature ovarian failure. *Reproduction* 140 (5), 633–641. doi:10.1530/REP-09-0567

Soncini, M., Vertua, E., Gibelli, L., Zorzi, F., Denegri, M., Albertini, A., et al. (2007). Isolation and characterization of mesenchymal cells from human fetal membranes. *J. Tissue Eng. Regen. Med.* 1 (4), 296–305. doi:10.1002/term.40

Stahl, P. D., and Raposo, G. (2019). Extracellular vesicles: Exosomes and microvesicles, integrators of homeostasis. *Physiol. (Bethesda)* 34 (3), 169–177. doi:10.1152/physiol.00045.2018

Su, Y., Song, X., Teng, J., Zhou, X., Dong, Z., Li, P., et al. (2021). Mesenchymal stem cells-derived extracellular vesicles carrying microRNA-17 inhibits macrophage apoptosis in lipopolysaccharide-induced sepsis. *Int. Immunopharmacol.* 95, 107408. doi:10.1016/j.intimp.2021.107408

Sun, B., Ma, Y., Wang, F., Hu, L., and Sun, Y. (2019). miR-644-5p carried by bone mesenchymal stem cell-derived exosomes targets regulation of p53 to inhibit ovarian granulosa cell apoptosis. *Stem Cell Res. Ther.* 10 (1), 360. doi:10.1186/s13287-019-1442-3

Sun, L., Li, D., Song, K., Wei, J., Yao, S., Li, Z., et al. (2017). Exosomes derived from human umbilical cord mesenchymal stem cells protect against cisplatin-induced ovarian granulosa cell stress and apoptosis *in vitro*. *Sci. Rep.* 7 (1), 2552. doi:10.1038/s41598-017-02786-x

Szeliga, A., Calik-Ksepka, A., Maciejewska-Jeske, M., Grymowicz, M., Smolarczyk, K., Kostrzak, A., et al. (2021). Autoimmune diseases in patients with premature ovarian insufficiency-our current state of knowledge. *Int. J. Mol. Sci.* 22 (5), 2594. doi:10.3390/ijms22052594

Tang, Y., Zhou, Y., and Li, H. J. (2021). Advances in mesenchymal stem cell exosomes: A review. *Stem Cell Res. Ther.* 12 (1), 71. doi:10.1186/s13287-021-02138-7

Tavakoli Dargani, Z., and Singla, D. K. (2019). Embryonic stem cell-derived exosomes inhibit doxorubicin-induced TLR4-NLRP3-mediated cell death-pyroptosis. *Am. J. Physiol. Heart Circ. Physiol.* 317 (2), H460–H471. doi:10.1152/ajpheart.00056.2019

Tracy, S. A., Ahmed, A., Tigges, J. C., Ericsson, M., Pal, A. K., Zurakowski, D., et al. (2019). A comparison of clinically relevant sources of mesenchymal stem cell-derived exosomes: Bone marrow and amniotic fluid. *J. Pediatr. Surg.* 54 (1), 86–90. doi:10.1016/j.jpedsurg.2018.10.020

van Niel, G., D'Angelo, G., and Raposo, G. (2018). Shedding light on the cell biology of extracellular vesicles. *Nat. Rev. Mol. Cell Biol.* 19 (4), 213–228. doi:10.1038/nrm.2017.125

Villarroya-Beltri, C., Baixauli, F., Gutierrez-Vazquez, C., Sanchez-Madrid, F., and Mittelbrunn, M. (2014). Sorting it out: Regulation of exosome loading. *Semin. Cancer Biol.* 28, 3–13. doi:10.1016/j.semcancer.2014.04.009

Vohra, M., Sharma, A., Bagga, R., and Arora, S. K. (2020). Human umbilical cord-derived mesenchymal stem cells induce tissue repair and regeneration in collagen-induced arthritis in rats. *J. Clin. Transl. Res.* 6 (6), 203–216.

Wang, L., Mei, Q., Xie, Q., Li, H., Su, P., Zhang, L., et al. (2022). A comparative study of Mesenchymal Stem Cells transplantation approach to antagonize age-associated ovarian hypofunction with consideration of safety and efficiency. *J. Adv. Res.* 38, 245–259. doi:10.1016/j.jare.2021.09.001

Wang, W., Peng, X., Zhao, L., Zhao, H., and Gu, Q. (2022). Extracellular vesicles from bone marrow mesenchymal stem cells inhibit apoptosis and autophagy of ischemia-hypoxia cardiomyocyte line *in vitro* by carrying miR-144-3p to inhibit ROCK1. *Curr. Stem Cell Res. Ther.* 18, 247–259. doi:10.2174/1574888X17666220503192941

Watanabe, Y., Tsuchiya, A., and Terai, S. (2021). The development of mesenchymal stem cell therapy in the present, and the perspective of cell-free therapy in the future. *Clin. Mol. Hepatol.* 27 (1), 70–80. doi:10.3350/cmh.2020.0194

Wen, T., Wang, H., Li, Y., Lin, Y., Zhao, S., Liu, J., et al. (2021). Bone mesenchymal stem cell-derived extracellular vesicles promote the repair of intervertebral disc degeneration by transferring microRNA-199a. *Cell Cycle* 20 (3), 256–270. doi:10.1080/15384101.2020.1863682

Williams, K. J., Picou, A. A., Kish, S. L., Giraldo, A. M., Godke, R. A., and Bondioli, K. R. (2008). Isolation and characterization of porcine adipose tissue-derived adult stem cells. *Cells Tissues Organs* 188 (3), 251–258. doi:10.1159/000121431

Xia, L., Zhang, C., Lv, N., Liang, Z., Ma, T., Cheng, H., et al. (2022). AdMSC-derived exosomes alleviate acute lung injury via transferring mitochondrial component to improve homeostasis of alveolar macrophages. *Theranostics* 12 (6), 2928–2947. doi:10.7150/thno.69533

Xiao, G. Y., Cheng, C. C., Chiang, Y. S., Cheng, W. T., Liu, I. H., and Wu, S. C. (2016). Exosomal miR-10a derived from amniotic fluid stem cells preserves ovarian follicles after chemotherapy. *Sci. Rep.* 6, 23120. doi:10.1038/srep23120

Xiong, W. P., Yao, W. Q., Wang, B., and Liu, K. (2021). BMSCs-exosomes containing GDF-15 alleviated SH-SY5Y cell injury model of Alzheimer's disease via AKT/GSK-3β/β-catenin. *Brain Res. Bull.* 177, 92–102. doi:10.1016/j.brainresbull.2021.09.008

Xu, M., Feng, T., Liu, B., Qiu, F., Xu, Y., Zhao, Y., et al. (2021). Engineered exosomes: Desirable target-tracking characteristics for cerebrovascular and neurodegenerative disease therapies. *Theranostics* 11 (18), 8926–8944. doi:10.7150/thno.62330

Xu, R., Rai, A., Chen, M., Suwakulsiri, W., Greening, D. W., and Simpson, R. J. (2018). Extracellular vesicles in cancer - implications for future improvements in cancer care. *Nat. Rev. Clin. Oncol.* 15 (10), 617–638. doi:10.1038/s41571-018-0036-9

Yamanaka, S. (2020). Pluripotent stem cell-based cell therapy-promise and challenges. *Cell Stem Cell* 27 (4), 523–531. doi:10.1016/j.stem.2020.09.014

Yang, M., Lin, L., Sha, C., Li, T., Zhao, D., Wei, H., et al. (2020). Bone marrow mesenchymal stem cell-derived exosomal miR-144-5p improves rat ovarian function after chemotherapy-induced ovarian failure by targeting PTEN. *Lab. Invest* 100 (3), 342–352. doi:10.1038/s41374-019-0321-y

Yang, Z., Du, X., Wang, C., Zhang, J., Liu, C., Li, Y., et al. (2019). Therapeutic effects of human umbilical cord mesenchymal stem cell-derived microvesicles on premature ovarian insufficiency in mice. *Stem Cell Res. Ther.* 10 (1), 250. doi:10.1186/s13287-019-1327-5

Yin, N., Wu, C., Qiu, J., Zhang, Y., Bo, L., Xu, Y., et al. (2020). Protective properties of heme oxygenase-1 expressed in umbilical cord mesenchymal stem cells help restore the ovarian function of premature ovarian failure mice through activating the JNK/Bcl-2 signal pathway-regulated autophagy and upregulating the circulating of CD8(+) CD28(-) T cells. *Stem Cell Res. Ther.* 11 (1), 49. doi:10.1186/s13287-019-1537-x

Yu, T., Chu, S., Liu, X., Li, J., Chen, Q., Xu, M., et al. (2021). Extracellular vesicles derived from EphB2-overexpressing bone marrow mesenchymal stem cells ameliorate DSS-induced colitis by modulating immune balance. *Stem Cell Res. Ther.* 12 (1), 181. doi:10.1186/s13287-021-02232-w

Zhang, J., Yin, H., Jiang, H., Du, X., and Yang, Z. (2020). The protective effects of human umbilical cord mesenchymal stem cell-derived extracellular vesicles on cisplatin-damaged granulosa cells. *Taiwan J. Obstet. Gynecol.* 59 (4), 527–533. doi:10.1016/j.tjog.2020.05.010

Zhang, L., Zhang, S., Yao, J., Lowery, F. J., Zhang, Q., Huang, W. C., et al. (2015). Microenvironment-induced PTEN loss by exosomal microRNA primes brain metastasis outgrowth. *Nature* 527 (7576), 100–104. doi:10.1038/nature15376

Zhang, Q., Sun, J., Huang, Y., Bu, S., Guo, Y., Gu, T., et al. (2019). Human amniotic epithelial cell-derived exosomes restore ovarian function by transferring MicroRNAs against apoptosis. *Mol. Ther. Nucleic Acids* 16, 407–418. doi:10.1016/j.omtn.2019.03.008

Zhang, S., Huang, B., Su, P., Chang, Q., Li, P., Song, A., et al. (2021). Concentrated exosomes from menstrual blood-derived stromal cells improves ovarian activity in a rat model of premature ovarian insufficiency. *Stem Cell Res. Ther.* 12 (1), 178. doi:10.1186/s13287-021-02255-3

Zhang, Y., Xu, J., Liu, S., Lim, M., Zhao, S., Cui, K., et al. (2019). Embryonic stem cell-derived extracellular vesicles enhance the therapeutic effect of mesenchymal stem cells. *Theranostics* 9 (23), 6976–6990. doi:10.7150/thno.35305

Zhu, X., Liu, J., Pan, H., Geng, Z., Huang, W., Liu, T., et al. (2021). Thymopentin treatment of murine premature ovarian failure via attenuation of immune cell activity and promotion of the BMP4/Smad9 signalling pathway. *Int. J. Med. Sci.* 18 (15), 3544–3555. doi:10.7150/ijms.61975

Zou, G., Liu, T., Zhang, L., Liu, Y., Li, M., Du, X., et al. (2011). Induction of pancreatic beta-cell-like cells from CD44+/CD105+ human amniotic fluids via epigenetic regulation of the pancreatic and duodenal homeobox factor 1 promoter. *DNA Cell Biol.* 30 (9), 739–748. doi:10.1089/dna.2010.1144

frontiers | Frontiers in Cell and Developmental Biology

TYPE Original Research
PUBLISHED 24 February 2023
DOI 10.3389/fcell.2023.1090593

OPEN ACCESS

EDITED BY
Vanina Gabriela Da Ros,
CONICET Institute of Biology and Experimental Medicine (IBYME), Argentina

REVIEWED BY
María Laura Ribeiro,
CONICET Centro de Estudios Farmacológicos y Botánicos (CEFYBO), Argentina
Emin Turkay Korgun,
Akdeniz University, Türkiye
Alejandro Tapia-Pizarro,
University of Chile, Chile

*CORRESPONDENCE
Jing Yang,
dryangqing@hotmail.com
Peter C. K. Leung,
peter.leung@ubc.ca

†These authors have contributed equally to this work

SPECIALTY SECTION
This article was submitted to Molecular and Cellular Reproduction, a section of the journal Frontiers in Cell and Developmental Biology

RECEIVED 05 November 2022
ACCEPTED 17 February 2023
PUBLISHED 24 February 2023

CITATION
Luo J, Wang Y, Chang H-M, Zhu H, Yang J and Leung PCK (2023), ID3 mediates BMP2-induced downregulation of ICAM1 expression in human endometiral stromal cells and decidual cells. *Front. Cell Dev. Biol.* 11:1090593. doi: 10.3389/fcell.2023.1090593

ID3 mediates BMP2-induced downregulation of ICAM1 expression in human endometiral stromal cells and decidual cells

Jin Luo[1,2†], Yaqin Wang[1†], Hsun-Ming Chang[3], Hua Zhu[2], Jing Yang[1*] and Peter C. K. Leung[2*]

[1]Reproductive Medicine Center, Hubei Clinic Research Center for Assisted Reproductive Technology and Embryonic Development, Renmin Hospital of Wuhan University, Wuhan, China, [2]Department of Obstetrics and Gynaecology, BC Children's Hospital Research Institute, University of British Columbia, Vancouver, BC, Canada, [3]Reproductive Medicine Center, Department of Obstetrics and Gynecology, China Medical University Hospital, Taichung, Taiwan

Recurrent pregnancy loss (RPL) remains an unsolved problem in obstetrics and gynecology, and up to 50% of RPL cases are unexplained. Unexplained RPL (uRPL) is widely considered to be related to an aberrant endometrial microenvironment. BMP2 is an important factor involved in endometrial decidualization and embryo implantation, and intercellular adhesion molecule 1 (ICAM1) is a critical inflammatory regulator in the endometrium. In this study, we found that endometrial samples obtained from Unexplained RPL patients have significantly lower BMP2 and higher ICAM1 levels than fertile controls. For further research on the relationship between BMP2 and ICAM1 and the potential molecular mechanisms in Unexplained RPL, immortalized human endometrial stromal cells (HESCs) and primary human decidual stromal cells (HDSCs) were used as study models. Our results showed that BMP2 significantly decreased ICAM1 expression by upregulating DNA-binding protein inhibitor 3 (ID3) in both HESCs and HDSCs. Using kinase receptor inhibitors (dorsomorphin homolog 1 (DMH-1) and dorsomorphin) and siRNA transfection, it has been found that the upregulation of ID3 and the following downregulation of ICAM1 induced by BMP2 is regulated through the ALK3-SMAD4 signaling pathway. This research gives a hint of a novel mechanism by which BMP2 regulates ICAM1 in the human endometrium, which provides insights into potential therapeutics for unexplained RPL.

KEYWORDS

recurrent pregnancy loss (RPL), endometrium, BMP2, ICAM1, Id3

Introduction

Recurrent pregnancy loss (RPL), which is defined as the loss of two or more pregnancies before 24 weeks of gestation in the same couple based on the European Society of Human Reproduction and Embryology (ESHRE) guideline (ESHRE Guideline Group on RPL et al., 2018), affects approximately 5% of couples trying to conceive (Garrido-Gimenez and Alijotas-Reig, 2015). Although various etiological factors have been shown to lead to RPL (El Hachem et al., 2017), nearly 50% of RPL cases cannot find identifiable causes

or risk factors, which are classified as unexplained RPL (uRPL) (Garrido-Gimenez and Alijotas-Reig, 2015; El Hachem et al., 2017). The profound negative impact of RPL on both physical and mental health combined with the uncertainties in regard to the etiology and management options makes uRPL an ongoing challenge for both the clinical and scientific community. Therefore, exploring the pathogenesis of uRPL is essential for developing early interventions and ensuring a better pregnancy outcome.

As a unique tissue that indirectly contacts with the embryo, the endometrium plays a vital role in the establishment and maintenance of pregnancy. In recent decades, extensive research has been carried out to elucidate the biomolecular mechanisms that promote the acceptance of the embryo by the endometrium and the specific molecules and cellular pathways involved in endometrial receptivity. A number of studies have shown that various factors are dysregulated in the endometrium of women with uRPL (Comba et al., 2015; Dambaeva et al., 2021; Heidari et al., 2021; Zhu et al., 2022), including intercellular adhesion molecule 1 (ICAM1). ICAM1 is a single-chain, 90 kDa inducible cell-surface glycoprotein and a member of the immunoglobulin superfamily (Rothlein et al., 1991). In the human endometrium, ICAM1 is localized to the apical surface of the glandular epithelium, the vascular endothelium, and endometrial stromal cells throughout the menstrual cycle, and its expression in stromal cells is upregulated during menstruation (Thomson et al., 1999). The expression of ICAM1 has also been found in first-trimester human decidual stromal cells (Marzusch et al., 1993). Studies have found that inappropriate expression of ICAM1 may contribute to various gynecological and obstetric disorders, including endometriosis (Pino et al., 2009), gestational diabetes mellitus (Xie et al., 2008), preeclampsia (Austgulen et al., 1997) and RPL (Comba et al., 2015). The wide distribution of ICAM1 and these findings indicate that ICAM1 is involved in the menstrual process, glands, blood vessels and stroma function in the human endometrium and plays a crucial role in a successful pregnancy. However, the regulatory mechanism of ICAM1 during the menstrual cycle and early pregnancy in the human endometrium and decidua is largely unknown.

Bone formation protein 2 (BMP2) is a member of the transforming growth factor β (TGF-β) superfamily which serves as a key regulator of both endometrial degeneration (Li et al., 2007; Stoikos et al., 2008) and trophoblast cell invasion (Zhao et al., 2018a; Zhao et al., 2018b; Zhao et al., 2020). Functionally, Sma- and Mad-related (SMAD) proteins SMAD1/5/8 are phosphorylated when BMP2 binds to the TGF-β type II receptor and recruits the TGF-β type I receptors (ALK2, ALK3 and ALK6). After associating with the SMAD4 protein, the activated SMAD1/5/8 complex migrates to the nucleus wherein it regulates the target genes expression (Zhao et al., 2018a; Zhang et al., 2020; Luo et al., 2021a; Luo et al., 2021b). BMP2 is significantly elevated during decidualization in immortalized human endometrial stromal cells (HESCs) and primary human endometrial stromal cells (HDSCs) in response to steroid hormones and cyclic adenosine monophosphate (cAMP) (Luo et al., 2020). In addition, exogenous BMP2 treatment promotes the decidual response of these two kinds of cells (Luo et al., 2020). Our previous studies also demonstrated that BMP2 plays an essential role in endometrial stromal remodeling (Luo et al., 2020). However, the expression of BMP2 in the endometrium of patients with RPL has not been reported. We hypothesize that the overexpression of ICAM1 in the endometrium of uRPL patients may be controlled by BMP2 given the spatiotemporal variations in the expression of BMP2 and ICAM1 in the human endometrium throughout the menstrual cycle and pregnancy. To test this hypothesis, we analyzed the endometrial BMP2 and ICAM1 expression levels between uRPL patients and healthy women and explored the underlying molecular mechanisms and signaling pathways using HESCs and primary HDSCs.

Materials and methods

Patient recruitment and tissue collection

The use of endometrial tissue in the research received clearance from the ethics committee of Renmin Hospital, Wuhan University. A total of 16 women diagnosed with uRPL and 12 normal fertile women were recruited. The inclusion and exclusion criteria refer to previously published literature (Comba et al., 2015; Benner et al., 2022). Briefly, uRPL was defined as two or more fetal losses before 24 weeks of gestation without known causes of miscarriages. The control group was made up of normal fertile women with regular periods who had had at least one live birth and no spontaneous miscarriages in the past. The exclusion criteria were the use of immunosuppressive drugs, steroid hormones, antibiotics, diabetes mellitus and smoking. Endometrial biopsies were obtained from women who attended the reproductive center of Renmin Hospital of Wuhan University and received a endometrial biopsy on day 21 or day 22 of menstrual cycle which were identified as mid-secretory phase by pathological examination. In order to isolate primary HDSCs, first-trimester decidual specimens (between the 7th and 12th weeks of gestation) were collected from healthy women who were having an elective abortion as part of the CARE Program at the BC Women's Hospital and Health Centre. The research was authorized by the University of British Columbia's Research Ethics Board. All participants in this study were between 20 and 40 years of age and provided written informed consent.

Cell models

Considering that both BMP2 and ICAM1 are expressed in human endometrial stromal cells throughout the menstrual cycle, and endometrial decidualization is a critical physiological event in the female menstrual cycle, thus immortalized human endometrial stromal cells (HESCs; ATCC® CRL-4003) and primary HDSCs were used as study cell models, representing non-decidual and decidual stromal cells respectively, to systematically study the regulatory effect of BMP2 on ICAM1 in human endometrium at different stages of the menstrual cycle.

Culture and treatment of immortalized HESCs

HESCs were grown in DMEM/F12 medium without phenol red (Sigma-Aldrich, St. Louis, MO, United States of America), added with 10% charcoal dextran-treated fetal bovine serum (FBS;

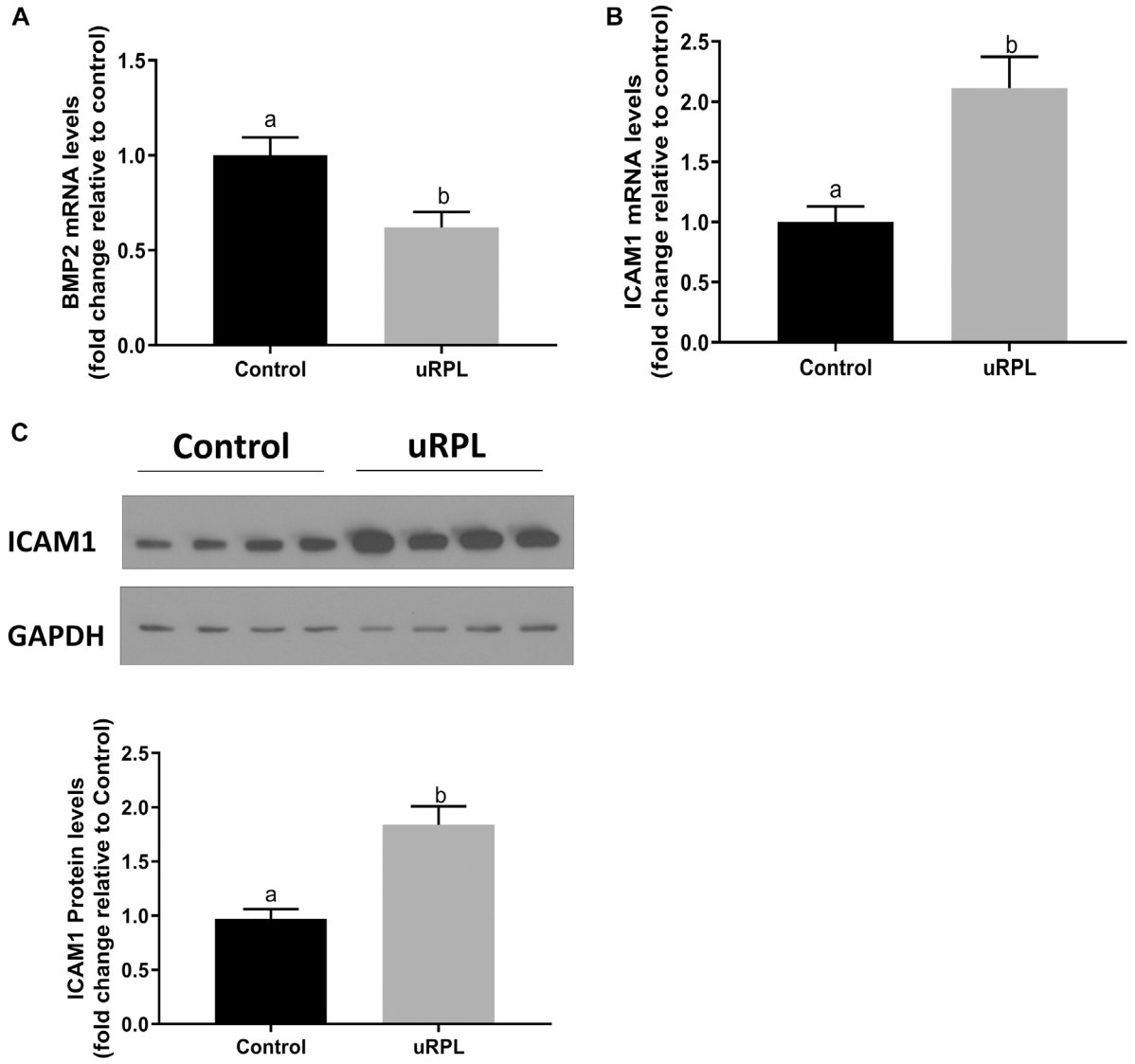

FIGURE 1
Expression levels of BMP2 and ICAM1 in the endometrium obtained from patients with unexplained recurrent pregnancy loss (uRPL) and fertile women (as a control). The endometrial samples were obtained from 12 uRPL patients and 16 fertile women (Control) during their mid-secretory phases. **(A,B)** The mRNA levels of BMP2 **(A)** and ICAM1 **(B)** of the endometrial tissues obtained from uRPL and controls were examined using RT-qPCR. **(C)** The protein levels of ICAM1 of the endometrial tissues obtained from uRPL and controls were examined using Western blot analysis. The results are expressed as the mean ± S.E.M. Different letters indicate a significant difference ($p < 0.05$).

HyClone Laboratories, Inc., Logan, UT, United States of America), 1% ITS - Premix (BD Biosciences, San Jose, CA, United States of America) and 5 ng/mL puromycin (Thermo Fisher Scientific, Ottawa, ON, CAN). Every culture was kept at 37 °C in an incubator with 5% CO_2. HESCs were cultivated for a day after being seeded at a density of 4×10^5 cells per plate in 60-mm tissue culture dishes with full culture media. HESCs were treated with BMP2 (0, 10, 25, or 50 ng/ml) for the concentration-dependent research or with 25 ng/mL BMP2 for the time-course study after serum deprivation in DMEM/F12 media without FBS for 18 h. For the concentration-dependent investigation, cells were taken at 24 h, while for the time-course study, cells were taken at 3, 6, 12, 24 h, and 48 h.

Isolation and cultivation of primary HDSCs

Primary HDSCs were separated from decidual tissues by means of enzymatic dispersion and mechanical dissociation, as mentioned before (Zhu et al., 2007). Generally, the samples were washed in cold phosphate-buffered saline (Gibco, Life Technologies, Inc., Carlsbad, CA, United States of America) three times, and then minced and treated with 0.1% collagenase (type IV; Sigma–Aldrich), 0.1% hyaluronidase (type I-S; Sigma–Aldrich) and 0.5 mg/ml DNase I (Sigma–Aldrich) and subsequently digested in a shaking water bath for 60 min at 37°C. The supernatant was neutralized by the addition of phenol red-free DMEM/F12 medium supplemented with 10% FBS before the cells were passed through a 40 m nylon filter (BD

10.3389/fcell.2023.1090593

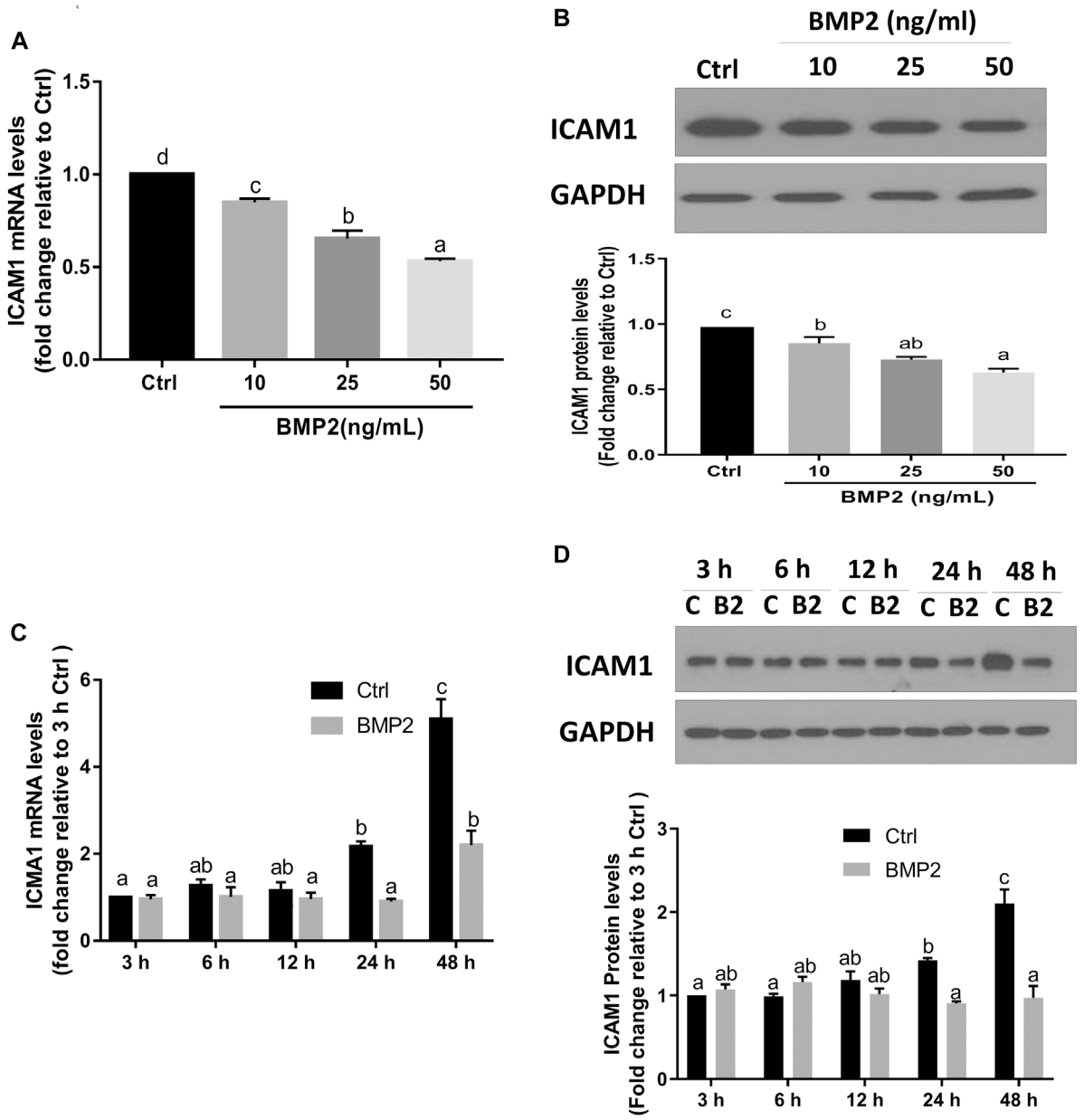

FIGURE 2
BMP2 downregulates the expression of ICAM1 in non-decidualized HESCs. **(A,B)** HESCs were treated with different concentrations (0, 10, 25, 50 ng/mL) of recombinant human BMP2 (BMP2) for 24 h, and the mRNA **(A)** and protein **(B)** levels of ICAM1 were examined using RT-qPCR and Western blot analysis, respectively. **(C,D)** HESCs were treated with 25 ng/mL of BMP2 for 3, 6, 12, 24 or 48 h, and the mRNA **(C)** and protein **(D)** levels of ICAM1 were examined using RT-qPCR and Western blot analysis, respectively. The results are expressed as the mean ± S.E.M. of at least three independent experiments. Different letters indicate significant a difference ($p < 0.05$). In detail, if the letters on two columns are different (E.g., "a" vs. "b" or "b" vs. "c"), it means that the difference between the two groups is significant, on the other hand, if the letters on the column of two groups are the same (E.g., "a" vs. "a" or "b" vs. "b"), it means there is no significant difference between two groups. C, Ctrl, Control; B2, BMP2.

Biosciences, Bedford, UK). The undigested tissue fragments were left on the filter, and the stromal cell-containing eluate was transferred into a 50 ml tube. The cells were then pelleted by centrifuging them at 1200 g for 3 min at room temperature. Following that, the cell pellets were washed, resuspended, and seeded in phenol red-free DMEM/F12 media with antibiotics (100 U/ml penicillin and 100 μg/ml streptomycin, Life Technologies, Inc.), 10% FBS, 30 nM 17β estradiol (E2; Sigma Aldrich), and 1 μM progesterone (P4; Sigma Aldrich). All decidual stromal cell cultures were afterwards maintained at 37°C in a humid incubator with 5% CO2, unless otherwise stated, in this culture medium. The purity of the HDSCs was determined by immunofluorescent staining for vimentin and cytokeratin-7 as described previously (Zhu et al., 2007). HDSCs were cultivated at a density of 5×10^5 cells per plate in 60-mm tissue culture dishes for the time- and concentration-dependent studies, and BMP2 was added in the same manner as HESCs.

10.3389/fcell.2023.1090593

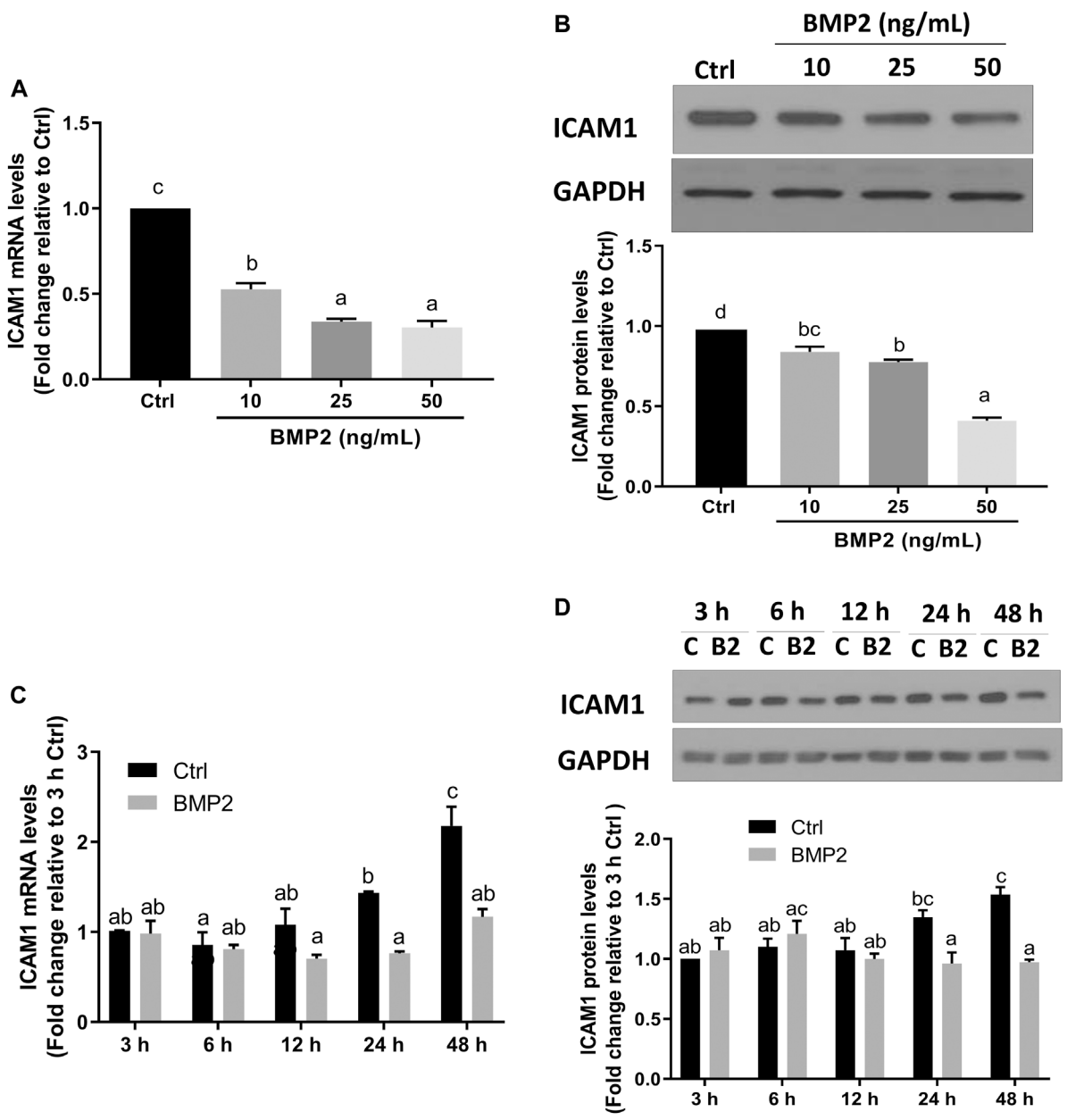

FIGURE 3
BMP2 downregulates the expression of ICAM1 in primary human endometrial stromal cells (HDSCs). (A,B) HDSCs (n = 3) were treated with different concentrations (0, 10, 25, 50 ng/mL) of BMP2 for 24 h, and the mRNA **(A)** and protein **(B)** levels of ICAM1 were examined using RT-qPCR and Western blot analysis, respectively. **(C,D)** HDSCs (n = 3) were treated with 25 ng/mL of BMP2 for 3, 6, 12, 24 or 48 h, and the mRNA **(C)** and protein **(D)** levels of ICAM1 were examined using RT-qPCR and Western blot analysis, respectively. The results are expressed as the mean ± S.E.M. Each experiment was performed in duplicate. Different letters indicate a significant difference ($p < 0.05$). C, Ctrl, Control; B2, BMP2.

Antibodies and reagents

Recombinant human BMP2, dorsomorphin homolog 1 (DMH-1) and dorsomorphin dihydrochloride (DM) were obtained from R&D Systems (Minneapolis, MN, United States of America). Monoclonal rabbit anti-DNA-binding protein inhibitor 3 (ID3), monoclonal mouse anti-ICAM1 and polyclonal rabbit anti-SMAD4 antibodies were obtained from Cell Signaling Technology (Beverly, MA, United States of America). Santa Cruz Biotechnology supplied the monoclonal mouse GAPDH antibody sc-47,724 (Santa Cruz, CA, United States of America). Bio-Rad Laboratories, Inc. supplied goat anti-mouse and goat anti-rabbit IgG that had been conjugated with horseradish peroxidase (Hercules, CA, United States of America).

Reverse transcription-quantitative real-time PCR (RT–qPCR)

Total RNA was extracted from collected endometrial tissue or cultured cells using TRIzol reagent (Invitrogen, Life Technologies,

Inc.) according to the manufacturer's instructions. Each reverse transcription procedure used 2 μg of RNA to create first-strand complementary DNA (cDNA) utilizing random primers and Moloney murine leukemia virus reverse transcriptase (Promega, Madison, WI, United States of America). Using an Applied Biosystems 7300 Real-Time PCR System, SYBR Green or TaqMan was used for RT-qPCR assays. Each 25 μl qPCR reaction comprised 12.5 μl of SYBR Green PCR Master Mix (Applied Biosystems, Foster City, CA), 100 ng of cDNA, and 7.5 nM of each specific primer. These primers were used in this study: ICAM-1, 5′-CTCCAATGTGCCAGGCTTG-3' (forward) and 5′- 5′-CAGTGGGAAAGTGCCATCCT-3' (reverse); ID3, 5′- CAG CTTAGCCAGGTGGAAATCC-3' (forward) and 5′-GTCGTTGGA GATGACAAGTTCCG-3' (reverse); SMAD4, 5′-TGGCCCAGGATCAGT AGGT-3′ (forward) and 5′-CATCAA CACCAATTCCAGCA-3′ (reverse); and GAPDH, 5' -GAGTCA ACGGATTTGGTCGT-3' (forward) and 5'- GACAAGCTTCCC GTTCTCAG-3' (reverse). Alternatively, TaqMan gene expression assay kits for BMP2 (Hs00154192_m1), ALK2 (Hs00153836_m1), ALK3 (Hs01034913_g1), and GAPDH (Hs02758991_g1) were bought from Applied Biosystems. Each 20 μL TaqMan RT-qPCR reaction comprised 1 × TaqMan Gene Expression Master Mix (Applied Biosystems), 20 ng of cDNA, and 1 × specific TaqMan assay Mix containing primers and probes. Relative quantification of the mRNA levels of target genes was determined based on the comparative cycle threshold (Ct) method, and the $2^{-\Delta\Delta Ct}$ method was used specifically, with the results standardized to endogenous GAPDH.

Western blot analysis

Total protein extracts were produced using lysis buffer (Cell Signaling Technology) containing protease inhibitor cocktail (Sigma Aldrich) from homogenized endometrial tissues or cultured cells. A DC Protein Assay (Bio-Rad Laboratories, Inc.) was used to measure the protein concentrations. Proteins of same concentration were put onto gels and transferred onto polyvinylidene fluoride (PVDF) membranes (Bio-Rad) after being separated by sodium dodecyl sulfate–polyacrylamide gel electrophoresis. After blocking the membranes for 1 h at room temperature in Tris-buffered saline containing 0.1% Tween-20 (TBST) and 5% nonfat milk, they were immunoblotted overnight at 4°C with the appropriate primary antibodies. After three washes with TBST, the membranes were incubated with peroxidase-conjugated secondary antibodies for 1 hour. Enhanced chemiluminescent or SuperSignal West Femto chemiluminescent substrates (Thermo Fisher Scientific) were used to identify immunoreactive bands, which were subsequently subjected to X-ray film (Thermo Fisher Scientific). Image-Pro Plus software was used to calculate the band intensities (v4.5; Media Cybernetics, Carlsbad, CA).

Small interfering RNA transfection

RNA interference was enabled by the transfection of small interfering RNA (siRNA). ON-TARGET plus non-targeting control pool siRNA or an ON-TARGET plus SMART pool targeting ALK2, ALK3, ID3 and SMAD4 were purchased from Dharmacon Inc. A total of 2×10^5 HESCs or primary HDSCs were simultaneously seeded with full culture media 1 day before transfection. Lipofectamine RNA iMAX (Life Technologies) was used to transfect control siRNA or siRNA against ALK2, ALK3, ID3 and SMAD4 into the cells at a dose of 25 nM in accordance with the manufacturer's instructions. The cells were then cultured for 24 h at 37 °C in a CO2 incubator untill starvation (synchronization of all the cells to the same cell cycle phase and removal of various ligands in serum). RT–qPCR or Western blot analysis was used to assess the knockdown effectiveness of each target.

Statistical analysis

All statistical analyses were conducted using PRISM software (GraphPad Software, Inc., San Diego, CA). Using the unpaired Student's t-test, comparisons were made between two sets of independent samples. Multiple comparisons of means were examined using one-way ANOVA and Newman–Keuls testing. The results are reported as the mean ± S.E.M. of at least three independent experiments. The significance threshold was established at $p < 0.05$.

Results

Decreased BMP2 and increased ICAM1 expression in the endometrium of patients with uRPL

High expression levels of BMP2 and ICAM1 have been reported in human endometrium in prior studies (Thomson et al., 1999; Bai et al., 2020). Here, the expression levels of these two factors in secretory endometrial tissues were compared between uRPL patients and healthy fertile women by using RT–qPCR and Western immunoblotting. As shown in Figure 1, compared with normal fertile controls, the expression of BMP2 in the endometrial tissues of uRPL patients was dramatically lower at mRNA level (Figure 1A), whereas the expression of ICAM1 at both mRNA (Figure 1B) and protein (Figure 1C) levels were considerably increased in the endometrium of women with uRPL.

BMP2 suppresses the expression of ICAM1 in HESCs and primary HDSCs

To investigate if BMP2 affects ICAM1 expression in HESCs, serum-starved cells were initially treated with vehicle control or various concentrations (10, 25, or 50 ng/ml) of recombinant human BMP2 for 24 h. The expression levels of ICAM1 were detected by RT–qPCR and Western immunoblotting. The results revealed that both the mRNA (Figure 2A) and protein levels (Figure 2B) of ICAM1 were markedly downregulated in a concentration-dependent fashion in response to the BMP2 treatment in HESCs. The time-course study showed that cultivation with 25 ng/mL BMP2 dramatically decreased the mRNA (Figure 2C) and protein levels of ICAM1 at 24 h and 48 h (Figure 2D). We also evaluated the

10.3389/fcell.2023.1090593

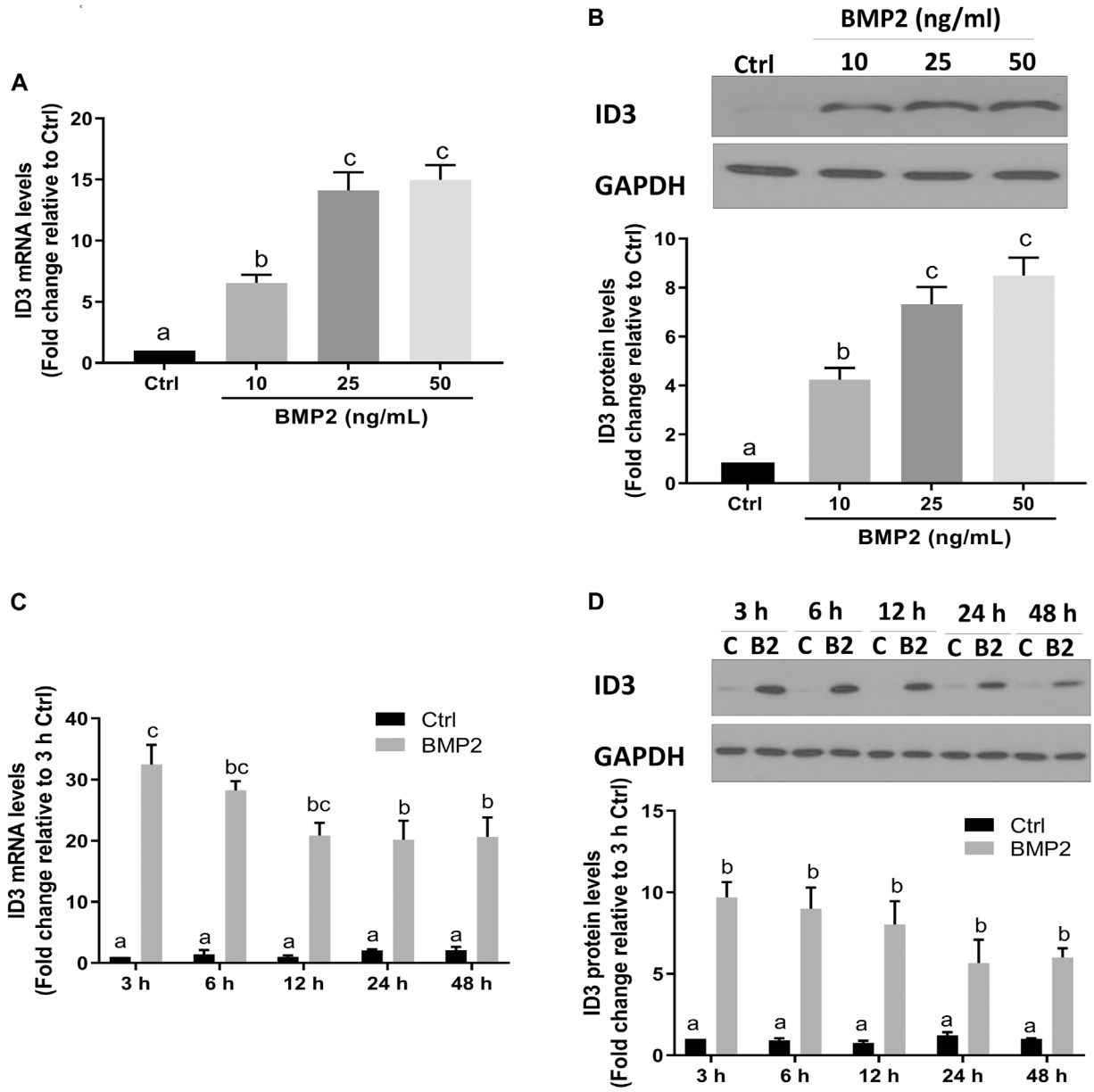

FIGURE 4
BMP2 upregulates the expression of ID3 in HESCs. (A and B) HESCs were treated with different concentrations (0, 10, 25, 50 ng/mL) of BMP2 for 24 h, and the mRNA **(A)** and protein **(B)** levels of ID3 were examined using RT-qPCR and Western blot analysis, respectively. **(C,D)** HESCs were treated with 25 ng/mL of BMP2 for 3, 6, 12, 24 or 48 h, and the mRNA **(C)** and protein **(D)** levels of ID3 were examined using RT-qPCR and Western blot analysis, respectively. The results are expressed as the mean ± S.E.M. of at least three independent experiments. Different letters indicate a significant difference ($p < 0.05$).

influence of BMP2 on the expression of ICAM1 in primary HDSCs in addition to HESCs. The purity of HDSCs was determined by immunofluorescent staining with markers specific to mesenchymal cells (vimentin) and epithelial cells (cytokeratin-7). HDSCs used in these studies were approximately 98% pure as assessed by vimentin-positive and cytokeratin-negative staining (Supplementary Figure S1). In accordance with the findings in HESCs, treatment with various dosages (10, 25, or 50 ng/mL) of BMP2 for 24 h dramatically decreased the mRNA (Figure 3A) and protein (Figure 3B) levels of ICAM1 in a concentration-dependent way. The time-course analysis revealed that 25 ng/mL BMP2 treatment substantially decreased ICAM1 mRNA (Figure 3C) and protein (Figure 3D) levels at 24 h, and 48 h.

BMP2 upregulates the expression of ID3 in HESCs and primary HDSCs

Transcriptional regulator inhibitor of DNA-binding/differentiation-3 (ID3) is a member of the helix-loop-helix

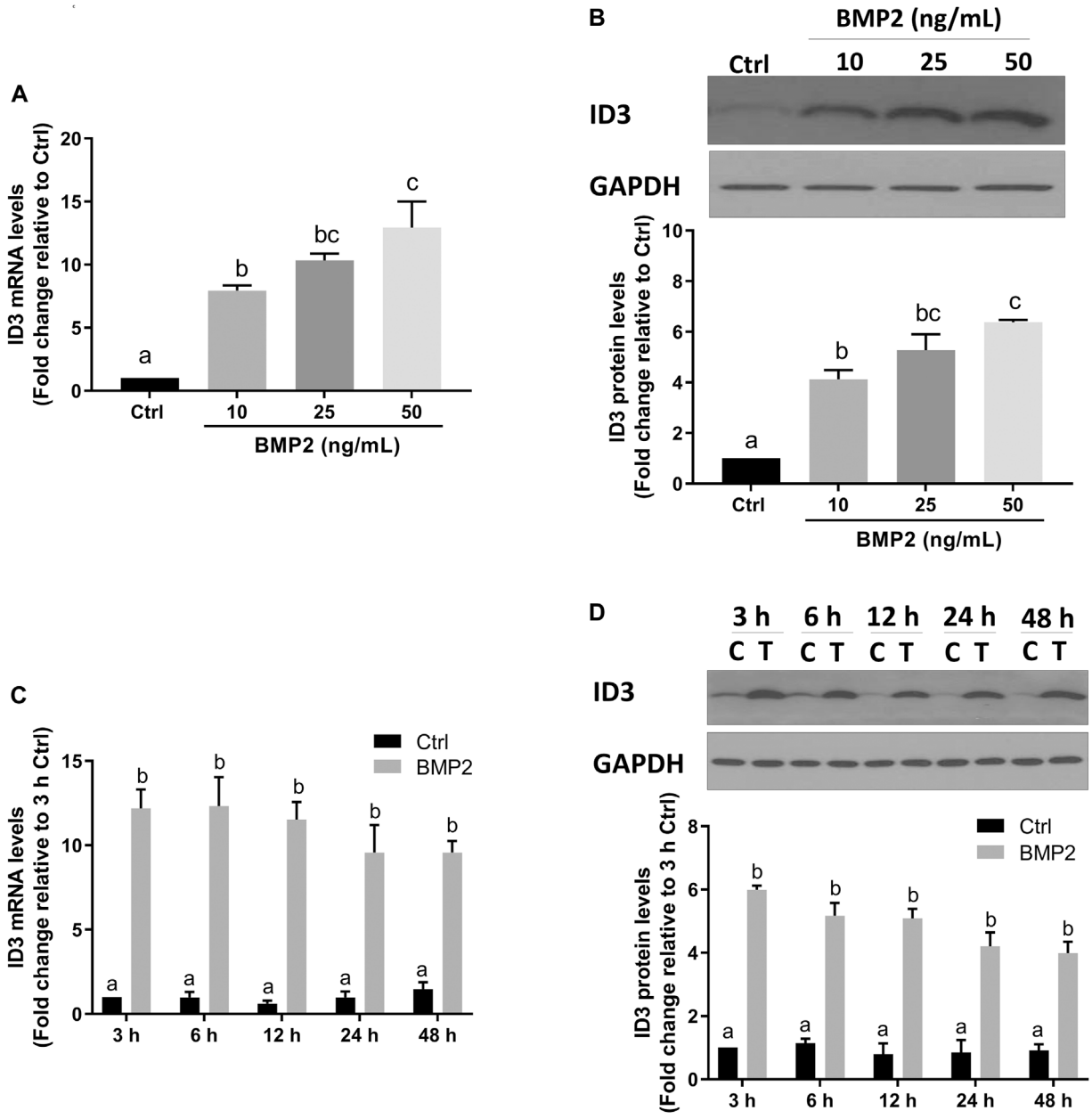

FIGURE 5
BMP2 upregulates the expression of ID3 by BMP2 in HDSCs. (A and B) HDSCs were treated with different concentrations (0, 10, 25, 50 ng/mL) of recombinant human BMP2 for 24 h, and the mRNA **(A)** and protein **(B)** levels of ID3 were examined using RT-qPCR and Western blot analysis, respectively. **(C,D)** HDSCs were treated with 25 ng/mL of BMP2 for 3, 6, 12, 24 or 48 h, and the mRNA **(C)** and protein **(D)** levels of ID3 were examined using RT-qPCR and Western blot analysis, respectively. The results are expressed as the mean ± S.E.M. of at least three independent experiments. Different letters indicate a significant difference ($p < 0.05$).

(HLH) protein family. Several previous studies have demonstrated that ID3 is a downstream target of BMPs [28–30]. To determine if ID3 is a downstream target of BMP2 in this assay system, the expression levels of ID3 in HESCs and HDSCs were assessed using RT–qPCR and Western blot analysis following BMP2 treatment. As shown in Figure 4, the mRNA (Figure 4A) and protein (Figure 4B) the expression levels of ID3 were remarkably increased after treatment with gradually increased concentrations of BMP2 in HESCs. In time-response experiments, the mRNA (Figure 4C) and protein (Figure 4D) levels of ID3 markedly rose 3 h after 25 ng/ml BMP2 treatment and persisted for 48 h in HESCs. Similar results were noted in the primary HDSCs. Increasing BMP2 doses resulted in a considerable rise in mRNA (Figure 5A) and protein (Figure 5B) expression levels of ID3, and 25 ng/ml BMP2 treatment markedly enhanced the mRNA (Figure 5C) and protein (Figure 5D) levels of ID3 at 3 h and persisted for 48 h in HDSCs. When cells were treated with BMP2 at a concentration of 10 ng/ml, the expression levels of

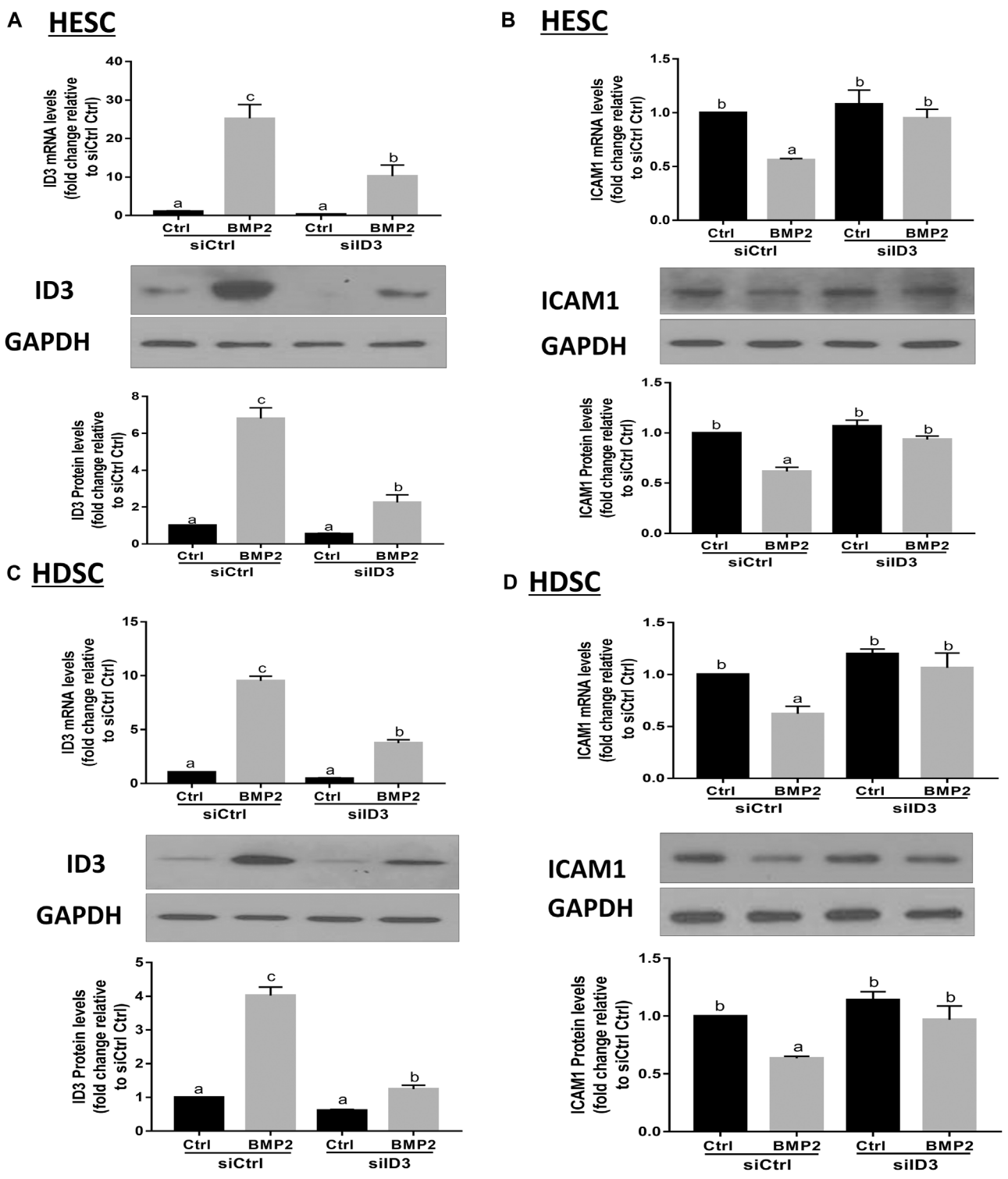

FIGURE 6
ID3 mediates the BMP2-induced downregulation of ICAM1 expression in HESCs and HDSCs. **(A,B)** HESCs were transfected with 25 nM control siRNA (siCtrl) or 25 nM siRNA targeting ID3 (siID3) for 48 h, and the cells were then treated with vehicle control (Ctrl) or 25 ng/mL BMP2 for an additional 24 h. The mRNA and protein levels of ID3 **(A)** and ICAM1 **(B)** were examined using RT-qPCR and Western blot analysis respectively. **(C,D)** HDSCs were transfected with 25 nM siCtrl or 25 nM siID3 for 48 h, and the cells were then treated with Ctrl or 25 ng/ml of BMP2 for an additional 24 h. The mRNA and protein levels of ID3 **(C)** and ICAM1 **(D)** were examined using RT-qPCRand Western blot analysis, respectively. The results are expressed as the mean ± S.E.M. of at least three independent experiments. Different letters indicate significant a difference ($p < 0.05$).

10.3389/fcell.2023.1090593

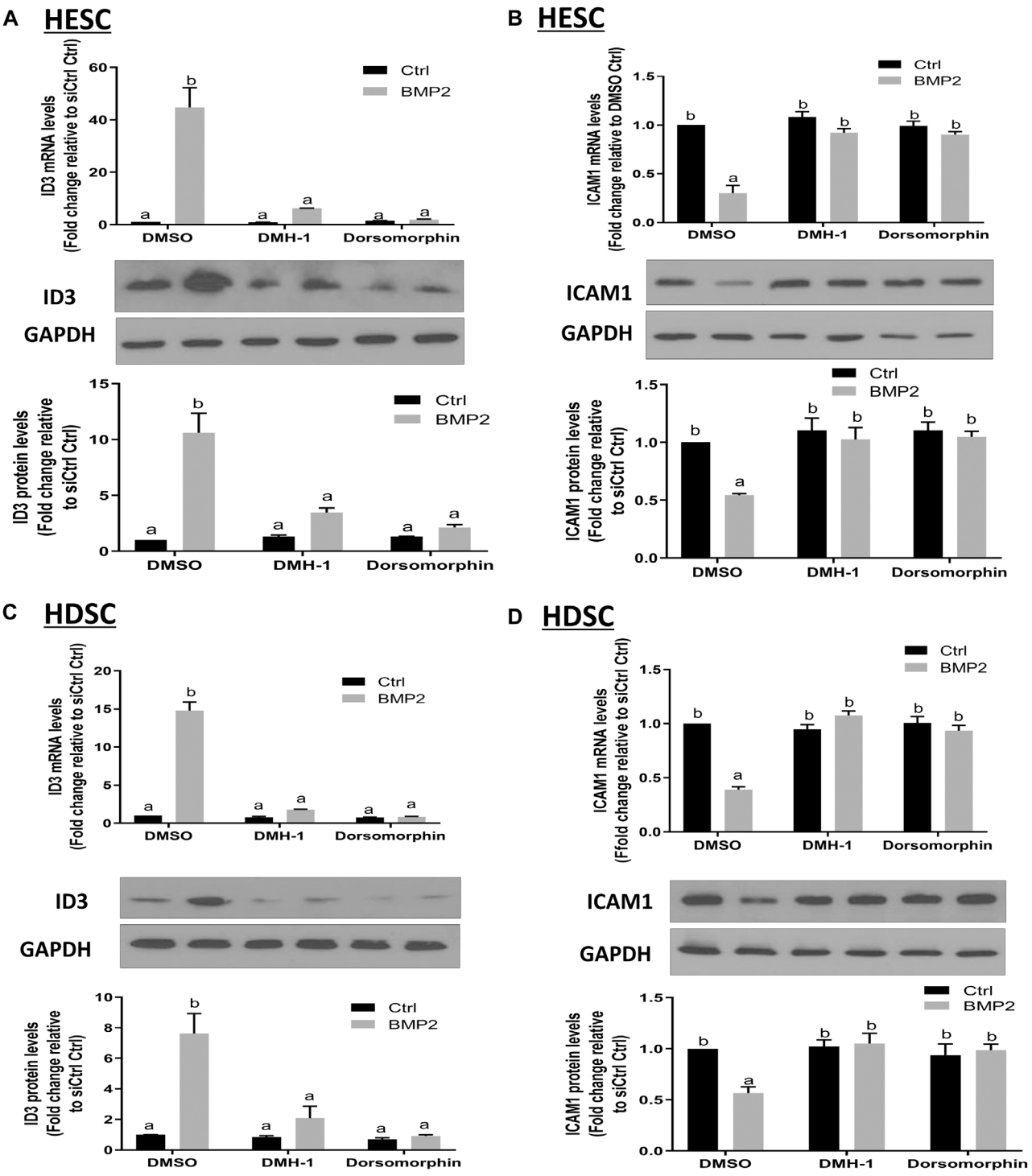

FIGURE 7
The effects of specific TGF-β type I inhibitors on BMP2-induced upregulation of ID3 expression and downregulation of ICAM1 expression in HESCs and HDSCs. (A and B) HESCs were pretreated with dimethyl sulfoxide (DMSO), DMH-1 (0.25 μM), or dorsomorphin (10 μM) for 1 h, and the cells were then treated with 25 ng/ml BMP2 for an additional 24 h. The mRNA and protein levels of ID3 **(A)** and ICAM1 **(B)** were examined using RT-qPCR and Western blot analysis, respectively. **(C,D)** HDSCs were pretreated with DMSO, DMH-1 (0.25 μM), or dorsomorphin (10 μM) for 1 h, and the cells were then treated with 25 ng/mL BMP2 for an additional 24 h. The mRNA and protein levels of ID3 **(C)** and ICAM1 **(D)** were examined using RT-qPCR and Western blot analysis, respectively. The results are expressed as the mean ± S.E.M. of at least three independent experiments. Different letters indicate a significant difference ($p < 0.05$).

10.3389/fcell.2023.1090593

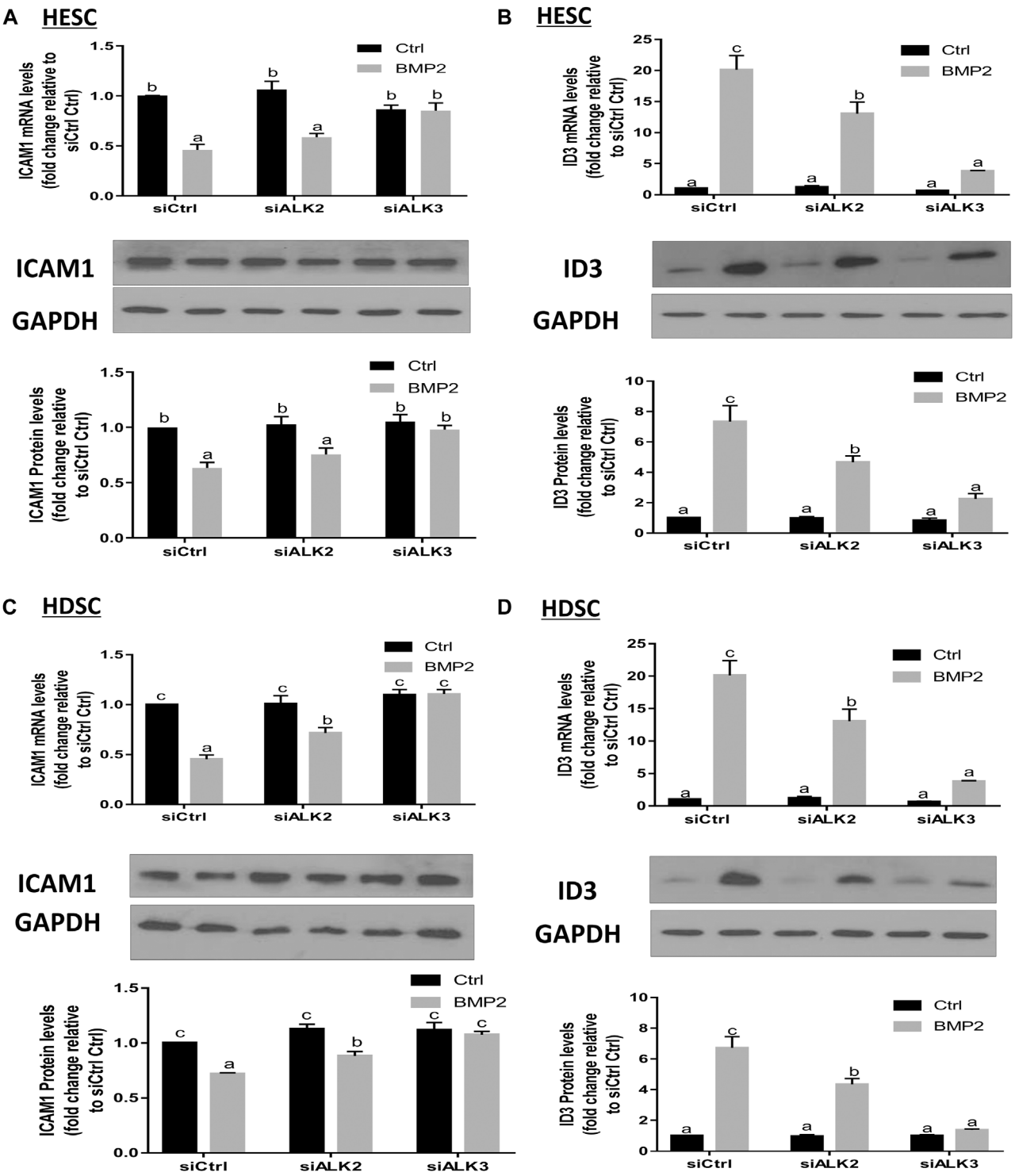

FIGURE 8
ALK3 type I mediates the BMP2-induced downregulation of ICAM1 and ID3 in HESCs and HDSCs. **(A,B)** HESCs were transfected with 25 nM siCtrl, siRNA targeting ALK2 (siALK2) or siRNA targeting ALK3 (siALK3) for 48 h, and the cells were then treated with Ctrl or 25 ng/mL of BMP2 for an additional 24 h. The mRNA levels of ICAM1 **(A)** and ID3 **(B)** were examined using RT-qPCR and the protein levels of ICAM1 and ID3 were examined using Western blot analysis. **(C,D)** HDSCs were transfected with 25 nM siCtrl, 25 nM siALK2 or 25 nM siALK3 for 48 h, and the cells were then treated with Ctrl or 25 ng/mL BMP2 for an additional 24 h. The mRNA levels of ICAM1 **(C)** and ID3 **(D)** were examined using RT-qPCR, and the protein levels of ICAM1 and ID3 were examined using Western blot analysis. The results are expressed as the mean ± S.E.M. of at least three independent experiments. Different letters indicate significant a difference ($p < 0.05$).

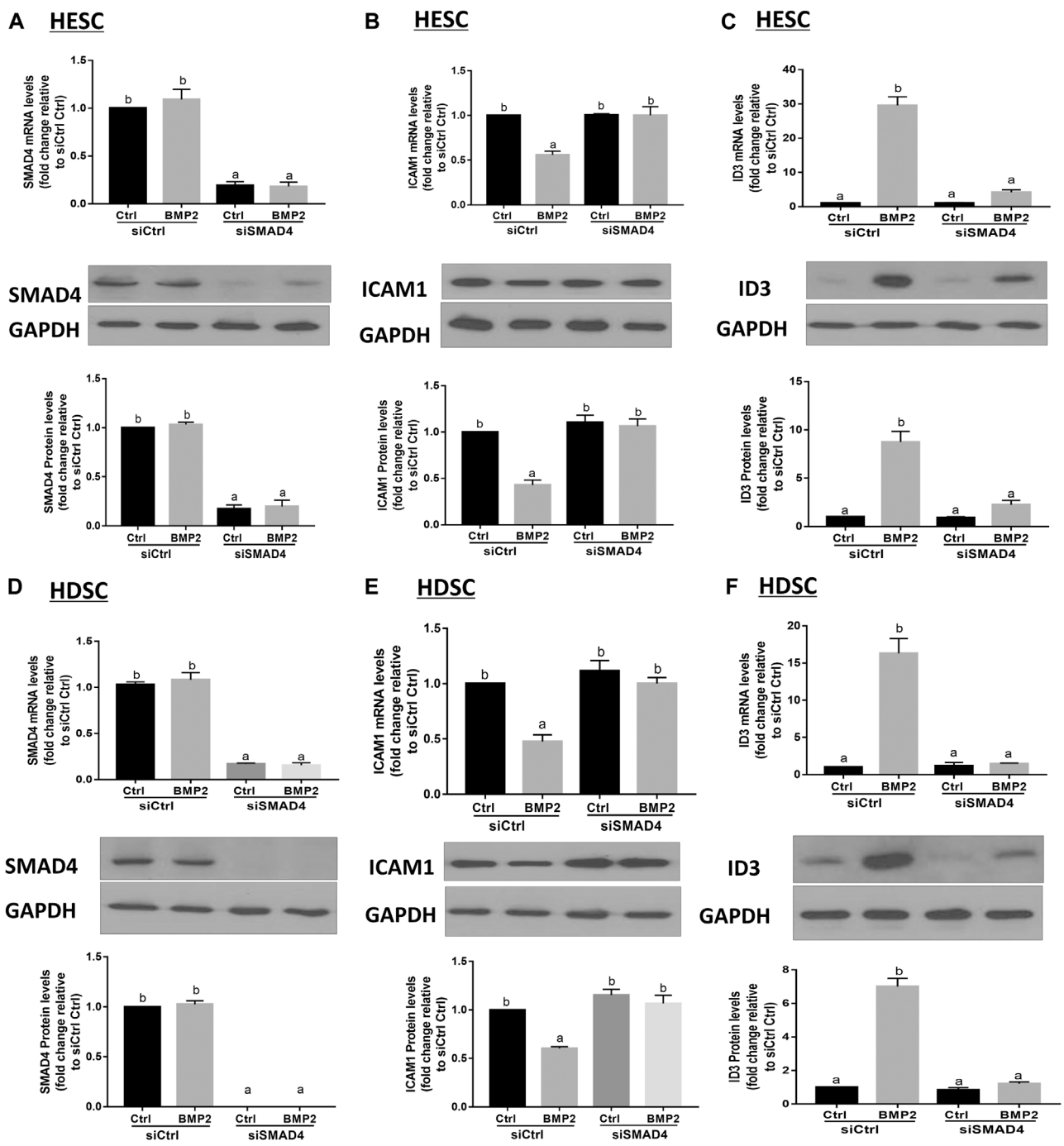

FIGURE 9
SMAD4 is involved in the BMP2-induced upregulation of ID3 expression and downregulation of ICAM1 expression in HESCs and HDSCs. **(A–C)** HESCs were transfected with 25 nMsiCtrl or 25 nM siRNA targeting SMAD4 (siSMAD4) for 48 h, and the cells were then treated with BMP2 (25 ng/mL) for an additional 24 h. The mRNA and protein levels of SAMD4 **(A)**, ICAM1 (B) and ID3 **(C)** were examined using RT-qPCR and Western blot analysis, respectively. **(D–F)** HDSCs were transfected with 25 nM siCtrl or 25 nM siSMAD4 for 48 h, and the cells were then treated with BMP2 (25 ng/mL) for an additional 24 h. The mRNA and protein levels of SAMD4 **(D)**, ICAM1 **(E)** and ID3 **(F)** were examined using RT-qPCR and Western blot analysis. Respectively. The results are expressed as the mean ± S.E.M. of at least three independent experiments. Different letters indicate significant a difference ($p < 0.05$).

ID3 and ICAM1 were significantly changed both in HESCs and HDSCs, but the decreased range of ICAM1 expression in protein was mild (0.84-fold change relative to Ctrl in HESCs and 0.85-fold change relative to Ctrl in HDSCs). Therefore, we chose a concentration of 25 ng/ml for the follow-up studies to ensure the stability and reproducibility of the experiment.

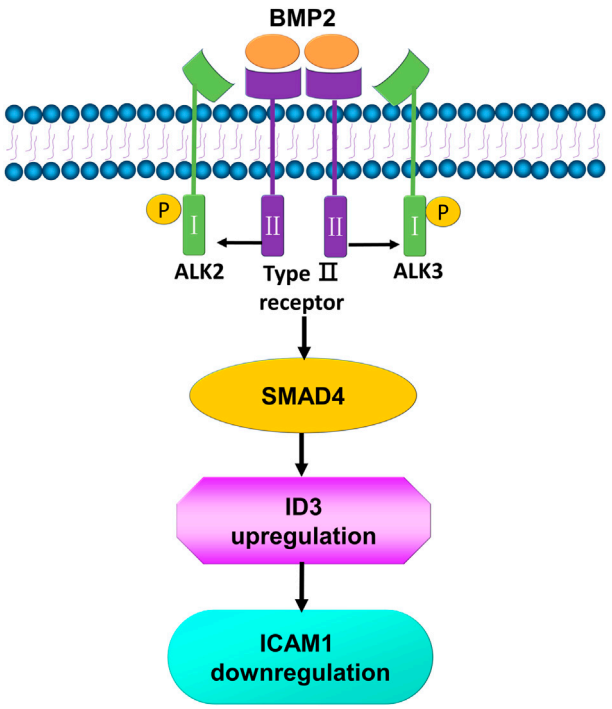

FIGURE 10
Schematic diagram of the proposed molecular mechanisms by which BMP2 downregulates the expression of ICAM1 in human endometrial stromal cells and decidual cells. BMP2 binds to a pair of ALK3 type 1 receptor and BMP type II receptors, leading to the activation of canonical R-SMADs, which are associated with a common SMAD (SMAD4) and further increases the transcription of ID3. The increase in ID3 suppresses the expression of ICAM1.

ID3 mediates the BMP2-induced downregulation of ICAM1 in HESCs and primary HDSCs

By transfecting HESCs and primary HDSCs with ID3-targeting siRNA (siID3), siRNA-based knockdown studies were carried out to investigate the functions of ID3 in BMP2-induced downregulation of ICAM1. The HESCs and primary HDSCs were transfected with siID3 for 24 h, starved in serum-free media for 18 h, and then cocultured with recombinant BMP2 (25 ng/mL) for 24 h. Our results showed that knockdown of ID3 significantly reduced the ID3 expression induced by BMP2 at the mRNA and protein levels (Figure 6A) as well as reversed the mRNA and protein levels of the BMP2-induced downregulation of ICAM1 (Figure 6B) in HESCs. Similar findings were also obtained in primary HDSCs (Figures 6C,D). However, silencing ID3 does not seem to alter basal levels of ICAM1. The same phenomenon has been found in some other studies (Li et al., 2019; Li et al., 2021). We believe that the possible reason is that in the non-stimulated HESCs and HDSCs, the expression of ID3 was very low, and silencing ID3 cannot alter the constitutive expression of ICAM1 but can only affect the inducible ICAM1 expression. These findings imply that ID3 mediates the BMP2-induced downregulation of ICAM1 in HESCs and primary HDSCs.

DMH-1 or dorsomorphin abolishes the BMP2-induced upregulation of ID3 and downregulation of ICAM1 expression in HESCs and primary HDSCs

BMPs transduce signals through transmembrane serine/kinases composed of type I (ALK2, ALK3, and ALK6) and type II receptors (Salazar et al., 2016). To further clarify the role of these type I receptors in the BMP2-induced upregulation of ID3 and downregulation of ICAM1 expression in HESCs and primary HDSCs, these two kinds of cells were pretreated with different TGF-β type I receptor inhibitors, namely, DMH-1 (an inhibitor of ALK2 and ALK3) or dorsomorphin (an inhibitor of ALK2, ALK3, and ALK6) for 1 h, followed by treatment with 25 ng/mL BMP2 for another 24 h. The cells in the control group were treated with equal volumes of DMSO, which has been widely used to formulate compounds for cell administration. Several studies have confirmed that there is no interference with the cell experiment if the final concentration of DMSO is controlled within 0.1% (v/v) (Qi et al., 2008; Dludla et al., 2018). In the present study, the final concentration of DMSO is 0.05% (v/v), which is considered to be a safe vehicle of reagents for almost all cells. The results showed that either DMH-1 or dorsomorphin completely abolished BMP2-induced upregulation of ID3 (Figures 7A, C) and downregulation of ICAM1 (Figures 7B, D) mRNA and protein expression in the HESCs (Figures 7A, B) and primary HDSCs (Figures 7C, D). These results indicate that BMP2 regulates the expression of ID3 and ICAM1 through ALK2 and/or ALK3 receptors.

ALK3 type I receptor mediates the BMP2-induced upregulation of ID3 and downregulation of ICAM1 expression in HESCs and primary HDSCs

To learn more about the particular type I receptor that BMP2 uses to upregulate ID3 expression and to reduce ICAM1 expression in HESCs and primary HDSCs, the effects of ALK2 or ALK3 were suppressed using a siRNA-based suppression strategy. The cells were pretreated with specific siRNAs targeting ALK2 (siALK2) or ALK3 (siALK3) for 48 h, followed by treatment with 25 ng/mL BMP2 for an additional 24 h. Our results showed that pretreated with siALK2 or siALK3 significantly reduced the target gene expression in HESCs and HDSCs without affecting the expression of the other one, and the expression levels of ALK2 and ALK3 were not affected by BMP2 treatment (Supplementary Figure S2). As shown in Figure 8, knockdown of ALK3 completely abolished the downregulation of ICAM1 (Figure 8A) and upregulation of ID3 (Figure 8B) induced by BMP2 at both the mRNA and protein levels in HESCs. Interestingly, knockdown of ALK2 partially inhibited the BMP2-induced downregulation of ICAM1 (Figure 8C) and upregulation of ID3 expression (Figure 8D) in HDSCs. However, it seemed to have no significant effect on the downregulation of ICAM1 mRNA or protein expression (Figure 8A) induced by BMP2 in HESCs. These results suggest that ALK3 is the major receptor for upregulating ID3 and downregulating ICAM1 expression by BMP2 in HESCs and primary HDSCs.

SMAD4 mediates the BMP2-induced upregulation of ID3 and downregulation of ICAM1 expression in HESCs and primary HDSCs

Prior to moving into the nucleus to control target genes, phosphorylated R-SMADs join forces with SMAD4 to create a heterotrimeric transcription factor complex. We transfected HESCs and primary HDSCs with siSMAD4 to inhibit endogenous SMAD4 expression in order to better understand if the SMAD signaling pathway is involved in the BMP2-induced overexpression of ID3 and downregulation of ICAM1. Following a 48-h siSMAD4 transfection, the cells were given 25 ng/mL BMP2 treatment for an additional 24-h period. SMAD4 knockdown effectiveness was confirmed by Western blot and RT-qPCR analysis. Our results showed that the expression of SMAD4 almost eliminated after siSMAD4 transfection and treatment with 25 ng/mL BMP2 did not alter SMAD4 expression in HESCs and HDSCs (Figures 9A, D). The siRNA-mediated depletion of SMAD4 completely abolished the downregulation of ICAM1(Figure 9B) and upregulation of ID3 (Figure 9C) mRNA and protein expression in HESCs. Notably, SMAD4 knockdown also completely abolished BMP2-induced cell activity in HDSCs (Figures 9E, F).

Discussion

Due to the unclear underlying pathogenesis and the lack of effective interventions, uRPL remains one of the most challenging and frustrating fertility-related diseases. In the present study, we found that mid-secretory endometrium samples obtained from uRPL patients had significantly lower BMP2 and higher ICAM1 levels than fertile controls. Additionally, we demonstrate for the first time that BMP2 suppresses ICAM1 expression through a mechanism reliant on ID3 overexpression both in non-decidual and decidual stromal cells. This information will aid in the development of new pharmacological strategies for unexplained RPL.

There are a large number of cell adhesion molecules in the human endometrium that appear to be necessary to successfully establish the physical interaction between the embryo and the endometrium (van Mourik et al., 2009). One of the best-characterized cell adhesion molecules is ICAM1, which is a ligand for integrin molecule 1 (LFA-1). The expression of ICAM1 has previously been examined in endometrial stromal cells and endometrial epithelial cells in multiple species (Blois et al., 2005; Defrere et al., 2005; Lecce et al., 2011). A previous study demonstrated that ICAM1 was substantially increased in the uterine epithelium and the stroma of high-stress sensing induced abort-prone mice compared to control mice, resulting in more LFA-1-expressing lymphocytes being recruited from the blood into the uterus. Neutralization of the adhesion molecules ICAM1/LFA-1 radically eliminated the effect of stress on the embryonic abortion (Blois et al., 2005). Further research revealed that upregulated ICAM1 in the decidua promoted Th1 polarization *via* mature dendritic cells, leading to Th1/Th2 imbalance (Blois et al., 2005), which is known to contribute to the pathogenesis of RPL. Notably, evidence from a clinical study showed that elevated ICAM1 levels detected by ELISA in human endometrial tissue correlated with idiopathic RPL (Comba et al., 2015). Similar results were obtained by examining the RNA and protein expression levels of ICAM1 in endometrial tissue obtained from uRPL patients and normal fertile women in our study. At the same time, we also detected that BMP2 expression in the endometrium of these two groups exhibited an opposite phenotype to ICMA1. It has been demonstrated that the upregulation of ICAM1 in HESCs can be induced by various inflammatory mediators such as IL-1 β (Vigano et al., 1994), TNF-α (Thomson et al., 1999), and INF-γ (Mangioni et al., 2005). However, the regulation of ICAM1 by BMP2 has not yet been reported. Definitive evidence shows that BMP2 is essential for pregnancy establishment and maintenance by regulating blastocyst implantation, uterine decidualization and placental/fetal development (Lee et al., 2007; Yi et al., 2021). Transcriptome analysis revealed that BMP2 targets primarily play a key role in regulating cell adhesion and extracellular matrix (ECM) transformation in human endometrium (Yi et al., 2021). By controlling the expression of IGFBP3, our prior work also showed that BMP2 contributes to endometrial remodeling in human non-decidual and decidual stromal cells (Luo et al., 2020). In this study, our *in vitro* analysis showed that the expression of ICAM1 in HESCs and primary HDSCs can also be regulated by BMP2 *via* ID3.

The inhibitors of DNA binding proteins (ID) are dominant negative antagonists of basic helixloop-helix (bHLH) transcription factors. To date, four ID family proteins have been identified in mammalian cells and have been demonstrated to be expressed in the uterine endometrium as well as the maternal-fetal interface (Han et al., 2018). Our studies showed that ID1 (Luo et al., 2020), ID2 (Supplementary Figure S3), and ID3 (Figure 4; Figure 5) are among the most significantly upregulated genes upon stimulation of BMP2. Further studies based on the siRNA-based knockdown experiments found that it was ID3 but not ID1 or ID2 that mediated BMP2-induced downregulation of ICAM1 in HESCs and primary HDSCs (Figure 6 and Supplementary Figure S4). ID3 expression can be differentially regulated by members of the TGF-β superfamily in various cell types; for example, TGF-β1 represses ID3 expression in adult neural stem/precursor cells (Bohrer et al., 2015), while TGF-β1 increases ID3 mRNA and nuclear ID3 protein levels in immortalized human granulosa cells (Li et al., 2019). In addition, other TGF-β superfamily members, such as BMP4 and BMP6, upregulate ID3 expression in a range of different cell lines, including embryonic stem cells, human B progenitor cells, intestinal stem cells, and neuronal stem cells (Hollnagel et al., 1999; Kersten et al., 2006; Hu et al., 2021). Importantly, a previous study revealed that ID3 was dramatically upregulated by BMP2 in adult neural stem/precursor cells and was essential for BMP2- induced differentiation of neural stem/precursor cells into astrocytes (Bohrer et al., 2015). In this study, our findings add to growing evidence that the overexpression of ID3 induced by BMP2 was required for BMP2-suppressed ICAM1 expression in HESCs and primary HDSCs. Furthermore, we explored the underlying molecular mechanism by which BMP2 regulates the ID3 and ICAM1 expression by pretreating HESCs and primary HDSCs with different TGF-β type I receptor inhibitors, including DMH-1 (an inhibitor of ALK2/3) and dorsomorphin (an inhibitor of ALK2/3/6) prior to BMP2 treatment. Our results show that the inhibitors DMH-1 and

dorsomorphin can significantly eliminate the upregulation of ID3 and downregulation of ICAM1 induced by BMP2, but the siRNA-mediated gene downregulation provided more accurate evidence that it is ALK3 rather than ALK2 mainly responsible for the downstream pathway of BMP2 induction. We suppose that although ALK3 and ALK2 are paralogous genes and both are downstream receptors of BMPs, their protein primary structures are about 10% different, which may lead to some functional divergence. This will be interesting research content in the future. Ligand–receptor complexes induce downstream signaling in a SMAD-dependent manner following BMP2 binding to specific receptors (Shi and Massague, 2003). SMAD1/5 is thought to be the main downstream signaling pathway that mediates BMP2 signaling pathway in HESCs and primary HDSCs (Zhang et al., 2020; Zhang et al., 2022). Upon phosphorylation of type I receptors in the majority of tissues, phosphorylated SMAD1/5 bind to a common SMAD (SMAD4) to create a heterotrimer complex, which translocates into the nucleus to control the expression of target genes. Here, knocking down SMAD4 totally reversed the effects of BMP2 on ID3 and ICAM1 expression, suggesting that SMAD4 is required for BMP2-induced intracellular signaling in HESCs and primary HDSCs.

In conclusion, our data reveal that downregulation of BMP2 in the endometrium may contribute to the pathogenesis of uRPL by increasing ICAM1 expression *via* the ALK3-SMAD4-ID3 signaling pathway (Figure 10). These findings not only deepen the understanding of the molecular regulatory mechanisms of ICAM1 expression in the human endometrium but also suggest that it may be possible to improve the pregnancy outcomes in patients with uRPL by regulating the local expression of BMP2 or ICAM1 in the endometrium.

Data availability statement

The original contributions presented in the study are included in the article/Supplementary Material, further inquiries can be directed to the corresponding authors.

Ethics statement

The studies involving human participants were reviewed and approved by Ethics Committee of Renmin Hospital, Wuhan University. The patients/participants provided their written informed consent to participate in this study.

Author contributions

JL, JY, and PL conceived and designed the research; JL and YW performed experiments; JL and YW analyzed and interpreted the results of the experiments; JL and HZ drafted the manuscript; H.-MC and PL edited and revised the manuscript. All the authors approved the final version of the manuscript.

Funding

JL is the recipient of a scholarship from the China Scholarship Council. This work was supported by the Canadian Institutes of Health Research Foundation Scheme Grant (#143317) to P.C.K.L. This work was also supported by the National Natural Science Foundation of China (Grant no. 81501306) to JL.

Conflict of interest

The authors declare that the research was conducted in the absence of any commercial or financial relationships that could be construed as a potential conflict of interest.

Publisher's note

All claims expressed in this article are solely those of the authors and do not necessarily represent those of their affiliated organizations, or those of the publisher, the editors and the reviewers. Any product that may be evaluated in this article, or claim that may be made by its manufacturer, is not guaranteed or endorsed by the publisher.

Supplementary material

The Supplementary Material for this article can be found online at: https://www.frontiersin.org/articles/10.3389/fcell.2023.1090593/full#supplementary-material

References

Austgulen, R., Lien, E., Vince, G., and Redman, C. W. (1997). Increased maternal plasma levels of soluble adhesion molecules (ICAM-1, VCAM-1, E-selectin) in preeclampsia. *Eur. J. Obstet. Gynecol. Reprod. Biol.* 71 (1), 53–58. doi:10.1016/s0301-2115(96)02647-4

Bai, L., Chang, H. M., Zhang, L., Zhu, Y. M., and Leung, P. C. K. (2020). BMP2 increases the production of BDNF through the upregulation of proBDNF and furin expression in human granulosa-lutein cells. *FASEB J.* 34 (12), 16129–16143. doi:10.1096/fj.202000940R

Benner, M., Feyaerts, D., Lopez-Rincon, A., van der Heijden, O. W. H., van der Hoorn, M. L., Joosten, I., et al. (2022). A combination of immune cell types identified through ensemble machine learning strategy detects altered profile in recurrent pregnancy loss: a pilot study. *F. S Sci.* 3 (2), 166–173. doi:10.1016/j.xfss.2022.02.002

Blois, S., Tometten, M., Kandil, J., Hagen, E., Klapp, B. F., Margni, R. A., et al. (2005). Intercellular adhesion molecule-1/LFA-1 cross talk is a proximate mediator capable of disrupting immune integration and tolerance mechanism at the feto-maternal interface in murine pregnancies. *J. Immunol.* 174 (4), 1820–1829. doi:10.4049/jimmunol.174.4.1820

Bohrer, C., Pfurr, S., Mammadzada, K., Schildge, S., Plappert, L., Hils, M., et al. (2015). The balance of Id3 and E47 determines neural stem/precursor cell differentiation into astrocytes. *EMBO J.* 34 (22), 2804–2819. doi:10.15252/embj.201591118

Comba, C., Bastu, E., Dural, O., Yasa, C., Keskin, G., Ozsurmeli, M., et al. (2015). Role of inflammatory mediators in patients with recurrent pregnancy loss. *Fertil. Steril.* 104 (6), 1467–1474.e1. doi:10.1016/j.fertnstert.2015.08.011

Dambaeva, S., Bilal, M., Schneiderman, S., Germain, A., Fernandez, E., Kwak-Kim, J., et al. (2021). Decidualization score identifies an endometrial dysregulation in samples from women with recurrent pregnancy losses and unexplained infertility. *F. S Rep.* 2 (1), 95–103. doi:10.1016/j.xfre.2020.12.004

Defrere, S., Van Langendonckt, A., Moulin, P., Befahy, P., Gonzalez, D., Martinez-Madrid, B., et al. (2005). Human endometrial epithelial cells (EEC) constitutively express more intercellular adhesion molecule (ICAM)-1 than endometrial stromal cells (ESC) in culture. *Am. J. Reprod. Immunol.* 54 (1), 5–12. doi:10.1111/j.1600-0897.2005.00272.x

Dludla, P. V., Jack, B., Viraragavan, A., Pheiffer, C., Johnson, R., Louw, J., et al. (2018). A dose-dependent effect of dimethyl sulfoxide on lipid content, cell viability and oxidative stress in 3T3-L1 adipocytes. *Toxicol. Rep.* 5, 1014–1020. doi:10.1016/j.toxrep.2018.10.002

El Hachem, H., Crepaux, V., May-Panloup, P., Descamps, P., Legendre, G., and Bouet, P. E. (2017). Recurrent pregnancy loss: current perspectives. *Int. J. Womens Health* 9, 331–345. doi:10.2147/IJWH.S100817

ESHRE Guideline Group on RPLBender Atik, R., Christiansen, O. B., Elson, J., Kolte, A. M., Lewis, S., et al. (2018). ESHRE guideline: recurrent pregnancy loss. *Hum. Reprod. Open* 2018 (2), hoy004. doi:10.1093/hropen/hoy004

Garrido-Gimenez, C., and Alijotas-Reig, J. (2015). Recurrent miscarriage: causes, evaluation and management. *Postgrad. Med. J.* 91 (1073), 151–162. doi:10.1136/postgradmedj-2014-132672

Han, J., Seo, H., Choi, Y., Lee, C., Kim, M. I., Jeon, Y., et al. (2018). Expression and regulation of inhibitor of DNA binding proteins ID1, ID2, ID3, and ID4 at the maternal-conceptus interface in pigs. *Theriogenology* 108, 46–55. doi:10.1016/j.theriogenology.2017.11.029

Heidari, Z., Moudi, B., Sheibak, N., Asemi-Rad, A., Keikha, N., Mahmoudzadeh-Sagheb, H., et al. (2021). Interleukin 22 expression during the implantation window in the endometrium of women with unexplained recurrent pregnancy loss and unexplained infertility compared to healthy parturient individuals. *J. Interferon Cytokine Res.* 41 (12), 461–468. doi:10.1089/jir.2021.0160

Hollnagel, A., Oehlmann, V., Heymer, J., Ruther, U., and Nordheim, A. (1999). Id genes are direct targets of bone morphogenetic protein induction in embryonic stem cells. *J. Biol. Chem.* 274 (28), 19838–19845. doi:10.1074/jbc.274.28.19838

Hu, L., Xu, J., Wang, X., Feng, L., Zhang, C., Wang, J., et al. (2021). Bone morphogenetic protein 4 alleviates DSS-induced ulcerative colitis through activating intestinal stem cell by target ID3. *Front. Cell Dev. Biol.* 9, 700864. doi:10.3389/fcell.2021.700864

Kersten, C., Dosen, G., Myklebust, J. H., Sivertsen, E. A., Hystad, M. E., Smeland, E. B., et al. (2006). BMP-6 inhibits human bone marrow B lymphopoiesis-upregulation of Id1 and Id3. *Exp. Hematol.* 34 (1), 72–81. doi:10.1016/j.exphem.2005.09.010

Lecce, L., Kaneko, Y., Madawala, R. J., and Murphy, C. R. (2011). ICAM1 and fibrinogen-gamma are increased in uterine epithelial cells at the time of implantation in rats. *Mol. Reprod. Dev.* 78 (5), 318–327. doi:10.1002/mrd.21307

Lee, K. Y., Jeong, J. W., Wang, J., Ma, L., Martin, J. F., Tsai, S. Y., et al. (2007). Bmp2 is critical for the murine uterine decidual response. *Mol. Cell Biol.* 27 (15), 5468–5478. doi:10.1128/MCB.00342-07

Li, Q., Kannan, A., Wang, W., Demayo, F. J., Taylor, R. N., Bagchi, M. K., et al. (2007). Bone morphogenetic protein 2 functions via a conserved signaling pathway involving Wnt4 to regulate uterine decidualization in the mouse and the human. *J. Biol. Chem.* 282 (43), 31725–31732. doi:10.1074/jbc.M704723200

Li, H., Chang, H. M., Shi, Z., and Leung, P. C. K. (2019). ID3 mediates the TGF-β1-induced suppression of matrix metalloproteinase-1 in human granulosa cells. *FEBS J.* 286 (21), 4310–4327. doi:10.1111/febs.14964

Li, H., Chang, H. M., Lin, Y. M., Shi, Z., and Leung, P. C. K. (2021). TGF-β1 inhibits microvascular-like formation by decreasing VCAM1 and ICAM1 via the upregulation of SNAIL in human granulosa cells. *Mol. Cell Endocrinol.* 111395, 111395. doi:10.1016/j.mce.2021.111395

Luo, J., Zhu, H., Chang, H. M., Lin, Y. M., Yang, J., and Leung, P. C. K. (2020). The regulation of IGFBP3 by BMP2 has a role in human endometrial remodeling. *FASEB J.* 34 (11), 15462–15479. doi:10.1096/fj.202000508R

Luo, X., Chang, H. M., Yi, Y., Leung, P. C. K., and Sun, Y. (2021a). Bone morphogenetic protein 2 upregulates SERPINE2 expression through noncanonical SMAD2/3 and p38 MAPK signaling pathways in human granulosa-lutein cells. *FASEB J.* 35 (9), e21845. doi:10.1096/fj.202100670RR

Luo, X., Chang, H. M., Yi, Y., Sun, Y., and Leung, P. C. K. (2021b). Bone morphogenetic protein 2 inhibits growth differentiation factor 8-induced cell signaling via upregulation of gremlin2 expression in human granulosa-lutein cells. *Reprod. Biol. Endocrinol.* 19 (1), 173. doi:10.1186/s12958-021-00854-6

Mangioni, S., Vigano, P., Florio, P., Borghi, O., Vignali, M., Petraglia, F., et al. (2005). Effect of activin A on tumor necrosis factor-alpha/intercellular adhesion molecule-1 pathway in endometrial stromal cells. *Eur. J. Obstet. Gynecol. Reprod. Biol.* 123 (2), 218–223. doi:10.1016/j.ejogrb.2005.03.017

Marzusch, K., Ruck, P., Geiselhart, A., Handgretinger, R., Dietl, J. A., Kaiserling, E., et al. (1993). Distribution of cell adhesion molecules on CD56++, CD3-CD16-large granular lymphocytes and endothelial cells in first-trimester human decidua. *Hum. Reprod.* 8 (8), 1203–1208. doi:10.1093/oxfordjournals.humrep.a138229

Pino, M., Galleguillos, C., Torres, M., Sovino, H., Fuentes, A., Boric, M. A., et al. (2009). Association between MMP1 and MMP9 activities and ICAM1 cleavage induced by tumor necrosis factor in stromal cell cultures from eutopic endometria of women with endometriosis. *Reproduction* 138 (5), 837–847. doi:10.1530/REP-09-0196

Qi, W., Ding, D., and Salvi, R. J. (2008). Cytotoxic effects of dimethyl sulphoxide (DMSO) on cochlear organotypic cultures. *Hear Res.* 236 (1-2), 52–60. doi:10.1016/j.heares.2007.12.002

Rothlein, R., Czajkowski, M., and Kishimoto, T. K. (1991). Intercellular adhesion molecule-1 in the inflammatory response. *Chem. Immunol.* 50, 135–142.

Salazar, V. S., Gamer, L. W., and Rosen, V. (2016). BMP signalling in skeletal development, disease and repair. *Nat. Rev. Endocrinol.* 12 (4), 203–221. doi:10.1038/nrendo.2016.12

Shi, Y., and Massague, J. (2003). Mechanisms of TGF-beta signaling from cell membrane to the nucleus. *Cell* 113 (6), 685–700. doi:10.1016/s0092-8674(03)00432-x

Stoikos, C. J., Harrison, C. A., Salamonsen, L. A., and Dimitriadis, E. (2008). A distinct cohort of the TGFbeta superfamily members expressed in human endometrium regulate decidualization. *Hum. Reprod.* 23 (6), 1447–1456. doi:10.1093/humrep/den110

Thomson, A. J., Greer, M. R., Young, A., Boswell, F., Telfer, J. F., Cameron, I. T., et al. (1999). Expression of intercellular adhesion molecules ICAM-1 and ICAM-2 in human endometrium: regulation by interferon-gamma. *Mol. Hum. Reprod.* 5 (1), 64–70. doi:10.1093/molehr/5.1.64

van Mourik, M. S., Macklon, N. S., and Heijnen, C. J. (2009). Embryonic implantation: cytokines, adhesion molecules, and immune cells in establishing an implantation environment. *J. Leukoc. Biol.* 85 (1), 4–19. doi:10.1189/jlb.0708395

Vigano, P., Pardi, R., Magri, B., Busacca, M., Di Blasio, A. M., and Vignali, M. (1994). Expression of intercellular adhesion molecule-1 (ICAM-1) on cultured human endometrial stromal cells and its role in the interaction with natural killers. *Am. J. Reprod. Immunol.* 32 (3), 139–145. doi:10.1111/j.1600-0897.1994.tb01104.x

Xie, L., Galettis, A., Morris, J., Jackson, C., Twigg, S. M., and Gallery, E. D. (2008). Intercellular adhesion molecule-1 (ICAM-1) expression is necessary for monocyte adhesion to the placental bed endothelium and is increased in type 1 diabetic human pregnancy. *Diabetes Metab. Res. Rev.* 24 (4), 294–300. doi:10.1002/dmrr.793

Yi, Y., Zhu, H., Klausen, C., Chang, H. M., Inkster, A. M., Terry, J., et al. (2021). Dysregulated BMP2 in the placenta may contribute to early-onset preeclampsia by regulating human trophoblast expression of extracellular matrix and adhesion molecules. *Front. Cell Dev. Biol.* 9, 768669. doi:10.3389/fcell.2021.768669

Zhang, Y., Zhu, H., Chang, H. M., and Leung, P. C. K. (2020). ALK3-SMAD1/5 signaling mediates the BMP2-induced decrease in PGE2 production in human endometrial stromal cells and decidual stromal cells. *Front. Cell Dev. Biol.* 8, 573028. doi:10.3389/fcell.2020.573028

Zhang, Y., Chang, H. M., Zhu, H., and Leung, P. C. K. (2022). BMP2 suppresses the production of pentraxin 3 in human endometrial stromal and decidual stromal cells. *FASEB J.* 36 (5), e22319. doi:10.1096/fj.202200081RR

Zhao, H. J., Chang, H. M., Zhu, H., Klausen, C., Li, Y., and Leung, P. C. K. (2018a). Bone morphogenetic protein 2 promotes human trophoblast cell invasion by inducing activin A production. *Endocrinology* 159 (7), 2815–2825. doi:10.1210/en.2018-00301

Zhao, H. J., Klausen, C., Li, Y., Zhu, H., Wang, Y. L., and Leung, P. C. K. (2018b). Bone morphogenetic protein 2 promotes human trophoblast cell invasion by upregulating N-cadherin via non-canonical SMAD2/3 signaling. *Cell Death Dis.* 9 (2), 174. doi:10.1038/s41419-017-0230-1

Zhao, H. J., Klausen, C., Zhu, H., Chang, H. M., Li, Y., and Leung, P. C. K. (2020). Bone morphogenetic protein 2 promotes human trophoblast cell invasion and endothelial-like tube formation through ID1-mediated upregulation of IGF binding protein-3. *FASEB J.* 34 (2), 3151–3164. doi:10.1096/fj.201902168RR

Zhu, H., Leung, P. C., and MacCalman, C. D. (2007). Expression of ADAMTS-5/implantin in human decidual stromal cells: regulatory effects of cytokines. *Hum. Reprod.* 22 (1), 63–74. doi:10.1093/humrep/del356

Zhu, R. H., Dai, F. F., Yang, D. Y., Liu, S. Y., Zheng, Y. J., Wu, M. L., et al. (2022). The mechanism of insulin-like growth factor II mRNA-binging protein 3 induce decidualization and maternal-fetal interface cross talk by TGF-β1 in recurrent spontaneous abortion. *Front. Cell Dev. Biol.* 10, 862180. doi:10.3389/fcell.2022.862180

frontiers | Frontiers in Cell and Developmental Biology

TYPE Original Research
PUBLISHED 31 March 2023
DOI 10.3389/fcell.2023.1148831

OPEN ACCESS

EDITED BY
Vanina Gabriela Da Ros,
CONICET Institute of Biology and Experimental Medicine (IBYME), Argentina

REVIEWED BY
Maria Jiménez-Movilla,
University of Murcia, Spain
Claudia Sánchez,
National Autonomous University of Mexico, Mexico

*CORRESPONDENCE
Silvia A. Belmonte,
belmonte.silviaalejandra@gmail.com,
sbelmonte@mendoza-conicet.gob.ar

†These authors share first authorship

SPECIALTY SECTION
This article was submitted to Molecular and Cellular Reproduction, a section of the journal Frontiers in Cell and Developmental Biology

RECEIVED 20 January 2023
ACCEPTED 22 March 2023
PUBLISHED 31 March 2023

CITATION
Vaquer CC, Suhaiman L, Pavarotti MA, Arias RJ, Pacheco Guiñazú AB, De Blas GA and Belmonte SA (2023), The pair ceramide 1-phosphate/ceramide kinase regulates intracellular calcium and progesterone-induced human sperm acrosomal exocytosis.
Front. Cell Dev. Biol. 11:1148831.
doi: 10.3389/fcell.2023.1148831

The pair ceramide 1-phosphate/ceramide kinase regulates intracellular calcium and progesterone-induced human sperm acrosomal exocytosis

Cintia C. Vaquer[1†], Laila Suhaiman[1,2†], Martín A. Pavarotti[1], Rodolfo J. Arias[1,3], Anahí B. Pacheco Guiñazú[1], Gerardo A. De Blas[1,3] and Silvia A. Belmonte[1,2*]

[1]Instituto de Histología y Embriología de Mendoza (IHEM) "Dr. Mario H. Burgos", CONICET, Universidad Nacional de Cuyo, Mendoza, Argentina, [2]Facultad de Ciencias Médicas, Universidad Nacional de Cuyo, Mendoza, Argentina, [3]LaTIT. Área Farmacología, Facultad de Ciencias Médicas, Universidad Nacional de Cuyo, Mendoza, Argentina

Before fertilization, spermatozoa must undergo calcium-regulated acrosome exocytosis in response to physiological stimuli such as progesterone and zona pellucida. Our laboratory has elucidated the signaling cascades accomplished by different sphingolipids during human sperm acrosomal exocytosis. Recently, we established that ceramide increases intracellular calcium by activating various channels and stimulating the acrosome reaction. However, whether ceramide induces exocytosis on its own, activation of the ceramide kinase/ceramide 1-phosphate (CERK/C1P) pathway or both is still an unsolved issue. Here, we demonstrate that C1P addition induces exocytosis in intact, capacitated human sperm. Real-time imaging in single-cell and calcium measurements in sperm population showed that C1P needs extracellular calcium to induce $[Ca^{2+}]i$ increase. The sphingolipid triggered the cation influx through voltage-operated calcium (VOC) and store-operated calcium (SOC) channels. However, it requires calcium efflux from internal stores through inositol 3-phosphate receptors (IP_3R) and ryanodine receptors (RyR) to achieve calcium rise and the acrosome reaction. We report the presence of the CERK in human spermatozoa, the enzyme that catalyzes C1P synthesis. Furthermore, CERK exhibited calcium-stimulated enzymatic activity during the acrosome reaction. Exocytosis assays using a CERK inhibitor demonstrated that ceramide induces acrosomal exocytosis, mainly due to C1P synthesis. Strikingly, progesterone required CERK activity to induce intracellular calcium increase and acrosome exocytosis. This is the first report, implicating the bioactive sphingolipid C1P in the physiological progesterone pathway leading to the sperm acrosome reaction.

KEYWORDS

human sperm, ceramide 1-phosphate/ceramide kinase, acrosome exocytosis, calcium channels, sphingolipids

Introduction

Sphingolipids are ubiquitous components of eukaryotic cells that accomplish vital roles in cell growth, death, and survival. Ceramide 1-phosphate (C1P) is a bioactive sphingolipid metabolite considered a signaling lipid. Ceramide kinase (CERK), phosphorylates ceramide to ceramide C1P in mammalian cells (Presa et al., 2020). This enzyme was initially characterized as a calcium-stimulated lipid kinase in synaptic vesicles (Bajjalieh et al., 1989). The C1P/CERK pathway has been involved in the regulation of essential pathophysiological functions such as phagocytosis and inflammation (Presa et al., 2016).

C1P regulates directly the activities of the cytosolic phospholipase A2 (cPLA2α) (Nakamura et al., 2006), sphingosine kinase (SK1) (Nishino et al., 2019; Hori et al., 2020), and tumor necrosis factor *a*-converting enzyme (Lamour et al., 2011). Further, C1P governs many cellular responses like cell migration and exocytosis by acting directly or indirectly *via* cell signaling involving putative receptors (Mitsutake et al., 2004; Presa et al., 2016; Hori et al., 2020).

The exocytosis, as the last step of the secretory pathway, is a precisely ordered and calcium-controlled process entailing tethering, docking, and fusion of vesicles to the plasma membrane for cargo release (Zhang and Staiger, 2021). Exocytosis is regulated by sphingolipids in PC12 cells. E.g., dopamine release by calcium ionophores is mediated by the production of ceramide from sphingomyelin (Jeon et al., 2005) and extracellular application of ceramide caused exocytosis in PC12 cells (Tang et al., 2007). C1P/CERK pathway regulates dopamine transporters recycling (Won et al., 2018). Some studies have identified the role of CERK in arachidonic acid release in a lung epithelial cell line (Pettus et al., 2003; Pettus et al., 2004; Subramanian et al., 2005).

Mitsutake et al. (2004) described that the enzyme CERK is a mediator of calcium-dependent mast cell degranulation (Mitsutake et al., 2004). Hewson et al. (2011) demonstrated that C1P induced histamine and PGD2 release in mast cells. CERK was involved in the exocytosis of these mediators and some molecules of the signaling pathway have been identified (Hewson et al., 2011).

The acrosome is the main calcium store of the male gamete. The exocytosis of the sperm granule, termed acrosome reaction (AR), is crucial for mammal fertilization. It involves complex biological changes that culminate with the release of the granule content and the plasma membrane reorganization (Belmonte et al., 2016). The last step enables sperm to interact and fuse with the oocyte (Inoue et al., 2011; Bianchi et al., 2014; Bianchi and Wright, 2020). Innumerable physiological events involved in the AR remain elusive, although it is known that during the AR there is an increase in the intracellular Ca^{2+} concentration ($[Ca^{2+}]i$) (Darszon et al., 2005; Stival et al., 2016). Therefore, orchestrated $[Ca^{2+}]i$ augments are necessary for the AR to occur. Briefly, the canonical mechanism described proposes that a temporary calcium entry through plasma membrane channels induces inositol 3-phosphate (IP_3) synthesis and IP_3R activation in the granule elicits calcium efflux from the acrosome calcium reservoir. The stromal interaction molecule, STIM, senses the acrosome calcium content decrease and bestows calcium store-depletion into the opening of Orai channels at the PM (Darszon et al., 2011; Sosa et al., 2015; Sosa et al., 2016). This event triggers a prolonged and continuous calcium increase due to SOC channels opening (Aldana et al., 2021). Abundant evidence exists for another functional calcium store present at the neck piece: the redundant nuclear envelope (RNE). Its membrane contains IP_3R and ryanodine receptors (RyR) (Harper and Publicover, 2005; Harper et al., 2006; Suarez, 2008). It is necessary to highlight the presence of CatSper (calcium channel of sperm), present at the flagellum principal piece. It is a voltage- and pH-dependent gated calcium channel, activated by Pg and required for male fertility (Kirichok et al., 2006; Lishko et al., 2011).

Our laboratory has elucidated the signaling cascades accomplished by different sphingolipids during sperm acrosomal exocytosis (Suhaiman et al., 2010; Vaquer et al., 2020). We have not only demonstrated the presence and activity of some enzymes of the sphingolipid metabolism in a terminal cell like the human sperm but we defined how some of these enzymes and lipids regulate exocytosis. The bioactive sphingolipid, sphingosine 1-phosphate (S1P), triggers AR by interacting with Gi-coupled receptors and activating extracellular calcium influx through voltage and store-operated calcium channels as well as efflux from intracellular stores through IP_3-sensitive calcium channels. We showed for the first time that human spermatozoa produce S1P, which induces exocytosis through an autocrine/paracrine action (Suhaiman et al., 2010). Recently, we established the effect of ceramide, a metabolic precursor of S1P, during acrosomal exocytosis. Both, exogenous and endogenous ceramide induces AR by raising $[Ca^{2+}]i$ during the first 40 s activating calcium influx through CatSper and SOC channels. The sphingolipid also promotes calcium efflux through RyR from RNE. A striking finding was that even though ceramide is a precursor of S1P its action is exerted in an S1P-independent manner (Vaquer et al., 2020). However, whether ceramide induces exocytosis by itself or activates the CERK/C1P pathway, or whether both mechanisms are related is still an unresolved issue. In the present study, we demonstrated that the pair C1P/CERK regulates intracellular calcium concentration and induces human sperm acrosomal exocytosis. Further, the CERK activity and thus C1P synthesis are required for progesterone-elicited AR. This research is unique in determining the effect of C1P during acrosomal exocytosis and its involvement in the progesterone (Pg) physiological pathway.

Materials and methods

Reagents

Spermatozoa were maintained in Human Tubal Fluid medium (HTF), which contains 0.35 g/L KCl, 5.94 g/L NaCl, 0.05 g/L KH_2PO_4, 0.05 g/L $MgSO_4{\cdot}7H_2O$, 0.3 g/L $CaCl_2$ $.2H_2O$, 2.1 g/L $NaHCO_3$, 0.51 g/L D-glucose, 2.39 g/L Na lactate, 0.036 g/L Na pyruvate, 0.05 g/L streptomycin, 0.06 g/L penicillin, 0.01 g/L phenol red. Sphingosine kinase inhibitor (SKI), 2-aminoethoxydiphenylborate (2-APB), and adamantane-1-carboxylic acid (2-benzoylamino-benzothiazol-6-yl)amide, N-[2-(benzoylamino)-6-benzothiazolyl]-Tricyclo [3.3.1.13,7]decane-1-carboxamide (NVP-231) were from Calbiochem (MERCK Argentina). C2 Ceramide-1-Phosphate (d18:1/2:0) and C6-ceramide were from Avanti Polar Lipids, Inc. (Alabaster, AL, United States). A23187 and dantrolene were from Alomone

(Alomone Labs. Ltd. Jerusalem, Israel). TLC aluminum sheets silica gel 60 were from MERCK KGaA (Darmstadt, Germany). Verapamil, 4-methyl-4′-[3,5-bis (trifluoromethyl)-1H-pyrazol-1-yl]-1,2,3-thiadiazole-5-carboxanilide (YM-58483) and 1-[b-[3-(4-methoxyphenyl)propoxy]-4-methoxyphenethyl]- 1H-imidazole (SKF-96365), xestospongin C, and progesterone were from Sigma (Sigma-Aldrich Argentina SA). Albumin and fluorescein-isothiocyanate-coupled Pisum sativum lectin were from ICN (Eurolab SA, Buenos Aires, Argentina). Horseradish peroxidase- and Cy™3-conjugated goat anti-rabbit antibodies were from Jackson ImmunoResearch (West Grove, PA). Anti-CERK (Abcam). N-Lauroyl-D-erythro-sphingosine, ruthenium red, ionomycin, 1,2-bis amino phenoxy)ethane-N,N,N0,N0-tetraacetic acid (BAPTA), and glycine, 4-(6-Acetoxymethoxy-2,7-dichloro-3-oxo-9-xanthenyl)-4′-methyl-2,2′(ethylenedioxy) dianiline-N,N,N′,N′-tetraacetic acid tetrakis (acetoxymethyl) ester (Fluo-3 AM) were from Molecular Probes (Invitrogen Argentina). Ted Pella Inc. provided the electron microscopy supplies. Recombinant streptolysin O (SLO) was from Dr. Bhakdi (University of Mainz, Mainz, Germany). Any other reagents were purchased from Sigma-Aldrich™, Tecnolab, or Genbiotech.

Ethics statement and human sperm preparation

Healthy male donors provided ejaculates by masturbation, after at least 48 h of sexual abstinence. We used only semen samples that accomplished the World Health Organization (WHO, 2021) specifications, for the experiments shown here. Data collection adheres to the guidelines established in Argentina (ANMAT 5330/97) and the International Declaration of Helsinki. All donors signed an informed consent according to supply semen samples. The protocol for semen manipulation was accepted by the Ethics Committee of the School of Medicine, National University of Cuyo.

After semen liquefaction (30–60 min at 37°C), motile sperm were retrieved after a swim-up procedure for 1 h at 37°C in HTF. We adjusted sperm concentration to 10^6 cells/mL and further incubated for 2 h under non-capacitating (HTF, 5% CO_2/95% air, 37°C) or 2–5 h under capacitating (HTF supplemented with 0.5% BSA, 5% CO_2/95% air, 37°C) conditions. When permeabilized sperm are required, we washed capacitated cells and resuspended them in cold PBS with 3 U/mL SLO, and incubated for 15 min at 4°C. We washed sperm twice with PBS and suspended in ice-cold sucrose buffer (20 mM Hepes-K, 0.5 mM EGTA, 250 mM sucrose, pH 7.0) with 2 mM DTT. Then, we follow the procedures for AR assays, Western blot, enzyme activities, and calcium measurements.

Sperm acrosome exocytosis measurements

We incubated capacitated or non-capacitated sperm suspensions consecutively with inhibitors and stimulants as described in the legends to figures. We kept the cells for 10–15 min at 37°C after each addition. The acrosome status was assessed by FITC-PSA (25 μg/mL in PBS) staining as described in Mendoza et al., 1992 (Mendoza et al., 1992) and as detailed in our publications (Suhaiman et al., 2010; Belmonte & Suhaiman, 2012; Vaquer et al., 2020; Suhaiman et al., 2021). We scored at least 300 cells using a Nikon Optiphot II microscope equipped with epifluorescence optics. In each experiment, negative controls (no stimulation) and positive controls (stimulated with A23187 or progesterone) were included. For each experiment, the data were normalized by subtracting the number of reacted spermatozoa in the negative control from all values and expressing the result as a percentage of the acrosome reaction observed in the positive control (100%). The actual percentages of reacted sperm for negative and positive controls ranged between 6% and 25% and 25% and 40%, respectively. Experiments in which the difference between positive and negative controls was less than 10% were discarded. The average difference between positive and negative controls was 14%.

We performed one-way ANOVA to analyze the data. Conditions used for data normalization were not included in the evaluation (0% and 100%). Dunnett *post hoc* test or Tukey-Kramer were utilized to compare the means with a control condition. When specified, we utilized a Student's t-test or Newman-Keuls Multiple Comparison Test. We considered significant differences at the $p > 0.05$ level.

Indirect immunofluorescence

We fixed capacitated sperm (5×10^6 cells) in 2% paraformaldehyde for 15 min at RT and resuspended them in 100 mM glycine in PBS. We attached sperm to poly-L-coated, coverslips. Next, we permeabilized the plasma membrane with 0.1% Triton X-100 in PBS for 10 min at RT, and washed twice with 0.1% polyvinylpyrrolidone in PBS for 1 h at 37°C. To block non-specific marks, we incubated the sample with 5% BSA in PBS/PVP for 1 h at 37°C. Then, we incubated the cells with anti-CERK (Abcam, 20 μg/mL) for 1 h at RT in a moisturized chamber. As a second antibody, we used Cy™3-conjugated anti-rabbit in BSA 1%/PBS/PVP. Then, we fixed/permeabilized the acrosome membrane with cold methanol (−20°C) for 20 s and stained the cells with FITC-PSA as described in here *Sperm acrosome exocytosis measurements*. Sperm were observed by confocal microscopy (Olympus FluoViewTM FV1000 confocal microscope, Olympus, Argentina), with the FV10-ASW software. Images were processed with MetaMorph, ImageJ, and Corel Draw. The protocol is detailed in our previous publications (Suhaiman et al., 2010; Belmonte and Suhaiman, 2012; Suhaiman et al., 2021).

SDS-PAGE and Western blot

We electrophoresed proteins on 8% Tris-glycine SDS gels and transferred them to nitrocellulose membranes. We blocked non-specific reaction with 3% BSA in washing buffer (PBS pH 7.4, 0.1% Tween 20) for 1 h at RT. Blots were incubated with anti-CERK (Abcam, 0.1 μg/mL) for 2 h at RT. As a secondary antibody, we utilized horseradish peroxidase-conjugated goat anti-rabbit IgG (0.1 μg/mL in washing buffer) with 1 h incubation at RT. We detected the protein with a chemiluminescence system (Kalium

Technologies SRL, Argentina) on a Luminescent Image Analyzer LAS-4000 (Fujifilm, Tokyo, Japan).

Transmission electron microscopy

Capacitated sperm were treated with 10 μM C1P or 10 μM A23187 (used as a positive control), and incubated for 15 min at 37°C. As a negative control, we included a sample without any treatment. We washed sperm twice in PBS and fixed them in 2.5% v/v glutaraldehyde in 0.1 M sodium cacodylate buffer for 2 h at 10°C. We centrifuged the samples for 30 s at 10,000 rpm. The sperm pellets obtained were further fixed in 1% OsO_4 for 1 h at RT. We used graded acetone series to dehydrate cells and embedded them in low-viscosity epoxy resin. The resin was polymerized at 70°C for 48 h. Using a diamond knife, we obtained ultrathin sections in an ultramicrotome (Ultracut R; Leica, Austria) with an interference color grey. We collected ultrathin sections on 200-mesh copper grids and stained them with uranyl acetate and lead citrate as described in (Belmonte et al., 2005). We observed the samples under the electron microscope Zeiss 900 (Zeiss, Jena, Germany) at 80 kV. Micrographs were obtained with a Gatan Orius SC1000 (model 832) charge-coupled device. The samples were processed by A. Morales, Ph.D. and P. López, MS from the STAN: ST3371 of TEM and SEM samples preparation, IHEM-CONICET-UNCuyo. At least 100 cells per condition were scored and sorted the acrosomal patterns as intact, swollen (swollen and waving), and reacted (lost and vesiculated acrosomes). Newman-Keuls Multiple Comparison Test allowed us to analyze all these data by using the GraphPad program Prism 5. Significant differences were considered at the $p < 0.05$ level.

Tetanus toxin conjugation with cell-penetrating peptides

We prepared the protein as detailed in Mayorga et al. (2020) (Mayorga et al., 2020). In short, we transformed the plasmid's DNA coding 6His-light chain of tetanus toxin (pQE3plasmid, Qiagen) into *E. coli* XL-1Blue (Stratagene). We induced protein expression with 0.2 mM isopropyl 1-thio-D-galactopyranoside, ON at 20°C. We purified the 6His-tagged proteins according to the QIAexpressionist (www.qiagen.com). We used Trilinks Biotechnology Kits and followed the manufacturer's instructions, to conjugate the CPP peptides (KRRRRRRRRRC) and tetanus toxin. SDS-PAGE analysis allowed us to validate purity.

Sphingosine kinase activity measurement

We measured sphingosine kinase 1 (SK1) activity in permeabilized sperm as described in Suhaiman et al. (2010) (Suhaiman et al., 2010). We washed 50×10^6 spermatozoa with cold PBS, after permeabilization with SLO (Pelletan et al., 2015), and resuspended them in SK1 buffer (20 mM Tris-HCl, pH 7.4, 1 mM EDTA, 0.5 mM deoxypyridoxine, 15 mM NaF, 1 mM *ß*-mercaptoethanol, 1 mM sodium orthovanadate, 40 mM *ß*-glycerophosphate, 0.4 mM phenylmethylsulfonyl fluoride, 10% glycerol, 0.5% Triton X-100, 10 mM $MgCl_2$, and Complete protease inhibitors). Then, we incubated sperm in 100 μL of SK1 buffer: sphingosine (50 μM, delivered in 4 mg/mL fatty acid-free bovine serum albumin) and [γ-^{32}P]ATP (5 μCi) for 30 min at 37°C. We used HeLa cells incubated with sphingosine as a positive control (30 μg of proteins) and without sphingosine addition as a negative control. When indicated, sperm were incubated for 15 min at 37°C with 1 μM SKI (specific Sphingosine Kinase Inhibitor). Subsequently, we added 10 μM C6-ceramide (C6), washed it with cold PBS, and suspended it in SK1 buffer. We stopped the reaction with 10 μL of 1 N HCl and 400 μL of chloroform/methanol/HCl (100:200:1, v/v). Then, we added 120 μL of chloroform and 120 μL of 2 M KCl. We centrifuged the samples at 3,000 g for 10 min. We transferred 200 μL of the organic phase to new glass tubes and dried them. We resuspended the samples in chloroform/methanol/HCl (100:100:1, v/v). Then we resolved the lipids on TLC plates utilizing 1-butanol/methanol/acetic acid/water (8:2:1:2, v/v) as a solvent system and observed by autoradiography.

Ceramide kinase (CERK) activity measurement

We determined CERK as detailed in Tada et al. (2010) (Tada et al., 2010) and introduced the modifications described for sperm in Vaquer et al. (2020) (Vaquer et al., 2020). In brief, we incubated 100×10^6 cells with 10 μM C12-NBD dissolved in 4 mg/mL fatty acid-free BSA (FAF-BSA) for 1 h at 37 °C. We kept sperm in the dark to prevent NBD degradation. After that, sperm were washed with HTF/0.4% FAF-BSA. Phosphatase inhibitors were added to the mixture: 1 mM sodium orthovanadate and 15 mM NaF. When indicated, we incubated sperm with 200 nM NVP-231 (CERK inhibitor) for 20 min at 37°C. After that, we added A23187 (10 μM) and treated the cells for 20 min. We ended the reaction by adding 500 μL methanol, 250 μL chloroform, and mixed-up. Afterward, we incorporated 500 μL of chloroform and 250 μL of water. Sperm were centrifuged at 600 *g* for 10 min. In the organic phase, we observed the C12-NBD (data not shown), and in the aqueous phase, two bands appear corresponding to lauric acid-NBD, produced due to ceramidase activity, as shown in our previous publication (Vaquer et al., 2020) and another band that matches with the retention factor (Rf) of C1P. Lipids were resolved on TLC plates by using 1-butanol/acetic acid/water (3:1:1, v/v/v) and visualized by fluorescence with LAS-4000 (Fujifilm (λEx: 498 nm - λEm: 522 nm). A semiquantitative evaluation of the spots was performed with ImageJ.

[Ca^{2+}]i measurements in single-cell

Sperm (10×10^6) were loaded with Fluo-3 AM. Male gametes were immobilized on poly-L-lysine-coated coverslips, mounted on a chamber, and placed on the stage of an inverted microscope (Eclipse TE300 Nikon). Fluo-3 AM was excited with a stroboscopic LED-based fluorescence illumination system as detailed in (Pocognoni et al., 2013). We compiled images (7 frames/min). A filter with the following bandwidths: excitation 450–490 nm, dichroic mirror 505 nm, and emission 520–560 nm were used. We utilized a Plan Fluor 40×/0.6 Nikon objective and compiled images using NIS Element software (Nikon). C1P was microinjected to the sperm suspension (injection speed: 73 nL per second). Intracellular calcium was measured once ionomycin was added to calibrate the maximal

response. We performed fluorescence measurements as detailed in Suhaiman et al. (2010) (Suhaiman et al., 2010). Fluorescence data were processed offline with ImageJ. We normalized raw intensity values imported with the following equations: a) (F/Fo) − 1. F is the fluorescence intensity at time t and Fo is the mean of F taken during the control period. We graphed all the results of (F/Fo) −1 vs. time. %Δ(F/Fo) −1 is the difference between the fluorescence before stimulation and the maximal fluorescence obtained after the addition of C1P. We analyzed and graphed the data with GraphPad Prism 5 (four independent experiments).

Calcium measurements in cell population

We loaded 5–10 × 10^6 sperm/mL of motile sperm with the permeable Fluo-3 AM dye (2 μM). Afterwards, we washed sperm and suspended them in nominally calcium-free (~1 μM) medium (10 mM Hepes-Na, 4 mM KCl, 120 mM NaCl, 15 mM $NaHCO_3$, 5 mM D-glucose, 1 mM sodium pyruvate, 10 mM lactic acid, 1 mM $MgCl_2$, pH 7.4). We used cuvettes at 37°C to perform sperm fluorescence measurements. At the times indicated, we added 15 μM Pg or 10 μM C1P to the samples. We recorded Fluo-3 AM fluorescence (λEx = 505, λEm = 525 nm) in an Aminco Bowman II spectrofluorometer. To assess $[Ca^{2+}]$i movements, we chelated extracellular calcium with 0.75 mM EGTA and 0.5 mM Ca^{2+} to the medium (calculated by MAXCHELATOR, https://web.stanford.edu/~cpatton/, Chris Patton, Stanford University, Stanford, CA, United States) resulting in a final extracellular $[Ca^{2+}] \leq 100$ nM. Cells were loaded with Fluo-3 AM, washed once, and suspended in buffer (0.75 mM EGTA, 0.5 mM Ca^{2+}, 10 mM Hepes-Na, 120 mM NaCl, 15 mM $NaHCO_3$, 5 mM D-glucose, 4 mM KCl, 1 mM $MgCl_2$, 10 mM lactic acid, 1 mM sodium pyruvate, pH 7.4). When indicated, we added to sperm suspension 15 μM Pg or 10 μM C1P. We recorded Fluo-3 fluorescence as stated above. To test which calcium channels are involved in the calcium increment induced by C1P, we run experiments using different calcium channel blockers in a media with a final $[Ca^{2+}]$ concentration of 2 mM. Cells loaded with Fluo-3 AM were incubated for 10 min with 200 μM lanthanum, 100 μM Verapamil, 1 μM XC, 100 μM 2-APB, 1 mM YM-58483, 50 mM SKF-96365, 1 μM NNC 55–0396 (NNC), 100 μM dantrolene, or 20 nM Ruthenium red (RR), previous the addition of C1P (10 μM). We collected the data for 600 s at a frequency of 4 Hz (2 fps). We calibrated the maximal $[Ca^{2+}]$i response after Triton X-100 (0.1%) addition. We used five different batches of sperm to perform independent measurements. We utilized the Tukey-Kramer *post hoc* test for pairwise comparisons. We considered significant differences at the $p \geq 0.05$ level.

Results

C1P induces exocytosis in human sperm capacitated *"in vitro"*

First, we started by testing if C1P was able to directly accomplish the AR. Considering that C1P acts, as an extracellular and intracellular signaling molecule, we performed experiments using intact and plasma membrane-permeabilized human spermatozoa.

First, we challenged intact spermatozoa with increasing C1P concentrations (from 0 to 10 μM) and measured the exocytotic response. Exogenous C1P triggered exocytosis in a dose-dependent way (Figure 1A) achieving a maximum at 0.1 μM. Even when C1P concentration was increased, the percentage of reacted cells remained in the same range. C1P elicited the acrosome exocytosis as effectively as Pg, the physiological inducer of the AR, used as a positive control (Figures 1A,B). It is worth highlighting that C1P did not induce exocytosis in permeabilized sperm (Figure 1A). As shown in Figure 1A (Ca^{2+}), permeabilized cells treated with calcium (control) underwent exocytosis. Both, C1P 0.1 and 10 μM did not affect sperm viability assessed by using 0.1% eosin to stain dead cells (control, 92.6% ± 1.10; 0.1 μM C1P, 88.2% ± 2.98; 10 uM C1P 89.7% ± 1.73; mean ± S.E.).

Human sperm are not able to fertilize straight away after ejaculation. They acquire this ability during a lapse of permanence in the female reproductive tract. There, sperm undergo numerous complex physiological changes called capacitation. Sperm capacitation can be accomplished *in vitro* by incubating spermatozoa in artificial media mimicking the composition of the fluids present in the female reproductive tract. The exocytic response of human sperm to progesterone is a hallmark of capacitation (Belmonte et al., 2005; Mayorga et al., 2020). To elucidate if C1P requires sperm capacitation to induce exocytosis we performed AR experiments by incubating male gametes under capacitating (HTF media supplemented with 5 mg/mL BSA) or non-capacitating conditions (HTF without BSA). After 3 h incubation, we challenged the cells with 10 μM C1P. As shown in Figure 1B, capacitated sperm underwent AR when treated with C1P. In contrast, non-capacitated cells were not able to respond to the sphingolipid stimulus (non-cap, gray bars). We used 15 μM Pg to determine the capacitation status of the gametes (Belmonte et al., 2005; Muratori et al., 2008).

Handling lipids is tricky given that when added to the culture media they can be embedded in membranes affecting directly their integrity and/or function. Therefore, we ran various controls. First, we evaluated the physiological behavior of human sperm after C1P treatment. Swelling of secretory vesicles is a previous step occurring before the fusion of the granules with the plasma membrane (Finkelstein et al., 1986). The acrosome granule swelling was observed by electron microscopy in human sperm that have started exocytosis before they completely lose their acrosomes (Zanetti and Mayorga, 2009). Upon AR stimulation, the outer acrosome membrane (OAM) waves and the invagination edges encounter the plasma membrane. Both membranes form tight appositions finally stabilized by the assembly of SNAREs. Calcium rise leads to membrane fusion, the opening of fusion pores, hybrid vesicles (mixed composition containing OAM and plasma membrane), and acrosome content release (Suhaiman et al., 2021).

To discard the possibility of acrosome loss due to C1P-induced membrane destabilization, we searched for possible ultrastructural changes by TEM in human sperm after challenging them with C1P. Then, we incubated sperm for 15 min with 10 μM of C1P or the calcium ionophore, A23187. The percentage of swollen plus waving acrosomes increased up to ~50% compared to the control (Figures 1C,D). Our data provide direct evidence indicating that C1P can induce the intermediate step necessary for sperm AR, the granule

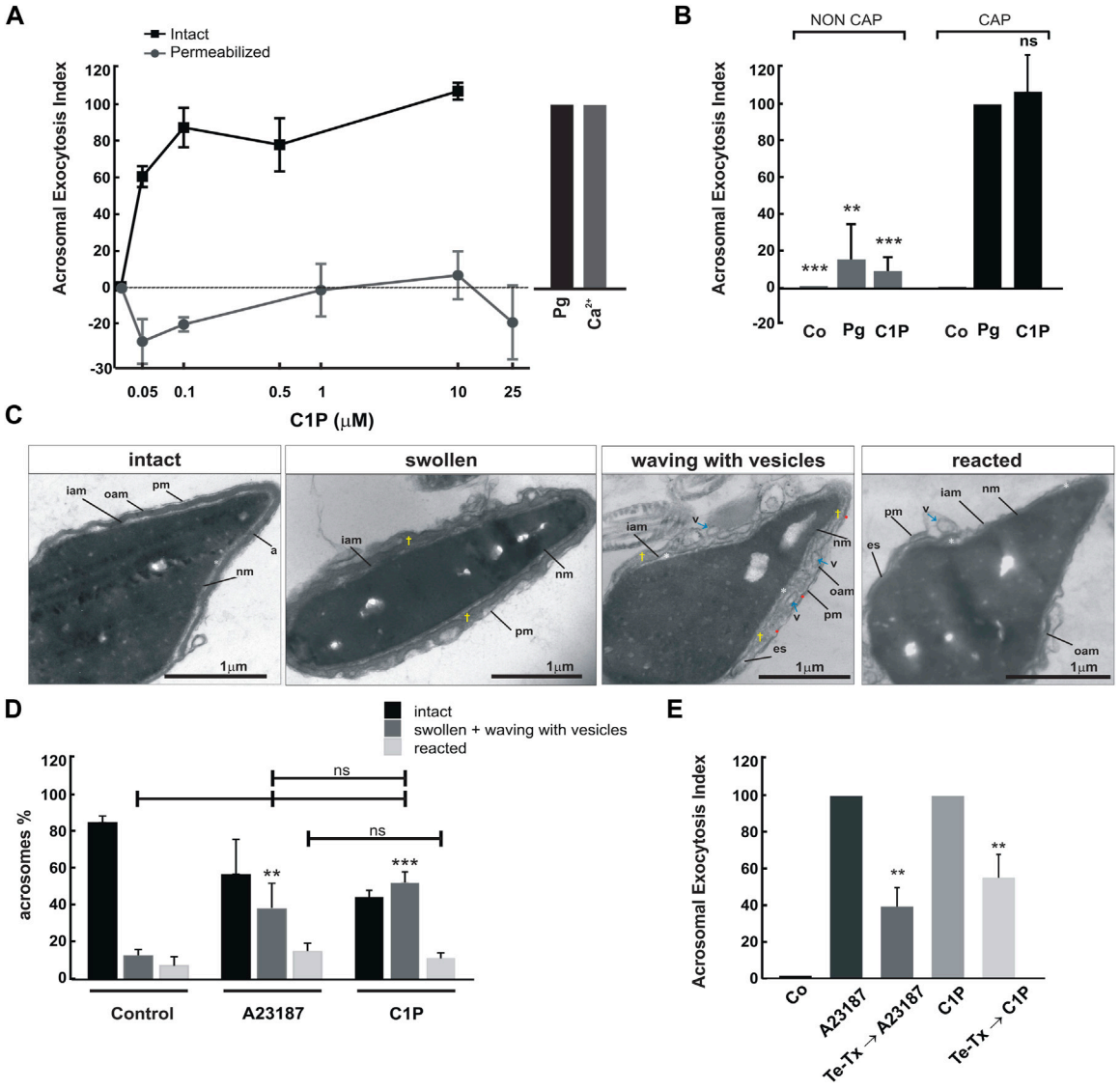

FIGURE 1
C1P triggers acrosomal exocytosis in capacitated intact human spermatozoa. **(A)** After swim-up in HTF (5 mg/ml bovine serum albumin) at 37°C, 5% CO_2, sperm were incubated for at least 3 h under capacitating conditions. Intact and controlled plasma membrane SLO-permeabilized sperm were treated with increasing concentrations of C1P (0–10 μM) for 15 min at 37°C in 5% CO_2. As a positive control, permeabilized spermatozoa were stimulated with 10 μM free Ca^{2+} (gray bar) and intact sperm with 15 μM Pg (black bar). Sperm were fixed and acrosomal exocytosis was evaluated by FITC-PSA binding with at least 300 cells per condition scored. The data represent the mean ± S.E. from three to five independent experiments. **(B)** An aliquot of a sperm sample was subjected to swim-up in HTF medium under non-capacitating conditions (37°C, 5% CO_2, without bovine serum albumin). Another aliquot was processed in capacitating conditions: swim-up in HTF (supplemented with 5 mg/ml bovine serum albumin, 37°C, 5% CO_2). Cells recovered from swim-up were incubated for an additional 3 h under non-capacitating or capacitating conditions as indicated. Sperm were treated or not (control, Co) with 15 μM progesterone (Pg) or 10 μM C1P for 15 min at 37°C 5% CO_2. Acrosomal exocytosis was evaluated as explained under "Materials and Methods". The data represent the mean ± S.E. of at least four independent experiments. The means of groups NON CAP and CAP were compared with the corresponding control (Pg) using Dunnett's test and classified as non-significant (ns, $p < 0.05$), or significant (**, $p < 0.01$; ***, $p < 0.001$). **(C)** Capacitated sperm were incubated for 15 min at 37°C with 10 μM C1P or 10 μM A23187 and processed as described in "Materials and Methods" for electron microscopy. Transmission electron micrographs of spermatozoa after C1P treatment showing different morphological stages: intact, swollen + waving with vesicles and reacted. pm: plasma membrane; oam: outer acrosomal membrane; iam: inner acrosomal membrane; nm nuclear membrane; es: equatorial segment; v: vesicle; †: swollen acrosome. Scale bars, 1 μm. **(D)** Quantification of the percentage of intact, swollen (swollen and waving with vesicles) and reacted sperm (lost acrosomes). The means of groups swollen plus waving with vesicles were compared with the corresponding control s, *$p < 0.05$; ns, $p > 0.05$ (Newman-Keuls Multiple Comparison Test). **(E)** Capacitated sperm were incubated with 1.5 μM recombinant cell-permeant light chain of Tetanus toxin (Te-Tx). After that, the AR was stimulated with 10 μM C1P or 10 μM A23187 for 15 min. Sperm was fixed and acrosomal exocytosis was evaluated by FITC-PSA binding with at least 300 cells scored.

swelling. Further, this result allows us to rule out membrane disruption. The sperm AR is a synchronized process occurring once in the gamete life. It depends on neurotoxin-sensitive SNAREs activation. Calcium sparks tangled signaling in spermatozoa that ultimately disassembles neurotoxin-resistant cis and triggers toxin-sensitive loose trans-SNARE complexes assembly.

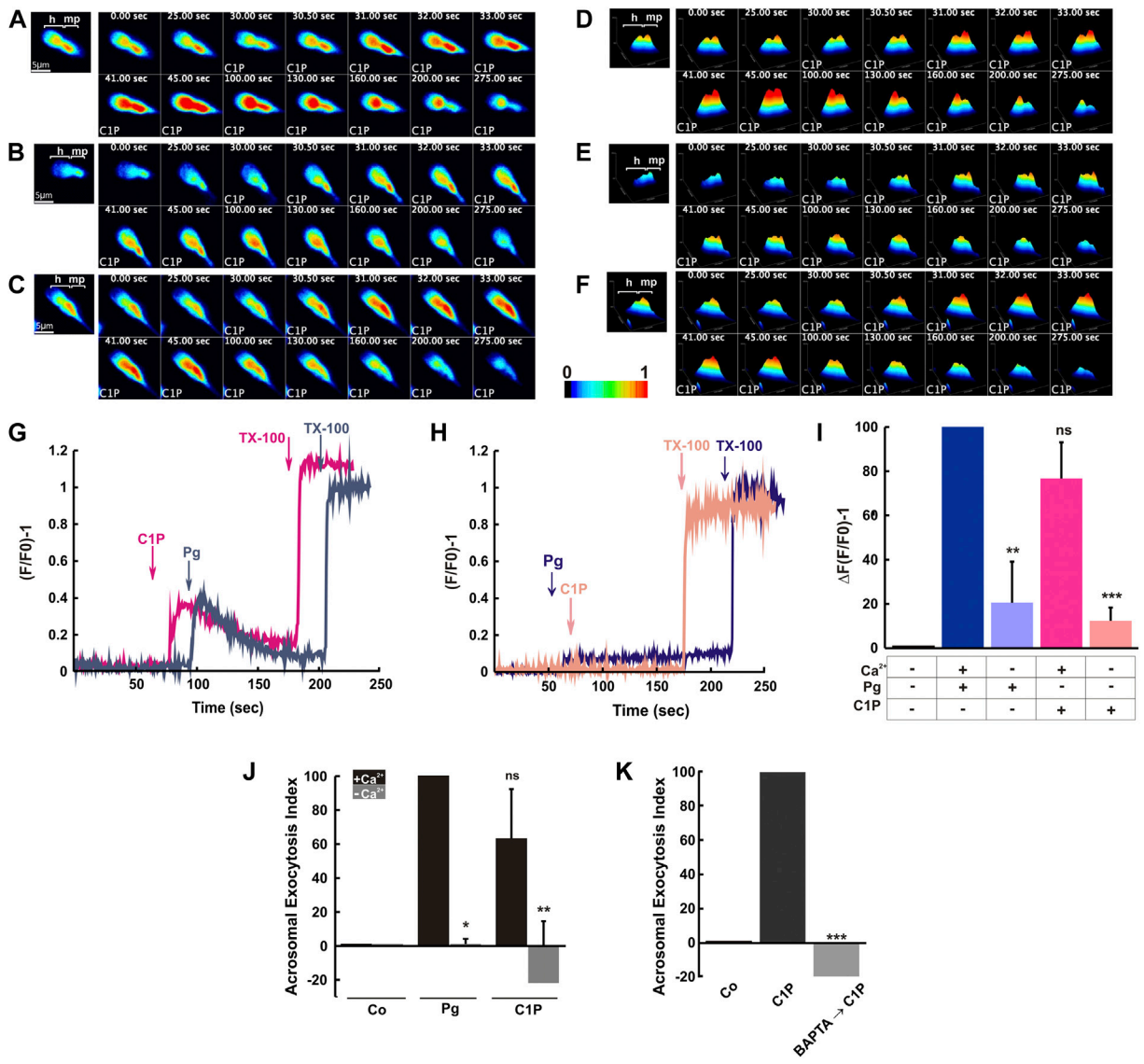

FIGURE 2
C1P-triggers extracellular calcium influx leading to sperm acrosomal exocytosis. Capacitated human sperm were loaded with Fluo-3 AM (2 µM) and suspended in HTF medium containing a final concentration of 2 mM $CaCl_2$. The fluorescence intensity was visualized before and after C1P addition as described under "Materials and Methods". **(A–C)** Sequence of fluorescence images from human sperm capacitated and loaded with Fluo-3AM showing changes in $[Ca^{2+}]i$ before (0 s) and after (25, 30, 30.5, 31, 32, 33, 41, 45, 100, 130, 160, 200, and 275 s) the application of 10 µM C1P. Shown are representative images of three individual human sperm. **(D–F)** Surface plots of the cells shown in panels A–C, also plots indicate the increase in fluorescence intensity in response to 10 µM C1P. Fluorescence is expressed as (F/F0) –1 *versus* time. Pseudocolor from black to red represents low to high $[Ca^{2+}]i$, respectively. h: head, mp: midpiece. **(G)** Calcium sperm response to C1P in population. Human sperm were loaded with 2 µM Fluo-3 AM for 30 min at 37°C. At the indicated times (arrows) 10 µM C1P or 15 µM progesterone (Pg) were added. Maximal $[Ca^{2+}]i$ response was calibrated with 0.1% Triton X-100 (TX-100) at the end of the incubation period. Shown are traces representative of 6 experiments. The increase in fluorescence is expressed as (F/F0) –1 ((maximum fluorescence intensity/initial fluorescence) - 1) *versus* time in seconds. **(H)** Capacitated male gametes were suspended in the same medium including 0.75 mM EGTA to chelate the calcium leaving the HTF with a $[Ca^{2+}] \leq 100$ nM. Then, cells were loaded with 2 µM Fluo-3 AM for 30 min at 37°C. At the indicated times (arrows), 10 µM C1P or 15 µM progesterone (Pg) were added. Maximal $[Ca^{2+}]i$ response was calibrated with 0.1% Triton X-100 (TX-100) at the end of the incubation period. **(I)** Summary of Figures 2G,H. The data represent the mean ± S.E. of five experiments. **(J)** Acrosomal exocytosis was evaluated by FITC-PSA binding. We scored at least 300 cells per condition. Sperm batches incubated in normal calcium concentrations (black bars) and treated with 0.75 mM EGTA (gray bars) were challenged with 10 µM C1P or 15 µM progesterone (Pg). The data represent the mean ± S.E. of at least five independent experiments. The means of groups + Ca^{2+} and -Ca^{2+} were compared to Pg treatment (2 mM Ca^{2+}) using Dunnett's test and classified as non-significant (ns, $p > 0.05$) or significant (*, $p \leq 0.05$; **, $p \leq 0.01$). **(K)** Capacitated sperm were incubated with 5 mM BAPTA for 15 min and after that, C1P was added and further incubated for 15 min. Acrosomal exocytosis was evaluated by FITC-PSA binding scoring at least 300 cells per condition. The data represent the mean ± S.E. of four independent experiments. We used Dunnett's test to compare the means of all groups against the Control condition and classified them as significant (***, $p \leq 0.001$).

Acrosome exocytosis requires all these steps to proceed (De Blas et al., 2005) (Lopez et al., 2012; Pelletan et al., 2015). To elucidate if C1P-induced exocytosis is a physiological process that requires functional SNAREs to proceed, we cleaved VAMP2 with a tool developed in the laboratory before adding the lipid. We utilized a recombinant Tetanus toxin (Te-Tx) coupled to a cell-penetrating peptide (Mayorga et al., 2020). This peptide permits plasma membrane translocation and toxin delivery to the cytosol. To assess our hypothesis, we first incubated human spermatozoa with the permeable Te-Tx light chain and after that, the sperm AR was stimulated with 10 μM C1P for 15 min. Te-Tx cleaved VAMP2 and significantly inhibited both, the calcium ionophore (A23187) and C1P-triggered AR (Figure 1E). This last result demonstrates that C1P requires the SNAREs assembly to induce the AR.

C1P-triggers extracellular calcium influx leading to sperm acrosomal exocytosis

Hence, if C1P is inducing regulated exocytosis, we assumed that the sphingolipid should be increasing intracellular calcium. Then, we tested whether C1P addition to the sperm media was able to induce an $[Ca^{2+}]i$ augment in live cells.

First, we suspended the live gametes in HTF medium containing a final concentration of 2 mM $CaCl_2$. After that, we performed single-cell experiments by loading spermatozoa with Fluo-3 AM dye, a permeant Ca^{2+} indicator, and measuring Ca^{2+} changes in an inverted fluorescence microscope. Figure 2A–C displays sequential images of human sperm after 10 μM C1P addition. We showed the $[Ca^{2+}]i$ changes in three live single cells from 0 to 275 s. We noticed the cells presented different kinetic responses after the stimulus addition. Further, the cells recovered the basal calcium values indicating that the ion homeostasis has been restored. The kinetic of the calcium changes can be observed in the Supplementary Movies S1–S3. Figure 2D–F illustrated a surface plot of each cell. Summarizing, exogenous C1P provokes an $[Ca^{2+}]i$ rise in human sperm. Next, we analyzed calcium sperm response to C1P in the population. Sperm suspended in HTF and loaded with the calcium indicator were incubated with C1P or Pg. C1P caused a sperm $[Ca^{2+}]i$ augment followed by a gradual drop to almost resting levels (Figure 2G). This transient calcium increase is coincident with that induced by 15 μM Pg treatment (control).

To establish whether the C1P-induced $[Ca^{2+}]i$ increase was due to calcium influx from the extracellular medium or calcium mobilization from the internal reservoirs, we decided to measure $[Ca^{2+}]i$ in the sperm population in a free calcium media. For this purpose, we resuspended capacitated sperm in the same medium including 0.75 mM EGTA to chelate the calcium leaving the HTF with a $[Ca^{2+}] \leq 100$ nM as previously described in Vaquer et al. (2020) (Vaquer et al., 2020). Afterward, we loaded the male gametes with the permeant calcium probe. Under this extremely low extracellular $[Ca^{2+}]$ C1P did not cause an increase in sperm $[Ca^{2+}]i$. The same result was obtained by adding Pg under the same conditions (Figure 2H). Different sperm batches achieved equivalent results that were depicted and compared in Figure 2I. These results indicate that C1P elicited human sperm transitory $[Ca^{2+}]i$ rise is due to extracellular calcium entry.

We evaluated the C1P effect on the AR in a calcium free media. As shown in Figure 2J, incubating the cells in HTF media with $[Ca^{2+}] \leq 100$ nM abolished the exocytotic effect of C1P and Pg. Pg-induced AR depends on calcium entry (Carlson et al., 2022), and the result was reproduced here in Figure 2J as a control. Further, sperm incubated in normal HTF (2 mM $CaCl_2$) and then treated with 5 mM BAPTA for 15 min were not able to respond to the C1P stimulus. The incubation with the chelating agent for a short time was enough to inhibit the AR (Figure 2K).

The last results indicate that C1P induces Ca^{2+} influx from the extracellular media, which is necessary for the lipid-triggered exocytosis.

C1P increases intracellular Ca^{2+} in human sperm through the activation of VOCCs, SOCCs, CatSper, RyR, and IP_3-dependent calcium channels

The classical calcium channels pathway requires different calcium waves produced by the sequential activation of these channels. In short, an exocytotic stimulus provokes VOCCs opening that generates a transient calcium increase inducing reservoirs (acrosome and RNE) emptying. The voiding of the stores causes a sustained calcium influx through SOCCs. We decided to analyze which calcium channel/s are implicated in the C1P-triggered mechanism. To test this premise, we incubated Fluo-3 AM-loaded sperm in HTF medium containing 2 mM $CaCl_2$. Then, we added specific inhibitors of calcium channels and measured, in the sperm population, the variations in $[Ca^{2+}]i$ after cells were challenged with 10 μM C1P. First, we treated sperm with 200 μM lanthanum, which is a general calcium channel blocker. C1P-induced calcium rise was sensitive to lanthanum suggesting the requirement of plasma membrane calcium channels (Figure 3G).

To block L-type high voltage-activated Ca^{2+} currents we used 100 μM verapamil. The arylalkylamine treatment abolished completely the C1P-induced calcium increase (Figures 3A,G). It is expected that an early transient calcium rise through VOCCs, activates the emptying of calcium stores through IP_3R and this calcium efflux is mandatory for the AR. Therefore, we incubated sperm with IP_3-sensitive calcium channel blockers before C1P addition. Both 2-APB and Xestospongin C (XC) inhibited significantly the C1P-triggered calcium increase (Figures 3D, E, G). The RNE has been described as a calcium reservoir in mammalian sperm (Harper and Publicover, 2005; Suarez, 2008). Both IP_3R and RyR are present in its membrane (Reviewed in Darszon et al., 2011 (Darszon et al., 2011)). Since we described a function for these RyRs in the ceramide-elicited acrosome exocytosis we asked if they are required for calcium signal induced by C1P. We incubated the cells with 20 nM ruthenium red (RR) or 100 μM dantrolene to block the RyR function. The treatments prevented the sphingolipid-induced calcium augment, indicating that the RNE is an important store involved in C1P-elicited calcium signaling (Figures 3F,G). To elucidate if plasma membrane calcium channels like SOCCs, are required for the C1P-stimulated calcium rise we resorted to specific blockers: SKF-96365 (Kachoei et al., 2006; Trevino et al., 2006) and YM-58483 (Yoshino et al., 2007). Both inhibitors blocked calcium increment elicited by C1P

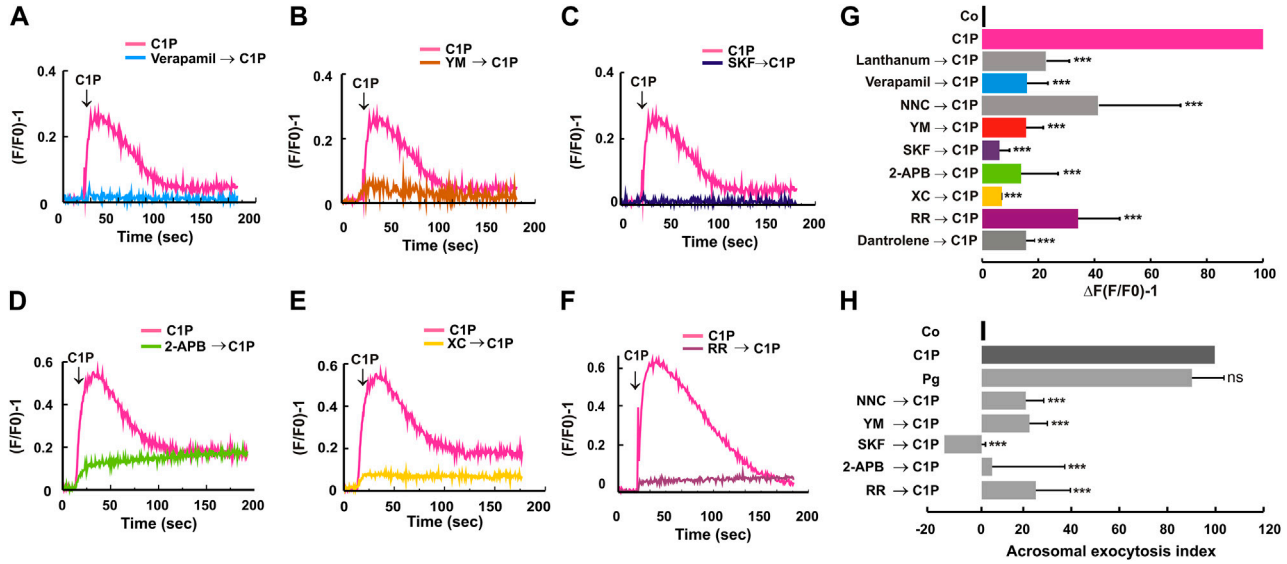

FIGURE 3
C1P-elicited intracellular Ca^{2+} increase relies on extracellular calcium influx and the ion release from intracellular stores. Capacitated human sperm recovered after swim-up were loaded with Fluo-3 AM (2 μM), and the fluorescence intensity was observed as described under "Materials and Methods". Representative spatiotemporal $[Ca^{2+}]$i changes and their corresponding traces are shown. The arrow indicates the addition of 10 μM C1P. When indicated, cells were previously incubated for 10 min at 37°C with: **(A)** 100 μM Verapamil, **(B)** 1 μM YM-58483 (YM), **(C)** 50 μM SKF-96365 (SKF), **(D)** 100 μM 2-APB, **(E)** 1 μM Xestospongin C (XC), **(F)** 20 nM ruthenium red (RR). **(G)**, ΔF(F/F0) – 1 is the average of the changes in fluorescence of each condition measured. Here, we represented in addition results obtained after the treatment with 200 μM Lanthanum, 1 μM NNC, and 100 μM Dantrolene. Bars represent the mean ± S.E of five independent experiments. Different conditions were compared using Dunnett's test and C1P as a control, and differences were classified as significant (***, $p \leq 0.001$). **(H)** To determine if calcium channels inhibitors affect the AR we incubated capacitated human sperm without any treatment (control, Co) or treated when indicated with, 1 μM NNC, 1 μM YM, 50 μM SKF, 100 μM 2-APB, or 20 nM RR for 15 min at 37°C. When specified, acrosomal exocytosis was initiated by adding 10 μM C1P and the incubation continued for an additional 15 min. We used 15 μM Pg as a positive control of the experiment. Sperm were then fixed, and acrosomal exocytosis was measured. The data represent the mean ± S.E. from 3 to 5 independent experiments. Dunnett's test was used to compare the means of all groups against the C1P-stimulated condition in the absence of inhibitors and classified as non-significant (ns, $p > 0.05$) or significant (***, $p \leq 0.001$).

(Figures 3B,C,G). CatSper has been proposed as the plasma membrane Ca^{2+} channel responsible for the initial Ca^{2+} transient current (Kirichok et al., 2006). NNC was reported as a CatSper blocker (Lishko et al., 2011; Strunker et al., 2011). NNC inhibited significantly C1P-triggered $[Ca^{2+}]$i augment (Figure 3G). These last results suggest that even though the extracellular calcium entry is necessary for C1P-induced $[Ca^{2+}]$i augment both plasma membrane and store channels participate in calcium rise and the acrosomal exocytosis.

Since not all the calcium augments observed lead to the sperm AR, we measured exocytosis after inhibiting the aforementioned channels under the same conditions. The use of these channel blockers significantly inhibited the C1P-provoked exocytosis (Figure 3H).

CERK is present and catalyzes C1P synthesis in response to calcium increase in human spermatozoa

Previously, our laboratory demonstrated a crucial role for S1P as a sperm acrosomal exocytosis inducer. Spermatozoa exocytic stimuli elicit S1P synthesis, which can reach the extracellular medium and bind to Gi-coupled receptor/s triggering a signaling cascade that drives the AR (Suhaiman et al., 2010). Next, we described that ceramide triggers the acrosomal exocytosis by inducing calcium mobilization from internal stores and external calcium entry conducting, finally to sperm AR (Vaquer et al., 2020). In that last publication, we first hypothesized that the ceramide increase could be inducing S1P synthesis given the presence in sperm of the sphingolipid metabolism enzymes required (Suhaiman et al., 2010). However, against our prediction, the sphingosine kinase inhibitor does not hinder the ceramide-stimulated AR. This demonstrates that ceramide elicits exocytosis in an S1P-independent way (Vaquer et al., 2020). Moreover, we described the ceramide pathway that differs at the early stages from that induced by S1P.

Here, we decided to measure if ceramide can induce the synthesis of a phosphorylated bioactive sphingolipid once added to sperm. Then, spermatozoa were incubated or not with 10 μM ceramide (C6) in the presence of [γ-^{32}P] ATP. The ceramide treatment did not induce S1P synthesis in human sperm. HeLa cells incubated with sphingosine proved the Rf of S1P (Figure 4A). However, here we identified a spot in sperm samples incubated with ceramide consistent with the Rf of C1P. The sperm incubation with the Sphingosine Kinase Inhibitor (SKI) before the C6 addition did not affect the C1P synthesis (Figure 4A, C6, and SKI →C6). These results demonstrate that an increase of ceramide in sperm provokes an acute C1P rise. Furthermore, they imply the existence of an active CERK in human sperm. To determine if this kinase was present in

10.3389/fcell.2023.1148831

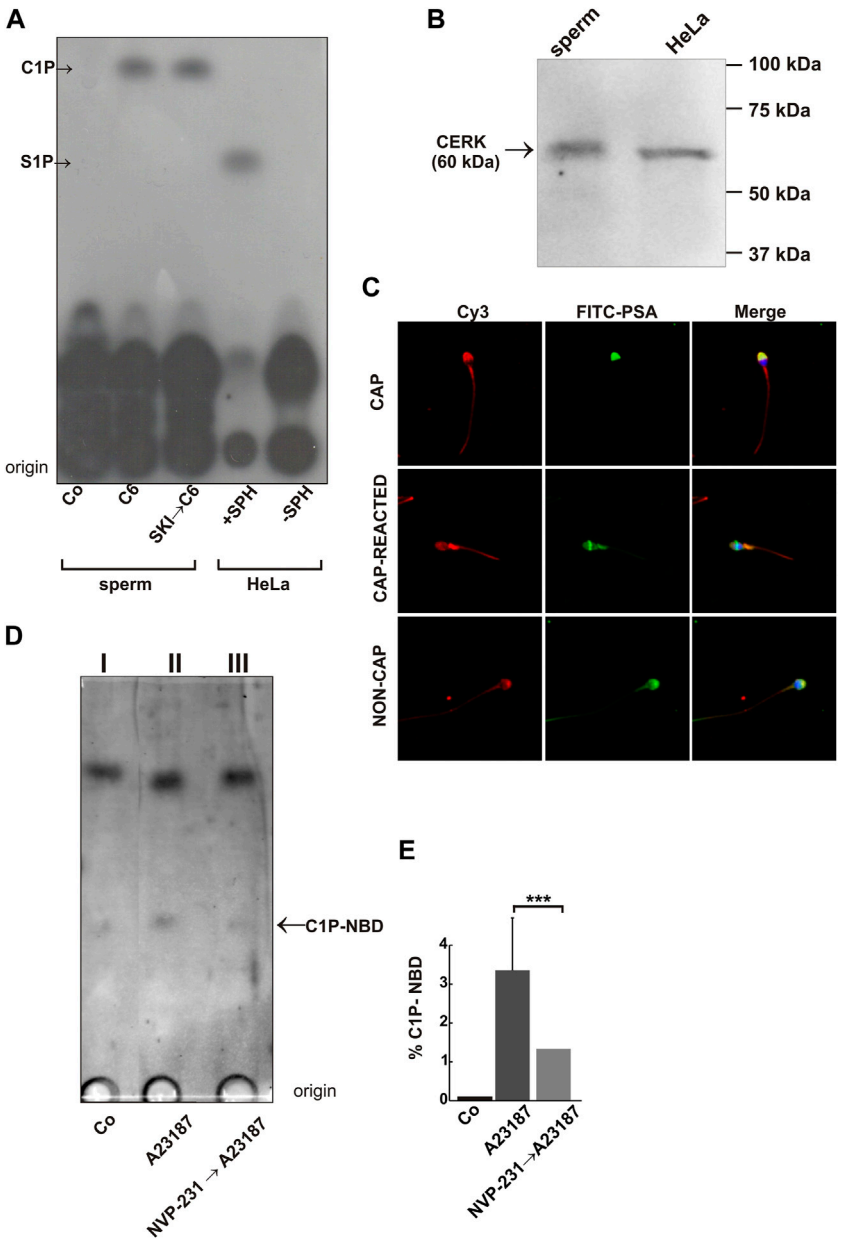

FIGURE 4
C6-Ceramide induces C1P synthesis in human spermatozoa. **(A)** After swim-up in HTF at 37°C, 5% CO_2, sperm were incubated under capacitating conditions for 2 h, and permeabilized with streptolysin O as described in our previous publications (Lopez et al., 2012; Pelletan et al., 2015). When indicated, we incubated permeabilized sperm in SK1 buffer containing 1 μM SKI (specific Sphingosine Kinase Inhibitor) for 15 min at 37°C. We further incubated the samples for 15 min at 37°C with 50 μM fatty acid free bovine serum albumin-sphingosine, 1 μL of [γ-^{32}P]ATP in the absence of any stimulus (Control, Co) or 10 μM C6-Cer (C6, SKI→C6). HeLa cells (positive control, incubated with sphingosine; +SPH, and negative control with no sphingosine added; -SPH) were prepared as described under "Materials and Methods". Thin-layer chromatograms were developed in 1-butanol/methanol/acetic acid/water (8:2:1:2, v/v) and observed by autoradiography. The figure is representative of three experiments. **(B)** CerK is present and catalyzes C1P synthesis in response to calcium increase in human spermatozoa. Sperm proteins were extracted in Laemmli sample buffer (10×10^6 cells) and analyzed by Western blot with a rabbit polyclonal anti-CERK antibody (sperm). HeLa extract (HeLa) was used as a control. **(C)** Capacitated (CAP) and non-capacitated (NON-CAP) human sperm were fixed and double-stained with an anti-CERK antibody followed by an anti-rabbit Cy3 (red: Cy3) and FITC-PSA to differentiate between reacted and intact sperm (green: FITC-PSA). The middle panel shows a capacitated cell that in response to the Pg stimuli lost its acrosome (CAP-REACTED) and Cy3 staining remains diffuse. Merged images are shown (stained sperm nuclei are visualized in blue, Merge). **(D)** Capacitated sperm were loaded with a fluorescent ceramide (4-nitrobenzo-2-oxa-1,3-diazole–labeled C12-ceramide, NBD-ceramide). After that, cells were incubated or not (Co, basal activity) with a calcium ionophore, A23187, to increase the [Ca^{2+}]i. One batch of ionophore-treated cells was previously incubated with the CERK inhibitor, NVP-231 (adamantane-1-carboxylic acid (2-benzoylamino-benzothiazol-6-yl)amide) 200 nM. Before resolving ceramide metabolites by TLC, we separated them according to their lipophilicity as described in "Materials and Methods". **(E)**. Quantification of spot intensity of three thin-layer chromatograms corresponding to C1P-NBD. A significant increase of C1P-NBD was assessed by *t*-test for single group mean significant (***, $p \leq 0.001$).

spermatozoa we performed Western blot assays. We utilized a specific polyclonal antibody (Abcam) to reveal the presence of CERK in sperm extracts. Figure 4B (whole sperm extract, sperm) showed a single band of an apparent MW of ~60 kDa equivalent to the MW described for human CERK, and an identical band in a homogenate of HeLa cells (control, Figure 4B, HeLa lane). To analyze the CERK localization we used indirect immunofluorescence. To differentiate between intact and reacted spermatozoa we performed double labeling with FITC-PSA (Figure 4C, FITC-PSA, and Cy3). Both, capacitated and non-capacitated (CAP, NON-CAP) sperm showed strong labeling in the acrosomal region and the midpiece of the flagellum. This pattern was present in 82% of the non-reacted cells (n = 4 samples). When capacitated samples where stimulated with Pg (CAP-REACTED), the cells lost their acrosomes and the acrosomal region labeling is replaced by a diffuse staining pattern.

CERK catalyzes the phosphorylation of ceramide to synthesize the bioactive sphingolipid C1P. The kinase contains a Ca^{2+}/calmodulin (Ca^{2+}/CaM) binding motif (Rhoads and Friedberg, 1997), which is required for C1P production in response to $[Ca^{2+}]i$ increase (Mitsutake and Igarashi, 2005; Hinkovska-Galcheva and Shayman, 2010). Hence, we decided to evaluate if the sperm CERK is active, upregulated by calcium, and inhibited by a specific CERK blocker. For this purpose, we made use of the thin-layer chromatography (TLC) method we published recently for sperm sphingolipid metabolites (Vaquer et al., 2020). First, we loaded sperm with a fluorescent ceramide (4-nitrobenzo-2-oxa-1,3-diazole–labeled C12-ceramide, NBD-ceramide). After that, cells were incubated or not (Co, basal activity) with a calcium ionophore, A23187, to increase the $[Ca^{2+}]i$. One batch of ionophore-treated cells was previously incubated with the CERK inhibitor, NVP-231. A potent, specific, and reversible CERK inhibitor that competitively inhibits ceramide binding to CERK. It abrogates phosphorylation of ceramide, resulting in decreased endogenous C1P levels (Graf et al., 2008). Before resolving ceramide metabolites by TLC, we separated them according to their lipophilicity. Then, we measured C1P levels in the aqueous phase. Figures 4D,E showed a low basal activity of the enzyme (Co) in human sperm. The calcium ionophore, A23187, increased significantly the kinase activity, which was almost abolished in the presence of NVP-231. Thus, calcium is a CERK activator in human sperm AR and NVP inhibits the kinase activity allowing us to use this permeant inhibitor as a tool for exocytosis experiments.

Ceramide induces sperm acrosomal exocytosis, partly, due to C1P synthesis

A few years ago, we unveiled the exocytic pathway triggered by ceramide. The sphingolipid induces a multicomponent calcium rise driving exocytosis. The calcium channels described to be regulated by ceramide constitute a calcium signaling partly similar to that induced by C1P. Here we demonstrated that ceramide induces C1P synthesis in human sperm. Strikingly, C1P elicited exocytosis by itself. Then, we asked whether ceramide-accomplished exocytosis is due to C1P synthesis. To answer this question, we incubated capacitated sperm with NVP-231, the CERK inhibitor, before adding the ceramide stimulus. We hypothesized that if ceramide was exerting its effect through C1P the exocytosis will be completely abolished. As shown in Figure 5A, the NVP-231, inhibited significantly ceramide-triggered exocytosis. Even so, 36% of the relative AR remained. C1P completely rescued the inhibition of ceramide-triggered exocytosis caused by the CERK blocker, evincing the specificity of the NVP-231.

Progesterone requires C1P to trigger acrosome exocytosis

There are two well-known physiological inducers of the AR: Pg and zona pellucida (ZP) glycoproteins (Aldana et al., 2021). However, the complete network of molecules involved in both pathways is largely unknown. In particular, the function of lipids has been relegated to a secondary role in a signaling cascade dominated by proteins. To determine the physiological importance of C1P in the progesterone pathway, we stimulated the AR with Pg in the presence of the CERK inhibitor. NVP-231 inhibited significantly (80%) the Pg-elicited exocytosis. C1P reversed the inhibitory effect. This result highlight the role of the bioactive sphingolipid C1P as a molecule implied in the acrosomal exocytosis physiology.

Trying to understand which is the role of the C1P in the Pg pathway, we inquired if the CERK activity was necessary for the Pg-induced calcium increase. Then, we resort to calcium measurements in cell population. We loaded capacitated sperm with the calcium indicator Fluo3-AM. Next, we added the CERK inhibitor NVP-231, followed by the Pg stimulus. NVP decreased the calcium sperm response to Pg addition, causing a significantly drop in the (F/F0) – 1 (Figure 5D) compared to the transient calcium increase induced by Pg (Figure 5C). As a specificity control we added 10 μM C1P after NVP-231 treatment. C1P induced a calcium augment, which was not significantly different to that induced by incubating the cells with NVP before C1P addition (Figures 5E,F). The ΔF of all experimental conditions were compared in Figure 5G. To sum up, the calcium rise induced by Pg, partially, relies on CERK activity and consequently on C1P synthesis.

Discussion

Whilst protein complexes implicated in exocytosis are relatively well characterized, few data are showing directly the mechanistic role of lipids during membrane fusion.

Further, scarce information exists about the biological significance of different lipids in human sperm AR. Given that the spermatozoa are conveniently fitted to study this issue, our laboratory has elucidated the signaling cascades accomplished by different sphingolipids during human sperm acrosomal exocytosis establishing a dynamic protein-membrane interface (Suhaiman et al., 2010; Belmonte & Suhaiman, 2012; Vaquer et al., 2020). Recently, we described that ceramide increases intracellular calcium by activating SOCCs, CatSper, and RyRs triggering human sperm AR (Vaquer et al., 2020). Ceramide is considered a main hub in the *de novo* sphingolipids synthesis generating a large variety of molecules. Given this, we focused on the bioactive metabolites synthesized. As previously demonstrated, ceramide, a precursor

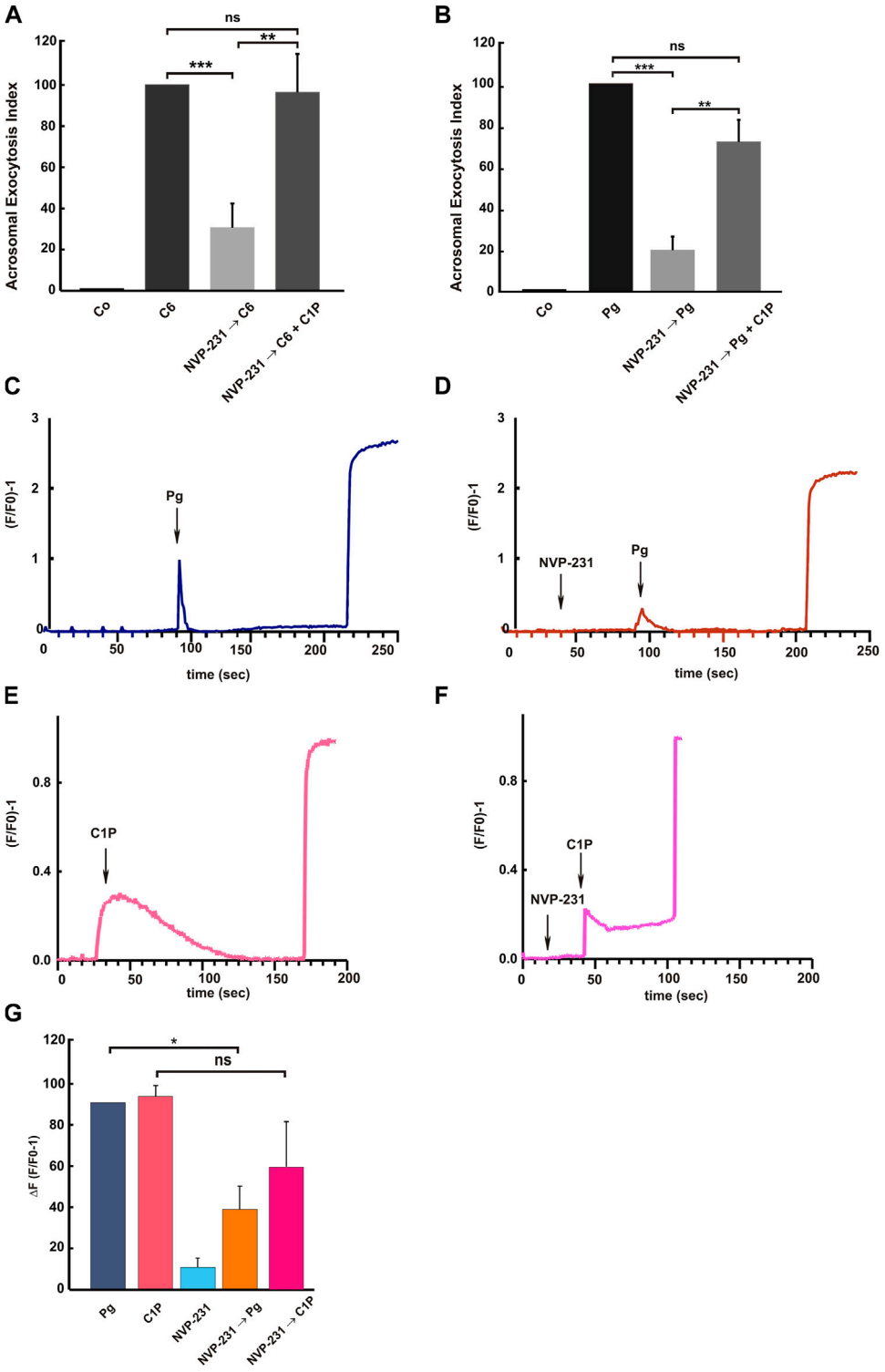

FIGURE 5
Ceramide and Progesterone require C1P to trigger acrosome exocytosis. After swim-up in HTF (5 mg/ml BSA) at 37°C, 5% CO_2, sperm were incubated for an additional 2 h under capacitating conditions. **(A)** Capacitated sperm were treated with 200 nM NVP-231 for 15 min at 37 °C in 5% CO_2 and further incubated with 10 μM C6-Cer (NVP-231→C6) or with 10 μM C6-Cer plus 10 μM C1P (NVP-231→C6+C1P). C6-Cer (C6) was used as a positive control **(B)** We incubated capacitated spermatozoa with 200 nM NVP-231 for 15 min at 37°C in 5% CO_2 then we treated the cells for an additional 15 min with 15 μM Pg (NVP-231→Pg, Pg) or with 15 μM Pg plus 10 μM C1P (NVP-231→Pg + C1P). Sperm were fixed and acrosomal exocytosis was evaluated by FITC-PSA binding with at least 300 cells per condition scored. Tukey's test was used to compare mean groups of treatments and classified as non-significant (ns, $p > 0.05$) or significant (**, $p < 0.01$ or ***, $p < 0.001$). **(C–F)** Capacitated human sperm were loaded with 2 μM Fluo-3 AM for 30 min at 37°C. At the indicated times (arrows) 15 μM Pg was added. Maximal $[Ca^{2+}]i$ response was calibrated with 0.1% Triton X-100 (TX-100) at the end of the incubation period. When indicated, 200 nM NVP-231 was added before Pg or C1P addition. Shown are traces representative of 4 experiments. The increase in fluorescence is expressed as (F/F0) −1 ((maximum fluorescence intensity/initial
(*Continued*)

FIGURE 5 (Continued)
fluorescence) - 1) *versus* time in seconds. **(G)** ΔF(F/F0) – 1 is the average of the changes in fluorescence of each condition measured. Bars represent the mean ± S.E of 4 independent experiments. Different conditions were compared using Tukey's test and the differences were classified as significant (*, $p < 0.05$; NVP-231→Pg, Pg), or as non-significant (ns, $p > 0.05$; NVP-231→C1P, C1P).

of S1P, does not require S1P presence to activate exocytosis. Herein, we confirmed that ceramide addition to sperm does not induce acute S1P synthesis but the small bioactive lipid C1P. The specific aim of this research was to analyze whether C1P is involved in sperm AR. To the best of these authors' knowledge, the implication of C1P in sperm AR has not been investigated, nor has its physiological importance. Here, for the first time, we evaluated this issue using human sperm allowing an extrapolation and transference to the clinical interests.

Given that we added exogenous C1P to the extracellular media, which is not a membrane-permeant molecule, and observed its ability to induce the AR we conclude that our results support the idea of an extracellular role of C1P. Since C1P acts intra and extracellularly in other cells, we corroborated that the sphingolipid did not exert any effect in controlled plasma membrane permeabilized sperm (Figure 1). It is important to highlight that, C1P can be found in the intracellular and extracellular media. The sphingolipid is synthesized intracellularly in somatic cells. A calcium-dependent CERK catalyzes ceramide phosphorylation. The sphingolipid produced intracellularly can elicit numerous biological effects. On the other hand, C1P can be transported through the plasma membrane to the extracellular environment by a C1P transfer protein (CPTP) (Presa et al., 2020). C1P is present in plasma at concentrations ranging from 0.5 to 1.5 μM. Extracellular C1P stimulates cell migration, glucose uptake, and adipogenesis inhibition through a Gi protein-coupled receptor-mediated mechanism. However, even if a putative C1P receptor has been in part characterized, receptor/s have not yet been isolated nor cloned (Arana et al., 2013; Ouro et al., 2013). In intact human sperm, 0.1 μM C1P evoked the maximal exocytic response indicating that a high-affinity receptor is mediating C1P action. Our results support the idea that C1P interacts with a C1P receptor in the sperm plasma membrane allowing the bioactive sphingolipid to trigger a signaling mechanism leading to AR.

In addition, the capacitation is a requirement for C1P-induced acrosome exocytosis, suggesting a physiological behavior of the lipid. We assessed by TEM that C1P provokes the physiological activation of the AR at the ultrastructural level. The results obtained are comparable to that induced by Pg, which have been demonstrated to be similar to that elicited by the calcium ionophore, A23187 (Zanetti & Mayorga, 2009; Sosa et al., 2015; Sosa et al., 2016). Further, the necessity of a functional VAMP2 to engage the fusion of the outer acrosomal membrane with the plasma membrane during C1P-elicited exocytosis rule out the possibility of an artifactual effect of the lipid on exocytosis. These results discard the probability of acrosome loss due to C1P-induced membrane destabilization.

C1P has been proposed to stimulate exocytosis by rising the fusion ability of the synaptic vesicle membranes. Both C1P phosphatase and CERK, are associated with these organelles (Bajjalieh et al., 1989; Sugiura et al., 2002). Liposomes shifted the rate and extent of their calcium-reliant fusion when C1P is added (Hinkovska-Galcheva et al., 1998). Hori et al. (2020) demonstrated that in PC12 cells the CERK/C1P pathway plays a pivotal role in stimulating noradrenaline release. The sphingolipid seems to be directly stimulating the exocytic machinery (Hori et al., 2020). Even though the molecular mechanisms activated by this lipid in exocytosis have not been elucidated yet. However, given that regulated exocytosis requires a fine-tuning of $[Ca^{2+}]i$, how the activation of the CERK/C1P pathway regulates this ion leading to exocytosis, is an unresolved topic. This complex function requires multiple channels, transporters, and pumps. Our calcium measurement results performed in single-cell and population (Figure 2), lead us to conclude that C1P induced calcium entry from the extracellular media through VOC and SOC channels and CatSper. However, the calcium release from internal stores *via* RyR and IP_3R-dependent calcium channels was essential for C1P-triggered exocytosis to proceed. We hypothesize that exogenous C1P interacts with a Gi-coupled receptor activating a transient VOCCs opening and triggering the canonical exocytotic pathway described for sperm (Suhaiman et al., 2010; Darszon et al., 2011). We aim to emphasize that the calcium kinetics during the first 200 s is coincident with that activated by progesterone, the physiological AR inducer rising the physiological importance of the findings.

We described previously the exocytic pathway triggered by endogenous and exogenous added ceramide, the immediate precursor of C1P, to the male gamete (Vaquer et al., 2020). Given that, both, ceramide and its phosphorylated product, trigger the AR is imperative to compare the effect of the sphingolipids on calcium channels. Ceramide was able to raise $[Ca^{2+}]i$ even in the absence of extracellular calcium ($[Ca^{2+}] \leq 100$ nM) due to its ability to mobilize the ion from internal stores. We introduced evidence demonstrating that after ceramide treatment, RyRs are activated. Notwithstanding, calcium efflux from internal reservoirs did not result sufficient to trigger the AR. Calcium entry from SOCCs and CatSper were mandatory for ceramide-elicited AR, as well as, a late calcium efflux from IP_3-dependent calcium channels. Further, ceramide-evoked exocytosis does not require the VOCC's activation. However, C1P, the metabolite synthesized 10 min after ceramide addition to sperm (Figure 4), provoked an $[Ca^{2+}]i$ increase that relies on different calcium channels that ceramide although needed extracellular calcium entry and intracellular stores calcium release. Even though, both lipids share some channels. We thought, that probably ceramide can initiate the pathway, increasing the $[Ca^{2+}]i$ which activates the CERK, generating C1P. Our hypothesis is that ceramide and C1P are in the same pathway leading to acrosome exocytosis. Probably, both sphingolipids are inducing temporally different calcium waves.

Our results are similar to those published by Colina et al., 2005 (Colina et al., 2005) where C1P increases $[Ca^{2+}]i$ in Jurkat T Cells. C1P causes an IP_3 rise releasing calcium from the ER and provoking the

opening of SOCCs at the plasma membrane. Hogback et al., 2003 (Hogback et al., 2003) described that in thyroid FRTL-5 cells, C1P evokes a pertussis toxin-sensitive G protein-mediated mechanism that activates a PLC and the sphingosine kinase (SK), leading to S1P synthesis. This result caught our attention because our group outlined the S1P pathway during acrosomal exocytosis (Suhaiman et al., 2010). In GH4C1 rat pituitary cells, C1P elicited Ca^{2+} influx from the media through VOC channels (Tornquist et al., 2004). Thus, C1P is a molecule able to induce calcium increase in different somatic cells using diverse mechanisms and probably by activating a receptor. Some of these molecular mechanisms are shared with those described for the male gamete in this study.

hCERK is a protein of 537 amino acids. It contains a catalytic domain with a high degree of analogy to the glycerol kinase catalytic region. The enzyme carries a Ca^{2+}/calmodulin binding motif which regulates its activity and consequently, the C1P synthesis when $[Ca^{2+}]i$ increases (Mitsutake et al., 2004; Mitsutake and Igarashi, 2005). In this work, we demonstrated for the first time the presence of the CERK in the human male gamete, a protein with a MW of 60 kDa. The MW is coincident with that shown in somatic cells described in the literature (Sugiura et al., 2002) and HeLa cells (Figure 4). Moreover, Wang et al. (2013) reported the presence of the CERK in the human sperm proteome (Wang et al., 2013) supporting our findings. Concerning the localization, the kinase resides in several somatic cell compartments, e.g., the nucleus, the cytosol, and the plasma membrane. However, its main location is the Golgi apparatus. It has been described as a cytosolic enzyme that migrates to the membranes when active in somatic cells (Presa et al., 2020). The spermatozoa are polarized and very compartmentalized cells so, the enzyme is distributed in defined zones. At least, its presence in the acrosomal region matches its exocytic function, and this particular staining is lost after the AR. Remarkably, we found that the CERK activity is upregulated by calcium during human sperm AR and blocked by a specific CERK inhibitor. The kinase has been involved in the exocytosis of numerous cells. The CERK inhibition abolishes mast cells degranulation (Kim et al., 2005) and histamine and PGD2 release (Hewson et al., 2011). In addition, the CERK/C1P pathway plays a stimulatory role in the noradrenaline release in PC12 cells (Hori et al., 2020). Calmodulin directly interacts with CERK and is involved in the regulation of exocytosis, including acrosomal exocytosis (Lopez-Gonzalez et al., 2001; Yunes et al., 2002; Xue et al., 2021). On the other hand, CERK binds to a crucial lipid for sperm acrosomal exocytosis like PIP_2 (Lopez et al., 2012; Pelletan et al., 2015), we believe that fits the lipid pathway we have described for sperm AR. In addition, CERK binding could be regulating the availability of the phospholipid for the IP_3 and DAG synthesis thanks to PLC activation. Taking into account, that Ca^{2+} activates CERK during the AR and that C1P activates sphingosine kinase (SK1) (Nishino et al., 2019), we cannot discard that C1P could be inducing SK1 activation and consequently, S1P synthesis, which triggers the pathway we described for the AR (Suhaiman et al., 2010).

Both calcium and ceramide provoked C1P synthesis (Figure 4). Ceramide elicits the AR activating multiple calcium channels but here, we evinced that the sphingolipid requires the C1P synthesis to exert its full action (Figure 5). Moreover, the inhibition of the CERK restrained significantly Pg-induced AR and the Pg-elicited $[Ca^{2+}]i$ calcium augment. Consequently, Pg physiological activity in human sperm relies on ceramide (Vaquer et al., 2020) and C1P, however, is independent of S1P (Suhaiman et al., 2010). It is important to remark that, during exocytosis, there is an increase in intracellular C1P, nevertheless, the phosphosphingolipid only causes a biological effect when added to the extracellular media.

In light of these new and previous results, we built a working model shown in Figure 6. We hypothesize that C1P binds to a putative Gi-coupled receptor, and induces heterotrimeric Gi-protein and VOCCs activity driving the PLC activation. PLC hydrolyzes PIP_2 producing IP_3 and DAG. IP_3 binds to IP_3-sensitive calcium channels present in the sperm acrosome and RNE membranes, releasing calcium from these stores and, stimulating SOCCs' opening. Besides, cytosolic calcium increase could activate RyR at the sperm neck and, consequently, calcium efflux from the RNE. The activation of CatSper by C1P, a voltage-reliant, and pH-sensitive calcium channel, made us think about the molecular mechanism triggered by the sphingolipid. Evidence in the literature shows that ceramide 1-(2-cyanoethyl) phosphate (C1CP), a molecule generated during the final phase of C1P synthesis, induces ion changes in different cells. In thyroid FRTL-5 cells, patch-clamp assays demonstrated that C1CP hyperpolarized the membrane potential of the cells (Tornquist et al., 2002; Tornquist et al., 2004). We could hypothesize that C1P could be activating CatSper by modulating intracellular voltage. Even that, we cannot discard a direct effect of the phosphosphingolipid on the channel. In order to determine whether C1P/CERK signaling has a direct impact on CatSper currents in the Pg pathway, it would be required to conduct electrophysiological recordings.

It is easy to have straightforward thinking about ceramide and C1P connection given that the former is the immediate precursor of the phosphorylated sphingolipid and, we showed that ceramide acute increase produces C1P synthesis. In general, our results support the idea that they can act sequentially in the same pathway.

How would it be possible that Pg necessitates C1P synthesis to carry on exocytosis and $[Ca^{2+}]i$ increase? We propose that Pg, present in the human tubal fluid, induces a calcium increase that stimulates human sperm CERK to generate C1P. It is well known that Pg once coupled to its membrane receptor, activates an α/β hydrolase domain-containing protein 2 (ABHD2) (Miller et al., 2016). ABHD proteins play a crucial role in lipid metabolism, metabolic diseases, and lipid signaling. ABHD2 is a lipid hydrolase that acts depleting endocannabinoid 2-arachidonoylglycerol (2-AG), a natural inhibitor of CatSper, releases glycerol, arachidonic acid (AA), and increases $[Ca^{2+}]i$. The $[Ca^{2+}]i$ increase elicited by Pg can activate the CERK in the male gamete generating C1P, which could be delivered to the extracellular media through the C1P transfer protein (CPTP). Once outside, C1P may bind to a putative C1P receptor sparking an exocytotic signaling cascade. Our research evinces that C1P is not only a booster producing a positive feedback loop for the AR. The inhibition of the CERK almost abolishes the Pg-induced acrosomal exocytosis and calcium augment pointing out the requirement of the phosphorylated sphingolipid during the physiological road to fertilization.

Recently, Shan et al. (2020) demonstrated that a specific hydrolase form (ABHD16B) is associated with bull infertility in Holstein cattle (Shan et al., 2020). Sperm lipidomics proved that the absence of ABHD16B influenced the content of ceramide, phosphatidylcholine, sphingomyelin, and diacylglycerol. The ABHD16B impaired function

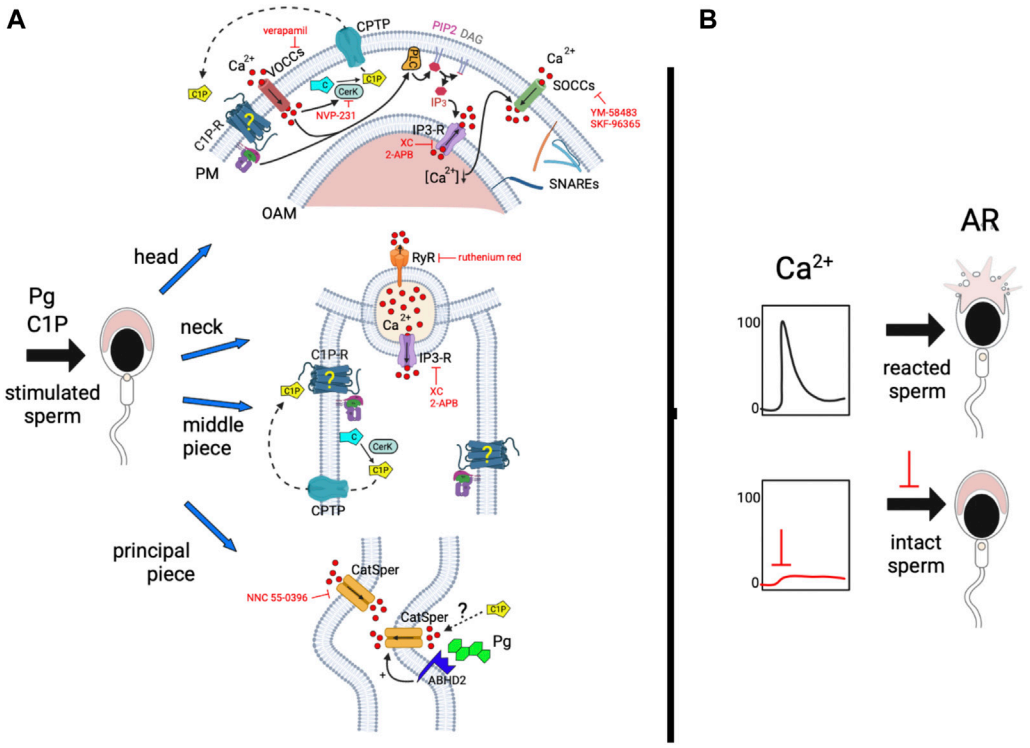

FIGURE 6
Scheme of the working model hypothesized for C1P/CERK pathway in acrosome exocytosis. **(A)** We propose that C1P interacts with a Gi-coupled receptor (C1P-R) activating VOC channels and a heterotrimeric Gi-protein. The transient calcium augment could be activating the CERK through the Ca^{2+}/calmodulin-binding motif. The kinase phosphorylates ceramide to C1P, which can be transported through the plasma membrane to the extracellular environment by a C1P transfer protein (CPTP). Once outside, it can interact with its receptor amplifying the signaling pathway. Calcium increase and the heterotrimeric Gi-protein switch on a PLC which hydrolyzes phosphatidylinositol 4,5-bisphosphate (PIP_2) producing DAG and IP_3. The last one binds to IP_3-sensitive calcium channels, present on the outer acrosomal and redundant nuclear envelope (RNE) membranes, inducing calcium efflux from the reservoirs. The voiding of the stores triggers the opening of SOCCs at the plasma membrane allowing a sustained calcium increase. At the same time, C1P, due to the first calcium wave can be causing the opening of ryanodine sensitive-calcium channels (RyR) present in the RNE. CatSper is a multimeric voltage-activated channel, negatively regulated by 2-arachidonoylglycerol (2-AG), which is hydrolyzed by the lipid α/β hydrolase domain-containing protein 2 when Pg binds its receptor. Given that C1P-induced AR requires CatSper activity, we suppose that the sphingolipid can set off CatSper *via* an unknown, alternative mechanism or by using the same machinery utilized by Pg. The last possibility makes sense due to the CERK activity requirement for Pg-triggered exocytosis. On the other hand, C1P drives SNARE (SNAP receptor) complex assembly during sperm. **(B)** C1P-elicited exocytosis is a complex mechanism that demands the participation of multiple calcium channels to reach a sustained $[Ca^{2+}]i$ necessary for the efficient signaling conducting human sperm AR.

provoked an alteration of the sperm membrane composition. Therefore, we believe that the Pg signaling involves more lipids than we had thought until now. This follows our results published previously (Vaquer et al., 2020) and supports the role of ceramide and C1P in the Pg pathway.

Considering that, C1P is present at low concentrations in different biological fluids is a stable, slowly metabolized molecule, and possesses a long half-life (Gomez-Munoz et al., 1995; Gangoiti et al., 2012) we cannot discard that extracellular C1P in the female genital tract could trigger acrosomal exocytosis when the gamete transits near the oocyte. Further, Dr. Parborell's group demonstrated that C1P reduces ovarian injury during chemotherapy with alkylating agents (Pascuali et al., 2018) assigning a crucial role to the sphingolipid.

Our findings are laying the groundwork for additional research about the physiological Pg pathway that remains to be fully ascertained. This study uncovers the sphingolipids' function during exocytosis, particularly, the role of the critical bioactive lipid C1P. Here, we emphasize the indispensable lipid balance required for fertilization. The data provided here may open novel scenarios about the pathways that could be affected in male infertility bringing basic knowledge closer to translational medicine.

Data availability statement

The original contributions presented in the study are included in the article/Supplementary Material, further inquiries can be directed to the corresponding author.

Ethics statement

The studies involving human participants were reviewed and approved by the Ethics Committee of the Medical School, Universidad Nacional de Cuyo. The Committee approved the signed informed consent and the protocol for semen handling

(CUDAP: EXP-CUY:0025793/2016). Data collection adheres to the guidelines established in Argentina (ANMAT 5330/97) and followed the principles outlined in the Declaration of Helsinki. All donors signed an informed consent agreeing to supply their own anonymous information and semen samples. The patients/participants provided their written informed consent to participate in this study.

Author contributions

CV contributed to investigation, conceptualization, methodology, formal analysis, and review. LS: investigation, methodology, formal analysis, writing—review, and editing. MP: methodology, investigation, formal analysis, and review. RA: methodology and formal analysis. APG: methodology. GDB: investigation, methodology, formal analysis, visualization, editing, and review. SB: conceptualization, methodology, funding acquisition, project administration, writing—original draft preparation, writing—review and editing. All authors have read and agreed to the published version of the manuscript.

Funding

This research was funded by grants from Agencia Nacional de Promoción Científica y Tecnológica (ANPCYT), Fondo para la Investigación Científica y Tecnológica (FONCYT) (PICT-2015-1222, Argentina); CONICET (PIP N° 11220120100267, Argentina), and SIIP-Universidad Nacional de Cuyo (grant number 06/J003-T1, Argentina) to SB. CONICET awarded a doctoral fellowship to CV and RA.

Acknowledgments

The authors thank E. Bocanegra for excellent technical assistance. We also thank A. Morales, Ph.D. and P. López, MS from the STAN: ST3371 of TEM and SEM samples preparation, IHEM-CONICET-UNCuyo. We are thankful to Dr. L. Mayorga for useful discussions and substantial contributions to the interpretation of data. Dr. Mayorga revised this manuscript critically for important intellectual content.

Conflict of interest

The authors declare that the research was conducted in the absence of any commercial or financial relationships that could be construed as a potential conflict of interest.

Publisher's note

Supplementary material

The Supplementary Material for this article can be found online at: https://www.frontiersin.org/articles/10.3389/fcell.2023.1148831/full#supplementary-material

References

Aldana, A., Carneiro, J., Martinez-Mekler, G., and Darszon, A. (2021). Discrete dynamic model of the mammalian sperm acrosome reaction: The influence of acrosomal pH and physiological heterogeneity. *Front. Physiol.* 12, 682790. doi:10.3389/fphys.2021.682790

Arana, L., Ordonez, M., Ouro, A., Rivera, I. G., Gangoiti, P., Trueba, M., et al. (2013). Ceramide 1-phosphate induces macrophage chemoattractant protein-1 release: Involvement in ceramide 1-phosphate-stimulated cell migration. *Am. J. Physiol. Endocrinol. Metab.* 304 (11), E1213–E1226. doi:10.1152/ajpendo.00480.2012

Bajjalieh, S. M., Martin, T. F., and Floor, E. (1989). Synaptic vesicle ceramide kinase. *J. Biol. Chem.* 264 (24), 14354–14360. doi:10.1016/s0021-9258(18)71685-2

Belmonte, S. A., Lopez, C. I., Roggero, C. M., De Blas, G. A., Tomes, C. N., and Mayorga, L. S. (2005). Cholesterol content regulates acrosomal exocytosis by enhancing Rab3A plasma membrane association. *Dev. Biol.* 285 (2), 393–408. doi:10.1016/j.ydbio.2005.07.001

Belmonte, S. A., Mayorga, L. S., and Tomes, C. N. (2016). The molecules of sperm exocytosis. *Adv. Anat. Embryol. Cell Biol.* 220, 71–92. doi:10.1007/978-3-319-30567-7_4

Belmonte, S. A., and Suhaiman, L. (2012). Optimized protocols to analyze sphingosine-1-phosphate signal transduction pathways during acrosomal exocytosis in human sperm. *Methods Mol. Biol.* 874, 99–128. doi:10.1007/978-1-61779-800-9_9

Bianchi, E., Doe, B., Goulding, D., and Wright, G. J. (2014). Juno is the egg Izumo receptor and is essential for mammalian fertilization. *Nature* 508 (7497), 483–487. doi:10.1038/nature13203

Bianchi, E., and Wright, G. J. (2020). Find and fuse: Unsolved mysteries in sperm-egg recognition. *PLoS Biol.* 18 (11), e3000953. doi:10.1371/journal.pbio.3000953

Carlson, E. J., Francis, R., Liu, Y., Li, P., Lyon, M., Santi, C. M., et al. (2022). Discovery and Characterization of Multiple Classes of Human CatSper Blockers. *ChemMedChem.* 17 (15), e202000499. doi:10.1002/cmdc.202000499

Colina, C., Flores, A., Castillo, C., Garrido Mdel, R., Israel, A., DiPolo, R., et al. (2005). Ceramide-1-P induces Ca2+ mobilization in Jurkat T-cells by elevation of Ins(1,4,5)-P3 and activation of a store-operated calcium channel. *Biochem. Biophys. Res. Commun.* 336 (1), 54–60. doi:10.1016/j.bbrc.2005.08.039

Darszon, A., Nishigaki, T., Beltran, C., and Trevino, C. L. (2011). Calcium channels in the development, maturation, and function of spermatozoa. *Physiol. Rev.* 91 (4), 1305–1355. doi:10.1152/physrev.00028.2010

Darszon, A., Nishigaki, T., Wood, C., Trevino, C. L., Felix, R., and Beltran, C. (2005). Calcium channels and Ca2+ fluctuations in sperm physiology. *Int. Rev. Cytol.* 243, 79–172. doi:10.1016/S0074-7696(05)43002-8

De Blas, G. A., Roggero, C. M., Tomes, C. N., and Mayorga, L. S. (2005). Dynamics of SNARE assembly and disassembly during sperm acrosomal exocytosis. *PLoS. Biol.* 3, e323. doi:10.1371/journal.pbio.0030323

Finkelstein, A., Zimmerberg, J., and Cohen, F. S. (1986). Osmotic swelling of vesicles: Its role in the fusion of vesicles with planar phospholipid bilayer membranes and its possible role in exocytosis. *Annu. Rev. Physiol.* 48, 163–174. doi:10.1146/annurev.ph.48.030186.001115

Gangoiti, P., Bernacchioni, C., Donati, C., Cencetti, F., Ouro, A., Gomez-Munoz, A., et al. (2012). Ceramide 1-phosphate stimulates proliferation of C2C12 myoblasts. *Biochimie* 94 (3), 597–607. doi:10.1016/j.biochi.2011.09.009

Gomez-Munoz, A., Duffy, P. A., Martin, A., O'Brien, L., Byun, H. S., Bittman, R., et al. (1995). Short-chain ceramide-1-phosphates are novel stimulators of DNA synthesis and cell division: Antagonism by cell-permeable ceramides. *Mol. Pharmacol.* 47 (5), 833–839.

Graf, C., Klumpp, M., Habig, M., Rovina, P., Billich, A., Baumruker, T., et al. (2008). Targeting ceramide metabolism with a potent and specific ceramide kinase inhibitor. *Mol. Pharmacol.* 74 (4), 925–932. doi:10.1124/mol.108.048652

Harper, C. V., Barratt, C. L., Publicover, S. J., and Kirkman-Brown, J. C. (2006). Kinetics of the progesterone-induced acrosome reaction and its relation to intracellular

calcium responses in individual human spermatozoa. *Biol. Reprod.* 75 (6), 933–939. doi:10.1095/biolreprod.106.054627

Harper, C. V., and Publicover, S. J. (2005). Reassessing the role of progesterone in fertilization--compartmentalized calcium signalling in human spermatozoa? *Hum. Reprod.* 20 (10), 2675–2680. doi:10.1093/humrep/dei158

Hewson, C. A., Watson, J. R., Liu, W. L., and Fidock, M. D. (2011). A differential role for ceramide kinase in antigen/FcεRI-mediated mast cell activation and function. *Clin. Exp. Allergy* 41 (3), 389–398. doi:10.1111/j.1365-2222.2010.03682.x

Hinkovska-Galcheva, V., and Shayman, J. A. (2010). Ceramide-1-phosphate in phagocytosis and calcium homeostasis. *Adv. Exp. Med. Biol.* 688, 131–140. doi:10.1007/978-1-4419-6741-1_9

Hinkovska-Galcheva, V. T., Boxer, L. A., Mansfield, P. J., Harsh, D., Blackwood, A., and Shayman, J. A. (1998). The formation of ceramide-1-phosphate during neutrophil phagocytosis and its role in liposome fusion. *J. Biol. Chem.* 273 (50), 33203–33209. doi:10.1074/jbc.273.50.33203

Hogback, S., Leppimaki, P., Rudnas, B., Bjorklund, S., Slotte, J. P., and Tornquist, K. (2003). Ceramide 1-phosphate increases intracellular free calcium concentrations in thyroid FRTL-5 cells: Evidence for an effect mediated by inositol 1,4,5-trisphosphate and intracellular sphingosine 1-phosphate. *Biochem. J.* 370, 111–119. doi:10.1042/BJ20020970

Hori, M., Gokita, M., Yasue, M., Honda, T., Kohama, T., Mashimo, M., et al. (2020). Down-regulation of ceramide kinase via proteasome and lysosome pathways in PC12 cells by serum withdrawal: Its protection by nerve growth factor and role in exocytosis. *Biochim. Biophys. Acta Mol. Cell Res.* 1867 (7), 118714. doi:10.1016/j.bbamcr.2020.118714

Inoue, N., Ikawa, M., and Okabe, M. (2011). The mechanism of sperm-egg interaction and the involvement of IZUMO1 in fusion. *Asian J. Androl.* 13 (1), 81–87. doi:10.1038/aja.2010.70

Jeon, H. J., Lee, D. H., Kang, M. S., Lee, M. O., Jung, K. M., Jung, S. Y., et al. (2005). Dopamine release in PC12 cells is mediated by Ca(2+)-dependent production of ceramide via sphingomyelin pathway. *J. Neurochem.* 95 (3), 811–820. doi:10.1111/j.1471-4159.2005.03403.x

Kachoei, B. A., Knox, R. J., Uthuza, D., Levy, S., Kaczmarek, L. K., and Magoski, N. S. (2006). A store-operated Ca(2+) influx pathway in the bag cell neurons of Aplysia. *J. Neurophysiol.* 96 (5), 2688–2698. doi:10.1152/jn.00118.2006

Kim, J. W., Inagaki, Y., Mitsutake, S., Maezawa, N., Katsumura, S., Ryu, Y. W., et al. (2005). Suppression of mast cell degranulation by a novel ceramide kinase inhibitor, the F-12509A olefin isomer K1. *Biochim. Biophys. Acta* 1738 (1-3), 82–90. doi:10.1016/j.bbalip.2005.10.007

Kirichok, Y., Navarro, B., and Clapham, D. E. (2006). Whole-cell patch-clamp measurements of spermatozoa reveal an alkaline-activated Ca2+ channel. *Nature* 439 (7077), 737–740. doi:10.1038/nature04417

Lamour, N. F., Wijesinghe, D. S., Mietla, J. A., Ward, K. E., Stahelin, R. V., and Chalfant, C. E. (2011). Ceramide kinase regulates the production of tumor necrosis factor α (TNFα) via inhibition of TNFα-converting enzyme. *J. Biol. Chem.* 286 (50), 42808–42817. doi:10.1074/jbc.M111.310169

Lishko, P. V., Botchkina, I. L., and Kirichok, Y. (2011). Progesterone activates the principal Ca2+ channel of human sperm. *Nature* 471 (7338), 387–391. doi:10.1038/nature09767

Lopez, C. I., Pelletan, L. E., Suhaiman, L., De Blas, G. A., Vitale, N., Mayorga, L. S., et al. (2012). Diacylglycerol stimulates acrosomal exocytosis by feeding into a PKC- and PLD1-dependent positive loop that continuously supplies phosphatidylinositol 4,5-bisphosphate. *Biochim. Biophys. Acta* 1821 (9), 1186–1199. doi:10.1016/j.bbalip.2012.05.001

Lopez-Gonzalez, I., De La Vega-Beltran, J. L., Santi, C. M., Florman, H. M., Felix, R., and Darszon, A. (2001). Calmodulin antagonists inhibit T-type Ca(2+) currents in mouse spermatogenic cells and the zona pellucida-induced sperm acrosome reaction. *Dev. Biol.* 236 (1), 210–219. doi:10.1006/dbio.2001.0314

Mayorga, L., Altamirano, K., Zanni Ruiz, E., and Pavarotti, M. (2020). Human sperm capacitation is necessary for SNARE assembly in neurotoxin-resistant complexes. *Andrology* 8 (2), 442–449. doi:10.1111/andr.12706

Mendoza, C., Carreras, A., Moos, J., and Tesarik, J. (1992). Distinction between true acrosome reaction and degenerative acrosome loss by a one-step staining method using Pisum sativum agglutinin. *J. Reprod. Fertil.* 95 (3), 755–763. doi:10.1530/jrf.0.0950755

Miller, M. R., Mannowetz, N., Iavarone, A. T., Safavi, R., Gracheva, E. O., Smith, J. F., et al. (2016). Unconventional endocannabinoid signaling governs sperm activation via the sex hormone progesterone. *Science* 352 (6285), 555–559. doi:10.1126/science.aad6887

Mitsutake, S., and Igarashi, Y. (2005). Calmodulin is involved in the Ca2+-dependent activation of ceramide kinase as a calcium sensor. *J. Biol. Chem.* 280 (49), 40436–40441. doi:10.1074/jbc.M501962200

Mitsutake, S., Kim, T. J., Inagaki, Y., Kato, M., Yamashita, T., and Igarashi, Y. (2004). Ceramide kinase is a mediator of calcium-dependent degranulation in mast cells. *J. Biol. Chem.* 279 (17), 17570–17577. doi:10.1074/jbc.M312885200

Muratori, M., Luconi, M., Marchiani, S., Forti, G., and Baldi, E. (2008). Molecular markers of human sperm functions. *Int. J. Androl.* 32, 25–45. doi:10.1111/j.1365-2605.2008.00875.x

Nakamura, H., Hirabayashi, T., Shimizu, M., and Murayama, T. (2006). Ceramide-1-phosphate activates cytosolic phospholipase A2alpha directly and by PKC pathway. *Biochem. Pharmacol.* 71 (6), 850–857. doi:10.1016/j.bcp.2005.12.027

Nishino, S., Yamashita, H., Tamori, M., Mashimo, M., Yamagata, K., Nakamura, H., et al. (2019). Translocation and activation of sphingosine kinase 1 by ceramide-1-phosphate. *J. Cell Biochem.* 120 (4), 5396–5408. doi:10.1002/jcb.27818

Ouro, A., Arana, L., Gangoiti, P., Rivera, I. G., Ordonez, M., Trueba, M., et al. (2013). Ceramide 1-phosphate stimulates glucose uptake in macrophages. *Cell Signal* 25 (4), 786–795. doi:10.1016/j.cellsig.2013.01.009

Pascuali, N., Scotti, L., Di Pietro, M., Oubina, G., Bas, D., May, M., et al. (2018). Ceramide-1-phosphate has protective properties against cyclophosphamide-induced ovarian damage in a mice model of premature ovarian failure. *Hum. Reprod.* 33 (5), 844–859. doi:10.1093/humrep/dey045

Pelletan, L. E., Suhaiman, L., Vaquer, C. C., Bustos, M. A., De Blas, G. A., Vitale, N., et al. (2015). ADP ribosylation factor 6 (ARF6) promotes acrosomal exocytosis by modulating lipid turnover and Rab3A activation. *J. Biol. Chem.* 290, 9823–9841. doi:10.1074/jbc.M114.629006

Pettus, B. J., Bielawska, A., Spiegel, S., Roddy, P., Hannun, Y. A., and Chalfant, C. E. (2003). Ceramide kinase mediates cytokine- and calcium ionophore-induced arachidonic acid release. *J. Biol. Chem.* 278 (40), 38206–38213. doi:10.1074/jbc.M304816200

Pettus, B. J., Bielawska, A., Subramanian, P., Wijesinghe, D. S., Maceyka, M., Leslie, C. C., et al. (2004). Ceramide 1-phosphate is a direct activator of cytosolic phospholipase A2. *J. Biol. Chem.* 279 (12), 11320–11326. doi:10.1074/jbc.M309262200

Pocognoni, C. A., De Blas, G. A., Heuck, A. P., Belmonte, S. A., and Mayorga, L. S. (2013). Perfringolysin O as a useful tool to study human sperm physiology. *Fertil. Steril.* 99 (1), 99–106.e2. doi:10.1016/j.fertnstert.2012.08.052

Presa, N., Gomez-Larrauri, A., Dominguez-Herrera, A., Trueba, M., and Gomez-Munoz, A. (2020). Novel signaling aspects of ceramide 1-phosphate. *Biochim. Biophys. Acta Mol. Cell Biol. Lipids* 1865 (4), 158630. doi:10.1016/j.bbalip.2020.158630

Presa, N., Gomez-Larrauri, A., Rivera, I. G., Ordonez, M., Trueba, M., and Gomez-Munoz, A. (2016). Regulation of cell migration and inflammation by ceramide 1-phosphate. *Biochim. Biophys. Acta* 1861 (5), 402–409. doi:10.1016/j.bbalip.2016.02.007

Rhoads, A. R., and Friedberg, F. (1997). Sequence motifs for calmodulin recognition. *FASEB J.* 11 (5), 331–340. doi:10.1096/fasebj.11.5.9141499

Shan, S., Xu, F., Bleyer, M., Becker, S., Melbaum, T., Wemheuer, W., et al. (2020). Association of α/β-Hydrolase D16B with bovine conception rate and sperm plasma membrane lipid composition. *Int. J. Mol. Sci.* 21 (2), 627. doi:10.3390/ijms21020627

Sosa, C. M., Pavarotti, M. A., Zanetti, M. N., Zoppino, F. C., De Blas, G. A., and Mayorga, L. S. (2015). Kinetics of human sperm acrosomal exocytosis. *Mol. Hum. Reprod.* 21 (3), 244–254. doi:10.1093/molehr/gau110

Sosa, C. M., Zanetti, M. N., Pocognoni, C. A., and Mayorga, L. S. (2016). Acrosomal swelling is triggered by cAMP downstream of the opening of store-operated calcium channels during acrosomal exocytosis in human sperm. *Biol. Reprod.* 94 (3), 57. doi:10.1095/biolreprod.115.133231

Stival, C., Puga Molina Ldel, C., Paudel, B., Buffone, M. G., Visconti, P. E., and Krapf, D. (2016). Sperm capacitation and acrosome reaction in mammalian sperm. *Adv. Anat. Embryol. Cell Biol.* 220, 93–106. doi:10.1007/978-3-319-30567-7_5

Strunker, T., Goodwin, N., Brenker, C., Kashikar, N. D., Weyand, I., Seifert, R., et al. (2011). The CatSper channel mediates progesterone-induced Ca2+ influx in human sperm. *Nature* 471 (7338), 382–386. doi:10.1038/nature09769

Suarez, S. S. (2008). Control of hyperactivation in sperm. *Hum. Reprod. Update* 14 (6), 647–657. doi:10.1093/humupd/dmn029

Subramanian, P., Stahelin, R. V., Szulc, Z., Bielawska, A., Cho, W., and Chalfant, C. E. (2005). Ceramide 1-phosphate acts as a positive allosteric activator of group IVA cytosolic phospholipase A2 alpha and enhances the interaction of the enzyme with phosphatidylcholine. *J. Biol. Chem.* 280 (18), 17601–17607. doi:10.1074/jbc.M414173200

Sugiura, M., Kono, K., Liu, H., Shimizugawa, T., Minekura, H., Spiegel, S., et al. (2002). Ceramide kinase, a novel lipid kinase. Molecular cloning and functional characterization. *J. Biol. Chem.* 277 (26), 23294–23300. doi:10.1074/jbc.M201535200

Suhaiman, L., Altamirano, K. N., Morales, A., and Belmonte, S. A. (2021). Different approaches to record human sperm exocytosis. *Methods Mol. Biol.* 2233, 139–168. doi:10.1007/978-1-0716-1044-2_10

Suhaiman, L., De Blas, G. A., Obeid, L. M., Darszon, A., Mayorga, L. S., and Belmonte, S. A. (2010). Sphingosine 1-phosphate and sphingosine kinase are involved in a novel signaling pathway leading to acrosomal exocytosis. *J. Biol. Chem.* 285 (21), 16302–16314. doi:10.1074/jbc.M109.072439

Tada, E., Toyomura, K., Nakamura, H., Sasaki, H., Saito, T., Kaneko, M., et al. (2010). Activation of ceramidase and ceramide kinase by vanadate via a tyrosine kinase-mediated pathway. *J. Pharmacol. Sci.* 114 (4), 420–432. doi:10.1254/jphs.10181fp

Tang, N., Ong, W. Y., Zhang, E. M., Chen, P., and Yeo, J. F. (2007). Differential effects of ceramide species on exocytosis in rat PC12 cells. *Exp. Brain Res.* 183 (2), 241–247. doi:10.1007/s00221-007-1036-7

Tornquist, K., Blom, T., Shariatmadari, R., and Pasternack, M. (2004). Ceramide 1-phosphate enhances calcium entry through voltage-operated calcium channels by a protein kinase C-dependent mechanism in GH4C1 rat pituitary cells. *Biochem. J.* 380, 661–668. doi:10.1042/BJ20031637

Tornquist, K., Ramstrom, C., Rudnas, B., Klika, K. D., Dugue, B., Adams, J., et al. (2002). Ceramide 1-(2-cyanoethyl) phosphate enhances store-operated Ca2+ entry in thyroid FRTL-5 cells. *Eur. J. Pharmacol.* 453 (1), 1–11. doi:10.1016/s0014-2999(02)02362-2

Trevino, C. L., Jl, D. l. V.-B., Nishigaki, T., Felix, R., and Darszon, A. (2006). Maitotoxin potently promotes Ca2+ influx in mouse spermatogenic cells and sperm, and induces the acrosome reaction. *J. Cell Physiol.* 206 (2), 449–456. doi:10.1002/jcp.20487

Vaquer, C. C., Suhaiman, L., Pavarotti, M. A., De Blas, G. A., and Belmonte, S. A. (2020). Ceramide induces a multicomponent intracellular calcium increase triggering the acrosome secretion in human sperm. *Biochim. Biophys. Acta Mol. Cell Res.* 1867 (7), 118704. doi:10.1016/j.bbamcr.2020.118704

Wang, G., Guo, Y., Zhou, T., Shi, X., Yu, J., Yang, Y., et al. (2013). In-depth proteomic analysis of the human sperm reveals complex protein compositions. *J. Proteomics* 79, 114–122. doi:10.1016/j.jprot.2012.12.008

WHO (2021). WHO laboratory manual for the examination and processing of human semen, sixth edition. *Geneva: World Health Organization; 2021. Licence: CC BY-NC-SA 3.0 IGO.*

Won, J. H., Kim, S. K., Shin, I. C., Ha, H. C., Jang, J. M., Back, M. J., et al. (2018). Dopamine transporter trafficking is regulated by neutral sphingomyelinase 2/ceramide kinase. *Cell Signal* 44, 171–187. doi:10.1016/j.cellsig.2018.01.006

Xue, R., Meng, H., Yin, J., Xia, J., Hu, Z., and Liu, H. (2021). The role of calmodulin vs. Synaptotagmin in exocytosis. *Front. Mol. Neurosci.* 14, 691363. doi:10.3389/fnmol.2021.691363

Yoshino, T., Ishikawa, J., Ohga, K., Morokata, T., Takezawa, R., Morio, H., et al. (2007). YM-58483, a selective CRAC channel inhibitor, prevents antigen-induced airway eosinophilia and late phase asthmatic responses via Th2 cytokine inhibition in animal models. *Eur. J. Pharmacol.* 560 (2-3), 225–233. doi:10.1016/j.ejphar.2007.01.012

Yunes, R., Tomes, C., Michaut, M., De, B. G., Rodriguez, F., Regazzi, R., et al. (2002). Rab3A and calmodulin regulate acrosomal exocytosis by mechanisms that do not require a direct interaction. *FEBS Lett.* 525 (1-3), 126–130. doi:10.1016/s0014-5793(02)03102-2

Zanetti, N., and Mayorga, L. S. (2009). Acrosomal swelling and membrane docking are required for hybrid vesicle formation during the human sperm acrosome reaction. *Biol. Reprod.* 81 (2), 396–405. doi:10.1095/biolreprod.109.076166

Zhang, W., and Staiger, C. J. (2021). Revising the role of cortical cytoskeleton during secretion: Actin and myosin XI function in vesicle tethering. *Int. J. Mol. Sci.* 23 (1), 317. doi:10.3390/ijms23010317

frontiers | Frontiers in Cell and Developmental Biology

TYPE Original Research
PUBLISHED 11 July 2023
DOI 10.3389/fcell.2023.1177279

OPEN ACCESS

EDITED BY
Vanina Gabriela Da Ros,
CONICET Institute of Biology and Experimental Medicine (IBYME), Argentina

REVIEWED BY
Thomas Ebner,
Kepler University Hospital, Austria
Jessica Eastick,
IVF Australia, Australia

*CORRESPONDENCE
Kata Joo,
joo.kata@med.semmelweis-univ.hu

RECEIVED 01 March 2023
ACCEPTED 19 June 2023
PUBLISHED 11 July 2023

CITATION
Joo K, Nemes A, Dudas B, Berkes-Bara E, Murber A, Urbancsek J and Fancsovits P (2023), The importance of cytoplasmic strings during early human embryonic development.
Front. Cell Dev. Biol. 11:1177279.
doi: 10.3389/fcell.2023.1177279

The importance of cytoplasmic strings during early human embryonic development

Kata Joo*, Annamaria Nemes, Beata Dudas, Eva Berkes-Bara, Akos Murber, Janos Urbancsek and Peter Fancsovits

Division of Assisted Reproduction, Department of Obstetrics and Gynaecology, Semmelweis University, Budapest, Hungary

Objectives: During human *in vitro* fertilisation (IVF) treatments, embryologists attempt to select the most viable embryos for embryo transfer (ET). Previously, embryos were evaluated based on light microscopic morphological parameters. However, this is currently accomplished by morphokinetic analysis of time-lapse recordings. This technique provides us the opportunity to observe cytoplasmic strings at the blastocyst stage. The aim of this work was to examine the relationship between the presence of cytoplasmic strings (CS) and the embryo viability in human *in vitro* fertilised embryos.

Study design: Herein, we present an evaluation of the morphokinetic data on the development of embryos obtained during IVF treatments performed at the Division of Assisted Reproduction between December 2020 and March 2021. The dynamics of embryo development, embryo morphology, and morphokinetic scores generated by a time-lapse system were compared between the presence of cytoplasmic strings (CS+) and their absence (CS-) at the blastocyst stage.

Results: The development of 208 embryos from 78 patients was examined. Moreover, 81.2% of the embryos had CS in the blastocyst stage; 77% of CS existed in embryos created by conventional IVF, while 86% of CS existed in embryos fertilised by intracytoplasmic sperm injection (ICSI) (p = 0.08). A greater number of CS+ embryos developed into a higher quality blastocyst (52.1% vs. 20.5%, p = 0.02). The morphokinetic score values characterising the development of embryos, such as Known Implantation Data Score (KIDScore) and Intelligent Data Analysis (iDAScore), were higher in CS+ groups (KID: 6.1 $\pm$ 2.1 vs. 4.7 $\pm$ 2.07; iDA: 8.0 $\pm$ 1.9 vs. 6.8 $\pm$ 2.3, $p < 0.01$). The dynamics of the early embryo development were similar between the two groups; however, CS+ embryos reached the blastocyst stage significantly earlier (tB: 103.9 h vs. tB: 107.6 h; p = 0.001).

Conclusion: Based on our results, the number of embryos with cytoplasmic strings was higher than that without cytoplasmic strings, and its presence is not related to the fertilisation method. These embryos reached the blastocyst stage earlier, and their morphokinetic (KIDScore and iDAScore) parameters were

Abbreviations: CS+, blastocyst with cytoplasmic strings; CS-, blastocyst without cytoplasmic strings; ET, embryo transfer; FSH, follicular stimulating hormone; GnRH, gonadotropin-releasing hormone antagonist; hCG, human chorion gonadotropin; hMG, human menopausal gonadotropin; ICM, inner cell mass; ICSI, intracytoplasmic sperm injection; iDAScore, Intelligent Data Analysis Score; IVF, *in vitro* fertilisation (treatment); KIDScore, Known Implantation Data Score; TE, trophectoderm cells; tPNf, time of the pronucleus fading; t2, t4, . . . tn, time taken to divide into 2, 4, . . . n cells; tM, time of end of compaction; tB, time of the full blastocyst stage.

better. All these results suggest that the presence of CS indicates higher embryo viability. The examination of this feature may help us make decisions about the embryos with higher implantation potential.

KEYWORDS

human *in vitro* fertilisation, embryo quality, cytoplasmic strings, time lapse, embryo development, human blastocyst, Intelligent Data Analysis Score, Known Implantation Data Score

Introduction

During *in vitro* fertilisation (IVF-ET) treatments, embryologists attempt to select the best developing and most viable embryo for embryo transfer (ET). Previously, conventional embryo selection methods were based on morphology grading systems. In addition to the traditional morphological grading techniques (Gardner & Schoolcraft, 1999; Alpha Scientists in Reproductive Medicine and ESHRE Special Interest Group of Embryology, 2011; Prados et al., 2012), the morphokinetic evaluation of embryo development by time-lapse recordings commenced in practice (Meseguer et al., 2012). Conventional embryo culture and traditional morphological evaluations were performed at static time points, which has a limited ability to predict the most viable embryo (Guerif et al., 2007), since they provide a "snap-shot" of the embryo development.

The appearance and clinical application of the time-lapse system create new opportunities for the detailed evaluation of embryo morphology. The system records embryo development at regular intervals of 5–15 min (Rubio et al., 2014).

Embryo development can be analysed by several morphology evaluation programs. The KIDScore decision support tool (Vitrolife, Göteborg, Sweden) is based on the known implantation data of the world's largest embryo development database, and it provides a morphokinetic score to annotated embryos. Those embryos, which ranked low by the tool, have statistically lower chances of implantation (Berntsen et al., 2022). Intelligent Data Analysis Score (iDAScore) (Vitrolife) () is a grading system with artificial intelligence. This artificial intelligent system compares the examined embryo with a similar developmental pattern. The system has the ability to recognise the developmental stage and morphology of embryos without any human interaction and generate a score for the possibility of implantation (Kragh et al., 2019; Ueno et al., 2021).

Literature has heavily focused on the prediction of morphokinetic-based embryo assessment and implantation and pregnancy outcomes during the previous years. Furthermore, the analysis of the time-lapse videos made it possible to identify and observe the behaviour of dynamically changing structures like cytoplasmic strings. This observation is impossible during the conventional microscopic morphology assessment.

In addition to the frequent presence of cytoplasmic strings in different cell functions, we have limited information about their function in human embryos. The observation of morphology and behaviour of these cytoplasmic strings can aid us to reach a closer understanding of the early embryonic development.

In the early 2000s, the occurrence of cytoplasmic strings at the blastocyst stage was classified as a negative sign of embryo viability (Scott, 2000), but more recently, it has been described as a positive feature (The ESHRE Capri Workshop Group, 2010; Ebner et al., 2020; Ma, Jin, and Huang, 2020; The ESHRE Capri Workshop Group, 2020; Eastick et al., 2021). However, the importance and clinical significance of this structure are still controversial. Previous proposals suggested that signalling molecules could migrate through cytoplasmic strings by vesicle transport or via cytoplasmic material exchange (Gustafson and Wolpert, 1961; Miller et al., 1995; Salas-Vidal and Lomelí, 2004). The authors observed retrograde transport, but it is still not known exactly what molecules are required for the transport of particles through the cytoplasmic strings.

The aim of our study was to investigate the occurrence and morphological characteristics of cytoplasmic strings in the human blastocyst and to examine the relationship between the occurrence of strings and embryo viability during human blastocyst formation.

Materials and methods

Study design

This retrospective study was conducted at the Division of Assisted Reproduction, Department of Obstetrics and Gynaecology, Semmelweis University, Budapest, Hungary. A total of 78 IVF treatment (IVF-ET) cycles performed routinely due to infertility at our department between December 2020 and March 2021 were included in the study. The exclusion criteria did not include maternal age, male infertility parameter, method of fertilisation, BMI, and treatment indication. Those IVF treatment cycles were examined to identify at least one normally fertilised (two pronuclei) oocyte that developed into blastocyst by day 5. More embryos of the same IVF-ET cycle were examined to analyse the development of 208 embryos which reached the expanded blastocyst stage until the ET. Blastocyst development was analysed in detail, particularly the occurrence and morphology of cytoplasmic strings. Embryo development and implantation were compared between blastocysts containing cytoplasmic strings (CS+ group) and blastocysts without CS (CS- group) (Figure 1).

Ovarian stimulation and oocyte collection

A gonadotropin ovarian stimulation protocol with gonadotropin-releasing hormone (GnRH) antagonist was used to achieve multiple follicular growth. Human menopausal gonadotropin (hMG) (Menopur, Parsippany, New Jersey; Ferring, Saint-Prex, Switzerland) or follicular stimulating hormone (FSH) (Fostimon HP, IBSA, Pambio Noranco, Switzerland) was used for ovarian stimulation, which was monitored by estradiol measurements and transvaginal ultrasound examination on alternate days. A dose of 0.25 mg/day cetrorelix (Cetrotide;

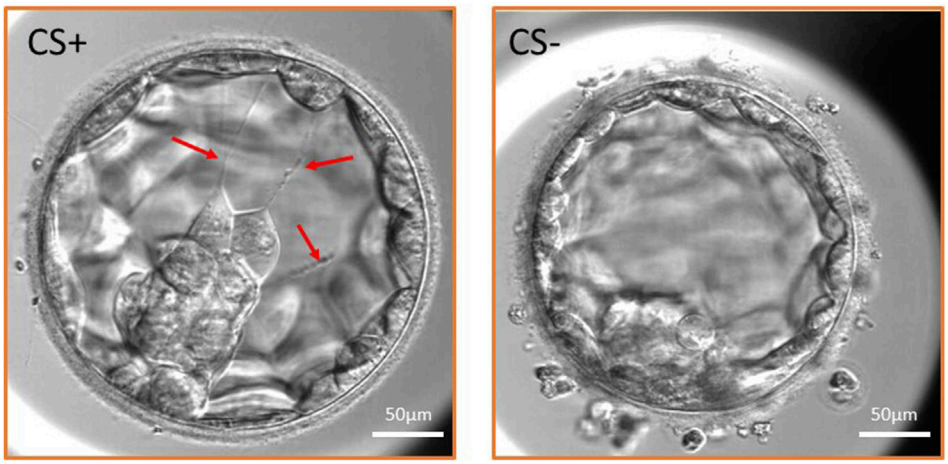

FIGURE 1
Expanded blastocyst with cytoplasmic strings (CS+ group) and without CS (CS- group). Three cytoplasmic strings are shown in the CS+ embryo traversing the blastocoel cavity (red arrows) and maintaining connection between the inner cell mass and the mural trophectoderm cells.

Serono, Rome, Italy) was administered from the day of ovarian stimulation where the diameter of the leading follicle was ≥14 mm. Ovulation was induced with 5,000 IU of human chorionic gonadotropin (hCG) (Ovitrelle; Serono, Geneva, Switzerland) when at least one follicle with a diameter of 18 mm and three or more follicles with a diameter of 16 mm were seen on ultrasound and serum estradiol levels reached 2–300 pg/mL per ≥16 mm follicle. Transvaginal ultrasound-guided aspiration of follicles was performed 36 h after hCG administration. Oocytes were collected from the follicular fluid and cultured at 37°C and 6% CO_2 and 5% O_2 levels until fertilisation.

Sperm preparation and fertilisation

All laboratory procedures were performed using the standard protocol (Fancsovits et al., 2015). Oocyte and embryo culture was performed in a culture media product line called "G-series" produced by Vitrolife. A semen sample was prepared for fertilisation by density gradient centrifugation followed by the swim-up technique to isolate progressive motile sperms. Two-layer density gradient centrifugation (90% and 45% SpermGrade (Vitrolife) solution) was performed for the separation of motile sperm cells from the semen sample. Samples were centrifuged at 400 g for 20 min (Centrifuge 5702; Eppendorf, Hamburg, Germany). Viable sperms gathered at the bottom of the centrifuge tube were washed two times with warm sperm preparation media (G-MOPS+; Vitrolife) at 400 g for 10 min. The sperm fraction was resuspended with 0.1–0.5 mL fertilisation media (G-IVF$^+$; Vitrolife) according to the semen quality. Sperm concentration and motility were counted again after sperm preparation.

Fertilisation was carried out by conventional IVF or intracytoplasmic sperm injection (ICSI), depending on the patient's history and the semen quality. In case of conventional IVF, a maximum of five cumulus–oocyte complexes/well in a four-well culture dish (NUNC; Thermo Fisher, Waltham, Massachusetts) were co-incubated with 3×10^5 progressive motile sperms/mL in G-IVF+ (Vitrolife) culture fertilisation media.

During ICSI treatment, oocytes were injected following enzymatic removal of cumulus cells using hyaluronidase solution. Fertilisation by injecting a single sperm cell into the oocyte is recommended, if andrological parameters or previous fertilisation rate justifies the treatment. Intracytoplasmic sperm injection (ICSI) was performed 4–6 h after oocyte retrieval (Ebner et al., 2001). Only mature oocytes with a visible first polar body were injected. Oocytes were placed into a EmbryoSlide$^+$ time-lapse dish (Vitrolife) containing embryo culture media (G-TL; Vitrolife) and inserted into the EmbryoScope$^+$ time-lapse incubator (Vitrolife) after sperm injection.

Zygotes were assessed for signs of fertilisation 16–18 h after insemination and were considered normally fertilised if two pronuclei were clearly visible.

Embryo culture and embryo transfer

Embryos were cultured for at least 5 days in the EmbryoScope$^+$ time-lapse incubator in EmbryoSlide$^+$ dishes at 37°C under 6% CO_2 and 5% O_2 conditions, according to the manufacturer's instruction. This culture technique was carried out in a microwell culture dish, which contains 8 or 16 microwells. The application of this embryo culture technique made it possible to monitor the full course of embryo development under undisturbed culture conditions without removing the embryos from the safe environment of the time-lapse incubator (Figure 2). Embryo development and morphology were evaluated by the analysis of time-lapse videos each day by embryologists (Alpha Scientists in Reproductive Medicine and ESHRE Special Interest Group of Embryology, 2011; Kovacs et al., 2019), according to standard criteria.

Embryos at an optimal developmental stage and of highest morphology grade were selected for ET 5 days after fertilisation.

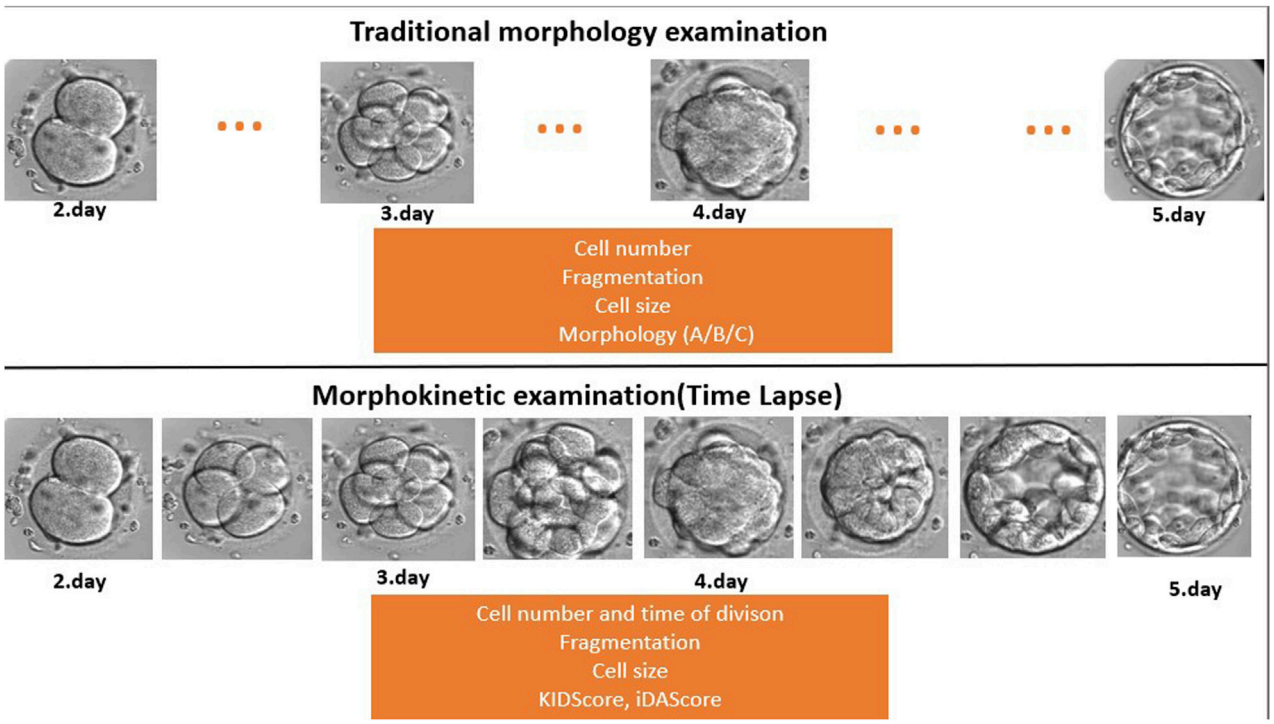

FIGURE 2
Traditional morphology examination compared to time-lapse-based morphokinetic examination. During the traditional microscopic evaluation, the embryologists miss developmental events and stages because they check the embryos once a day (dots . . . mean the missed/not seen developmental stage). On the other hand, the time-lapse system makes a recording every 10 min, which provides a continuous follow-up.

One or two embryos were transferred at a time depending on the female patient's age and history. The transfer media used were the EmbryoGlue (Vitrolife). Wallace (SIMS Portex Ltd., Målov, Denmark) or Tight Difficult Transfer (TDT) catheters (Laboratoire CCD, Paris, France) were used for the ET. Non-transferred embryos, which were considered showing the normal blastocyst development and morphology according to the Gardner's criteria (Gardner and Schoolcraft, 1999), were vitrified and stored in liquid nitrogen according to the patient's request.

Pregnancy was confirmed by the presence of a gestational sac with foetal heart activity 4 weeks after ET. The implantation rate was calculated by the number of gestational sacs with foetal heart activity divided by the number of transferred embryos. When calculating the implantation rate, only embryos with known implantation data were taken into account. This means that those cycles were excluded where two embryos were transferred at the same time but only one implanted. Since it was not possible to determine which embryo was implanted, data on mixed embryo transfer, when CS+ and CS- embryos were transferred and implanted together, were also excluded.

Assessment of embryo morphology

Morphology and kinetics of embryo development were also monitored and analysed using EmbryoViewer (version: 7.8.4.28428; Vitrolife) and iDAScore (version: 1.2.0.0.; Vitrolife) software. The time of the pronuclear fading (tPNF); 2-cell (t2), 3-cell (t3), 4-cell (t4), 5-cell (t5), and 8-cell (t8) stages; end of compaction (tM); initiation of blastocyst formation (tsB); and full blastocyst stage (tB) was recorded. The fragmentation rate; morphology at 4- and 8-cell and blastocyst stages; and the presence of cytoplasmic strings were also observed.

Detailed evaluation of the embryo morphology was performed on the third and fifth days of embryo development, without removing the culture dishes from the incubator. The morphology grade and amount of fragmentation were recorded at the 8-cell stage on day 3 (48 h post-insemination). The developmental stage and the morphology of the trophectoderm layer (TE) and inner cell mass (ICM) were recorded according to Gardner's grading system on day 5 (112–114 h post-insemination) (Gardner and Schoolcraft, 1999).

Embryos with stage-appropriate cell sizes and low fragmentation were graded as good quality embryos on day 3. Embryos on day 5 were considered of good quality, if they reached at least the blastocyst stage with grade A or B TE and grade A or B ICM (Alpha Scientists in Reproductive Medicine and ESHRE Special Interest Group of Embryology, 2011). KIDScore and iDAScore were also calculated for each blastocyst on day 5.

A cytoplasmic string assessment was performed after ET and vitrification. The time-lapse videos and their images were analysed in 11 focal planes. The annotation was carried out by one embryologist, who has experience in time-lapse embryo annotation, to minimise personal bias. We determined the frequency of occurrence of cytoplasmic strings and their relation to the female age and the method of fertilisation. The dynamics of embryo development, embryo morphology at the 8-cell stage and at the blastocyst stage, KIDScore, iDAScore, and the implantation rate were compared between CS+ and CS- groups.

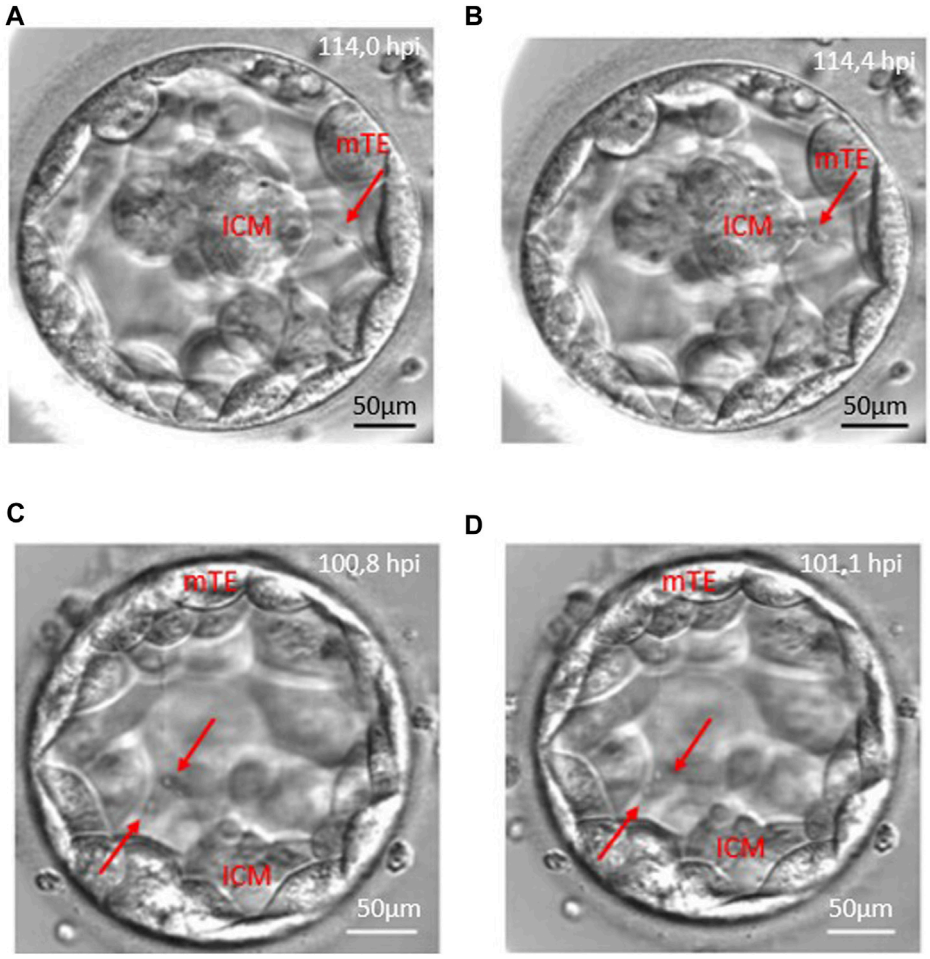

FIGURE 3
Anterograde and retrograde transport along the cytoplasmic string. Red arrows point to vesicle-like structures moving along cytoplasmic strings. Panels **(A, B)** demonstrate the retrograde transport which starts from the mural trophoblast (mTE) to the inner cell mass (ICM). Panels **(C, D)** show an anterograde transport from the inner cell mass (ICM) to the mural trophoblast (mTE) moving of two vesicles.

Statistical analysis

All statistical analyses were performed using Statistica software (TIBCO Software Inc.). Continuous variables were presented as mean and standard deviation, and proportional variables were presented as percentages. The Mann–Whitney *U*-test was used to compare mean values, while chi-squared and Fisher tests were used to compare proportional values. Statistical significance was set at $p < 0.05$.

Results

The appearance of cytoplasmic strings

Of the total of 498 retrieved oocytes, 354 zygotes showed normal fertilisation (two pronuclei), and 208 embryos reached the blastocyst stage (58.8%) until the fifth day during the study period. Detailed morphokinetic analysis was performed on the embryos, which fulfilled our criteria. According to our observations, the long traversing cytoplasmic strings were visible during blastocyst formation and the full blastocyst stage. Of the 169 CS+ blastocysts, there were 135 cases (79.8%) where the string was single-ending (non-branching) and 34 cases (20.1%) where the string was multiple-ending (branching). In 128 blastocysts (75.7%), the cytoplasmic strings were thin, while 41 blastocysts (24.3%) contained thick strings. There were single- and multiple-stranded forms, and they showed considerable variation in thickness. The CS always maintain connection between the ICM and mural TE cells, and there might be a transport along the strings as shown in Figure 3 with red arrows (Figure 3).

The analysis of the CS+ embryo videos suggests that there is a transport along the cytoplasmic string that moves in both directions, anterograde and retrograde, related to the ICM, or the migration could be bidirectional (Figure 3; Supplementary Video S1).

Development of CS+ and CS- embryos

Cytoplasmic strings can be observed from the expansion of the blastocyst. All the blastocysts, developed from the normally fertilised

TABLE 1 Kinetics of embryo development in cytoplasmic string containing (CS+) and not containing (CS-) groups.

	CS+ (hour)	CS-(hour)	*p*-value
tPNf	22.9 ± 3.1	23.3 ± 2.7	0.48
t2	25.5 ± 3.2	25.8 ± 2.8	0.56
t3	34.9 ± 4.8	35.2 ± 4.7	0.69
t4	36.9 ± 4.5	36.1 ± 4.9	0.69
t5	46.7 ± 8.2	47.1 ± 8.2	0.72
t8	55.8 ± 8.2	57.2 ± 9.4	0.51
tM	85.2 ± 7.6	85.2 ± 7.4	0.93
tsB	96.2 ± 6.8	99.2 ± 6.4	<0.01
tB	103.9 ± 7.7	107.6 ± 7.0	<0.01

Data are mean ± SD.
tPnf: time of pronuclei fading.
t2: time to the 2-cell stage.
t3: time to the 3-cell stage.
t4: time to the 4-cell stage.
t5: time to the 5-cell stage.
t8: time to the 8-cell stage.
tM: time of end of compaction.
tsB: time of initiation of blastulation.
tB: time to full blastocyst stage.

zygote, were examined, and 81% contained cytoplasmic strings, while 19% of the embryos did not contain cytoplasmic strings. The rate of CS+ embryos was 77% in conventional IVF and 86% in ICSI cycles. The difference between the two fertilisation methods was not significant (p = 0.08). The presence of cytoplasmic strings is not related to the maternal age (CS+: 35.7 ± 4.6 years; CS-:35.8 ± 4.04 years, p = 0.89).

The dynamics of embryo development were similar between CS+ and CS- groups until the compaction and morula stages. However, as shown in Table 1, CS+ embryos began blastocyst formation earlier and took, on average, 3 h less time than CS- embryos to reach the entire blastocyst stage (Table 1.).

In both the CS+ and CS- groups, the proportion of good quality embryos at the 8-cell stage was similar. However, significantly more CS+ embryos developed into good quality blastocysts (AA, AB, BB, and BA) compared to CS- embryos. KIDScore and iDAScore were significantly higher in CS+ blastocysts than CS- blastocysts, as shown in Table 2.

Out of the 208 analysed embryos, 83 were transferred. However, only 70 embryos with known implantation data were used for the calculation of implantation. The implantation rate was 39.7% in the CS+ group and 14.3% in the CS- group, but this difference did not reach the level of significance (p = 0.16).

Discussion

Investigation of the presence and function of cytoplasmic strings in the human blastocyst is a controversial topic among embryologists (Scott, 2000; Hardarson, Van Landuyt, and Jones, 2012; Ebner et al., 2020; Ma, Jin, and Huang, 2020; Eastick et al., 2022a). In addition, the study on the relationship between the presence of cytoplasmic strings and the embryo viability in human *in vitro* fertilised embryos has received considerable attention. The analysis of the embryo development, using time-lapse videos, made it possible to identify and observe the behaviour of dynamically changing structures. This observation would be impossible during conventional microscopic morphology assessment. Embryologists can better understand the development and condition of early embryos by observing the appearance and behaviour of cytoplasmic strings.

Cytoplasmic strings were detected in 81.2% of the examined embryos, which is almost two times higher than the CS+ embryo ratio (43.9%) published by Ebner et al. (2020). However, the presence of CS is similar in scale to the results of Eastick et al. (2021) just in the case of the proportion of CS after conventional IVF and ICSI fertilisation, which suggests that the method of fertilisation does not affect the formation of CS (Eastick et al., 2022b).

Data did not reveal great differences neither in the early embryonic development nor in the cleavage stage morphology among the CS+ and CS- groups. However, embryos in the CS+ group developed into a higher quality blastocyst. Although it seems that other working groups who examine cytoplasmic strings do not apply traditional morphology assessment for early embryo morphology evaluation, the use of Gardner's blastocyst

TABLE 2 Embryo quality and morphokinetic scores in cytoplasmic string containing (CS+) and not containing (CS-) groups.

	CS+	CS-	*p*-value
Number of embryos	169 (81.2%)	39 (18.8%)	
Good quality 8-cell stage embryo	58 (34.3%)	10 (25.6%)	0.30
Good quality blastocyst (AA, AB, BA, and BB)	88 (52.1%)	8 (20.5%)	0.02
KIDScore[a]	6.1 ± 2.1	4.7 ± 2.1	<0.01
iDAScore[a]	8.0 ± 1.9	6.8 ± 2.3	<0.01
Implantation rate	25/63 ET (39.7%)	1/7 ET (14.3%)	0.19

[a]Values are mean ± SD.
CS+: blastocyst with cytoplasmic strings.
CS-: blastocyst without cytoplasmic strings.
KIDScore: Known Implantation Data Score.
iDAScore: Intelligent Data Analysis Score.

morphology assessment revealed similar results (Eastick et al., 2022b).

The implantation rate was also higher in the case of CS+ embryos, but this difference was not significant. The reason is probably due to the low number of cases and the limitations of multiple pregnancy follow-ups. In addition to the limitations, a recent study examined the relationship between the cytoplasmic strings and the clinical pregnancy rate (Eastick et al., 2021). This result also supports our hypothesis that CS-containing blastocysts have a higher implantation potential.

The kinetics of early embryo development were similar within the two groups. On the other hand, the CS-containing embryos reached the blastocyst stage significantly earlier. Compared to our results, Eastick et al. (2021) found significant differences in early embryo development (PN appearance, tPNf, t2, t3, t4, t5, t6, and t8) and the time to reach blastocyst stages (Eastick et al., 2021) between embryos with and without CS. These results suggest that CS+ embryos have a better ability to develop and implant into the uterus. Based on our results, we can conclude that the early embryo development and quality were not related to the presence of CS, but the presence of cytoplasmic strings is accompanied by accelerating development and better morphology in the blastocyst stage.

KIDScore and iDAScore were significantly higher in CS+ blastocysts than CS- blastocysts. This result implies that KIDScore and iDAScore are correlated with the embryo viability (Berntsen et al., 2022; Kim, Lee, and Jun 2022; Lassen, 2022). The higher score of the CS+ embryos indicates that based on the analysis of the large IVF database, the artificial intelligence system considered the CS+ embryos most viable. To the best of our knowledge, this is the first report which shows the relationship between the morphokinetic scores (KID and iDA) and the presence of cytoplasmic string.

Time-lapse imaging allows us to follow the preimplantation embryo development including the whole cavitation process. In addition to these benefits, we were unable to detect the growth of the traversing cytoplasmic strings through the blastocoelic cavity similar to the Salas-Vidal and Lomelí's working groups in the case of the mouse embryos (Salas-Vidal and Lomelí, 2004). This observation may indicate the fact that CS must be formed within the early stages of cavitation, and this suggestion is supported by our morphokinetic results. Cytoplasmic string formation probably occurs during compaction, and the blastulation process is responsible for their elongation and string-like structure formation in the blastocyst stage (Salas-Vidal and Lomelí, 2004; Fierro-González et al., 2013).

The observation of the morphology of the cytoplasmic string in our time-lapse images shows transport processes in both anterograde (from the inner cell mass to the mural trophectoderm cells) and retrograde (from the mTE to the ICM) directions, while Salas-Vidal and Lomelí's groups concluded that they observed only retrograde transport in the mouse blastocyst. They also described connections between the ICM and polar trophectoderm cells in mouse blastocysts (Salas-Vidal and Lomelí, 2004). Our research group could not observe this connection, which may be due to the difference in magnitude of the time-lapse microscopes.

The observation of cytoplasmic strings in human embryos by other embryologists also suggests that bulb-like vesicle transport occurs along the strings (Ebner et al., 2020) in a bidirectional movement (antero- and retrograde) (Eastick et al., 2022b). Ebner and his colleagues also investigated the relationship between cytoplasmic extension and the blastocyst collapse, as well as the characterisation of filaments. In addition to that, this study does not focus on these phenomena, but we consider it necessary to validate these observations. This observation can raise the question whether the strings have different purposes at the blastocyst stage. However, we would like to pay more attention to vesicle transport along the cytoplasmic filaments in the future.

Transport was observed along the strings in all of our cases. We assume that there is a communication between the 2-cell population which may stimulate them to divide further or help them differentiate (Salas-Vidal and Lomelí, 2004). Although these results are preliminary observations and a deeper analysis of the vesicle-like transport was out of scope of this study, we consider it important to mention that there is a clearly visible communication which motivates us for further microscopic examination of this structure.

Conclusion

The investigation of the importance and behaviour of cytoplasmic strings with time-lapse technology in human embryos is a new field, and there are still lots of questions to be answered: is vesicular transport taking place along the cytoplasmic strings? What kinds of molecules are transported between the cells? Which differentiated cell population (ICM or mural TE) produces signalling factors? Is the presence of cytoplasmic strings related to the quality of compaction and morula formation? Further examination of CS in embryos would be necessary. The identification of cell structures and molecules along the cytoplasmic strings could help us understand the origin, meaning, and importance of these structures in the blastocyst stage. Although the topic of cytoplasmic strings in the human blastocyst is not defined yet, more and more importance is being attached to its research, and further results are expected in the near future. Based on our results, CS were observed in most of the examined human blastocysts. The CS+ embryos developed into blastocysts faster, and their morphokinetic parameters were better. The scoring systems based on artificial intelligence also consider the CS+ blastocysts more viable, and it looks like that their implantation ability was higher.

All these results prove us that the presence of cytoplasmic strings was accompanied by good embryo viability. The examination of this phenomenon could help us select the most viable embryo in terms of implantation. Evaluation of the presence of cytoplasmic strings could be an additional morphologic feature in the future embryo grading system. These results put the following question in the spotlight: what is the certain function of the cytoplasmic strings during early embryogenesis?

Data availability statement

The raw data supporting the conclusion of this article will be made available by the authors, without undue reservation.

Ethics statement

The studies involving human participants were reviewed and approved by the National Public Health Centre (NPHC) (60728-8/2022/EÜIG). Written informed consent for participation was not required for this study in accordance with the national legislation and the institutional requirements.

Author contributions

Embryologists AN, BD, and PF contributed to this research and carried out the technical processes and fertilisations during the research period. EB-B, AM, and JU contributed to this report as clinical gynaecologists. PF contributed to the study design and helped perform the statistical analysis. All authors contributed to the article and approved the submitted version.

Conflict of interest

The authors declare that the research was conducted in the absence of any commercial or financial relationships that could be construed as a potential conflict of interest.

Publisher's note

All claims expressed in this article are solely those of the authors and do not necessarily represent those of their affiliated organizations, or those of the publisher, the editors, and the reviewers. Any product that may be evaluated in this article, or claim that may be made by its manufacturer, is not guaranteed or endorsed by the publisher.

Supplementary material

The Supplementary Material for this article can be found online at: https://www.frontiersin.org/articles/10.3389/fcell.2023.1177279/full#supplementary-material

References

Alpha Scientists in Reproductive Medicine and ESHRE Special Interest Group of Embryology (2011). The istanbul consensus Workshop on embryo assessment: Proceedings of an expert meeting. *Hum. Reprod.* 26 (6), 1270–1283. doi:10.1093/humrep/der037

Berntsen, J., Rimestad, J., Lassen, J. T., Tran, D., and Kragh, M. F. (2022). Robust and generalizable embryo selection based on artificial intelligence and time-lapse image sequences. *PLoS ONE* 17 (2), e0262661. doi:10.1371/journal.pone.0262661

Eastick, J., Venetis, C., Cooke, S., and Chapman, M. (2022b). Detailed analysis of cytoplasmic strings in human blastocysts: New insights. *Zygote* 31, 78–84. doi:10.1017/S0967199422000570

Eastick, J., Venetis, C., Cooke, S., and Chapman, M. (2021). The presence of cytoplasmic strings in human blastocysts is associated with the probability of clinical pregnancy with fetal heart. *J. Assisted Reproduction Genet.* 38 (8), 2139–2149. doi:10.1007/s10815-021-02213-1

Eastick, J., Venetis, C., Cooke, S., and Chapman, M. (2022a). *Inter- and intra-observer agreement between embryologists for cytoplasmic string assessment in day 5/6 human blastocysts*. Thousand Oaks, Calif: Reproductive Sciences. doi:10.1007/s43032-022-01151-2

Ebner, T., Sesli, Ö., Kresic, S., Enengl, S., Stoiber, B., Reiter, E., et al. (2020). Time-lapse imaging of cytoplasmic strings at the blastocyst stage suggests their association with spontaneous blastocoel collapse. *Reprod. Biomed. Online* 40 (2), 191–199. doi:10.1016/j.rbmo.2019.11.004

Ebner, T., Yaman, C., Moser, M., Sommergruber, M., Jesacher, K., and Tews, G. (2001). A prospective study on oocyte survival rate after ICSI: Influence of injection technique and morphological features. *J. Assisted Reproduction Genet.* 18 (12), 623–628. doi:10.1023/A:1013171505702

Fancsovits, P., Adam, L., Murber, A., Kaszas, Z., Rigo, J., and Urbancsek, J. (2015). Effect of hyaluronan-enriched embryo transfer medium on IVF outcome: A prospective randomized clinical trial. *Archives Gynecol. Obstetrics* 291 (5), 1173–1179. doi:10.1007/s00404-014-3541-9

Fierro-González, J. C., White, M. D., Silva, J. C., and Plachta, N. (2013). Cadherin-dependent filopodia control preimplantation embryo compaction. *Nat. Cell Biol.* 15 (12), 1424–1433. doi:10.1038/ncb2875

Gardner, D. K., and Schoolcraft, W. B. (1999). Culture and transfer of human blastocysts. *Curr. Opin. Obstetrics Gynecol.* 11 (3), 307–311. doi:10.1097/00001703-199906000-00013

Guerif, F., Le Gouge, A., Giraudeau, B., Poindron, J., Bidault, R., Gasnier, O., et al. (2007). Limited value of morphological assessment at days 1 and 2 to predict blastocyst development potential: A prospective study based on 4042 embryos. *Hum. Reprod. Oxf. Engl.* 22 (7), 1973–1981. doi:10.1093/humrep/dem100

Gustafson, T., and Wolpert, L. (1961). Studies on the cellular basis of morphogenesis in the sea urchin embryo. Gastrulation in vegetalized larvae. *Exp. Cell Res.* 22, 437–449. doi:10.1016/0014-4827(61)90120-3

Hardarson, T., Van Landuyt, L., and Jones, G. (2012). The blastocyst. *Hum. Reprod.* 27 (1), i72–i91. doi:10.1093/humrep/des230

Kim, J., Lee, J., and Jun, J. H. (2022). Non-invasive evaluation of embryo quality for the selection of transferable embryos in human *in vitro* fertilization-embryo transfer. *Clin. Exp. Reproductive Med.* 49 (4), 225–238. doi:10.5653/cerm.2022.05575

Kovacs, P., Matyas, S., Forgacs, V., Sajgo, A., Molnar, L., and Pribenszky, C. (2019). Non-invasive embryo evaluation and selection using time-lapse monitoring: Results of a randomized controlled study. *Eur. J. Obstetrics Gynecol. Reproductive Biol.* 233, 58–63. doi:10.1016/j.ejogrb.2018.12.011

Kragh, M. F., Rimestad, J., Berntsen, J., and Karstoft, H. (2019). Automatic grading of human blastocysts from time-lapse imaging. *Comput. Biol. Med.* 115, 103494. doi:10.1016/j.compbiomed.2019.103494

Lassen, J. T. (2022). *Development and validation of deep learning based embryo selection across multiple days of transfer*. arXiv. doi:10.48550/arXiv.2210.02120

Ma, B.-X., Jin, L., and Huang, B. (2020). *Cytoplasmic string between ICM and mte is a positive predictor of clinical pregnancy and live birth outcomes in elective frozen-thawed single blastocyst transfer cycles: A time-lapse study*. Preprint. doi:10.21203/rs.3.rs-122470/v1

Meseguer, M., Rubio, I., Cruz, M., Basile, N., Marcos, J., and Requena, A. (2012). Embryo incubation and selection in a time-lapse monitoring system improves pregnancy outcome compared with a standard incubator: A retrospective cohort study. *Fertil. Steril.* 98 (6), 1481–1489.e10. doi:10.1016/j.fertnstert.2012.08.016

Miller, J., Fraser, S. E., and McClay, D. (1995). Dynamics of thin filopodia during sea urchin gastrulation. *Dev. Camb. Engl.* 121 (8), 2501–2511. doi:10.1242/dev.121.8.2501

Prados, F. J., Debrock, S., Lemmen, J. G., and Agerholm, I. (2012). The cleavage stage embryo. *Hum. Reprod.* 27 (1), i50–i71. doi:10.1093/humrep/des224

Rubio, I., Galán, A., Larreategui, Z., Ayerdi, F., Bellver, J., Herrero, J., et al. (2014). Clinical validation of embryo culture and selection by morphokinetic analysis: A randomized, controlled trial of the EmbryoScope. *Fertil. Steril.* 102 (5), 1287–1294.e5. doi:10.1016/j.fertnstert.2014.07.738

Salas-Vidal, E., and Lomelí, H. (2004). Imaging filopodia dynamics in the mouse blastocyst. *Dev. Biol.* 265 (1), 75–89. doi:10.1016/j.ydbio.2003.09.012

Scott, L. A. (2000). Oocyte and embryo polarity. *Seminars Reproductive Med.* 18 (2), 171–183. doi:10.1055/s-2000-12556

The ESHRE Capri Workshop Group (2020). Erratum to: IVF, from the past to the future: The inheritance of the Capri Workshop group. *Hum. Reprod. Open* 2020 (4), hoaa051. doi:10.1093/hropen/hoaa051

The ESHRE Capri Workshop Group (2010). Europe the continent with the lowest fertility. *Hum. Reprod. Update* 16 (6), 590–602. doi:10.1093/humupd/dmq023

Ueno, S., Ito, M., Uchiyama, K., Okimura, T., Yabuuchi, A., and Kato, K. (2021). O-220 an annotation-free embryo scoring system (IDAScore®) based on deep learning shows high performance for pregnancy prediction after single-vitrified blastocyst transfer. *Hum. Reprod.* 36 (1)–044. doi:10.1093/humrep/deab128.044

frontiers | Frontiers in Cell and Developmental Biology

TYPE Original Research
PUBLISHED 28 July 2023
DOI 10.3389/fcell.2023.1217808

OPEN ACCESS

EDITED BY
Vanina Gabriela Da Ros,
CONICET Institute of Biology and Experimental Medicine (IBYME), Argentina

REVIEWED BY
Fuxin Wang,
Suzhou Municipal Hospital, China
Shuzhen Liu,
Shandong Normal University, China

*CORRESPONDENCE
Brigita Vaigauskaitė-Mažeikienė,
brigita.vaigauskaite@gmc.vu.lt
Rūta Navakauskienė,
ruta.navakauskiene@bchi.vu.lt

RECEIVED 05 May 2023
ACCEPTED 20 July 2023
PUBLISHED 28 July 2023

CITATION
Vaigauskaitė-Mažeikienė B, Baušytė R, Valatkaitė E, Maželytė R, Kazėnaitė E, Ramašauskaitė D and Navakauskienė R (2023), Assisted reproductive technology outcomes and gene expression in unexplained infertility patients. *Front. Cell Dev. Biol.* 11:1217808. doi: 10.3389/fcell.2023.1217808

Assisted reproductive technology outcomes and gene expression in unexplained infertility patients

Brigita Vaigauskaitė-Mažeikienė[1,2]*, Raminta Baušytė[1,2], Elvina Valatkaitė[1], Rūta Maželytė[2], Edita Kazėnaitė[3], Diana Ramašauskaitė[2] and Rūta Navakauskienė[1]*

[1]Department of Molecular Cell Biology, Institute of Biochemistry, Life Sciences Center, Vilnius University, Vilnius, Lithuania, [2]Centre of Obstetrics and Gynaecology of the Institute of Clinical Medicine, Faculty of Medicine, Vilnius University, Vilnius, Lithuania, [3]Faculty of Medicine, Vilnius University Hospital Santaros Klinikos, Vilnius University, Vilnius, Lithuania

Background: Unexplained infertility (UI) can be a frustrating and challenging diagnosis for doctors and couples as it can be difficult to understand why they are unable to conceive despite increasing diagnostic tools. Assisted reproductive technology (ART) procedures have been successfully applied to many couples aiming to overcome UI. However, they can be not only expensive but also require multiple cycles to achieve a successful pregnancy. The endometrium and the follicular fluid have been investigated as target tissues not only to determine the cause of UI but also to increase conception rates.

Results: In this study, we analyzed the outcomes of ART in 223 UI couples and gene expression associated with DNA modification, cell death, immune response and senescence (*TET1, TET2, BCL2, BAK1, HMGA2, IL-6, IL-8*) in infertile women's endometrium and follicular fluid. We found significant differences in women who successfully got pregnant compared to women unable to conceive depending on age, duration of infertility, number of retrieved oocytes, zygotes, transferred embryos. Further, the expression of genes *BAK1* (pro-apoptotic), *TET2* (associated with epigenetic DNA modification) and *IL-6* (associated with immune responses) were significantly higher in the endometrium of women who successfully got pregnant.

Conclusion: Younger parental age couples showed higher ART success rates, shorter duration of infertility, higher number of retrieved oocytes, zygotes and transferred embryos. The gene expression analysis revealed significant changes in the endometrium depending on genes associated with cell death and immune response which were upregulated in females with diagnosed unexplained infertility.

KEYWORDS

unexplained infertility, assisted reproductive technology, gene expression, endometrium, follicular fluid (FF)

Introduction

Infertility is a disease of the reproductive system defined by the failure to achieve a clinical pregnancy after 12 months or more of regular unprotected sexual intercourse. *Unexplained infertility (UI)* term exists longer than 50 years with the definition of couples who both have normal genito-urinary anatomy, normal semen quality and adequate sexual

intercourse (Zegers-Hochschild et al., 2017). However, when defining the term "unexplained", emphasis is laid on the quality of diagnostic tests and tools (Sadeghi, 2015). According to different authors (Evers, 2002; Gelbaya et al., 2014), UI varies approximately from 10 to 30 percent in all infertile couples, although discussions among clinicians with reference to "unexplained" actually as "undiagnosed" are present (Gleicher and Barad, 2006; Sadeghi, 2015). Other tempting and possible causes of infertility such as minor ovarian and testicular dysfunctions, the quality of sperm and oocyte, endometrial receptivity, implantation failures, immune factors dysfunction are still underway to daily clinical practice. Some studies suggest that up to 15% of these young couples (less than 30 years old) will conceive over a 1-year period and up to 30% over the second year, therefore expectant management is suggested (Isaksson and Tiitinen, 2004). On the other hand, it has been highlighted that women over 35 years of age are diagnosed with unexplained infertility twice as often as younger women (less than 30 years old) (Maheshwari et al., 2008). Even though up to six cycles of ovarian stimulation or/and intrauterine insemination can be offered to couples with UI by many fertility organization guidelines, yet *in vitro* fertilization procedure (IVF) is considered an effective first-line treatment in UI patients (Pandian et al., 2001; Buckett and Sierra, 2019). In the couples who received IVF, subtle changes were observed in oocyte fertilization rates indicating that the pathogenesis of UI may lie in the fertilization process itself which remains indistinct for diagnosis (Hull, 1994). Also, more attention has been brought to a search of molecular mechanisms underlying UI. Some studies indicate that the endometrium is a key tissue in the UI pathogenesis considering, for instance, the reduced expression of Foxp3 (a master regulator of Treg cell differentiation) decreases the endometrial Treg cell population resulting in implantation failure (Jasper et al., 2006). Other researchers indicate that UI is associated with a compromised endometrial receptivity during the implantation window in mechanisms such as the reduction of αVβ3 integrin in the endometrium (Elnaggar et al., 2017), overexpression of endometrial estrogen receptor-alpha (ER-α) in the mid-luteal phase (Dorostghoal et al., 2018). Furthermore, follicular fluid (FF) components have been investigated to discover some new insights. Some authors showed that the lipid compound in FF could affect oocyte development: not only higher amounts of phospholipid but also phospholipid/apoA-I ratio in FF were associated with poor oocyte fertilization rates (Fayezi et al., 2014). Also, some studies indicate that the reduction of some components (triglycerides, lactate, alkaline phosphatase and lactate dehydrogenase) is negatively associated with follicle size indicating impaired oocyte maturation (Nandi et al., 2007). In addition, increased triacylglycerol levels with a lower amount of monoacylglycerols, phospholipids and sphingolipids were found in the FF of UI population (Batushansky et al., 2020).

Gene expression in either the endometrium or the follicular fluid has been investigated to determine underlying molecular variations partially contributing to UI. The study conducted by Altmäe et al. detected several important genes (such as the mucin-associated peptide *TFF3*; metalloproteinases *MMP8*, *MMP10*, *MMP26*; chemokines *SCBG3A1*, *FAM3D*, *FAM3B*; the integrin-binding protein *COL16A1*), *etc.*) which were dysregulated in infertile women with UI (Altmäe et al., 2009). It shows the occurrence of subtle changes in the immune responses, signal transduction, binding, transport, lipid metabolism and extracellular matrix component at the time of embryo implantation in women with unexplained infertility compared to fertile women. Furthermore, complement-coagulation cascades, morphine addiction pathway, and PI3K-Akt signalling pathway were determined to be differentially expressed in UI patients which reveals the complexity of UI diagnosis (Keleş et al., 2022). It is known that TET family genes are associated with DNA demethylation process and its decrease was noticed in infertile endometriosis patients (Adamczyk et al., 2022a). *BCL2* and *BAK1* genes are cell death regulators and sometimes irregular patterns of the expression of these genes could reveal some underlying issues, for example, cancer (Witek et al., 2016). In this case, we wanted to see if there are any changes in expression patterns in unexplained infertility patients. Further, some evidence suggests that the decrease of high mobility group AT-hook 2 (*HMGA2*) expression reduces stem cell frequency and function (Nishino et al., 2008). These major pathways are responsible in ensuring that all cellular processes are being regulated normally and are not being altered like in the cases of diseases. For example, some pro-inflammatory cytokines (IL-6, IL-8) are related to inflammation, which may be responsible not only for failed IVF, but also could be associated with unexplained infertility (An et al., 2015; Fortin et al., 2019). Our goal was to search for unconventional genes related to this topic and see if there is a significant difference between infertile patients who conceived successfully and failed to conceive as well as investigate possible associations with infertility and pregnancy outcome. When analyzing follicular fluid gene expression, some studies suggest that an imbalance between pro-inflammatory and anti-inflammatory mediators could be the underlying reason in the failure of conception after ART cycles (Fortin et al., 2019). Unfortunately, there is a lack of research of the gene expression in follicular fluid in humans concerning oocyte maturation, fertilization, aging processes.

While focusing on long term outcomes of UI couples, the bright side is that most UI couples were able to achieve a live birth either spontaneously or when treated (Pandian et al., 2001; Vaughan et al., 2022). An important conclusion was drawn that couples who do not delay the treatment have greater odds to achieve more than one live birth.

In the current study, we analyzed the reproductive outcomes of UI couples who received ART and performed the subgroup analysis addressing the conceived and failed to conceive populations. Moreover, to carry out the gene expression analysis in the endometrial and follicular fluid tissues, selected women from these populations. Our study investigated seven genes (*TET1, TET2, BCL2, BAK1, HMGA2, IL-6, IL-8*) associated with the DNA modification, cell death, immune response and senescence. The findings of this study not only could help understand the unexplained infertility diagnosis but also improve the conception outcomes when treating these couples.

Primary and secondary outcomes

Our primary outcome measure in this study was the cumulative overall ongoing pregnancy rate (OPR). Our secondary outcome measure was the conception predicting factors.

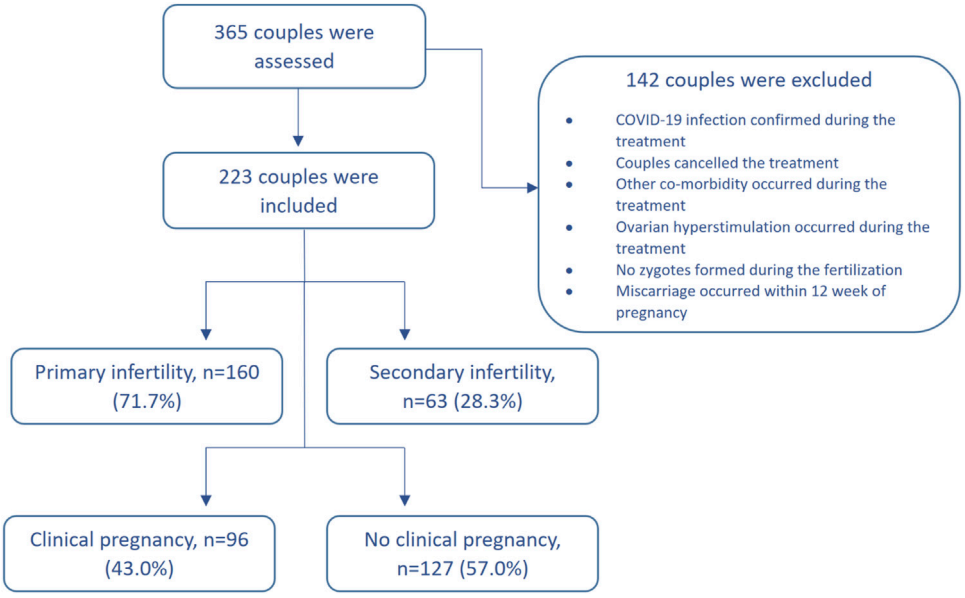

FIGURE 1
Study flowchart.

Materials and methods

We have conducted an interventional prospective cohort study. The patients with unexplained infertility who received ART and were treated in Santaros Fertility Center of Vilnius University Hospital Santaros Klinikos were enrolled for the study from 1 January 2020 to 30 March 2021 (until the COVID-19 lockdown). The inclusion criteria were as follows: 1) age of women at the time of enrollment was 25–40 years, 2) average duration of infertility at least 2 years, 3) unexplained infertility diagnosis was confirmed after laboratory and instrumental investigation (testing failed to reveal any abnormality), 4) informed consent of all the subjects was received. The exclusion criteria were as follows: 1) oncological disease was confirmed for a woman during the last 3 years, 2) other infertility causes, except unexplained infertility, were confirmed, 3) women who were addicted to alcohol or other substances, 4) uncontrolled endocrine or other medical conditions, such as prolactinemia or thyroid diseases, 5) COVID-19 infection was confirmed during the treatment. The flow chart of the study population is presented in Figure 1.

All women received endometrial scratching procedure without the dilatation of the cervix, using a pipelle catheter during the natural luteal cycle phase (approximately 7–9 days before the menstrual cycle and the start of ovarian stimulation). The hormones (estradiol, luteinizing hormone and progesterone) were investigated during the second-third day of the cycle before starting ART. All women underwent controlled ovarian stimulation by the GnRH antagonist protocol or short GnRH agonist protocol. The ovarian response was assessed by transvaginal ultrasound. Human chorionic gonadotropin was administered to induce the final oocyte maturation 36 h before oocyte retrieval. Oocyte retrieval was performed under general anesthesia using transvaginal aspiration with 16–17-gauge needles under ultrasonography guidance. Oocytes were extracted by an embryologist, and the residual FF was pooled and spun down to collect FF and discard blood and granulosa cells. Fertilization was accomplished by IVF or intracytoplasmic sperm injection. Day 3 or day 5 embryos were transferred according to the age of the woman, anamnesis of infertility, the embryo morphologic grading. For the luteal phase support, a total of 600 mg intravaginal progesterone was prescribed. A human chorionic gonadotropin (HCG) pregnancy test was carried out 14 days after the oocyte retrieval procedure. An ongoing pregnancy was defined with each pregnancy showing a positive heartbeat of the fetus at ultrasound after 12 weeks of gestation.

Collection of follicular fluid and endometrial tissue

Endometrium samples were collected during the scratching procedure. Follicular fluid containing heterogenic population was collected at the time of oocyte aspiration without flushing (36 h after human chorionic gonadotropin (6500 IU) trigger administration) into sterile tubes. Follicular fluid samples used for analysis were macroscopically clear and not contaminated with blood. Once collected, follicular fluid was transferred into 50 mL tubes and centrifuged at 500× g for 10 min, supernatant removed and 20 mL of 1× red blood cell (RBC) lysis buffer (10×, 155 mM NH_4Cl (Sigma-Aldrich, St. Louis, MO, United States), 12 mM $NaHCO_3$ (Sigma-Aldrich, St. Louis, MO, United States), 0.1 mM EDTA (Sigma-Aldrich, St. Louis, MO, United States), pH 7.3) was added to the pellet. Further, the samples were incubated for 5 min at room temperature and centrifuged at 500× g for 10 min. After

10.3389/fcell.2023.1217808

TABLE 1 Primer sequences used in gene expression analysis.

Name	Primer sequence	Product size, bp
TET1	F: TTCGTCACTGCCAACCTTAG	149
	R: ATGCCTCTTTCACTGGGTG	
TET2	F: CCCTTCTCCGATGCTTTCTG	136
	R: TGGGTTATGCTTGAGGTGTTC	
BCL2	F: CGGAGGCTGGGATGCCTTTG	166
	R: TTTGGGGCAGGCATGTTGAC	
BAK1	F: TCATCGGGGACGACATCAAC	120
	R: CAAACAGGCTGGTGGCAATC	
IL-6	F: ACAGCCACTCACCTCTTCAG	168
	R: CCATCTTTTTCAGCCATCTTT	
IL-8	F: CATACTCCAAACCTTTCCACCCC	175
	R: TCAGCCCTCTTCAAAAACTTCTCCA	
HMGA2	F: CCCAAAGGCAGCAAAAACAA	81
	R: GCCTCTTGGCCGTTTTTCTC	
GAPDH	F: GTGAACCATGAGAAGTATGACAAC	123
	R: CATGAGTCCTTCCACGATACC	

centrifugation, the isolated heterogenic cell pellet was mixed with DNA/RNA lysis buffer (Zymo research, Irvine, CA, United States) and incubated at room temperature up to 10 min. After this, RNA isolation followed as described below.

RNA isolation and gene expression analysis

For the total RNA extraction from follicular fluid cells, the Quick-DNA/RNA Miniprep Kit (Zymo Research, CA, United States) was used in line with manufacturer's recommendations. The RNA isolation from the endometrium tissue required an additional step prior to using the kit. A piece of the tissue was first submerged in liquid nitrogen and ground to a powder using a mortar and pestle. Then the powder was mixed well with DNA/RNA lysis buffer and the lysate was transferred to a Zymo-Spin™ Column. The following isolation steps were carried out according to manufacturer's recommendations. After this, cDNA was synthesized with the LunaScript® RT SuperMix Kit (New England Biolabs, Ipswich, MA, United States) following manufacturer's guidelines. cDNA was then amplified using the RT-qPCR with Luna® universal qPCR Master Mix (New England Biolabs, Ipswich, MA, United States) and the Rotor-Gene 6000 Real-time Analyzer (Corbett Life Science, QIAGEN, Hilden, Germany) with experimental conditions as follows: 95°C 1 min, 95°C 15 s, 60°C 30 s (40 cycles). Primer sequences used in RT-qPCR analysis are listed in Table 1. The acquired data from RT-qPCR was further analyzed using the ΔΔCt method, mRNA expression was normalized using *GAPDH* gene expression and therefore the relative gene expression was calculated.

Results

Two hundred twenty-three couples were enrolled in the study of whom 127 (57%) were unable to conceive (Group A) while 96 (43%) couples successfully got pregnant (Group B). The characteristics of the total cohort and study groups are presented in Table 2.

A statistically positive correlation was found between the age of both groups (Group B r = 0.26; p = 0.01) (Group A r = 0.30; p = 0.001) and the duration of infertility (Figure 2).

When analyzing the spermogram indicator values of the participating men, the sperm of Group B men had statistically higher values of sperm count, however, the values of live sperm, sperm motility A (rapid progressive motility) and sperm motility B (slow or sluggish progressive motility) were higher in Group A (Table 3).

To evaluate the correlations of the conception success with endometrium thickness, the influence of seven different female hormones, the number of retrieved oocytes, zygotes and transferred embryos, the non-parametric values of the Spearman's correlation coefficients were calculated. Our analysis revealed a significant conception success correlation with estradiol and progesterone hormones, the number of retrieved oocytes, zygotes and the number of the total transferred embryos (in all cases Spearman; $p < 0.05$), whereas no significant correlation was found between the successful conception and endometrial thickness and the remaining female hormones (in all cases Spearman; $p > 0.05$) (Table 4).

A detailed correlational analysis showed very a weak negative significant statistical correlation between the successful conception and estradiol hormone (on day 2/3 when the ovarian stimulation was started), indicating that as the concentration of the hormone increased, the probability of conception reliably decreased (r = −0.14; p = 0.04) (Table 4). The opposite result was obtained between the successful conception and hormone progesterone, as a very weak positive statistical correlation was formed between these criteria (r = 0.15; p = 0.03). This suggested that the increasing concentration of hormone progesterone significantly increases the chances of conception (Table 4). It is important to recall that all women have started an IVF cycle and ovarian stimuliation when their progesterone levels were in normal range at day 2/3 (≦ 1.0 ng/mL).

During further statistical analysis, weak positive correlations were observed between the successful conception and the number of retrieved oocytes (r = 0.34; $p < 0.001$); number of zygotes (r = 0.34; $p < 0.001$) and the number of the total transferred embryos (r = 0.31; $p < 0.001$). A very weak positive (r = 0.28; $p < 0.001$) significant statistical correlation was found between the successful conception and the number of transferred blastocysts (Table 5). Statistically significant relations between the age of women of Group A and the duration of infertility and an anti-Mullerian hormone were found implying that the increased age is also related to a longer duration of infertility and a decreased chance to conceive.

With the help of RT-qPCR, we tested seven genes associated with the epigenetic DNA modification (*TET1*, *TET2*), senescence (*HMGA2*), apoptosis (*BCL2, BAK1*) and the immune response (*IL-6, IL-8*) in the endometrium tissue (End) and the follicular fluid (FF). Nevertheless, our interest was set not only within these groups, but also between Group A and Group B under our analysis. To conduct

TABLE 2 Patient characteristics for the total cohort and study groups.

Characteristics	Study cohort (*n* = 223)	Group A (*n* = 127)	Group B (*n* = 96)	*p* values
Women age, in years	33.4 ± 3.7	34.1 ± 3.8	32.6 ± 3.6 years	p = **0.006**
Mean ± SD				
Men age, in years	35.3 ± 5.1	36.0 ± 5.1	34.5 ± 5.2	p = **0.03**
Mean ± SD				
Women BMI, kg/m2	22.4 ± 3.7	22.3 ± 3.2	22.8 ± 4.3	p = 0.99
Mean ± SD				
Smoking male, number	58	28	30	p = 0.12
The duration on infertility, in years	4.8 ± 2.9	5.2 ± 3.2	4.4 ± 2.5	p = **0.01**
Mean ± SD				
Type on infertility, number	160	88	72	p = 0.35
Primary				
Secondary	63	39	24	
Stimulation protocol, number	176	125	51	p = 0.29
Antagonist				
Agonist	47	10	37	
Retrieved oocytes, number	11.3 ± 9.0	6.7 ± 9.2	12.3 ± 9.7	p < **0.001**
Mean ± SD				
Zygotes, number	5.7 ± 5.5	3.4 ± 5.3	7.0 ± 6.8	p < **0.001**
Mean ± SD				
Total transferred embryos: 44.2% of day3 embryos; 55.8% of day5 embryos; number	1.3 ± 1.1	1.0 ± 1.0	2.0 ± 1.0	p = **0.016**
Mean ± SD				

p values marked in bold indicate statistically significant results.

TABLE 3 Mean, minimum (Min), maximum (Max) values and standard deviations of spermogram indicators of men from both groups.

Spermogram indicator	Group	Mean	Standard deviation	Minimal value	Maximal value	*p*-value
Sperm count, mln./ml	A	77.5	59.4	0.0	285.0	**0.01**
	B	97.9	61.7	3.0	322.0	
Live sperms, %	A	52.1	18.7	10.0	150.0	0.25
	B	49.2	20.3	10.0	160.0	
Motility A, number	A	24.5	26.1	0.0	232.0	**0.01**
	B	18.1	16.7	0.0	70.0	
Motility B, number	A	20.6	10.4	0.0	61.0	**0.02**
	B	17.5	12.5	0.0	66.0	

p values marked in bold indicate statistically significant results.

this analysis, we selected 10 samples to represent End group (Group A n = 5; Group B n = 5) and 10 samples to represent FF group (Group A n = 5; Group B n = 5).

The *TET1* and *TET2* gene expression involved in the DNA demethylation process is seen to be slightly upregulated in End group compared to FF group. In the case of *TET1* gene expression

10.3389/fcell.2023.1217808

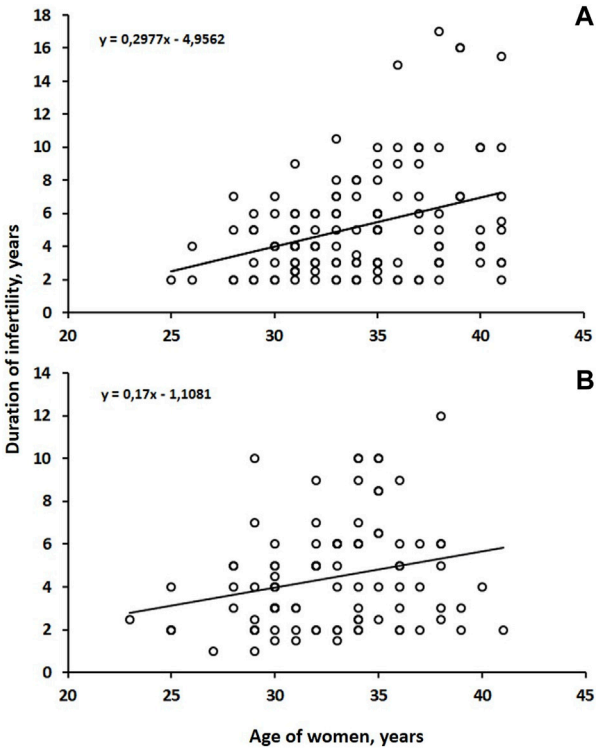

FIGURE 2
Correlations between the age and duration of infertility in both groups.

TABLE 4 Pregnancy success correlation with endometrial thickness, values of different female sex hormones concentration, number of retrieved oocytes, zygotes, and number of transferred embryos.

Characteristics	Success in conception	
	r	p
Endometrium thickness	0.13	0.30
Luteinizing hormone	−0.04	0.47
Follicle-stimulating hormone	0.07	0.30
Estradiol	−0.14	**0.04**
Progesterone	0.15	**0.03**
Prolactin	−0.006	0.92
Anti-Mullerian hormone	0.13	0.06
Thyroid stimulating hormone	0.05	0.49
Retrieved oocytes	0.34	< **0.001**
Zygotes	0.34	< **0.001**
Total transferred embryos	0.31	< **0.001**
Transferred blastocysts	0.28	< **0.001**

p values marked in bold indicate statistically significant results.

TABLE 5 Association between unsuccessfully and successfully conceived women age and duration of infertility, number of retrieved oocytes, number of fertilized oocytes and AMH hormone.

Characteristics	Women age			
	Group A women		Group B women	
	r	p	r	p
Duration of infertility	0.30	**0.001**	0.26	**0.01**
Number of retrieved oocytes	0.27	0.08	−0.14	0.23
Number of zygotes	0.12	0.17	−0.17	0.10
Anti-Mullerian hormone	−0.32	< **0.001**	−0.18	0.09

p values marked in bold indicate statistically significant results.

profile, no significant differences were detected between Group A and Group B, however, *TET2* gene was significantly upregulated in Group A in End group compared to Group B (Figure 3A). Similar tendency can be observed in the anti-apoptotic gene *BCL2* expression profile where the expression of this gene was very similar between Group A and Group B in both End and FF groups (Figure 3B). On the other hand, we detected that the expression of pro-apoptotic gene *BAK1* was significantly higher in Group A End group compared to Group B (Figure 3B). However, no such difference was observed in FF group. Senescence associated *HMGA2* gene expression showed a slight tendency to be upregulated in Group B FF group, however, in End group, the expression remained the same between Group A and Group B (Figure 3C). Further genes under our focus were *IL-6* and *IL-8* associated with immune responses. The *IL-6* gene expression analysis revealed that in the endometrium of Group A the expression of this gene increased significantly compared to Group B (Figure 3D). On the contrary, FF group showed no significant changes. Moreover, *IL-8* expression remained at low levels in all of the groups including Group A and Group B.

Discussion

Unexplained infertility diagnosis remains challenging both for the patients and clinicians. Not only the patients delay the infertility treatment due to the knowledge to be a "healthy" couple, but also the lack of understanding what does not function in the body triggers the couples. From the clinicians' perspective, understanding the pathogenesis of the diagnosis is the key to the proper evaluation and treatment the disease. Our study investigates the clinical data and gene expression of the UI patients. The findings of our research help to understand the clinical and molecular view of the UI and indicates the direction for further investigation.

Age is widely known as the key element not only in terms of the ovarian reserve and function but also possible conception. It is estimated that female fertility declines significantly after the age of 35 leaving them with a chance to conceive spontaneously of around 66% and a dramatic drop later in years (Delbaere et al., 2020). What is more, according to some studies, women of the same age with 2 years of primary unexplained infertility have even lower chances to conceive (Chua et al., 2020). Interestingly, some authors even raise an idea that age-related infertility and UI diagnosis are contradictory and should not be assimilated (Somigliana et al., 2016). Despite the

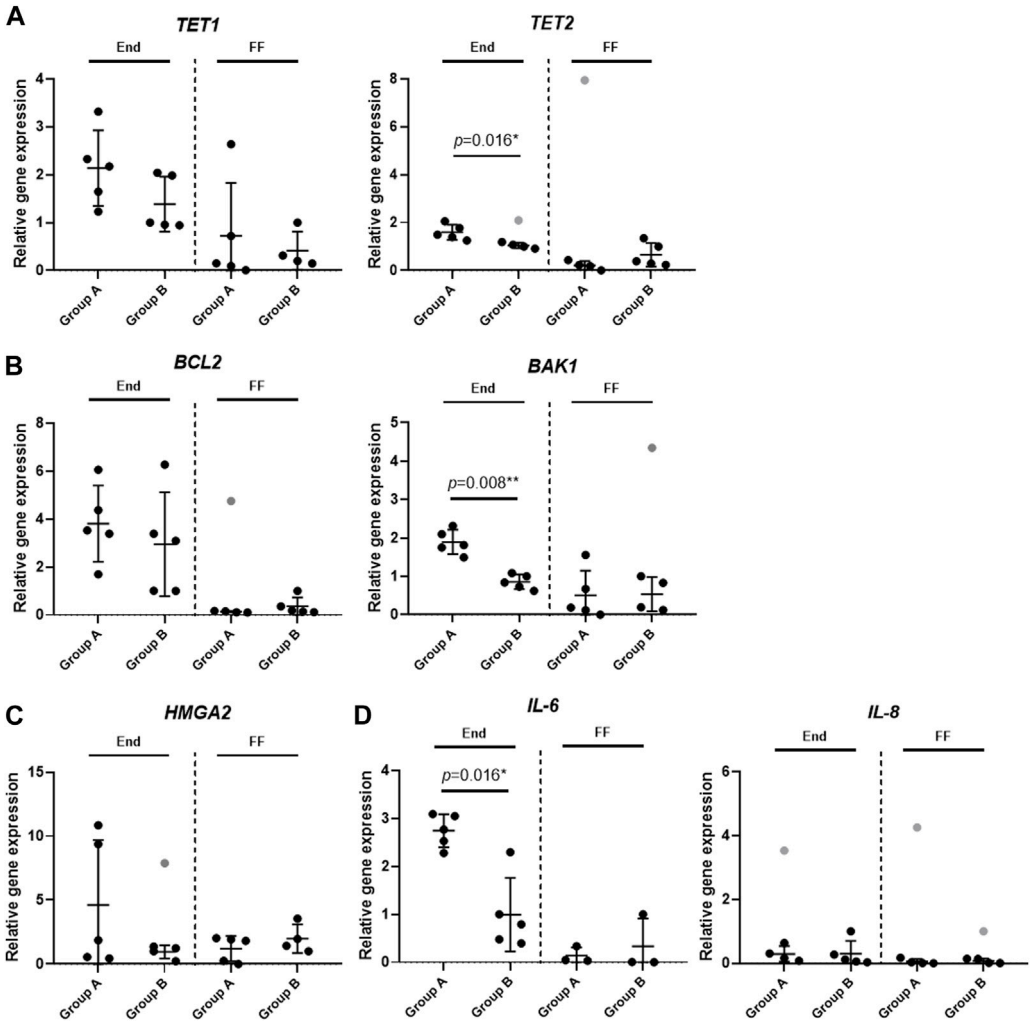

FIGURE 3
Analysis of gene expression profiles in endometrium and follicular fluid. Gene expression was analyzed in Group A (unexplained infertility patients; n = 5) and Group B (fertile patients; n = 5) using RT-qPCR. **(A)** Epigenetic DNA modification-related genes (*TET1, TET2*) expression analysis. **(B)** Gene expression analysis of cell death associated genes (*BCL2, BAK1*). **(C)** Senescence associated *HMGA2* gene expression analysis. **(D)** Gene analysis of genes related to immune response (*IL-6, IL-8*). Relative gene expression analysis was calculated using ΔΔCt method and *GAPDH* was used as a reference gene. Data are presented as mean ± SD; grey data points depict outliers as determined by ROUT (Q = 2%). Statistical significance was determined with Mann–Whitney *U* test and significance was set to $*p \leq 0.05$; $**p \leq 0.01$. Unmarked data points show no significance.

diagnosis, older women have naturally lower number of oocytes which leads to a lower amount of embryos in IVF cycles and a decreasing implantation rate (Spandorfer et al., 1998). A very important study revealed that embryo implantation rates in IVF cycles remain constant until the age of 35 and later decrease by 2.77% per year (Spandorfer et al., 2000). This could be associated with such factors as the decreased uterine receptivity, older paternal age, embryo aneuploidy, *etc.* Our study found that younger female age is a statistically reliable factor in prognosing the conception in UI patients after IVF. Also, the male age was significantly lower in the clinical pregnancy group. We believe that it should be emphasized for the UI couples that the treatment delay (especially when considering IVF) could negatively affect their conception rate.

A fertilization method is always a matter of question in performing the ART cycle for UI patients. The purpose of performing the intracytoplasmic sperm injection (ICSI) procedure prior to a conventional *in vitro* fertilization (IVF) in UI couples was to increase fertilization rates as a possible reason of infertility (Practice Committees of ASRM and SART, 2020). Several studies have been conducted to estimate whether the conception rates were higher in ICSI groups when treating UI patients. Unfortunately, most of the authors did not find any higher clinical pregnancy rates associated with ICSI although higher fertilization rates were observed (Ruiz et al., 1997; Foong et al., 2006). Similarly, our study showed that ICSI for UI couples did not improve clinical pregnancy rates. These findings suggest that ICSI should not be performed as a "rescue" procedure for UI patients especially if it is the first ART cycle.

A growing number of recent research studies suggest that the impaired quality of oocyte could be the key factor in UI patients' conception likely to lead to a poor-quality embryo formation (Tejera et al., 2005). However, in ART cycles, patients usually have several embryos thus the best quality embryo can be transferred. In this study, we did not investigate the correlation between the conception rate and the quality of the transferred embryo, however, we did find

a positive correlation with not only a higher number of transferred embryos but also with a higher number of received oocytes during the retrieval procedure. These correlations confirm the opinion that "every oocyte counts" as they could form more good quality embryos and increase pregnancy rates.

The day-2 serum progesterone has been estimated as a key hormone in predicting the ART outcome. Studies suggest that a high value of day-2 serum progesterone level was associated with a lower clinical pregnancy rate (Mahapatro and Radhakrishan, 2017). Likewise, other authors found the same result in IVF cycles using the GnRH antagonist protocol (Kolibianakis et al., 2004). Our research determined a positive statistical correlation between progesterone on day 2–3 and a successful conception. Since we only perform an IVF cycle when the progesterone is within normal levels, this correlation suggests that the fluctuations of progesterone under 1.0 ng/mL does not affect conception. We confirm that the progesterone measurement is an important clinical indicator for ensuring the chances of conception.

As mentioned above, infertility is a complex disorder influenced not only by one, but most commonly by multiple factors. In many cases the diagnosis does not provide useful insights, therefore, the causes of infertility may remain unknown. Difficulties in conceiving could also stem from the underlying molecular mechanisms in the endometrium or in other organs associated with reproduction (Gupta et al., 2014; Vázquez-Martínez et al., 2019; Fauque et al., 2020). Hoping that molecular analysis will give us useful insights, we investigated gene expression in the endometrial tissue and the follicular fluid cells between the two groups: in females unable to conceive (Group A) and in females who have successfully conceived (Group B). Aberrant gene expression patterns could be one of the causes of the endometrium dysfunction and, in turn, a contributing factor when it comes to difficulties conceiving (Garrido et al., 2002; Adamczyk et al., 2022b). The gene expression profiles obtained from RT-qPCR analysis demonstrated that Ten-eleven translocation (TET) genes *TET1* and *TET2* have a tendency to be upregulated in the endometrium of Group A. On the other hand, in the follicular fluid cells, these genes maintain a similar expression in both Group A and B. Proteins coded by these genes are associated with the changing DNA methylation pattern, more specifically, these proteins catalyze the DNA demethylation cascade (Ciesielski et al., 2017). Many studies suggest that the TET family plays a role in the endometriosis and endometrial cancer (Mahajan et al., 2020). One study investigated the *TET1* gene expression in the endometrium of the group of infertile endometriosis patients, infertile non-endometriosis patients, and in the group of patients without any reproductive disturbances (Adamczyk et al., 2022a). The study showed a significant decrease in the expression of *TET1* gene in the group of infertile endometriosis patients compared to fertile patients, however, the expression remained unchanged in idiopathic infertile patients. Moreover, lower *TET1* and *TET2* expression has been reported in the cases of endometrial cancer (Mahajan et al., 2020). Another gene of interest is a pro-apoptotic gene *BAK1* which is activated by p53 and BCL2. Our study found it to be significantly upregulated in the endometrium of Group A. This could suggest that apoptotic processes are induced by a greater degree in unexplained infertility patients than in fertile patients resulting in the stimulation of cell death. Most studies link BAK1 as well as BCL2 with the regulation of cancer. One of such studies by Witek et al. (2016) examined gene expression profiles in endometrial cancer and revealed that *BAK1* is overexpressed in grade 3 endometrial cancer which suggests that the tumor suppression system is still active and has yet to fulfil its role (Witek et al., 2016). There is evidence that augmented expression of a high mobility group AT-hook 2 (*HMGA2*) is associated with common benign mesenchymal tumors and rare aggressive cancers (Hammond and Sharpless, 2008). Moreover, HMGA2 plays a role in self-renewal and proliferation in neural stem cells since it was discovered that HMGA2 expression in mice decreases with age which in turn reduces the stem cell frequency and function (Nishino et al., 2008). Our research revealed a constant expression of *HMGA2* gene both in the endometrium and in the follicular fluid cells of both groups. As mentioned previously, many factors are possible contributors to infertility such as age, fertilization method, impaired quality of oocyte, hormonal imbalance. In addition to this list, the immune conditions may also lead to the reduced ability to conceive. A study by An et al. (2015) proposed that immunologic infertility could be caused by the upregulation of cytokines IL-2, IL-4, IL-6, IL-21, TNFα, IFNγ and IL-8 (An et al., 2015). Thirty infertile women were enrolled in this study and their blood was tested against mentioned cytokines. The analysis revealed a significant upregulation of these factors in the serums of infertility patients compared to healthy patients which led to a conclusion that the occurrence of immunologic infertility could be closely related to the changes in cytokine expression. Here we demonstrated the changes of the *IL-6* gene expression in the endometrium of infertile and fertile women. A significantly higher increase was recorded in the endometrium of infertile women (Group A), however, no significant changes were observed in the *IL-8* gene expression profile.

Conclusion

A successful conception after ART in UI patients is more likely to occur in couples of younger parental ages with a good ovarian reserve and a higher number of transferred embryos. The duration of infertility can negatively affect conception rates, therefore, ART treatment should not be delayed in young UI couples. The gene expression analysis revealed significant changes in the endometrium regarding the genes associated with cell death (*BAK1*), epigenetic DNA modification (*TET2*) and the immune response (*IL-6*) which were upregulated in females with the diagnosed unexplained infertility.

Data availability statement

The datasets presented in this study can be found in online repositories. The names of the repository/repositories and accession number(s) can be found in the article/Supplementary Material.

Ethics statement

The study was conducted in accordance with the Declaration of Helsinki and approved by the Vilnius Regional Biomedical Research Ethics Committee (No. 158200-18/7-1049-550, protocol number P-3/2019; 9 October 2019). The patients/participants provided their written informed consent to participate in this study.

Author contributions

Study design, RN, EK, DR; execution, BV-M, RB, RM; analysis: BV-M, RB, and EV; manuscript drafting: BV-M, RB, RM, and EV; critical discussion: RN, EK, DR. All authors contributed to the article and approved the submitted version.

Conflict of interest

The authors declare that the research was conducted in the absence of any commercial or financial relationships that could be construed as a potential conflict of interest.

Publisher's note

All claims expressed in this article are solely those of the authors and do not necessarily represent those of their affiliated organizations, or those of the publisher, the editors and the reviewers. Any product that may be evaluated in this article, or claim that may be made by its manufacturer, is not guaranteed or endorsed by the publisher.

References

Adamczyk, M., Rawłuszko-Wieczorek, A. A., Wirstlein, P., Nowicki, M., Jagodziński, P. P., Wender-Ozegowska, E., et al. (2022a). Assessment of TET1 gene expression, DNA methylation and H3K27me3 level of its promoter region in eutopic endometrium of women with endometriosis and infertility. *Biomed. Pharmacother.* 150, 112989. doi:10.1016/j.biopha.2022.112989

Adamczyk, M., Wender-Ozegowska, E., and Kedzia, M. (2022b). Epigenetic factors in eutopic endometrium in women with endometriosis and infertility. *Int. J. Mol. Sci.* 23, 3804. doi:10.3390/ijms23073804

Altmäe, S., Martínez-Conejero, J. A., Salumets, A., Simón, C., Horcajadas, J. A., and Stavreus-Evers, A. (2009). Endometrial gene expression analysis at the time of embryo implantation in women with unexplained infertility. *Mol. Hum. Reprod.* 16, 178–187. doi:10.1093/molehr/gap102

An, L. F., Zhang, X. H., Sun, X. T., Zhao, L. H., Li, S., and Wang, W. H. (2015). Unexplained infertility patients have increased serum IL-2, IL-4, IL-6, IL-8, IL-21, TNFα, IFNγ and increased tfh/CD4 T cell ratio: Increased tfh and IL-21 strongly correlate with presence of autoantibodies. *Immunol. Investig.* 44, 164–173. doi:10.3109/08820139.2014.932377

Batushansky, A., Zacharia, A., Shehadeh, A., Bruck-Haimson, R., Saidemberg, D., Kogan, N. M., et al. (2020). A shift in glycerolipid metabolism defines the follicular fluid of IVF patients with unexplained infertility. *Biomolecules* 10, 1135. doi:10.3390/biom10081135

Buckett, W., and Sierra, S. (2019). The management of unexplained infertility: An evidence-based guideline from the Canadian fertility and andrology society. *Reprod. Biomed. Online* 39, 633–640. doi:10.1016/j.rbmo.2019.05.023

Chua, S. J., Danhof, N. A., Mochtar, M. H., Van Wely, M., Mclernon, D. J., Custers, I., et al. (2020). Age-related natural fertility outcomes in women over 35 years: A systematic review and individual participant data meta-analysis. *Hum. Reprod.* 35, 1808–1820. doi:10.1093/humrep/deaa129

Ciesielski, P., Jóźwiak, P., Wójcik-Krowiranda, K., Forma, E., Cwonda, Ł., Szczepaniec, S., et al. (2017). Differential expression of ten-eleven translocation genes in endometrial cancers. *Tumor Biol.* 39, 1010428317695017. doi:10.1177/1010428317695017

Delbaere, I., Verbiest, S., and Tydén, T. (2020). Knowledge about the impact of age on fertility: A brief review. *Ups. J. Med. Sci.* 125, 167–174. doi:10.1080/03009734.2019.1707913

Dorostghoal, M., Ghaffari, H. O., Marmazi, F., and Keikhah, N. (2018). Overexpression of endometrial estrogen receptor-alpha in the window of implantation in women with unexplained infertility. *Int. J. Fertil. Steril.* 12, 37–42. doi:10.22074/ijfs.2018.5118

Elnaggar, A., Farag, A. H., Gaber, M. E., Hafeez, M. A., Ali, M. S., and Atef, A. M. (2017). AlphaVBeta3 integrin expression within uterine endometrium in unexplained infertility: A prospective cohort study. *BMC Womens Health* 17, 90. doi:10.1186/s12905-017-0438-3

Evers, J. L. (2002). Female subfertility. *Lancet* 360, 151–159. doi:10.1016/s0140-6736(02)09417-5

Fauque, P., De Mouzon, J., Devaux, A., Epelboin, S., Gervoise-Boyer, M.-J., Levy, R., et al. (2020). Reproductive technologies, female infertility, and the risk of imprinting-related disorders. *Clin. Epigenetics* 12, 191. doi:10.1186/s13148-020-00986-3

Fayezi, S., Darabi, M., Darabi, M., Nouri, M., Rahimipour, A., and Mehdizadeh, A. (2014). Analysis of follicular fluid total phospholipids in women undergoing *in-vitro* fertilisation. *J. Obstet. Gynaecol.* 34, 259–262. doi:10.3109/01443615.2013.851657

Foong, S. C., Fleetham, J. A., O'keane, J. A., Scott, S. G., Tough, S. C., and Greene, C. A. (2006). A prospective randomized trial of conventional *in vitro* fertilization versus intracytoplasmic sperm injection in unexplained infertility. *J. Assist. Reprod. Genet.* 23, 137–140. doi:10.1007/s10815-005-9008-y

Fortin, C. S., Leader, A., Mahutte, N., Hamilton, S., Léveillé, M. C., Villeneuve, M., et al. (2019). Gene expression analysis of follicular cells revealed inflammation as a potential IVF failure cause. *J. Assist. Reprod. Genet.* 36, 1195–1210. doi:10.1007/s10815-019-01447-4

Garrido, N., Navarro, J., García-Velasco, J., Remohí, J., Pellicer, A., and Simón, C. (2002). The endometrium versus embryonic quality in endometriosis-related infertility. *Hum. Reprod. Update* 8, 95–103. doi:10.1093/humupd/8.1.95

Gelbaya, T. A., Potdar, N., Jeve, Y. B., and Nardo, L. G. (2014). Definition and epidemiology of unexplained infertility. *Obstet. Gynecol. Surv.* 69, 109–115. doi:10.1097/ogx.0000000000000043

Gleicher, N., and Barad, D. (2006). Unexplained infertility: Does it really exist? *Hum. Reprod.* 21, 1951–1955. doi:10.1093/humrep/del135

Gupta, S., Ghulmiyyah, J., Sharma, R., Halabi, J., and Agarwal, A. (2014). Power of proteomics in linking oxidative stress and female infertility. *BioMed Res. Int.*, 2014, 916212. doi:10.1155/2014/916212

Hammond, S. M., and Sharpless, N. E. (2008). HMGA2, MicroRNAs, and stem cell aging. *Cell.* 135, 1013–1016. doi:10.1016/j.cell.2008.11.026

Hull, M. G. R. (1994). Effectiveness of infertility treatments: Choice and comparative analysis. *Int. J. Gynecol. Obstetrics* 47, 99–108. doi:10.1016/0020-7292(94)90348-4

Isaksson, R., and Tiitinen, A. (2004). Present concept of unexplained infertility. *Gynecol. Endocrinol.* 18, 278–290. doi:10.1080/0951359042000199878

Jasper, M. J., Tremellen, K. P., and Robertson, S. A. (2006). Primary unexplained infertility is associated with reduced expression of the T-regulatory cell transcription factor Foxp3 in endometrial tissue. *Mol. Hum. Reprod.* 12, 301–308. doi:10.1093/molehr/gal032

Keleş, I. D., Günel, T., Özgör, B. Y., Ülgen, E., Gümüşoğlu, E., Hosseini, M. K., et al. (2022). Gene pathway analysis of the endometrium at the start of the window of implantation in women with unexplained infertility and unexplained recurrent pregnancy loss: Is unexplained recurrent pregnancy loss a subset of unexplained infertility? *Hum. Fertil.*, 1–13. doi:10.1080/14647273.2022.2143299

Kolibianakis, E. M., Zikopoulos, K., Smitz, J., Camus, M., Tournaye, H., Van Steirteghem, A. C., et al. (2004). Elevated progesterone at initiation of stimulation is associated with a lower ongoing pregnancy rate after IVF using GnRH antagonists. *Hum. Reprod.* 19, 1525–1529. doi:10.1093/humrep/deh272

Mahajan, V., Osavlyuk, D., Logan, P. C., Amirapu, S., and Ponnampalam, A. P. (2020). Expression and steroid hormone regulation of TETs and DNMTs in human endometrium. *Reproduction* 160, 247–257. doi:10.1530/rep-19-0562

Mahapatro, A. K., and Radhakrishan, A. (2017). Day-2 serum progesterone level and IVF/ICSI outcome: A comparative study. *Int. J. Reproduction, Contracept. Obstetrics Gynecol.* 6, 1871–1875. doi:10.18203/2320-1770.ijrcog20171939

Maheshwari, A., Hamilton, M., and Bhattacharya, S. (2008). Effect of female age on the diagnostic categories of infertility. *Hum. Reprod.* 23, 538–542. doi:10.1093/humrep/dem431

Nandi, S., Kumar, V. G., Manjunatha, B. M., and Gupta, P. S. P. (2007). Biochemical composition of ovine follicular fluid in relation to follicle size. *Dev. Growth & Differ.* 49, 61–66. doi:10.1111/j.1440-169X.2007.00901.x

Nishino, J., Kim, I., Chada, K., and Morrison, S. J. (2008). Hmga2 promotes neural stem cell self-renewal in young but not old mice by reducing p16Ink4a and p19Arf expression. *Cell.* 135, 227–239. doi:10.1016/j.cell.2008.09.017

Pandian, Z., Bhattacharya, S., and Templeton, A. (2001). Review of unexplained infertility and obstetric outcome: A 10 year review. *Hum. Reprod.* 16, 2593–2597. doi:10.1093/humrep/16.12.2593

Ruiz, A., Remohí, J., Minguez, Y., Guanes, P. P., Simón, C., and Pellicer, A. (1997). The role of *in vitro* fertilization and intracytoplasmic sperm injection in couples with unexplained infertility after failed intrauterine insemination. *Fertil. Steril.* 68, 171–173. doi:10.1016/S0015-0282(97)81497-5

Sadeghi, M. R. (2015). Unexplained infertility, the controversial matter in management of infertile couples. *J. Reprod. Infertil.* 16, 1–2.

Somigliana, E., Paffoni, A., Busnelli, A., Filippi, F., Pagliardini, L., Vigano, P., et al. (2016). Age-related infertility and unexplained infertility: An intricate clinical dilemma. *Hum. Reprod.* 31, 1390–1396. doi:10.1093/humrep/dew066

Spandorfer, S. D., Avrech, O. M., Colombero, L. T., Palermo, G. D., and Rosenwaks, Z. (1998). Effect of parental age on fertilization and pregnancy characteristics in couples treated by intracytoplasmic sperm injection. *Hum. Reprod.* 13, 334–338. doi:10.1093/humrep/13.2.334

Spandorfer, S. D., Chung, P. H., Kligman, I., Liu, H. C., Davis, O. K., and Rosenwaks, Z. (2000). An analysis of the effect of age on implantation rates. *J. Assist. Reprod. Genet.* 17, 303–306. doi:10.1023/a:1009422725434

Tejera, A., Munoz, E., Meseguer, M., De Los Santos, M., Remohi, J., and Pellicer, A. (2005). Oocyte and embryo quality in women with unexplained infertility. *Fertil. Steril.* 84, S294–S295. doi:10.1016/j.fertnstert.2005.07.767

Vaughan, D. A., Goldman, M. B., Koniares, K. G., Nesbit, C. B., Toth, T. L., Fung, J. L., et al. (2022). Long-term reproductive outcomes in patients with unexplained infertility: Follow-up of the fast track and standard treatment trial participants. *Fertil. Steril.* 117, 193–201. doi:10.1016/j.fertnstert.2021.09.012

Vázquez-Martínez, E. R., Gómez-Viais, Y. I., García-Gómez, E., Reyes-Mayoral, C., Reyes-Muñoz, E., Camacho-Arroyo, I., et al. (2019). DNA methylation in the pathogenesis of polycystic ovary syndrome. *Reproduction* 158, R27-R40–R40. doi:10.1530/rep-18-0449

Witek, Ł., Janikowski, T., Bodzek, P., Olejek, A., and Mazurek, U. (2016). Expression of tumor suppressor genes related to the cell cycle in endometrial cancer patients. *Adv. Med. Sci.* 61, 317–324. doi:10.1016/j.advms.2016.04.001

Zegers-Hochschild, F., Adamson, G. D., Dyer, S., Racowsky, C., De Mouzon, J., Sokol, R., et al. (2017). The international glossary on infertility and fertility care. *Fertil. Steril.*, 108, 393–406. doi:10.1016/j.fertnstert.2017.06.005

frontiers | Frontiers in Cell and Developmental Biology

TYPE Original Research
PUBLISHED 15 August 2023
DOI 10.3389/fcell.2023.1234221

OPEN ACCESS

EDITED BY
Dolores Busso,
Universidad de los Andes, Chile

REVIEWED BY
Rossana Sapiro,
Rossana Sapiro, Uruguay
Haim Breitbart,
Bar-Ilan University, Israel
Bart M. Gadella,
Utrecht University, Netherlands

*CORRESPONDENCE
Ana Romarowski,
anaromarowski@ibyme.conicet.gov.ar
Pablo E. Visconti,
pvisconti@vasci.umass.edu

RECEIVED 03 June 2023
ACCEPTED 02 August 2023
PUBLISHED 15 August 2023

CITATION
Romarowski A, Fejzo J, Nayyab S, Martin-Hidalgo D, Gervasi MG, Balbach M, Violante S, Salicioni AM, Cross J, Levin LR, Buck J and Visconti PE (2023), Mouse sperm energy restriction and recovery (SER) revealed novel metabolic pathways.
Front. Cell Dev. Biol. 11:1234221.
doi: 10.3389/fcell.2023.1234221

Mouse sperm energy restriction and recovery (SER) revealed novel metabolic pathways

Ana Romarowski[1,2]*, Jasna Fejzo[3], Saman Nayyab[1], David Martin-Hidalgo[4], Maria G. Gervasi[1], Melanie Balbach[5], Sara Violante[6], Ana M. Salicioni[1], Justin Cross[6], Lonny R. Levin[5], Jochen Buck[5] and Pablo E. Visconti[1]*

[1]Department of Veterinary and Animal Sciences, University of Massachusetts, Amherst, MA, United States, [2]Instituto de Biología y Medicina Experimental, Consejo Nacional de Investigaciones Científicas y Técnicas (IBYME-CONICET), Buenos Aires, Argentina, [3]Institute for Applied Life Sciences, University of Massachusetts, Amherst, MA, United States, [4]Hospital San Pedro de Alcántara, Cáceres, Spain, [5]Department of Pharmacology, Weill Cornell Medicine, New York, NY, United States, [6]Memorial Sloan Kettering Cancer Center, New York, NY, United States

Mammalian sperm must undergo capacitation to become fertilization-competent. While working on mice, we recently developed a new methodology for treating sperm *in vitro,* which results in higher rates of fertilization and embryo development after *in vitro* fertilization. Sperm incubated in media devoid of nutrients lose motility, although they remain viable. Upon re-adding energy substrates, sperm resume motility and become capacitated with improved functionality. Here, we explore how sperm energy restriction and recovery (SER) treatment affects sperm metabolism and capacitation-associated signaling. Using extracellular flux analysis and metabolite profiling and tracing via nuclear magnetic resonance (NMR) and mass spectrometry (MS), we found that the levels of many metabolites were altered during the starvation phase of SER. Of particular interest, two metabolites, AMP and L-carnitine, were significantly increased in energy-restricted sperm. Upon re-addition of glucose and initiation of capacitation, most metabolite levels recovered and closely mimic the levels observed in capacitating sperm that have not undergone starvation. In both control and SER-treated sperm, incubation under capacitating conditions upregulated glycolysis and oxidative phosphorylation. However, ATP levels were diminished, presumably reflecting the increased energy consumption during capacitation. Flux data following the fate of ^{13}C glucose indicate that, similar to other cells with high glucose consumption rates, pyruvate is converted into ^{13}C-lactate and, with lower efficiency, into ^{13}C-acetate, which are then released into the incubation media. Furthermore, our metabolic flux data show that exogenously supplied glucose is converted into citrate, providing evidence that in sperm cells, as in somatic cells, glycolytic products can be converted into Krebs cycle metabolites.

KEYWORDS

sperm, assisted reproductive technologies, metabolism, AMP, ATP, citrate, L-carnitine

Introduction

After leaving the testis, mammalian sperm undergo two post-testicular maturation processes, one in the male epididymis, known as epididymal maturation (Gervasi and Visconti, 2017), and the second in the female genital tract, known as capacitation (Austin, 1951; Chang, 1951). Contrary to epididymal maturation, capacitation can be mimicked *in vitro* in a defined medium. While there are some species-specific variations, mammalian sperm capacitation media are isotonic physiological solutions containing bicarbonate (HCO_3^-), calcium (Ca^{2+}), a protein source that is usually serum albumin, and energy substrates. Functionally, capacitation results in sperm changing their motility pattern (e.g., hyperactivation) (Ho and Suarez, 2001) and being able to undergo a physiologically induced acrosome reaction. At the molecular level, capacitation is initiated as soon as sperm are exposed to HCO_3^- in the seminal plasma or *in vitro* capacitation media. HCO_3^- stimulates the activity of soluble adenylyl cyclase ADCY10 (aka sAC) with the consequent increase in cAMP and protein kinase A (PKA) activity (Gervasi and Visconti, 2016). Activation of this pathway occurs in less than 1 min and triggers signaling cascades that include increases in intracellular pH, intracellular Ca^{2+}, protein tyrosine phosphorylation, and hyperpolarization of the sperm plasma membrane potential. These sperm signaling pathways elicit processes with increased energy demand. In capacitating sperm, most of the energy consumed is used for movement mediated by dynein ATPases; however, many other functions also require ATP, including ion homeostasis, enzymatic reactions, and exocytotic events.

Like somatic cells, spermatozoa harbor the molecular machinery for glycolysis and oxidative phosphorylation. However, contrary to other cell types, these two metabolic pathways are postulated to be physically separated in different sperm compartments; glycolytic enzymes are most abundantly found in the principal piece, while mitochondria and oxidative phosphorylation (OxPhos) machinery are found exclusively in the mid-piece (Visconti, 2012; Ferramosca and Zara, 2014; Amaral, 2022). We recently used extracellular flux analysis to show that, during capacitation, mouse sperm incubated only in the presence of glucose upregulated both glycolysis and OxPhos (Balbach et al., 2020b). Under these conditions, inhibitors of glycolysis prevented the stimulation of OxPhos, suggesting that these metabolic pathways are coupled in sperm (Balbach et al., 2020b) as they are in somatic cells.

During our investigations of sperm metabolism, we explored the effects of nutrient starvation. When cauda epididymal mouse sperm are incubated in nutrient-free media, their motility ceases within 30–40 min. These "starved" sperm remain viable, and when they are allowed to capacitate in the presence of restored nutrients (i.e., glucose and/or pyruvate), the "recovered" sperm show improved functionality relative to sperm directly capacitated after collection from the epididymis. We refer to this procedure as sperm energy restriction and recovery (SER), and relative to untreated sperm, a higher percentage of SER-treated sperm undergo hyperactivation and more efficiently fertilized metaphase II-arrested oocytes after *in vitro* fertilization (IVF). More surprisingly, zygotes derived from SER-treated sperm had an increased probability to develop into blastocysts, and when transferred into pseudo-pregnant females, blastocysts derived from SER treatment were three times more likely to successfully develop into pups (Navarrete et al., 2019). SER treatment also increased cleavage and blastocyst development in bovines after intracytoplasmic sperm injection (Navarrete et al., 2019), as well as the obtention of ram blastocysts after IVF (Al-Hafedh and Cedden, 2023).

In this work, we used metabolic flux assays, along with sperm metabolite profiling and tracing, to investigate the metabolic consequences of starvation and subsequent recovery. The most significant differences from normally capacitated sperm we observed were that starved sperm have significantly increased levels of AMP and L-carnitine. Both metabolites recovered to pre-starvation levels during rescue. Regardless of the sperm treatment, capacitation conditions increased glycolysis and OxPhos. However, despite this upregulation of energy pathways, capacitated sperm have reduced ATP levels, suggesting increased energy consumption. Finally, using NMR, we observed the conversion of ^{13}C-glucose into ^{13}C-citrate, indicating that glycolysis has the potential to couple with the mitochondrial Krebs cycle.

Results

Phosphorylation pathways are blocked under starvation conditions and recovered upon rescue

We used Western blotting with anti-phospho-PKA substrates (anti-pPKAs) (Figures 1A–C, upper panels) and anti-phosphotyrosine (anti-pY) (Figures 1A–C, lower panels) antibodies to explore the effect of SER on capacitation-dependent protein phosphorylation signaling cascades. As expected, in non-capacitating (NC) media, there were no significant changes in the PKA substrates or pY phosphorylation patterns under any condition (Figures 1A–C, NC), whereas in CAP media, PKA phosphorylation of substrates increased in less than 1 min (Figure 1A, CAP, upper panel) and that of pY increased after 15 min of capacitation (Figure 1A, CAP, lower panel). Under starving conditions, PKA phosphorylation of substrates was initially stimulated, followed by dephosphorylation at 30 min, which coincides with the time point when sperm stop moving (see arrow in Figure 1B). In the absence of nutrients, whether under NC or CAP conditions, pY did not change. Importantly, upon recovery (i.e., when glucose and pyruvate are added back) under conditions that support capacitation, phosphorylation of PKA substrates and tyrosine residues recovered (Figure 1C, SER-CAP). Densitometric analysis confirmed that PKA substrates and pY phosphorylation patterns after recovery, under either NC or CAP conditions, are indistinguishable from their respective controls persistently incubated in the presence of nutrients (Figures 1D, E).

Glucose alone is sufficient for sperm capacitation and to maintain glycolysis and oxidative phosphorylation pathways

Using glucose alone in the recovery step, we observed similar PKA substrates and pY phosphorylation patterns as when using

10.3389/fcell.2023.1234221

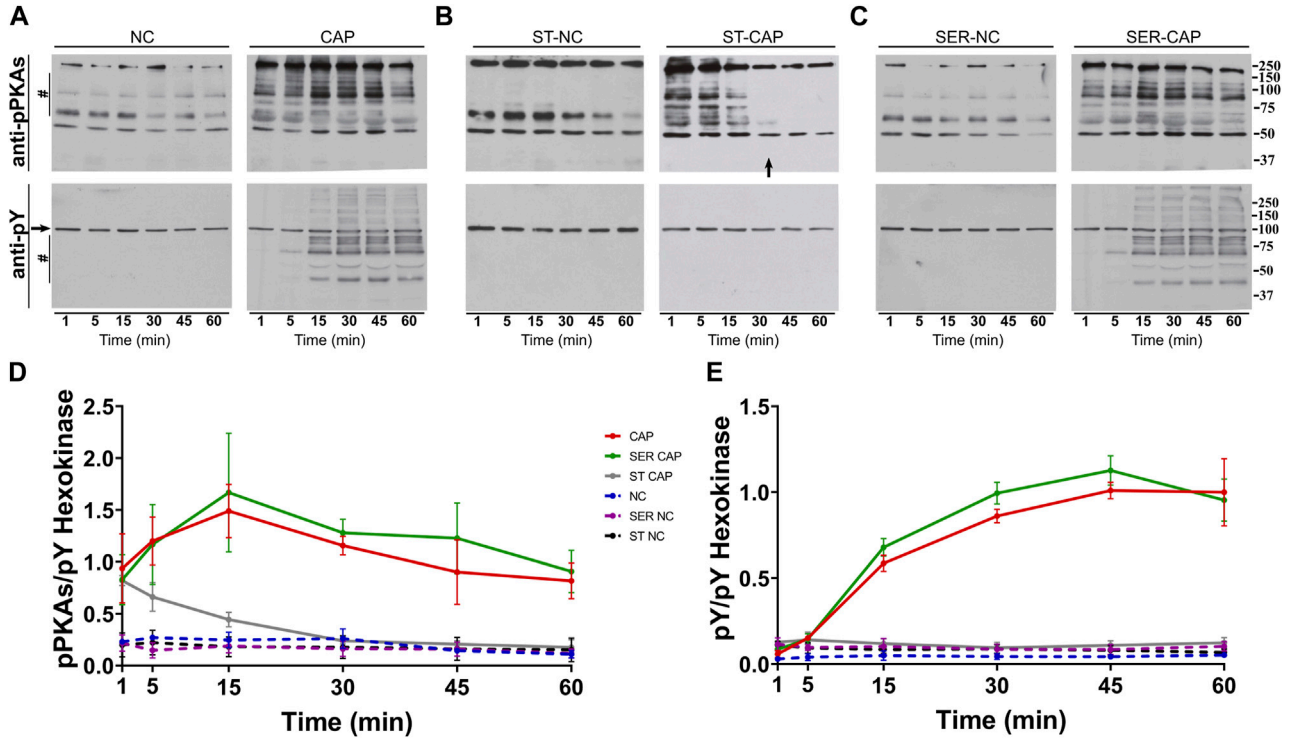

FIGURE 1
SER treatment recovers the activation of the PKA/pY pathway. Sperm were incubated under the following different conditions: **(A)** continuously incubated with glucose and pyruvate under the NC (without BSA and without HCO_3^-) or CAP (with BSA and HCO_3^-) condition; **(B)** continuously incubated without glucose and pyruvate under the NC (ST-NC) or CAP (ST-CAP) condition; or **(C)** incubated without glucose and pyruvate under the NC condition until motility stopped (~30–40 min) and recovered with glucose and pyruvate in non-capacitated medium (SER-NC) or in capacitated medium (SER-CAP). At the indicated time points, proteins were extracted and separated by 8% SDS-PAGE and immunoblotted using anti-phosphorylated PKA substrates (pPKAs) and anti-phospho-tyrosine (pY) antibodies. Equal loading was visualized by tyrosine-phosphorylated hexokinase. Representative images are shown. The arrow in (B) ST-CAP indicates that PKA substrate dephosphorylation occurs at the time when sperm stop moving. **(D–E)** The respective quantitative analysis was performed by measuring the optical density of the bands in the region marked by # and normalized using tyrosine-phosphorylated hexokinase as the control. The results are expressed as the mean ± SEM of at least three independent experiments.

glucose and pyruvate combined (Figures 2A, B); thus, glucose alone was sufficient to recover capacitation-induced changes in PKA and tyrosine phosphorylation. In contrast, pyruvate alone was only partially able to recover phosphorylation of PKA substrates and did not support the capacitation-induced increase in pY. In addition to phosphorylation, capacitation is accompanied by changes in the sperm motility pattern, known as hyperactivation. Recovery with glucose, but not pyruvate, was sufficient to increase the percentage of hyperactivated sperm to the same level as observed for media containing glucose and pyruvate (Figure 2C). Finally, assessing the definitive readout of capacitation, i.e., the ability to fertilize an oocyte, glucose, but not pyruvate, supported the fertilizing capacity of SER sperm to levels comparable to those obtained in media containing glucose and pyruvate (Figures 2D, E). Altogether, these data support the use of glucose alone to explore how metabolite levels are altered during capacitation and SER treatments.

We previously showed that glucose consumption is increased in capacitating sperm ((Hidalgo et al., 2020) and Figure 3A, left panel), and both glycolysis and OxPhos are stimulated during capacitation (Balbach et al., 2020b). In SER-treated sperm (i.e., following nutrient deprivation), glucose consumption was also increased in CAP conditions (Figure 3A, right panel). Because glucose was measured using glucose oxidase coupling to hydrogen peroxide formation (H_2O_2), we should consider H_2O_2 is released by capacitated sperm (Takei et al., 2021), implying that glucose consumption might be slightly higher than that shown in Figure 3A. Overall, this observation does not change our main conclusion regarding the increase in glucose consumption during capacitation. Consistently, the capacitation-associated increase in glucose consumption was accompanied by upregulation of glycolysis. We used an extracellular flux analyzer to measure real-time changes in proton release (ECAR) and oxygen consumption rate (OCR) (Ferrick et al., 2008). While ECAR and OCR serve as readouts of the changes in the rate of glycolysis and oxidative phosphorylation, respectively, proton release and oxygen consumption may occur via other metabolic pathways. We have previously shown that the capacitation-induced changes in ECAR and OCR in mouse sperm are completely inhibited upon addition of 2-deoxyglucose (inhibits the first step of glycolysis) or antimycin A and rotenone (inhibits complex III and complex I of the electron transport chain, respectively), respectively (Balbach et al., 2020b; Balbach et al., 2020a), implying that the Seahorse measurements reflect glycolysis by proton release and OxPhos by oxygen consumption. As anticipated, under starvation conditions, the ECAR (Figures 3B, C, lower panel and right panel; Supplementary Figure 1A, right panel) and OCR (Figures 4A, B,

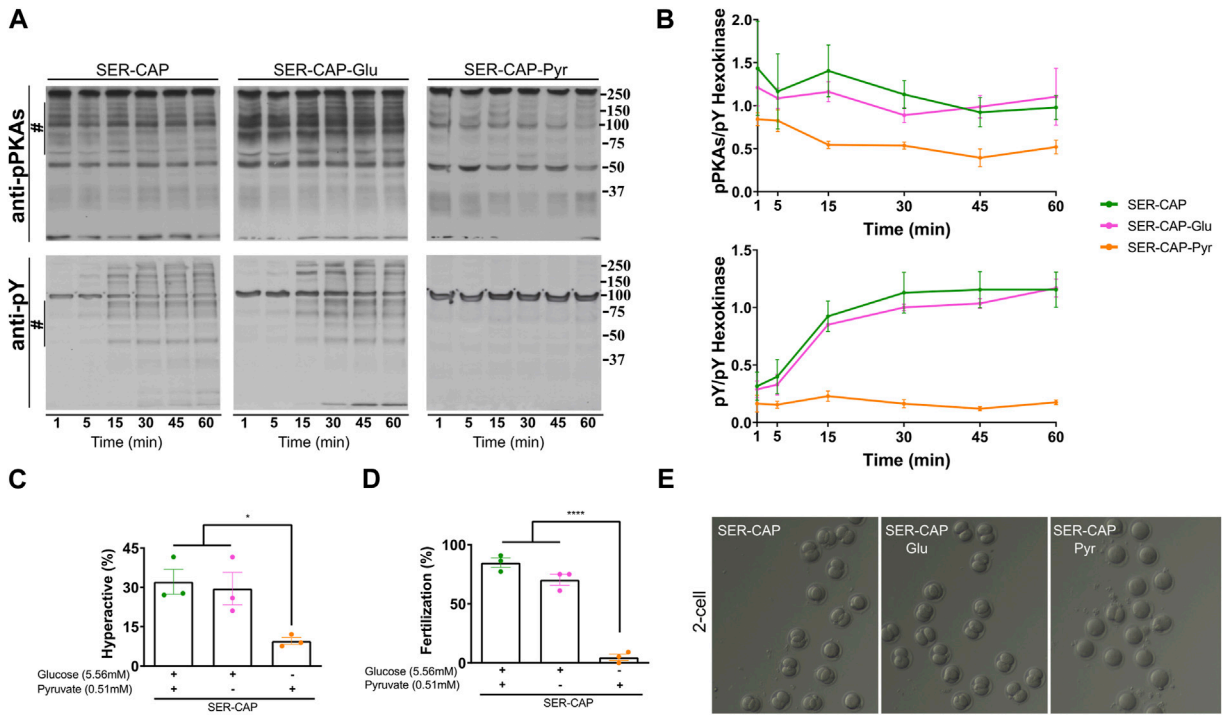

FIGURE 2
Glucose is sufficient to induce the activation of the PKA/pY pathway and the increased hyperactivation and fertilization rates obtained after SER. **(A)** Sperm were incubated without glucose and pyruvate under the NC condition until motility stopped (~30–40 min) and recovered with glucose and pyruvate in capacitated medium (SER-CAP) or with glucose only in capacitated medium (SER-CAP-Glu) or with pyruvate only in capacitated medium (SER-CAP-Pyr). At the indicated time points, proteins were extracted and separated by 8% SDS-PAGE and immunoblotted using anti-phosphorylated PKA substrates (pPKAs) and anti-phospho-tyrosine (pY) antibodies. As a loading control, hexokinase was used. Representative images are shown. **(B)** The respective quantitative analysis was performed by measuring the optical density of the bands in the region marked by # and normalized using tyrosine-phosphorylated hexokinase as the control. The results are expressed as the mean ± SEM of at least three independent experiments. **(C)** Percentage of hyperactivated out of the total motile sperm after 1 h incubation under the different conditions. The results are expressed as the mean ± SEM of three independent experiments. ANOVA with Tukey's multiple comparison test was performed. * indicates a significant difference with $p < 0.05$. **(D)** Percentage of fertilization indicated by oocytes that reached the two-cell embryo stage. The results are expressed as the mean ± SEM of three independent experiments. ANOVA with Tukey's multiple comparison test was performed. **** indicates a significant difference with $p < 0.0001$. **(E)** Representative images of two-cell embryos obtained after IVF with CD-1 female oocytes and CD1 male sperm, SER-treated recovered with glucose and pyruvate or SER-treated recovered with glucose only or SER-treated recovered with pyruvate only.

right panel and right panel; Supplementary Figure 1B, right panel) decreased to almost undetectable levels. Interestingly, the rates of glycolysis and OxPhos transiently increased when starved sperm were placed in capacitating media (Supplementary Figures 1A, B, right panels). Presumably, the capacitation-induced increases in glycolysis and OxPhos were initiated but could not be sustained in the absence of exogenous nutrients. When glucose was added back to starved sperm, the increase in the ECAR (Figures 3B, C lower panel and right panel; Supplementary Figure 1A, right panel) and OCR (Figure 4A, right panel; B, right panel; and Supplementary Figure 1B, right panel) was rescued, and this recovery was higher under capacitating conditions as observed in control conditions. It appears that the ECAR (Figure 3B, lower panel vs. upper panel) and OCR (Figure 4A, right panel vs. left panel) in SER-treated sperm have faster kinetics than those of sperm persistently incubated in the presence of nutrients. However, it is important to be careful when comparing these samples because in control sperm, glucose was present from the beginning of the measurements, while in SER-treated sperm, glucose was added to starved sperm during the measurements. Overall, these results are consistent with those of our previous experiments demonstrating that a glycolytic substrate can support the increase in OCR (Balbach et al., 2020b), suggesting that sperm can couple glycolysis and mitochondrial OxPhos as observed in somatic cells.

NMR and MS metabolomics studies revealed significant changes in sperm incubated under starvation conditions

We used NMR and MS metabolomics profiling to assess changes in sperm metabolites during the different treatments. Metabolite profiles measured via NMR are summarized in Table 1, and metabolites identified via MS are listed in Table 2. Principal component analysis of the NMR spectra revealed that extracts from sperm incubated in the presence of glucose under any condition clustered together, while starved samples defined a distinct cluster (Figure 5A). Similar results were observed with MS data (Figure 5B). When starved sperm samples were excluded from PCA, metabolites from non-capacitated and capacitated sperm formed distinct clusters, regardless of when glucose was added (Supplementary Figure S2). Not surprisingly,

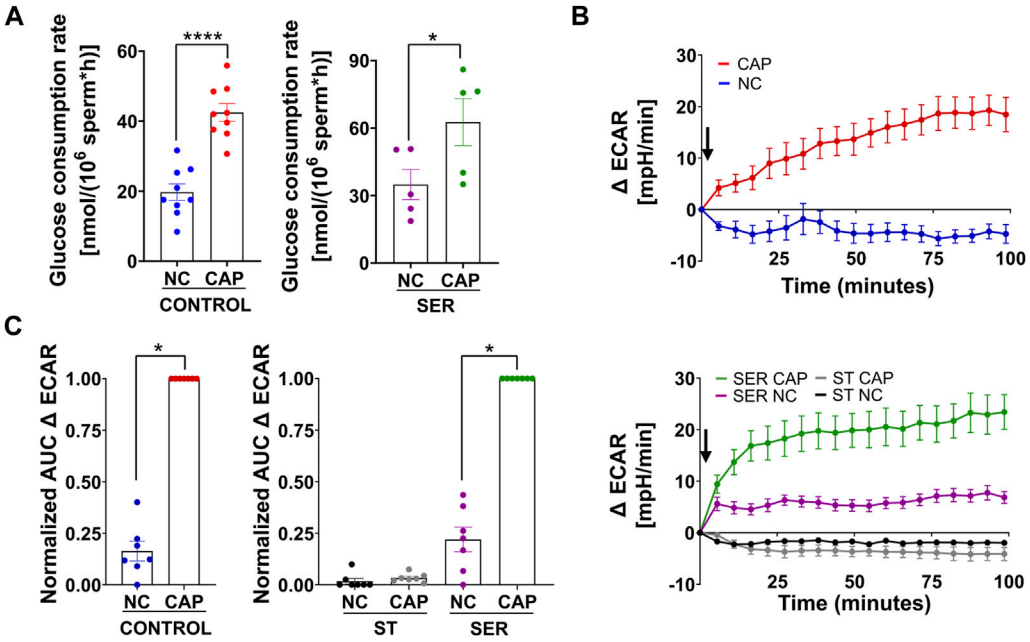

FIGURE 3
Glucose alone is sufficient to maintain glycolysis pathways. **(A)** The glucose consumption rate was determined using the Amplex™ Red Glucose/Glucose Oxidase Assay Kit. Sperm were subjected to different incubation conditions as follows: continuously incubated with glucose in NC (without BSA and without HCO_3^-) or CAP (with BSA and HCO_3^-); incubated without glucose under the NC condition until motility stopped (~30–40 min) and recovered with glucose in non-capacitated medium (SER-NC) or in capacitated medium (SER-CAP). The results are expressed as the mean ± SEM of at least five independent experiments. T-tests between NC and CAP (control and SER) conditions were performed. **** indicates a significant difference with $p < 0.0001$; * indicates a significant difference with $p < 0.05$. **(B)** Measurement of the extracellular acidification rate (ECAR) by Seahorse. Upper panel: the arrow indicates the release of the content of port B (5.6 mM glucose TYH medium with DMSO (vehicle) for wells with NC sperm; 5.6 mM glucose TYH medium with 10 mM dbcAMP and 1 mM IBMX for wells with CAP sperm). Lower panel: the arrow indicates the release of the content of port B (starving TYH medium with DMSO (vehicle) for wells with ST NC sperm; starving TYH medium with 10 mM dbcAMP and 1 mM IBMX for wells with ST CAP sperm; 56 mM glucose TYH medium with DMSO (vehicle) for wells with SER NC sperm; 56 mM glucose TYH medium with 10 mM dbcAMP and 1 mM IBMX for wells with SER CAP sperm). **(C)** Area under the curve (AUC) of ECAR−ECAR at time 0 min for each time point (=Δ ECAR), normalized to CONTROL CAP (left panel) or to SER CAP (right panel). The results are expressed as the mean ± SEM of seven independent experiments. T-tests with Wilcoxon's matched-pair signed rank test between NC and CAP (control, ST, and SER) conditions were performed. * indicates a significant difference with $p < 0.05$.

glycolytic intermediates, which are significantly reduced upon starvation (Table 2), are recovered after rescue to levels comparable to those of their respective control (NC and CAP, respectively). Metabolic profiles of SER-NC and NC sperm, as well as those of SER-CAP and CAP sperm, are very similar. For example, in capacitating sperm, in both control and SER, cAMP is elevated (Table 2), consistent with what is known about signal transduction in capacitating sperm (Gervasi and Visconti, 2016) and the increase in phosphorylation of PKA substrates (Figure 1, Figures 2A, B). Thus, most changes in metabolites caused by starvation did not persist following glucose recovery, and the steady-state concentrations of metabolites depend more on the regulation of signaling pathways during capacitation than on whether the sperm recover from starvation.

As predicted from extracellular flux analyzer experiments (Figure 3C) and our previously work (Balbach et al., 2020b; Hidalgo et al., 2020), both NMR and MS analyses confirm that lactate production is increased during capacitation in both CAP and SER-CAP (Figures 6A–C). Here, we also show that most of the lactate produced during glycolysis is extruded into the media (Figures 6D, E). Unexpectedly, we identified lactate in the starved sperm and supernatant via one-dimensional (1D) ^{1}H-NMR that was not derived from ^{13}C-labeled glucose (Supplementary Figures S3A, B), as it was 0 via two-dimensional (2D) ^{1}H-^{13}C HSQC NMR spectra (Figures 6A–B, D–E). Similarly, we observed ^{13}C-acetate derived from ^{13}C-glucose (Supplementary Figures S4A, B), indicating that sperm can metabolize the conversion of pyruvate to acetate, as in other cell types with high glucose consumption (Liu et al., 2018). As observed with lactate, 1D ^{1}H-NMR indicates that this metabolite is also produced under starving conditions (Supplementary Figures S4C, D). Altogether, these results suggest that sperm can form lactate and acetate from glycolysis, as well as using endogenous sources. This possibility needs to be explored in future studies. Among Krebs cycle metabolites, we were only able to identify citrate by NMR and MS. Importantly, in NMR ^{1}H-^{13}C 2D HSQC spectra, citrate is labeled with ^{13}C, which means it is derived from exogenously supplied ^{13}C-glucose (Figures 6F–H). These data confirm the observations from extracellular flux analysis [(Figure 4) and (Balbach et al., 2020b)] that in sperm, as in somatic cells, glycolytic products can feed the Krebs cycle and OxPhos.

As expected, ATP levels were significantly reduced under starvation conditions when measured by NMR (Figure 7A), MS (Figure 7B), or chemiluminescence (Figure 7C). The reduced ATP in starved mouse sperm is a likely reason why they become quiescent; they have insufficient ATP to maintain dynein ATPase function throughout the axoneme. Unexpectedly, ATP levels are also reduced

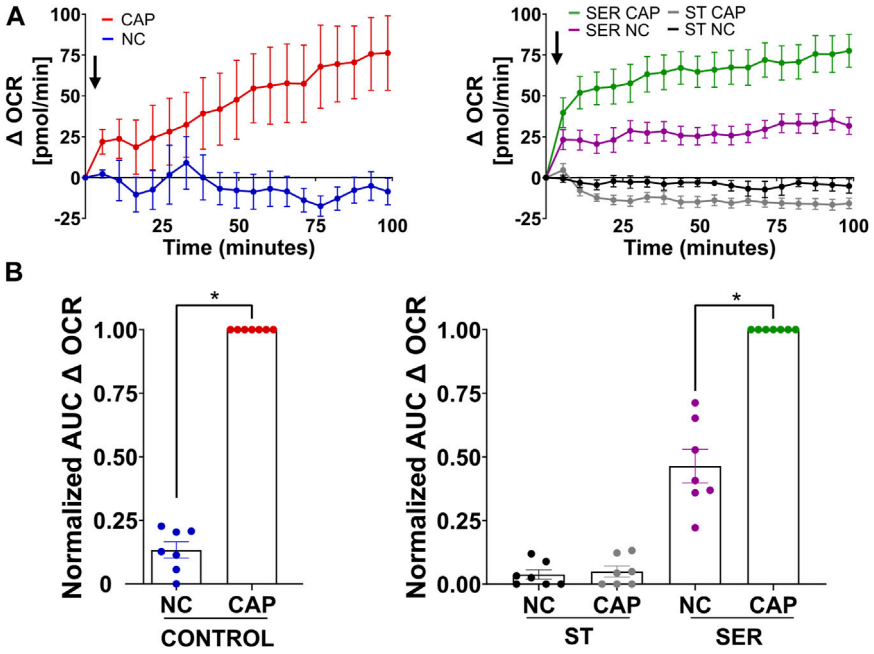

FIGURE 4
Glucose alone is sufficient to maintain oxidative phosphorylation pathways. **(A)** Measurement of the oxygen consumption rate (OCR) by Seahorse under the following incubation conditions: continuously incubated with glucose in NC (without BSA and without HCO_3^-) or CAP (with dbcAMP and IBMX); continuously incubated without glucose in NC (ST-NC) or CAP (ST-CAP); incubated without glucose under NC condition until motility stopped (~30–40 min) and recovered with glucose in non-capacitated medium (SER-NC) or in capacitated medium (SER-CAP). Left panel: the arrow indicates the release of the content of port B (5.6 mM glucose TYH medium with DMSO (vehicle) for wells with NC sperm; 5.6 mM glucose TYH medium with 10 mM dbcAMP and 1 mM IBMX for wells with CAP sperm). Right panel: the arrow indicates the release of the content of port B (starving TYH medium with DMSO (vehicle) for wells with ST NC sperm; starving TYH medium with 10 mM dbcAMP and 1 mM IBMX for wells with ST CAP sperm; 56 mM glucose TYH medium with DMSO (vehicle) for wells with SER NC sperm; 56 mM glucose TYH medium with 10 mM dbcAMP and 1 mM IBMX for wells with SER CAP sperm). **(B)** AUC of OCR−OCR at time 0 min for each time point (=Δ OCR), normalized to CONTROL CAP (left panel) or to SER CAP (right panel). The results are expressed as the mean ± SEM of seven independent experiments. T-tests with Wilcoxon's matched-pair signed rank test between NC and CAP (control, ST and SER) conditions were performed. * indicates a significant difference with $p < 0.05$.

TABLE 1 Sperm metabolites identified by NMR, indicating whether or not they were present in the supernatant of sperm samples. The type of the NMR experiment used for data analysis is indicated and explained in the *Methods* section.

Metabolite	Sperm	Supernatant	Experiment
Glucose	Yes	Yes	1H, TOCSY, HSQC
Lactic acid	Yes	Yes	1H, TOCSY, HSQC
Citric acid	Yes	No	1H, TOCSY, HSQC
Beta-nicotinamide adenine dinucleotide	Yes	No	1H, TOCSY
Adenosine 5-triphosphate	Yes	No	1H
Adenosine 5-diphosphate	Yes	No	1H
Adenosine 5-monophosphate	Yes	No	1H
L-Acetyl carnitine	Yes	No	1H, TOCSY, HSQC
L-Carnitine	Yes	No	1H, TOCSY, HSQC
Acetic acid	Yes	Yes	1H, TOCSY, HSQC

in sperm incubated in capacitating media. Metabolic profiling provides an indication of steady-state levels of metabolites, which can change due to alterations in rates of production and/or consumption. Thus, the decrease in ATP levels, despite the observed capacitation-induced increase in glycolytic activity (ECAR), OxPhos activity (OCR), and lactate production, suggests that higher ATP consumption during capacitation decreases ATP levels, alleviating the feedback inhibition of glycolytic enzymes. Consistently, the new, lower steady-state level of ATP would support the essential increased ATP production. In capacitating

10.3389/fcell.2023.1234221

TABLE 2 Sperm metabolites identified by MS. Quadruplicate AUC values of each condition for each experiment were averaged, and all conditions values within the same experiment were normalized against the corresponding CAP value. Finally, the values were averaged across all the independent experiments.

	NC		CAP		ST-NC		ST-CAP		SER-NC		SER-CAP	
Metabolite	Mean	SEM	Mean	SEM	Mean	SEM	Mean	SEM	Mean	SEM	Mean	SEM
2-Phosphoglyceric acid	0.37	0.04	1	0	0.02	0.01	0.02	0.00	0.18	0.06	0.57	0.09
Adenine	1.46	0.25	1	0	1.63	0.30	0.85	0.30	1.38	0.25	1.22	0.16
Adenosine	1.62	0.49	1	0	0.92	0.34	2.82	1.18	1.38	0.24	1.04	0.18
Adenosine 3-5-cyclic monophosphate	0.31	0.04	1	0	0.35	0.16	0.21	0.03	0.36	0.17	0.79	0.17
Adenosine 5-diphosphate	3.49	0.79	1	0	2.98	1.55	1.26	0.21	3.82	1.59	1.55	0.41
Adenosine 5-monophosphate	1.83	0.19	1	0	13.60	4.52	8.80	1.89	2.05	0.28	1.22	0.15
Adenosine 5-triphosphate	2.44	0.36	1	0	0.28	0.10	0.07	0.01	2.06	0.55	0.72	0.07
alpha-D(+)Mannose 1-phosphate	0.61	0.20	1	0	0.05	0.02	0.04	0.02	0.51	0.22	0.93	0.18
alpha-D-Glucose-1-phosphate	0.68	0.06	1	0	0.04	0.01	0.03	0.01	0.62	0.10	0.70	0.08
Arabinose-5-phosphate	1.83	0.47	1	0	0.19	0.07	0.28	0.17	1.43	0.37	0.97	0.25
Beta-nicotinamide adenine dinucleotide	1.32	0.17	1	0	1.34	0.34	0.87	0.13	1.24	0.27	0.81	0.07
Citric acid	0.65	0.10	1	0	0.24	0.01	0.34	0.02	0.42	0.06	0.70	0.10
Cytidine	0.92	0.23	1	0	1.00	0.15	0.59	0.18	1.04	0.42	1.12	0.58
D-Fructose 6-phosphate	1.39	0.24	1	0	0.02	0.01	0.00	0.00	1.07	0.23	0.73	0.14
D-Glucose 6-phosphate	1.35	0.23	1	0	0.01	0.00	0.00	0.00	1.17	0.27	0.74	0.11
Dihydroxyacetone phosphate	0.71	0.18	1	0	0.35	0.15	0.44	0.24	0.68	0.23	1.00	0.39
D-pantothenic acid	1.13	0.26	1	0	1.93	0.29	2.72	1.42	1.09	0.21	1.25	0.48
D-Ribose 5-phosphate	2.12	0.62	1	0	0.14	0.04	0.11	0.04	1.44	0.38	0.75	0.11
D-Xylulose-5-phosphate	1.65	0.62	1	0	0.25	0.08	0.49	0.17	1.30	0.39	0.71	0.15
Flavin adenine dinucleotide	1.30	0.17	1	0	1.40	0.39	0.96	0.16	1.20	0.23	1.06	0.15
Guanosine	0.87	0.12	1	0	0.65	0.07	0.60	0.37	0.77	0.16	0.65	0.14
Hypoxanthine	0.94	0.09	1	0	0.78	0.09	0.79	0.28	0.98	0.21	1.04	0.20
Inosine	0.81	0.09	1	0	0.45	0.05	0.70	0.24	0.81	0.18	1.00	0.16
Inosine 5-diphosphate	2.11	0.25	1	0	0.49	0.02	1.24	0.20	1.33	0.33	0.96	0.11
Inosine 5-monophosphate	1.76	0.21	1	0	13.21	4.49	8.38	1.82	2.00	0.27	1.21	0.14
Inosine 5-triphosphate	1.72	0.39	1	0	0.06	0.03	0.07	0.04	0.68	0.18	0.58	0.08
Ketoisovaleric acid	1.06	0.25	1	0	0.93	0.06	0.95	0.13	1.00	0.30	0.82	0.17
Lactic acid	0.56	0.04	1	0	0.04	0.01	0.08	0.00	0.51	0.09	0.72	0.13
L-Aspartic Acid	1.47	0.31	1	0	1.33	0.24	1.20	0.13	1.37	0.22	1.22	0.43
L-Carnitine	2.04	0.66	1	0	2.96	0.69	3.06	0.86	1.84	0.57	1.10	0.26
L-Dihydroorotic acid	1.24	0.13	1	0	1.75	0.34	1.02	0.44	1.37	0.34	0.81	0.19
L-Glutamic acid	1.49	0.26	1	0	1.52	0.25	1.03	0.18	1.30	0.18	1.02	0.14
L-Gluthathione (oxidized)	1.42	0.26	1	0	1.34	0.43	1.74	0.48	1.29	0.29	1.02	0.16
L-Hydroxyglutaric acid	1.00	0.11	1	0	0.45	0.04	0.48	0.05	0.78	0.12	0.70	0.13
L-Kynurenine	1.27	0.17	1	0	1.83	0.50	1.20	0.31	0.96	0.26	0.79	0.14
L-Malic acid	0.70	0.04	1	0	0.70	0.08	0.80	0.05	0.74	0.02	0.82	0.19
L-Methionine	1.08	0.33	1	0	0.76	0.16	0.64	0.16	0.88	0.20	0.93	0.13

(Continued on following page)

TABLE 2 (*Continued*) Sperm metabolites identified by MS. Quadruplicate AUC values of each condition for each experiment were averaged, and all conditions values within the same experiment were normalized against the corresponding CAP value. Finally, the values were averaged across all the independent experiments.

	NC		CAP		ST-NC		ST-CAP		SER-NC		SER-CAP	
Metabolite	Mean	SEM	Mean	SEM	Mean	SEM	Mean	SEM	Mean	SEM	Mean	SEM
L-Phenylalanine	0.84	0.09	1	0	0.66	0.06	0.74	0.14	0.73	0.12	0.97	0.09
L-Tyrosine	1.29	0.38	1	0	0.86	0.14	0.77	0.18	0.83	0.14	0.99	0.14
N-carbamoyl-DL-aspartic acid	1.19	0.13	1	0	1.01	0.29	0.26	0.06	1.07	0.25	0.80	0.17
Orotic acid	1.06	0.07	1	0	1.33	0.29	0.65	0.10	0.72	0.14	0.62	0.08
Phenylpyruvic acid	0.99	0.26	1	0	1.46	0.75	0.60	0.13	0.62	0.24	1.04	0.56
Phosphoenolpyruvic acid	1.18	0.41	1	0	0.06	0.02	0.02	0.00	1.16	0.49	0.77	0.14
Pyruvic acid	1.30	0.14	1	0	0.35	0.07	0.45	0.19	1.12	0.26	0.90	0.16
Succinic acid	0.87	0.02	1	0	0.94	0.09	0.94	0.04	0.94	0.07	0.92	0.13
Taurine	5.14	3.52	1	0	3.48	1.59	1.95	0.66	4.62	3.22	1.14	0.32
Uracil	0.86	0.20	1	0	0.81	0.25	0.89	0.21	1.19	0.19	0.73	0.20
Uric acid	1.00	0.26	1	0	0.82	0.18	0.65	0.22	0.72	0.18	0.77	0.05
Uridine	0.97	0.12	1	0	0.83	0.07	0.91	0.34	0.89	0.18	0.85	0.15
Uridine 5-diphosphoglucose	3.93	2.02	1	0	1.51	0.73	1.06	0.70	0.68	0.19	1.22	0.61
Xanthine	0.93	0.10	1	0	0.82	0.06	0.87	0.30	0.97	0.24	0.85	0.15
Xanthosine	0.67	0.13	1	0	0.66	0.19	0.64	0.30	0.57	0.15	0.71	0.12

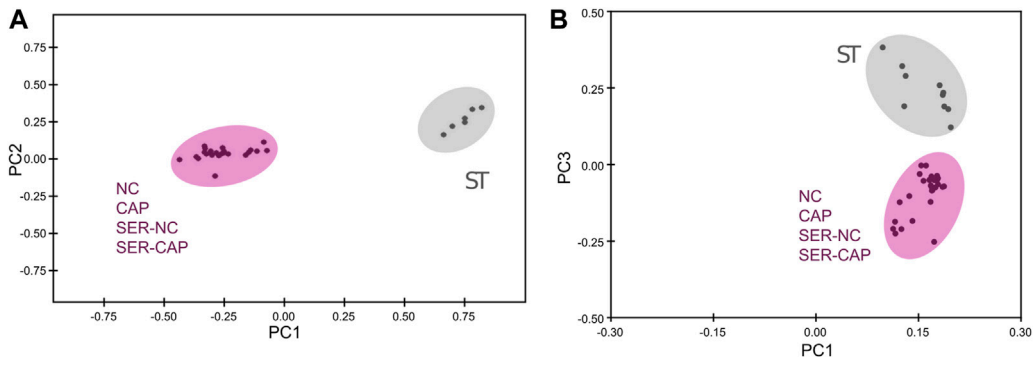

FIGURE 5
Significant metabolomic changes at the starving step. Measurement of metabolites by NMR and MS was performed after incubation under the following conditions: continuously incubated with glucose in NC (without BSA and without HCO_3^-) or CAP (with BSA and HCO_3^-); continuously incubated without glucose in NC (ST); incubated without glucose in NC condition until motility stopped (~30–40 min) and recovered with glucose in non-capacitated medium (SER-NC) or in capacitated medium (SER-CAP). **(A)** PCA score plot of metabolite profiles generated by 1D ^{1}H NMR spectra. ST sperm are surrounded by a gray circle (*N* = 6); NC, CAP, SER-NC, and SER-CAP are surrounded by a pink circle (*N* = 5) to show the different clusters. **(B)** PCA score plot of metabolite profiles generated by MS data. ST sperm are surrounded by a gray circle (*N* = 10); NC, CAP, SER-NC, and SER-CAP are surrounded by a pink circle (*N* = 7) to show the different clusters.

SER sperm during recovery, when glucose is added to starved sperm, ATP levels increase for the first 5 min, and then, in cap, but not in non-cap conditions, they decrease again (Figure 7C, right panel), indicating the time at which energy consumption pathways begin to overtake the capacitation-induced increase in ATP production via glycolysis and OxPhos.

While most metabolites either decreased or remained stable during starvation (Tables 1, 2; Supplementary Figure S5), two metabolites, AMP and carnitine, were significantly increased (Figures 8A–F). AMP levels were approximately 10-fold higher in ST sperm relative to control and SER sperm as quantitated by 1D ^{1}H-NMR (Figure 8B). In concert with their increased carnitine levels

10.3389/fcell.2023.1234221

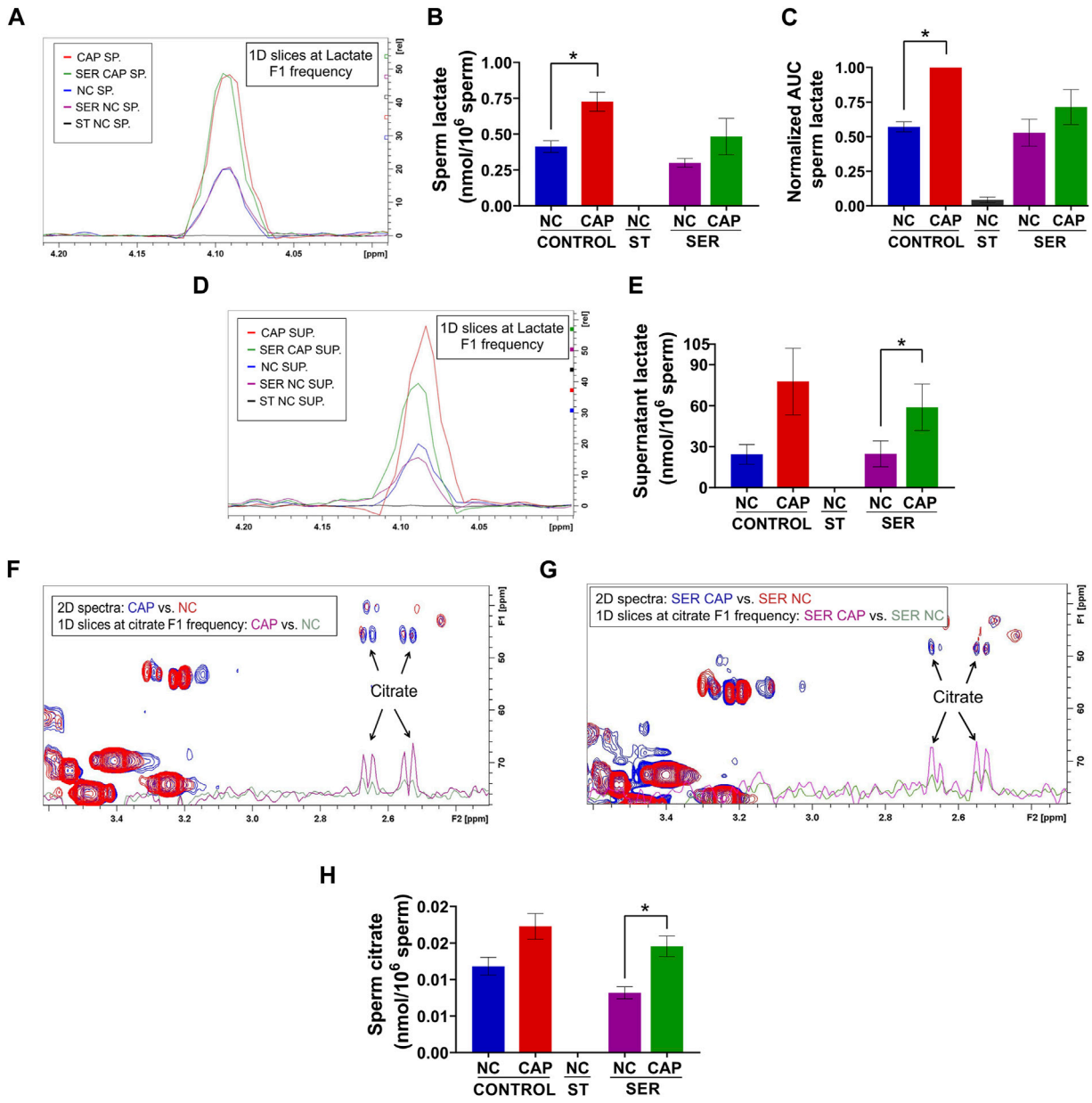

FIGURE 6
Capacitated sperm upregulate energy production metabolic pathways. Measurement of metabolites by NMR and MS was performed after incubation under the following conditions: continuously incubated with glucose in NC (without BSA and without HCO_3^-) or CAP (with BSA and HCO_3^-); continuously incubated without glucose in NC (ST); incubated without glucose in NC condition until motility stopped (~30–40 min) and recovered with glucose in non-capacitated medium (SER-NC) or in capacitated medium (SER-CAP). **(A)** Following ^{13}C-labeled glucose metabolites, 1D slices at a lactate F1 frequency of a representative 2D NMR ^1H-^{13}C HSQC experiment of sperm (SP) incubated for 60 min under the different conditions. **(B)** Sperm lactate amount determined by 2D NMR ^1H-^{13}C HSQC experiments. The results are expressed as the mean ± SEM of three independent experiments. Lactate was undetectable in NC ST sperm. T-tests between NC and CAP (control and SER) conditions were performed. * indicates a significant difference with $p < 0.05$. **(C)** AUC of the lactate MS peak of sperm incubated under the different conditions, normalized to CONTROL CAP. The results are expressed as the mean ± SEM of seven independent experiments. T-tests with Wilcoxon's matched-pair signed rank test between NC and CAP (control and SER) conditions were performed. * indicates significant difference with $p < 0.05$. **(D–E)** Idem A-B but for the supernatant (SUP) of sperm incubated for 60 min in the different conditions. * indicates a significant difference with $p < 0.05$. **(F–G)** Following ^{13}C-labeled glucose metabolites, the representative 2D NMR ^1H-^{13}C HSQC experiment showing citrate together with the 1D slices at citrate F1 frequency of the 2D spectrum of sperm incubated for 60 min under the different conditions. **(H)** Sperm citrate amount determined by 2D NMR ^1H-^{13}C HSQC experiments. The results are expressed as the mean ± SEM of three independent experiments. Citrate was undetectable in NC ST sperm. T-tests between NC and CAP (control and SER) conditions were performed. * indicates a significant difference with $p < 0.05$.

(Figures 8D–F), ST sperm had decreased levels of acetyl carnitine compared to control and SER sperm (Figures 8G, H). These two metabolites comprise the carnitine shuttle involved in lipid oxidation pathways, and our observation that their levels change during starvation suggests that, in the absence of external nutrients, sperm use lipid oxidation to get energy from endogenous sources.

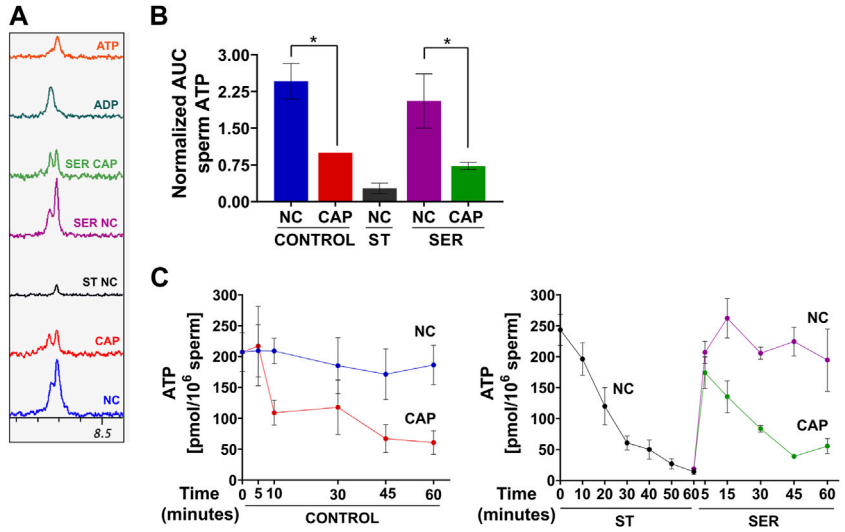

FIGURE 7
Sperm capacitation decreases intracellular ATP content. Measurement of metabolites by NMR, MS, and chemiluminescence was performed after incubation under the following conditions: continuously incubated with glucose in NC (without BSA and without HCO_3^-) or CAP (with BSA and HCO_3^-); continuously incubated without glucose in NC (ST); incubated without glucose in NC condition until motility stopped (~30–40 min) and recovered with glucose in non-capacitated medium (SER-NC) or in capacitated medium (SER-CAP). **(A)** Representative 1D ^{1}H NMR spectra showing ATP and ADP peaks of sperm incubated for 60 min under the different conditions. **(B)** AUC of the ATP MS peak of sperm incubated under the different conditions, normalized to CONTROL CAP. The results are expressed as the mean ± SEM of seven independent experiments. T-tests with Wilcoxon's matched-pair signed rank test between NC and CAP (control and SER) conditions were performed. * indicates a significant difference with $p < 0.05$. **(C)** Intracellular sperm ATP amount measured using the ATP/ADP-Glo™ Assay kit under the different conditions. The results are expressed as the mean ± SEM of at least four independent experiments.

Discussion

When mouse sperm are incubated in the absence of external nutrients (starvation step), they stop moving but remain viable. During the rescue step, the addition of energy substrates in media which support capacitation, sperm exhibit enhanced hyperactivation, fertilization, and embryo development rates (Navarrete et al., 2019; Tourzani et al., 2022). Moreover, when transferred into pseudo-pregnant females, blastocysts derived from SER-treated sperm resulted in more pups than blastocysts derived from control sperm (Navarrete et al., 2019). As a first step to understand the molecular mechanisms underlying the benefits of SER treatment, we analyzed how this treatment affected signaling and metabolic pathways involved in sperm capacitation. Capacitation is initiated when sperm are exposed to HCO_3^-, which stimulates sAC to produce cAMP and consequent activation of PKA. Activation of PKA results in an FERT tyrosine kinase-dependent increase in tyrosine phosphorylation (Alvau et al., 2016). Both pathways can be monitored by Western blotting using anti-phospho-PKA substrates and anti-pY antibodies, respectively (Krapf et al., 2010). Sperm under ST-CAP conditions exhibited a transient increase in PKA-dependent phosphorylation, followed by a sustained period of dephosphorylation extending through the time when sperm stop moving (Figure 1B). These results indicate that Ser/Thr phosphatases remain active under starvation conditions. During rescue, phosphorylation pathways recovered upon re-addition of energy metabolites, and their kinetics were indistinguishable from those of controls (Figures 1C–E).

We next sought to identify changes in the metabolic profile in sperm during starvation and recovery. Our previous studies defining SER (Navarrete et al., 2015; 2016) were performed in TYH media containing glucose and pyruvate as energy substrates. We confirmed that glucose alone is sufficient to support enhanced capacitation and fertilization in SER (Figure 2) in CD1 mice, which permitted the use of media containing only glucose-derived metabolites in the absence of external pyruvate to explore the metabolic consequences of individual nutrients. Importantly, these experiments were designed to validate the use of glucose alone for metabolomics purposes, not to explore the best capacitation media for which the addition of pyruvate might be positive as was shown for human sperm (Hereng et al., 2011). Glucose can be metabolized via glycolysis and/or the pentose phosphate pathway (PPP), both cases leading to the generation of two molecules of ATP and pyruvate. In both SER and control sperm, we showed that the pyruvate formed from exogenously metabolized glucose can enter the Krebs cycle in the mitochondrial mid-piece. This conclusion is consistent with our NMR data indicating the formation of ^{13}C citrate from ^{13}C glucose (Figures 6F–H) (see discussion of alternatives given as follows).

We used both NMR and MS metabolomics approaches to evaluate how sperm metabolite levels change during the different treatments. Each technique has specific strengths and weaknesses, and when combined, they provide synergic and complementary knowledge. NMR spectra reveal molecules present in sperm extracts without the need for prior purification. Moreover, the same sample can be used to obtain different types of spectra, including two-dimensional ^{1}H-^{1}H and ^{1}H-^{13}C. We used NMR to follow the fate of

10.3389/fcell.2023.1234221

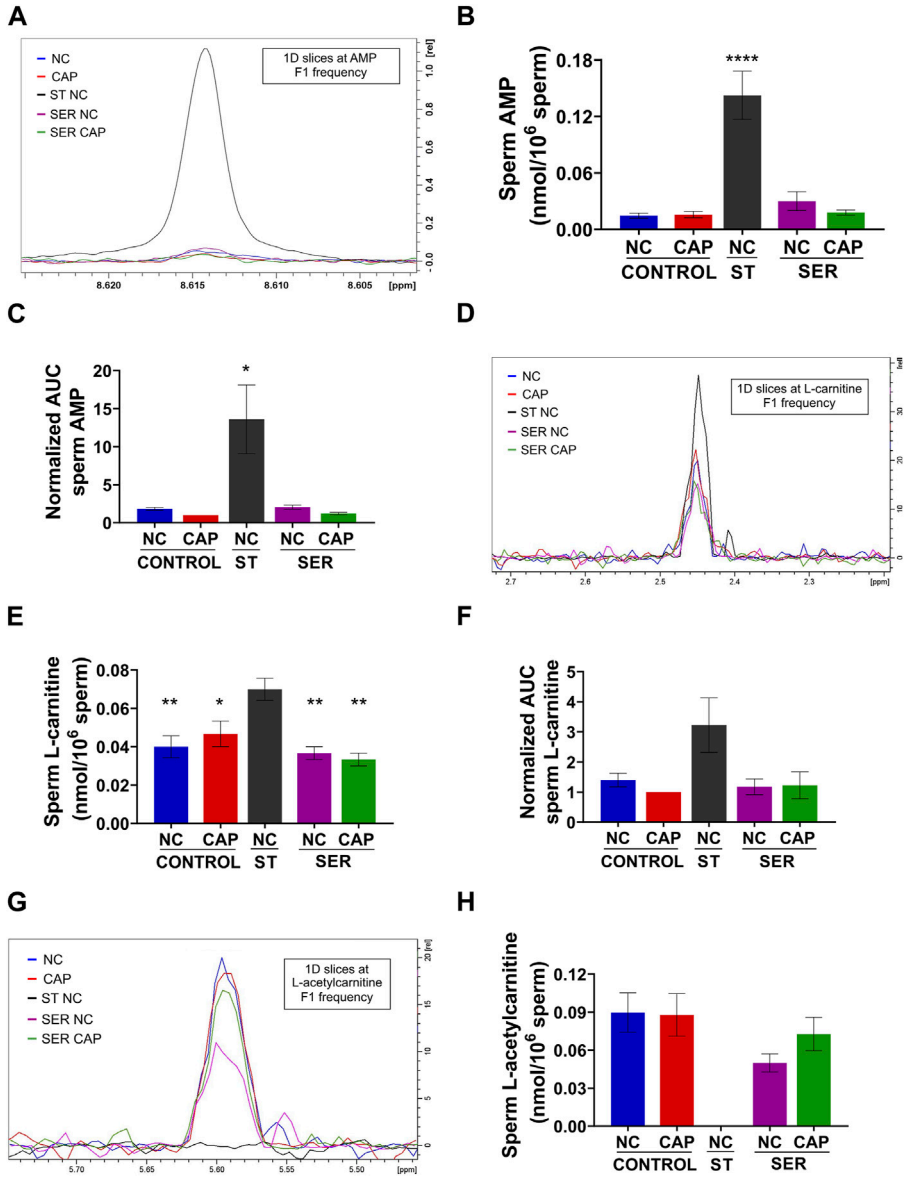

FIGURE 8
Metabolites that are significantly changed at the starving step. Measurement of metabolites by NMR and MS was performed after incubation under the following conditions: continuously incubated with glucose in NC (without BSA and without HCO_3^-) or CAP (with BSA and HCO_3^-); continuously incubated without glucose in NC (ST); incubated without glucose in NC condition until motility stopped (~30–40 min) and recovered with glucose in non-capacitated medium (SER-NC) or in capacitated medium (SER-CAP). **(A)** Representative 1D ^{1}H NMR spectra showing AMP peaks of sperm incubated for 60 min under the different conditions. **(B)** Sperm AMP amount determined by 1D NMR ^{1}H experiments. The results are expressed as the mean ± SEM of four independent experiments. ANOVA with Dunnett's multiple comparison test, comparing every condition with NC ST, was performed. **** indicates a significant difference with $p < 0.0001$. **(C)** AUC of the AMP MS peak of sperm incubated under the different conditions, normalized to CONTROL CAP. The results are expressed as the mean ± SEM of seven independent experiments. T-tests with Wilcoxon's matched-pairs signed rank test between every condition and NC ST condition were performed. * indicates a significant difference with $p < 0.05$. **(D)** 1D slices at L-carnitine F1 frequency of a representative 2D NMR ^{1}H-^{13}C HSQC experiment of sperm incubated for 60 min under the different conditions. **(E)** Sperm L-carnitine amount determined by 2D NMR ^{1}H-^{13}C HSQC experiments. The results are expressed as the mean ± SEM of three independent experiments. ANOVA with Dunnett's multiple comparisons test, comparing every condition with NC ST, was performed. * indicates a significant difference with $p < 0.05$; ** indicates a significant difference with $p < 0.01$. **(F)** AUC of the L-carnitine MS peak of sperm incubated under the different conditions, normalized to CONTROL CAP. The results are expressed as the mean ± SEM of four independent experiments. T-tests with Wilcoxon's matched-pairs signed rank test between every condition and NC ST condition were performed. **(G–H)** Idem D-E but for L-acetyl carnitine. The results are expressed as the mean ± SEM of three independent experiments. L-acetyl carnitine was undetectable in NC ST sperm. T-tests between NC and CAP (control and SER) conditions were performed.

^{13}C-glucose. However, NMR has low sensitivity, and the identification relies on comparison with available databases. In contrast, MS, which requires purification of samples under different ionization protocols for different types of molecules, provides unmatched sensitivity with more reliable metabolite identification.

In starved sperm, glycolytic intermediates were significantly reduced, and they recovered upon the addition of glucose (Table 2; Supplementary Figure S5). As predicted from extracellular flux analysis, which shows that metabolism is stimulated during capacitation (Figures 3B, C, Figure 4; Supplementary Figure S1), the metabolite profile of sperm depends on their state of capacitation (Supplementary Figure S2). The difference between non-capacitating and capacitating sperm was observed in sperm whether they were SER-treated or when they remain in the continuous presence of glucose (Supplementary Figure S2). We have shown that during capacitation sperm consume increased amounts of glucose [(Hidalgo et al., 2020) and Figure 3A]. Glucose consumed during capacitation is converted into lactate (Figures 6A–E), which is mostly secreted out of the cell (Figures 6D, E). The conversion of pyruvate, the product of glycolysis, into lactate is catalyzed by lactate dehydrogenases, including the sperm-specific lactate dehydrogenase, LDHC4. This conversion is coupled to the production of NADH oxidation to NAD^+, a metabolite essential to maintain glycolysis at the level of the sperm-specific glyceraldehyde-3-phosphate dehydrogenase (GAPDHS) (Odet et al., 2011). Consistently, LDHC4 knockout genetic mouse models are sterile (Odet et al., 2008).

In addition to lactate secretion, we also found ^{13}C acetate in the sperm incubation supernatant. This observation is consistent with that of previous work in ram (Scott et al., 1967) and bull (Melrose and Terner, 1953; Mann and Lutwak-Mann, 1981), indicating that ejaculated sperm from these species secretes ^{14}C acetate when incubated in the presence of ^{14}C glucose. Two independent pathways can explain pyruvate decarboxylation to form acetate. In one of them, radical oxygen species catalyze the oxidative decarboxylation of pyruvate to form acetate and CO_2. This conversion involves the nucleophilic attack of pyruvate by H_2O_2 and has been shown to occur in culture mammalian cells following the fate of ^{18}O-labeled H_2O_2. The second mechanism involved ketoacid dehydrogenases such as pyruvate dehydrogenase or alpha ketoglutarate dehydrogenase in a thiamine-dependent manner (Liu et al. (2018) to provide a detailed explanation of these molecular pathways of pyruvate decarboxylation).

In sperm, glucose is also metabolized via the PPP (Urner and Sakkas, 1999), and we detected two metabolites, xylulose-5-phosphate and ribose-5-phosphate (Table 2), which were reduced under starving conditions and restored after the addition of glucose. The PPP provides cells with NADPH. In most cells, the reducing power of NADPH is required to maintain biosynthetic anabolic reactions, but because sperm are terminally differentiated, anabolic reactions are not considered to play relevant roles during capacitation. Instead, NADPH is thought to be needed to protect sperm DNA, lipids, and other molecules from oxidative damage. While it remains unclear in which sperm compartment the PPP is active, hexokinase type I, which is the first step in both glycolysis and the PPP, is present in both the mid-piece (i.e., along with the mitochondria) and the principal piece (Visconti et al., 1996).

Extracellular flux analysis suggested that OxPhos is stimulated during capacitation (Figure 4; Supplementary Figure S1), and metabolite profiling confirmed that more exogenous glucose is metabolized into citrate in capacitated sperm relative to non-capacitated sperm (Figures 6F–H). Stimulation of OxPhos may also be relevant for sperm utilizing endogenous energy sources. Recently, we demonstrated that human sperm remain motile in the absence of external metabolites (Marín-Briggiler et al., 2021), which predicts that sperm can use endogenous energy sources such as lipids or amino acids, which is in agreement with previous reports in other sperm species (for review see Mann and Lutwak-Mann book, 1981). Although mouse sperm incubated in starvation media stopped moving in ~ 30 min, we found that starved mouse sperm showed increased levels of carnitine with a corresponding decrease in acetyl-carnitine (Figures 8D–H). These data suggest that starved mouse sperm stimulate lipid oxidation pathways, consistent with the hypothesis that these cells can also utilize endogenous nutrients.

Not surprisingly, another metabolite that is increased in starved sperm is AMP (Figures 8A–C). Because AMP can regulate multiple aspects of metabolism, it could contribute to SER metabolic effects. AMP binds to and activates AMP-activated kinase (AMPK), which is present in mouse sperm [Supplementary Figure S6 and (Vadnais et al., 2014)] and other mammalian sperm (Tartarin et al., 2012; Martin-Hidalgo et al., 2018), senses a low energy state, stimulates glucose uptake and lipid oxidation, and inhibits anabolic reactions (Herzig and Shaw, 2018). AMP can also regulate phosphofructokinase (PFK), the rate-limiting step of glycolysis (Kamp et al., 2007). Interestingly, PFK is regulated by the ATP: AMP ratio inside cells; PFK is stimulated when AMP is high or ATP is low. While the AMP level increases during starvation, ATP levels decrease during capacitation (Figure 7C). Thus, the ATP: AMP ratio remains favorable for high PFK activity to sustain high glycolytic rates.

Although glycolysis and OxPhos are believed to occur in different compartments, we found ^{13}C-citrate produced from ^{13}C-glucose (Figures 6F–H). These data indicate that, at least a fraction of the pyruvate formed can render the metabolites in the Krebs cycle. How pyruvate arrives in the mitochondria is not known. Some alternatives are 1) that pyruvate diffuses from the principal piece of the mitochondria where glycolysis occurs to the mitochondria in the mid-piece; 2) that lactate derived from pyruvate is the molecule diffusing from the principal piece to the mid-piece; 3) considering that lactate and acetate are released into the incubation media (Figures 6D, E; Supplementary Figure S4B), we cannot discard the fact that once secreted, these molecules can reenter the sperm by transporters localized in the mid-piece; 4) although glycolytic enzymes have been shown to be in the principal piece (Nakamura et al., 2008; Nakamura et al., 2010), it is not possible to discard the fact that lower levels of these enzymes are present in the mid-piece. The efficiency of this coupling warrants further studies. Coupling between glycolysis and oxidative phosphorylation has been reported for sperm of other species (Mann and Lutwak-Mann, 1981), and it is suggested by our previous and current findings that glucose alone is sufficient for the capacitation-induced increase in OCR Seahorse parameters; 5) despite this evidence, as a fifth alternative, we cannot discard the fact that the glucose-derived citrate formed as a result of a cytosolic reaction since cytosolic citrate synthase has been shown to be present in mammalian sperm outside the mitochondrial compartment (Kang et al., 2022).

In summary, in this paper, we applied methods for studying metabolism in sperm during capacitation as well as following

starvation and recovery. Following the fate of ^{13}C-glucose by NMR allowed quantitative assessment of glycolysis and provided direct evidence that large amounts of glucose-derived pyruvate are released into the media after conversion to lactate and acetate (Figures 6D, E; Supplementary Figure S4B). In addition, our results indicate a significant increase in AMP (Figures 8A–C), which is likely the consequence of ATP hydrolysis. In addition to the aforementioned possible roles of AMP and carnitine, reduced levels of ATP are expected to affect multiple signaling pathways relevant for sperm capacitation, such as phosphorylation and ion homeostasis. For example, we recently showed that when sperm incubated under starving conditions become immotile, intracellular Ca^{2+} ($[Ca^{2+}]_i$) levels are highly increased (Sánchez-Cárdenas et al., 2021). This increase in $[Ca^{2+}]_i$ is likely due to inactivation of the ATP-dependent Ca^{2+} ATPase PMCA4. The starvation-induced increase in $[Ca^{2+}]_i$ also occurs in sperm lacking the sperm-specific Ca^{2+} channel complex CatSper (Sánchez-Cárdenas et al., 2021), suggesting that, in addition to the CatSper complex, other Ca^{2+} transporters are present in mouse sperm. It is noteworthy that SER treatment rescued the infertile phenotype of sperm *in vitro* from mice deficient in C2CD6, one of the CatSper subunits (Yang et al., 2022). In bovine sperm, an increase in $[Ca^{2+}]_i$ under ATP starvation by pharmacological inhibition of glycolysis and OxPhos was reported, but the calcium influx was reported to be via CatSper (Dahan and Breitbart, 2022). Finally, one of the most surprising consequences of starvation and recovery is the effects on post-fertilization events such as embryo development (Navarrete et al., 2019; Tourzani et al., 2022; Al-Hafedh and Cedden, 2023). We speculate that SER improvements in embryo development rates are due to changes in the sperm epigenetic information. In somatic cells, it is well-established that histone-modifying enzymes are regulated by changes in metabolites (Reid et al., 2017). Although the sperm chromatin is highly condensed due to histone replacement by protamine during spermiogenesis, a considerable number of histones remain in mature sperm (Jung et al., 2017). Then, the metabolite changes observed during SER treatment could impact posttranslational modifications of sperm-retained histones and affect early embryo development after fertilization. Alternatively, reduced levels of ATP can affect the concentration of small non-coding RNAs in sperm, which have also been proposed to mediate epigenetic transmission to the embryo (Sharma et al., 2016; Conine et al., 2018). Although, at the moment, it is too early to understand how the SER sperm regulates early embryo development, studies such as ours are a necessary step to gain an insight into why SER-treated sperm exhibit increased sperm functionality.

Material and methods

Reagents

The following chemicals were purchased from the given sources (codes between parentheses indicate the catalog number of the respective compound): sodium bicarbonate ($NaHCO_3$) (S-5761); bovine serum albumin (BSA) (fatty acid-free) (A0281), Tween-20 (P7949), fish skin gelatin (G-7765), concanavalin A (L7647), dbcAMP (D0627), IBMX (I5879), and rabbit monoclonal anti-phospho-PKA substrates (anti-pPKAS) (7,906) were purchased from Sigma (St. Louis, MO, United States). Anti-phosphotyrosine (anti-pY) monoclonal antibody (clone 4G10) was obtained from Millipore (Billerica, MA, United States). Horseradish peroxidase-conjugated anti-mouse and anti-rabbit IgGs were purchased from Jackson ImmunoResearch Laboratories (West Grove, PA, United States) and GE Life Sciences (Pittsburgh, PA, United States), respectively. Acrylamide/bis solution (30%) (161-0138) and β-mercaptoethanol (BP176-100) were obtained from Bio-Rad (Hercules, CA, United States). HEPES (BP310-100) was purchased from Roche (Hatfield, PA, United States), and the Amplex®Red Glucose/Glucose Oxidase Assay Kit was obtained from Invitrogen (Grand Island, NY, United States) (A22189). D-glucose (U-13C6, 99%) (CLM-1396), TMSP-2,2,3,3-D4 (D, 98%), sodium-3-trimethylsilylpropionate (DLM-48), maleic acid disodium salt monohydrate (13C4, 99%) (CLM-10892), deuterium oxide (D, 99.9%) (DLM-4-100), and HEPES (D18, 98%) (DLM-3786) were purchased from Cambridge Isotope Laboratories (Tewksbury, MA, United States). ADP/ATP-GloTM was obtained from Promega (Madison, WI, United States), and Seahorse XFe96 FluxPak mini was purchased from Agilent (102601-100) (Santa Clara, CA, United States).

Animals

All procedures involving experimental animals were performed in accordance with Protocol 2019–0008 approved by the University of Massachusetts Amherst Institutional Animal Care and Use Committee (IACUC). Cauda epididymal mouse sperm were collected from CD1 retired male breeders (Charles River Laboratories, Wilmington, MA, United States). Mouse oocytes were collected from 8–10-week-old superovulated CD1 females (Charles River Laboratories, Wilmington, MA, United States). For superovulation, females were injected with 5 IU pregnant mare serum gonadotropin (PMSG) (Lee BioSolutions, cat #493-10) and 5 IU human chorionic gonadotrophin (hCG) (Sigma, cat #CG5) 48 h later, and cumulus–oocyte complexes (COCs) were collected 13 h post-hCG injection.

Media

Modified Toyoda–Yokoyama–Hosi (mTYH) medium was used for sperm (Toyoda et al., 1971). The non-capacitating (NC) medium used contained the following: NaCl (119.3 mM), KCl (4.7 mM), $CaCl_2.2H_2O$ (1.71 mM), KH_2PO_4 (1.2 mM), $MgSO_4.7H_2O$ (1.2 mM), HEPES (20 mM), glucose (5.56 mM), and sodium pyruvate (0.51 mM). For capacitating (CAP) conditions, 15 mM $NaHCO_3$ and 5 mg/mL BSA were added. These media were also used containing only glucose (5.56 mM) or only pyruvate (0.51 mM) or devoid of both energy substrates (starving (ST) medium). In all cases, pH was adjusted to 7.2–7.4 with NaOH. For glucose consumption measurements, glucose was used at a final concentration of 1 mM (Hidalgo et al., 2020). For NMR experiments, ^{13}C uniformly labeled glucose (5.56 mM) and deuterated HEPES (20 mM) were used (NMR TYH). For Seahorse experiments, HEPES was used at a final concentration of 1 mM (Seahorse TYH). Both non-capacitating and capacitating

media contained 5 mg/mL BSA. The capacitating medium also contained dbcAMP (1 mM) and IBMX (0.1 mM), as shown previously (Balbach et al., 2020a).

The Toyoda–Yokoyama–Hosi (TYH) medium (IVF TYH) was used for sperm fertilization assay, consisting of NaCl (119.3 mM), KCl (4.7 mM), $CaCl_2.2H_2O$ (1.71 mM), KH_2PO_4 (1.2 mM), $MgSO_4.7H_2O$ (1.2 mM), glucose (5.56 mM), sodium pyruvate (0.51 mM), $NaHCO_3^-$ (25.1 mM), 4 mg/mL BSA, 10 μg/mL gentamicin, and 0.0006% phenol red at pH 7.4 equilibrated with 5% CO_2. This medium was also used containing only glucose (5.56 mM) or only pyruvate (0.51 mM) or devoid of both energy substrates (ST medium). For oocyte collection, Tyrodes's lactate–HEPES (TL-HEPES) was used, consisting of NaCl (114 mM), KCl (3.22 mM), $CaCl_2.2H_2O$ (2.04 mM), $NaH_2PO_4.2H_2O$ (0.35 mM), $MgCl_2.6H_2O$ (0.49 mM), $NaHCO_3^-$ (2.02 mM), lactic acid (sodium salt) (10 mM), and HEPES (10.1 mM) at pH 7.4.

Sperm incubation and SER treatment

Male mice were culled, and both cauda with 3–5 excisions were placed in 2 mL ST medium. We let sperm swim out for 15 min at 37°C. Cauda were removed, and sperm were washed for 5 min at 300 × g and resuspended in 2 mL ST medium. Samples were centrifuged for an additional 5 min at 150 × g at RT, supernatants removed, and sperm resuspended in ST medium. Sperm from the different mice were pooled together, and an aliquot was separated for sperm counting. During collection and washing (~20 min), sperm remained motile, which were then separated and incubated under six different conditions. Incubation conditions 1 (NC) and 2 (CAP): for regular NC and CAP conditions, immediately after washing, sperm were resuspended in new tubes containing media to create 1× NC and CAP conditions. After 60 min of incubation, these tubes were processed. Incubation conditions 3 (ST-NC) and 4 (ST-CAP): for starved in NC and for starved in CAP conditions, pooled sperm were resuspended in either the same ST media or in ST media containing BSA and HCO_3^-. Upon resuspension, sperm were continuously checked until they stopped moving (~30–40 min). Once sperm stopped moving, they were processed to be used. Incubation conditions 5 (SER-NC) and 6 (SER-CAP): sperm were incubated in the ST medium and continuously checked until they stopped moving. Once they stopped, they were transferred to be rescued in new tubes containing media with the respective nutrient (either glucose or pyruvate or both) either under 1× NC (SER-NC) or 1x CAP (SER-CAP) conditions. These last two conditions were ready to be processed after 60 min of incubation. In all experiments, sperm concentration varied between 2 and 5 million/ml. For IVF experiments SER treatment was carried out as previously stated by Navarrete et al. (2019); Navarrete et al. (2016). Briefly, sperm were incubated in the IVF TYH ST medium. Once the sperm stopped moving, a fraction of them was resuspended in IVF TYH medium containing glucose, pyruvate, or both energy substrates and was used for insemination.

For Seahorse experiments, we adapted the procedure previously described (Balbach et al., 2020a). Briefly, after washing in the ST Seahorse TYH medium, sperm were aliquoted to tubes containing the NC medium with glucose and BSA or to tubes containing the ST medium with BSA. Then, sperm under both conditions were plated (180 μL) in Seahorse-compatible well plates, and after centrifuging, the cell cartridge was placed in the Seahorse equipment. At this point, sperm in the ST medium were already starved for ~20 min. Because those sperm inside the Seahorse will be under starving conditions for an additional 10 min (before the addition of the medium with glucose for SER sperm or before more starving medium for ST and never rescued sperm), sperm under the SER condition will be starved for a total time of ~30–40 min (the time that it usually takes for the sperm to stop moving).

Western blot

Upon the completion of the aforementioned different treatments, sperm were collected by gentle centrifugation (3,000 × g), washed in 1 mL of PBS, resuspended in Laemmli sample buffer (Laemmli, 1970) without β-mercaptoethanol, boiled for 5 min, and centrifuged at 12,100 × g. The pellets were discarded and supernatants supplemented with 5% β-mercaptoethanol and boiled for 4 min. Protein extracts were separated by 8% SDS-PAGE and electro-transferred to PVDF membranes (Millipore). Immunoblotting was conducted with anti-pPKAs and anti-pY antibodies sequentially as previously described (Krapf et al., 2010). Briefly, PVDF membranes were blocked with 5% fat-free milk in TBS containing 0.1% Tween 20 (T-TBS) for anti-pPKAs and with 5% fish gelatin for anti-pY in PBS containing 0.1% Tween 20 (T-PBS). Antibodies were used at a final concentration of 1:10.000. Secondary antibodies were diluted in T-TBS or T-PBS (1:10.000) for anti-pPKAs and anti-pY, respectively. Before conducting anti-pY Western blotting, the PVDF membranes used for pPKAs were stripped at 55°C for 20 min in 2% SDS, 0.74% β-mercaptoethanol, and 62.5 mM Tris, pH 6.5, and then washed six times for 5 min each in T-TBS prior to reprobing. An enhanced chemiluminescence ECL Plus Kit (GE Healthcare) and ECL regular were used for the detection of pPKAs and pY signals, respectively. Quantitative analysis was performed using ImageJ 1.47 V software (National Institutes of Health, United States). Regions of interest (ROIs) used for quantification are indicated by a # on the left of the respective Western blot. The extent of hexokinase tyrosine phosphorylation (see arrow in Figure 1A, lower panel) does not change during capacitation (Porambo et al., 2012; Chung et al., 2014) and was used as the loading control. The optical density of the bands was measured and relativized to tyrosine-phosphorylated hexokinase.

Computer-assisted sperm analysis measurements

Sperm suspensions (30 μL; 2×10^6 sperm/ml) from the different treatments were loaded into a pre-warmed chamber slide (depth 100 μm) (Leja slide, Spectrum Technologies, Aurora, IL, United States) and placed on a microscope stage at 37°C. Sperm motility was examined using the CEROS computer-assisted sperm analysis (CASA) system (Hamilton Thorne Research, Beverly, MA, United States). The default settings include the following

parameters: frames acquired: 90; frame rate: 60 Hz; minimum cell size: 4 pixels; static head size: 0.13–2.43; static head intensity: 0.10–1.52; static head elongation: 5–100. At least five microscopy fields corresponding to a minimum of 200 sperm were analyzed for each treatment in each experiment. Hyperactivated sperm were those having the following parameters: curvilinear velocity (VCL) > 271.00 μm/s, linearity (LIN) < 50.00%, and amplitude of lateral head (ALH) > 3.50 μm.

In vitro fertilization

COCs were collected in TL-HEPES 13 h post hCG and washed under respective TYH medium conditions (with glucose and pyruvate, with glucose only, or with pyruvate only) prior to being placed in the insemination droplet under the proper TYH medium conditions (with glucose and pyruvate, with glucose only, or with pyruvate only). Sperm were incubated as described previously, and approximately 100,000 sperm were added to a 90 μL insemination droplet. After 4 h, oocytes were washed in TYH (containing glucose and pyruvate) and allowed to culture for 20 h. The following day, fertilization was determined by visualization of cleavage into a 2-cell stage embryo.

Glucose consumption measurement

Glucose consumption measurement was performed as previously described by Hidalgo et al. (2020)); Hidalgo et al. (2020). Briefly, sperm under the different conditions were prepared as described previously, and 50 μL of the sperm suspension was taken every hour for 3 h of incubation. Sperm were then removed by centrifugation at 12,000 × g for 3 min, and the supernatant was recovered and frozen at −80°C until analysis. The glucose concentration was measured using the fluorescent Amplex®Red Glucose/Glucose Oxidase Assay Kit. Fluorescence was measured in duplicate in 96-well plates (Corning®#3915, New York, United States). In each well, 3 μL of the sample was added to 47 μL of 1x reaction buffer followed by 50 μL of the reaction mix. The reaction mix contained (concentrations are given in parentheses) Amplex®Red reagent (100 μM), horseradish peroxidase (0.2 U/ml), and glucose oxidase (2 U/ml). After 30 min of incubation at 23°C, fluorescence was measured using the fluorimeter capabilities of the POLARstar Omega equipment (BMG LABTECH, Germany) with a wavelength excitation of 540 nm and wavelength emission of 590 nm. Each assay included a "blank" sample containing the mTYH medium without glucose and standard concentration curves obtained in the presence and in the absence of BSA. After correction of all relative light unit (RLU) values with background measurement (blank sample), RLU values were averaged for each sample, and the glucose concentration was determined using the linear equation of the glucose standard curve (y = mx + b), where "y" was RLU, "x" is the glucose concentration, "m" is the slope, and "b" is the y-intercept. To calculate glucose consumption, we subtracted the remnant glucose concentration in the media that we measured after 1, 2, and 3 h of incubation from the initial glucose concentration, equal to 1 mM (time 0). These glucose concentration data were represented over time. Each equation line was calculated, and the slope represented the average of glucose consumption by unit time (hour) over a 3-h incubation period corrected by the sperm concentration in each experiment. This value was used to calculate the average ± SEM of each independent measurement indicated as the glucose consumption rate.

Seahorse measurements

Seahorse measurements were performed as previously described by Balbach et al. (2020a). In brief, the sensor cartridge was hydrated with H_2O overnight in a 37°C non-CO_2 incubator. The extracellular flux analyzer 96-well cell plate was coated with 0.5 mg/mL (w/v) concanavalin A and dried overnight at RT. The following morning, H_2O in the utility plate was replaced with 200 μL calibrant per well and incubated for at least 1 h in a 37°C non-CO_2 incubator. Port A was filled with Seahorse TYH containing glucose or with ST Seahorse TYH. Port B was filled with 10 mM dbcAMP and 1 mM IBMX in every even number column and 1 mM DMSO (vehicle) in every uneven column, in the corresponding medium (Seahorse TYH containing glucose or with ST Seahorse TYH). The injection of the port B content to sperm starts the recovery process and capacitation in the corresponding wells (as the addition creates dilution of 10 times, glucose, dbcAMP, and IBMX are 10 X). For one plate, sperm from six mice were isolated as described previously. After washing with the ST Seahorse TYH medium, sperm were aliquoted to tubes containing 3 mL NC Seahorse TYH medium with glucose and BSA or to tubes containing ST Seahorse TYH medium with BSA. Then, 180 μL of sperm suspension (1.2×10^6 sperm/well) under both conditions was plated in the corresponding wells of the concanavalin A-coated cell plate. The four corner wells were filled with the Seahorse TYH medium only for background correction. The plate was centrifuged at 250 × g for 1 min, rotated by 180°, and centrifuged again at 250 × g for 1 min.

A template was generated in the Agilent Seahorse XFe96 analyzer according to these details: one cycle of basal measurement, port A injection and one cycle of measurement, and port B injection and 18 cycles of measurement. Each cycle of measurement was 2 min of mixing plus 3 min of measurement. For each condition, 7/8 replicates were measured. After successful calibration, the utility plate was replaced with the sperm plate. The Seahorse analyzer kinetically and simultaneously measures glycolysis and OxPhos. The conversion of glucose to lactate by glycolysis with lactate being the primary source of free protons acidifies the medium. Glycolysis is determined by measuring the rate of proton release or the extracellular acidification rate (ECAR). OxPhos is determined by measuring the oxygen consumption rate (OCR).

Data were analyzed by first removing the first data point (basal measurement) and subtracting the first time point to every other time point to make all data start at the zero time point. Then, every replicate was subtracted with its initial value to make all of them start at 0, showing the change from its initial value (Δ ECAR or Δ OCR). The mean of all the replicates was obtained, and the area under that curve (AUC) was calculated. To compare between experiments, AUC data were normalized: all AUCs were subtracted with the minor of them and then divided by the value of control CAP (for control conditions) or by the value of the SER-CAP condition (for starved and SER conditions) (normalized AUC Δ ECAR or normalized AUC Δ OCR).

Nuclear magnetic resonance

NMR sample preparation

For every condition, sperm from six mice (~90 × 10^6 sperm/condition) were isolated and incubated as described previously. When tubes were ready to be processed, the supernatant and sperm were separated by centrifugation for 5 min at 300 × g at RT. The supernatant was transferred to a 15-mL falcon tube. A volume of 100 µL of the supernatant was transferred to a new tube, and ice-cold methanol was added to obtain a final concentration of 80% methanol. The tubes were incubated for 5 min in dry ice and then vortexed and then moved to wet ice and stored at −80°C overnight. Sperm were washed with PBS twice, and the supernatant was removed. Ice-cold methanol was added to the sperm pellet to obtain a final concentration of 80% methanol. The tubes were incubated for 5 min in dry ice and vortexed until the pellet was resuspended. The tubes were moved to wet ice and stored at −80°C overnight. As controls, the different media were also treated with 80% methanol, in the same way used for the samples. Supernatant samples, sperm samples, and control media were centrifuged for 20 min at 20,000 × g at 4°C. Supernatants were transferred to a new tube on ice, dried using a compact, integrated vacuum concentrator (SpeedVac™), and stored at −80°C until NMR analysis. Samples and controls were resuspended in 520 µL of 5 µM 3-(trimethylsilyl) propionic-(2,2,3,3-d4) acid sodium salt (TSP) and 25 µM ^{13}C maleic acid solution in D_2O. TSP was used as the frequency standard (δ = 0.00 ppm), and ^{13}C maleic acid was used for quantification of ^{13}C glucose metabolites in 2D ^{1}H-^{13}C HSQC spectra. Aliquots of 520 µL were transferred into standard 5-mm NMR tubes for NMR measurements.

NMR experiments and data processing

All NMR spectra were acquired on a Bruker AVANCE III solution-state NMR spectrometer equipped with a liquid helium-cooled QCI (H/F, C, N, P), deuterium lock, and a cryoprobe operating at a frequency of 600.259972 MHz for proton and 150.934614 MHz for carbon. All NMR data were collected at T = 298 K. Nonuniform sampling (NUS) schedules were generated using a Poisson gap distribution with a sinusoidal weight of 2 and a random seed generator. The same 50% NUS schedule and seed were used for all ^{1}H-^{13}C HSQC experiments. The spectral widths along the direct ^{1}H and the indirect ^{13}C dimensions were set at 6,009.615 and 19,623.264 Hz, respectively. The number of complex points in the direct dimension was set at 1 K, and in the indirect dimension, it was set at 105 with a 50% NUS sampling schedule for ^{1}H-^{13}C HSQC experiments. The 50% NUS schedule and seed were used for ^{1}H-^{1}H TOCSY experiments. The spectral width along both the direct and indirect ^{1}H dimensions was set at 6,009.615 Hz. The number of complex points in the direct dimension was set at 1,024, and in the indirect dimension, it was set at 512 with a 50% NUS sampling schedule. The number of scans for the 1D ^{1}H experiments was set to 256 (d1 = 10.0 s). The number of scans for the 2D ^{1}H-^{13}C HSQC experiments was set to 96 (d1 = 2.0 s). The transmitter frequency offset was set to 75 ppm in the ^{13}C dimension and 4.7 ppm in the ^{1}H dimension. The number of scans for the 2D ^{1}H-^{1}H TOCSY experiments was set to 16 (d1 = 2.0 s). The transmitter frequency offset was set to 4.7 ppm in both the ^{1}H dimensions. The spectral data were processed using the TopSpin 3.6.4 software package. The NUS data were reconstructed using the cs mode in TopSpin 3.6.4 to generate the same number of direct dimension data points and twice the number of indirect dimension data points. Both the NUS and uniform sampling (US) NMR data were zero-filled, Fourier-transformed, and manually phase-corrected to yield a final digital resolution of 2,048 (N2) 2,048 (N1) points.

Data analysis

We assigned the metabolite peaks by comparing the chemical shifts of the 1D ^{1}H, 2D ^{1}H-^{13}C HSQC, and ^{1}H-^{1}H TOCSY NMR spectra with those from the reference spectra available in the Biological Magnetic Resonance Data Bank (BMRB) (Ulrich et al., 2008) and the Human Metabolome Database (HMDB) (Wishart et al., 2007). Quantification of metabolites was performed using Bruker TopSpin 3.6.4 software. Most metabolites (lactate, glucose, citrate, carnitine, acetyl carnitine, and acetic acid) were quantified in 2D ^{1}H-^{13}C HSQC spectra using 25 µM ^{13}C-labeled maleic acid as an internal standard. NAD, ATP, ADP, and AMP were quantified in 1D ^{1}H spectra using 5 µM TSP as an internal standard.

Mass spectrometry

LC-MS sample preparation

For every condition, sperm (5 × 10^6 sperm/tube) were isolated and incubated as described previously. Sperm conditions and control media were run in quadruplicates. Sample prep for MS was the same as for NMR. Briefly, when tubes were ready to be processed, sperm were separated by centrifugation for 5 min at 300 × g, RT and washed with PBS twice. Ice-cold methanol was added to the sperm pellet to obtain a final concentration of 80% methanol, incubated for 5 min in dry ice, and vortexed until the pellet was resuspended. The tubes were then moved to wet ice and incubated at −80°C overnight. The following day, sperm samples were centrifuged for 20 min at 20,000 × g at 4°C. Supernatants were transferred to a new tube on ice, SpeedVacced, and stored at −80°C until running MS. Samples were sent on dry ice to the Memorial Sloan Kettering Cancer Center, New York, NY, United States. For sample resuspension for LC-MS/MS analysis, the tubes were placed on wet ice, and 30 µL of mobile phase A (MPA) was added and vortexed until the pellet was resuspended. Tubes were incubated on ice for 20 min, vortexing every 5 min. Samples were centrifuged for 20 min at 20,000 × g, 4°C, and 25 µL of the supernatant was transferred into LC vials for injection.

LC-MS/MS analysis

Ion-pair LC-MS/MS analysis was performed by LC separation on a Zorbax RRHD Extend-C18 column (150 mm × 2.1 mm, 1.8 µm particle size, Agilent Technologies) and using a gradient of solvent A (10 mM tributylamine and 15 mM acetic acid in 97:3 water: methanol) and solvent B (10 mM tributylamine and 15 mM acetic acid in methanol) according to the manufacturer's instructions (MassHunter Metabolomics dMRM Database and Method, Agilent Technologies).

Intracellular ATP measurements

For every condition, sperm were isolated and incubated as described previously. To determine nucleotide concentration, sperm were centrifuged at 1,700 × g for 5 min, and supernatants were discarded. Sperm pellets were resuspended in 80 µL of boiling lysis buffer (Tris 100 mM and EDTA 4 mM, pH 7.75), and the suspension was incubated at 95°C for 5 min to allow the release of nucleotides. Finally, cells were removed by centrifugation at 12,000 × g for 5 min, and the final volume of the remaining supernatant was corrected to 100 µL with lysis buffer and stored at −80°C until use. ATP concentration was measured using a commercial firefly luciferin–luciferase assay following the manufacturer's instructions (ADP/ATP-Glo™). Briefly, 15 µL of each sample (sperm lysate) was added to a well of a 96-well white wall clear bottom plate (Corning® # 3392, New York, United States). Then, 5 µL of 4% trichloroacetic acid solution (TCA) was added to each well and incubated for 10 min at 23°C. Then, 5 µL of the neutralization solution was added to each well and incubated for 5 min at 23°C. Then, 25 µL of the ATP detection reagent was added, and after 10 min of incubation at 23°C, bioluminescence was measured using a microplate luminometer (POLARstar Omega, BMG LABTECH, Germany) controlled by Omega software (Version 5.11, BGM LABTECH, Germany). Standard curves were generated according to the manufacturer's instructions using ATP concentrations ranging from 0 to 200 picomoles. All samples and standards were measured in duplicate. Relative light units (RLU) obtained from the blank sample were subtracted from the RLU measured for each ATP standard concentration and samples incubated under different conditions. After correction, RLU were averaged for each sample, and the ATP concentration was determined by using the linear equation generated using the ATP standard curve (y = mx + b), where "y" was the RLU, "x" was the ATP concentration, "m" was the slope, and "b" was the y-intercept.

Statistical analysis

Statistical analyses were performed using GraphPad Prism 8.0.2 (GraphPad Software). All data are shown as the mean ± SEM. Statistical significance between two groups was determined using two-tailed t-tests for parametric data and the Wilcoxon matched-pair signed rank test for nonparametric data. Statistical significance between multiple groups was determined using one-way ANOVA with Tukey's or Dunnett's multiple comparison test for parametric data and with Friedman's test and Dunn's multiple comparison test for nonparametric data. The statistical test performed in each figure is indicated in the Figure legend. Differences were considered significant if $*p < 0.05$, $**p < 0.01$, $***p < 0.001$, and $****p < 0.0001$. For NMR data statistical analysis, each NMR spectrum was reduced to 250 frequency bins (0.04 ppm bin size) using Bruker AMIX software version 4.01. A bin is the sum of the intensity values for a fixed number of consecutive points. Spectral regions within the range of 0 ppm–10 ppm were analyzed after deleting the regions between 4.7 and 4.86 ppm and between 3.06 and 3.34 ppm that contained the residual water peak and the methanol signal, respectively. NMR spectra were normalized (such that the total intensity of each spectrum is equal to 1) and mean-centered prior to statistical analysis. PCA was performed using the AMIX tool-kit, suitable for performing various types of multivariate data analysis and multi-group data analysis and visualizing the results. For MS PCA, AUC values for each condition were z-scored. PCA was performed using the Python scikit-learn library.

Data availability statement

The original contributions presented in the study are included in the article/Supplementary Material, further inquiries can be directed to the corresponding authors.

Ethics statement

The animal study was reviewed and approved by the University of Massachusetts-Amherst Institutional Animal Care and Use Committee (IACUC).

Author contributions

Conceptualization: AR, PV, LL, and JB. Methodology: AR, JF, SN, JC, and AS. Investigation: AR, SN, DM-H, MG, MB, SV, AS, and JF. Visualization: AR, JF, and PV. Funding acquisition: PV, LL, and JB. Supervision: PV. Writing—original draft: AR, MB, LL, JB, and PV. All authors contributed to the article and approved the submitted version.

Funding

This study was supported by NIH grants HD-038082 (to PV) and HD088571 (to JB, LL, and PV). DM-H was the recipient of a post-doctoral award from the Government of Extremadura (Spain) and by Fondo Social Europeo (PO14005). AR was supported by a fellowship from the Lalor Foundation.

Conflict of interest

The authors declare that the research was conducted in the absence of any commercial or financial relationships that could be construed as a potential conflict of interest.

Publisher's note

Supplementary material

The Supplementary Material for this article can be found online at: https://www.frontiersin.org/articles/10.3389/fcell.2023.1234221/full#supplementary-material

References

Al-Hafedh, S., and Cedden, F. (2023). The massive impact of ram's sperm starvation on the fertilization and blastocyst rates in terms of sperm quality and capacitation. *Tarim. Bilim. Derg.* 29, 455–463. doi:10.15832/ankutbd.998067

Alvau, A., Battistone, M. A., Gervasi, M. G., Navarrete, F. A., Xu, X., Sánchez-Cárdenas, C., et al. (2016). The tyrosine kinase FER is responsible for the capacitation-associated increase in tyrosine phosphorylation in murine sperm. *Dev* 143, 2325–2333. doi:10.1242/dev.136499

Amaral, A. (2022). Energy metabolism in mammalian sperm motility. *WIREs Mech. Dis.* 14, e1569. doi:10.1002/wsbm.1569

Austin, C. R. (1951). Observations on the penetration of the sperm in the mammalian egg. *Aust. J. Sci. Res.* 4, 581–596. doi:10.1071/BI9510581

Balbach, M., Buck, J., and Levin, L. R. (2020a). Using an extracellular flux analyzer to measure changes in glycolysis and oxidative phosphorylation during mouse sperm capacitation. *J. Vis. Exp.*, 1–7. doi:10.3791/60815

Balbach, M., Gervasi, M. G., Hidalgo, D. M., Visconti, P. E., Levin, L. R., and Buck, J. (2020b). Metabolic changes in mouse sperm during capacitation. *Biol. Reprod.* 103, 791–801. doi:10.1093/biolre/ioaa114

Chang, M. C. (1951). Fertilizing capacity of spermatozoa deposited into the fallopian tubes. *Nature* 168, 697–698. doi:10.1038/168697b0

Chung, J.-J. J., Shim, S.-H. H., Everley, R. A., Gygi, S. P., Zhuang, X., and Clapham, D. E. (2014). Structurally distinct Ca2+ signaling domains of sperm flagella orchestrate tyrosine phosphorylation and motility. *Cell* 157, 808–822. doi:10.1016/j.cell.2014.02.056

Conine, C. C., Sun, F., Song, L., Rivera-Pérez, J. A., and Rando, O. J. (2018). Small RNAs gained during epididymal transit of sperm are essential for embryonic development in mice. *Dev. Cell* 46, 470–480.e3. doi:10.1016/J.DEVCEL.2018.06.024

Dahan, T., and Breitbart, H. (2022). Involvement of metabolic pathway in the sperm spontaneous acrosome reaction. *Theriogenology* 192, 38–44. doi:10.1016/J.THERIOGENOLOGY.2022.08.018

Ferramosca, A., and Zara, V. (2014). Bioenergetics of mammalian sperm capacitation. *Biomed. Res. Int.* 2014, 902953. doi:10.1155/2014/902953

Ferrick, D. A., Neilson, A., and Beeson, C. (2008). Advances in measuring cellular bioenergetics using extracellular flux. *Drug Discov. Today* 13, 268–274. doi:10.1016/J.DRUDIS.2007.12.008

Gervasi, M. G., and Visconti, P. E. (2016). Chang's meaning of capacitation: A molecular perspective. *Mol. Reprod. Dev.* 83, 860–874. doi:10.1002/mrd.22663

Gervasi, M. G., and Visconti, P. E. (2017). Molecular changes and signaling events occurring in spermatozoa during epididymal maturation. *Andrology* 5, 204–218. doi:10.1111/andr.12320

Hereng, T. H., Elgstøen, K. B. P., Cederkvist, F. H., Eide, L., Jahnsen, T., Sklhegg, B. S., et al. (2011). Exogenous pyruvate accelerates glycolysis and promotes capacitation in human spermatozoa. *Hum. Reprod.* 26, 3249–3263. doi:10.1093/humrep/der317

Herzig, S., and Shaw, R. J. (2018). Ampk: guardian of metabolism and mitochondrial homeostasis. *Nat. Rev. Mol. Cell Biol.* 19, 121–135. doi:10.1038/NRM.2017.95

Hidalgo, D. M., Romarowski, A., Gervasi, M. G., Navarrete, F., Balbach, M., Salicioni, A. M., et al. (2020). Capacitation increases glucose consumption in murine sperm. *Mol. Reprod. Dev.* 87, 1037–1047. doi:10.1002/mrd.23421

Ho, H. C., and Suarez, S. S. (2001). Hyperactivation of mammalian spermatozoa: function and regulation. *Reproduction* 122, 519–526. doi:10.1530/rep.0.1220519

Jung, Y. H., Sauria, M. E. G., Lyu, X., Cheema, M. S., Ausio, J., Taylor, J., et al. (2017). Chromatin states in mouse sperm correlate with embryonic and adult regulatory landscapes. *Cell Rep.* 18, 1366–1382. doi:10.1016/J.CELREP.2017.01.034

Kamp, G., Schmidt, H., Stypa, H., Feiden, S., Mahling, C., and Wegener, G. (2007). Regulatory properties of 6-phosphofructokinase and control of glycolysis in boar spermatozoa. *Reproduction* 133, 29–40. doi:10.1530/REP-06-0082

Kang, W., Katano, D., Kawano, N., Miyado, M., and Miyado, K. (2022). Extra-mitochondrial citrate synthase controls cAMP-dependent pathway during sperm acrosome reaction in mice. *microPublication Biol.* 2022. doi:10.17912/MICROPUB.BIOLOGY.000579

Krapf, D., Arcelay, E., Wertheimer, E. V., Sanjay, A., Pilder, S. H., Salicioni, A. M., et al. (2010). Inhibition of ser/thr phosphatases induces capacitation-associated signaling in the presence of src kinase inhibitors. *J. Biol. Chem.* 285, 7977–7985. doi:10.1074/jbc.M109.085845

Laemmli, U. K. (1970). Cleavage of structural proteins during the assembly of the headof bacteriophage T4. *Nature* 227 (5259), 680–685. doi:10.1038/227680a0

Liu, X., Cooper, D. E., Cluntun, A. A., Warmoes, M. O., Zhao, S., Reid, M. A., et al. (2018). Acetate production from glucose and coupling to mitochondrial metabolism in mammals. *Cell* 175, 502–513.e13. doi:10.1016/J.CELL.2018.08.040

Mann, T., and Lutwak-Mann, C. (1981). *Male reproductive function and semen: Themes and trends in physiology, biochemistry and investigative andrology*.

Marín-Briggiler, C. I., Luque, G. M., Gervasi, M. G., Oscoz-Susino, N., Sierra, J. M., Mondillo, C., et al. (2021). Human sperm remain motile after a temporary energy restriction but do not undergo capacitation-related events. *Front. Cell Dev. Biol.* 9, 777086. doi:10.3389/fcell.2021.777086

Martin-Hidalgo, D., de Llera, A. H., Calle-Guisado, V., Gonzalez-Fernandez, L., Garcia-Marin, L., and Bragado, M. J. (2018). AMPK function in mammalian spermatozoa. *Int. J. Mol. Sci.* 19, 3293. doi:10.3390/ijms19113293

Melrose, D. R., and Terner, C. (1953). The metabolism of pyruvate in bull spermatozoa. *Biochem. J.* 53, 296–305. doi:10.1042/BJ0530296

Nakamura, N., Miranda-Vizuete, A., Miki, K., Mori, C., and Eddy, E. M. (2008). Cleavage of disulfide bonds in mouse spermatogenic cell-specific type 1 hexokinase isozyme is associated with increased hexokinase activity and initiation of sperm motility. *Biol. Reprod.* 79, 537–545. doi:10.1095/BIOLREPROD.108.067561

Nakamura, N., Mori, C., and Eddy, E. M. (2010). Molecular complex of three testis-specific isozymes associated with the mouse sperm fibrous sheath: hexokinase 1, phosphofructokinase M, and glutathione S-transferase mu class 5. *Biol. Reprod.* 82, 504–515. doi:10.1095/BIOLREPROD.109.080580

Navarrete, F. A., Aguila, L., Martin-Hidalgo, D., Tourzani, D. A., Luque, G. M., Ardestani, G., et al. (2019). Transient sperm starvation improves the outcome of assisted reproductive Technologies. *Front. Cell Dev. Biol.* 7, 262. doi:10.3389/fcell.2019.00262

Navarrete, F. A., Alvau, A., Lee, H. C., Levin, L. R., Buck, J., Leon, P. M.-D., et al. (2016). Transient exposure to calcium ionophore enables *in vitro* fertilization in sterile mouse models. *Sci. Rep.* 6, 33589. doi:10.1038/srep33589

Navarrete, F. A., García-Vázquez, F. A., Alvau, A., Escoffier, J., Krapf, D., Sánchez-Cárdenas, C., et al. (2015). Biphasic role of calcium in mouse sperm capacitation signaling pathways. *J. Cell. Physiol.* 230, 1758–1769. doi:10.1002/jcp.24873

Odet, F., Duan, C., Willis, W. D., Goulding, E. H., Kung, A., Eddy, E. M., et al. (2008). Expression of the gene for mouse lactate dehydrogenase C (ldhc) is required for male fertility. *Biol. Reprod.* 79, 26–34. doi:10.1095/BIOLREPROD.108.068353

Odet, F., Gabel, S. A., Williams, J., London, R. E., Goldberg, E., and Eddy, E. M. (2011). Lactate dehydrogenase C and energy metabolism in mouse sperm. *Biol. Reprod.* 85, 556–564. doi:10.1095/biolreprod.111.091546

Porambo, J. R., Salicioni, A. M., Visconti, P. E., and Platt, M. D. (2012). Sperm phosphoproteomics: historical perspectives and current methodologies. *Expert Rev. Proteomics* 9, 533–548. doi:10.1586/epr.12.41

Reid, M. A., Dai, Z., and Locasale, J. W. (2017). The impact of cellular metabolism on chromatin dynamics and epigenetics. *Nat. Cell Biol.* 19, 1298–1306. doi:10.1038/NCB3629

Sánchez-Cárdenas, C., Romarowski, A., Orta, G., De la Vega-Beltrán, J. L., Martín-Hidalgo, D., Hernández-Cruz, A., et al. (2021). Starvation induces an increase in intracellular calcium and potentiates the progesterone-induced mouse sperm acrosome reaction. *FASEB J.* 35, e21528. doi:10.1096/fj.202100122R

Scott, T. W., Voglmayr, J. K., and Setchell, B. P. (1967). Lipid composition and metabolism in testicular and ejaculated ram spermatozoa. *Biochem. J.* 102, 456–461. doi:10.1042/BJ1020456

Sharma, U., Conine, C. C., Shea, J. M., Boskovic, A., Derr, A. G., Bing, X. Y., et al. (2016). Biogenesis and function of tRNA fragments during sperm maturation and fertilization in mammals. *Science* 351, 391–396. doi:10.1126/SCIENCE.AAD6780

Takei, G. L., Tourzani, D. A., Paudel, B., and Visconti, P. E. (2021). Activation of cAMP-dependent phosphorylation pathways is independent of ROS production during mouse sperm capacitation. *Mol. Reprod. Dev.* 88, 544–557. doi:10.1002/mrd.23524

Tartarin, P., Guibert, E., Touré, A., Ouiste, C., Leclerc, J., Sanz, N., et al. (2012). Inactivation of AMPKα1 induces asthenozoospermia and alters spermatozoa morphology. *Endocrinology* 153, 3468–3481. doi:10.1210/en.2011-1911

Tourzani, D. A., Yin, Q., Jackson, E. A., Rando, O. J., Visconti, P. E., and Gervasi, M. G. (2022). Sperm energy restriction and recovery (SER) alters epigenetic marks during the first cell cycle of development in mice. *Int. J. Mol. Sci.* 24, 640. doi:10.3390/IJMS24010640

Toyoda, Y., Yokoyama, M., and Hosi, T. (1971). Studies on the fertilization of mouse eggs fertilization of eggs by fresh epididymal sperm. *Jpn. J. Anim. Reprod.* 16, 147–151. doi:10.1262/jrd1955.16.147

Ulrich, E. L., Akutsu, H., Doreleijers, J. F., Harano, Y., Ioannidis, Y. E., Lin, J., et al. (2008). *BioMagResBank.* Nucleic Acids Res. 36, 402–408. doi:10.1093/nar/gkm957

Urner, F., and Sakkas, D. (1999). A possible role for the pentose phosphate pathway of spermatozoa in gamete fusion in the mouse. *Biol. Reprod.* 60, 733–739. doi:10.1095/BIOLREPROD60.3.733

Vadnais, M. L., Lin, A. M., and Gerton, G. L. (2014). Mitochondrial fusion protein MFN2 interacts with the mitostatin-related protein MNS1 required for mouse sperm flagellar structure and function. *Cilia* 3, 5–15. doi:10.1186/2046-2530-3-5

Visconti, P. E., Olds-Clarke, P., Moss, S. B., Kalab, P., Travis, A. J., De Las Heras, M., et al. (1996). Properties and localization of a tyrosine phosphorylated form of hexokinase in mouse sperm. *Mol. Reprod. Dev.* 43, 82–93. doi:10.1002/(SICI)1098-2795(199601)43:1<82::AID-MRD11>3.0.CO;2-6

Visconti, P. E. (2012). Sperm bioenergetics in a nutshell. *Biol. Reprod.* 87, 72. doi:10.1095/biolreprod.112.104109

Wishart, D. S., Tzur, D., Knox, C., Eisner, R., Guo, A. C., Young, N., et al. (2007). Hmdb: the human metabolome database. *Nucleic Acids Res.* 35, 521–526. doi:10.1093/nar/gkl923

Yang, F., Gracia Gervasi, M., Orta, G., Tourzani, D. A., De la Vega-Beltrán, J. L., Ruthel, G., et al. (2022). C2CD6 regulates targeting and organization of the CatSper calcium channel complex in sperm flagella. *Development* 149, dev199988. doi:10.1242/DEV.199988

frontiers | Frontiers in Cell and Developmental Biology

TYPE Original Research
PUBLISHED 16 August 2023
DOI 10.3389/fcell.2023.1240152

OPEN ACCESS

EDITED BY
Vanina Gabriela Da Ros,
CONICET, Argentina

REVIEWED BY
Murid Javed,
Embryogenex Inc., Canada
Debora Cohen,
National Scientific and Technical Research Council (CONICET), Argentina

*CORRESPONDENCE
Rossana Sapiro,
rossanasapiro@gmail.com
Dana Kimelman,
danakimelmanf@gmail.com

†These authors have contributed equally to this work

RECEIVED 14 June 2023
ACCEPTED 03 August 2023
PUBLISHED 16 August 2023

CITATION
Kimelman D, Torrens A, Bonelli C and Sapiro R (2023), Fertility preservation in male cancer patients. Counseling and reproductive outcomes.
Front. Cell Dev. Biol. 11:1240152.
doi: 10.3389/fcell.2023.1240152

Fertility preservation in male cancer patients. Counseling and reproductive outcomes

Dana Kimelman[1,2,3*†], Andrea Torrens[2], Carla Bonelli[2] and Rossana Sapiro[4*†]

[1]Oncofertility Program, Centro Hospitalario Pereira Rossell, Administración de los Servicios de Salud del Estado (ASSE), Montevideo, Uruguay, [2]Reprovita Lab and Biobank, Montevideo, Uruguay, [3]Clínica Ginecotocológica "B", Facultad de Medicina, Universidad de la República, Montevideo, Uruguay, [4]Unidad Académica Histologia y Embriologia, Facultad de Medicina, Universidad de la República, Montevideo, Uruguay

Introduction: Advances in cancer treatments have determined an increase in survival rates. However, these lifesaving therapies may have a negative impact on reproductive health. To diminish the infertility risk; different fertility preservation strategies have been designed. Sperm freezing is the gold standard fertility preservation method in the case of post-pubertal men. The main objective of this study is to evaluate the fertility status of Uruguayan male cancer survivors who have gone through sperm freezing, as well as to assess oncofertility counseling received by these patients.

Methods: This is a descriptive, cross-sectional, observational, and transversal study. A survey was conducted on male cancer survivors who cryopreserved sperm between 1985 and 2021 in "Reprovita Lab and Biobank" which is the only sperm bank in this country.

Results: One hundred thirty-five participants answered the survey. At the time of diagnosis, the mean age of patients was 28.8 ± 6.4 years old. Testicular was the most frequent type of cancer (64%). Only, 12% (n = 15) already had children at the time of diagnosis. Among the interviewed survivors, 50% (n = 62) attempted to conceive after cancer treatment, and 68% (n = 42) achieved natural pregnancy. Patients who did not achieve spontaneous conception (n = 11), used their cryopreserved samples, and 45.4% achieved pregnancy. About 86% (n = 107) of survivors believed that the timing of oncofertility referrals was appropriate and 97% considered that having the possibility of protecting their fertility was very important. Eighty percent (n = 101), were advised by their attending physicians, 14% (n = 18) sought advice from family members or friends, and 4% (n = 5) from oncofertility specialists.

Discussion: To our knowledge, this is the first study evaluating the reproductive outcomes of male cancer survivors in our country and the region. Most of the interviewed survivors considered fertility preservation as a positive initiative, independent of their reproductive outcomes, reflecting the importance of fertility preservation counseling as one of the most important aspects for futurequality of life of young cancer patients.

KEYWORDS

fertility preservation, male infertility, male cancer, reproductive outcomes, counseling

1 Introduction

Six percent of male cancer diagnoses in Uruguay occur in patients who are under the age of 40 (Incidencia cancer, 2019). Advances in cancer diagnosis and treatments have improved the survival rates of this population. However, these treatments may have a negative impact on future fertility affecting the quality of life of young cancer survivors (Kohler et al., 2011; Alsharhrani et al., 2017). For this reason, health providers should focus their attention on the quality-of-life aspects, which are usually as relevant as the disease for survivors (Mulder et al., 2021). Cancer treatments may affect future fertility in different ways. Drugs have different grades of gonadotoxicity and this also depends on doses, age of the patient, and previous fertility status (Alsharhrani et al., 2017; Ono et al., 2022). Gonadotoxic risks are cataloged as high, moderate, low, and unknown risks (El Issaoui et al., 2016). The toxicity of radiotherapy depends on the doses of radiation, and the target area, low doses of radiation as 0.1 and 1.2 Gy may negatively impact spermatogenesis, and doses over 4 Gy may cause permanent azoospermia (De Felice et al., 2019).

In some cases, spermatogenesis may be affected temporally after treatment and there may be recovery of the function that may take years depending on the treatment and the patient's age. Sperm cryopreservation should be done ideally before initiating cancer treatments (El Issaoui et al., 2016).

In order to diminish the infertility risk; different fertility preservation strategies have been designed. Sperm, egg, and embryo freezing are some of the available fertility preservation techniques. International guidelines (Practice Committee of the American Society for Reproductive Medicine, 2019; Ono et al., 2022) recommend that every young patient with a cancer diagnosis should receive complete oncofertility counseling before treatment initiation (Lambertini et al., 2020). For patients that had been through puberty, gamete cryopreservation (sperm or oocytes) should be offered (Lambertini et al., 2020). In Uruguay, physicians guide their clinical practice on international guidelines when counseling young cancer patients but there are no national guidelines, national registries, or reports that had evaluated the success rates of fertility preservation strategies or their use. Within male fertility preservation strategies, whenever possible, gamete cryopreservation is the standard and preferred technique. As it is recommended; sperm cryopreservation should be performed prior to starting oncologic treatments. This is why timely referrals from the treating medical team are so relevant. The strategy of testicular tissue cryopreservation and potential re-implantation is only performed in an experimental framework (Eugeni et al., 2022) and there is no experience in our country.

Reprovita Lab and Biobank laboratory is a private center specialized in human reproduction. Gamete and embryo cryopreservation are some of the services provided by this institution. Reprovita is the only sperm bank in our country; therefore, all male gametes cryopreserved for oncological reasons are stored there.

The main objective of this work is to know whether male cancer survivors who underwent sperm cryopreservation achieved their reproductive goals. Secondary outcomes are to evaluate the fertility status of patients that cryopreserved semen samples before cancer treatment, to know how frequently cryopreserved specimens had been used, and to investigate whether patients who underwent sperm cryopreservation are satisfied with the reproductive counseling they received prior to starting oncological treatment.

2 Materials and methods

2.1 Study population

This descriptive and cross-sectional study includes all male cancer patients who cryopreserved semen samples in a single country at the only sperm bank available in the period from 1985 to 2021. Inclusion and exclusion criteria were established. Inclusion criteria: male patients between 15 and 50 years of age at the time of cryopreservation, who cryopreserved gametes in Reprovita sperm bank due to oncological reasons, and who have given their informed consent to participate in this research. The exclusion criteria established were age <15 and >50 at the time of cryopreservation and/or deceased patients. Data collection was done through telephone interviews conducted by the research team. Telephone lines intended for this work were used for the interviews, in order to facilitate and maintain confidentiality. The collected variables are related to patronymic, demographic, and oncological pathology data, oncological treatment, reproductive counseling, reproductive desires, and events. The collected data were coded and registered anonymously.

2.2 Procedure and data management

The whole database of the cryobank was reviewed. Out of 2045 male patients who stored semen samples at our bank between 1985 and 2021, 755 of them did so specifically for oncologic reasons so they all were identified as possible participants. Technical laboratory specialists intended to phone call all 755 men through the period from June to September 2022. When the contact was established, the laboratory staff requested their consent to be contacted by the research team. This phone call was recorded.

2.3 Semen analyses and cryopreservation procedure

Semen analyses at the time of cryopreservation were requested for the patients included in the study. Sperm concentration, progressive and total motility (progressive and non-progressive motility), vitality, and sperm morphology were evaluated. The sperm analysis was performed based on reference parameters from the World Health Organization (WHO) guidelines of 1999 and 2010, respectively (Alsharhrani et al., 2017; Boitrelle et al., 2021). Concentration and sperm motility post cryopreservation were also evaluated in the 12 patients that attended our clinic for assisted reproductive treatments (ART).

Sperm samples conditioned with cryoprotectant media were cryopreserved at −196°C in liquid nitrogen. Samples were stored in straws with high biological safety freezing, sealed at both ends, and labeled with the patient's name, identification document number, and processing date. The patient received a report with the characteristics of the cryopreserved sample.

2.4 Statistical analysis

Data were entered into a password-protected secure database. All respondents did not reply to all questions, and the missing data

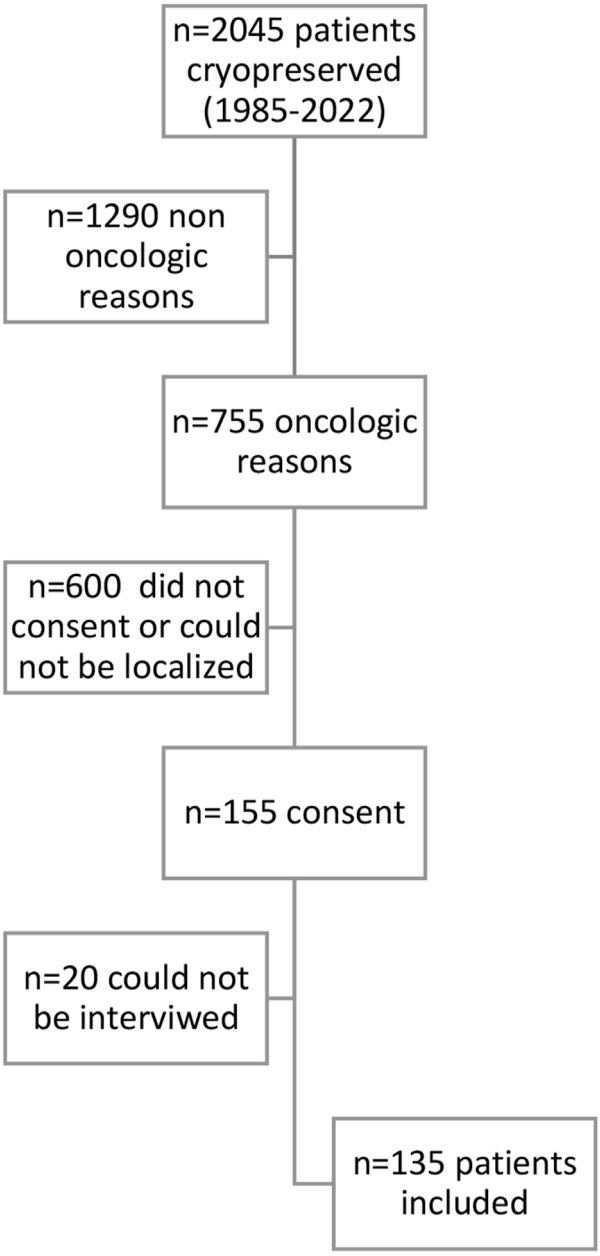

FIGURE 1
Flow chart of included patients. N=Number of patients included in each step of the analysis.

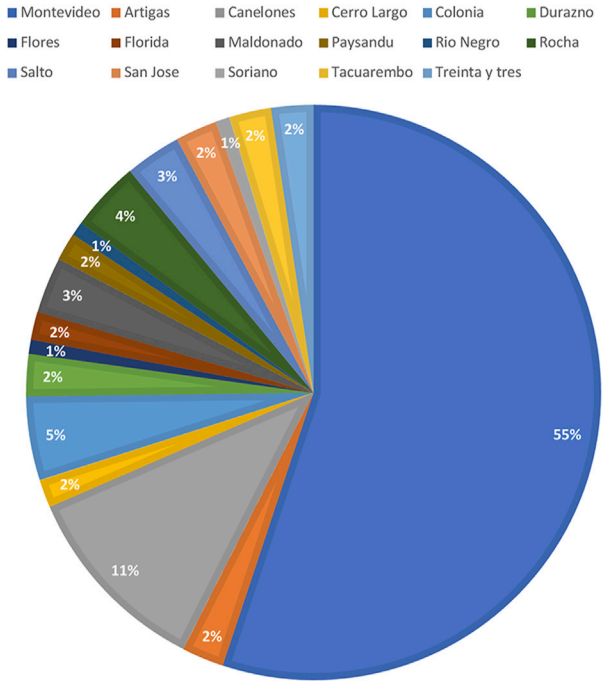

FIGURE 2
City of residence of surveyed participants. Values are presented as percentages (%).

2.5 Ethical considerations

This study has been evaluated and approved by the Institutional Review Board of the School of Medicine at the Universidad de la República (UdelaR).

3 Results

3.1 Characteristics of the analyzed population

Out of the 2045 patients who stored semen samples at our bank between 1985 and 2021, 755 of them did so specifically for oncologic reasons (Figure 1). Only 155 patients (20%) accepted to participate in the study through a survey that was performed through a second call (Figure 1). Different reasons for not participating were: patients who could not be localized, patients who did not answer the phone calls, and patients who did not consent. The recruitment was done through personal phone calls, so patients who died during the period were not registered. Finally, 135 participants that fitted the inclusion criteria answered the questionnaire and were included in the study. Of these patients, 55.1% (n = 70) resided in the capital city (Figure 2). The mean age of patients who underwent cryopreservation was 28.8 ± 6.4 years old, whereas the current mean age of this population is 38.1 ± 7.7 years old (Table 1). Among these patients, 64% (n = 81) cryopreserved sperm samples due to a testicular cancer diagnosis, while 24% (n = 30) had hemato-oncological diseases (Figure 3).

were not computed. Data analysis was performed on Version 26 of the IBM SPSS Statistics software package (Armonk, NY). No power calculation was performed as the sample size directly resulted from the number of respondents to the questionnaire.

Categorical variables were presented as percentages. Continuous variables were expressed by arithmetic means and the corresponding standard errors. The normal distribution of the data was tested using the Shapiro-Wilk normality test. Semen parameters previous and post cryopreservation were compared with paired Student's t-test. The chi-square test was applied to analyze the percentage of men acquiring pregnancy. A p-value <0.05 was considered statistically significant.

TABLE 1 Demographic characteristics of participants. The values are Mean ± SD.

Age at time of survey (mean ± SD)	38.1 ± 7.7
Age at diagnosis (Mean ± SD)	28.8 ± 6.4
City of residence (%)	
Montevideo	55 (n = 70)
Others	45 (n = 57)
Financial coverage for Fertility preservation (%)	
Yes	18.4 (n = 23)
No	80 (n = 100)
Parenthood before cancer diagnosis (%)	
Yes	11.9 (n = 15)
No	88.1 (n = 111)

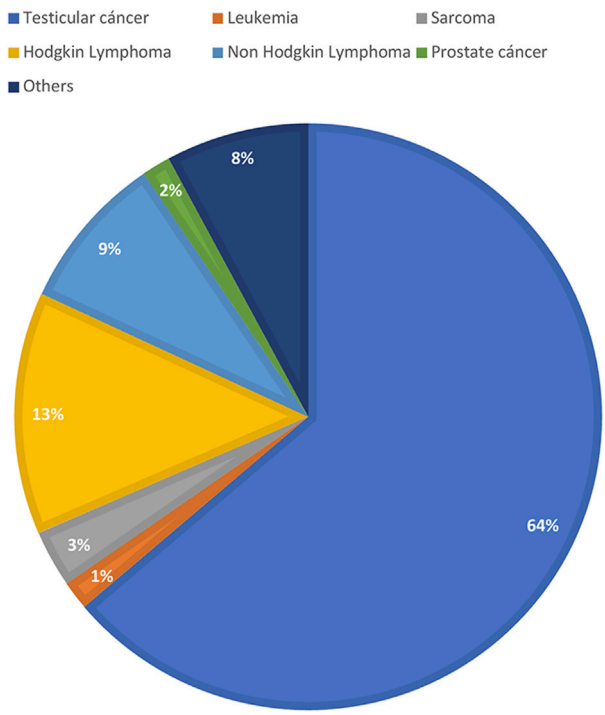

FIGURE 3
Diagnosis of men that responded the questionnaire. Values are presented as percentasge of patients (%).

3.2 Reproductive outcomes

When analyzing reproductive outcomes of the interviewed population, our findings showed that at the time of diagnosis, 88% (N = 111) of the patients did not have children, whereas 12% (*n* = 15) already had children (Table 1). Among the interviewees, 56% (*n* = 76) attempted to conceive. All of them had been counseled on not seeking pregnancy before 6 months to 1 year after finalizing oncologic treatment. Out of those survivors who tried to conceive after cancer treatment, 55% (*n* = 42) were successful in achieving pregnancy without the need to use cryopreserved sperm samples. When asked how long they had been trying to conceive, we found that out of 39 respondents, 51% (*n* = 20) achieved pregnancy between one and 2 years of unprotected intercourse. 33% (*n* = 13) achieved pregnancy in two to 3 years, and 13% (*n* = 5) after 3 years. When analyzing the results, we found that 69% (*n* = 29) of testicular cancer survivors and 31% (*n* = 13) of other types of cancer survivors who attempted to conceive were able to achieve pregnancy spontaneously (Table 2). Twelve patients tried to achieve pregnancy through assisted reproductive technologies using cryopreserved samples. Among these patients, 46% (*n* = 5) successfully achieved pregnancy, one patient had no motile sperm in the thawed sample. A comparison between testicular cancer survivors and survivors of other types of cancer who used cryopreserved samples revealed that 67% (*n* = 4) of testicular cancer survivors achieved pregnancy, while only 20% (*n* = 1) of survivors of other types of cancer achieved the same outcome. This comparison did not result statistically significant probably due to the low number of patients included (Table 2).

3.3 Sperm usage

Semen analyses at the time of post-cryopreservation were available for 12 of the patients (those who decided to use the cryopreserved sample for reproductive purposes). One of the samples did not have any motile sperm after thawing. The results of the remaining eleven semen analyses are shown in Table 1. Mean sperm concentration ± standard deviation (61.3 ± 56.0 million/mL), progressive (61.4% ± 13.0%), and total sperm motility (72.7% ± 8.9%) of patients who cryopreserved sperm before initiating gonadotoxic therapy were normal. At the time of thawing, the mean ± standard deviation of sperm concentration significantly decreased to 28.1 ± 27.6 million/mL ($p < 0.05$). The progressive motility was 54.4% ± 20.9% and the total motility 68.5% ± 20.8% (Table 3). All patients that intended to use the cryopreserved samples finalized their cancer treatment more than 1 year before.

3.4 Counseling

Out of 124 participants who answered this question; 86% (*n* = 107) believed that the timing of oncofertility referrals was appropriate, while 12% (*n* = 15) would have preferred an earlier referral. However, 97% of patients feel that having the opportunity to pursue fertility preservation strategies was greatly valuable. When asked about who discussed the potential impact of cancer treatments on fertility, most patients 80% (*n* = 101) indicated that their attending physicians had raised this topic. A small percentage, 4% (*n* = 5), received counseling from oncofertility specialists, and 14% (*n* = 18) sought advice from family members or friends. In interviews with testicular cancer survivors, we inquired about the timing of counseling regarding surgical treatment (orchiectomy). It was revealed that 65% (*n* = 49) received counseling after the surgery, while 36% (*n* = 27) were counseled prior to the procedure. All patients were counseled by oncologists not to seek pregnancy until

TABLE 2 Reproductive outcomes of participants after treatment.

Spontaneous pregnancy n (%)				Pregnancy using cryopreserved samples (ART) n (%)		
	Yes	No	Total	Yes	No	Total
Testicular cancer	29 (67.4%)	14 (32.6%)	43 (100%)	4 (66.7%)	2 (33.3%)	6 (100%)
Other	13 (59.1%)	9 (40.9%)	22 (100%)	1 (20%)	4 (80%)	5 (100%)
Total	42 (64.6) %	23 (35.4%)	65 (100%)	5 (45.5%)	6 (54.5%)	11 (100%)

Chi square test. Differences between groups were not statistically significant. *n* = number of patients, values are no (%).

TABLE 3 Semen characteristics at the time of cryopreservation and at the time of use of sample.

Group	Sperm concentration (10^6/mL)	Progressive motility (%)	Total motility (%)
	Mean ± SD	Mean ± SD	Mean ± SD
Pre-cryopreservation	61.3 ± 56.0	61.4 ± 13.0	72.7 ± 8.9
Post-cryopreservation	28.1 ± 27.6*	54.4 ± 20.9	68.5 ± 20.8

n = 11. *$p < 0.01$, paired Student's t-test.

6 months after treatment. When it came to financial coverage for fertility preservation strategies, 80% of patients (*n* = 100) paid out of pocket for these techniques and the storage of cryopreserved samples, while 18.4% (*n* = 23) received financial support from their health insurance.

4 Discussion

Cancer treatments can lead to impaired fertility (Green et al., 2010). International guidelines recommend that patients should receive complete oncofertility counseling soon after diagnosis and during treatment planning so that fertility preservation strategies may be offered and pursued before treatment (Ono et al., 2022). The attending physician should promote the conversation about possible fertility impairment with every young cancer patient early after the diagnosis (Ono et al., 2022). This exchange not only improves the likelihood that the patient will achieve their reproductive goal, but also improves adherence to the proposed treatments and quality of life (Mulder et al., 2021). For our study, 135 male cancer survivors that cryopreserved sperm samples in the context of cancer diagnosis had been interviewed, this population represents 17.9% of the whole number of patients that cryopreserved semen samples due to oncologic reasons. Most of interviewees had testicular cancer (64%). Consistent with our findings, a study published by Kohler et al. (2011) in 2011, the most common type of cancer among patients who decided to cryopreserve semen samples was Non-Hodgkin's Lymphoma, Hodgkin's Lymphoma, and Testicular Cancer; being this the most frequent cancer diagnosis of young male patients worldwide (Hayes-Lattin and Nichols, 2009). Testicular cancer is the most common cancer in men between 20 and 40 years old. During the period 2015–2019, 475 patients between 15 and 39 years old had been diagnosed with testicular cancer in our country; this represents 32% of all cases during the same time range (Incidencia cancer, 2019). Most patients were residents of Montevideo City, the capital of Uruguay. Even though almost 50% of the population of the country lives in the capital city; the underlying reasons for why patients from Montevideo were more likely to undergo fertility preservation is multifactorial. The main reason is that the sperm bank is in this city, which makes access easier. This shows a clear difference in access to cryopreservation treatments in patients from the countryside compared to patients from the capital city. It also seems to be more referrals from physicians from the capital city. Our results suggest the need to generate strategies that allow access throughout the national territory so that patients from the countryside do not miss the opportunity to pursue these treatments. Regarding counseling prior to cryopreservation, most interviewees were advised by their treating physician prior to the start of oncospecific treatment.

Regarding financial coverage and costs of gamete cryopreservation, our findings show that most patients did not receive any financial support from the healthcare system. In the study published by Lackamp et al. in Frontiers Oncology it is indicated that costs may affect cryopreservation rates and future sperm usage (Lackamp et al., 2021), in addition to the lack of information and counseling on cryopreservation, the economic component is a barrier when resorting to this strategy. We must mention that there have been legal changes regarding financing gamete cryopreservation treatments for cancer patients. In July 2022, there was a modification to the assisted reproductive technology regulation law (Law number 19.167). This amendment stipulates that the Uruguayan State is now obligated to provide financial coverage for gamete cryopreservation treatments to all post-pubertal cancer patients under 40 years old. This development is significant in terms of reproductive rights, as the cost of preservation can be a barrier to accessing these strategies. Adequate counseling is part of the recommendations of the Clinical Practice Guideline of the American Society of Clinical Oncology (ASCO), which also considers it appropriate before starting treatment, accompanied by a consultation with an oncofertility specialist (Oktay et al., 2018).

Our results show that most interviewees achieved their reproductive desire through spontaneous pregnancy. However, the number of interviewed patients is low, and these results cannot be extrapolated to all cancer patients. Sheth et al. showed similar

outcomes in their study published in 2012 (Sheth et al., 2012), of the 249 patients who cryopreserved semen samples between 2002 and 2010, 21 patients (8.4%) used their sample for assisted reproduction treatments. While in another study conducted at Erasmus Medical Center in the Netherlands (van Casteren et al., 2008), it was shown that 7.5% of patients who cryopreserved between 1983 and 2004 used the sample, and 49% achieved pregnancy. In our research, 12 survivors of all participants intended to use their cryopreserved semen samples, and a total of 45.5% achieved pregnancy with it. Therefore, the results obtained were similar in both studies. In the case of patients who did not achieve pregnancy using cryopreserved samples, several factors that may have determined this result, such as the timing of the sample collection relative to the treatment stage, its quality, and female factors, among others.

Most patients with testicular cancer diagnosis did sperm cryopreservation after orchiectomy, it is important to notice that Emmanuel et al. have shown that there is no evidence showing that expedited radical orchiectomy has an oncological benefit (Emmanuel et al., 2021). Also, Moody et al. demonstrated that effective cryopreservation can be achieved within 1 week of initial diagnosis (Moody et al., 2019). Both conclude in their published work that it is critical to recommend cryopreservation to all patients prior to orchiectomy and/or neoadjuvant chemotherapy regardless of cancer staging even if there is a short temporary delay in orchiectomy (Emmanuel et al., 2021).

We have no knowledge of a study of similar characteristics being conducted neither in our country nor in another Latin American country. In 2021 Lackamp et al. published a survey evaluating "Long- Term Experiences of Sperm Cryopreservation in Oncological and Non-Oncological Patients." This group evaluated respective outcomes related to different treatment protocols and their results showed that 20.7% of all survivors reported to have fathered at least one naturally conceived child after treatment, especially if they had been treated with less or potentially gonadotoxic therapies (Lackamp et al., 2021). Most of the interviewed patients who cryopreserved sperm and tried to conceive in our study did not have impaired fertility, being able to achieve spontaneous pregnancy. This is consistent with what Brydoy et al.(2005) have published stating that the spermatogenesis function of many patients recovers after cancer treatment. Like us, Nalesnik et al. (2004) published that 64% of testicular cancer survivors have naturally conceived children. A cohort study of 8.670 male cancer survivors from Denmark and Sweden indicated that 8.162 of the survivors experienced spontaneous pregnancies (Stahl et al., 2011). Although our findings are similar to what our colleagues published before, in our study, only 17.88% of the patients who cryopreserved due to cancer diagnosis were included, which is a deficient percentage. This small percentage may not be representative of the whole population, which is one of our study's major limitations. Due to the size of the sample studied, it is not possible to conclude whether there was a relationship between the type of cancer, or the received treatment and the rates of spontaneous pregnancy. Of all interviewed survivors, 64% had testicular cancer, and the treatment protocol for this group of patients includes etoposide, cisplatin, and bleomycin from one to four cycles. Of testicular cancer survivors, 69% (n = 29) could conceive spontaneously after cancer treatment. Due to the low number of participants, we may not conclude that these chemotherapeutic agents are not gonadotoxic; in fact, there is enough evidence showing the gonad toxicity of these mentioned agents (Sheth et al., 2012; Eugeni et al., 2022).

Even though many survivors achieved spontaneous pregnancy; they still consider that being counseled in oncofertility was very valuable. As the international guidelines have established, every reproductive-aged patient with a cancer diagnosis should be advised in oncofertility before cancer treatment, no matter type of cancer, stage, or prognosis (Lambertini et al., 2020; Ono et al., 2022). Counseling will positively impact how patients will face treatment thinking about life after cancer (Practice Committee of the American Society for Reproductive Medicine, 2019; Lambertini et al., 2020; Ono et al., 2022).

Our work provides valuable data. To our knowledge, this is the first study evaluating the reproductive outcomes of male cancer survivors in our country and the region. The main strength of our work is the fact that our country has only one sperm bank, and this allowed us to include some of the patients who underwent sperm cryopreservation treatment due to oncologic reasons. Our study has some important limitations: the first one is that, as previously mentioned, we only had access to 17.9% of the men who cryopreserved semen samples for cancer reasons. This limitation means that it is only possible to make conclusions based on a small percentage of the population. Another area of improvement to be acknowledged is that the study's design (through personal phone calls) does not distinguish the causes of why some of the patients cannot be localized. Consequently, valuable data is missing, e.g.: how many patients died for oncological reasons. The third main limitation is not having access to the specific cancer treatment. That information was not asked at the time of cryopreservation, and some patients, while being interviewed for this study, did not remember the treatment they received. It should be noted that although patients who cryopreserved their samples are satisfied with the counseling they received, to objectively evaluate the population of young cancer patients in general, a study would be needed that should include patients who did not undergo cryopreservation. It would be important to continue this research in 5–10 years to follow up on patients who cryopreserved but have not yet expressed reproductive desire. Our future objective will be to compare access to fertility preservation strategies of patients using financial coverage, we believe that much more patients will be able to cryopreserve gametes not only because of financial access but also because of better referrals. We will also need to develop better registries in order to follow up with cancer survivors and have better database information on their disease, treatment, and fertility status after cancer treatment.

Data availability statement

The original contributions presented in the study are included in the article/Supplementary Material, further inquiries can be directed to the corresponding authors.

Ethics statement

The studies involving humans were approved by Comité de ética de Facultad de Medicina, UdelaR. The studies were conducted

in accordance with the local legislation and institutional requirements. Informed consent for participation in this study was provided by the participants or the participants' legal guardians/next of kin.

Author contributions

The conceptualization of the study: DK and RS. Data acquisition and analysis DK, CB, AT, and RS. Writing the manuscript: DK and RS. All authors contributed to the article and approved the submitted version.

Funding

This work was partially founded by the Programa de Desarrollo de Ciencias Básicas (PEDECIBA, Uruguay) and Universidad de la República (I+D = # 22520220100126UD, CSIC).

Acknowledgments

We kindly acknowledge the technical laboratory specialists from Reprovita Lab and Biobank who performed the first call to patients and the patients who participated. And Doctor Luciano Amarelle who helped with the data analysis.

Conflict of interest

The authors declare that the research was conducted in the absence of any commercial or financial relationships that could be construed as a potential conflict of interest.

Publisher's note

All claims expressed in this article are solely those of the authors and do not necessarily represent those of their affiliated organizations, or those of the publisher, the editors and the reviewers. Any product that may be evaluated in this article, or claim that may be made by its manufacturer, is not guaranteed or endorsed by the publisher.

Supplementary material

The Supplementary Material for this article can be found online at: https://www.frontiersin.org/articles/10.3389/fcell.2023.1240152/full#supplementary-material

References

Alsharhrani, K., Aldossari, K., Al-Zahrani, J., Gabr R, A. H., Henkel, R., and Ahmad, G. (2017). Interpretation of semen analysis using WHO 1999 and WHO 2010 reference values: abnormal becoming normal. *First Int. J. Androl.* 50 (2), e12838. doi:10.1111/and.12838

Boitrelle, F., Shah, R., Saleh, R., Henkel, R., Kandil, H., Chung, E., et al. (2021). The sixth edition of the WHO manual for human semen analysis: a critical Review and swot analysis. *Life (Basel)* 11 (12), 1368. doi:10.3390/life11121368

Brydoy, M., Fossa, S. D., Klepp, O., Bremnes, R. M., Wist, E. A., Wentzel-Larsen, T., et al. (2005). Paternity following treatment for testicular cancer. *J. Natl. Cancer Inst.* 97 (21), 1580–1588. doi:10.1093/jnci/dji339

De Felice, F., Marchetti, C., Marampon, F., Cascialli, G., Muzii, L., and Tombolini, V. (2019). Radiation effects on male fertility. *Andrology* 7 (1), 2–7. doi:10.1111/andr.12562

El Issaoui, M., Giorgione, V., Mamsen, L. S., Rechnitzer, C., Birkebaek, N., Clausen, N., et al. (2016). Effect of first line cancer treatment on the ovarian reserve and follicular density in girls under the age of 18 years. *Fertil. Steril.* 106 (7), 1757–1762.e1. doi:10.1016/j.fertnstert.2016.09.001

Emmanuel, A., Kanthabalan, A., Alexander, C., Bhatt, N., Chan, V., Kasivisvanathan, V., et al. (2021). Expedited radical orchidectomy for testicular cancer: compromising fertility outcomes without oncological benefit? *Eur. Urol.* 80 (6), 766–767. doi:10.1016/j.eururo.2021.08.025

Eugeni, E., Arato, I., Del Sordo, R., Sidoni, A., Garolla, A., Ferlin, A., et al. (2022). Fertility preservation and restoration options for pre-pubertal male cancer patients: current approaches. *Front. Endocrinol. (Lausanne)* 13, 877537. doi:10.3389/fendo.2022.877537

Green, D. M., Kawashima, T., Stovall, M., Leisenring, W., Sklar, C. A., Mertens, A. C., et al. (2010). Fertility of male survivors of childhood cancer: a report from the childhood cancer survivor study. *J. Clin. Oncol.* 28 (2), 332–339. doi:10.1200/JCO.2009.24.9037

Hayes-Lattin, B., and Nichols, C. R. (2009). Testicular cancer: a prototypic tumor of young adults. *Semin. Oncol.* 36 (5), 432–438. doi:10.1053/j.seminoncol.2009.07.006

Incidencia cancer *Incidencia cancer 2015 - 2019 por edad*. Montevideo, Uruguay: Regsitro Nacional del Cancer, Comisiòn Honoraria de Lucha Contra el Càncer. 2019.

Kohler, T. S., Kondapalli, L. A., Shah, A., Chan, S., Woodruff, T. K., and Brannigan, R. E. (2011). Results from the survey for preservation of adolescent reproduction (SPARE) study: gender disparity in delivery of fertility preservation message to adolescents with cancer. *J. Assist. Reprod. Genet.* 28 (3), 269–277. doi:10.1007/s10815-010-9504-6

Lackamp, N., Wilkemeyer, I., Jelas, I., Keller, U., Bullinger, L., Stintzing, S., et al. (2021). Survey of long-term experiences of sperm cryopreservation in oncological and non-oncological patients: usage and reproductive outcomes of a large monocentric cohort. *Front. Oncol.* 11, 772809. doi:10.3389/fonc.2021.772809

Lambertini, M., Peccatori, F. A., Demeestere, I., Amant, F., Wyns, C., Stukenborg, J. B., et al. (2020). Fertility preservation and post-treatment pregnancies in post-pubertal cancer patients: esmo clinical practice guidelines†. *Ann. Oncol.* 31 (12), 1664–1678. doi:10.1016/j.annonc.2020.09.006

Moody, J. A., Ahmed, K., Yap, T., Minhas, S., and Shabbir, M. (2019). Fertility managment in testicular cancer: the need to establish a standardized and evidence-based patient-centric pathway. *BJU Int. Androl.* 123 (1), 160–172. doi:10.1111/bju.14455

Mulder, R. L., Font-Gonzalez, A., Hudson, M. M., van Santen, H. M., Loeffen, E. A. H., Burns, K. C., et al. (2021). Fertility preservation for female patients with childhood, adolescent, and young adult cancer: recommendations from the PanCareLIFE consortium and the international late effects of childhood cancer guideline harmonization group. *Lancet Oncol.* 22 (2), e45–e56. doi:10.1016/S1470-2045(20)30594-5

Nalesnik, J. G., Sabanegh, E. S., Eng, T. Y., and Buchholz, T. A. (2004). Fertility in men after treatment for stage 1 and 2A seminoma. *Am. J. Clin. Oncol.* 27, 584–588. doi:10.1097/01.coc.0000135736.18493.dd

Oktay, K., Harvvey, B. E., Patridge, A. H., Quinn, G. P., Reinecke, J., Taylor, H. S., et al. (2018). Fertility preservation in patients with cancer: asco clinical practice guideline update. *J. Clin. Oncol.* 36 (19), 1994–2001. doi:10.1200/JCO.2018.78.1914

Ono, M., Matsumoto, K., Boku, N., Fujii, N., Tsuchida, Y., Furui, T., et al. (2022). Indications for fertility preservation not included in the 2017 Japan society of clinical Oncology guideline for fertility preservation in pediatric, adolescent, and young adult patients treated with gonadal toxicity, including benign diseases. *Int. J. Clin. Oncol.* 27 (2), 301–309. doi:10.1007/s10147-021-02082-9

Practice Committee of the American Society for Reproductive Medicine (2019). Fertility preservation in patients undergoing gonadotoxic therapy or gonadectomy: a committee opinion. *Fertil. Steril.* 112 (6), 1022–1033. doi:10.1016/j.fertnstert.2019.09.013

Sheth, K. R., Sharma, V., Helfand, B. T., Cashy, J., Smith, K., Hedges, J. C., et al. (2012). Improved fertility preservation care for male patients with cancer after establishment of formalized oncofertility program. *J. Urol.* 187 (3), 979–986. doi:10.1016/j.juro.2011.10.154

Stahl, O., Boyd, H. A., Giwercman, A., Lindholm, M., Jensen, A., Kjaer, S. K., et al. (2011). Risk of birth abnormalities in the offspring of men with a history of cancer: a cohort study using Danish and Swedish national registries. *J. Natl. Cancer Inst.* 103 (5), 398–406. doi:10.1093/jnci/djq550

van Casteren, N. J., van Santbrink, E. J., van Inzen, W., Romijn, J. C., and Dohle, G. R. (2008). Use rate and assisted reproduction technologies outcome of cryopreserved semen from 629 cancer patients. *Fertil. Steril.* 90 (6), 2245–2250. doi:10.1016/j.fertnstert.2007.10.055

frontiers | Frontiers in Cell and Developmental Biology

TYPE Original Research
PUBLISHED 05 September 2023
DOI 10.3389/fcell.2023.1227487

OPEN ACCESS

EDITED BY
Dolores Busso,
Universidad de los Andes, Chile

REVIEWED BY
Anna Lange-Consiglio,
University of Milan, Italy
Ruiwei Jiang,
Nanjing Drum Tower Hospital, China
Marta Tesone,
University of Buenos Aires, Argentina

*CORRESPONDENCE
Raminta Bausyte,
raminta.bausyte@gmc.vu.lt
Ruta Navakauskiene,
ruta.navakauskiene@bchi.vu.lt

RECEIVED 23 May 2023
ACCEPTED 15 August 2023
PUBLISHED 05 September 2023

CITATION
Bausyte R, Vaigauskaite - Mazeikiene B, Borutinskaite V, Valatkaite E, Besusparis J, Valkiuniene RB, Kazenaite E, Ramasauskaite D and Navakauskiene R (2023), Human endometrium-derived mesenchymal stem/stromal cells application in endometrial-factor induced infertility.
Front. Cell Dev. Biol. 11:1227487.
doi: 10.3389/fcell.2023.1227487

Human endometrium-derived mesenchymal stem/stromal cells application in endometrial-factor induced infertility

Raminta Bausyte[1,2]*, Brigita Vaigauskaite - Mazeikiene[1,2], Veronika Borutinskaite[1], Elvina Valatkaite[1], Justinas Besusparis[3,4], Ruta Barbora Valkiuniene[3,4], Edita Kazenaite[5], Diana Ramasauskaite[2] and Ruta Navakauskiene[1]*

[1]Life Sciences Center, Department of Molecular Cell Biology, Institute of Biochemistry, Vilnius University, Vilnius, Lithuania, [2]Center of Obstetrics and Gynaecology of Institute of Clinical Medicine, Faculty of Medicine, Vilnius University, Vilnius, Lithuania, [3]Faculty of Medicine, Vilnius University, Vilnius, Lithuania, [4]National Center of Pathology, Vilnius University Hospital Santaros Klinikos, Vilnius, Lithuania, [5]Faculty of Medicine, Vilnius University Hospital Santaros Klinikos, Vilnius University, Vilnius, Lithuania

Endometrial-factor induced infertility remains one of the most significant pathology among all fertility disorders. Stem cell-based therapy is considered to be the next-generation approach. However, there are still issues about successfully retrieving human endometrium-derived mesenchymal stem/stromal cells (hEnMSCs). Moreover, we need to establish a better understanding of the effect of hEnMSCs on the endometrial recovery and the clinical outcome. According to these challenges we created a multi-step study. Endometrium samples were collected from females undergoing assisted reproductive technology (ART) procedure due to couple infertility. These samples were obtained using an endometrium scratching. The hEnMSCs were isolated from endometrium samples and characterized with flow cytometry analysis. Groups of endometrium injured female mice were established by the mechanical injury to uterine horns and the intraperitoneal chemotherapy. The hEnMSCs suspension was injected to some of the studied female mice at approved time intervals. Histological changes of mice uterine horns were evaluated after Masson's trichrome original staining, hematoxylin and eosin (H&E) staining. The fertility assessment of mice was performed by counting formed embryo implantation sites (ISs). The expression of fibrosis related genes (*Col1a1*, *Col3a1*, *Acta2*, and *CD44*) was evaluated by the reverse transcription—quantitative polymerase chain reaction (RT-qPCR). Results showed that endometrium scratching is an effective procedure for mesenchymal stem/stromal cells (MSCs) collection from human endometrium. Isolated hEnMSCs met the criteria for defining MSCs. Moreover, hEnMSCs-based

Abbreviations: Acta2, Actin alpha 2, smooth muscle; ALCAM, Activated Leukocyte Cell Adhesion Molecule; ART, Assisted reproductive technology; BSA, Bovine serum albumin; Col1a1, Collagen, type I, alpha 1; Col3a1, Collagen, type III, alpha 1; FBS, Fetal bovine serum; H&E, Hematoxylin and eosin; hEnMSCs, Human endometrium-derived mesenchymal stem/stromal cells; ICSI, Intracytoplasmic sperm injection; ISCT, The International Society for Cellular Therapy; ISs, Implantation sites; IVF, *In vitro* fertilization; LCA, Leukocyte common antigen; MHC, Major histocompatibility complex; MSCs, Mesenchymal stem/stromal cells; PBS, Phosphate-buffered saline; PMNs, Polymorphonuclear cells; RBCs, Red blood cells; RT-qPCR, Reverse transcription-quantitative polymerase chain reaction; S.D., Standard deviation.

therapy had a demonstrably positive effect on the repair of damaged uterine horns, including a reduction of fibrosis, intensity of inflammatory cells such as lymphocytes and polymorphonuclear cells (PMNs) and the number of apoptotic bodies. The injured mice which recieved hEnMSCs had higher fertility in comparison to the untreated mice. Gene expression was reflected in histology changes and outcomes of conception. In conclusion, hEnMSCs demonstrated a positive impact on endometrium restoration and outcomes of endometrial-factor induced infertility. Further exploration is required in order to continue exploring the multifactorial associations between stem cell therapy, gene expression, endometrial changes and reproductive health, so we can identify individually effective and safe treatment strategies for endometrial-factor induced infertility, which is caused by mechanical effect or chemotherapy, in daily clinical practise.

KEYWORDS

infertility, endometrium-derived mesenchymal stem cells, stromal cells, endometrial-factor, mechanical injury, chemotherapy, histology, genes

Introduction

Infertility has become a significant health problem. Overall, approximately one in six heterosexual couples (or 8%–12% women aged 20–44 years) around the world may experience difficulty getting pregnant (ESHRE Capri Workshop Group, 2001). Studies on the mechanisms of fertility disorders have identified human endometrial tissue as one of the key elements in reproductive health field.

Regardless of the method of conception, endometrial receptivity—the ability of endometrium to successfully attach and maintain the embryo—is an essential condition for conception and further pregnancy development (Heger et al., 2012; Lessey and Young, 2019). Unfortunately, the endometrial receptivity can be impaired by the endometrial dysfunction such as intrauterine adhesions, Asherman's syndrome, a persistently thin endometrium or an endometrial atrophy. In this way, these pathologies have been associated with infertility (Liu et al., 2018; Mahutte et al., 2022), increased risk of miscarriage (Yuan et al., 2016; Bu et al., 2020), ectopic pregnancy (Rombauts et al., 2015; Liu et al., 2020), placenta previa (Jing et al., 2019), low birthweight (Moffat et al., 2017; Oron et al., 2018; Ribeiro et al., 2018; Guo et al., 2020) and other obstetric complications (Oron et al., 2018).

The main treatment strategy for the mentioned endometrial dysfunction consists of medical therapy (estrogen therapy, vitamin E, pentoxifylline, L-arginine, aspirin, tamoxifen, sildenafil), surgical procedures (dilatation and curettage, hysteroscopy), devices and materials of re-adhesion prevention (intrauterine device, uterine stent, Foley's catheter, adhesion barriers), autologous cellular therapy (intrauterine infusion of granulocyte colony stimulating factor or autologous platelet-rich plasma) and assisted reproductive technology (ART) procedures (AAGL Elevating Gynecologic Surgery, 2017; Ranisavljevic et al., 2019; Santamaria et al., 2020; Mouanness et al., 2021; Strug and Aghajanova, 2021). Although multiple approaches to treatment are available, the overall curative outcome is quite inconsistent. Therefore, stem cell-based therapy is being explored as a potential next-generation approach for endometrial-factor induced infertility.

Stem cells have been recognized as a potential treatment strategy for endometrium pathology caused infertility due to self-renewal and multilineage differentiation, disruption of fibrosis and promotion of angiogenesis, immune regulation and paracrine stimulation (Fossett et al., 2012; Song et al., 2021; Wu et al., 2022). Much attention has been paid to mesenchymal stem/stromal cells (MSCs) as a potential therapy tool due to their properties in contrast to other stem cell types: MSCs are a well-characterized population of adult stem cells, with no ethical or moral issues attached to their usage; they have a wide range of differentiation potential; they can be easily grown and multiplied in culture to create the required amount, without losing differentiation potential; they have a low immunogenicity; they lack tumorigenesis properties; they can act through different mechanisms and, they are even easily available commercially (Tipnis et al., 2010; Lee, 2018; Lukomska et al., 2019; Musiał-Wysocka et al., 2019; Wang et al., 2019). MSCs can be isolated from different adult tissues (bone marrow, adipose tissue, dental pulps, peripheral blood, skin, synovial fluid, muscle, menstrual blood or endometrial tissue) (Taylor, 2004; Mints et al., 2008; Figueira et al., 2011; Phermthai et al., 2016; Chen et al., 2019; Fuoco et al., 2020) and neonatal tissues (umbilical cord, Wharton's jelly, amniotic fluid, placenta or amniotic membrane) (Phermthai et al., 2010; Figueira et al., 2011; Zhang et al., 2018; Ouyang et al., 2020; Lin et al., 2022). While the best-known and most prevalent sources of MSCs are bone marrow, adipose tissue and umbilical cord, increasing evidence from basic and preclinical studies suggests that human endometrium-derived mesenchymal stem/stromal cells (hEnMSCs) show great promise as an autologous source for regenerative medicine, including reproductive health (Abuwala and Tal, 2021). While quite a lot of knowledge has been accumulated about hEnMSCs, their role in the repair process of the endometrium and the impact on fertility disorders treatment, remains elusive.

The aim of the present study is to evaluate the endometrium as a potential source of multipotent MSCs, while specifying hEnMSCs collecting methods, and investigating their impact on endometrial-factor induced infertility according to the multifactorial background

along with an analysis of histological findings, gene expression and fertility assay.

Materials and methods

Patient recruitment

The study "Therapeutic potential of human endometrial stem cells" was approved by the Ethics Committee of Biomedical Research of Vilnius Region, No. 158200-18/7-1049-550 (29/06/2018). All endometrial tissue samples were collected during routine procedure at Vilnius University Hospital Santaros Klinikos Obstetrics and Gynaecology Center Santaros Fertility Center. The female subjects of the present study signed consent forms to confirm their agreement to providing their endometrium specimens.

Endometrial tissue samples were taken from a total 20 females undergoing ART procedures due to couple infertility. The inclusion criteria were as follows: (a) age of female at the time of enrollment is 18–45 years; (b) the minimum duration of infertility—1 year; (c) female is undergoing ART procedures due to couple infertility; (d) female confirms the participation in the study and signed informed consent. The exclusion criteria were as follows: (a) confirmed oncological disease for female during the last 3 years; (b) female smokes or is addicted to alcohol or other substances; (c) pregnancy is contraindicated for female; (d) female is diagnosed with uncontrolled endocrine or other medical conditions, such as hyperprolactinemia or thyroid diseases; (e) female was diagnosed with mental disorders or illness in the past medical history.

A reproductive medicine professional collected the specimens using 3 mm wide pipelle, endometrial sampling catheter, while performing a scratching procedure on the inner wall of uterine lining. The procedure was carried out once on Day 20–22 of the menstrual cycle prior to *in vitro fertilization* (IVF)/intracytoplasmic sperm injection (ICSI) procedure.

Isolation and cultivation of human endometrium-derived mesenchymal stem/stromal cells

The isolation of hEnMSCs was performed according to Tavakol et al. (2018). Shortly, endometrial tissue samples were washed with Hank's media, cut into small pieces and incubated with collagenase I (1 mg/ml) for approximately 60 min. The growth medium was then added and the sample was passed through a 70 µm Falcon cell strainer. Passed cells were centrifuged and purified from red blood cells (RBCs) by using Ficoll gradient. Isolated cells were cultured in a growth medium DMEM/F12 (DMEM, Dulbecco's Modified Eagle Medium/Nutrient Mixture F-12) supplemented with 10% Fetal Bovine Serum (FBS), 100 U/mL penicillin and 100 µg/mL streptomycin (Gibco, Thermo Fisher Scientific, Waltham, MA, United States) at 37°C in a 5% CO_2 atmosphere with humidity. Cells were plated into T75 cm^2 culture flasks at a density of 0.5–0.6 × 10^6 cells. The medium was replaced every 2–3 days and cells were replated according to their confluence. Cell viability was evaluated during passaging using Neubauer's chamber and Trypan Blue test. Preparation of hEnMSCs for the injection into female mice was done by washing cells twice with sterile phosphate-buffered saline (PBS) solution.

Flow cytometry analysis

To determine hEnMSCs surface markers, cells were collected (about 0.1 × 10^6 cells for one marker), centrifuged at 500 *g* speed for 5 min and washed twice with 1xPBS and 1% Bovine serum albumin (BSA) solution. Washed cells were then incubated for 30 min in the dark on ice with appropriate antibodies against cell surface markers (CD44, CD146, CD166, CD140b, CD34, CD45, HLA-DR). After that, the labelled cells were washed twice with PBS +1% BSA solution by centrifuging at 550 g for 5 min, 4°C. Since flow cytometry analysis was not done immediately, cells were fixated with 2% paraformaldehyde solution and later analyzed with Partec flow cytometer (Sysmex Corporation, Cobe, Hioko, Japan). Results were processed with Flowing Software 2 software.

Animal study

Animal testing "Possibilities of stem cells application for restoration of endometrium" was approved by the State Food and Veterinary Service of the Republic of Lithuania. Veterinary approval for that study was No. G2-115 (20/05/2019).

Procedures with animal were performed by trained specialists using appropriate equipment.

A total of 58 NOD. CB-17-Prkdc scid/Rj female mice, 6 weeks of age, 18 g ± 0.5 g were purchased from JANVIER LABS (France) and allowed to adapt to the new environment for at least a week. The mice were maintained in specific-pathogen free conditions.

The anesthetized mice were euthanized by cervical dislocation procedure. Mice were removed from their cages, anesthetized by 1%–3% isoflurane inhalation (100 mg/g, Isoflurin, Vetpharma, Spain) and gently restrained while resting on the operating tables with aseptic pads. Cervical dislocation was performed mechanically and resulted in euthanasia within approximately 10 s.

The Control mice group *(n = 11)* did not receive any interventions. The group of female mice with mechanically damaged endometrium and the chemotherapy-induced female mice were designed by the following procedures.

A design of mechanically damaged endometrium model in female mice

To construct a mechanically damaged endometrium model, 23 female mice were anesthetized by 1%–3% isoflurane inhalation (100 mg/g, Isoflurin, Vetpharma, Spain). Once the mice had no limb reaction, they were placed in a supine position with the limbs gently fixed on the operating table with aseptic pads. The operation area was disinfected by 75% alcohol, and a longitudinal incision of 1.5 cm was made in the low midline abdomen. Ophthalmic forceps were used to lift the skin, and ophthalmic scissors were used to cut the skin layer-by-layer longitudinally. A 21-gauge needle was inserted into the connection between the left and right uterine horns, and the right horn was scratched back and forth carefully until the uterus became hyperemic (approximately 10 times) while continuing to maintain the wholeness of the horn. The abdominal cavity was subsequently closed.

After 7 days, the affected female mice were divided into three groups: a) the mice group which was euthanized right away and its uterine horns were sent for further analysis (the MechI mice group, $n = 8$); b) the mice group which was housed together with male mice for 2 weeks ($n = 5$); and c) the mice group which was being prepared for the investigation of hEnMSCs treatment impact on the injured endometrium (the MechI-hEnMSCs mice group, $n = 10$). A few additional steps were required to achieve this goal. First, the abdominal cavity of the mice in the MechI-hEnMSCs group was reopened according to the previous protocol. When in the back of the bladder, the bilateral uterus was touched, then straight forceps were used to clamp the right horn in the upper third and in the lower third. hEnMSCs (0.5×10^6 cells/20 µl PBS) suspension was injected directly to the right horn. Subsequently, the abdominal cavity was closed. After 7 days, the MechI-hEnMSCs group of mice were divided into another two groups: a) mice that were euthanized right away with their uterine horn sent for further analysis ($n = 5$); and b) mice that were housed together with male mice for 2 weeks ($n = 5$). At the end of the study, the mated female mice were euthanized to evalute their fertility by counting embryo implantation sites (ISs). The number of embryo ISs in uterine horns was visually recorded after uterine horns dissection.

A design of chemotherapy-induced female mice model

To construct a chemotherapy-induced female mice model, 24 mice were injected once intraperitoneally with cyclophosphamide 120 mg/kg and busulfan 30 mg/kg. After 7 days, the affected female mice were divided into three groups: a) the mice group which was euthanized right away with its uterine horn were sent for further analysis (the CheI mice group, $n = 9$); b) the mice group housed together with male mice for 2 weeks ($n = 5$); and c) the mice group prepared for the investigation of hEnMSCs treatment impact on injured endometrium (the CheI-hEnMSCs mice group, $n = 10$). The anesthesia and the operation procedure for female mice with the aim to infused hEnMSCs suspension was performed according to procedures described in the section "A design of mechanically damaged endometrium model in female mice". After 7 days, the CheI-hEnMSCs mice were divided into two groups: a) mice that were euthanized right away with their uterine horn sent for further analysis ($n = 5$); and b) mice that were housed together with male mice for 2 weeks ($n = 5$).

A fertility assessment of the female mice was performed after 14 days. The studied mice were then euthanized to evalute their fertility by counting embryo ISs. The number of embryo ISs in uterine horns was visually recorded after uterine horns dissection.

RNA isolation from female mice uterine horns and gene expression analysis using RT-qPCR

Quick-DNA/RNA Miniprep Kit (Zymo Research, CA, United States) was used to facilitate the total RNA extraction from mice uterine horns. Frozen tissue was first submerged in liquid nitrogen and ground to a powder using a mortar and pestle. Then powder was mixed with about 600 µl of DNA/RNA Lysis Buffer, pipetted and transferred to a Zymo-Spin™ Column and centrifuged at 13,000 g for 1 min at room temperature. The following isolation steps were done in accordance with manufacturer's recommendations to ensure high yield and purity of the RNA samples. cDNA was synthesized using Luna® Universal One-Step the reverse transcription—quantitative polymerase chain reaction (RT-qPCR) Kit (New England Biolabs, Ipswich, MA, United States) in accordance with the manufacturer's recommendations. cDNA was then amplified by RT-qPCR using Luna® Universal qPCR Master Mix (New England Biolabs, Ipswich, MA, United States) in accordance with the manufacturer's guidelines. RT-qPCR was performed using Rotor-Gene 6,000 Real-time Analyzer (Corbett Life Science, QIAGEN, Hilden, Germany) and cycling conditions were set as follows: initial denaturation 95°C 1 min (1 cycle), denaturation 95°C 15 s, primer Tm 60°C 30 s (40 cycles). The sequences of forward and reverse primers used in this study are detailed in Table 1. Relative gene expression of *Col1a1 (Collagen, type I, alpha 1), Col3a1 (Collagen, type III, alpha 1), Acta2 (Actin alpha 2, smooth muscle)* and *CD44* was calculated using ΔΔCt method and mRNA levels were normalized according to *18S* expression.

Evaluation of uterine horns histology

Samples of uterine horns collected from female mice were fixed in 10% neutral buffered formalin with subsequent paraffin embedding. 3 µm-thick sections were stained with hematoxylin and eosin (H&E) and Masson's trichrome original in accordance with standard protocol. Digital whole slide images were recorded using a ScanScope XT Slide Scanner (Leica Aperio Technologies, Vista, CA, United States) under ×20 objective magnification (0.5-µm resolution) and subsequently subjected to digital image analysis by using HALOTM software (version 3.0311.174; Indica Labs, Corrales, New Mexico, United States). The positive pixel counts based HALO Area Quantification v2.1.3 algorithm was calibrated to recognize fibrosis areas and other surrounding tissues. Pixel intensity values were manually determined by the pathologist. Examples of image analysis output are presented in Figure 4 and Figure 6. The repeated manual measurements of the thickness of the total uterine horn wall and its separate layers (10 measurements per each tissue sample) were performed by using HALOTM software.

Statistical analysis

Statistical analysis was performed using GraphPad Prism version 8.0.1 for Windows, GraphPad Software, San Diego, California United States, www.graphpad.com. Data in graphs are represented as mean ± standard deviation (S.D.), while triangular data points indicate outliers determined by ROUT (Q = 5%). The statistical significance of difference was calculated using Mann-Whitney U test, Kruskal-Wallis test and Bonferroni test, significance was set at $p \leq 0.05$ (*), $p \leq 0.01$ (**), $p \leq 0.001$ (***).

Results

In this work, the effect of cells isolated from human endometrium on the female mice of mechanically damaged and

TABLE 1 List of primers used for RT-qPCR analysis.

Gene name	Forward primer (5′-3′)	Reverse primer (5′-3′)
18S	GGAAGGGCACCACCAGGAGT	TGCAGCCCCGGACATCTAAG
Col1a1	TCACCAAACTCAGAAGATGTAGGA	GACCAGGAGGACCAGGAAG
Col3a1	ACAGCAGTCCAACGTAGATGAAT	TCACAGATTATGTCATCGCA
Acta2	TTGCTGACAGGATGCAGAAGGAGA	ATCTGCTGGAAGGTAGACAGCGAA
CD44	ATCAGCAGATCGATTTGAATGTAA	CATTTCCTTCTATGAACCCATACC

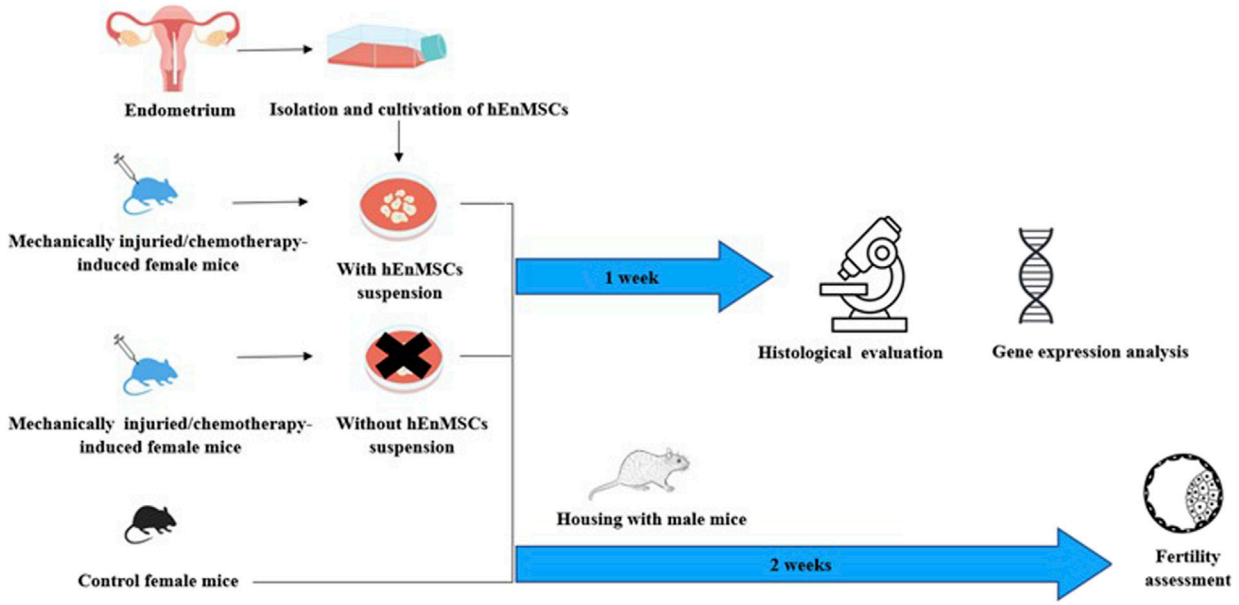

FIGURE 1
Schematic view of the study performed on different female mice groups: the Control mice group, the mechanically injuried endometrium mice group and the chemotherapy-induced mice group *(Adopted images from Shutterstock system)*.

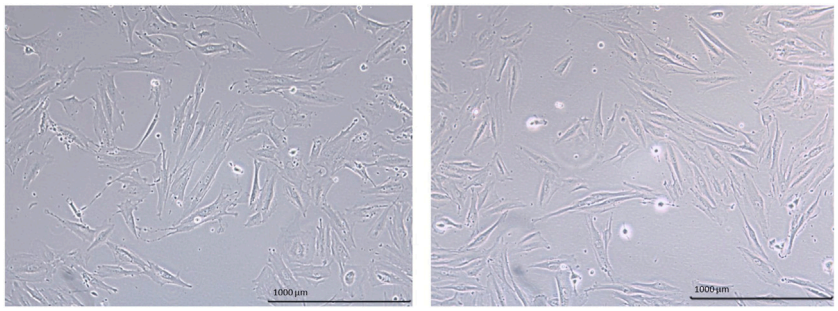

FIGURE 2
Morphology of hEnMSCs early passages. Images were taken with ×10 objective, scale bar—1000 µm.

chemotherapy-induced model was investigated (Figure 1). During the study, cells isolated from endometrium were characterized using flow cytometry. After, the cells were subsequently injected into the uterine horns of injured female mice. Changes in the uterine horn tissue were investigated by histological analysis, expression of genes related to the process of fibrosis. The therapeutic effect of cells to restore infertility has also been established.

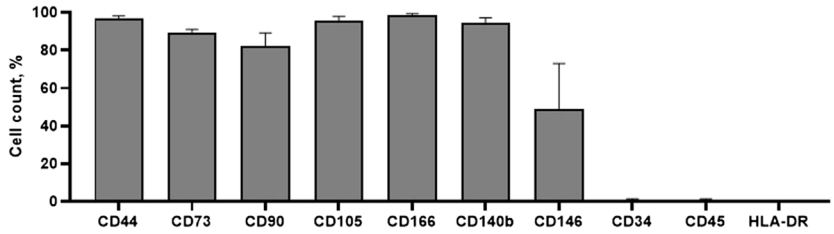

FIGURE 3
Characterization of hEnMSCs by the expression of surface markers. The cells were tested against mesenchymal stem cells markers: CD44, CD73, CD90, CD105, CD166; endometrial stromal cells markers: CD140b, CD146; hematopoietic and immune cells markers: CD34, CD45, HLA-DR. Analysis was performed using flow cytometry. Results are presented as mean ± S.D.

Characterization of hEnMSCs

The morphology of hEnMSCs was observed during cultivation and prior to the injection into different female mice models (Figure 2). The images indicate that cells had spindle-shaped morphology, were adherent and formed a consistent monolayer. The cells were cultured and further characterized at early passages.

Cell surface analysis by flow cytometry was carried out to ensure that our isolated cells corresponded with basic MSCs properties. We have founded that hEnMSCs were identified as positive with CD44, CD73, CD90, CD105, CD146, CD166 and CD140b cell surface markers (Figure 3). CD44 and CD166 were determined to be highly positive, exceeding 95%. Positive expression of CD146 and CD140b markers are characteristic to endometrial stromal cells and positive expression of CD44, CD73, CD90, CD105 surface markers confirms mesenchymal origin of stem cells. Moreover, hEnMSCs did not express hematopoietic cell surface markers CD34, CD45 and HLA-DR, which were all measured at less than 1%. Histograms of analyzed surface markers are presented in Supplementary Figure S1. In order to further characterize hEnMSCs by their differentiational abilities, we induced hEnMSCs to specialize into adipogenic, osteogenic, myogenic, neurogenic, and chondrogenic lineages in our previous research (Žukauskaitė et al., 2023). According to our results, we showed that hEnMSCs were able to successfully differentiate into adipogenic, osteogenic, neurogenic, and chondrogenic directions.

Establishment a multi-step analysis of different female mice models

The mechanically damaged endometrium model of NOD. CB-17-Prkdc scid/Rj female mice was established via endometrial scratching of the right uterine horn of female mice. Meanwhile, chemotherapy-induced female mice model was established using intraperitoneally chemotherapy. The Control mice model did not receive any interventions.

Uterine horns were collected and histologically evaluated 7 days after the endometrium injury (the MechI mice group) or intraperitoneally chemotherapy induction (the CheI mice group), and 7 days after hEnMSCs-treatment usage for endometrium regeneration in the MechI-hEnMSCs mice group and the CheI-hEnMSCs mice group, accordingly. Masson's trichrome original staining and H&E staining was used to evaluate histological changes in layers of uterine horns: the total wall, the myometrium-endometrium, the myometrium and the endometrium.

A fertility assessment was performed by visually counting of embryo ISs after 14 days of housing female mice and male mace together in these groups: female mice with mechanically damaged endometrium (MechI) or chemotherapy induction (CheI) and female mice with mechanically damaged endometrium or chemotherapy induction which received hEnMSCs-treatment usage for endometrium regeneration—the MechI-hEnMSCs mice group and the CheI-hEnMSCs mice group, accordingly. In the mechanically injured endometrium model, we counted the number of embryo ISs only in the one uterine horn which was affected. Meanwhile, in the chemotherapy-induced female mice, the number of embryo ISs was counted in two uterine horns due to the systematic effect of the medication.

Expression analysis of genes involved in fibrosis process *(Col1a1, Col3a1, Acta2 and CD44*) was performed with study's female mice groups using RNA extracted from their uterine horn tissue samples.

Fibrotic transformation under the influence of hEnMSCs-treatment in mechanically damaged endometrium model of female mice

An evaluation of fibrosis in different layers of uterine horns (the total wall, the myometrium-endometrium, the myometrium and the endometrium) was performed in 3 different female mice groups (the Control, the MechI and the MechI-hEnMSCs) using Masson's trichrome original staining (Figures 4D, H, L) and was subsequently statistically analyzed (Figure 5).

Statistical analysis showed significant differences in the fibrotic area between the Control mice group (Figure 4D), the MechI mice group (Figure 4H) and the MechI-hEnMSCs mice group (Figure 4L) in separate layers of mechanically injured uterine horns such as the total wall of uterine horn (Kruskal-Wallis; H = 8.38; df = 2; $p = 0.02$), the myometrium-endometrium (Kruskal-Wallis; H = 7.28; df = 2; $p = 0.03$) and the myometrium (Kruskal-Wallis; H = 7.53; df = 2; $p = 0.02$) (Figure 5). Conversely, the endometrial fibrosis was significant similar (Kruskal-Wallis; H = 5.58; df = 2; $p = 0.06$), although this related to the tendencies of the widest fibrotic area in the MechI mice group (Figure 4H) and the narrowest fibrotic area in the MechI-

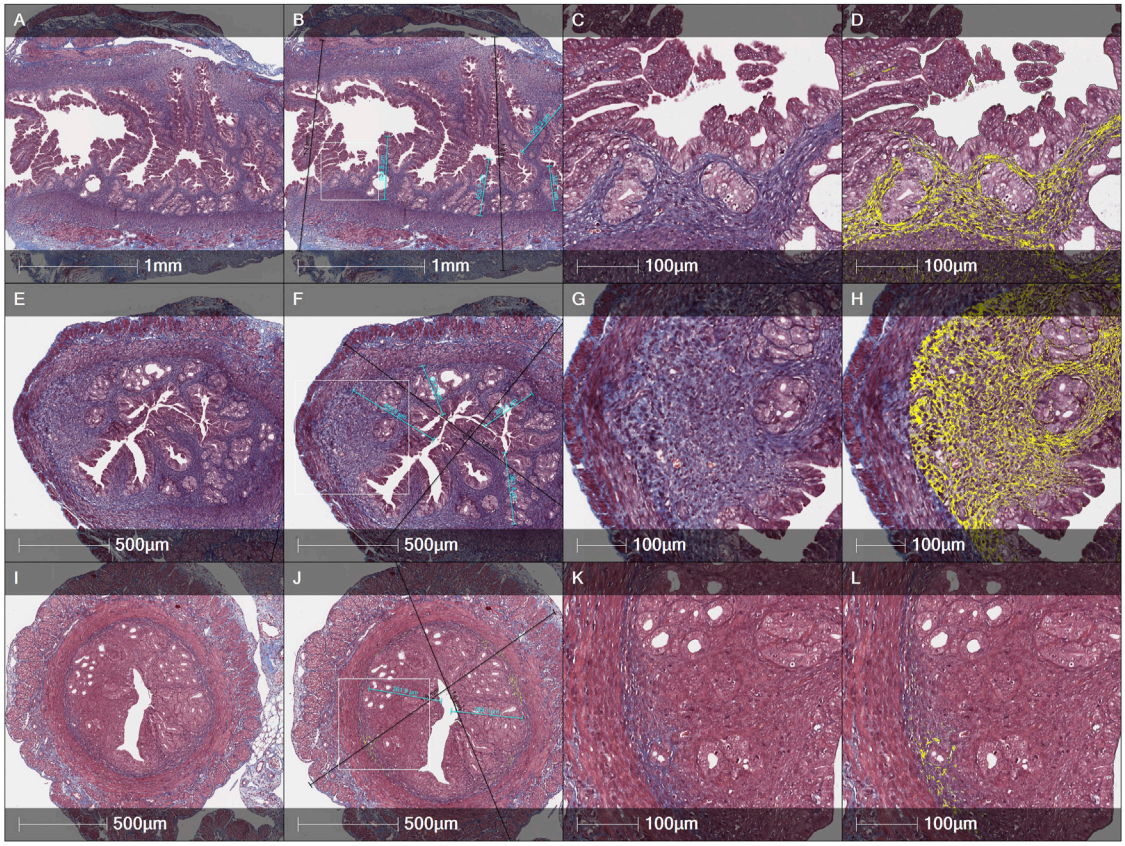

FIGURE 4
Histological evaluation of the thickness of endometrial and the total wall of uterine horn and fibrosis spread by Masson's trichrome original staining in different female mice groups: **(A–D)**—the Control, **(E–H)**—the MechI, (**I–L)**—the MechI-hEnMSCs. Figures **(B, F and J)** indicating measurements of endometrial thickness *(light blue)* and the total wall of uterine horn *(black)*. Fibrosis mark-up area *(in yellow)* on digitized slide obtained by automated image analysis Area Quantification algorithm **(D, H, L)**. Scale bar—1 mm, 500 µm and 100 µm. Figures **(B, F and J)**: white rectangle indicates higher magnification reference frames for Figures (**C, D, G, H, K, L)**.

hEnMSCs mice group (Figure 4L) (Figure 5). Overall, the lowest spread of fibrosis was observed of all layers of uterine horns in MechI-hEnMSCs mice group (Figure 4L)—the total wall 6.3% (±1,3%), the myometrium-endometrium 4.1% (±2.9%), the myometrium 6.0% (±0.8%) and the endometrium 1.1% (±1.7%) compared to other study's groups (Figure 5).

The Bonferroni *post hoc* test revealed that the percentage of fibrosis spread in the total wall and its separate layers—the myometrium and the myometrium-endometrium—was significantly higher in Mech I mice group (Figure 4H) compared to MechI-hEnMSCs mice group (Figure 4L) (Bonferroni test in all cases; $p < 0.05$), although the differences in mean values between the Control mice group (Figure 4D), the MechI mice group (Figure 4H) and the MechI-hEnMSCs mice group (Figure 4L) were not statistically significant (in all cases Bonferroni test; $p > 0.05$) (Figure 5).

Fibrotic transformation under the influence of hEnMSCs-treatment in chemotherapy-induced female mice model

Evaluation of fibrosis in different layers of uterine horns (the total wall of uterine horn, the myometrium-endometrium, the myometrium and the endometrium) was performed in 3 different female mice groups (the Control, the CheI and the CheI-hEnMSCs) using Masson's trichrome original staining (Figures 6D, H, L) and then they were statistically analyzed (Figure 5).

Analysing the intensity of fibrotic area, we detected no significant differences in separate uterine horn layers within the different female mice groups: the total wall of uterine horn (Kruskal-Wallis; H = 1.62; df = 2; $p = 0.45$), the myometrium-endometrium (Kruskal-Wallis; H = 1.06; df = 2; $p = 0,59$), the myometrium (Kruskal-Wallis; H = 1.66; df = 2; $p = 0.44$) and the endometrium (Kruskal-Wallis; H = 0.35; df = 2; $p = 0.84$) (Figure 5). However, the highest level of fibrosis was observed in the CheI mice group (Figure 6H) in all layers of uterine horns: the total wall of uterine horn 16.9% (±8.4%), the myometrium-endometrium 14.8% (±11.3%), the myometrium 21.4% (±9.8%) and endometrium 8.4% (±8.3%) (Figure 5).

Evaluation of the thickness of uterine horn layers and other histological changes in different female mice groups

An evaluation of the thickness of different uterine horns layers (the total wall of uterine horn and the endometrium) was performed

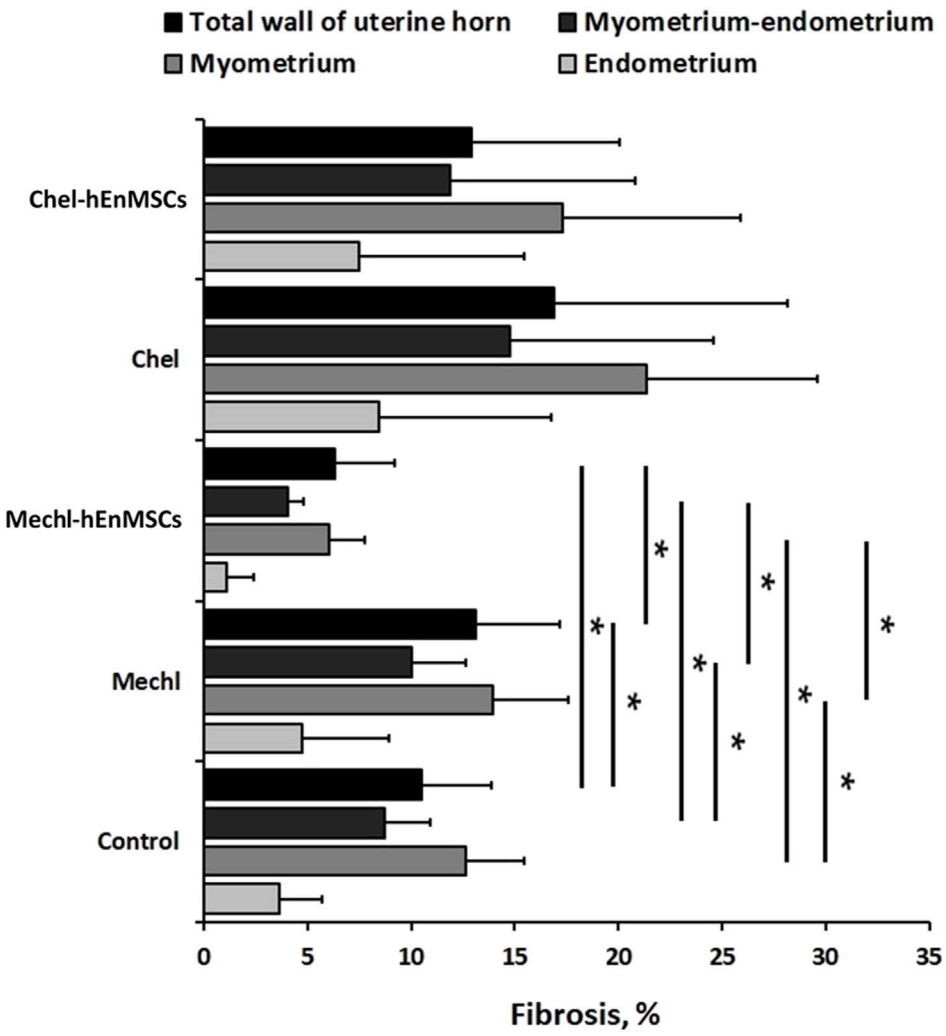

FIGURE 5
Statistical analysis of fibrotic transformation in different layers of uterine horns (the total wall of uterine horn, the myometrium-endometrium, the myometrium, and the endometrium). Uterine horns samples were collected from different female mice groups: the Control *(n = 4)*, the MechI *(n = 6)*, the MechI-hEnMSCs *(n = 4)*, the ChelI *(n = 3)* and the ChelI-hEnMSCs *(n = 3)*. Results are presented as mean and ±S.D. Statistical significance was evaluated using the Kruskal-Wallis test and Bonferroni test, where *denotes $p \leq 0.05$.

in the Control mice group (Figure 4B; Figure 6B), mechanically injured endometrium model (Figures 4F, 4J) and chemotherapy-induced model (Figures 6F, J) using Masson's trichrome original staining and, after that, statistically analyzed (Figure 7).

During the study, it was revealed that the widest total wall thickness of uterine horns was observed in the Che-EnMSCs mice group (1645.3 ± 203.0 μm) (Figure 6J), a slightly lower thickness was detected in the CheI group (1539.7 ± 190.5 μm) (Figure 6F) and the Control mice group (1500.7 ± 189.7 μm) (Figure 6B; Figure 7). Overall, the total wall thickness was significantly smaller in the MechI mice group (1315.1 ± 222.0 μm) (Figure 4F) and the MechI-EnMSCs mice group (1220.8 ± 241.5 μm) (Figure 4J; Figure 7).

An evaluation of the endometrial area in all female mice groups revealed that the widest endometrial area, as well as the total wall thickness of uterine horns, was observed in the Che-EnMSCs mice group (485.1 ± 50.0 μm) (Figure 6J; Figure 7). In contrast, the result of the Control mice group (367.2 ± 50.6 μm) (Figure 4B), the MechI mice group (388.0 ± 72.6 μm) (Figure 4F) and the MechI-hEnMSCs mice group (320.5 ± 69.3 μm) (Figure 4J) showed a thickening of the narrower endometrial area (Figure 7). It was also seen that the endometrial diameter in all female mice groups was significantly reduced compared to the total wall thickness (in all cases Mann-Whitney U; $p \leq 0.05$).

The nonparametric one-way analysis of variance revealed that the endometrial thickness of the Control mice group (Figure 6B) and the CheI mice group (Figure 6J) was statistically significant (Kruskal-Wallis; H = 6.56; df = 2; $p = 0.04$) and, moreover, the endometrial thickness in the Control group (Figure 6B) was significantly narrow in comparison with the CheI mice group (Figure 6F) and the Che-EnMSCs mice group (both Bonferroni test; $p < 0.05$) (Figure 7). Contrary to the endometrial area, the total wall thickness of uterine horns was not statistically different between the Control mice group (Figure 6B), the CheI mice group (Figure 6F) and the Che-EnMSCs mice group (Kruskal-Wallis; H = 1.62; df = 2;

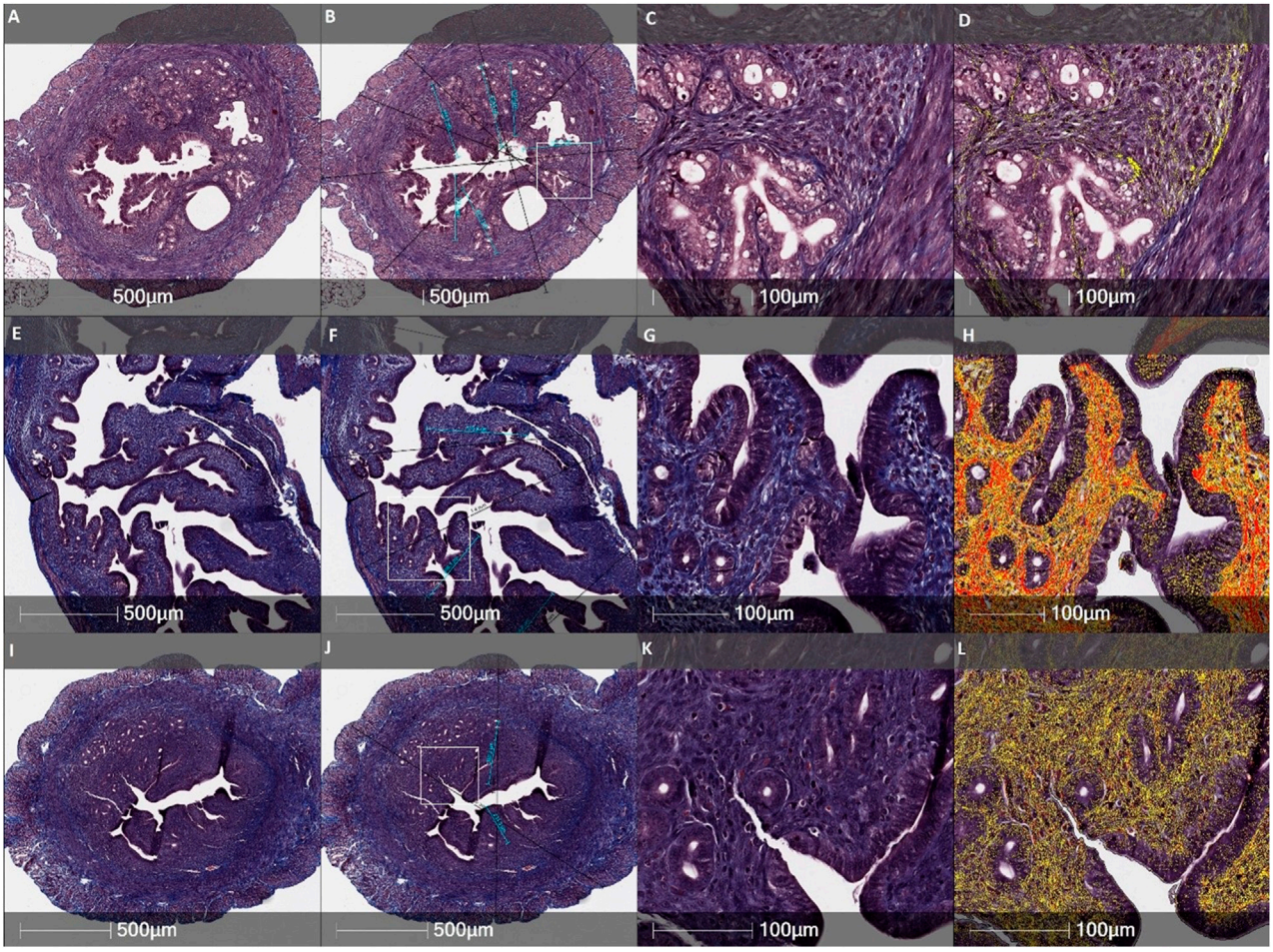

FIGURE 6
Histological evaluation of the thickness of endometrial and the total wall of uterine horn and fibrosis by Masson's trichrome original staining in different female mice groups: **(A–D)**—the Control mice group, **(E–H)**—the ChemI mice group, **(I–L)**—the ChemI-hEnMSCs mice group. Figures **(B, F and J)** indicate measurements of the endometrial thickness *(light blue)* and the total diameter of uterine horn *(black)*. Fibrosis mark-up area *(in yellow and red)* on digitized slide obtained by automated image analysis Area Quantification algorithm **(D, H, L)**. Scale bar –500 μm and 100 μm. Figures **(B, F and J)**: white rectangle indicates higher magnification reference frames for Figures (**C, D, G, H, K, L**).

$p = 0.45$) (Figure 6J; Figure 7). There was also a similarity between the Control mice group (Figure 4B), the MechI mice group (Figure 4F) and the MechI-hEnMSCs mice group (Figure 4J) in relation to the thickness of endometrium (Kruskal-Wallis; H = 1.67; df = 2; $p = 0.44$) and the total wall thickness of uterine horns (Kruskal-Wallis; H = 3.72; df = 2; $p = 0.16$) (Figure 7).

Some tendencies could be seen according to the histology assessment by H&E, also. It was observed that in the MechI mice group, the smooth cavity of uterine horn was damaged with the detaching of the endometrium and glandular dilatation (Figures 8D–F). Meanwhile, these findings were less pronounced in the MechI-EnMSCs mice group (Figures 8G–I) and not expressed in the Control mice group (Figures 8A–C). Assessing the intensity of inflammatory cells infiltration, absent or scant number of lymphocytes and polymorphonuclear cells (PMNs) was observed in the Control mice group (Figures 8A–C) and the MechI-EnMSCs mice group (Figures 8G–I) in contrast with the MechI mice group (Figures 8D–F), where moderate amount of PMNs were seen. Evaluating results of apoptosis rate, the moderate number of apoptotic bodies in the MechI mice group (Figures 8D–F) were observed. None of these pathological changes were detected in the Control mice group (Figures 8A–C) and they showed improvement in the MechI-hEnMSCs mice group (Figures 8G–I). However, the distribution results of inflammatory cells and apoptotic bodies when comparing chemotherapy-induced mice groups (Figures 8J–O) and the Control mice group (Figures 8A–C) were quite scattered. Overall, the similar tendencies were also seen in the evaluation of mitotic bodies formation in different study's groups (Figure 8).

Fertility assessment in different female mice groups

A fertility assessment was performed to evaluate the direct effect of stem cell-based treatment on reproductive function in

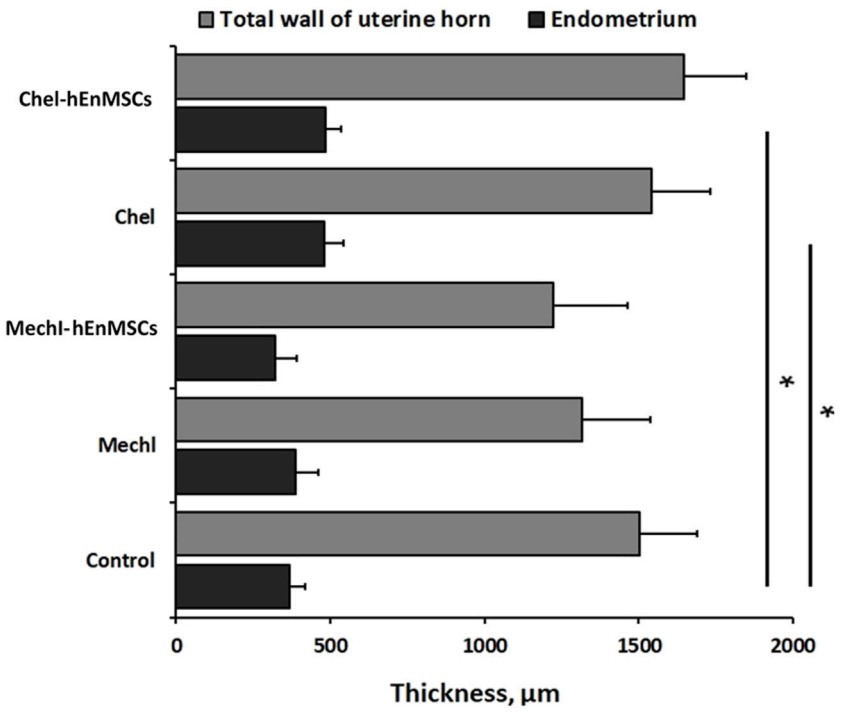

FIGURE 7
Analysis of the total wall and the endometrium thickness of uterine horns in different female mice groups: the Control mice group *(n = 4)*, the MechI mice group *(n = 6)*, the MechI-hEnMSCs mice group *(n = 4)*, the CheI mice group *(n = 3)* and the CheI-hEnMSCs mice group (n = 3). Results are presented as mean and ±S.D. Statistical significance was evaluated using the Kruskal-Wallis test and Bonferroni test, where *denotes $p \leq 0.05$.

5 different female mice groups (the Control, the MechI, the MechI-hEnMSCs, the CheI and the CheI-hEnMSCs) (Supplementary Table S1). In the mechanically injured endometrium model, we counted the number of embryo ISs only in the one uterine horn which was affected. Meanwhile, in the chemotherapy-induced female mice, the number of embryo ISs was counted in two uterine horns due to the specific effect of the medication. Chemotherapy drugs exert cytotoxic effects systemically and therefore can damage the ovaries, leading to infertility, premature ovarian failure, and, have indirect or direct deleterious effects on the uterus, that can be recognized clinically.

First of all, results from mechanically injured endometrium model showed a lower number of mice embryo ISs in the MechI mice group (2.6 ± 1.1 units) and the MechI-hEnMSCs mice group (3.8 ± 1,3 units) in comparison to the Control mice group (5.2 ± 0.8 units) (Figure 9). The Bonferroni *post hoc* test analysis revealed that the number of mice embryo ISs was significantly different between the Control mice group and the MechI mice group, also (Bonferroni test; $p < 0.05$) (Figure 9).

During the study of chemotherapy-induced female mice, the Control mice group was observed to have the highest number of mice embryo IS (10.8 ± 0.8 units), more than twice the number of embryo ISs was determined in the CheI-hEnMSCs mice group (4.6 ± 0.5 units) while the lowest number of embryo ISs was observed in the CheI mice group (0.2 ± 0.4 units) (Figure 10). Statistical analysis revealed that the number of embryo IS in the Control mice group, the CheI mice group and the CheI-hEnMSCs mice group was significantly different from each other (Kruskal-Wallis; H = 12.89; df = 2; $p = 0.002$; Bonferroni test; $p < 0.001$) (Figure 10).

Col1a1, *Col3a1*, *Acta2* and *CD44* gene expression analysis in uterine horn tissue from different female mice groups

Expression analysis of genes involved in fibrosis process was performed with 5 different female mice groups (the Control, the MechI, the MechI-hEnMSCs, the CheI and the CheI-hEnMSCs) using RNA extracted from their uterine horn tissue samples (Figure 11).

The discussed genes *Col1a1*, *Col3a1*, *Acta2* have been shown to have an association with excess fibrosis and wound healing (Liu et al., 1997; Cutroneo et al., 2007; Szóstek-Mioduchowska et al., 2019), and *CD44* gene is associated with the binding of extracellular matrix molecules, such as collagen, fibronectin and osteopontin (Foster et al., 1998). Gene expression analysis revealed that *Col1a1* gene was upregulated in all of the female mice groups receiving interventions, compared to Control mice group, although, only two of which were considered to be statistically significant (Figure 11). *Col1a1* gene was upregulated significantly in the MechI mice group and the CheI mice group (Figure 11). The expression of *Col3a1* gene throughout different group was determined to be at a very similar

10.3389/fcell.2023.1227487

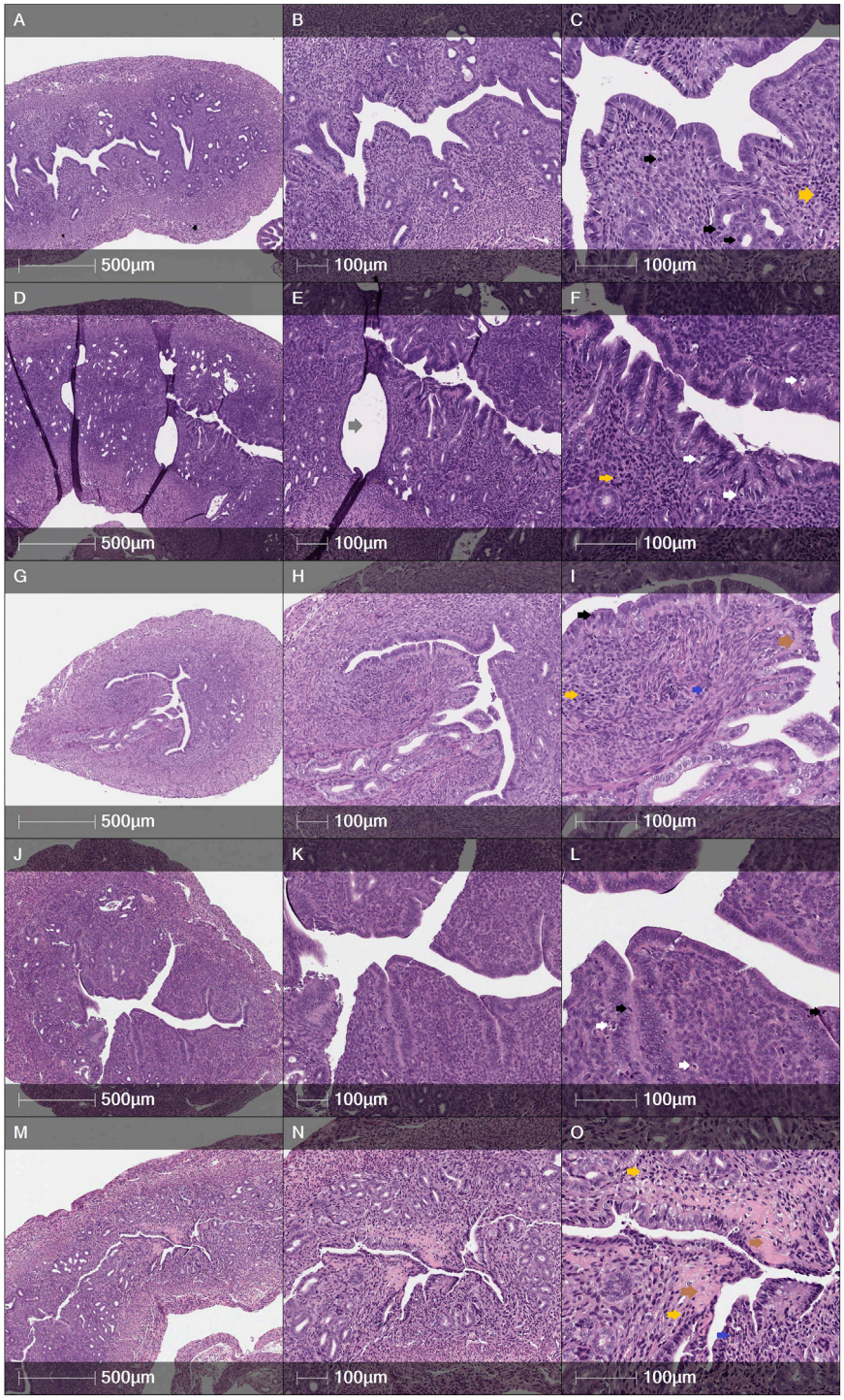

FIGURE 8
Cross sections of female mice uterine horns after H&E staining: **(A–C)**—the Control mice group, **(D–F)** - the MechI mice group, **(G–I)**—the MechI-hEnMSCs mice group, **(J–L)**—the ChemI mice group, **(M–O)**—the ChemI-hEnMSCs mice group. **(A–C)** Tall columnar epithelium with numerous mitotic figures in glands and stroma. Few apoptotic bodies. PMNs absent. No fibrosis. **(D–F)** Dilated glands, lined by tall columnar epithelium. Moderate apoptotic bodies, scant mitoses, moderate amount of PMNs. No fibrosis. **(G–I)** Compact endometrial stroma with few mitoses. Apoptotic bodies are scant. Few PMNs. Scant fibrosis. **(J–L)** Abundant mitosis in glands and stroma. Dense cellular endometrial stroma. Few apoptotic bodies and PMNs. No fibrosis. **(M–O)** Marked stromal fibrosis, distorted glands. Moderate mitotic figures and apoptotic bodies. Focal PMNs infiltration. Scale bar—500 μm and 100 μm. *Mitoses - black arrows; apoptotic bodies - white arrows; PMNs - blue arrows; lymphocytes - yellow arrows; fibrosis - brown arrows; dilated glands - grey arrows.*

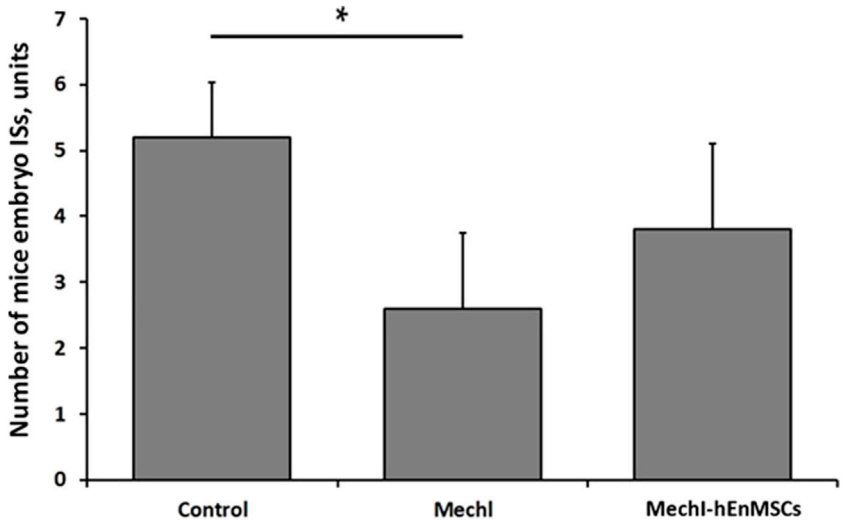

FIGURE 9
Fertility assessment in mechanically damaged endometrium model of female mice, accordingly to the number of embryo ISs in the one uterine horn: the Control mice group *(n = 5)*, the MechI mice group *(n = 5)* and the MechI-hEnMSCs mice group *(n = 5)*. Results are presented as mean and ±S.D. Statistical significance was evaluated using Kruskal-Wallis test and Bonferroni test, where *denotes $p \leq 0.05$.

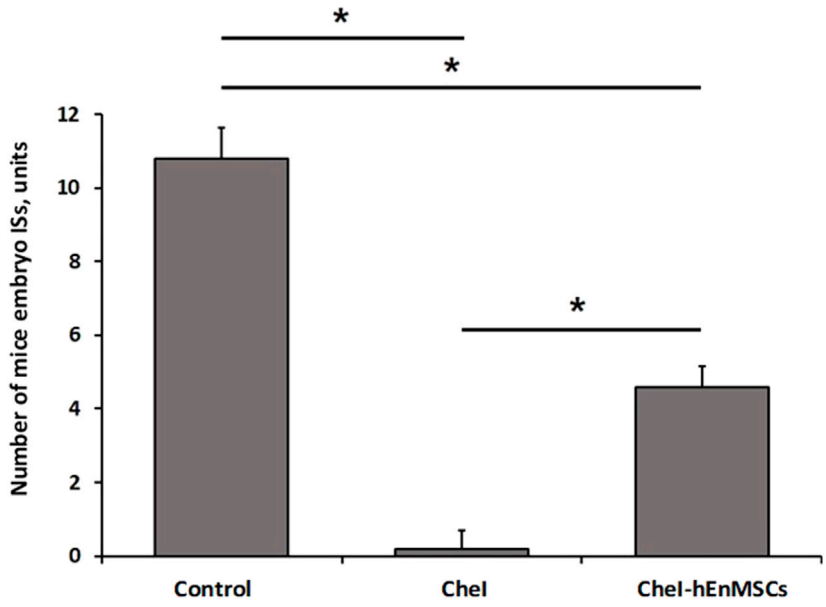

FIGURE 10
Fertility assessment in chemotherapy-induced female mice model, accordingly to the number of embryo ISs in both of uterine horns: the Control mice group *(n = 5)*, the ChemI mice group *(n = 5)* and the ChemI-hEnMSCs mice group *(n = 5)*. Results are presented as mean and ±S.D. Statistical significance was evaluated using Kruskal-Wallis and Bonferroni test, where *denotes $p \leq 0.05$.

level to the Control mice group, although a slight upregulation can be seen in the ChemI-hEnMSCs mice group when compared to the ChemI group. In all groups, *CD44* was downregulated in comparison to the Control mice group while values of relative gene expression remained at a similar level between the different mice groups. *Acta2* gene was upregulated in the MechI-hEnMSCs mice group in comparison to the MechI mice group, although the results were not significant.

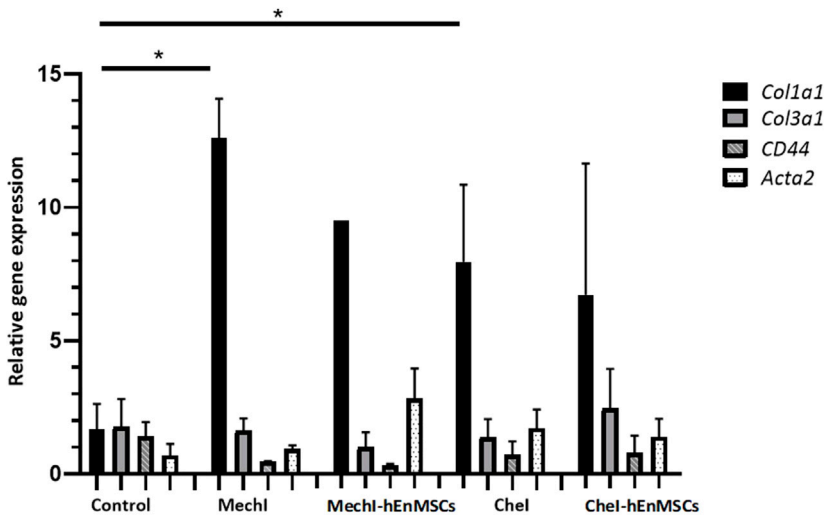

FIGURE 11
Analysis of differentially expressed *Col1a1, Col3a1, Acta2* and *CD44* genes in uterine horns samples collected from female mice groups: the Control mice group *(n = 2)*, the MechI mice group *(n = 2)*, the MechI-hEnMSCs mice group *(n = 1)*, the CheI mice group *(n = 6)* and the CheI-hEnMSCs mice group *(n = 2)* groups. Results are presented as mean and ±S.D. Relative mRNA expression was measured using RT-qPCR and results were calculated using ΔΔCt method and mRNA levels were normalized according to 18S expression. Statistical significance was evaluated using Mann–Whitney U test, where *denotes $p \leq 0.05$.

Discussion

Fertility is an issue that affects many parameters of peoples' lives, as individuals and as a couple. Nevertheless, while the main factors for the successful implantation are recognized as implantation competency of the embryo, a receptive state for the endometrium along with synchronized development for both of them, reproductive health disorders remain a significant problem (Teh et al., 2016), especially, endometrial-factor induced infertility. The lack of clear understanding of this pathology, along with conflicting theoretical and practical results from different studies have aggravated the impact of this situation to the point where couples facing this issue turn to alternatives such as surrogacy, uterine transplantation, adoption or they even choose to remain childless. Meanwhile, new strategies of diagnosis and treatment are being investigated.

Stem cell-based therapies have proved to be a promising treatment option for treating autoimmune, inflammatory, neurological, orthopaedic conditions and traumatic injuries, and could also be used for infertility. MSCs have several mechanisms of action, that could be utilized for the repair of reproductive dysfunction. The best known mode of action involves the migration of stem cells to the injured site in response to chemokines, which is followed by the differentiation into cells of the residing tissue and in the end resulting in the regeneration of the affected tissue (Wu et al., 2022). However, MSCs exhibit regenerative abilities not only through differentiation and integration, but also through paracrine signaling and immunoregulation (Jimenez-Puerta et al., 2020).

The human endometrium provides unique material in comparison to other adult tissues due to the cyclical nature of endometrial expansion, maturation and shedding, after which it again remarkably regenerates. Therefore the endometrium itself is considered to be an excellent source of stem cells and, moreover, hEnMSCs are considered to have great promise for the therapy of reproductive system disorders (Figueira et al., 2011).

The aim of this study was to deepen the investigation of the endometrial-factor induced infertility and hEnMSCs-based treatment role on it using multifactorial analysis consisted from the histological assessment, gene expression analysis and fertility assay.

First of all, in the present study we confirmed that the endometrium scratching procedure performed for female undergoing ART procedures due to couple infertility is an effective tool for the collection of stem cells. Isolated stem cells from endometrium samples, which were collected through endometrium scratching procedures, had a fibroblastic-like appearance with adherent property to the culture plate, expressed MSCs markers CD44 and CD166 and, did not express hematopoietic cell surface markers CD34, CD45 and HLA-DR. These findings fulfil the minimal criteria to define human MSCs proposed by Mesenchymal and Tissue Stem Cell Committee of the International Society for Cellular Therapy (ISCT) (Dominici et al., 2006; Machado et al., 2013; Baghaei et al., 2017). The findings negate the uncertainty about endometrium scratching usage for stem cells collection and lead us to clearly confirm that not only *stratum basalis*, but, also, *stratum functionalis* could be used for the isolation of stem cells with high proliferation, self-renewal and differentiation potential characteristics of hEnMSCs (Schwab and Gargett, 2007; Gargett and Masuda, 2010; Hu et al., 2019; Cousins et al., 2022). The evidence that hEnMSCs can be easily and repeatedly isolated without leading to major technical problems or causing

inconvenience to patients—such as the need for hospitalization or anaesthesia—is worthwhile for stem cells-based therapy implementation in clinical practise (Mobarakeh et al., 2012; Stem Cell Research & Therapy | Full Text, n. d.).

Further, embryo implantation is a precise process, in which various factors come into play one after the other, so we decided to extended used models to evaluate the effectiveness of hEnMSCs therapy for induced infertility (Archibong et al., 2011; Jiang et al., 2013; Alawadhi et al., 2014; Hu et al., 2019; Stem Cell Research & Therapy | Full Text, n. d.). In this way, we combined three evaluation methods—histological assessment, gene expression analysis and fertility assay—in pursuit of a broader view which could provide new insights for understanding related mechanisms and investigate treatment strategies.

According to multivarious study results, mechanically injury of the endometrium or intraperitoneal chemotherapy was observed to be capable of causing clear negative impact on uterine tissues and, most importantly, conceiving. The fibrotic area of the total wall of uterine horns and their separate layers—the myometrium and the myometrium-endometrium was significantly wider in untreated mice group with the mechanically injured endometrium compared to the mice group with mechanically injured endometrium, which received hEnMSCs.

The same tendencies were seen in the chemotherapy-induced mice group where the highest level of fibrosis in all uterine horns' layers was observed in the mice group which did not receive hEnMSCs in comparison with treated mice group and the Control mice group. These findings could be explained by the activity of hEnMSCs. The regeneration capacity of stromal cells is defined by the broad differentiation potential, highly efficient self-renewal, and remarkable immunomodulatory capacity and paracrine activity to migrate to the injured reproductive tissues caused by chemokines, before they differentiate and integrate somatic cells with non-tumorigenic properties (Jimenez-Puerta et al., 2020; Wiśniewska et al., 2021; Wu et al., 2022). It creates conditions for slowing down the progression of fibrosis and (or) replacing damaged tissues (Nie et al., 2011; Park et al., 2018; Wiśniewska et al., 2021). The ability of MSCs to relieve the fibrotic diseases by modulating inflammation, regenerating damaged tissues and modulating the death of stressed cells was also confirmed in the following results Qin et al., 2023.

According to the assessment of other histology elements, it was observed that hEnMSCs-based therapy can reduce the infiltration of inflammation factors such as PMNs and lymphocytes, and apoptotic bodies in uterine horns. The density of inflammatory cells and the rate of apoptotic bodies was higher in the mechanically injured female mice model, which did not receive hEnMSCs suspension, compared to the mechanically injured female mice model which received hEnMSCs suspension and the Control mice group. These repeated tendencies were also seen in fertility assessment of female mice.

During the study, the higher fertility rate was observed in harmfully affected mice groups which received stem cells therapy, even with a significant difference between the chemotherapy-induced female mice model, which did not receive stem cells and the chemotherapy-induced female mice model, which were treated.

The observed tendencies of histological changes and fertility assessment in different groups of female mice are fairly strong confirmation of the relationships between both of them and could be explained by several known physiological mechanisms.

First of all, the fibrotic endometrium is characterized by poor epithelial growth, poor vascular development, impaired endometrium function and the displacement of extracellular matrix by the fibrous connective tissues, which can lead to uterine cavity degeneration, progression to intrauterine adhesions or Asherman's syndrome and, ultimately to embryo implantation dysfunction and consequent infertility or spontaneous abortion (Deans and Abbott, 2010; Cai et al., 2016; Bai et al., 2019). Secondly, apoptosis is a form of programmed cell death in which cells condense and fragment their nuclear material, cytoplasmic material, and then release their contents in membrane-bound apoptotic bodies (Kerr et al., 1972). In this way, apoptotic bodies may contain a wide variety of cellular components such as micronuclei, chromatin remnants, cytosol portions, degraded proteins, DNA fragments, or even intact organelles and other metabolites which could negatively affect even gene expression (Battistelli and Falcieri, 2020; Medina et al., 2020; Zeng et al., 2020). An imbalance of apoptotic bodies clearance could cause harmful exposure to the inflammatory and immunogenic contents of dying cells, ultimately causing implantation failure and consecutive pregnancy complications (Fadok et al., 1998; Savill et al., 2002; Maderna and Godson, 2003). Moreover, few studies concluded that some substance derived from PMNs may exert toxic effects on fertilized oocytes or on spermatozoa and could thus be responsible for the endometrial-factor induced infertility (Parr et al., 1967). Also, a variation of endometrial natural killer, T and B lymphocyte populations including upregulation of them, have all been proposed as contributory factors to adverse reproductive failure outcome such as repeated implantation failure and recurrent pregnancy loss (Robertson et al., 2018; Marron and Harrity, 2019; Csabai et al., 2020). However, there is still a lack of study into each subtype, including their concentrations in the endometrium and mechanisms of activity. Further research is essential not only in the inflammatory process, but also in other fields.

The measurement of the endometrial thickness and the total diameter of the uterine horns showed controversial results, especially when studying the chemotherapy-induced mice groups. The endometrial thickness in the Control mice group was significantly narrow compared with the chemotherapy-induced mice groups that nevertheless received hEnMSCs-based therapy. The total wall thickness of uterine horns was not statistically different between these three groups of female mice, although the shortest diameter was measured in the Control mice group. Moreover, the frequency of the distribution of inflammatory cells and apoptotic bodies between chemotherapy-induced mice groups and the Control mice group was quite scattered. These results are quite unexpected because it is well known that chemotherapy is one of the main cause of premature ovarian failure (Torrealday et al., 2017; Mauri et al., 2020; Spears et al., 2019) which is characterized by hypoestrogenism and, eventually, the endometrium atrophy. This limitation might be related to several factors, including the need for more time to develop premature ovarian failure. Some pre-processing issues were also agreed: during gross examination, the cross sections of uterine

horns were selected as thick as possible for further paraffin-embedding procedure in order to receive well-represented cross-sections of tissues and facilitate the whole procedure. Future perspective for overcoming this limitation is applying a more standardised gross section procedure which targets for more systemic tissue sampling regardless of the thickness of uterine horns.

Meanwhile, the last step of our study was to evaluate relationships between the expression of certain genes profile and different groups of female mice. It was observed that *Col1a1* gene was upregulated in all mice groups with mechanically injured endometrium and chemotherapy-induced mice groups with the statistically significant increase in the harmfully affected mice groups without hEnMSCs therapy. *Col1a1* encodes the major component of type I collagen, the fibrillar collagen found in most connective tissues. According to the fact that gene expression is regulated by both extrinsic and intrinsic factors to the cell and interplay between them (Scitable by nature education, 2008; Kabir and O'Connor, 2019), it could be hypothesized that stem cells-based therapy can reduce or even prevent formation of excessive fibrosis through transcriptional changes. Also, interesting insights could be made after the evaluation of *Acta2* gene profile expression in different female mice groups. *Acta2* encodes smooth muscle actin - Actin alpha 2. It was seen upregulation of *Acta2* gene expression in the mechanically injured mice group which received hEnMSCs compared with the same affected mice group which was not treated. Actin proteins are essential for the cell structure, and they are also involved in the process of cell motility, integrity, and intercellular signalling (NCBI, 2023). Moreover, *Acta2* is one of 6 different actin isoforms and is involved in the contractile apparatus of smooth muscle; mutation in this gene can cause a variety of vascular diseases, such as multisystemic smooth muscle dysfunction syndrome (NCBI, 2023). In this way, downregulation of *Acta2* gene expression can be associated with the abnormal uterine contractility which may contribute to endometrium-factor induced infertility. Considering the extensive growth of the genetic and epigenetic studies, it is believed that more clarification of actual relations between stem cells activity, gene profile expression and reproductive health disorders will come.

Conclusion

Failure to achieve a pregnancy and successful live birth due to the endometrial-factor induced infertility is one of the major challenges in the field of reproductive medicine.

Given the study results, hEnMSCs are an attractive target for endometrial-factor induced infertility. Isolated hEnMSCs have demonstrated a positive impact on the repair of mechanically injured endometrium and chemotherapy-induced endometrium with—most importantly—successful pregnancy outcomes. Moreover, it becomes apparent that multipotent MSCs can be successfully isolated from endometrium samples collected through routine gynaecological procedure such as endometrium scratching or endometrium biopsy. This finding increases the flexibility and effectiveness of MSCs collection procedure with help to decrease inconvenience to patients. Also, our study presented that a combination of multifactorial analysis could be valuable for the deeper understanding of the endometrial-factor induced infertility and, probably other endometrium pathologies.

Overall, generated results encourage the continuation of further research in order to discover new insights in this field with the hope of identifying safe and individually effective treatment strategies in mechanical injured or chemotherapy induced endometrial-factor infertility in daily clinical practise.

Data availability statement

The data and materials used and analyzed underlying this article are available from the corresponding authors on reasonable request.

Ethics statement

The studies involving humans were approved by the Ethics Committee of Biomedical Research of Vilnius Region, No. 158200-18/7-1049-550 (29/06/2018). The studies were conducted in accordance with the local legislation and institutional requirements. The participants provided their written informed consent to participate in this study. The animal study was approved by the State Food and Veterinary Service of the Republic of Lithuania. Veterinary approval for that study No. G2-115 (20/05/2019). The study was conducted in accordance with the local legislation and institutional requirements.

Author contributions

RB: designed the study, selected patients, performed clinical procedures and experiments with animals, summarized results of the histological changes, gene expression and fertility assessment, performed statistical analysis, wrote the original draft. BV-M: designed the study, selected patients, performed clinical procedures and experiments with animals, reviewed and edited the manuscript. VB: designed the study, performed experiments with animals, reviewed and edited the manuscript. EV: isolated and cultivated hEnMSCs from collected endometrium samples, analyzed gene expression by the RT-qPCR and interpretated obtained results, performed statistical analysis and visualization of the manuscript. JB: applied Masson's trichrome original staining and H&E staining, calibrated digital image analysis algorithms and performed measurements on digitalized images of female mice uterine horns, analyzed and interpretated results of histological changes, performed visualization of the manuscript. RV: applied Masson's trichrome original staining and H&E staining, evaluated histological changes of layers of female mice uterine horns, analyzed and interpretated results of histological changes, performed visualization of the manuscript. EK: validated data, performed review and editing of the manuscript. DR: conceptualized the study, curated the data, validated the data, performed review and editing of the manuscript. RN: conceptualized the study, supervised study performing and writing processes, performed review and editing of the article. All authors contributed to the article and approved the submitted version.

Conflict of interest

The authors declare that the research was conducted in the absence of any commercial or financial relationships that could be construed as a potential conflict of interest.

Publisher's note

All claims expressed in this article are solely those of the authors and do not necessarily represent those of their affiliated organizations, or those of the publisher, the editors and the reviewers. Any product that may be evaluated in this article, or claim that may be made by its manufacturer, is not guaranteed or endorsed by the publisher.

Supplementary material

The Supplementary Material for this article can be found online at: https://www.frontiersin.org/articles/10.3389/fcell.2023.1227487/full#supplementary-material

References

AAGL Elevating Gynecologic Surgery (2017). AAGL practice report: practice guidelines on intrauterine adhesions developed in collaboration with the European society of gynaecological endoscopy (ESGE). *J. Minim. Invasive Gynecol.* 24, 695–705. doi:10.1016/j.jmig.2016.11.008

Abuwala, N., and Tal, R. (2021). Endometrial stem cells: origin, biological function, and therapeutic applications for reproductive disorders. *Curr. Opin. Obstet. Gynecol.* 33, 232–240. doi:10.1097/GCO.0000000000000702

Alawadhi, F., Du, H., Cakmak, H., and Taylor, H. S. (2014). Bone Marrow-Derived Stem Cell (BMDSC) transplantation improves fertility in a murine model of Asherman's syndrome. *PLoS One* 9, e96662. doi:10.1371/journal.pone.0096662

Archibong, A. E., Sharan, C., and Al-Hendy, A. (2011). Intervention of chemotherapy-induced ovarian failure/infertility using diploid cell therapy. *Fertil. Steril.* 96, S125. doi:10.1016/j.fertnstert.2011.07.488

Baghaei, K., Hashemi, S. M., Tokhanbigli, S., Asadi Rad, A., Assadzadeh-Aghdaei, H., Sharifian, A., et al. (2017). Isolation, differentiation, and characterization of mesenchymal stem cells from human bone marrow. *Gastroenterol. Hepatol. Bed Bench* 10 (3), 208–213. doi:10.22037/ghfbb.v0i0.1089

Bai, X., Liu, J., Cao, S., and Wang, L. (2019). Mechanisms of endometrial fibrosis and the potential application of stem cell therapy. *Discov. Med.* 27, 267–279.

Battistelli, M., and Falcieri, E. (2020). Apoptotic bodies: particular extracellular vesicles involved in intercellular communication. *Biol. (Basel)* 9, E21. doi:10.3390/biology9010021

Bu, Z., Hu, L., Su, Y., Guo, Y., Zhai, J., and Sun, Y.-P. (2020). Factors related to early spontaneous miscarriage during IVF/ICSI treatment: an analysis of 21,485 clinical pregnancies. *Reprod. Biomed. Online* 40, 201–206. doi:10.1016/j.rbmo.2019.11.001

Cai, H., Li, H., and He, Y. (2016). Interceed and estrogen reduce uterine adhesions and fibrosis and improve endometrial receptivity in a rabbit model of intrauterine adhesions. *Reprod. Sci.* 23, 1208–1216. doi:10.1177/1933719116632923

Chen, L., Qu, J., Cheng, T., Chen, X., and Xiang, C. (2019). Menstrual blood-derived stem cells: toward therapeutic mechanisms, novel strategies, and future perspectives in the treatment of diseases. *Stem Cell. Res. Ther.* 10, 406. doi:10.1186/s13287-019-1503-7

Cousins, F. L., Filby, C. E., and Gargett, C. E. (2022). Endometrial stem/progenitor cells–their role in endometrial repair and regeneration. *Front. Reproductive Health* 3, 811537. doi:10.3389/frph.2021.811537

Csabai, T., Pallinger, E., Kovacs, A. F., Miko, E., Bognar, Z., and Szekeres-Bartho, J. (2020). Altered immune response and implantation failure in progesterone-induced blocking factor-deficient mice. *Front. Immunol.* 11, 349. doi:10.3389/fimmu.2020.00349

Cutroneo, K. R., White, S. L., Phan, S. H., and Ehrlich, H. P. (2007). Therapies for bleomycin induced lung fibrosis through regulation of TGF-beta1 induced collagen gene expression. *J. Cell. Physiol.* 211, 585–589. doi:10.1002/jcp.20972

Deans, R., and Abbott, J. (2010). Review of intrauterine adhesions. *J. Minim. Invasive Gynecol.* 17, 555–569. doi:10.1016/j.jmig.2010.04.016

Dominici, M., Le Blanc, K., Mueller, I., Slaper-Cortenbach, I., Marini, F., Krause, D., et al. (2006). Minimal criteria for defining multipotent mesenchymal stromal cells. The International Society for Cellular Therapy position statement. *Cytotherapy* 8, 315–317. doi:10.1080/14653240600855905

ESHRE Capri Workshop Group (2001). Social determinants of human reproduction. *Hum. Reprod.* 16, 1518–1526. doi:10.1093/humrep/16.7.1518

Fadok, V. A., Bratton, D. L., Frasch, S. C., Warner, M. L., and Henson, P. M. (1998). The role of phosphatidylserine in recognition of apoptotic cells by phagocytes. *Cell. Death Differ.* 5, 551–562. doi:10.1038/sj.cdd.4400404

Figueira, P. G. M., Abrão, M. S., Krikun, G., Taylor, H. S., and Taylor, H. (2011). Stem cells in endometrium and their role in the pathogenesis of endometriosis. *Ann. N. Y. Acad. Sci.* 1221, 10–17. doi:10.1111/j.1749-6632.2011.05969.x

Fossett, E., Khan, W. S., Longo, U. G., and Smitham, P. J. (2012). Effect of age and gender on cell proliferation and cell surface characterization of synovial fat pad derived mesenchymal stem cells. *J. Orthop. Res.* 30, 1013–1018. doi:10.1002/jor.22057

Foster, L. C., Arkonac, B. M., Sibinga, N. E., Shi, C., Perrella, M. A., and Haber, E. (1998). Regulation of CD44 gene expression by the proinflammatory cytokine interleukin-1beta in vascular smooth muscle cells. *J. Biol. Chem.* 273, 20341–20346. doi:10.1074/jbc.273.32.20341

Fuoco, N. L., de Oliveira, R. G., Marcelino, M. Y., Stessuk, T., Sakalem, M. E., Medina, D. A. L., et al. (2020). Efficient isolation and proliferation of human adipose-derived mesenchymal stromal cells in xeno-free conditions. *Mol. Biol. Rep.* 47, 2475–2486. doi:10.1007/s11033-020-05322-9

Gargett, C. E., and Masuda, H. (2010). Adult stem cells in the endometrium. *Mol. Hum. Reprod.* 16, 818–834. doi:10.1093/molehr/gaq061

Guo, Z., Xu, X., Zhang, L., Zhang, L., Yan, L., and Ma, J. (2020). Endometrial thickness is associated with incidence of small-for-gestational-age infants in fresh *in vitro* fertilization-intracytoplasmic sperm injection and embryo transfer cycles. *Fertil. Steril.* 113, 745–752. doi:10.1016/j.fertnstert.2019.12.014

Heger, A., Sator, M., and Pietrowski, D. (2012). Endometrial receptivity and its predictive value for IVF/ICSI-outcome. *Geburtsh Frauenheilk* 72, 710–715. doi:10.1055/s-0032-1315059

Hu, J., Song, K., Zhang, J., Zhang, Y., and Tan, B.-Z. (2019). Effects of menstrual blood-derived stem cells on endometrial injury repair. *Mol. Med. Rep.* 19, 813–820. doi:10.3892/mmr.2018.9744

Jiang, Y., Zhao, J., Qi, H., Li, X., Zhang, S., Song, D. W., et al. (2013). Accelerated ovarian aging in mice by treatment of busulfan and cyclophosphamide. *J. Zhejiang Univ. Sci. B* 14, 318–324. doi:10.1631/jzus.B1200181

Jimenez-Puerta, G. J., Marchal, J. A., López-Ruiz, E., and Gálvez-Martín, P. (2020). Role of mesenchymal stromal cells as therapeutic agents: potential mechanisms of action and implications in their clinical use. *J. Clin. Med.* 9, 445. doi:10.3390/jcm9020445

Jing, S., Li, X., Zhang, S., Gong, F., Lu, G., and Lin, G. (2019). The risk of placenta previa and cesarean section associated with a thin endometrial thickness: a retrospective study of 5251 singleton births during frozen embryo transfer in China. *Arch. Gynecol. Obstet.* 300, 1227–1237. doi:10.1007/s00404-019-05295-6

Kabir, M. H., and O'Connor, M. D. (2019). Stems cells, big data and compendium-based analyses for identifying cell types, signalling pathways and gene regulatory networks. *Biophys. Rev.* 11, 41–50. doi:10.1007/s12551-018-0486-4

Kerr, J. F., Wyllie, A. H., and Currie, A. R. (1972). Apoptosis: a basic biological phenomenon with wide-ranging implications in tissue kinetics. *Br. J. Cancer* 26, 239–257. doi:10.1038/bjc.1972.33

Lee, S. H. (2018). The advantages and limitations of mesenchymal stem cells in clinical application for treating human diseases. *Osteoporos. Sarcopenia* 4, 150. doi:10.1016/j.afos.2018.11.083

Lessey, B. A., and Young, S. L. (2019). What exactly is endometrial receptivity? *Fertil. Steril.* 111, 611–617. doi:10.1016/j.fertnstert.2019.02.009

Lin, Y., Dong, S., Ye, X., Liu, J., Li, J., Zhang, Y., et al. (2022). Synergistic regenerative therapy of thin endometrium by human placenta-derived mesenchymal stem cells encapsulated within hyaluronic acid hydrogels. *Stem Cell. Res. Ther.* 13, 66. doi:10.1186/s13287-022-02717-2

Liu, H., Zhang, J., Wang, B., and Kuang, Y. (2020). Effect of endometrial thickness on ectopic pregnancy in frozen embryo transfer cycles: an analysis including 17,244 pregnancy cycles. *Fertil. Steril.* 113, 131–139. doi:10.1016/j.fertnstert.2019.09.003

Liu, K. E., Hartman, M., Hartman, A., Luo, Z.-C., and Mahutte, N. (2018). The impact of a thin endometrial lining on fresh and frozen-thaw IVF outcomes: an analysis of over 40 000 embryo transfers. *Hum. Reprod.* 33, 1883–1888. doi:10.1093/humrep/dey281

Liu, X., Wu, H., Byrne, M., Krane, S., and Jaenisch, R. (1997). Type III collagen is crucial for collagen I fibrillogenesis and for normal cardiovascular development. *Proc. Natl. Acad. Sci. U. S. A.* 94, 1852–1856. doi:10.1073/pnas.94.5.1852

Lukomska, B., Stanaszek, L., Zuba-Surma, E., Legosz, P., Sarzynska, S., and Drela, K. (2019). Challenges and controversies in human mesenchymal stem cell therapy. *Stem Cells Int.* 2019, 9628536. doi:10.1155/2019/9628536

Machado, C. de V., Telles, P. D. da S., and Nascimento, I. L. O. (2013). Immunological characteristics of mesenchymal stem cells. *Rev. Bras. Hematol. Hemoter.* 35, 62–67. doi:10.5581/1516-8484.20130017

Maderna, P., and Godson, C. (2003). Phagocytosis of apoptotic cells and the resolution of inflammation. *Biochimica Biophysica Acta (BBA) - Mol. Basis Dis.* 1639, 141–151. doi:10.1016/j.bbadis.2003.09.004

Mahutte, N., Hartman, M., Meng, L., Lanes, A., Luo, Z.-C., and Liu, K. E. (2022). Optimal endometrial thickness in fresh and frozen-thaw *in vitro* fertilization cycles: an analysis of live birth rates from 96,000 autologous embryo transfers. *Fertil. Steril.* 117, 792–800. doi:10.1016/j.fertnstert.2021.12.025

Marron, K., and Harrity, C. (2019). Endometrial lymphocyte concentrations in adverse reproductive outcome populations. *J. Assist. Reprod. Genet.* 36, 837–846. doi:10.1007/s10815-019-01427-8

Mauri, D., Gazouli, I., Zarkavelis, G., Papadaki, A., Mavroeidis, L., Gkoura, S., et al. (2020). Chemotherapy associated ovarian failure. *Front. Endocrinol.* 11, 572388. doi:10.3389/fendo.2020.572388

Medina, C. B., Mehrotra, P., Arandjelovic, S., Perry, J. S. A., Guo, Y., Morioka, S., et al. (2020). Metabolites released from apoptotic cells act as tissue messengers. *Nature* 580, 130–135. doi:10.1038/s41586-020-2121-3

Mints, M., Jansson, M., Sadeghi, B., Westgren, M., Uzunel, M., Hassan, M., et al. (2008). Endometrial endothelial cells are derived from donor stem cells in a bone marrow transplant recipient. *Hum. Reprod.* 23, 139–143. doi:10.1093/humrep/dem342

Mobarakeh, Z. T., Ai, J., Yazdani, F., Sorkhabadi, S. M. R., Ghanbari, Z., Javidan, A. N., et al. (2012). Human endometrial stem cells as a new source for programming to neural cells. *Cell. Biol. Int. Rep.* 19, e00015. doi:10.1042/CBR20110009

Moffat, R., Beutler, S., Schötzau, A., De Geyter, M., and De Geyter, C. (2017). Endometrial thickness influences neonatal birth weight in pregnancies with obstetric complications achieved after fresh IVF-ICSI cycles. *Archives Gynecol. obstetrics* 296, 115–122. doi:10.1007/s00404-017-4411-z

Mouanness, M., Ali-Bynom, S., Jackman, J., Seckin, S., and Merhi, Z. (2021). Use of intra-uterine injection of platelet-rich plasma (PRP) for endometrial receptivity and thickness: a literature review of the mechanisms of action. *Reprod. Sci.* 28, 1659–1670. doi:10.1007/s43032-021-00579-2

Musiał-Wysocka, A., Kot, M., and Majka, M. (2019). The pros and cons of mesenchymal stem cell-based therapies. *Cell. Transpl.* 28, 801–812. doi:10.1177/0963689719837897

NCBI (2023). ACTA2 actin alpha 2, smooth muscle [Homo sapiens (human)]. Available at: https://www.ncbi.nlm.nih.gov/gene/59 (Accessed November 14, 2022).

Nie, C., Yang, D., Xu, J., Si, Z., Jin, X., and Zhang, J. (2011). Locally administered adipose-derived stem cells accelerate wound healing through differentiation and vasculogenesis. *Cell. Transpl.* 20, 205–216. doi:10.3727/096368910X520065

Oron, G., Hiersch, L., Rona, S., Prag-Rosenberg, R., Sapir, O., Tuttnauer-Hamburger, M., et al. (2018). Endometrial thickness of less than 7.5 mm is associated with obstetric complications in fresh IVF cycles: a retrospective cohort study. *Reprod. Biomed. Online* 37, 341–348. doi:10.1016/j.rbmo.2018.05.013

Ouyang, X., You, S., Zhang, Y., Zhang, C., Zhang, G., Shao, X., et al. (2020). Transplantation of human amnion epithelial cells improves endometrial regeneration in rat model of intrauterine adhesions. *Stem Cells Dev.* 29, 1346–1362. doi:10.1089/scd.2019.0246

Park, S.-R., Kim, J.-W., Jun, H.-S., Roh, J. Y., Lee, H.-Y., and Hong, I.-S. (2018). Stem cell secretome and its effect on cellular mechanisms relevant to wound healing. *Mol. Ther.* 26, 606–617. doi:10.1016/j.ymthe.2017.09.023

Parr, E. L., Schaedler, R. W., and Hirsch, J. G. (1967). The relationship of polymorphonuclear leukocytes to infertility in uteri containing foreign bodies. *J. Exp. Med.* 126, 523–538. doi:10.1084/jem.126.3.523

Phermthai, T., Odglun, Y., Julavijitphong, S., Titapant, V., Chuenwattana, P., Vantanasiri, C., et al. (2010). A novel method to derive amniotic fluid stem cells for therapeutic purposes. *BMC Cell. Biol.* 11, 79. doi:10.1186/1471-2121-11-79

Phermthai, T., Tungprasertpol, K., Julavijitphong, S., Pokathikorn, P., Thongbopit, S., and Wichitwiengrat, S. (2016). Successful derivation of xeno-free mesenchymal stem cell lines from endometrium of infertile women. *Reprod. Biol.* 16, 261–268. doi:10.1016/j.repbio.2016.10.002

Qin, L., Liu, N., Bao, C. L., Yang, D. Z., Ma, G. X., Yi, W. H., et al. (2023). Mesenchymal stem cells in fibrotic diseases—The two sides of the same coin. *Acta Pharmacol. Sin.* 44 (2), 268–287. doi:10.1038/s41401-022-00952-0

Ranisavljevic, N., Raad, J., Anahory, T., Grynberg, M., and Sonigo, C. (2019). Embryo transfer strategy and therapeutic options in infertile patients with thin endometrium: a systematic review. *J. Assist. Reprod. Genet.* 36, 2217–2231. doi:10.1007/s10815-019-01576-w

Ribeiro, V. C., Santos-Ribeiro, S., De Munck, N., Drakopoulos, P., Polyzos, N. P., Schutyser, V., et al. (2018). Should we continue to measure endometrial thickness in modern-day medicine? The effect on live birth rates and birth weight. *Reprod. Biomed. Online* 36, 416–426. doi:10.1016/j.rbmo.2017.12.016

Robertson, S. A., Care, A. S., and Moldenhauer, L. M. (2018). Regulatory T cells in embryo implantation and the immune response to pregnancy. *J. Clin. Investig.* 128, 4224–4235. doi:10.1172/JCI122182

Rombauts, L., McMaster, R., Motteram, C., and Fernando, S. (2015). Risk of ectopic pregnancy is linked to endometrial thickness in a retrospective cohort study of 8120 assisted reproduction technology cycles. *Hum. Reprod.* 30, 2846–2852. doi:10.1093/humrep/dev249

Santamaria, X., Liu, J. H., Lusine, A., Isaacson, K., Movilla, P., Fernandez, H., et al. (2020). Should we consider alternative therapies to operative hysteroscopy for the treatment of Asherman syndrome? *Fertil. Steril.* 113, 511–521. doi:10.1016/j.fertnstert.2020.01.022

Savill, J., Dransfield, I., Gregory, C., and Haslett, C. (2002). A blast from the past: clearance of apoptotic cells regulates immune responses. *Nat. Rev. Immunol.* 2, 965–975. doi:10.1038/nri957

Schwab, K. E., and Gargett, C. E. (2007). Co-expression of two perivascular cell markers isolates mesenchymal stem-like cells from human endometrium. *Hum. Reprod.* 22, 2903–2911. doi:10.1093/humrep/dem265

Scitable by nature education (2008) Gene expression regulates cell differentiation. Available at: https://www.nature.com/scitable/topicpage/gene-expression-regulates-cell-differentiation-931/[Accessed November 16, 2022].

Song, Y.-T., Liu, P.-C., Tan, J., Zou, C.-Y., Li, Q.-J., Li-Ling, J., et al. (2021). Stem cell-based therapy for ameliorating intrauterine adhesion and endometrium injury. *Stem Cell. Res. Ther.* 12, 556. doi:10.1186/s13287-021-02620-2

Spears, N., Lopes, F., Stefansdottir, A., Rossi, V., De Felici, M., Anderson, R. A., et al. (2019). Ovarian damage from chemotherapy and current approaches to its protection. *Hum. Reprod. Update* 25 (6), 673–693. doi:10.1093/humupd/dmz027

Strug, M., and Aghajanova, L. (2021). Making more womb: clinical perspectives supporting the development and utilization of mesenchymal stem cell therapy for endometrial regeneration and infertility. *J. Pers. Med.* 11, 1364. doi:10.3390/jpm11121364

Szóstek-Mioduchowska, A. Z., Lukasik, K., Skarzynski, D. J., and Okuda, K. (2019). Effect of transforming growth factor -β1 on α-smooth muscle actin and collagen expression in equine endometrial fibroblasts. *Theriogenology* 124, 9–17. doi:10.1016/j.theriogenology.2018.10.005

Tavakol, S., Azedi, F., Hoveizi, E., Ai, J., and Joghataei, M. T. (2018). Human endometrial stem cell isolation from endometrium and menstrual blood. *Bio Protoc.* 8, e2693. doi:10.21769/BioProtoc.2693

Taylor, H. S. (2004). Endometrial cells derived from donor stem cells in bone marrow transplant recipients. *JAMA* 292, 81–85. doi:10.1001/jama.292.1.81

Teh, W.-T., McBain, J., and Rogers, P. (2016). What is the contribution of embryo-endometrial asynchrony to implantation failure? *J. Assist. Reprod. Genet.* 33, 1419–1430. doi:10.1007/s10815-016-0773-6

Tipnis, S., Viswanathan, C., and Majumdar, A. S. (2010). Immunosuppressive properties of human umbilical cord-derived mesenchymal stem cells: role of B7-H1 and ido. *Immunol. Cell. Biol.* 88, 795–806. doi:10.1038/icb.2010.47

Torrealday, S., Kodaman, P., and Pal, L. (2017). Premature Ovarian Insufficiency - an update on recent advances in understanding and management. *F1000Res* 6, 2069. doi:10.12688/f1000research.11948.1

Wang, J., Liu, C., Fujino, M., Tong, G., Zhang, Q., Li, X.-K., et al. (2019). Stem cells as a resource for treatment of infertility-related diseases. *Curr. Mol. Med.* 19, 539–546. doi:10.2174/1566524019666190709172636

Wiśniewska, J., Sadowska, A., Wójtowicz, A., Słyszewska, M., and Szóstek-Mioduchowska, A. (2021). Perspective on stem cell therapy in organ fibrosis: animal models and human studies. *Life* 11, 1068. doi:10.3390/life11101068

Wu, J.-X., Xia, T., She, L.-P., Lin, S., and Luo, X.-M. (2022). Stem cell therapies for human infertility: advantages and challenges. *Cell. Transpl.* 31, 9636897221083252. doi:10.1177/09636897221083252

Yuan, X., Saravelos, S. H., Wang, Q., Xu, Y., Li, T.-C., and Zhou, C. (2016). Endometrial thickness as a predictor of pregnancy outcomes in 10787 fresh IVF-ICSI cycles. *Reprod. Biomed. Online* 33, 197–205. doi:10.1016/j.rbmo.2016.05.002

Zeng, C., Shao, Z., Li, J., Pan, H., and Xing, F. (2020). Commentary: metabolites released from apoptotic cells act as tissue messengers. *Front. Immunol.* 11, 1878. doi:10.3389/fimmu.2020.01878

Zhang, L., Li, Y., Guan, C.-Y., Tian, S., Lv, X.-D., Li, J.-H., et al. (2018). Therapeutic effect of human umbilical cord-derived mesenchymal stem cells on injured rat endometrium during its chronic phase. *Stem Cell. Res. Ther.* 9, 36. doi:10.1186/s13287-018-0777-5

Žukauskaitė, D., Vitkevičienė, A., Žlibinaitė, A., Baušytė, R., Ramašauskaitė, D., and Navakauskienė, R. (2023). Histone H4 hyperacetylation but not DNA methylation regulates the expression of decidualization-associated genes during induced human endometrial stromal cells decidualization. *Int. J. Biochem. Cell. Biol.* 156, 106362. doi:10.1016/j.biocel.2023.106362

frontiers | Frontiers in Cell and Developmental Biology

TYPE Original Research
PUBLISHED 06 October 2023
DOI 10.3389/fcell.2023.1231755

OPEN ACCESS

EDITED BY
Patricia S. Cuasnicu,
CONICET Institute of Biology and Experimental Medicine (IBYME), Argentina

REVIEWED BY
Anna Lange-Consiglio,
University of Milan, Italy
Ahmed Gad,
Colorado State University, United States

*CORRESPONDENCE
C. Soriano-Úbeda,
c.soriano.ubeda@unileon.es
C. Matás,
cmatas@um.es

RECEIVED 30 May 2023
ACCEPTED 21 September 2023
PUBLISHED 06 October 2023

CITATION
Toledo-Guardiola SM, Luongo C, Abril-Parreño L, Soriano-Úbeda C and Matás C (2023), Different seminal ejaculated fractions in artificial insemination condition the protein cargo of oviductal and uterine extracellular vesicles in pig.
Front. Cell Dev. Biol. 11:1231755.
doi: 10.3389/fcell.2023.1231755

Different seminal ejaculated fractions in artificial insemination condition the protein cargo of oviductal and uterine extracellular vesicles in pig

S. M. Toledo-Guardiola[1], C. Luongo[1], L. Abril-Parreño[1], C. Soriano-Úbeda[2]* and C. Matás[1,3]*

[1]Departamento de Fisiología, Facultad de Veterinaria, Campus de Excelencia Mare Nostrum Universidad de Murcia, Murcia, Spain, [2]Departamento de Medicina, Cirugía y Anatomía Veterinaria, Universidad de Léon, León, Spain, [3]Instituto Murciano de Investigación Biosanitaria Pascual Parrilla (IMIB-Arrixaca), Murcia, Spain

The seminal plasma (SP) is the liquid component of semen that facilitates sperm transport through the female genital tract. SP modulates the activity of the ovary, oviductal environment and uterine function during the periovulatory and early pregnancy period. Extracellular vesicles (EVs) secreted in the oviduct (oEVs) and uterus (uEVs) have been shown to influence the expression of endometrial genes that regulate fertilization and early embryo development. In some species, semen is composed of well-separated fractions that vary in concentration of spermatozoa and SP composition and volume. This study aimed to investigate the impact of different accumulative fractions of the porcine ejaculate (F1, composed of the sperm-rich fraction, SRF; F2, composed of F1 plus the intermediate fraction; F3, composed of F2 plus the post-SRF) on oEVs and uEVs protein cargo. Six days after the onset of estrus, we determined the oEVs and uEVs size and protein concentration in pregnant sows by artificial insemination (AI-sows) and in non-inseminated sows as control (C-sows). We also identified the main proteins in oEVs and uEVs, in AI-F1, AI-F2, AI-F3, and C-sows. Our results indicated that although the size of EVs is similar between AI- and C-sows, the protein concentration of both oEVs and uEVs was significantly lower in AI-sows ($p < 0.05$). Proteomic analysis identified 38 unique proteins in oEVs from AI-sows, mainly involved in protein stabilization, glycolytic and carbohydrate processes. The uEVs from AI-sows showed the presence of 43 unique proteins, including already-known fertility-related proteins (EZR, HSPAA901, PDS). We also demonstrated that the protein composition of oEVs and uEVs differed depending on the seminal fraction(s) inseminated (F1, F2, or F3). In conclusion, we found specific protein cargo in oEVs and uEVs according to the type of semen fraction the sow was inseminated with and whose functions these specific EVs proteins are closely associated with reproductive processes.

KEYWORDS

ejaculate fractions, extracellular vesicles, insemination, oviductal fluid, pregnant sows, uterine fluid

1 Introduction

The ejaculation in boars is characterized by the release of semen in three visually differentiated fractions, each with specific color and consistency, associated with different cellular concentrations and biochemical compositions (Rodríguez-Martínez et al., 2009). The two main fractions of boar ejaculate are the sperm-rich fraction (SRF), which exhibits the highest concentration of sperm and accounts for 10%–30% of the total ejaculate volume and is well recognized by its dense white color, and the post-SRF, which represents the largest volume (70%–90% of the total ejaculate) but contains low levels of spermatozoa and has a watery aspect (Mann et al., 1981). The transition fraction between the SRF and the post-SRF, called intermediate fraction that is constituted by a higher volume than SRF, low concentration of spermatozoa, and greyish color. In farms, boar ejaculates are typically manually collected, retaining only the SRF to prepare seminal doses for artificial insemination (AI). The post-SRF and remaining seminal plasma (SP) are commonly discarded. However, in an increasing number of farms, the collection method is shifting towards semi-automated techniques, which enable the collection of the entire ejaculate and preservation of the large volume of SP present in the post-SRF (Aneas et al., 2008). It is well established that SP modulates sperm viability, function, and the ability to interact with the uterine epithelium and oocyte for successful fertilization (Rodríguez-Martínez et al., 2021). Moreover, the influence of SP extends beyond fertility, as its infusion into the uterus during the estrus persists throughout the preimplantation period, leading to modifications in the endometrial and embryonic transcriptome by upregulating genes and pathways related to maternal immune tolerance, embryonic development, implantation, and pregnancy progress (Martínez et al., 2019; Parrilla et al., 2020). SP triggers genetic and epigenetic pathways in spermatozoa that produce lasting changes in the female immune response with significant implications for progeny (Watkins et al., 2018; Morgan and Watkins, 2020). Importantly, studies have demonstrated that including all ejaculate fractions within seminal doses does not negatively impact reproductive performance regarding fertility, prolificacy, and animal growth (Luongo et al., 2022). As well as increasing the chances of the sperm reaching and fertilizing the egg, SP also has the potential to influence the development of the embryo (Martínez et al., 2020). This influence is thought to occur through specialized signaling pathways that interact with the female reproductive system.

Qualitative and quantitative differences in the SP proteome have been identified between the most relevant parts of boar ejaculate (Perez-Patiño et al., 2016), as well as in specific communication particles such as extracellular vesicles (EVs) (Barranco et al., 2019). EVs from SP play a regulatory role in female reproductive physiology in sows by modulating immune-related gene expression at the uterine level, facilitating spermatozoa fertilization of oocytes (Bai et al., 2018) and beyond. The reciprocal communication conceptus-endometrium is necessary for a successful pregnancy (Bazer and Johnson, 2014). This communication occurs through EVs released from the uterus (Kusama et al., 2018) and oviduct (Mazzarella et al., 2021), which are essential for regulating pivotal cellular activities during the peri-implantation period (Mittelbrunn and Sánchez-Madrid, 2012). The EVs released at uterine level modulate reproductive processes, such as follicular development in the ovary, oocyte maturation (Machtinger et al., 2016), maternal-embryonic communication (Almiñana et al., 2017) and the establishment of mammalian pregnancy. All of this may suggest a specific mechanism used by the uterine microenvironment to facilitate the fertilization process (Burns et al., 2014) and early embryonic development (Burns et al., 2016).

In relation to spermatozoa and once in the female genital tract, oviductal and uterine EVs (oEVs and uEVs, respectively) are transferred to the male gamete to ensure hyperactive sperm motility and fertilization potential (Nguyen et al., 2016). EVs originated from different parts of the female tract can be taken up by spermatozoa and influence their competition (Bridi et al., 2020). In addition, it has been demonstrated that incubation of sperm with endometrial cell-derived EVs could increase sperm tyrosine phosphorylation and the proportion of sperm undergoing the acrosome reaction (Franchi et al., 2016). Based on this finding, the exchange of EVs can be suggested as an emerging pathway by which cells of the female reproductive tract can interact with sperm (Murdica et al., 2020). The secretion of oEVs and uEVs has been demonstrated to be time-dependent and specific to the physiological status (reviewed by Bidarimath et al., 2021).

In this work, we hypothesized that SP from different accumulative ejaculate fractions might differentially affect the content of EVs in the oviductal fluid (OF) and uterine fluid (UF). Therefore, this study aimed to characterize sows' oEVs and uEVs proteome in pregnant sows after AI with different accumulative fractions of the boar ejaculate and compare them to non-inseminated sows. The goal was to elucidate the potential effects of SP on reproductive events in the female reproductive tract.

2 Materials and methods

2.1 Reagents

All chemicals were obtained from Sigma-Aldrich Química, S.A. (Madrid, Spain) or Thermo Fisher Scientific (Waltham, MA, United States) unless otherwise indicated.

2.2 Animals

Fertile German Pietrain boars were housed in individual pens with sawdust, according to the European Commission Directive on the welfare of pigs, in the commercial farm Sergal Gestió Ramadera in Lleida (Spain). The temperature levels were automatically controlled by a system that kept constant the room temperature between 18°C and 22°C. Boars were fed with restricted diet according to their nutritional requirements. Water was provided *ad libitum*. Large White x Landrace crossbred sows (Danbred genetic) finalizing nursing were selected just after the weaning of their litters. The sows were selected according to specific criteria: similar body condition, age, and number of parities (between their third and fifth parity). After being separated from their litters, the selected sows were individually housed in gestation crates with unrestricted access to water and were provided with a daily feed allowance of 4.0 kg feed/

day. Oestrus detection was performed from the day of weaning and once daily in the presence of a mature boar.

2.3 Semen collection

Ejaculates from boars with proven fertility were collected using the manual method by an experienced technician. The sample was separated at the time of collection by the visual perception of the different seminal fractions of the ejaculate based on their volume, color, and consistency: i) the SRF, identified by its characteristic dense white color; ii) the intermediate fraction, which was characterized by larger volume than SRF and moderate dense white color; iii) the post-SRF, characterized by a watery liquid appearance due to the absence or very low number of spermatozoa. The pre-SRF and the gel fraction were discarded. Samples from each boar and seminal fraction were evaluated microscopically for sperm concentration, motility, acrosome integrity, and normal morphology using standard laboratory techniques and performed by experienced technicians to meet normal standards of seminal samples for AI under commercial requirements.

2.4 Preparation of semen doses and artificial insemination (AI)

Immediately after the collection of each ejaculate fraction, the samples were processed to obtain AI doses with a total final volume of 60 mL. The sperm concentration in the samples was first determined using a calibrated sperm analyzer (Androvision® Minitüb, Tiefenbach, Germany) and then diluted in the AndroStar® Plus extender (Minitüb, Tiefenbach, Germany) to achieve a final concentration of 33×10^6 spermatozoa/mL (2×10^6 total spermatozoa/dose 60 mL). Sows were inseminated in individual stalls using a post-cervical AI method at the onset of estrus and 24 h later. The AI was performed with the combined catheter-cannula kit Soft & Quick® (Tecno-Vet, S.L., Barcelona, Spain), which was inserted to the uterine body by an experienced technician according to the standard protocol for post-cervical AI commonly used in pig farms.

2.5 Fluids collection

Female reproductive tracts from sows were collected at the local abattoir and transported to the laboratory within 60 min. Once in the laboratory, the uterine tracts were washed twice in physiological saline (0.9% NaCl) supplemented with 0.1% antibiotic kanamycin. Tissue dissection was performed on a cooled surface, keeping the uterus and oviducts together from the same animal.

2.5.1 Oviductal fluid (OF) collection

The OF collection was performed as previously described by Kusama et al. (2018). Briefly, the oviductal lumen of the two oviducts from the same animal was flushed in the direction from the ampulla to the isthmus with 5 mL phosphate-buffered saline (PBS) at 4°C and using a catheter (24G BD Insyte™, 381212, Becton Dickinson Infusion Therapy Systems, Inc., Sandy, Utah, United States) adapted to a 10 mL syringe. The fluid collected after the oviduct flushing with PBS was processed to isolate EVs.

2.5.2 Uterine fluid (UF) collection

For the collection of UF, the uterus was irrigated in the direction from the caudal uterine horn to the utero-tubal junction with 10 mL PBS at 4°C using a 10 mL syringe. Immediately after collection, the flushing medium from both uterine horns was placed into Petri dishes and embryos were isolated from the obtained flushes under stereomicroscope to ensure pregnancy and were assessed for morphological quality and developmental stage classified as morula or blastocyst. The fluid collected after the uterus flushing with PBS was collected and processed to isolate EVs.

2.6 Isolation and characterization of extracellular vesicles (EVs)

EVs were isolated from oviductal and uterine flushings according to the protocol of serial ultracentrifugation described by Théry et al. (2006) and Almiñana et al. (2017) with some modifications. Briefly, each experimental group's flushings from the oviducts and uteri were centrifuged at $300 \times g$ for 15 min at 4°C to remove epithelial cells. The supernatant was collected and transferred to a new tube, then centrifuged at $2,000 \times g$ for 10 min at 4°C to remove cellular debris. The supernatant was then ultracentrifuged at $100,000 \times g$ for 70 min at 4°C (Beckman Coulter Optima L-100 XP ultracentrifuge with 70ti rotor) to pellet the EVs. The supernatant was discarded, and the pellet was resuspended in 3.5 mL PBS and ultracentrifuged again under the same conditions. The pellet was resuspended in a final volume of 300 µL PBS and aliquoted to 100 µL. One aliquot of EVs suspensions was analyzed fresh for protein concentration using the Coomassie Plus Bradford assay kit (23238, Fisher Scientific™, Waltham, MA, United States of America) according to the manufacturer's protocol. The same amount of protein was processed and analyzed in each sample within the same type of reproductive fluid, OF or UF, corresponding to the sample with the lowest total amount of protein. The rest of the aliquots were stored at −80°C until further analysis.

2.6.1 EVs morphology

The presence and morphology of EVs were determined by Transmission Electron Microscopy (TEM). Samples were processed according to the protocol described by Théry et al. (2006) with the following modifications. A 10 µL aliquot of the vesicle suspension was placed on a Formvar-Carbon-Coated grid for 30 s at room temperature. The vesicle-coated grids were washed once with distilled water for 1 min and then stained with 10 µL of 2% uranyl acetate for 1 min for negative contrast. The samples were air-dried at room temperature for 20 min. Photographs were taken using a JEOL1011 electron microscope slide at 80 kV (Jeol, Japan). Digital images were taken at 59,000–97,000 magnification.

2.6.2 EVs size

The size distribution of EVs was measured by Dynamic Light Scattering (DLS) according to Sabín et al. (2007) and using a

Malvern Autosizer 4,800 (Malvern Instruments, Malvern, United Kingdom) equipped with a solid state He-Ne laser at a wavelength of 488 nm. The intensity of the scattered light was measured at 25°C. A 10-µL aliquot of the vesicle suspension was diluted up to 1 mL in PBS and transferred to a disposable solvent-resistant cuvette specific for the DLS analysis. Data were acquired and analyzed using the PCS software (version 1.61, Rev. 1, Malvern Instruments, Malvern, United Kingdom) in the automatic acquisition mode. We chose to use the intensity values as they best represent the data of the pure sample, as they assume the least error (criterion taken from Malvern Instruments INC). In addition, particle intensity classification provides more accurate data on the size of the EVs.

2.6.3 EVs quantitation

EVs quantitation was performed using the EXOCET Exosome Quantitation Kit (System Biosciences, SBI) which is an enzymatic, colorimetric assay designed as a direct measurement of esterase activity known to be within exosomes.

Fresh EVs pooled pellets in a concentrated solution (corresponding to a protein concentration of 1–2 µg/µL) were resuspended with kit lysis Buffer at (1:4, v:v) to a total volume of 100 µL per reaction. EVs lysates were incubated at 37°C for 5 min and centrifuged at 1,500 *g* for 5 min to remove cell debris. 50 µL of transferred supernatants and standards were added to clear microtiter wells and mixed with 50 µL of reaction buffer (buffer A + buffer B) up to a total 100 µL volume in a 96 well plate (Nunclon Delta, Thermo Scientific). Replicates of each sample were made fourfold, and the microtiter plate was incubated for 20 min at room temperature. Optical density was read using a spectrophotometric plate reader (Apollo 11 LB913, Berthold Technologies GmbH & Co., TN, United States) at 405 nm. Finally, quantitate results were obtained by calculating the standard curve, previously calibrated by Nano Sight analysis, and plotting the sample readings on the standard curve. Quantitative results were represented in number of particles per mL.

2.6.4 EVs proteins immunoblotting

Protein extraction from 50 µL of the EVs suspension was carried out adding RIPA Lysis Buffer System (Santa Cruz Biotechnology Inc., Dallas, TX, United States) at 1:1 (v:v). The mixtures were pipetted up and down to resuspend the pellet for 5 min, incubated 30 min on ice, placed in an ice-cold sonication bath for 10 s at 20% amplitude and were centrifuged at 14,000 *g* for 5 min at 4°C to remove cell debris (Subedi et al., 2019). The supernatants were transferred to new tubes and the protein concentration was determined using the Bradford protein assay (Bio-Rad Laboratories, Inc., Hercules, CA, United States).

Equal protein amount of each sample (40 µg) was mixed with reducing Laemmli-buffer and was resolved on 10% sodium dodecyl sulphate polyacrylamide gel electrophoresis (10% Mini-PROTEAN® TGX™ Precast Protein Gels, Bio Rad®) and transferred to a 0.45 µm polyvinylidene difluoride nitrocellulose (PVDF) membrane (Immobilon®-P Transfer Membranes). Membranes were washed with distilled water and unspecific unions were blocked with Tris buffered saline containing 0.1% Tween 20 (T-TBS; P-1379, Sigma-Aldrich®, Madrid, Spain) supplemented with 5% skimmed milk for 1 h at room temperature. After that, membranes were incubated with the primary antibodies anti-HSP70 (Sigma Aldrich; Cat # H5147-2ML, 1:1.000) and anti-CD63 (Santa Cruz Biotechnology; Cat # sc-5275, 1:100) in blocking solution overnight at 4°C. After washing with fresh T-TBS, membranes were incubated for 1 h in goat anti-mouse IgG secondary antibody conjugated to horseradish peroxidase (HRP) in blocking solution (Du et al., 2016). Positive immunoreactive bands were detected by an enhanced chemiluminescence (ECL) substrate (Thermo Fisher Scientific, Waltham, MA, United States) and chemiluminescence was detected with Amersham™ Imager 600 (GE Healthcare) equipment.

2.7 Proteomic analysis of extracellular vesicles (EVs)

2.7.1 In-solution trypsin digestion

The EVs suspensions were thawed at 4°C and subsequently subjected to digestion. This digestion process took place in a solution containing 100 µL of a buffer consisting of 50 mM ammonium bicarbonate with a pH of 8.5. To aid in the digestion, a small amount (0.01%, v:v) of ProteaseMax (Promega, WI, United States) was added. In addition, the samples were reduced by introducing 20 mM of dithiothreitol (DTT) and incubating the mixture for 20 min at 56°C. Following this, the samples were alkylated by adding 100 mM of iodoacetic acid (IAA) and allowing it to react for 30 min at room temperature while keeping the environment dark. Once the alkylation was completed, the digestion process was initiated by adding Trypsin Gold Proteomics Grade (Promega) to the mixture at a ratio of 1:100 (w/w). The digestion was carried out for a duration of 3 h at 37 °C. To halt the reaction, 0.1% formic acid was added, and the resulting mixture was filtered through a filter with a pore diameter of 0.2 µm. Finally, the samples were dried using an Eppendorf Vacuum Concentrator 5301.

2.7.2 High-performance liquid chromatography-mass spectrometry analysis (HPLC-MS/MS analysis)

The separation and analysis of the digested peptides from the samples were performed using an HPLC/MS system. This system consisted of an Agilent 1290 Infinity II Series HPLC (Agilent Technologies, Santa Clara, CA, United States) equipped with an Automated Multisampler module and a High-Speed Binary Pump. The HPLC system was connected to an Agilent 6550 Q-TOF Mass Spectrometer, and the interface used was the Agilent Jet Stream Dual electrospray (AJS-Dual ESI). The experimental parameters for both the HPLC and Q-TOF components were configured in the MassHunter Workstation Data Acquisition software (Agilent Technologies, Rev. B.08.00).

To prepare the dry samples resulting from trypsin digestion, they were reconstituted in a 20 µL volume of resuspending buffer. This buffer, known as buffer A, was composed of a mixture of water, acetonitrile, and formic acid in the ratio of 94.9:5:0.1, respectively. The reconstituted samples were injected into an Agilent AdvanceBio Peptide Mapping HPLC column with dimensions of 2.7 µm × 100 × 2.1 mm, which was thermostatted at 50°C. The injection of the samples occurred at a flow rate of 0.4 mL/min. Subsequently, the column was washed with buffer A for a duration of 3 min, and the digested peptides were eluted using a linear gradient of buffer B

(acetonitrile:water:formic acid, 97:2.9:0.1). This gradient started at 0% and gradually increased to 40% over a period of 40 min. After that, there was a linear gradient from 40% to 95% of buffer B for 8 min, followed by a 95% concentration of buffer B for 3 min. Finally, the column was equilibrated in the initial conditions for 6 min before each subsequent injection. Ten μg of albumin were injected to check the purity of the samples.

The mass spectrometer was operated in the positive mode. The nebulizer gas pressure was set at 35 psi, while the drying gas flow rate was maintained at 14 L/min at a temperature of 300°C. The sheath gas flow rate was set at 11 L/min with a temperature of 250°C. The capillary spray, nozzle, fragmentor, and octopole RF Vpp voltages were configured at 3500 V, 100 V, 360 V, and 750 V, respectively. Profile data were collected for both MS and MS/MS scans using the extended dynamic range mode at a scan rate of 4 GHz. The mass range for both MS and MS/MS scans was set between 50–1700 m/z, and the scan rates were 8 spectra/sec for MS and 3 spectra/sec for MS/MS. Auto MS/MS mode was used, and precursor selection was based on abundance with a maximum of 20 precursors selected per cycle. A ramped collision energy was employed with a slope of 3.68 and an offset of −4.28. The exclusion of the same ion was applied after two consecutive spectra.

The data processing and analysis were conducted using the Spectrum Mill MS Proteomics Workbench software (Rev B.06.00.201, Agilent Technologies, Santa Clara, CA, United States). The raw data were extracted using default conditions, which included the identification of unmodified or carbamidomethylated cysteines, a range of [MH]+ 50–10,000 m/z, a maximum precursor charge of +5, and a minimum signal-to-noise MS (S/N) ratio of 25. The software also utilized specific parameters for peak finding, such as the identification of 12C signals.

For the MS/MS search, an appropriate and updated protein database was employed, and the search criteria included variable modifications (carbamidomethylated cysteines, STY phosphorylation, oxidized methionine, and N-terminal glutamine conversion to pyroglutamic acid), a tryptic digestion allowing for up to 5 missed cleavages, the use of an ESI-Q-TOF instrument, a minimum matched peak intensity of 50%, a maximum ambiguous precursor charge of +5, monoisotopic masses, a peptide precursor mass tolerance of 20 ppm, a product ion mass tolerance of 50 ppm, and the calculation of reversed database scores. The validation of peptide and protein data was performed using auto thresholds.

2.8 Experimental design

The semen samples were collected from six boars, and the AI doses were composed according to the study performed by Luongo et al. (2022). Briefly, three different types of AI doses were produced based on their appearance and composition in ejaculate fractions i) F1, composed of the SRF; ii) F2, composed of F1 plus the intermediate fraction; iii) F3, composed of F2 plus the post-SRF. A grand total of 20 female pigs (sows) were allocated randomly into four separate groups, with each group receiving a distinct type of AI dose (AI-F1, AI-F2, or AI-F3) or non-inseminated (control, C). On day six post-AI, all sows were sacrificed, and their uterine tracts were collected and identified according to the experimental group they belonged to. Each genital tract was dissected to obtain OF and UF for EVs' isolation, characterization, and proteomic analysis. Note that all AI-sows were pregnant at the time of slaughter. Figure 1 depicts a visual representation of the experimental design.

2.9 Bioinformatic analysis–Annotation of human homologs and gene ontology analysis

Raw Uniprot IDs obtained from the proteomics results were utilized to identify the most extensively annotated IDs in *Sus scrofa* and their corresponding homologs in the human species. This was achieved by querying the UniProt API (UniProt Consortium, 2018) using a custom Python 2.7 script. Subsequently, the UniProt IDs were annotated using the functional annotation tool of the Database for Annotation, Visualization, and Integrated Discovery (DAVID, version 6.8) (Bateman, 2019). The Gene Ontology (GO) includes three orthogonal ontologies: biological process (BP), molecular function (MF), and cellular component (CC). To eliminate redundant terms, the most statistically significant GO terms (FDR <5%) were assessed using REVIGO (Supek et al., 2011). The selected GO terms were then visualized by plotting the corresponding percentages using a custom R script incorporating the dplyr (Wickham et al., 2019) and ggplot2 (Wickham H., 2016) libraries. Additionally, a functional clustering analysis of the proteins present in extracellular vesicles (EVs) from each fluid was performed using the DAVID functional clustering tool. Venn diagrams comparing the five experimental groups were generated using Venn diagrams at https://bioinformatics.psb.ugent.be/webtools/Venn/.

2.10 Statistical analysis

All statistical analyses were performed using IBM SPSS 24.0 software package (SPSS Inc. Chicago, IL, United States). EVs quantitation, protein concentration, and size are presented as the mean ± standard error of the mean (SEM). The variables in all experiments were tested for their normality by Shapiro-Wilk and homogeneity of variances before analysis by two-way ANOVA considering the group of sows (AI-F1, AI-F2, AI-F3, and C) and pregnancy as factors, followed by a *post hoc* Tukey test. The non-parametric Kruskal Wallis test was used for the variables whose data were not normally distributed. Differences between treatments were considered statistically significant at $p < 0.05$.

3 Results

3.1 Characterization of EVs from the OF and UF

3.1.1 Presence of EVs and characterization by transmission electron microscopy (TEM)

TEM observations confirmed the presence of EVs in porcine oviductal and uterine flushings (Figures 2A, B). The presence of two

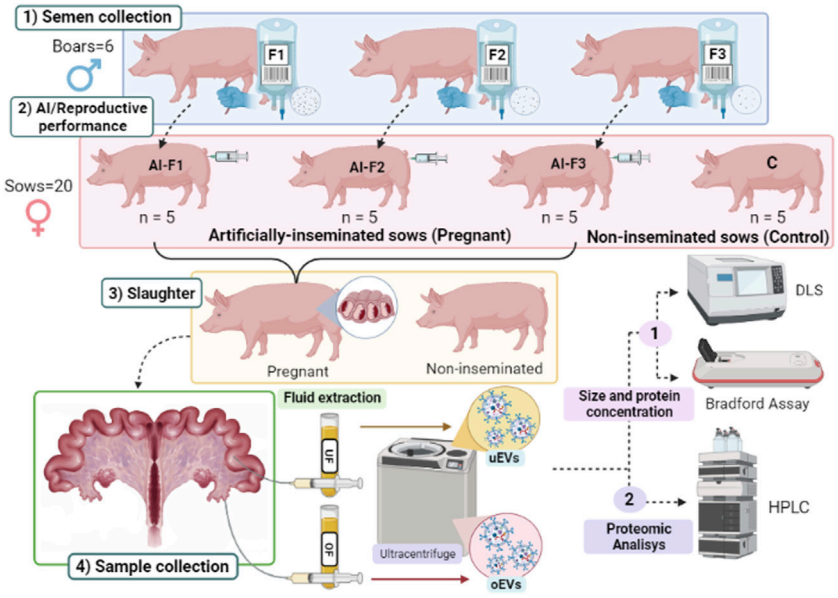

FIGURE 1
Diagram of the experimental design. 1) Semen samples were collected from six different boars and prepared as three types of ejaculate accumulative fractions: F1, composed of the rich-sperm fraction (SRF); F2, composed of the F1 plus the intermediate fraction; and F3, composed of F2 plus the post-SRF. 2) Artificial insemination (AI) was performed: Four experimental groups of sows (n = 5 sows/group) were inseminated with a type of AI dose (AI-F1, AI-F2, and AI-F3) or non-inseminated (C). 3) Sows were slaughtered on day six post-AI, and female genital tracts were collected and identified according to the experimental group they belonged. 4) Sampling of the female genital tracts: Oviductal and uterine flushing's were extracted for the isolation of extracellular vesicles (EVs) by ultracentrifugation, characterization analysis of the size distribution by dynamic light scattering, and determination of the protein concentration by the Bradford assay (protein concentration). The protein quantification of EVs from the oviductal fluid (oEVs) and uterine fluid (uEVs) were evaluated by HPLC/MS-MS.

populations of EVs in the fluid was observed as two different peaks detected in sows from the four experimental groups, either in OF or UF (Figures 2C, D). Diverse populations of EVs ranging in size (142.40–297.76 nm) were observed. These EVs appeared as round or cup-shaped membrane-surrounded vesicles in their native stage. We observed a population of small EVs (30–150 nm) resembling exosomes and a population of large EVs (>150 nm) resembling microvesicles. Very large EVs (>1,000 nm) were considered as aggregates of multiple EVs.

The size of the oEVs and uEVs was analyzed and compared and there were no statistically significant differences between groups of sows ($p > 0.05$; Table 1). In general terms, oEVs tended to be larger (ranging from 215.52 to 297.76 nm) than uEVs (ranging from 142.840 to 202.92 nm); however, there were no differences in size between groups of sows (Table 1).

The immunoblotting revealed that EVs were present both in the OF and UF of all sows in study (Figure 2) since EVs protein markers HSP70 (2E) and CD63 (2F) were detected in AI- and C-sows.

3.1.2 EVs quantitation and protein concentration

The results of the quantitation of oEVs particles were similar for all experimental groups (Table 1), ranging from 278.36 to 414.79 × 10^9 particles/mL ($p > 0.05$). However, the concentration of uEVs particles were lower ($p < 0.05$) in AI-F1 and AI-F2 (321.92 ± 8.05 and 395.14 ± 32.00 × 10^9 particles/mL) than in C (687.28 ± 85.19 × 10^9 particles/mL). AI-F3 showed an intermediate concentration of uEVs particles with respect to the rest of groups (525.14 ± 32.81 × 10^9 particles/mL; $p > 0.05$).

The oEVs and uEVs protein concentration (protein cargo) was also compared in AI- and C-sows (Table 1). No statistical differences were found in the protein cargo of the total intact oEVs, ranging from 0.51 to 0.58 μg/μL ($p > 0.05$). In uEVs, the protein cargo of AI-F1 and AI-F2 (0.86 ± 0.06 and 0.86 ± 0.04 μg/μL) were significantly lower than AI-F3 and C (1.19 ± 0.09 and 1.30 ± 0.06 μg/μL).

3.2 Proteomic analysis

3.2.1 Proteins identified in EVs from oviductal (oEVs) and uterine fluids (uEVs)

Initially, the purity of the samples was confirmed since the samples for all the experimental groups only showed between 0.00% and 7.61% of the albumin's spectra and between 0.00% and 0.66% of the albumin's intensity. A total of 645 proteins were identified in oEVs and uEVs. To minimize the risk of false positives, only proteins with a minimum of two peptides and present in at least three of the five replicates were considered, resulting in 362 final proteins. The list of proteins identified in the different accumulative ejaculate fractions, including the relative number of peptides of each protein, is shown in Supplementary Tables S1–4 (Supplementary File S1) and Supplementary File S2.

Interestingly, a comparison of the oEVs and uEVs proteome of AI- and C-sows revealed four proteins common to all groups: 15S Mg (2^+)-ATPase p97 subunit, annexin (ANXA), glyceraldehyde-3-phosphate dehydrogenase (GAPDH) and tubulin alpha 1 chain

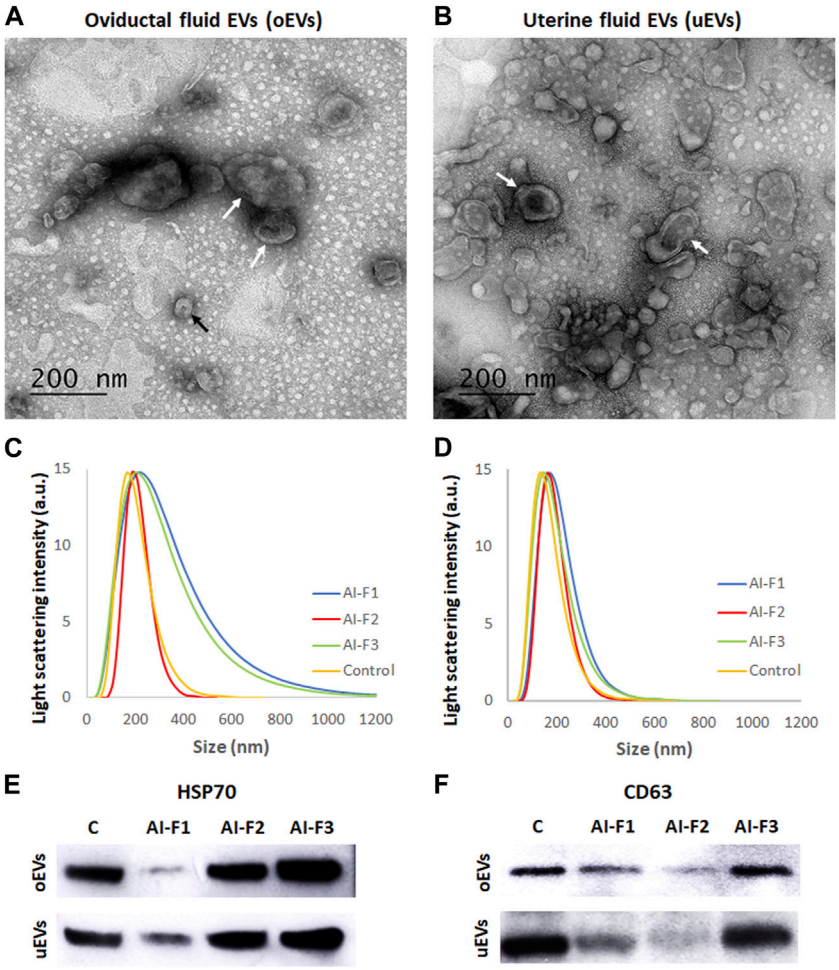

FIGURE 2
Characterization the extracellular vesicles' size from oviductal fluid (oEVs) and uterine fluid (uEVs). **(A)** Transmission electron microscopy (TEM) of oEVs after the OF ultracentrifugation. **(B)** Transmission electron microscopy (TEM) of uEVs after the UF ultracentrifugation. Concentration of uEVs was higher than oEVs, independently of the type of AI-dose inseminated (F1, F2 or F3). Arrows indicate the cup-shaped morphology of EVs. **(C)** Graphical distribution of the oEVs by size and sow depending on the type of AI-dose inseminated (AI-F1, AI-F2, or AI-F3) or non-inseminated (control, C). **(D)** uEVs populations by size and sow depending on the experimental group (AI-F1, AI-F2, AI-F3, or C). **(E)** EVs protein marker HSP70 in the experimental groups (AI-F1, AI-F2, AI-F3, or C). **(F)** EVs protein marker CD63 in the experimental groups (AI-F1, AI-F2, AI-F3, or C).

(TUBA1C). These four proteins are involved in calcium signaling, tissue remodeling, immune modulation, and antioxidant defense systems. They exert biological functions that are regulated in the fallopian tube and endometrium. We decided to compare the oEVs and uEVs proteins from AI- and C-sows since it provides valuable insights into the molecular mechanisms involved in reproductive events and potentially influences the outcome of offspring development. The nature of the proteins and the possible differences are described below.

3.2.2 Protein characterization of oEVs

A total of 220 proteins were detected across all experimental groups. Figure 3 shows specific proteins from each experimental group and the common ones in two or more experimental groups. In addition, all proteins from oEVs are listed in Supplementary Tables S1, S2 (Supplementary File S1). A total of 139 proteins were detected in oEVs from AI-sows and 92 of them were detected in oEVs from AI-F1 group 31 of which were exclusive to this group. A total of 72 proteins were detected in oEVs from AI-F2 sows, 10 of which were exclusive to this group. Finally, 93 proteins were detected in oEVs from AI-F3 sows, 24 of which were exclusive to this group. In addition, the comparison between the three experimental groups identified 44 common proteins (Figure 3A). When C-sows were compared with AI-sows, 82 proteins were common to both groups. Of these, 57 proteins were exclusive to AI-sows and 81 proteins were exclusive to C-sows (Figure 3B).

The number and comparative overlap of the identified oEVs proteins in AI- and C-sows are illustrated in Figure 3C and listed in Supplementary Tables S1, S2 (Supplementary File S1). Eighty-one of the 220 proteins were exclusively present in C-sows: 14-3-3 protein theta (YWHAQ), cadherin 13 (CDH13), galectin-3 binding protein (LGALS3), and ubiquitin C (UBC). Twenty-three proteins were characteristically exclusive of AI-F1 sows: 14-3-3 protein zeta/delta (YWHAZ), 6 phosphogluconate dehydrogenase decarboxylating

TABLE 1 EVs' size, quantitation, and protein concentration in the oviductal fluid (oEVs) and uterine fluid (uEVs) from artificially inseminated sows with three different types of accumulative fractions of the boar ejaculate: AI-F1 ($n = 5$), AI-F2 ($n = 5$), and AI-F3 ($n = 5$); and from non-inseminated sows: C ($n = 5$). F1, sperm-rich fraction (SRF); F2, F1 plus the intermediate fraction; F3, F2 plus the post-SRF.

		AI-F1	AI-F2	AI-F3	C
Size (nm)	oEVs	297.76 ± 89.45	262.60 ± 98.57	234.84 ± 5.67	215.52 ± 9.65
	uEVs	142.40 ± 30.53	202.92 ± 18.20	176.86 ± 8.45	163.86 ± 12.45
[EVs] (x 10^9 particles/mL)	oEVs	278.36 ± 10.32	392.28 ± 20.79	404.07 ± 26.29	414.79 ± 106.53
	uEVs	321.92 ± 8.05^a	395.14 ± 32.00^a	525.14 ± 32.81^{ab}	687.28 ± 85.19^b
[Protein] (μg/μL)	oEVs	0.51 ± 0.07	0.55 ± 0.05	0.53 ± 0.06	0.58 ± 0.05
	uEVs	0.86 ± 0.06^a	0.86 ± 0.04^a	1.19 ± 0.09^b	1.30 ± 0.06^b

Data are represented as the mean ± standard error of the mean (SEM). Different superscripts (^{a,b}) within the same row indicate statistical differences between experimental groups ($p < 0.05$).

(PGD), peptidyl-prolyl trans isomerase E (PPIE), and tubulin alpha-1A chain (TUBA1A). In addition, 7 proteins were exclusive of AI-F2 sows: GTP-binding nuclear protein Ran (RAN), NIMA-related kinase 1 (NEK1), peroxiredoxin-2 (PRDX2), and syndecan-binding protein (SDCBP). Finally, 8 proteins were found exclusively in AI-F3 sows: Heat shock protein 70 kDa 1B (HSPA1B), haemoglobin subunit epsilon (HBE), profilin (PFN1), and tyrosine 3-monooxygenase/tryptophan 5-monooxygenase activation protein zeta (YWHAZ).

3.2.3 Functional analysis of oEVs proteins

GO includes three orthogonal ontologies: biological process (BP), molecular function (MF), and cellular component (CC), although we only focused on BP, which is more relevant in our study. Identification of enriched pathways using GO analysis revealed 45 pathways related to oEVs proteins. In Figure 4, we have presented the results of the GO analysis, focusing on the ten most enriched pathways in artificially inseminated sows and non-inseminated control sows. All the enriched pathways involved in biological processes are listed in Supplementary File S3. The top 5 biological processes in F1 group included pathways involved in protein stabilization, protein folding, glycolytic process, proteasome-mediated ubiquitin-dependent protein catabolic process and positive regulation of RNA polymerase II transcriptional preinitiation complex assembly. We also identified enriched pathways in the F2 group that are involved in glycolytic process, vesicle-mediated transport, protein stabilization, protein folding and regulation of cell shape. However, the most enriched pathways in the sows inseminated with F3 were translation, protein stabilization, innate immune response, glycolytic process and DNA-templated transcription and initiation.

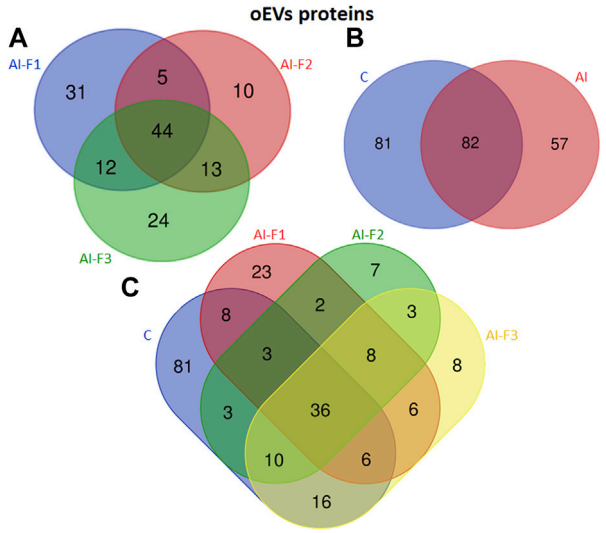

FIGURE 3
Venn diagram illustrating the number of different proteins from extracellular vesicles of oviductal fluid (oEVs) in sows ($n = 20$) inseminated with different semen doses from boars ($n = 6$) according to the seminal fraction(s) used for artificial insemination (AI): F1, composed by the sperm-rich fraction (SRF); F2, composed by F1 plus the intermediate fraction; F3, composed by F2 plus the post-SRF. Non-inseminated sows were considered as control (C). **(A)** The overlap of oEVs proteins from AI-F1, AI-F2, and AI-F3 sows. **(B)** The overlap of oEVs proteins of AI- and C-sows. **(C)** The overlap of oEVs protein in all the experimental groups.

3.2.4 Protein characterization of uEVs

A total of 142 proteins were identified in uEVs. Figure 5 illustrates the exclusive proteins found in each group, as well as the shared proteins among the different experimental groups. The detailed lists of exclusive and common proteins can be found in Supplementary Tables S3, S4 (Supplementary File S1), respectively.

A group of 112 proteins were detected in uEVs proteins from AI-sows. Ninety-three proteins were detected in AI-F1 sows, being 34 of them, exclusive to this group. In uEVs from AI-F2 sows, a total of 69 proteins were detected, being 6 of them, exclusive to this group. Fifty-three proteins were detected in uEVs from AI-F3 sows, being 7 of them exclusive to this group.

The analysis of uEVs detected 38 proteins present in the three groups of AI-sows. In addition, 19 proteins were common in AI-F1 and AI-F2 sows, two proteins between AI-F1 and AI-F3 sows, and six proteins between AI-F2 and AI-F3 sows (Figure 5A). Comparing AI- with C-sows (Figure 5B), 85 proteins were exclusive to AI-sows, 30 to C-sows, and 27 were shared by the two groups.

The number and comparative overlap of the identified oEVs proteins in AI- and C-sows are illustrated in Figure 5C and listed in Supplementary Tables S3, S4 (Supplementary File S1). Thirty of the 142 proteins were characteristically exclusive of C-sows and included beta-2-microglobulin (B2M), clathrin heavy chain

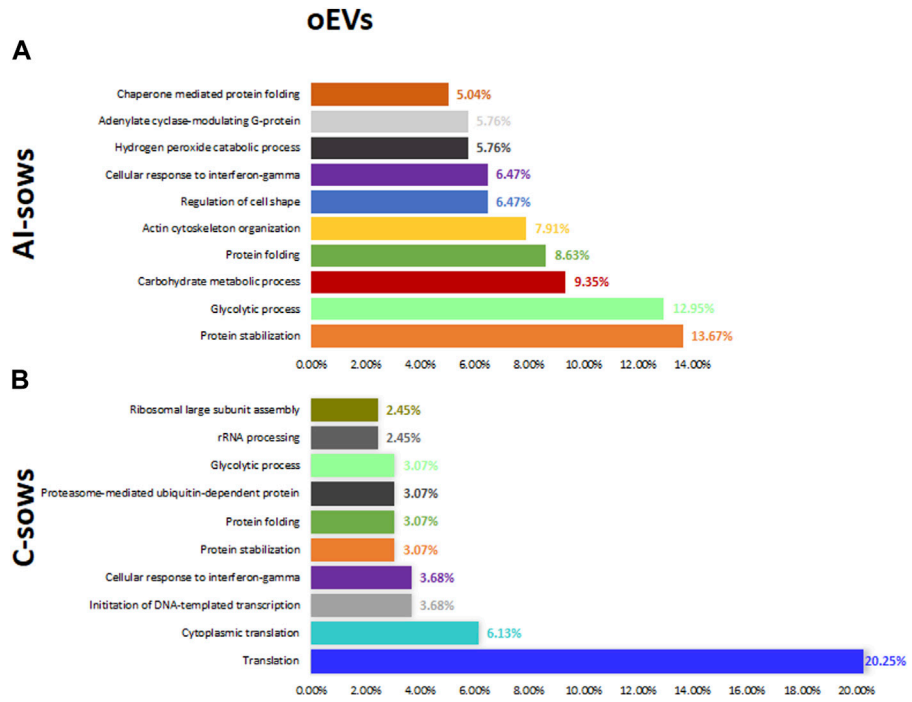

FIGURE 4
Biological processes and the percentage of extracellular vesicles detected in oviductal fluid (oEVs) in **(A)** artificially inseminated sows (AI-sows) and **(B)** non-inseminated sows (control, C-sows).

(CLTC), heat shock protein family A member 8 (HSPA8), and vitronectin (VTN). Thirty-one proteins were characteristically exclusive of AI-F1 sows, including 14-3-3 domain-containing protein (YWHAG), calmodulin-3 (CALM3), ezrin (EZR), and heat shock protein HSP90-alpha (HSP90AA1). In addition, six proteins were exclusive to AI-F2 sows: 14-3-3 protein zeta/delta (YWHAZ), adenylyl cyclase-associated protein (CAP1), heterogeneous nuclear ribonucleoprotein K (HNRNPK), and Na^+-dependent phosphate cotransporter 2B (NPT2B). Finally, six proteins were found exclusively in AI-F3 sows: ATP-binding cassette subfamily G member 2 (ABCG2), pendrin (SLC26A4), proline-rich transmembrane protein 1B (PRRT1B), and STEAP family member 4 (STEAP4).

3.2.5 Functional analysis of uEVs proteins

Identification of enriched pathways using GO analysis revealed 62 pathways in uEVs proteins. In Figure 6, we have presented the results of the GO analysis, focusing on the ten most enriched pathways in artificially inseminated sows and non-inseminated control sows. All the enriched pathways involved in biological processes are listed in (Supplementary File S4). The top 5 biological processes in F1 included protein stabilization, protein folding, glycolytic process, regulation of cell shape and protein localization to plasma membrane. The enriched pathways in F2 were also related to regulation of cell shape, protein folding, actin filament organization, protein stabilization and small GTPase mediated signal transduction. We also identified enriched pathways in the F3 group that are involved in regulation of cell shape, glycolytic process, actin filament organization, actin cytoskeleton organization and sensory perception of sound.

4 Discussion

The present study aimed to gain insight into the changes in EVs protein cargo in non-inseminated and pregnant sows artificially inseminated with three accumulative fractions of the boar ejaculate. The objective was to elucidate how the SP from different ejaculate fractions might influence the oviductal and endometrial EVs proteome. The oviduct and uterus of pregnant sows undergo significant physiological and biochemical changes to support the development and growth of the conceptus. One of these changes is a modification in the quantity and diversity of proteins present. However, the amount of protein in the uEVs cargo in pregnant and non-pregnant sows has not been determined yet.

Contrary to expectations, our results revealed that the protein concentration in EVs from the OF and UF was higher in non-pregnant compared to pregnant sows. An explanation for this result could be attributed to the analyzed day of gestation. We determined the protein cargo on day 6 of pregnancy, while maternal recognition typically occurs around day 11–12 (Bazer et al., 1997). This hypothesis is supported by the results obtained by Rudolf Vegas and co-workers (Rudolf Vegas et al., 2022), who observed that the EVs protein cargo of UF collected from pregnant mares was similar to that of cyclic control mares on day 10 of gestation, with an increase in protein concentration occurring later. Hu et al. (2022) obtained similar results in pigs on day

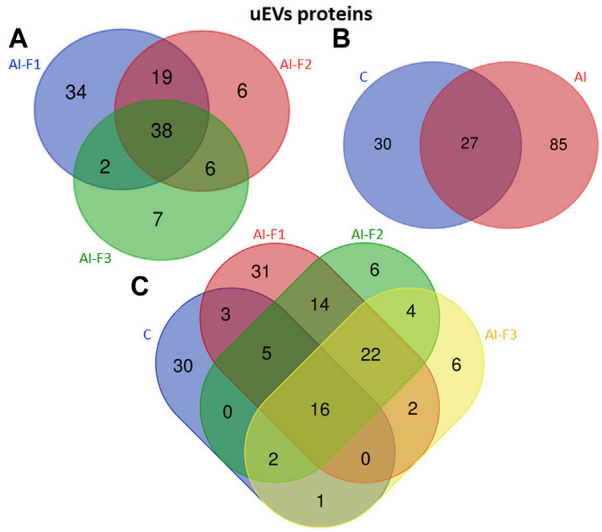

FIGURE 5
Venn diagram illustrating the number of different proteins from extracellular vesicles of uterine fluid (uEVs) in sows (n = 20) inseminated with different semen doses from boars (n = 6) according to the seminal fraction(s) used for artificial insemination (AI): F1, composed by the sperm-rich fraction (SRF); F2, composed by F1 plus the intermediate fraction; F3, composed by F2 plus the post-SRF. Non-inseminated sows were considered as control (C). **(A)** The overlap of uEVs proteins from AI-F1, AI-F2, and AI-F3 sows. **(B)** The overlap of uEVs proteins of AI- and non-inseminated sows (control, C). **(C)** The overlap of uEVs protein in all the experimental groups.

10 of gestation. It seems that the type of protein is likely more important than the amount of protein in early pregnancy. However, most studies have focused on the miRNAs carried by EVs, and only a limited number have determined the protein concentration of EVs.

TEM and WB observations from our study confirmed the presence of EVs in the oviduct and uterus. The characterization of these EVs was analyzed by TEM to confirm the presence and morphology of EVs, and by DLS to obtain populations of EVs of different sizes. DLS analysis showed an asymmetric size distribution of EVs, between 30 and 300 nm in diameter, which is in line with findings from other studies (Álvarez-Rodríguez et al., 2019). This distribution showed a higher frequency of larger vesicles (80%) compared to exosomes (8%) within the EVs population as in Almiñana et al. (2017). These results contradict the current measurement obtained by TEM, which differs from certain previous studies. Therefore, establishing methods to distinguish between exosomes and microvesicles is a major ongoing challenge in the field of EVs (Raposo and Stoorvogel, 2013). Besides, we believe that DLS results could be influenced by artifacts and measurements of aggregates of vesicles instead of single vesicles (Muller et al., 2014). Furthermore, some authors have shown that different techniques can give a different size distribution result and a different concentration for the same vesicle sample (van der Pol et al., 2014). Nevertheless, our results agree with previous studies that isolated exosomes and microvesicles from the bovine OF using a similar protocol to ours (centrifugating the samples at 100,000 *g* (Almiñana et al., 2017; Lopera-Vasquez et al., 2017). We also confirmed a higher proportion of larger EVs (size >150 nm) in inseminated pregnant sows compared to the non-inseminated ones, which is also in agreement with previous studies (Almiñana et al., 2017; Laezer et al., 2020). Additionally, no significant differences were observed in the size distribution of EVs in OF and UF, which is consistent with the findings of Almiñana et al. (2018). They demonstrated that the size of EVs remains constant throughout the various stages of the estrous cycle, despite the strong hormonal regulation of their molecular cargo.

4.1 Oviductal EVs cargo from inseminated pregnant sows

Proteomic analysis showed differences in the protein cargo of the oEVs across the sows inseminated with F1, F2 and F3. Of the 139 proteins identified in the oEVs across the three groups, 57 were exclusive in the inseminated sows, being the inseminated sows with the F1, the group with the higher number of exclusive proteins, a total of 31. Gene ontology analysis showed that the most enriched biological processes in the inseminated sows (including F1, F2 and F3) were protein stabilization, protein folding and glycolytic process. Exclusively in the oEVs from sows inseminated with F1, proteasome-mediated ubiquitin dependent protein catabolic process and positive regulation of RNA polymerase pathways were within the top five of most enriched biological processes, within these pathways we can find proteins such as 26S proteasome regulatory subunit 8 (PSMD8), proteasome 20S subunit alpha 2 (PSMA2), proteasome subunit alpha type (PSMA1), among others. The ubiquitin proteasome system (UPS) is a complex enzymatic machinery responsible for protein degradation which is involved in many biological processes such as cell cycle, cellular signalling, and transcription (Moore and Steitz, 2005). Research on UPS involvement in mammalian fertilization has demonstrated that it is related with sperm

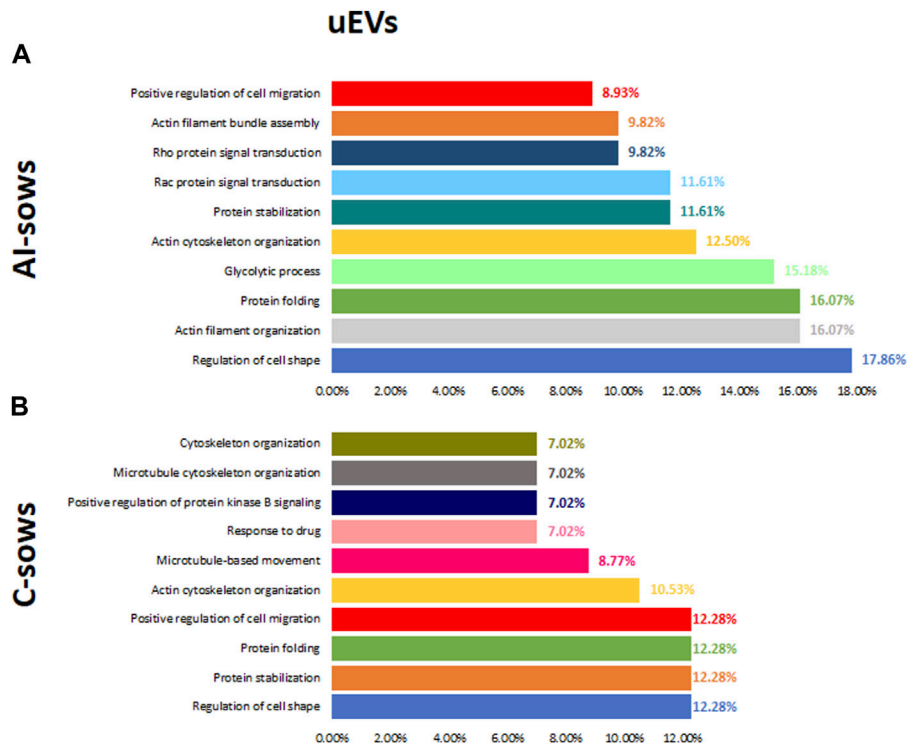

FIGURE 6
Biological processes and the percentage of extracellular vesicles detected in uterine fluid (uEVs) in **(A)** artificially inseminated sows (AI-sows) and **(B)** non-inseminated sows (control, C-sows).

capacitation process (reviewed by Kerns et al., 2016). Moreover, UPS is also involved in the redistribution and turnover of proteins implicated in the formation of oviductal sperm reservoir, which aids in reducing polyspermy and helps in the establishment of a sequential release of freshly capacitated spermatozoa. The removal of some proteins (i.e., spermadhesins) covering the surface of the spermatozoa seems to be necessary for the disruption of the sperm-oviductal epithelium interaction, where some studies have indicated that this event is regulated by UPS-dependent proteolysis (Zigo et al., 2019; Zigo et al., 2023). Although the role of the ubiquitin proteasome catabolic process in oEVs has not been elucidated yet, this study demonstrates the presence of proteins related with such a system playing a key role in the sperm surface remodelling during capacitation (Zigo et al., 2023).

Exclusively in the oEVs from sows inseminated with the F2, the second most enriched biological process was the vesicle mediated transport pathway containing proteins previously reported (Almiñana et al., 2017) in oEVs such as Heat-shock protein family A member 8 (HSPA8), Heat-shock protein family A (HSPA70) and Syntaxin-binding protein 2 (STXBP2) which are involved in important roles in the gamete/embryo-oviduct interactions. HSPA8 belongs to a cytosolic family of chaperones that are constitutively expressed in the cytoplasm of mammalian cells under normal conditions to maintain protein structural homeostasis and are induced upon environmental stress (Nollen and Morimoto, 2002; Liman, 2017). HSPA8 protein has been found in human fallopian tubes during the menstrual cycle (Fujii et al., 2021), the bovine (Lamy et al., 2017), ovine (Soleilhavoup et al., 2016), and sow (Seytanoglu et al., 2008) cyclic oviducts. In addition, HSP70 released from porcine oviductal epithelium has been shown to enhance *in vitro* survival of boar and bull spermatozoa when spermatozoa are briefly exposed to HSP70 before interacting with oocytes (Elliott et al., 2009). These proteins also have important roles in the sperm-oviduct interaction and early embryo development (Almiñana et al., 2017). Although the mechanism of released by the oviductal cells is not known yet, authors like (Campanella et al., 2014) suggested that heat-shock proteins might be released via exosomes. These findings are consistent with the results of the present study, which identified HSPA8 and HSP70 among the relevant proteins in oEVs.

In the oEVs from pregnant sows inseminated with F3, the innate immune response pathway was exclusive of this group compared to other groups. In this pathway we found proteins which have been found in all experimental groups, such as Glyceraldehyde-3-Phosphate Dehydrogenase (GAPDH). Some researchers such as Almiñana et al. (2018) and Nakano et al. (2017) found that GAPDH mRNA is also a component of murine oEVs isolated from oviductal mesenchymal cell lines, where they demonstrated that these specific mRNAs exert a functional effect by increasing the number of ciliated cells. In addition, GAPDH has been associated with better quality embryos (Lopera-Vasquez et al., 2017), increased cryotolerance (Gutiérrez-Adán et al., 2004). Another protein found in this pathway was CD59 which is a GPI-anchored membrane protein in the cell membrane and acts as a key regulator of the complement activation cascade, thus preventing the formation of

the membrane attack complex and a lytic lesion. CD59 has been found in reproductive tract cells such as sperm (Frolíková et al., 2012) and also in normal human fallopian tube, endometrium and cervical mucosa (Jensen et al., 1995). Since functional complement components are abundant in the female reproductive tract, it has been speculated that CD59 may be involved in protecting the sperm from complement-mediated damage that might be initiated by anti-sperm antibodies present in the female reproductive tract (Qian et al., 2000). Therefore, the current study demonstrated differences in protein cargo from oEVs of the sows inseminated with different sperm fractions, however essential functions involved in gamete/embryo-oviduct interactions were maintain across all the groups.

4.2 Uterine EVs cargo from inseminated pregnant sows

Of the 142 proteins identified in the uEVs across the three groups, 85 were exclusive in the inseminated sows, being the inseminated sows with the F1, the group with the highest number of exclusive proteins, a total of 34. In addition, 6 and 7 proteins were unique in the uEVs from sows inseminated with F2 and F3 (respectively). Gene ontology analysis showed that the most enriched biological processes (across the three groups) were protein stabilization, protein folding and cell development. These processes are related to endometrial receptivity and embryo implantation. Interestingly, GO analysis identified the protein stabilization pathway as one of the most enriched pathways in sows inseminated with F1 and F2 but not in the F3 group. Within this pathway, there are proteins such as Heat Shock Protein 90 Alpha Family Class B Member 1 (HSP90AB1), Heat Shock Protein 90 Alpha Family Class A Member 1 (HSP90AA1), Parkinson protein 7 (PARK7), Chaperonin containing TCP1, subunit 7 (CCT7), among others.

HSP90AB1 and HSP90AA1 are conserved chaperone proteins that play a key role in maintaining protein structural homeostasis and are induced by environmental stress (Neuer et al., 2000). HSP90 also plays an essential role in the controlled inflammatory response required for conceptus implantation and trophoblast growth (Jee et al., 2021). For example, HSPAA901 is a co-factor for steroid hormone receptors and is released from the receptor complex upon ligand hormone-receptor interaction produced by uterine cells (Neuer et al., 2000). This protein has previously been identified in the porcine OF (Mondéjar et al., 2013), and it has been suggested to be released via exosomes (Campanella et al., 2012) or lipid rafts (Pralle et al., 2000). On the other hand, Chaperonin containing TCP1 is necessary for folding newly synthesized proteins, including actin and tubulin (Yam et al., 2008). This has also been previously identified in the porcine endometrium of pregnant sows (Pierzchała et al., 2021), being higher expressed in healthy pregnancy compared to pregnancy lost. Therefore, these proteins seem to be involved in embryo maternal interaction and the signaling of maternal recognition of pregnancy.

In the uEVs from pregnant sows inseminated with F1, the protein localisation to plasma membrane pathway was only found in this group. Rap1, as a member of the GTPase family, is normally in the active GTP-bound form, which is the main regulator of cell-cell junction (Gaonac'h-Lovejoy et al., 2020), and cell adhesion (Boettner and Van Aelst, 2009). Moreover, Rap1 has been related to embryo implantation, as Rap1 can induce cell–cell junction stabilization (Gaonac'h-Lovejoy et al., 2020). The activation of Rap1 has been shown to be involved in the establishment of cell polarity (Freeman et al., 2017), where this epithelial cell polarity is rebuilt during uterine repair, then suggesting that Rap1a is involved in the reparation of endometrial injury (Zhang et al., 2023) including physiological processes occurring in the establishment of pregnancy such as embryo implantation and the development of uterine fibroids. Moreover, some pathways related to actin filament organization were found in the sows inseminated with F2 and F3. This suggests that all the fractions of the ejaculate are mediating in the uterine remodulation of the tissue during the establishment of pregnancy.

In summary, the results of this work demonstrated that the porcine EVs isolated from OF and UF exhibit different protein cargo depending on the semen plasma in the AI dose. We were also able to demonstrate that the AI with different sperm fractions results in the secretion of EVs with specific protein content, and these proteins are closely associated with reproductive processes.

5 Conclusion

In conclusion, to the best of our knowledge, the present study provides novel insights into the differential expression of some EVs-induced proteins in pregnant sows inseminated with three different accumulative fractions of the boar ejaculate compared to non-pregnant sows. These results contribute to a better understanding of the regulation of oviduct and uterine physiology, elucidating candidate proteins that may interact with gametes and embryos, thereby modulating reproductive events involved in fertilization. Our findings include already-known fertility-related proteins, several new candidates that may modulate sperm survival and embryo development, and functions related to fertilization. Further studies will be required to determine the exact role of these proteins and their interaction mechanism by binding or fusion with the sperm, the oocyte, or even the female genital tract epithelium. Understanding the contribution of EVs to the fine-tuning of the oviductal and uterine environment may help to better mimic the *in vitro* environment during *in vitro* production of porcine embryos to enhance their quality.

Data availability statement

The datasets presented in this study can be found in online repositories. The names of the repository/repositories and accession number(s) can be found below: https://www.ebi.ac.uk/pride/archive/, PXD044639.

Ethics statement

The animal study was approved by Ethical Committee of Animal Experimentation of the University of Murcia on 1 June 2020

(PID2019-106380RB-I00) and by the Animal Production Service for the Agriculture Department of the Region of Murcia (Spain) (A13230106). The study was conducted in accordance with the local legislation and institutional requirements.

Author contributions

ST-G, CL, LA-P, and CM performed the experiments. ST-G, CL, LA-P, CS-Ú, and CM analyzed the data and wrote the manuscript. CM conceived and designed all the experiments and assessed the discussion. All authors contributed to the article and approved the submitted version.

Funding

This research was supported by the Seneca Foundation (21656/21), Ministry of Science and Innovation (PID2019-106380RBI00/AEI/10.13039/501100011033) and European Union Next-Generation EU/PRTR (PDC2022-133589-I00).

Acknowledgments

The authors thank Dr. Alejandro Torrecillas for his valuable work with the proteomic analyses and for advising our research, Dr. F.A. García-Vázquez for the management of the farm and the aid in obtaining the reproductive tracts, and Dr. Sergio Navarro-Serna and Celia Piñeiro-Silva for the technical assistance. Thanks to the company Sergal Gestió Ramadera (Lleida, Spain) and the slaughterhouse of El Pozo S.A. (Murcia, Spain) for providing the biological material. Thank you to Centro de Apoyo a la Investigación y Desarrollo (CAID) at the University of Murcia for assisting with data protein concentration, DLS data, proteomic analysis, and Transmission Electron Microscopy technician support.

Conflict of interest

The authors declare that the research was conducted in the absence of any commercial or financial relationships that could be construed as a potential conflict of interest.

Publisher's note

Supplementary material

The Supplementary Material for this article can be found online at: https://www.frontiersin.org/articles/10.3389/fcell.2023.1231755/full#supplementary-material

References

Almiñana, C., Corbin, E., Tsikis, G., Alcântara-Neto, A. S., Labas, V., Reynaud, K., et al. (2017). Oviduct extracellular vesicles protein content and their role during oviduct–embryo cross-talk. *Reproduction* 154, 153–168. doi:10.1530/REP-17-0054

Almiñana, C., Tsikis, G., Labas, V., Uzbekov, R., da Silveira, J. C., Bauersachs, S., et al. (2018). Deciphering the oviductal extracellular vesicles content across the estrous cycle: implications for the gametes-oviduct interactions and the environment of the potential embryo. *BMC Genomics* 19, 622. doi:10.1186/s12864-018-4982-5

Álvarez-Rodríguez, M., Atikuzzaman, M., Venhoranta, H., Wright, D., and Rodríguez-Martínez, H. (2019). Expression of immune regulatory genes in the porcine internal genital tract is differentially triggered by spermatozoa and seminal plasma. *Int. J. Mol. Sci.* 20, 513. doi:10.3390/ijms20030513

Aneas, S. B., Gary, B. G., and Bouvier, B. P. (2008). Collectis® automated boar collection technology. *Theriogenology* 70, 1368–1373. doi:10.1016/j.theriogenology.2008.07.011

Bai, R., Latifi, Z., Kusama, K., Nakamura, K., Shimada, M., and Imakawa, K. (2018). Induction of immune-related gene expression by seminal exosomes in the porcine endometrium. *Biochem. Biophys. Res. Commun.* 495, 1094–1101. doi:10.1016/j.bbrc.2017.11.100

Barranco, I., Padilla, L., Parrilla, I., Álvarez-Barrientos, A., Pérez-Patiño, C., Peña, F. J., et al. (2019). Extracellular vesicles isolated from porcine seminal plasma exhibit different tetraspanin expression profiles. *Sci. Rep.* 9, 11584. doi:10.1038/s41598-019-48095-3

Bateman, A. (2019). UniProt: A worldwide hub of protein knowledge. *Nucleic Acids Res.* 47, D506–D515. doi:10.1093/nar/gky1049

Bazer, F. W., and Johnson, G. A. (2014). Pig blastocyst-uterine interactions. *Differentiation* 87, 52–65. doi:10.1016/j.diff.2013.11.005

Bazer, F. W., Spencer, T. E., and Ott, T. L. (1997). "Interferon tau: A novel pregnancy recognition signal," in *American journal of reproductive immunology* (China: Blackwell Publishing Ltd), 412–420. doi:10.1111/j.1600-0897.1997.tb00253.x

Bidarimath, M., Lingegowda, H., Miller, J. E., Koti, M., and Tayade, C. (2021). Insights into extracellular vesicle/exosome and miRNA mediated Bi-directional communication during porcine pregnancy. *Front. Vet. Sci.* 8, 654064. doi:10.3389/fvets.2021.654064

Boettner, B., and Van Aelst, L. (2009). Control of cell adhesion dynamics by Rap1 signaling. *Curr. Opin. Cell. Biol.* 21, 684–693. doi:10.1016/j.ceb.2009.06.004

Bridi, A., Perecin, F., and da Silveira, J. C. (2020). Extracellular vesicles mediated early embryo–maternal interactions. *Int. J. Mol. Sci.* 21, 1163. doi:10.3390/ijms21031163

Burns, G., Brooks, K., Wildung, M., Navakanitworakul, R., Christenson, L. K., and Spencer, T. E. (2014). Extracellular vesicles in luminal fluid of the ovine uterus. *PLoS One* 9, e90913. doi:10.1371/journal.pone.0090913

Burns, G. W., Brooks, K. E., and Spencer, T. E. (2016). Extracellular vesicles originate from the conceptus and uterus during early pregnancy in sheep. *Biol. Reprod.* 94, 56. doi:10.1095/biolreprod.115.134973

Campanella, C., Bavisotto, C. C., Marino Gammazza, A., Nikolic, D., Rappa, F., David, S., et al. (2014). Exosomal heat shock proteins as new players in tumour cell-to-cell communication. *J. Circ. Biomark.* 3, 4. doi:10.5772/58721

Campanella, C., Bucchieri, F., Merendino, A. M., Fucarino, A., Burgio, G., Corona, D. F. V., et al. (2012). The odyssey of Hsp60 from tumor cells to other destinations includes plasma membrane-associated stages and Golgi and exosomal protein-trafficking modalities. *PLoS One* 7, e42008. doi:10.1371/journal.pone.0042008

Du, J., Shen, J., Wang, Y., Pan, C., Pang, W., Diao, H., et al. (2016). Boar seminal plasma exosomes maintain sperm function by infiltrating into the sperm membrane. *Oncotarget* 7, 58832–58847. doi:10.18632/oncotarget.11315

Elliott, R. M. A., Lloyd, R. E., Fazeli, A., Sostaric, E., Georgiou, A. S., Satake, N., et al. (2009). Effects of HSPA8, an evolutionarily conserved oviductal protein, on boar and bull spermatozoa. *Reproduction* 137, 191–203. doi:10.1530/REP-08-0298

Franchi, A., Cubilla, M., Guidobaldi, H. A., Bravo, A. A., and Giojalas, L. C. (2016). Uterosome-like vesicles prompt human sperm fertilizing capability. *Mol. Hum. Reprod.* 22, 833–841. doi:10.1093/molehr/gaw066

Freeman, S. A., Christian, S., Austin, P., Iu, I., Graves, M. L., Huang, L., et al. (2017). Applied stretch initiates directional invasion through the action of Rap1 GTPase as a tension sensor. *J. Cell. Sci.* 130, 152–163. doi:10.1242/jcs.180612

Frolíková, M., Stopková, R., Antalíková, J., Johnson, P. M., Stopka, P., and Dvořáková-Hortova, K. (2012). Role of complement regulatory proteins CD46, CD55 and CD59 in reproduction. *Folia Zool. Brno* 61, 84–94. doi:10.25225/fozo.v61.i1.a12.2012

Fujii, D. T., Yohannes, E., Por, E. D., Gillette, L., Beesley, R. D., Heitmann, R. J., et al. (2021). The proteome of human Fallopian tube lavages during the phase of embryo transit reveals candidate proteins for the optimization of preimplantation embryo culture. *Hum. Reprod.* 36, 367–380. doi:10.1093/humrep/deaa333

Gaonac'h-Lovejoy, V., Boscher, C., Delisle, C., and Gratton, J. P. (2020). Rap1 is involved in Angiopoietin-1-induced cell-cell junction stabilization and endothelial cell sprouting. *Cells* 9, 155. doi:10.3390/cells9010155

Gutiérrez-Adán, A., Rizos, D., Fair, T., Moreira, P. N., Pintado, B., De La Fuente, J., et al. (2004). Effect of speed of development on mRNA expression pattern in early bovine embryos cultured *in vivo* or *in vitro*. *Mol. Reprod. Dev.* 68, 441–448. doi:10.1002/mrd.20113

Hu, Q., Zang, X., Ding, Y., Gu, T., Shi, J., Li, Z., et al. (2022). Porcine uterine luminal fluid-derived extracellular vesicles improve conceptus-endometrial interaction during implantation. *Theriogenology* 178, 8–17. doi:10.1016/j.theriogenology.2021.10.021

Jee, B., Dhar, R., Singh, S., and Karmakar, S. (2021). Heat shock proteins and their role in pregnancy: redefining the function of old rum in a new bottle. *Front. Cell. Dev. Biol.* 9, 648463. doi:10.3389/fcell.2021.648463

Jensen, T. S., Bjorge, L., Wollen, A.-L., and Ulstein, M. (1995). Identification of the complement regulatory proteins CD46, CD55, and CD59 in human Fallopian tube, endometrium, and cervical mucosa and secretion. *Am. J. Reproductive Immunol.* 34, 1–9. doi:10.1111/j.1600-0897.1995.tb00913.x

Kerns, K., Morales, P., and Sutovsky, P. (2016). Regulation of sperm capacitation by the 26S proteasome: an emerging new paradigm in spermatology. *Biol. Reprod.* 94 (5), 117–119. doi:10.1095/biolreprod.115.136622

Kusama, K., Nakamura, K., Bai, R., Nagaoka, K., Sakurai, T., and Imakawa, K. (2018). Intrauterine exosomes are required for bovine conceptus implantation. *Biochem. Biophys. Res. Commun.* 495, 1370–1375. doi:10.1016/j.bbrc.2017.11.176

Laezer, I., Palma-Vera, S. E., Liu, F., Frank, M., Trakooljul, N., Vernunft, A., et al. (2020). Dynamic profile of EVs in porcine oviductal fluid during the periovulatory period. *Reproduction* 159, 371–382. doi:10.1530/REP-19-0219

Lamy, J., Corbin, E., Blache, M. C., Garanina, A. S., Uzbekov, R., Mermillod, P., et al. (2017). Steroid hormones regulate sperm–oviduct interactions in the bovine. *Reproduction* 154, 497–508. doi:10.1530/REP-17-0328

Liman, N. (2017). Heat shock proteins (HSP)-60, -70, -90, and 105 display variable spatial and temporal immunolocalization patterns in the involuting rat uterus. *Anim. Reprod.* 14, 1072–1086. doi:10.21451/1984-3143-AR917

Lopera-Vasquez, R., Hamdi, M., Maillo, V., Gutierrez-Adan, A., Bermejo-Alvarez, P., Angel Ramirez, M., et al. (2017). Effect of bovine oviductal extracellular vesicles on embryo development and quality *in vitro*. *Reproduction* 153, 461–470. doi:10.1530/REP-16-0384

Luongo, C., Llamas-López, P. J., Hernández-Caravaca, I., Matás, C., and García-Vázquez, F. A. (2022). Should all fractions of the boar ejaculate be prepared for insemination rather than using the sperm rich only? *Biol. (Basel)* 11 1–15, 210. doi:10.3390/biology11020210

Machtinger, R., Laurent, L. C., and Baccarelli, A. A. (2016). Extracellular vesicles: roles in gamete maturation, fertilization and embryo implantation. *Hum. Reprod. Update* 22, 182–193. doi:10.1093/humupd/dmv055

Mann, T., Lutwak-Mann, C., and Dixon, R. L. (1981). Male reproductive function and semen. *Crit. Rev. Toxicol. II*, 1. –14.

Martínez, C. A., Cambra, J. M., Gil, M. A., Parrilla, I., Álvarez-Rodríguez, M., Rodríguez-Martínez, H., et al. (2020). Seminal plasma induces overexpression of genes associated with embryo development and implantation in day-6 porcine blastocysts. *Int. J. Mol. Sci.* 21, 3662. doi:10.3390/ijms21103662

Martínez, C. A., Cambra, J. M., Parrilla, I., Roca, J., Ferreira-Dias, G., Pallares, F. J., et al. (2019). Seminal plasma modifies the transcriptional pattern of the endometrium and advances embryo development in pigs. *Front. Vet. Sci.* 6, 465. doi:10.3389/fvets.2019.00465

Mazzarella, R., Bastos, N. M., Bridi, A., del Collado, M., Andrade, G. M., Pinzon, J., et al. (2021). Changes in oviductal cells and small extracellular vesicles miRNAs in pregnant cows. *Front. Vet. Sci.* 8, 639752. doi:10.3389/fvets.2021.639752

Mittelbrunn, M., and Sánchez-Madrid, F. (2012). Intercellular communication: diverse structures for exchange of genetic information. *Nat. Rev. Mol. Cell. Biol.* 13, 328–335. doi:10.1038/nrm3335

Mondéjar, I., Martínez-Martínez, I., Avilés, M., and Coy, P. (2013). Identification of potential oviductal factors responsible for zona pellucida hardening and monospermy during fertilization in mammals. *Biol. Reprod.* 89, 67. doi:10.1095/biolreprod.113.111385

Moore, P. B., and Steitz, T. A. (2005). The ribosome revealed. *Trends Biochem. Sci.* 30, 281–283. doi:10.1016/j.tibs.2005.04.006

Morgan, H. L., and Watkins, A. J. (2020). The influence of seminal plasma on offspring development and health. *Semin. Cell. Dev. Biol.* 97, 131–137. doi:10.1016/j.semcdb.2019.06.008

Muller, L., Hong, C. S., Stolz, D. B., Watkins, S. C., and Whiteside, T. L. (2014). Isolation of biologically-active exosomes from human plasma. *J. Immunol. Methods* 411, 55–65. doi:10.1016/j.jim.2014.06.007

Murdica, V., Giacomini, E., Makieva, S., Zarovni, N., Candiani, M., Salonia, A., et al. (2020). *In vitro* cultured human endometrial cells release extracellular vesicles that can be uptaken by spermatozoa. *Sci. Rep.* 10, 8856. doi:10.1038/s41598-020-65517-9

Nakano, S., Yamamoto, S., Okada, A., Nakajima, T., Sato, M., Takagi, T., et al. (2017). Role of extracellular vesicles in the interaction between epithelial and mesenchymal cells during oviductal ciliogenesis. *Biochem. Biophys. Res. Commun.* 483, 245–251. doi:10.1016/j.bbrc.2016.12.158

Neuer, A., Spandorfer, S. D., Giraldo, P., Dieterle, S., Rosenwaks, Z., and Witkin, S. S. (2000). The role of heat shock proteins in reproduction. *Hum. Reprod. Update* 6, 149–159. doi:10.1093/humupd/6.2.149

Nguyen, H. P. T., Simpson, R. J., Salamonsen, L. A., and Greening, D. W. (2016). Extracellular vesicles in the intrauterine environment: challenges and potential functions. *Biol. Reprod.* 95, 109. doi:10.1095/biolreprod.116.143503

Nollen, E., and Morimoto, R. (2002). Chaperoning signaling pathways: molecular chaperones as stress-sensing 'heat shock' proteins. *J. Cell. Sci.* 115, 2809–2816. doi:10.1242/jcs.115.14.2809

Parrilla, I., Martinez, C. A., Cambra, J. M., Lucas, X., Ferreira-Dias, G., Rodriguez-Martinez, H., et al. (2020). Blastocyst-bearing sows display a dominant anti-inflammatory cytokine profile compared to cyclic sows at day 6 of the cycle. *Animals* 10, 2028–2112. doi:10.3390/ani10112028

Perez-Patiño, C., Barranco, I., Parrilla, I., Valero, M. L., Martinez, E. A., Rodriguez-Martinez, H., et al. (2016). Characterization of the porcine seminal plasma proteome comparing ejaculate portions. *J. Proteomics* 142, 15–23. doi:10.1016/j.jprot.2016.04.026

Perez-Riverol, Y., Bai, J., Bandla, C., García-Seisdedos, D., Hewapathirana, S., Kamatchinathan, S., et al. (2022). The PRIDE database resources in 2022: A hub for mass spectrometry-based proteomics evidences. *Nucleic Acids Res.* 50, D543–D552. doi:10.1093/nar/gkab1038

Pierzchała, D., Liput, K., Korwin-Kossakowska, A., Ogłuszka, M., Poławska, E., Nawrocka, A., et al. (2021). Molecular characterisation of uterine endometrial proteins during early stages of pregnancy in pigs by maldi tof/tof. *Int. J. Mol. Sci.* 22, 6720. doi:10.3390/ijms22136720

Pralle, A., Keller, P., Florin, E.-L., Simons, K., and Hörber, J. K. H. (2000). Sphingolipid-cholesterol rafts diffuse as small entities in the plasma membrane of mammalian cells. *J. Cell. Biol.* 148, 997–1008. doi:10.1083/jcb.148.5.997

Qian, Y.-M., Qin, X., Miwa, T., Sun, X., Halperin, J. A., and Song, W.-C. (2000). Identification and functional characterization of a new gene encoding the mouse terminal complement inhibitor CD59. *J. Immunol.* 165, 2528–2534. doi:10.4049/jimmunol.165.5.2528

Raposo, G., and Stoorvogel, W. (2013). Extracellular vesicles: exosomes, microvesicles, and friends. *J. Cell. Biol.* 200, 373–383. doi:10.1083/jcb.201211138

Rodríguez-Martínez, H., Kvist, U., Saravia, F., Wallgren, M., Johannisson, A., Sanz, L., et al. (2009). The physiological roles of the boar ejaculate. *Control pig reproduction* VIII, 1–21.

Rodríguez-Martínez, H., Martinez, E. A., Calvete, J. J., Peña Vega, F. J., and Roca, J. (2021). Seminal plasma: relevant for fertility? *Int. J. Mol. Sci.* 22, 4368. doi:10.3390/ijms22094368

Rudolf Vegas, A., Hamdi, M., Podico, G., Bollwein, H., Fröhlich, T., Canisso, I. F., et al. (2022). Uterine extracellular vesicles as multi-signal messengers during maternal recognition of pregnancy in the mare. *Sci. Rep.* 12, 15616. doi:10.1038/s41598-022-19958-z

Sabín, J., Prieto, G., Ruso, J. M., and Sarmiento, F. (2007). Fractal aggregates induced by liposome-liposome interaction in the presence of Ca 2+. *Eur. Phys. J. E* 24, 201–210. doi:10.1140/epje/i2007-10231-3

Seytanoglu, A., Stephen Georgiou, A., Sostaric, E., Watson, P. F., Holt, W. V., and Fazeli, A. (2008). Oviductal cell proteome alterations during the reproductive cycle in pigs. *J. Proteome Res.* 7, 2825–2833. doi:10.1021/pr8000095

Soleilhavoup, C., Riou, C., Tsikis, G., Labas, V., Harichaux, G., Kohnke, P., et al. (2016). Proteomes of the female genital tract during the oestrous cycle. *Mol. Cell. Proteomics* 15, 93–108. doi:10.1074/mcp.M115.052332

Subedi, P., Schneider, M., Philipp, J., Azimzadeh, O., Metzger, F., Moertl, S., et al. (2019). Comparison of methods to isolate proteins from extracellular vesicles for mass spectrometry-based proteomic analyses. *Anal. Biochem.* 584, 113390. doi:10.1016/j.ab.2019.113390

Supek, F., Bošnjak, M., Škunca, N., and Šmuc, T. (2011). Revigo summarizes and visualizes long lists of gene ontology terms. *PLoS One* 6, e21800. doi:10.1371/journal.pone.0021800

Théry, C., Amigorena, S., Raposo, G., and Clayton, A. (2006). Isolation and characterization of exosomes from cell culture supernatants and biological fluids. *Curr. Protoc. Cell. Biol.* 30, Unit 3.22. doi:10.1002/0471143030.cb0322s30

van der Pol, E., Coumans, F. A. W., Grootemaat, A. E., Gardiner, C., Sargent, I. L., Harrison, P., et al. (2014). Particle size distribution of exosomes and microvesicles

determined by transmission electron microscopy, flow cytometry, nanoparticle tracking analysis, and resistive pulse sensing. *J. Thrombosis Haemostasis* 12, 1182–1192. doi:10.1111/jth.12602

Watkins, A. J., Dias, I., Tsuro, H., Allen, D., Emes, R. D., Moreton, J., et al. (2018). Paternal diet programs offspring health through sperm- and seminal plasma-specific pathways in mice. *Proc. Natl. Acad. Sci. U. S. A.* 115, 10064–10069. doi:10.1073/pnas.1806333115

Wickham, H., François, R., Henry, L., and Müller, K. (2019). *dplyr: A grammar of data manipulation*.

Wickham, H. (2016). *ggplot2: Elegant graphics for data analysis*. 2nd ed. Cham: Springer.

Yam, A. Y., Xia, Y., Lin, H. T. J., Burlingame, A., Gerstein, M., and Frydman, J. (2008). Defining the TRiC/CCT interactome links chaperonin function to stabilization of newly made proteins with complex topologies. *Nat. Struct. Mol. Biol.* 15, 1255–1262. doi:10.1038/nsmb.1515

Zhang, T., Hu, R., Wang, Y., Guo, S., Wu, Z., Liu, J., et al. (2023). Extracellular matrix stiffness mediates uterine repair via the Rap1a/ARHGAP35/RhoA/F-actin/YAP axis. *Cell. Commun. Signal.* 21, 22. doi:10.1186/s12964-022-01018-8

Zigo, M., Jonakova, V., Manaskova-Postlerova, P., Kerns, K., and Sutovsky, P. (2019). Ubiquitin-proteasome system participates in the de-aggregation of spermadhesins and DQH protein during boar sperm capacitation. *Reproduction* 157, 283–295. doi:10.1530/REP-18-0413

Zigo, M., Kerns, K., and Sutovsky, P. (2023). The ubiquitin-proteasome system participates in sperm surface subproteome remodeling during boar sperm capacitation. *Biomolecules* 13, 996. doi:10.3390/biom13060996

frontiers | Frontiers in Cell and Developmental Biology

TYPE Original Research
PUBLISHED 15 November 2023
DOI 10.3389/fcell.2023.1259421

OPEN ACCESS

EDITED BY
Dolores Busso,
Universidad de los Andes, Chile, Chile

REVIEWED BY
Ingrid Carvacho,
Universidad Católica del Maule, Chile
Atsushi Asano,
University of Tsukuba, Japan

*CORRESPONDENCE
María Victoria Berberian,
victoria.berberian@gmail.com
Marcela A. Michaut,
mmichaut@gmail.com

†These authors have contributed equally to this work and share last authorship

RECEIVED 15 July 2023
ACCEPTED 30 October 2023
PUBLISHED 15 November 2023

CITATION
Klinsky OG, Wetten PA, Zanni-Ruiz E, Pavarotti MA, Berberian MV and Michaut MA (2023), The light chain of tetanus toxin bound to arginine-rich cell-penetrating peptide inhibits cortical reaction in mouse oocytes.
Front. Cell Dev. Biol. 11:1259421.
doi: 10.3389/fcell.2023.1259421

The light chain of tetanus toxin bound to arginine-rich cell-penetrating peptide inhibits cortical reaction in mouse oocytes

Omar G. Klinsky[1,2], Paula A. Wetten[1,2], Emilia Zanni-Ruiz[3], Martín A. Pavarotti[3], María Victoria Berberian[3,4,5*†] and Marcela A. Michaut[1,4*†]

[1]Laboratorio de Biología Reproductiva y Molecular, Instituto de Histología y Embriología de Mendoza (IHEM), Universidad Nacional de Cuyo-Consejo Nacional de Investigaciones Científicas y Técnicas (CONICET), Mendoza, Argentina, [2]Facultad de Ciencias Médicas, Universidad Nacional de Cuyo, Mendoza, Argentina, [3]Laboratorio de Transporte Intracelular, Instituto de Histología and Embriología de Mendoza (IHEM), Universidad Nacional de Cuyo-Consejo Nacional de Investigaciones Científicas y Técnicas (CONICET), Mendoza, Argentina, [4]Facultad de Ciencias Exactas y Naturales, Universidad Nacional de Cuyo, Mendoza, Argentina, [5]Instituto Interdisciplinario de Ciencias Básicas, Facultad de Ciencias Exactas y Naturales, Universidad Nacional de Cuyo, Consejo Nacional de Investigaciones Científicas y Técnicas (CONICET), Mendoza, Argentina

Introduction: Cortical reaction is a secretory process that occurs after a spermatozoon fuses with the oocyte, avoiding the fusion of additional sperm. During this exocytic event, the cortical granule membrane fuses with the oocyte plasma membrane. We have identified several molecular components involved in this process and confirmed that SNARE proteins regulate membrane fusion during cortical reaction in mouse oocytes. In those studies, we microinjected different nonpermeable reagents to demonstrate the participation of a specific protein in the cortical reaction. However, the microinjection technique has several limitations. In this work, we aimed to assess the potential of cell-penetrating peptides (CPP) as biotechnological tools for delivering molecules into oocytes, and to evaluate the functionality of the permeable tetanus toxin (bound to CPP sequence) during cortical reaction.

Methods: Arginine-rich cell-penetrating peptides have demonstrated the optimal internalization of small molecules in mammalian cells. Two arginine-rich CPP were used in the present study. One, labeled with 5-carboxyfluorescein, to characterize the factors that can modulate its internalization, and the other, the permeable light chain of tetanus toxin, that cleaves the SNAREs VAMP1 and VAMP3 expressed in mouse oocytes.

Results: Results showed that fluorescent CPP was internalized into the oocyte cytoplasm and that internalization was dependent on the concentration, time, temperature, and maturation stage of the oocyte. Using our functional assay to study cortical reaction, the light chain of tetanus toxin bound to arginine-rich cell-penetrating peptide inhibited cortical granules exocytosis.

Discussion: Results obtained from the use of permeable peptides demonstrate that this CPP is a promising biotechnological tool to study functional macromolecules in mouse oocytes.

KEYWORDS

cortical granules, tetanus toxin, arginine-rich cell-penetrating peptides, exocytosis, oocytes, cortical reaction, biotechnology

1 Introduction

In mammals, the cortical reaction is a secretory process that occurs after a spermatozoon fuses with the oocyte during fertilization. This fusion event activates various molecular mechanisms in oocytes that are globally called oocyte activation. The first and more rapid sign of oocyte activation is the liberation of millions of zinc atoms, known as zinc sparks (Kim et al., 2011). After zinc sparks and in the following 15 min, granules localized in the oocyte cortical region -cortical granules-fuse with the oocyte plasma membrane (Cappa et al., 2018). This process is an exocytotic event triggered by an increase in cytoplasmatic calcium levels and avoids the fusion of additional spermatozoa. Therefore, cortical granules exocytosis -also named cortical reaction-is essential for ensuring the development of the preimplantation embryo.

Membrane fusion during cortical granule exocytosis is regulated by SNARE proteins. Our laboratory has made significant contributions to the identification of several proteins involved in this exocytosis process. We have demonstrated the participation of alpha-SNAP and NSF (Paola et al., 2015), Rab3A (Bello et al., 2016), as well as VAMP1 and VAMP3 (Paola et al., 2021). Furthermore, other groups have identified SNAP23 (Mehlmann et al., 2019), Rabphilin 3A (Masumoto et al., 1996), Rab27A (Wang et al., 2016), and Synaptotagmin I (Zhu et al., 2020). Collectively, these findings have allowed us to propose a comprehensive working model for membrane fusion during cortical granule exocytosis in mouse oocytes (Paola et al., 2021).

To identify the participation of a specific protein in the cortical reaction, we developed a functional assay based on cortical granules quantification during the cortical reaction parthenogenetically activated in mouse oocytes. To inhibit protein function, we performed microinjections of recombinant proteins, blocking antibodies, or toxins prior to parthenogenetic activation with strontium chloride (Paola et al., 2015; Bello et al., 2016; Paola et al., 2021). So far, oocyte microinjection is the standard method for introducing molecules into oocytes. However, this technique is associated with several limitations such as invasiveness, time-consuming nature, the requirement of specialized microinjection equipment, and skilled personnel (Rubino et al., 2016).

An alternative approach involves the use of cell-penetrating peptides (CPP), which are short peptides that have the capability to permeate cell membranes and deliver molecules directly into the cytoplasm. CPPs are derived from naturally occurring proteins and can be synthesized using solid-phase peptide synthesis. They can be used to deliver a wide range of cargo molecules, including proteins, nucleic acids, and small molecules, into the cell cytoplasm (Copolovici et al., 2014; Jafari et al., 2015; Dinca et al., 2016; Zhang et al., 2016; Mayorga et al., 2020; Xie et al., 2020).

One advantage of CPPs is their ease of use. Peptides can be readily synthesized and delivered into the cell cytoplasm using simple methods such as incubating cells in a CPP containing solution. In addition, this approach is less invasive than microinjection, and does not require specialized equipment or skilled personnel. Therefore, this investigation aims to ascertain whether CPP-mediated delivery can be utilized as a substitute method to intracytoplasmic microinjection for achieving intracellular delivery of macromolecules into oocytes.

Arginine-rich cell-penetrating peptides have demonstrated the optimal internalization of small molecules in mammalian cells (Mitchell et al., 2000; Mueller et al., 2008; Tünnemann et al., 2008). To assess the potential of cell-penetrating peptides as biotechnological tools for molecules deliver into oocytes, we first analyzed the ability of arginine-rich cell-penetrating peptide to cross both the zona pellucida and plasma membrane in immature and mature mouse oocytes, and then, determined the functionality of the light chain of tetanus toxin bound to this cell-penetrating peptide in the cortical granule exocytosis assay.

2 Materials and methods

2.1 Ethics statement

All animals were cared in accordance with the Guiding Principles in the Care and Use of Animals of the US National Institute of Health. All procedures were approved by the Institutional Animal Care and Use Committee of the School of Medical Science, Universidad Nacional de Cuyo (Protocol N° 169/2019).

2.2 Chemical and reagents

All chemicals and reagents, unless stated otherwise, were purchased from Sigma-Aldrich Chemical Inc. (St. Louis, United States).

2.3 Oocyte collection

Germinal Vesicle (GV, immature) and Metaphase II (MII, mature) oocytes were obtained from hormonally stimulated CF-1 female mice (8–12 weeks) and bred under controlled conditions of light and temperature. To obtain GV oocytes, females were injected intraperitoneally (i.p.) with 10 IU of purified equine chorionic gonadotropin hormone (PMSG) (Syntex, Argentina), and after 45–48 h cumulus oocyte-cell complexes (COC) were obtained by ovarian puncture. Earle's balanced salt solution with 0.01% PVA, 0.001% Gentamicin, and 25 mM HEPES buffer, pH 7.3 (MEM/HEPES) was used as the collection medium, supplemented with 2.5 μM Milrinone to inhibit oocyte maturation. To denude the GV oocytes, cumulus cells were

mechanically removed using fine-bore pipettes. MII oocytes were obtained from female mice stimulated with 10 IU (i.p.) of PMSG (Syntex, Argentina), followed by 10 IU (i.p.) of human chorionic gonadotropin hCG (Syntex, Argentina) 48 h later. After 13–17 h, the MII oocytes were obtained from the oviductal ampullae, denuded from cumulus cells by brief incubation in hyaluronidase (0.04%) and placed in CZB medium (81.62 mM NaCl, 4.83 mM KCl, 1.70 mM $CaCl_2.2H_2O$, 1.18 mM $MgSO_4.7H_2O$, 1.18 mM KH_2PO_4, 0.11 mM EDTA.2Na, 25.12 mM $NaHCO_3$, 52 mM sodium lactate, 0.27 mM sodium pyruvate, 7 mM taurine, 1 mM L-glutamine, 10 mg/mL gentamicin, supplemented with 0.3% BSA) and covered with mineral oil in a humidified chamber (37°C, 5% CO_2) for the shortest time possible until their use.

2.4 Cell penetrating peptide

The CPP used in this study possesses the following sequence: NH_2-K-(5-FAM)RRRRRRRRRC-$CONH_2$ (MW 2012,32 Da). It was custom-designed by our research team and was commercially synthesized by Innovagen AB using solid-phase synthesis, achieving a purity grade exceeding 98%. This CPP includes an amide group at the C-terminus of the cysteine to prevent undesired binding, a lysine residue at the N-terminus to provide a primary amino group suitable for protein conjugation, and a polyR sequence that confers a membrane-penetrating capability. Furthermore, 5-FAM(5-carboxyfluorescein) is conjugated covalently to CPP through the lysine residue, allowing the peptide to be visualized using fluorescence microscopy.

2.5 CPP incubations

After collection, GV and MII oocytes were incubated in CPP in CZB medium. To check the effect of the zona pellucida (ZP) in the CPP internalization, some GV and MII oocytes were subjected to a brief incubation in acid Tyrode to remove the ZP, prior to carrying out the corresponding treatments with CPP. If not, oocytes were incubated with ZP at different concentrations of FAM-CPP: 1, 2 and 3 μM (only for MII oocytes), and 4, 10 and 16 μM (for GV and MII oocytes); at different times: 15, 30, and 60 min; and different temperatures: 37°C in a humidified atmosphere of CO_2 (5%) or 4°C in a refrigerator. Likewise, as a control, a group of GV and MII oocytes was treated with CZB medium without CPP. Following, the ZP was removed by brief incubation in acid Tyrode (pH 2.2) and the oocytes were fixed in paraformaldehyde (3.7%) in Dulbecco's PBS (DPBS) for 1 h at room temperature (RT). Cells were then washed in blocking solution (BS) containing 3 mg/mL BSA, 100 mM glycine, and 0.01% Tween 20 in DPBS, and mounted in Vectashield mounting medium (Vector Laboratories, Burlingame, CA) following two types of mounting techniques: in chamber or flattened (Figure 1A). Chamber mounting consists of placing two lines of solid vaseline between the slide and the coverslip to create a space where the oocytes are contained with a minimal compression to keep their spherical shape. On the contrary, in the flattened mounting, the lines of solid vaseline are absent and the cells are compressed between the slide and coverslip. Then, samples were sealed and stored at 4°C until viewing.

2.6 Endocytosis inhibition assays

To inhibit endocytosis, oocytes were incubated in CZB medium containing either 80 μM Dyngo-4a (Abcam) or 20 μM Cytochalasin B (Abcam) for 90 min at 37°C in a humidified atmosphere of 5% CO_2. After washing, oocytes were incubated during 30 min in 10 μM FAM-CPP in the same conditions. Then, ZP was removed, and oocytes were fixed as described in section 2.5. Cells were separated in two groups. One cells group was flatten mounted to analyze the cytoplasmic FAM-CPP fluorescence. The other cells group was permeabilized with Triton X-100 for 15 min, stained with Rhodamine-Phalloidin 555 (1:1000) for 60 min and mounted in chamber. For DNA detection, Vectashield Mounting Medium (Vector Laboratories, Burlingame, CA) containing 1.5 μg/mL Hoechst 33342 (Molecular Probes, Invitrogen) was used. After sealing, slides were stored at 4°C until visualization.

2.7 Mitochondrial membrane potential (MMP) assay

MII oocytes with ZP were incubated with 10 μM FAM-CPP in CZB for 60 min, at 37 °C in a humidified atmosphere of CO_2 (5%). Likewise, as a control, a group of MII oocytes was treated with 5-FAM (without CPP) in CZB. Next, MII oocytes were incubated for 30 min in a solution of 2 μM Tetramethylrhodamine perchlorate ethyl ester (TMRE), which allowed the staining of the mitochondrial membranes to determine their potential. Then, cells were washed twice in MEM/HEPES drops and transferred to a real-time chamber with MEM/HEPES without PVP to fix them on the glass and prevent their movement. *In vivo* visualization was performed on a laser scanning confocal microscope (FV1000, Olympus) using a UPLSAPO 20X/NA:0.75 objective lens, a pixel resolution of ×512512, and the pinhole fully open (800) to obtain the total fluorescence of the cells. Equatorial images of oocytes were captured using the same microscope setup. The absolute total fluorescence intensity of the cell was quantified using ImageJ software (version 1.42L; NIH, MD).

2.8 Cortical granules (CG) staining

CG staining was performed as previously described (Paola et al., 2015). Briefly, after MII oocytes incubation in CPP (10 μM), at 37°C, and different times (15, 30, 60 min), ZP was removed by brief incubation in acid Tyrode and oocytes were fixed in paraformaldehyde for 1 h at RT. Then, oocytes were washed in BS, and permeabilized with Triton X-100 for 15 min. After 3 washes in BS, cells were incubated in 25 μg/mL Rhodamine-labeled Lens Culinaris Agglutinin (LCA) in BS for 30 min, after which they were washed again in BS. Cells were mounted in Vectashield mounting medium (Vector Laboratories, Burlingame, CA) between slide and coverslip (flattened mounting), sealed, and stored at 4°C until viewing.

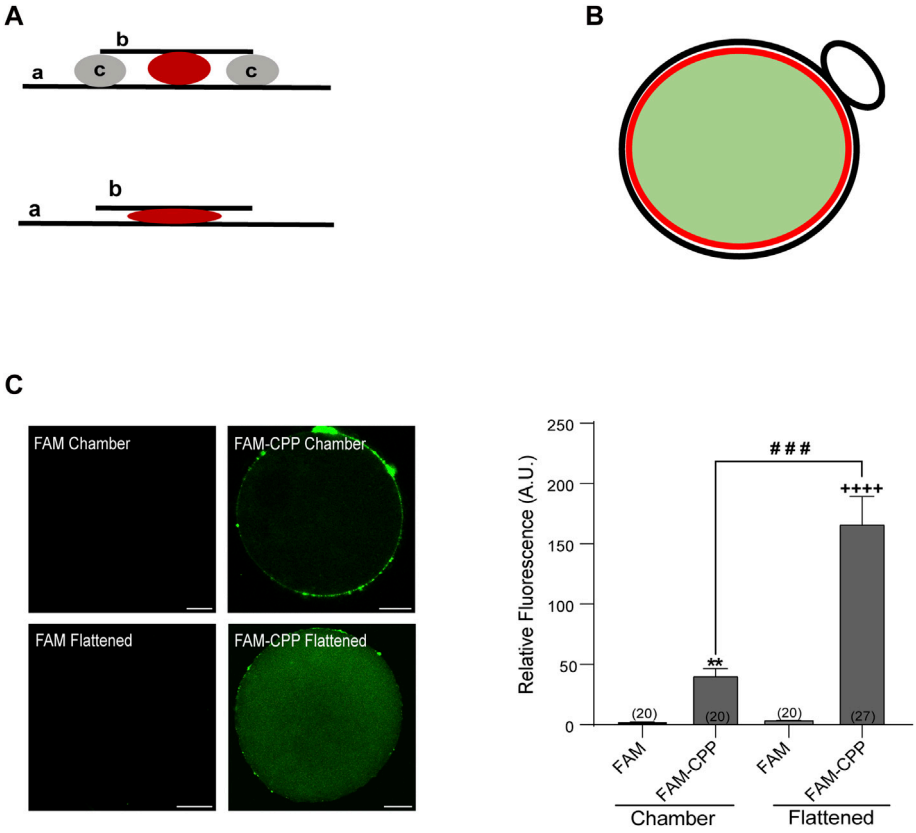

FIGURE 1
FAM-CPP is able to cross both zona pellucida and plasma membrane of mouse oocytes. **(A)** Schematic representation of mounting. Upper: chambered mounting. Lower: flattened mounting. **(A)** slide, **(B)** coverslip, **(C)** solid vaseline. **(B)** Schematic representation of absolute fluorescence quantification through Image J. Red circle represents the area taken to quantify the fluorescence intensity. It only takes the central area of the oocyte (light green area) and excludes the cortical area and polar body (black line). **(C)** Effect of mounting on the visualization of FAM-CPP internalization. MII oocytes with ZP were incubated with 10 μM FAM (control) or FAM-CPP during 1 h, washed, fixed, and mounted as indicated. Left: representative confocal microscopic images of oocytes taken at equatorial plane of the cell. Scale bar: 15 μm. Right: histogram showing relative fluorescence intensity (A.U.) for different mounting. The data represent mean ± SEM. Numbers in parentheses at the base of the bar represent the total number of oocytes. Comparisons between FAM and mounting types were made by Kruskal–Wallis and Dunn's multiple comparisons test ($p < 0.001$). * (chamber) and + (flattened) represent significant differences compared to FAM. # represent significant differences between mounting types.

2.9 Recombinant permeable tetanus toxin light chain (CPP-TeTx) design and purification

The TeTx light chain purification was performed as described by Mayorga et al., 2019 (Mayorga et al., 2020). The plasmid DNA encoding His6-tetanus toxin light chain in pQE3-Qiagen (previously provided by T. Binz from Medizinische Hochschule Hannover, Hannover, Germany) was transformed into *E. coli* XL-1Blue (Stratagene, La Jolla, CA, United States), and protein expression was induced overnight at 20°C with 0.2 mM IPTG. Purification of recombinant His_6-tetanus toxin (TeNT) was accomplished according to the QIAexpressionist (www.qiagen.com). The CPP peptide (RRRQRRKRRRRQ) and the recombinant toxin (His6-TeNT) were cross-linked by Trilinks Biotechnology under the manufacturing protocol. The primary amines of both toxin and peptide were linked to succinimidyl-4-formyl benzamide (S-4FB) and succinimidyl-6-hydrazino-nicotinamide (SHyNic), respectively. The modified proteins and peptides were then conjugated by a specific chemical reaction between HyNic and 4FB in a particular molar ratio (3:1 M equivalent) at RT by 3 h incubation with aniline 100 mM as a catalyst. After the conjugation reaction, the cross-linkers reagents surplus was removed and the CPP-TeTx was purified on a Sephadex G25 column (MP Biomedicals) in a medium suitable for oocyte incubation (MEM/HEPES). The purity was confirmed by SDS-PAGE analysis.

2.10 CPP-TeTx incubation and inmunofluorescence assay

Incubation of MII oocytes was performed in CPP-TeTx (4 μM) for 15, 30 and 60 min, at 37°C on a thermal stage. After that, ZP was removed by brief incubation in acid Tyrode and the oocytes were fixed in paraformaldehyde for 1 h at RT. Cells were then washed in BS, and permeabilized with Triton X-100 for 15 min. After 3 washes in BS, incubation was performed in Mouse Anti-6X His (Abcam) primary antibody (1:20) for 1 h at RT. After 3 washes in BS, oocytes were incubated for 1 h in DyLight 488 donkey anti-mouse secondary antibody (3 ng/μl, Jackson ImmunoReasearch). After 3 washes, cells

were flat mounted in Vectashield mounting medium (Vector Laboratories, Burlingame, CA) on a slide, sealed, and stored at 4°C until visualization.

2.11 Parthenogenetic activation with strontium chloride ($SrCl_2$)

After MII oocytes incubation in 10 μM FAM-CPP or 4 μM pTxTe for 60 min, at 37°C, the cortical reaction was induced by parthenogenetic activation with $SrCl_2$ (30 mM) in calcium and magnesium free CZB (85.35 mM NaCl, 4.83 mM KCl, 1.18 mM KH_2PO4, 110 μM EDTA.2Na, 12 mM $NaHCO_3$ 25, 270 μM Na pyruvate, 52 mM Na lactate, supplemented with 0.001% Gentamicin, 0.01% PVA, 1 mM Glutamine), for 1 h at 37°C in a humidified CO_2 (5%) atmosphere. Then, ZP was removed by brief incubation in acid Tyrode and oocytes were fixed in paraformaldehyde for 1 h at RT. Cells were washed in BS, and permeabilized with Triton X-100 for 15 min. After 3 washes in BS, cells were incubated in 25 μg/mL Rhodamine-labeled Lens Culinaris Agglutinin (LCA) in BS for 30 min, after which they were washed again in BS. Cells were flattened-mounted in Vectashield mounting medium (Vector Laboratories, Burlingame, CA) on a slide, sealed, and stored at 4°C. To demonstrate the specificity of the effect of pTxTe, a group of oocytes was incubated with N,N,N′,N′-Tetrakis (2-pyridylmethyl) ethylenediamine (TPEN), a zinc chelator permeable to cells with a high affinity for zinc. Oocytes were treated with 10 μM TPEN during 15 min at 37°C prior activation with $SrCl_2$.

2.12 Microscopy imaging and quantification

The images were acquired with a confocal laser scanning microscope (FV1000, Olympus), using a PLAPON 60x/NA1.42 oil immersion objective lens, at a pixel resolution of ×512 512. The cell images were taken at flat optical fields of the equatorial zone (to analyze either the fluorescence of CPP or the immunolabeled CPP-TeTx) or at the cortical zone (to analyze cortical granule density). The confocal acquisition parameters were constant for all images captured. Using the computer-assisted image quantification software ImageJ (version 1.42L; NIH, MD), the absolute fluorescence intensity of oocytes treated with CPP or CPP-TeTx was quantified by drawing a circumference that took the cytoplasm of the cell, but not the cortical zone, and whose diameter was maintained for all the cells analyzed (Figure 1B). To quantify the density of CG through ImageJ, images were deconvoluted to obtain greater sharpness. The mean obtained from the counting of CG present in four non overlapping equal areas from the oocyte cortex, was used to determine CG density per 100 μm^2 (CG/100 μm^2) for each cell.

2.13 Data analysis

Experiments were repeated at least three times. The number of oocytes used for each experiment is indicated in the figure or in legends. Data analysis was performed with GraphPad Prism 8 software. Depending on data distribution (whether parametric or not), statistical significance was determined by Student/Mann Whitney *t*-test or One-way Analysis of Variance (ANOVA)/Brown-Forsythe and Welch ANOVA/Kruskal–Wallis tests followed by *post hoc* test for multiple comparisons. Data are expressed as mean ± SEM and $p < 0.05$ is considered statistically significant.

3 Results

3.1 The fluorescent cell permeable peptide K(5-FAM)R_9C is able to cross both zona pellucida and plasma membrane of mouse oocytes

In this study, we investigated the internalization ability of cell-penetrating peptides across the zona pellucida and plasma membrane of mouse oocytes. As a representative CPP model, we selected KR_9C, a peptide comprising nine consecutive arginine residues. Previous research has indicated that oligoarginine sequences consisting of eight to twelve consecutive residues demonstrate optimal internalization capability for small molecules in mammalian cells (Mitchell et al., 2000; Mueller et al., 2008; Tünnemann et al., 2008). To observe the intracellular behavior of the CPP using fluorescence microscopy, we introduced the 5-FAM (5-carboxyfluorescein) into the peptide sequence. Specifically, FAM was conjugated covalently to the lysine residue (see Materials and Methods), resulting in the peptide sequence K(5-FAM)R_9C, which will be referred to as FAM-CPP hereinafter.

To evaluate if this FAM-CPP was able to cross the oocyte's plasma membrane, we analyzed the fluorescence intensity in Metaphase II (MII or mature) oocytes after cells incubation at 37 °C in the presence (or absence) of 10 μM CPP. For these assays, MII oocytes with zona pellucida were used.

After fixation, cells were mounted in two different manners: in "chamber" or "flattened" between slide and coverslip (see schematic representation of mountings in Figure 1A). To detect exclusively the cytoplasmic fluorescence, only equatorial zone of the cells was imaged. Confocal microscopy images of oocyte's equatorial zone showed that FAM-CPP accumulated on the outside of cells and in the polar body; thus, we only analyzed the fluorescence intensity of the equatorial region within the red circle as indicated in the scheme of Figure 1B. The analysis of fluorescence intensity showed that the flattened method was the best mounting manner to obtain a significant signal compared to control cells (Figure 1C). FAM-CPP showed a diffuse pattern of distribution in oocyte cytoplasm, while control cells incubated only with FAM (without CPP) did not shown fluorescence. These results indicated that the fluorescent CPP was able to cross the plasma membrane of mature oocytes with zona pellucida and that the flattened method was the best cell mounting to analyze the FAM-CPP internalization in the assayed conditions.

One of the fundamental conditions for a CPP to be viable as a biotechnological tool is that it has low or no cytotoxicity. Although there are studies with cationic peptides (such as the

10.3389/fcell.2023.1259421

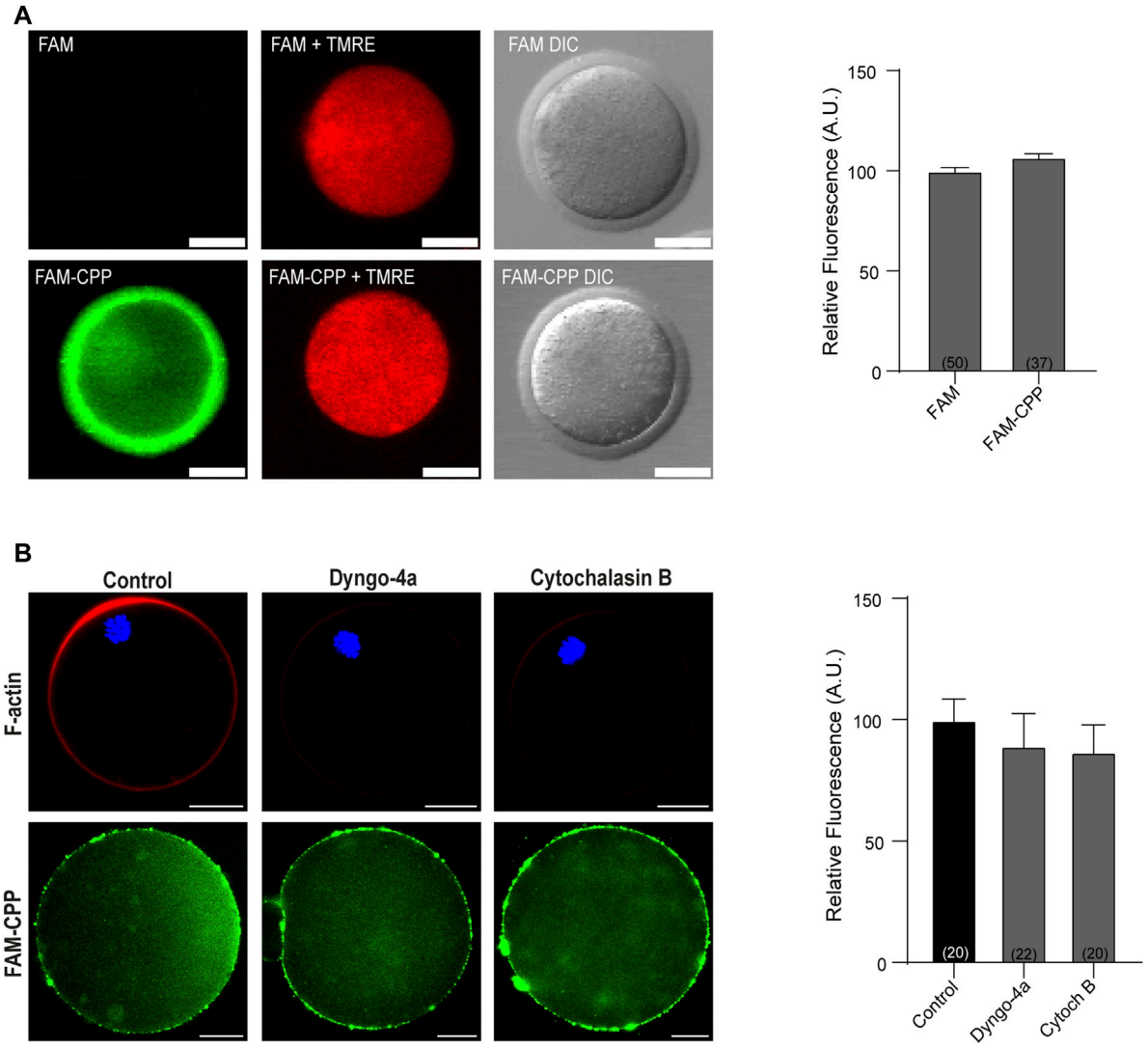

FIGURE 2
FAM-CPP does not affect cell viability and enters oocytes by translocation. (**A**) Effect of incubation with FAM-CPP on mitochondrial membrane potential (MMP). MII oocytes with ZP were incubated with 10 μM FAM or FAM-CPP during 1 h, and then incubated in the probe TMRE (red) to analyze MMP *in vivo*. Left: representative confocal microscopic images of oocytes. Scale bar: 5 μm. Right: relative fluorescence intensity at different treatments. The data represent mean ± SEM. Numbers in parentheses at the base of the bar represent the total number of oocytes. Comparisons between FAM and FAM-CPP were made by t Student test ($p < 0.12$). DIC: differential interference contrast. (**B**) Effect of endocytosis inhibition on FAM-CPP penetration. MII oocytes were preincubated with 80 μM Dyngo-4a or 20 μM Cytochalasin B (Cytoch B) prior the incubation with 10 μM FAM-CPP (green). Left: upper panel, representative confocal microscopic images of oocytes stained with Rhodamine-Phalloidin 555 (F-actin, red) and mounted in chamber; lower panel, representative confocal microscopic images of oocytes incubated in FAM-CPP after endocytosis inhibition. Right: relative fluorescence intensity at different treatments. The data represent mean ± SEM. Numbers in parentheses at the base of the bar represent the total number of oocytes. Comparisons between control, Dyngo and CB were made by Kruskal–Wallis and Dunn's multiple comparisons test (p = 021).

polyarginine used in this work) that indicate that they have low toxicity and are tolerated by cells at high concentrations (Dinca et al., 2016), we first analyzed the viability of mature oocytes incubated with CPP by determining the mitochondrial membrane potential (MMP). As shown in Figure 2A, after 1 h incubation at 37°C in presence of 10 μM CPP, mature oocytes were alive, indicating that the FAM-CPP was not toxic for the cells. Then, to rule out that that FAM-CPP was entering by endocytosis, we preincubated oocytes with two different endocytosis inhibitors before CPP incubation: Dyngo-4a and Cytochalasin B. Dyngo-4a is a dynamin inhibitor that inhibit clathrin-mediated endocytosis and perturb the actin dynamic (Ferguson and De Camilli, 2012; McCluskey et al., 2013). Cytochalasin B is a known reagent that disassembly F-actin cytoskeleton (Cooper, 1987). Mouse oocytes were preincubated in presence of the endocytosis inhibitors prior FAM-CPP incubation. After fixation, oocytes were either flatten mounted to analyze the cytoplasmic FAM-CPP fluorescence or permeabilized to stain F-actin (see details in Materials and Methods) As shown in Figure 2B, both Dyngo-4a and Cytochalasin B disrupted cortical F-actin when compared to control condition. However, FAM-CPP was observed in the

10.3389/fcell.2023.1259421

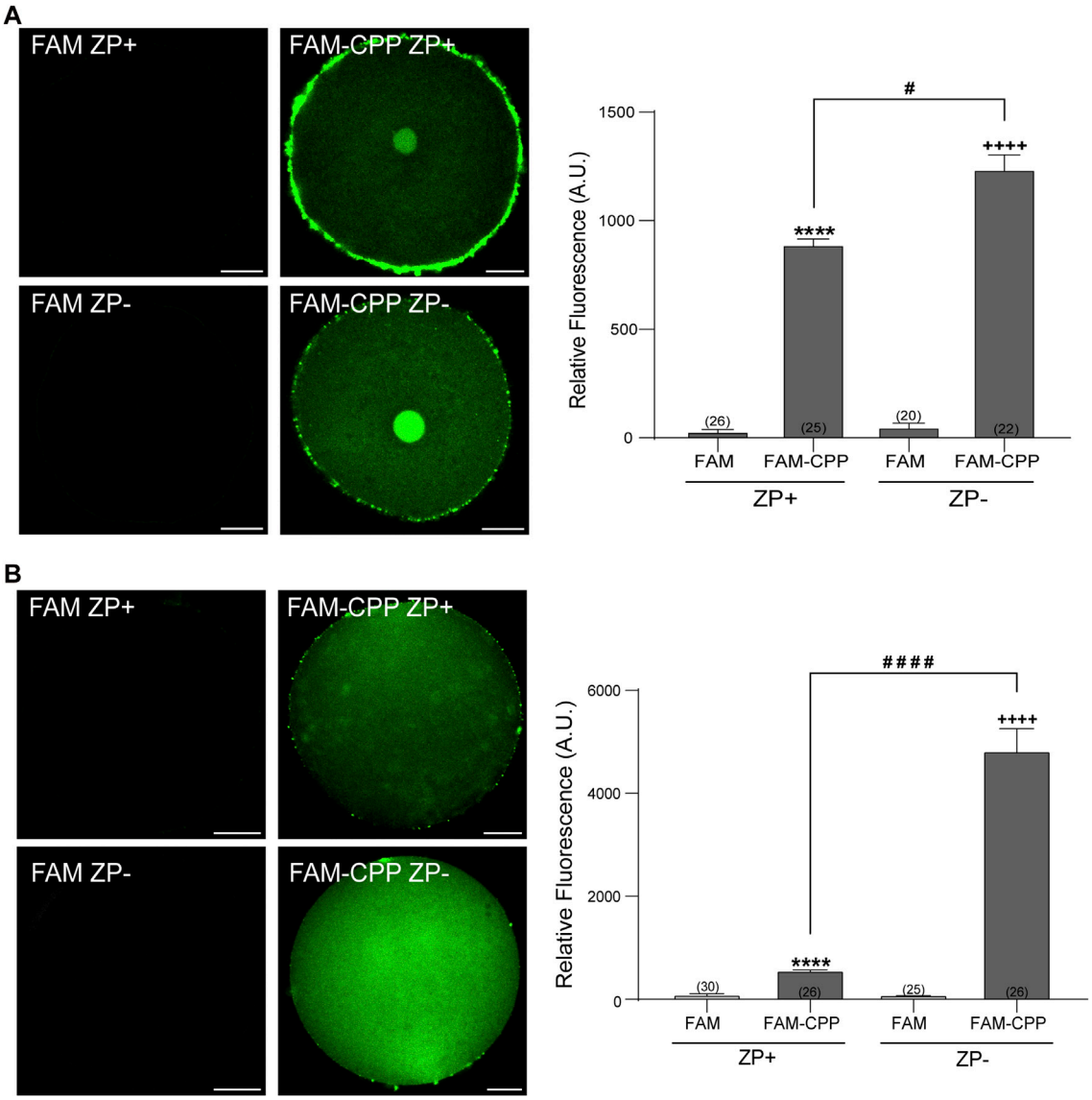

FIGURE 3
Effect of zona pellucida (ZP) on FAM-CPP internalization. GV oocytes **(A)** and MII oocytes **(B)** were incubated in FAM-CPP (4 and 10 μM, respectively) at 37°C, with (ZP+) or without (ZP-) zona pellucida. Left **(A,B)**. Representative confocal microscopy images taken at equatorial plane of the cell. Scale bar: 15 μm. Right **(A,B)**. Histogram showing relative fluorescence intensity for different treatments. The data represent mean ± SEM calculated from independent experiments. Numbers in parentheses at the base of the bar represent the total number of oocytes. Comparisons between FAM group and treatments were made by Kruskal–Wallis and Dunn's multiple comparisons test ($p < 0.0001$) for GV oocytes, and Brown-Forsythe and Welch ANOVA tests, and Games-Howell's multiple comparisons test ($p < 0.0001$) for MII oocytes. * (ZP+) and + (ZP-) represent statistically significant differences compared to control. # represent significant differences between groups.

cytoplasm indicating that, even when endocytosis was inhibited, the CPP was internalized. These results suggest that the translocation of FAM-CPP take place by a direct penetration mechanism.

The zona pellucida (ZP) is a glycoprotein matrix that functions as a protective barrier, filtering substances from the extracellular space (Gupta et al., 2012). Because this barrier must be crossed to introduce substances into the oocytes, we analyzed the effect of the presence/absence of ZP on the FAM-CPP internalization. For this assay, the ZP was removed before incubating with the fluorescent CPP as explained in Materials and Methods. As shown in Figure 3, both GV oocytes and MII eggs without ZP were able to incorporate significatively more FAM-CPP than cells with ZP, indicating that ZP hinders the fluorescent CPP incorporation. Nevertheless, for the following assays, we decided to use oocytes with ZP because they are easier to manipulate.

Taken together, these results showed that the FAM-CPP can cross both zona pellucida and plasma membrane of MII oocytes (with and without ZP) and does not affect cell viability. Nevertheless, it is worthy to mention that, even if the peptide can cross de ZP, the internalization is significatively reduced in oocytes with ZP.

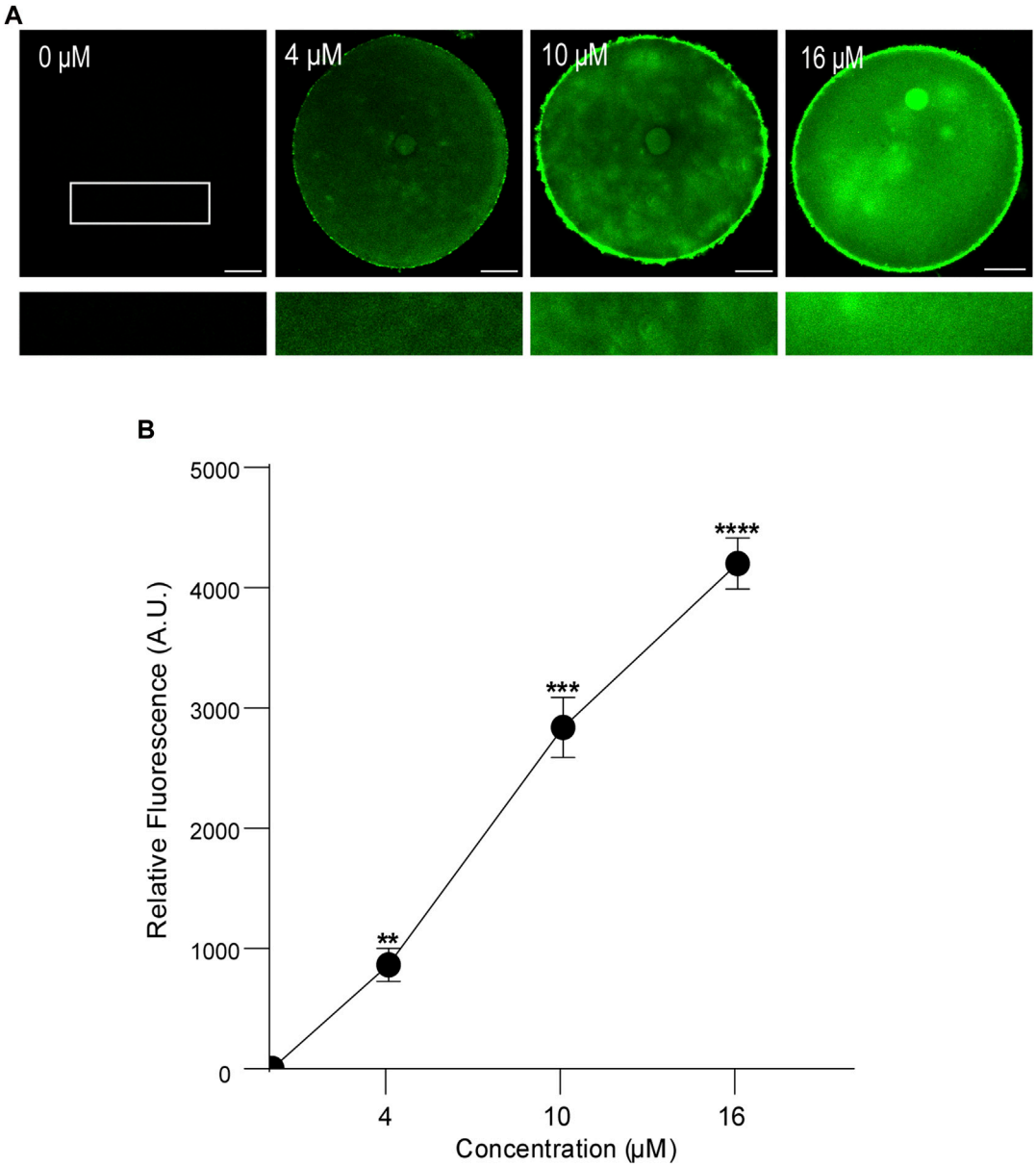

FIGURE 4
Effect of concentration on FAM-CPP internalization in GV mouse oocytes. Germinal Vesicle (GV) oocytes were incubated at different concentrations of FAM-CPP at 37 °C for 1 h. **(A)** Upper panels show representative confocal microscopy images taken at the equatorial plane of the cell inside the red circle (as represented in Figure 1B). Lower panels show magnification taken from rectangles of the same size represented only in 0 µM. Scale bar: 15 µm. **(B)** Relative fluorescence intensity at different FAM-CPP concentrations. The data represent mean ± SEM calculated from independent experiments. Comparisons with 0 µM were made by Kruskal–Wallis and Dunn's multiple comparisons test ($p < 0.0001$). * represents significant differences. Number of cells analyzed: 0 µM: 26; 4 µM: 32; 10 µM: 26; 16 µM: 27.

3.2 Effect of concentration, time, and temperature on CPP internalization during mouse oocyte maturation

There is evidence in the literature on the differential influence of concentration, time and temperature on the internalization of CPP (Fretz et al., 2007; Madani et al., 2011; Copolovici et al., 2014). However, often the mentioned factors act in conjunction with other factors such as the nature of the CPP and the type of cell used. For this reason, we tested how those parameters -concentration, time, and temperature-participate in the internalization of FAM-CPP in two different stages of mouse oocyte maturation: Germinal Vesicle (GV, immature) and Metaphase II (MII, mature) oocytes.

First, we analyzed the concentration effect on the FAM-CPP internalization in GV and MII mouse oocytes. Different concentrations (1–16 µM) were tested in immature and mature oocytes with ZP. Again, cells were imaged at equatorial region inside the red circle as explained previously. As shown in Figures 4A, B, the increasing of fluorescence intensity was directly proportional to FAM-CPP concentration in GV oocytes. CPP was homogeneously distributed

on the entire cytoplasm and reached the nucleus (or Germinal Vesicle). In other words, FAM-CPP internalization was concentration-dependent in immature oocytes. When the concentration effect on the FAM-CPP internalization was analyzed in MII oocytes, the fluorescence intensity reached a statistically significant plateau between 4 μM and 10 μM and diminished significantly at 16 μM (Figures 5A, B). These results indicate that, similarly to observed in GV oocytes, FAM-CPP internalization was concentration-dependent in MII oocytes until 4 uM, however it reached a plateau at higher concentrations.

Then, we analyzed the effect of time and temperature simultaneously on FAM-CPP internalization for each maturation stages. GV oocytes were collected and incubated in CZB medium with 10 μM FAM-CPP for 15, 30, and 60 min at 4°C or 37°C. As shown in Figure 6, the FAM-CPP internalization occurred at both temperatures and reached a statistically significant plateau at 15 min. Nevertheless, the FAM-CPP internalization at 4°C was statistically lower than 37°C (Figures 6A, B). Similar assays were performed using MII oocytes. Cells were collected and incubated in CZB medium with 10 μM FAM-CPP for 15, 30, and 60 min at 4°C or 37°C. As shown in Figure 7, similar results were obtained when MII oocytes were incubated at 37°C: the intensity of CPP fluorescence reached a plateau at 15 min. Nevertheless, when the FAM-CPP incubation took place at 4°C, the FAM-CPP internalization was dependent on the incubation time (Figures 7A, B).

Altogether, these results demonstrate that the FAM-CPP internalization in mouse oocytes depends on concentration, time, temperature, and the oocyte maturation stages.

3.3 The internalization of FAM-CPP does not affect the density of cortical granules in mature oocytes

Cortical granules (CG) are organelles localized in the cortical region of mature mouse oocytes and are involved in the cortical reaction. This process is an exocytotic event in which CG fuse with the oocyte plasma membrane after the fusion of the first spermatozoa. Thus, the secretion of CG content avoids the fusion of a second male gamete ensuring the embryo development. Considering that this work aimed to analyze the use of CPP to study cortical reaction in mature mouse oocytes, the next step was to investigate if the FAM-CPP internalization does perturb cortical granules density. Then, cortical granules density was evaluated for different incubation times in mature oocytes. For control and experimental conditions, cells were incubated with FAM and FAM-CPP, respectively. The results showed that, compared to control, the FAM-CPP incubation did not alter the cortical granule density at any assayed time in mature oocytes (Figure 8).

3.4 The permeable tetanus toxin is internalized into mature oocytes and inhibits cortical reaction

Cortical reaction is a calcium regulated exocytosis, in which cortical granules fuse with the oocyte plasma membrane after mouse oocyte activation. This fusion is mediated by SNARE proteins, and we have proposed a working model for cortical granules exocytosis in mouse oocytes (Paola et al., 2021). The SNARE proteins are proteolyzed by the light chains of the clostridial neurotoxins–tetanus toxin and botulinum toxin (Humeau et al., 2000; Schiavo et al., 2000). Tetanus toxin has two polypeptide chains: the heavy and the light chain. The heavy chain mediates binding, internalization, and translocation of the light chain to the cytosol, and the light chain inhibits exocytosis by cleaving VAMP1, VAMP2 or VAMP3 (Dong et al., 2019). In addition, the catalytic activity of the light chain is zinc-dependent and is used as a tool for the study of exocytosis in different secretory cells (Ahnert-Hilger et al., 1989; Bittner et al., 1989). Previously we have demonstrated that VAMP1 and VAMP3 are expressed in mouse oocytes (Paola et al., 2021). Considering that FAM-CPP internalization is innocuous for mouse oocytes (Figure 2A) and does not perturb cortical granules localization (Figure 8), we hypothesized that a permeable tetanus Toxin light chain (CPP-TeTx) might inhibit cortical reaction by cleaving the VAMPs isoforms expressed in mouse oocytes.

First, we purified the CPP-TeTx as a His6-tagged protein as described in Materials and Methods. We tested if this permeable toxin could internalize into mouse mature oocytes. Because CPP-TeTx is not fluorescent, we verified the protein internalization by immunofluorescence assays using a His6 antibody. As shown in Figure 9, CPP-TeTx was detected into mature oocytes incubated by 15, 30 and 60 min at 37°C (Figure 9A). In this case, two controls were performed: one, to determine the unspecific signal from the secondary antibody (0 min-, incubated only with secondary antibody), and the other, to determine the unspecific signal from histidines present in mature oocytes (0 min+, incubated with primary and secondary antibody). Figure 9B shows that the fluorescence intensity for all analyzed times was statistically higher than 0 min + control and time independent. These results are similar to that obtained with FAM-CPP (see Figure 7) and indicate that CPP-TeTx was internalized into mouse mature oocytes.

Second, to test the functionality of CPP-TeTx during parthenogenetically activated cortical reaction, we analyzed the function of CPP-TeTx using our functional assay. This functional assay consists of quantifying and comparing the cortical granules density in control oocytes (without activator) and in strontium-activated oocytes (positive control, with parthenogenetic activator). The difference between these two conditions is a functional measurement of cortical granule exocytosis (Supplementary Figure S1). Considering that the sequence of permeable peptide is similar for both FAM-CPP and CPP-TeTx, we tested if FAM-CPP internalization may affect the cortical reaction. As shown in Supplementary Figure S1, FAM-CPP did not perturb the cortical reaction activated by strontium chloride. Then, if prior strontium activation an inhibitor is present (CPP-TeTx), cortical granules exocytosis will be inhibited, and cortical granules density will be significantly higher than positive control. Mature oocytes with ZP were incubated in the presence of 4 μM CPP-TeTx at 37 °C during 1 h. Similarly to FAM-CPP (see Figure 5), 4 uM CPP-TeTx was the minimum concentration to reach the internalization plateau. Then, cortical reaction was activated by strontium chloride. Before fixation, ZP of the treated oocytes was removed and cortical granules were stained with Rhodamine-Lens Culinaris Agglutinin (LCA) to

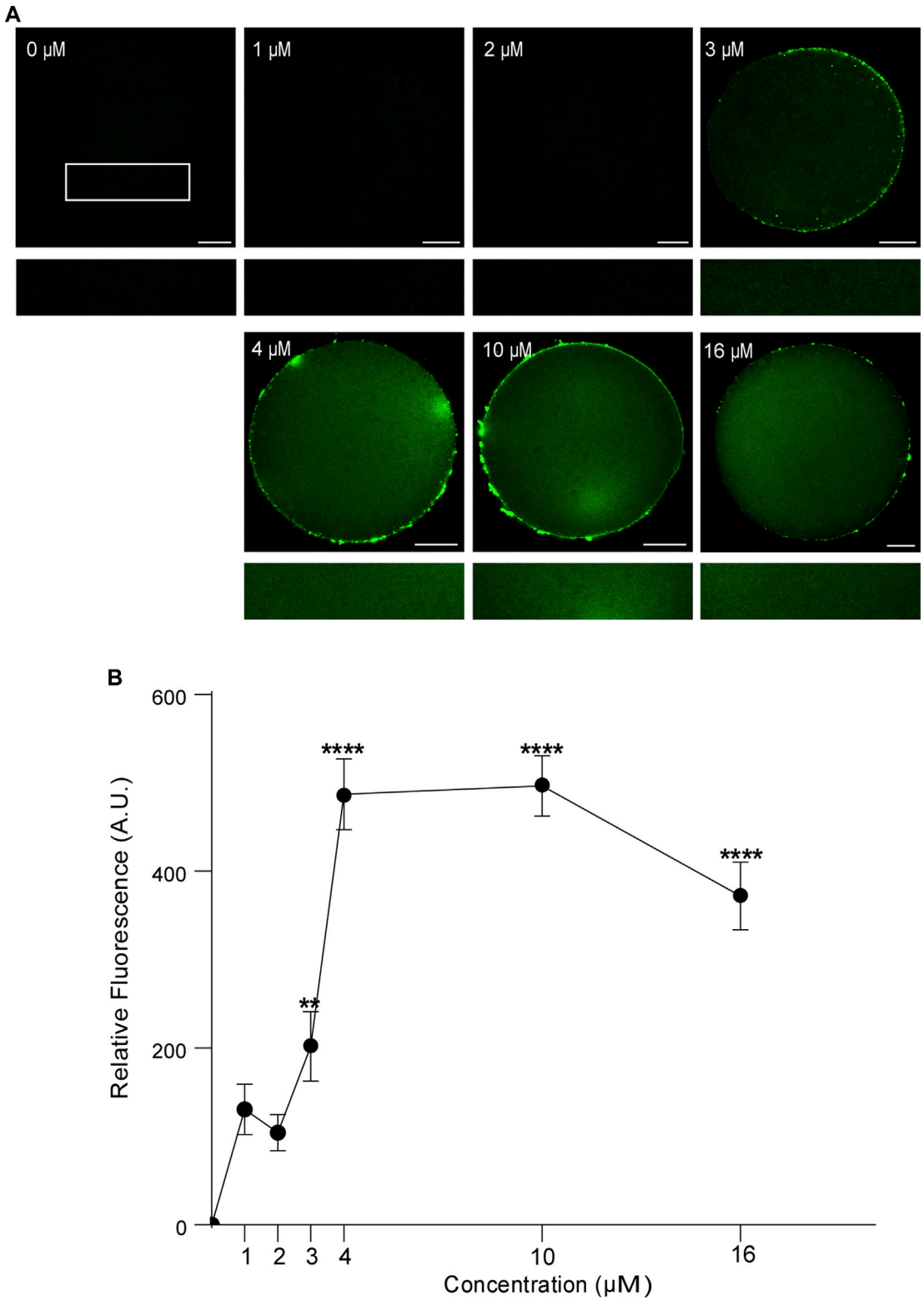

FIGURE 5
Effect of concentration on FAM-CPP internalization in MII mouse oocytes. Metaphase II (MII) oocytes were incubated at different concentrations of FAM-CPP at 37°C for 1 h. **(A)** Upper panels show representative confocal microscopy images taken at the equatorial plane of the cell inside the red circle (as represented in Figure 1B). Lower panels show magnification taken from rectangles of the same size represented only in 0 µM. Scale bar: 15 µm. **(B)** Relative fluorescence intensity at different FAM-CPP concentrations. The data represent mean ± SEM calculated from independent experiments. Comparisons with 0 µM were made by Kruskal–Wallis and Dunn's multiple comparisons test ($p < 0.0001$). * represents significant differences. Number of cells analyzed: 0 µM: 41; 1 µM: 31; 2 µM: 27; 3 µM: 26; 4 µM: 45; 10 µM: 54; 16 µM: 50.

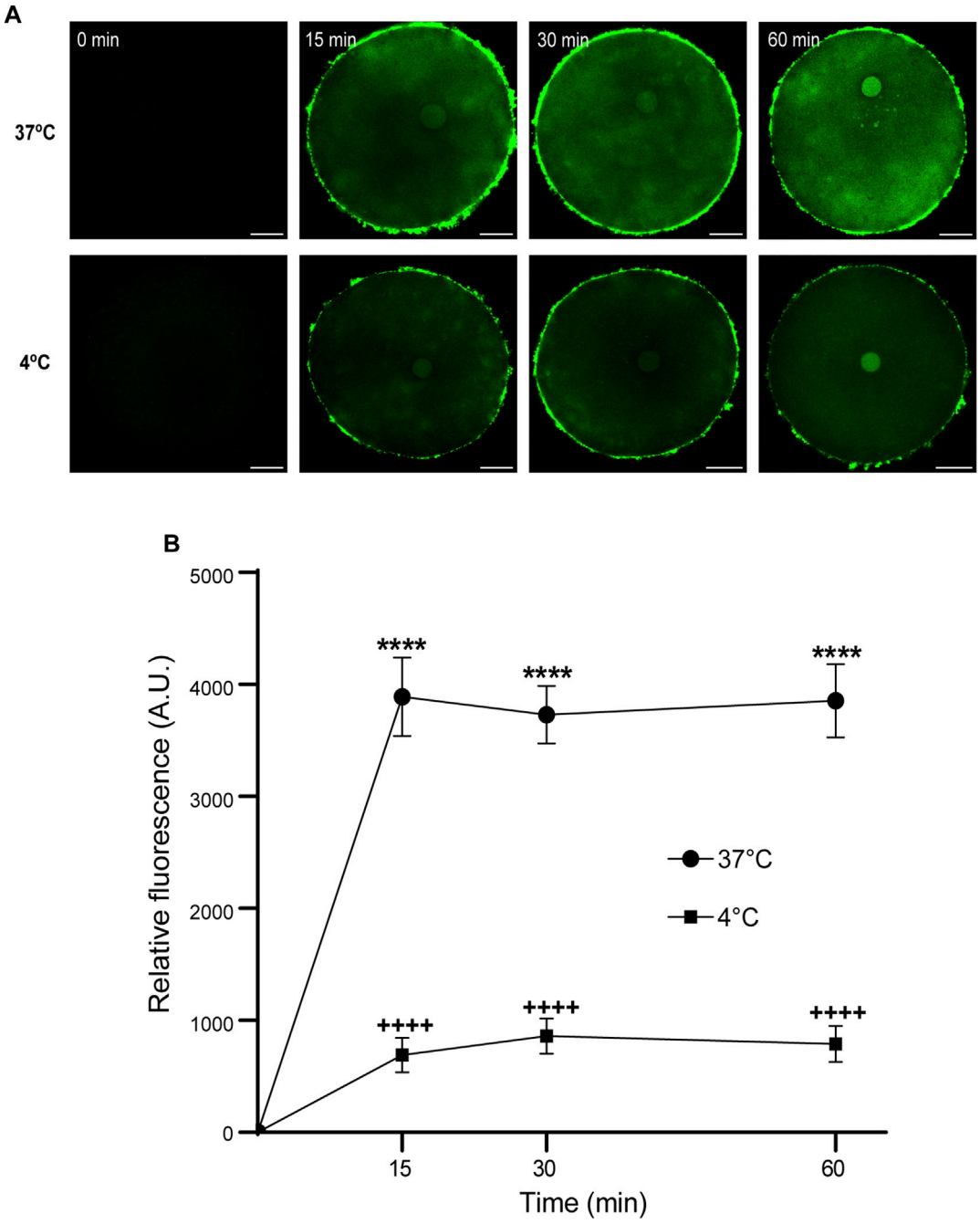

FIGURE 6
Effect of time and temperature on FAM-CPP internalization in GV oocytes. Oocytes were incubated with 10 μM FAM-CPP at 37 °C or 4°C, for 15, 30, and 60 min. **(A)** Representative confocal microscopy images taken at equatorial plane of the cell. Scale bar: 15 μm. **(B)** Relative fluorescence vs. time (min), at 4°C and 37°C, and relative to untreated group (0 min). The data represent mean ± SEM calculated from independent experiments. Comparisons between control and treatments were made by Kruskal–Wallis and Dunn's multiple comparisons test ($p < 0.0001$). * (37°C) and + (4°C) represent significant differences compared to 0 min. Number of cells analyzed: 4°C: 0 min: 27; 15 min: 30; 30 min: 29; 60 min: 24; 37°C: 0 min: 26; 15 min: 41; 30 min: 60; 60 min: 52.

evaluate cortical granules density as a measure of cortical reaction (see Materials and Methods for details). As shown in Figure 10, CPP-TeTx significantly inhibited the cortical reaction activated by $SrCl_2$. CPP-TeTx inhibited significantly cortical reaction by about 50%, suggesting that other tetanus toxin-insensitive protein might be involved in this secretory process. Next, considering that the catalytic activity of the light chain of tetanus Toxin is zinc-dependent, we analyzed the effect of zinc chelation to demonstrate the specificity of CPP-TeTx. We used N,N,N′,N′- Tetrakis(2-pyridylmethyl) ethylenediamine (TPEN), a cell-permeable zinc chelator with a high affinity for zinc. Incubation of CPP-TeTx treated oocytes

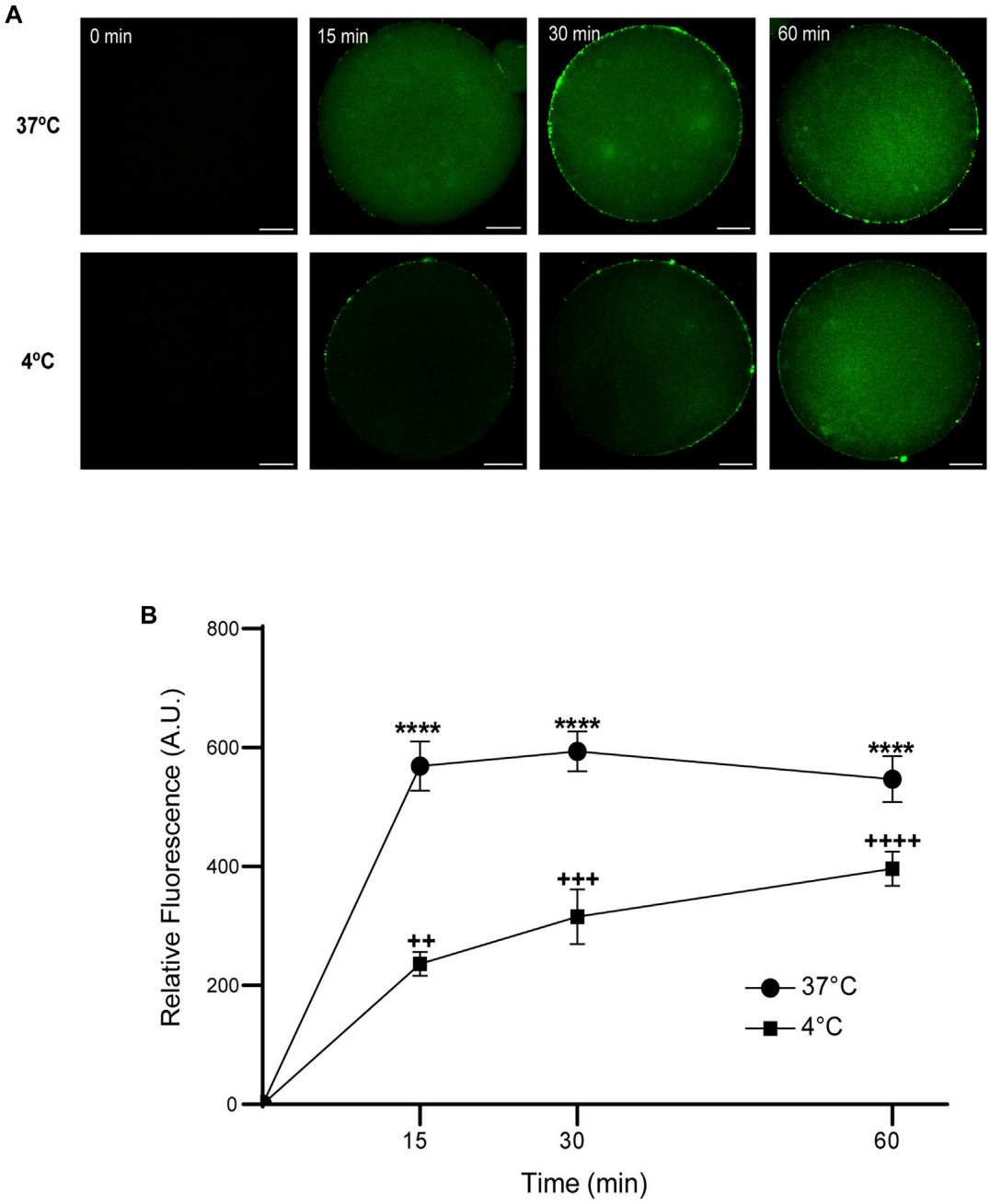

FIGURE 7
Effect of time and temperature on the internalization of FAM-CPP in MII oocytes. Oocytes were treated with 10 µM FAM-CPP at 37°C or at 4°C, for 15, 30 and 60 min. **(A)** Representative confocal microscopy images taken at equatorial plane of the cell. Scale bar: 15 µm. **(B)** Relative fluorescence vs. time (min), at 4°C and 37°C, and relative to untreated group (0 min). The data represent mean ± SEM calculated from independent experiments. Comparisons between control and treatments were made by Kruskal–Wallis and Dunn's multiple comparisons test ($p < 0.0001$). * (37°C) and + (4°C), represent significant differences compared to control. Number of cells analyzed: 4°C: 0 min: 47; 15 min: 38; 30 min: 45; 60 min: 59; 37°C: 0 min: 50; 15 min: 48; 30 min: 44; 60 min: 43.

in 10 µM TPEN prevented the inhibition of cortical granule exocytosis, confirming the specificity of the effect of CPP-TeTx (Figure 10). TPEN incubation alone did not alter the cortical reaction in presence or absence of $SrCl_2$ (Figure 10).

Altogether, these results confirmed our hypothesis and demonstrated that the permeable tetanus toxin inhibits cortical granule exocytosis in mouse oocytes.

4 Discussion

In this work, we aimed to assess the potential of cell-penetrating peptides (CPP) as a non-invasive approach for studying cortical reaction in mouse oocytes. We and other groups have characterized the molecular mechanism of this secretory process by microinjecting different proteins and antibodies into oocyte

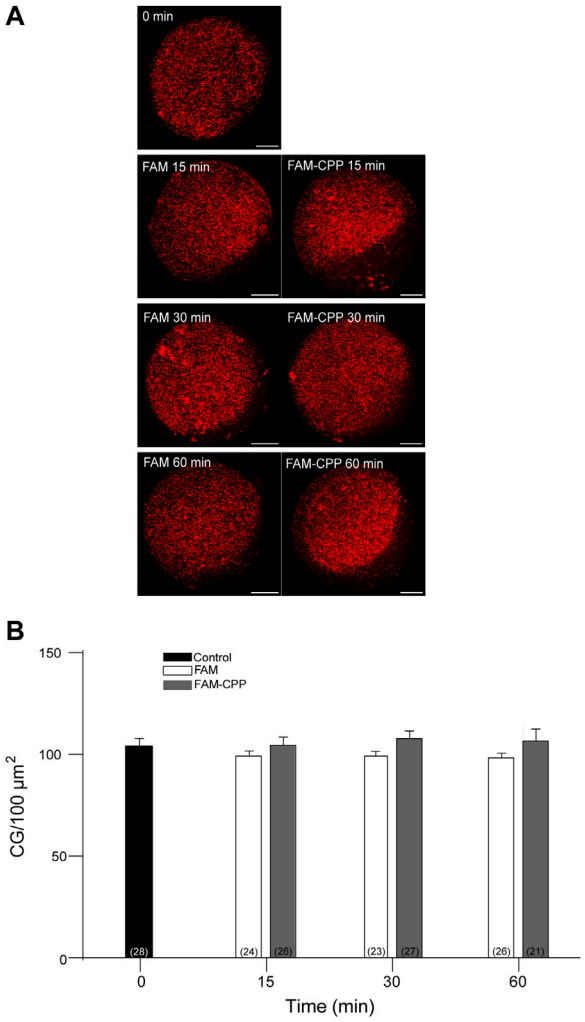

FIGURE 8
FAM-CPP internalization does not perturb cortical granules density in MII oocytes. Oocytes were incubated with 10 µM FAM-CPP and FAM (control) for 15, 30 and 60 min at 37 °C. After fixation, cortical granules (CG) were stained with Rhodamine-LCA (red). **(A)** Representative confocal microscopic images of oocytes taken at cortical plane of the cell. Scale bar: 15 µm. **(B)** Histogram showing CG density for different times and relative to untreated group (0 min) set as 100%. The data represent mean ± SEM calculated from at least three independent experiments. Comparisons between control and treatments were made by Ordinary one-way ANOVA and Tukey's multiple comparisons test ($p > 0.05$). Numbers in parentheses at the base of the bar represent total number of oocytes.

cytoplasm (Paola et al., 2015; Bello et al., 2016; Wang et al., 2016; Mehlmann et al., 2019; Zhu et al., 2020; Paola et al., 2021). The intracytoplasmic microinjection is an invasive method that requires specialized microinjection equipment and skilled personnel. Nevertheless, it is the only available method to cross both structures the zona pellucida (ZP) and the oocyte plasma membrane. ZP is a unique structure of female gamete, and is formed by glycoproteins that functions as a protective barrier, filtering substances from the extracellular space (Gupta et al., 2012). CPPs possess the ability to cross cell membranes naturally (Koren et al., 2012); however, the CPP ability to cross ZP has been poorly explored. Previous studies have demonstrated that hydrophilic arginine-rich cell-penetrating peptides have optimal internalization capability for small molecules in mammalian cells (Mitchell et al., 2000; Mueller et al., 2008; Tünnemann et al., 2008). Presently, there is a limited amount of literature available on the utilization of CPPs in oocytes (Kwon et al., 2009; Kwon et al., 2013; Yang et al., 2014; Jeon et al., 2019; Zhu et al., 2021), and none of these studies extensively examine the internalization of CPPs into mouse oocytes.

First, we evaluated the ability of CPPs to cross both the zona pellucida and plasma membrane of immature (GV) and mature (MII) mouse oocytes within a 1 h incubation period. To this end, we specifically used K(5-FAM)R_9C, a fluorescent peptide rich in arginine residues conjugated with FAM (FAM-CPP). Our results indicate that FAM-CPP successfully enters the oocytes (GV and MII), displaying a diffuse pattern of cytoplasmic distribution (Figure 1). Two primary mechanisms have been proposed for CPP internalization: endocytosis and direct penetration (Gestin et al., 2017). Direct penetration of fluorescent CPPs into living cells is expected to result in a uniform and diffuse labeling pattern, while endocytosis leads to a granular or punctuate

10.3389/fcell.2023.1259421

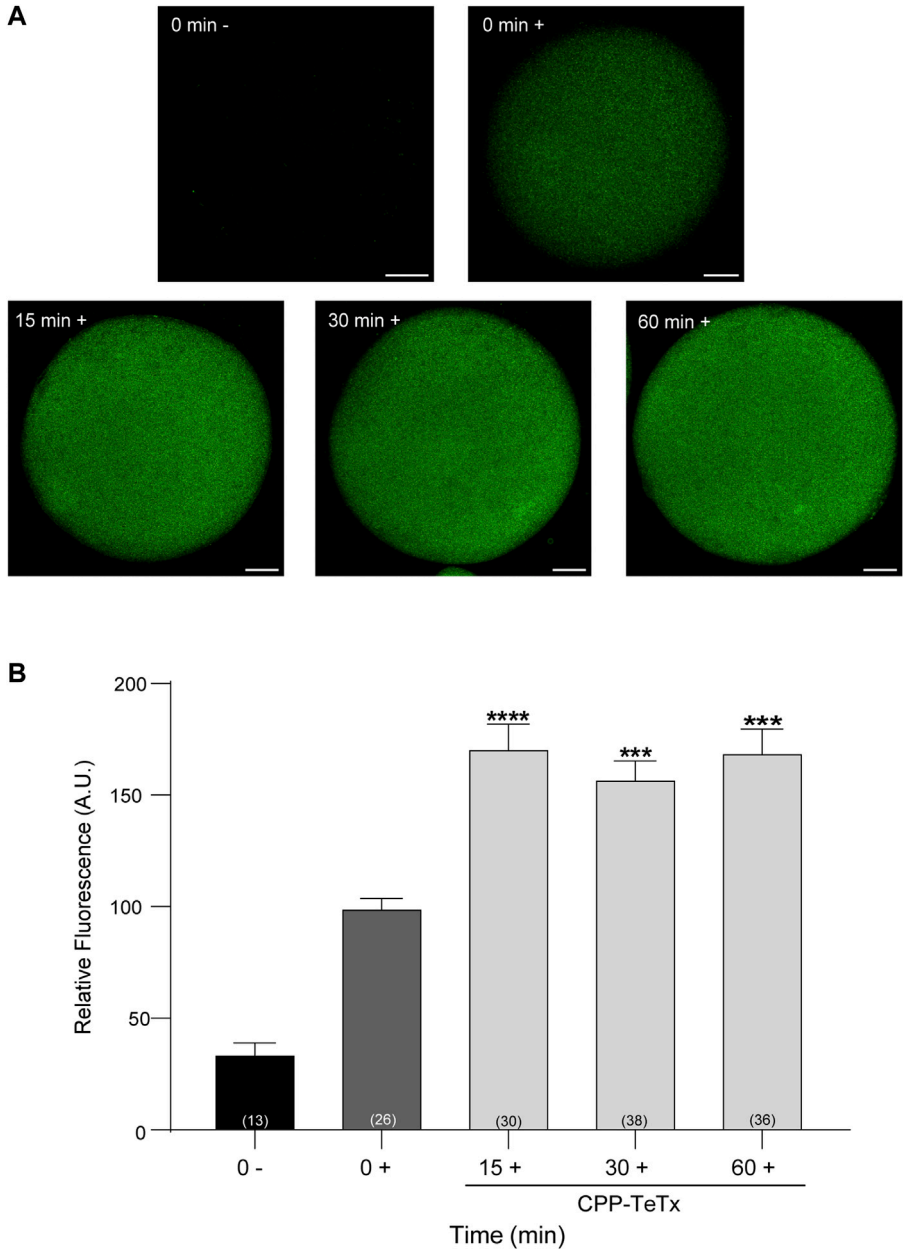

FIGURE 9
Permeable tetanus toxin (CPP-TeTx) is internalized into MII oocytes. Oocytes were incubated with 4 μM CPP-TeTx for 1 h at 37°C. The permeable TeTx was visualized by immunofluorescence assay. **(A)** Representative confocal microscopic images of oocytes taken at equatorial plane of the cell. Scale bar: 15 μm. **(B)** Histogram showing relative fluorescence intensity for different times and relative to 0+ group set as 100%. The data represent mean ± SEM calculated from independent experiments. Comparisons between control and treatments were made by Kruskal–Wallis and Dunn's multiple comparisons test ($p < 0.0001$). * represents significant differences between control (0+) and treatments. Numbers in parentheses at the base of the bar represent total number of oocytes. Minus sign (–): fixed oocytes were treated only with secondary antibody. Plus sign (+): fixed oocytes were treated with primary and secondary antibodies.

pattern due to the labeled CPP becoming trapped in vesicular organelles (Pooga and Langel, 2015). Therefore, based on our observations that FAM-CPP was internalized when endocytosis was inhibited, we propose that FAM-CPP is internalized by a direct penetration mechanism, which does not affect cell viability.

We also examined the effect of peptide concentration on FAM-CPP internalization in GV and MII oocytes. It is noteworthy that a significantly higher amount of CPP enters GV oocytes compared to MII oocytes. This discrepancy can be attributed to the distinct stages of maturation at which these oocytes were found. Each stage exhibits unique characteristics, among which the structure of the ZP and the plasma membrane potential (Vm) could explain the difference in CPP internalization between GV and MII oocytes. In effect, Novo and others have reported that in GV oocytes, the porosity of the ZP is 2.5 times higher than that of mature oocytes (Novo et al., 2012).

10.3389/fcell.2023.1259421

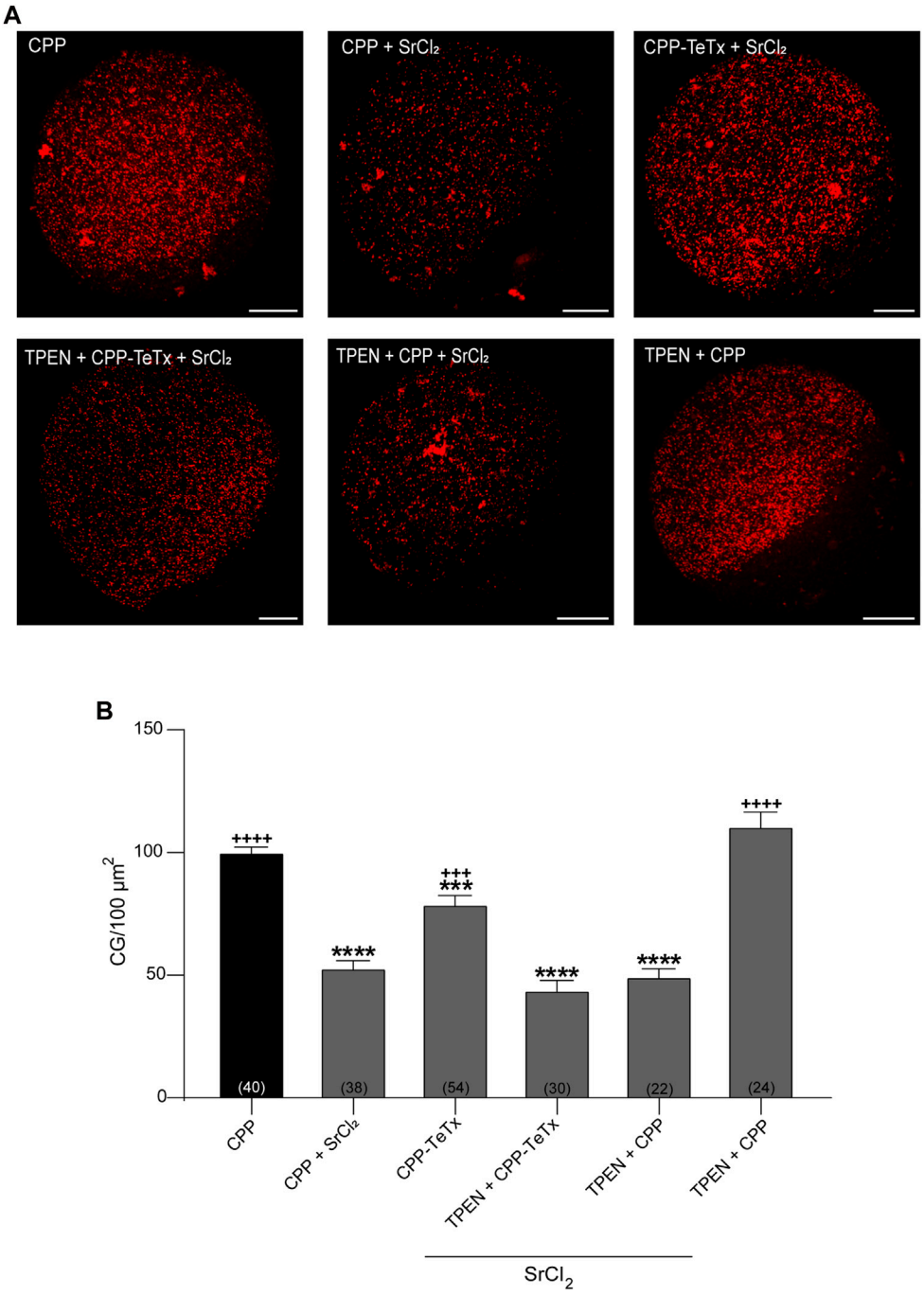

FIGURE 10
Permeable tetanus toxin (CPP-TeTx) inhibits cortical granules exocytosis in MII oocytes. Mature oocytes were incubated in 4 µM CPP-TeTx for 1 h at 37 °C before parthenogenetic activation with $SrCl_2$ (see text for details). **(A)** After fixation, cortical granules (GC) were stained with Rhodamine-LCA (red); representative confocal microscopic images of oocytes taken at cortical plane of the cell. Scale bar: 15 µm. **(B)** Histogram showing CG density for different treatments and relative to CPP (control) set as 100%. The data represent mean ± SEM calculated from independent experiments. Comparisons between CPP and different conditions were made by Brown-Forsythe and Welch ANOVA tests, and Games-Howell's multiple comparisons test ($p < 0.0001$). * represents significant differences compared to CPP; + represents significant differences compared to CPP + $SrCl_2$. Numbers in parentheses at the base of the bar represent total number of oocytes.

Regarding to Vm, electrophysiological investigations have shown that cell membrane depolarization occurs as *in vitro* meiotic maturation progresses from the GV stage (−46 mV) to the MII stage (−17 mV) in mouse oocytes. Moreover, hyperpolarization has been reported to increase CPP internalization, whereas depolarization impedes it. In silico modeling supports the idea that membrane hyperpolarization facilitates the formation of transient water pores, thereby enabling CPP translocation into

cells (Trofimenko et al., 2021). Altogether, the increased CPP internalization in GV oocytes could be explained by a higher ZP porosity and by the hyperpolarization of the plasma membrane.

Additionally, we explored the influence of time and temperature on FAM-CPP internalization. Our analysis revealed rapid internalization of fluorescent CPP by GV oocytes at both 37°C and 4 °C. Although internalization was significantly higher at 37°C, fluorescence intensity reached a plateau within 15 min at both temperatures (Figure 6). Similarly, in MII oocytes, internalization of FAM-CPP reached a plateau within 15 min of incubation at 37°C. However, internalization was directly proportional to incubation time when mature oocytes were incubated at 4°C (Figure 7). To the best of our knowledge, there are no comparative studies on CPP internalization between immature and mature oocytes. Furthermore, investigations on CPP use in mouse oocytes are scarce. Jeon and collaborators have showed that exogenous translationally controlled tumor protein (TCTP conjugated with mCherry) was able to translocate into mature oocytes across the ZP after 4 h of incubation; however, internalization of the fluorescent TCTP in immature oocytes was not assayed (Jeon et al., 2019). Kwon and others showed that MPG, -a designed CPP comprised of the first 17 amino acids of N-terminus derived from glycine-rich region of the viral gp41 and the hydrophilic C-terminus from nuclear localization signal of the SV40 large T antigen-, was internalized in immature ZP-free oocytes after 1 h incubation period (S.-J. Kwon et al., 2009). Interestingly, MPG-EGFP showed a diffuse distribution pattern in GV oocytes; nevertheless, the authors only highlighted that the fluorescent MPG was limited to the cell periphery probably because of the presence of cortical granules (S.-J. Kwon et al., 2009). The same group also tested a 12-mer CPP from the conserved region of the human papillomavirus L1 capsid protein, LDP12. Nevertheless, CPP was not internalized in mature oocytes (with or without ZP) and was not assayed in immature oocytes (S. Kwon et al., 2013). In this work, we have demonstrated that CPP internalization observation depends on the mounting method. In fact, we showed that the best mounting method for obtaining a significant signal was the flattened method (Figure 1).

The final aim of analyzing CPP permeation into mouse oocytes was to utilize CPP as a non-invasive tool for studying cortical reaction. Cortical reaction is a calcium regulated exocytosis, in which cortical granules fuse with the oocyte plasma membrane after mouse oocyte activation. This fusion process is mediated by SNARE proteins, and we have proposed a working model for cortical granules exocytosis in mouse oocytes (Paola et al., 2021). Previously, we demonstrated that VAMP1 and VAMP3 -two SNARE sensitive to tetanus toxin-are expressed in mouse oocytes (Paola et al., 2021). Tetanus toxin has two polypeptide chains: the heavy and the light chain. The heavy chain mediates binding, internalization, and translocation of the light chain to the cytosol, whereas the light chain inhibits exocytosis by cleaving VAMP1, VAMP2 or VAMP3 at specific and single sites (Dong et al., 2019). Consequently, after confirming that FAM-CPP internalization did not perturb cortical granules distribution (Figure 8), we proceeded to investigate whether permeable TeTx could inhibit cortical granule exocytosis during the parthenogenetically activated cortical reaction in mouse oocytes. CPP-TeTx effectively was able to cross the zona pellucida and the plasma membranes of oocytes (Figure 9), and inhibited the cortical reaction activated by strontium in mature oocytes (see Figure 10). Therefore, these findings indicate that CPP-TeTx demonstrated to be functional in the cortical granule exocytosis assay, exhibiting a similar behavior to TeTx administered via microinjection (Paola et al., 2021).

In this work, we have characterized for the first time the internalization of a fluorescent arginine-rich cell-penetrating peptide in immature and mature oocytes. We demonstrated that the internalization of this cell-penetrating peptide (CPP) depends on different factors such as presence or absence of ZP, CPP concentration, temperature, incubation time, and oocyte maturation stage. We also bound this CPP to the light chain of tetanus toxin to demonstrate that this permeable version of tetanus toxin can cross ZP and plasma membrane and conserves its function. In fact, the permeable light chain of tetanus toxin inhibited the cortical reaction activated parthenogenetically by strontium chloride in mature oocytes.

Our findings indicate that arginine-rich cell-penetrating peptides can be utilized as a substitute method to intracytoplasmic microinjection for intracellular delivery of macromolecules into oocytes to study cortical granules exocytosis. This approach has several advantages over the traditional microinjection technique, including ease of use, efficiency, and versatility. The use of permeable peptides not only provides a new avenue for studying oocyte physiology but also offers potential applications in developing new therapies and a better understanding of the molecular mechanisms that regulate oocyte *in vitro* maturation, fertilization, and early embryonic development.

Data availability statement

The original contributions presented in the study are included in the article/Supplementary Material, further inquiries can be directed to the corresponding authors.

Ethics statement

The animal study was approved by Institutional Animal Care and Use Committee of the School of Medical Science, Universidad Nacional de Cuyo (Protocol N° 169/2019). The study was conducted in accordance with the local legislation and institutional requirements.

Author contributions

OK: Formal Analysis, Investigation, Methodology, Validation, Visualization, Data curation, Writing–original draft. PW: Investigation, Methodology, Validation, Writing–review and editing, Data curation, Formal Analysis, Visualization. EZ-R: Methodology, Resources. MP: Methodology, Resources. MB: Formal Analysis, Funding acquisition, Resources, Supervision, Validation, Writing–original draft, Investigation, Methodology, Visualization. MM: Conceptualization, Funding acquisition, Project administration, Resources, Supervision, Visualization,

Writing–original draft, Formal Analysis, Investigation, Methodology, Validation.

Funding

The author(s) declare financial support was received for the research, authorship, and/or publication of this article. This work was funded by Proyecto de Fortalecimiento de la Investigación Científica y Tecnológica, Facultad de Ciencias Exactas y Naturales, Universidad Nacional de Cuyo (Res. 124-D/21) to MM; by Agencia Nacional de Promoción Científica y Tecnológica (grants PICT 2020–03627 to MM, PICT 2016-0894 and PICT 2018-04451 to MB and MP), by Agencia Nacional de Promoción Científica y Tecnológica and Universidad Nacional de Cuyo (grant PICTO 2016-0055 to MB), and Universidad Nacional de Cuyo (grant 06/M025-T1, and J050-T1 to MM), Argentina.

Acknowledgments

The authors are very grateful to Luis Mayorga for his critical reading of the manuscript. The authors acknowledge the help of Lucas Aldao and Veterinarian Julieta Scelta in the maintenance of the animal facility and E. Bocanegra, N. Domizio and J. Ibáñez for excellent technical assistance. OK and PW are thankful to CONICET, Argentina, for fellowships.

Conflict of interest

The authors declare that the research was conducted in the absence of any commercial or financial relationships that could be construed as a potential conflict of interest.

Publisher's note

All claims expressed in this article are solely those of the authors and do not necessarily represent those of their affiliated organizations, or those of the publisher, the editors and the reviewers. Any product that may be evaluated in this article, or claim that may be made by its manufacturer, is not guaranteed or endorsed by the publisher.

Supplementary material

The Supplementary Material for this article can be found online at: https://www.frontiersin.org/articles/10.3389/fcell.2023.1259421/full#supplementary-material

References

Ahnert-Hilger, G., Weller, U., Dauzenroth, M. E., Habermann, E., and Gratzl, y M. (1989). The tetanus toxin light chain inhibits exocytosis. *FEBS Lett.* 242 (2), 245–248. doi:10.1016/0014-5793(89)80478-8

Bello, O. D., Isabel Cappa, A., de Paola, M., Zanetti, M. N., Fukuda, M., Fissore, R. A., et al. (2016). Rab3A, a possible marker of cortical granules, participates in cortical granule exocytosis in mouse eggs. *Exp. Cell Res.* 347 (1), 42–51. doi:10.1016/j.yexcr.2016.07.005

Bittner, M. A., Habig, W. H., and Holz, R. W. (1989). Isolated light chain of tetanus toxin inhibits exocytosis: studies in digitonin-permeabilized cells. *J. Neurochem.* 53 (3), 966–968. doi:10.1111/j.1471-4159.1989.tb11800.x

Cappa, A. I., de Paola, M., Wetten, P., De Blas, G. A., and Michaut, M. A. (2018). Live imaging of cortical granule exocytosis reveals that *in vitro* matured mouse oocytes are not fully competent to secrete their content. *Biol. Open* 7 (12), bio031872. doi:10.1242/bio.031872

Cooper, J. A. (1987). Effects of Cytochalasin and phalloidin on actin. *J. Cell Biol.* 105 (4), 1473–1478. doi:10.1083/jcb.105.4.1473

Copolovici, D. M., Kent, L., Eriste, E., and Langel, Ü. (2014). Cell-penetrating peptides: design, synthesis, and applications. *ACS Nano* 8 (3), 1972–1994. doi:10.1021/nn4057269

Dinca, A., Chien, W.-M., and Chin, M. T. (2016). Intracellular delivery of proteins with cell-penetrating peptides for therapeutic uses in human disease. *Int. J. Mol. Sci.* 17 (2), 263. doi:10.3390/ijms17020263

Dong, M., Masuyer, G., and Stenmark, P. (2019). Botulinum and tetanus neurotoxins. *Annu. Rev. Biochem.* 88 (junio), 811–837. doi:10.1146/annurev-biochem-013118-111654

Ferguson, S. M., and De Camilli, P. (2012). Dynamin, a membrane-remodelling GTPase. *Nat. Rev. Mol. Cell Biol.* 13 (2), 75–88. doi:10.1038/nrm3266

Fretz, M. M., Neal, A. P., Al-Taei, S., Futaki, S., Takeuchi, T., Nakase, I., et al. (2007). Temperature-concentration- and cholesterol-dependent translocation of L- and D-octa-arginine across the plasma and nuclear membrane of CD34+ leukaemia cells. *Biochem. J.* 403 (2), 335–342. doi:10.1042/BJ20061808

Gestin, M., Dowaidar, M., and Langel, Ü. (2017). Uptake mechanism of cell-penetrating peptides. *Adv. Exp. Med. Biol.* 1030, 255–264. doi:10.1007/978-3-319-66095-0_11

Gupta, S. K., Bhandari, B., Shrestha, A., Biswal, B. K., Palaniappan, C., Malhotra, S. S., et al. (2012). Mammalian zona pellucida glycoproteins: structure and function during fertilization. *Cell Tissue Res.* 349 (3), 665–678. doi:10.1007/s00441-011-1319-y

Humeau, Y., Doussau, F., Grant, N. J., and Poulain, y B. (2000). How botulinum and tetanus neurotoxins block neurotransmitter release. *Biochimie* 82 (5), 427–446. doi:10.1016/s0300-9084(00)00216-9

Jafari, S., Solmaz, M. D., and Khosro, A. (2015). Cell-penetrating peptides and their analogues as novel nanocarriers for drug delivery. *BioImpacts BI* 5 (2), 103–111. doi:10.15171/bi.2015.10

Jeon, H., Bai, G.-Y., Park, Y., Kim, J.-S., and Su Oh, J. (2019). Prevention of quality decline and delivery of SiRNA using exogenous TCTP translocation across the zona pellucida in mouse oocytes. *Sci. Rep.* 9 (1), 18845. doi:10.1038/s41598-019-55449-4

Kim, A. M., Miranda, L. B., Betty, Y. K., Richard, W. A., Stefan, V., Woodruff, T. K., et al. (2011). Zinc sparks are triggered by fertilization and facilitate cell cycle resumption in mammalian eggs. *ACS Chem. Biol.* 6 (7), 716–723. doi:10.1021/cb200084y

Koren, E., Vladimir, Y., and Torchilin, P. (2012). Cell-penetrating peptides: breaking through to the other side. *Trends Mol. Med.* 18 (7), 385–393. doi:10.1016/j.molmed.2012.04.012

Kwon, S., Kwak, A., Shin, H., Choi, S., Kim, S., and Jade Lim, H. (2013). Application of a novel cell-permeable peptide-driven protein delivery in mouse blastocysts. *Reprod. Camb. Engl.* 146 (2), 145–153. doi:10.1530/REP-13-0203

Kwon, S.-J., Han, K., Jung, S., Lee, J. E., Park, S., Cheon, Y. P., et al. (2009). Transduction of the MPG-tagged fusion protein into mammalian cells and oocytes depends on amiloride-sensitive endocytic pathway. *BMC Biotechnol.* 9 73. doi:10.1186/1472-6750-9-73

Madani, F., Lindberg, S., Langel, U., Futaki, S., and Gräslund, A. (2011). Mechanisms of cellular uptake of cell-penetrating peptides. *J. Biophysics* 2011, 414729. doi:10.1155/2011/414729

Masumoto, N., Sasaki, T., Tahara, M., Mammoto, A., Ikebuchi, Y., Tasaka, K., et al. (1996). Involvement of rabphilin-3A in cortical granule exocytosis in mouse eggs. *J. Cell Biol.* 135 (6 Pt 2), 1741–1747. doi:10.1083/jcb.135.6.1741

Mayorga, L., Altamirano, K., Zanni Ruiz, E., and Pavarotti, M. (2020). Human sperm capacitation is necessary for SNARE assembly in neurotoxin-resistant complexes. *Andrology* 8 (2), 442–449. doi:10.1111/andr.12706

McCluskey, A., Daniel, J. A., Hadzic, G., Chau, N., Clayton, E. L., Anna, M., et al. (2013). Building a better dynasore: the Dyngo compounds potently inhibit dynamin and endocytosis. *Traffic (Copenhagen, Den.* 14 (12), 1272–1289. doi:10.1111/tra.12119

Mehlmann, L. M., Uliasz, T. F., and Lowther, K. M. (2019). SNAP23 is required for constitutive and regulated exocytosis in mouse oocytes. *Biol. Reproduction* 101 (2), 338–346. doi:10.1093/biolre/ioz106

Mitchell, D. J., Kim, D. T., Steinman, L., Fathman, C. G., and Rothbard, J. B. (2000). Polyarginine enters cells more efficiently than other polycationic homopolymers. *J. Peptide Res. Official J. Am. Peptide Soc.* 56 (5), 318–325. doi:10.1034/j.1399-3011.2000.00723.x

Mueller, J., Kretzschmar, I., Volkmer, R., and Boisguerin, P. (2008). Comparison of cellular uptake using 22 CPPs in 4 different cell lines. *Bioconjugate Chem.* 19 (12), 2363–2374. doi:10.1021/bc800194e

Novo, S., Barrios, L., Elena, I., and Nogués, C. (2012). The zona pellucida porosity: three-dimensional reconstruction of four types of mouse oocyte zona pellucida using a dual beam microscope. *Microsc. Microanal. Official J. Microsc. Soc. Am. Microbeam Analysis Soc. Microsc. Soc. Can.* 18 (6), 1442–1449. doi:10.1017/S1431927612013487

Paola, M., Daniel Bello, O., and Alejandra Michaut, M. (2015). Cortical granule exocytosis is mediated by alpha-SNAP and N-ethilmaleimide sensitive factor in mouse oocytes. *PloS One* 10 (8), e0135679. doi:10.1371/journal.pone.0135679

Paola, M., Garrido, F., Zanetti, M. N., and Alejandra Michaut, M. (2021). VAMPs sensitive to tetanus toxin are required for cortical granule exocytosis in mouse oocytes. *Exp. Cell Res.* 405 (1), 112629. doi:10.1016/j.yexcr.2021.112629

Pooga, M., and Langel, Ü. (2015). Classes of cell-penetrating peptides. *Methods Mol. Biol. Clift. N.J.)* 1324, 3–28. doi:10.1007/978-1-4939-2806-4_1

Rubino, P., Viganò, P., Luddi, A., and Piomboni, P. (2016). The ICSI procedure from past to future: a systematic review of the more controversial aspects. *Hum. Reprod. Update* 22 (2), 194–227. doi:10.1093/humupd/dmv050

Schiavo, G., Matteoli, M., and Montecucco, C. (2000). Neurotoxins affecting neuroexocytosis. *Physiol. Rev.* 80 (2), 717–766. doi:10.1152/physrev.2000.80.2.717

Trofimenko, E., Grasso, G., Heulot, M., Chevalier, N., Deriu, M. A., Dubuis, G., et al. (2021). Genetic, cellular, and structural characterization of the membrane potential-dependent cell-penetrating peptide translocation pore. *ELife* 10 (octubre), e69832. doi:10.7554/eLife.69832

Tünnemann, G., Ter-Avetisyan, G., Martin, R. M., Martin, S., Herrmann, A., and Cardoso, C. (2008). Live-cell analysis of cell penetration ability and toxicity of oligo-arginines. *J. Peptide Sci. Official Publ. Eur. Peptide Soc.* 14 (4), 469–476. doi:10.1002/psc.968

Wang, H. H., Cui, Q., Zhang, T., Wang, Z. B., Ouyang, Y. C., Shen, W., et al. (2016). Rab3A, Rab27A, and Rab35 regulate different events during mouse oocyte meiotic maturation and activation. *Histochem. Cell Biol.* 145 (6), 647–657. doi:10.1007/s00418-015-1404-5

Xie, J., Ye, B., Zhang, H., Dong, S., Teng, L., Lee, R. J., et al. (2020). Cell-penetrating peptides in diagnosis and treatment of human diseases: from preclinical research to clinical application. *Front. Pharmacol.* 11, 697. doi:10.3389/fphar.2020.00697

Yang, N. J., Seol, D.-W., Jo, J., Jang, H. M., Yoon, S.-Y., and Dong, R. (2014). Effect of cell-penetrating peptide-conjugated estrogen-related receptor β on the development of mouse embryos cultured *in vitro*. *Clin. Exp. Reproductive Med.* 41 (1), 1–8. doi:10.5653/cerm.2014.41.1.1

Zhang, D., Wang, J., and Xu, D. (2016). Cell-penetrating peptides as noninvasive transmembrane vectors for the development of novel multifunctional drug-delivery systems. *J. Control. Release Official J. Control. Release Soc.* 229 (mayo), 130–139. doi:10.1016/j.jconrel.2016.03.020

Zhu, F.-Y., Wang, L.-L., Meng, T.-G., Wang, R.-L., Yang, Z.-X., Cao, Y., et al. (2021). Inhibiting bridge integrator 2 phosphorylation leads to improved oocyte quality, ovarian health and fertility in aging and after chemotherapy in mice. *Nat. Aging* 1 (11), 1010–1023. doi:10.1038/s43587-021-00133-4

Zhu, X.-L., Li, S.-F., Zhang, X.-Q., Xu, H., Luo, Y.-Q., Yi, Y.-H., et al. (2020). Synaptotagmin 1 regulates cortical granule exocytosis during mouse oocyte activation. *Zygote Camb. Engl.* 28 (2), 97–102. doi:10.1017/S0967199419000704

frontiers | Frontiers in Cell and Developmental Biology

TYPE Mini Review
PUBLISHED 30 November 2023
DOI 10.3389/fcell.2023.1282579

OPEN ACCESS

EDITED BY
Marco G. Alves,
Independent Researcher, Portugal

REVIEWED BY
Mariana Pereira Antoniassi,
Federal University of São Paulo, Brazil
Jannette Marie Dufour,
Texas Tech University Health Sciences Center, United States

*CORRESPONDENCE
Vanesa A. Guazzone,
ciruba@fmed.uba.ar

RECEIVED 24 August 2023
ACCEPTED 12 October 2023
PUBLISHED 30 November 2023

CITATION
Guazzone VA and Lustig L (2023), Varicocele and testicular cord torsion: immune testicular microenvironment imbalance. *Front. Cell Dev. Biol.* 11:1282579. doi: 10.3389/fcell.2023.1282579

Varicocele and testicular cord torsion: immune testicular microenvironment imbalance

Vanesa A. Guazzone[1,2]* and Livia Lustig[1,2]

[1]Universidad de Buenos Aires, Facultad de Medicina, Departamento de Biología Celular e Histología/Unidad Académica II, Buenos Aires, Argentina, [2]Consejo Nacional de Investigaciones Científicas y Técnicas (CONICET)—Universidad de Buenos Aires, Instituto de Investigaciones Biomédicas (INBIOMED), Buenos Aires, Argentina

The main functions of the testis, steroidogenesis and spermatogenesis, depend on the endocrine axis and systemic and local tolerance mechanisms. Infectious or non-infectious diseases may disturb testicular immune regulation causing infertility. Literature has illustrated that bacterial and viral infections lead to autoimmune infertility: either sperm antibodies or autoimmune epididymo-orchitis. However, little is known about the association between non-infectious testicular pathologic diseases and autoimmunity. Here we review the novel aspect of varicocele and testicular cord torsion pathology linked to inflammation and discuss how immune factors could contribute to or modulate autoimmunity in ipsi- and contralateral testis.

KEYWORDS

testis, varicocele, testicular cord torsion, autoimmunity, testicular inflammation, infertility

Introduction

Infertility affects 10%–15% of couples, the male factor being present in around 50% of couples attempting to conceive. Moreover, global findings on sperm count strongly suggest a significant decline in male reproductive health, which seriously affects fertility (Turner et al., 2020).

The causes of male infertility or subfertility can be categorized mainly as genetic (autoimmune regulator (AIRE) gene deficiency), acquired, or idiopathic. Some acquired conditions are infections, testis tumors, environmental factors, hormonal factors, lifestyle, and systemic diseases. Numerous bacteria and viruses infect epididymis and testis through an ascending canalicular or haematogenous via, respectively. Hasan et al. (2022) describe these entities, mechanism of disease and negative impact on spermatogenesis and steroidogenesis. Microbial antigens may cross-react with testis antigen via molecular mimicry at the T- or B-cell level, and autoimmune orchitis may be the sequel of infections (Lustig et al., 2019).

Male infertility associated with immunological mechanisms may depend on the presence of: i) immune cells in the testis and excurrent ducts secreting cytokines and other inflammatory factors and/or ii) the presence of sperm antibodies. In the first case, immunopathological damage of the testis (and excurrent ducts) occurs through lymphomononuclear cell-mediated mechanisms triggered by antigens or pathogens that disrupt testicular immunoprivilege. In the second case, the antibodies generated may result in infertility by a variety of mechanisms (e.g., sperm agglutination, reduction of sperm

motility and ability to penetrate the cervical mucus, inhibition of sperm capacitation, acrosome reaction and impairment of sperm-egg interaction).

A severe reduction in the male fertility potential is also observed in varicocele (VC) and to lesser degree in testicular cord torsion (TCT), two pathologies originating in embryological/anatomical defects. Despite extensive literature on VC and TCT, mechanisms involved in damage to the contralateral testis and in long-term negative effects on fertility are not yet clear. With this review, we propose a different approach to this topic through the analysis and relevance of inflammation and immunologic mechanisms found in these two pathologies and discuss how immune factors may contribute to or modulate autoimmunity in ipsi- and contralateral testis.

Varicocele

VC is a vascular lesion manifested as abnormal dilatation and tortuosity of the pampiniform plexus veins, which occur by a pathological reflux of blood into the internal spermatic vein causing the elevation of scrotal temperature. It is most commonly observed on the left side (85% of cases), although some men are affected bilaterally. Isolated right-sided VC is rare. Reflux of blood is most often found on the left side as the hydrostatic pressure is higher on this side owing to the perpendicular drainage of the left internal spermatic vein into the left renal vein. VC can be observed in 35%–44% of men with primary infertility and 45%–81% with secondary infertility. Although VC repair (varicocelectomy) is a good way to improve a patient's semen quality, postoperative natural pregnancy outcomes are still being debated (Jensen et al., 2017).

A comprehensive review of the pathogenesis of VC is found elsewhere (Cho et al., 2016). Current consensus is that pathophysiological mechanisms of VC -induced infertility are scrotal hyperthermia, hypoxia and oxidative stress. The hypoxia-inducible factor 1 (HIF), an intrinsic marker for tissue hypoxia, and nitric oxide (NO) are more highly expressed in the internal spermatic vein of patients with VC (compared to control patients) (Ozbek et al., 2000; Lee et al., 2006). Oxidative stress results from an imbalance of reactive oxygen species (ROS) and protective antioxidant system. ROS make functional contributions at appropriate concentrations (i.e., condensation of sperm nuclear chromatin during spermatogenesis), but quickly become destructive in excess. Heat stress and hypoxia produce a large amount of ROS, producing a negative impact on sperm quality and function via lipid peroxidation, mitochondrial dysfunction, DNA damage, and apoptosis (Wang et al., 2022).

However, some phenomena are not fully explained by the factors mentioned above; it is likely that other acquired risk factors and testicular immune microenvironment disorder contribute to irreversible testicular damage. Testicular biopsies in subfertile/infertile patients with left VC showed bilateral pathological alterations of seminiferous epithelium, sloughing of immature cells into the lumen of the tubules, and an increase in the interstitium tissue area (Dubin and Hotchkiss, 1969; Terquem and Dadoune, 1981; Abdelrahim et al., 1993). An elevated number of leukocytes (La Vignera et al., 2015; Mongioì et al., 2020) and levels of proinflammatory cytokines (IL6, IL1ß, TNFα and IL18) and chemokines (IL8 and CXCL5) are observed in the seminal plasma of infertile patients with VC (Moretti et al., 2009; Nazari et al., 2017; Zeinali et al., 2017). In experimental rat model, the progression of VC induces upregulation of IL1ß, IL1α, IL6 and INFγ in ipsilateral testis (Sahin et al., 2006; Habibi et al., 2015). Fang et al. (2021) summarized cytokines reported in VC of human and animal model.

Immune factors alter the normal function of the blood testis barrier (BTB) by changing the expression of cell junction adhesion molecule and increasing its permeability. BTB, also known as the Sertoli cell seminiferous epithelium barrier, is formed by cell junctions of adjacent Sertoli cells at the base of the seminiferous tubules. It is constituted of multiple cell junction types including tight junctions, basal ectoplasmic specializations, gap junctions, and desmosome-like junctions. Testicular biopsies of men with VC but unknown reproductive potential revealed intact functionality of BTB by intercellular tracer studies utilizing lanthanum nitrate (Cameron and Snydle, 1980). Nevertheless, an experimentally induced VC demonstrated significantly decreased claudin-11 and N-cadherin expression in ipsilateral testis versus sham rat testis (Oh et al., 2016; Pan et al., 2018). Evidence also suggests that VC is associated with anti-sperm antibodies (ASAs) as summarized in Table 1.

Testicular cord torsion

TCT is a urological emergency affecting 1:4000 males under 25 years old. Early diagnosis (about 6 h) and immediate surgery (detorsion and orchiopexy) are important to avoid irreversible ischemia-induced damage of the testis (Danner et al., 1982). Most authors consider that gonad viability following testis torsion lasts 24 h, and that irreversible testis damage (edema, interstitial hemorrhage, apoptosis, sloughing of the germinal epithelium, and finally necrosis) occurs after that time. Prolonged testicular ischemia leads to an infarcted testis that should be removed (orchidectomy). Even patients treated by detorsion might become infertile or subfertile in the future, exhibiting ASA production, decreased sperm motility, and reduced sperm counts as long-term effects. Endocrine profiles are within normal range although serum testosterone is significantly lower only after orchidectomy or testicular atrophy which occurs in 47% of patients following surgical detorsion (Aggarwal et al., 2022).

Experimental models in rats and mice demonstrated that ischemia-inducing testicular torsion followed by torsion repair and reperfusion induces high levels of ROS and correlates with an inflammatory response expressed by upregulation of proinflammatory cytokines TNFα and IL1ß. These cytokines plus NO are involved in neutrophil recruitment into the testicular interstitium (Turner et al., 1997; Lysiak et al., 2003). In contrast, E-selectin knockout mice and wild-type mice rendered neutropenic showed a significant decrease and a reduction of germ cell specific apoptosis (Lysiak et al., 2001). E-selectin is an endothelial adhesion molecule in charge of tethering which allows rolling of neutrophils to endothelial cells.

Alterations of testis histopathology and function of the contralateral testis in TCT have been demonstrated by several authors in experimental TCT models (guinea pig, rabbits, and

TABLE 1 Antispermatic antibodies (ASA) in Varicocele and Testicular Cord Torsion (TCT).

		Reference	Time after surgical procedure for ASA detection	Sample	% rats sperm ASA+/ total # rats	
Varicocele	Experimental data	Shook et al. (1988)	28-32 days	Serum	100% / 8	
		Reference	ASA evaluation (before or after surgery)	Sample	% patients ASA+/ total # patients	
	Clinical data	Witkin and Toth (1983)	Before	Seminal plasma	30% / 10	
		Golomb et al. (1986)	Before	Semen and seminal plasma	62.5% / 32	
		Oshinsky et al. (1993)	Before	Semen	17% / 29	
		Knudson et al. (1994)	Before	Seminal plasma	28% / 32	
			After (6 months)		32% / 22	
		Solis et al. (2001)	Before	Seminal plasma	46.7% / 137	
		Bozhedomov et al. (2014)	Before	Seminal plasma	13% / 367	
		Reference	Surgical Procedure	Time after torsion for ASA detection	Sample	% rats sperm ASA+/ total # rats
Testicular Cord Torsion	Experiemental data	Rodriguez et al. (2006)	TCT	30 days	Serum	100% /12
		Reference	Surgical Procedure	Time after torsion for ASA evaluation	Sample	patients ASA+/ total # patients
	Clinical data	Mastrogiacomo et al. (1982)	Detorsion or orchidectomy	6 months to 2 years	Serum	23% / 13
				More than 2 years		33% / 12
		Zanchetta et al. (1984)	Not described	7 years	Serum	8.8 % anti-Leydig cells 4.4% anti-germ or Sertoli cells

rats) (Nagler and White, 1982; Cerasaro et al., 1984; Chakraborty et al., 1986; Pakyz et al., 1990; Vigueras and Reyes, 2004) whereas human data are more limited (Chakarborty et al., 1980; Laor et al., 1990).

Rodriguez et al., 2006, analyzing the contralateral testis of adult male rats subjected to unilateral spermatic cord torsion showed, 30 days after torsion, focal damage of seminiferous tubules associated with inflammation characterized by a significant increase in the number of resident and inflammatory macrophages, T lymphocytes, and mast cells localized in the testicular interstitium. Mast cells might indirectly trigger germ cell damage and fibrosis of the seminiferous tubule walls when tryptase increases microvascular permeability, stimulating inflammatory cell migration and releasing cytokines. TNFα content in testicular fluid of rats with TCT was significantly higher than in the sham group, suggesting it could be involved in apoptosis of TNFR1 positive germ cells. Serum sperm antibodies were detected in TCT rats and also in human subjects (Table 1).

Discussion

Systemic tolerance and local immune privilege are partners for complete immune protection of testis. Systemic tolerance involving antigen-specific regulatory T cells (Tregs) is maintained in peripheral lymphoid organs by continuously egressing germ cell antigens via transcytosis in Sertoli cells (Lustig et al., 2019). Testicular immune privilege also involves multiple mechanisms such as a BTB, secretion of numerous immunosuppressive factors mainly by macrophages, Sertoli, peritubular, and Leydig cells, and the presence of Tregs. Autoimmunity against spermatogenic cells develops as a consequence of the breakdown of local immune tolerance. Activation of lymphomonocyte cells during immune cell reactions against auto-antigens may trigger release of chemokines, cytokines and ROS (Lustig et al., 2020). Autoimmune infertility is often clinically silent and might be caused by VC and TCT. The higher VC incidence in men with secondary infertility suggests that men with prior fertility may suffer VC-mediated secondary infertility, and the presence of VC may cause a progressive decline in fertility (Naughton et al., 2001). Increased levels of proinflammatory cytokines, leukocytes, and ASAs in seminal plasma indicate that testis/epididymis inflammation occurs in VC and TCT. Proinflammatory cytokines appear to be a natural component of seminal plasma but their production increases in response to chronic inflammations, thereby playing a detrimental role in spermatogenesis. Sperm immaturity is more frequent in VC patients vs. controls, suggesting that it is associated with a detachment of cells from the seminiferous

TABLE 2 Effects of anti-inflammatory drugs in Varicocele and Testicular Cord Torsion.

		Drug	Effect	Reference
Varicocele	Experimental rat model	Resveratrol	< mRNA level NLRP3 inflammosome, caspase-1, Bax	Hajipour et al. (2018)
	Clinical data	Ketotifen fumarate (mast cell blocker)	Improves semen parameters, chromatin integrity and pregnancy rates	Azadi et al. (2010)
Testicular Cord Torsion	Experimental rat model	Cyclosporine + Prednisone	Improves sperm parameters	Pakyz et al. (1990)
			Reduces contralateral testis damage	
		Polydeoxy-ribonucleotide	> VEGF, VEGFR1, eNOS	Minutoli et al. (2011)
			Reduces ipsilateral testis damage	
		Melatonin	< Testis inflammation	Parlaktas et al. (2014)
			< Lipid peroxidation and enzymes activities	
			Improves spermatogenesis in the ipsilateral testis	Mirhoseini et al. (2017)
		Ketotifen fumarate	< Testis inflammation	Moreno et al. (2020)
			< Mast cell number	
			< Fibrosis of ST walls	
			Reduces damage of contralateral testis	
		Vitamin D3	Targeting ADAM 17 prevents germ cell apoptosis in the ipsilateral testis and protect contralateral testis	Mohamed et al. (2021)

Other drugs with exclusively anti- oxidative stress effects have not been included.

epithelium, also strengthened by the frequent presence of spermatocytes and spermatids in these ejaculates (Moretti et al., 2009). Disorganization of seminiferous epithelium and the presence of immune cells in ipsi- and contralateral testis observed in VC and TCT resembles the lesion in men with autoimmune orchitis. Orchitis is characterized by seminiferous tubules with progressive loss of germ cells that are replaced by granulomatous inflammation consisting of T cells, macrophages, dendritic cells, and multinucleated giant cells. These findings mimic the changes in experimental models of orchitis that have been valuable in understanding the pathogenic mechanism of testicular damage (Lustig et al., 2020).

Hypoxia and oxidative stress in the ipsilateral testis in VC and TCT induce dysfunctional testis consistent with apoptotic germ cells observed in men and rat testis. As in autoimmune orchitis, a hypoxic and oxidative microenvironment also induces HIF-1α and NO, respectively. In long-term experimental VC, damage to seminiferous tubules is more severe, apoptosis of spermatogenic cells and expression of HIF-1α gradually increase whereas antiapoptotic proteins Bcl-2 decrease in ipsilateral testis (Zhu et al., 2017). HIF-1α regulates the expression of vascular endothelial growth factor (VEGF) that could be involved in many VC and TCT pathophysiological effects. In an experimental model of autoimmune orchitis we demonstrate that involvement of VEGFA-VEGFR is associated with a significantly increased percentage of interstitial testicular blood vessels, suggesting that VEGFA might be an early marker of testicular inflammation (Gualdoni et al., 2021). Chakraborty et al. (1985) noted a significant increase in the percentage of total blood vessels in VC patients with severely affected testes compared to controls. An oxidative microenvironment is generated in orchitic testis by high levels of NO produced mainly by both resident and infiltrating macrophages. NO reaches seminiferous tubules and induces basal germ cell apoptosis by activating the mitochondrial pathway (Jarazo-Dietrich et al., 2012; Ferreiro et al., 2019).

Cytokines are produced and secreted by immune cells and by testicular somatic cells in response to external stimuli. Increased levels of proinflammatory cytokines IL1, TNFα, IL6, IL18 may be responsible for disruption of BTB in VC. To our knowledge, no study has evaluated BTB in TCT. During testicular inflammation BTB integrity is impaired—denoted by increased permeability to tracers. Concomitantly, changes in expression of cell junction adhesion molecules were detected (Pérez et al., 2011; Pérez et al., 2012).

Testicular injury via initial actions at the BTB to elicit subsequent damage to germ-cell adhesion, thereby leading to germ-cell loss, reduced sperm count, and male infertility or subfertility. In this context, there is an intricate relationship between the male gonad and the immune system resulting in production of antibodies against meiotic and postmeiotic germ cells. The presence of anti-sperm antibodies and the increase in the number of testicular immune cells in VC and TCT show that a humoral and cellular immune response occurs simultaneously with the histopathological damage, thereby suggesting involvement of an immunological mechanism that eventually impairs the contralateral testicular function. In fact, Gurdal et al. (2008) reported a trend of increasing apoptosis in bilateral testis correlating with increasing duration of VC. Wang et al. (2010) considered that the positive correlation between left- and right-testis HIF-1α expression and the

left- and right-sided apoptotic index of germ cells as confirmation that left-sided VC could cause similarly bilateral testicular damage.

In early publications on TCT, an immunologic mechanism was also suggested as a possible mechanism involved in contralateral testis damage (Chakraborty et al., 1980; Dondero et al., 1980; Mastrogiacomo et al., 1982). Ozkan et al. (2001) reported that serum inhibin B levels (marker of Sertoli cell function and state of spermatogenesis) decreases after unilateral TCT, reflecting contralateral testicular damage. Measurement of serum inhibin B levels is more effective than histopathological examination.

An early orchiectomy following TCT prevents the release of spermatic antigens, the formation of antibodies, and damage to the contralateral testis (Nagler and White, 1982). Anti-lymphocyte IgG and splenectomy or corticoids before detorsion also prevent damaging of the contralateral testis (Nagler and White, 1982; Pakyz et al., 1990; Mogilner et al., 2006). However, Jacobsen et al. (2020) suggest that contralateral testis damage results from multifactorial processes that also include pre-existing congenital testicular dysgenesis (a maldeveloped male urogenital tract) that may predispose to TCT (Laor et al., 1990; Osemlak et al., 2021) and/or contralateral hypoxia following ipsilateral torsion.

In this review, we emphasize that VC, TCT, and orchitis respond to common mechanisms of inflammation-related male infertility and theorize that prolonged VC and TCT negatively impact on contralateral testis through an autoimmune response. Consistent with this hypothesis, inhibition of inflammation can alleviate VC- and TCT-mediated pathogenesis (Table 2).

Author contributions

VAG: Writing–original draft. LL: Writing–original draft.

Funding

The author(s) declare financial support was received for the research, authorship, and/or publication of this article. Universidad de Buenos Aires (UBA). Consejo Nacional de Investigaciones Científicas y Técnicas (CONICET). Agencia Nacional de Promoción Científica y Tecnológica.

Conflict of interest

The authors declare that the research was conducted in the absence of any commercial or financial relationships that could be construed as a potential conflict of interest.

Publisher's note

References

Abdelrahim, F., Mostafa, A., Hamdy, A., Mabrouk, M., el-Kholy, M., and Hassan, O. (1993). Testicular morphology and function in varicocele patients: pre-operative and post-operative histopathology. *Br. J. Urology* 72 (5), 643–647. doi:10.1111/j.1464-410x.1993.tb16225.x

Aggarwal, D., Parmar, K., Sharma, A. P., Tyagi, S., Kumar, S., Singh, S. K., et al. (2022). Long-term impact of testicular torsion and its salvage on semen parameters and gonadal function. *Indian J. Urol.* 38, 135–139. doi:10.4103/iju.iju_328_21

Azadi, L., Abbasi, H., Deemeh, M. R., Tavalaee, M., Arbabian, M., Pilevarian, A. A., et al. (2011). Zaditen (Ketotifen), as mast cell blocker, improves sperm quality, chromatin integrity and pregnancy rate after varicocelectomy. *Int. J. Androl.* 34, 446–452. doi:10.1111/j.1365-2605.2010.01112.x

Bozhedomov, V. A., Lipatova, N. A., Rokhlikov, I. M., Alexeev, R. A., Ushakova, I. V., and Sukhikh, G. T. (2014). Male fertility and varicocoele: role of immune factors. *Andrology* 2 (1), 51–58. doi:10.1111/j.2047-2927.2013.00160.x

Cameron, D. F., and Snydle, F. E. (1980). The blood-testis barrier in men with varicocele: a lanthanum tracer study. *Fertil. Steril.* 34 (3), 255–258. doi:10.1016/s0015-0282(16)44958-7

Cerasaro, T. S., Hachtsheim, D. A., Otero, F., and Lowell Parsons, L. (1984). The effect of testicular torsion on contralateral testis and the production of antisperm antibodies in rabbits. *J. Urol.* 132, 577–579. doi:10.1016/s0022-5347(17)49750-3

Chakraborty, I. J., Jhunjhunwala, P., Nelson, L., and Young, M. (1980). Effects of unilateral torsion of the spermatic cord on the contralateral testis in human and Guinea pig. *Arch. Androl.* 4 (2), 95–108. doi:10.3109/01485018008986475

Chakraborty, J., Hikim, A. P., and Jhunjhunwala, J. S. (1985). Stagnation of blood in the microcirculatory vessels in the testes of men with varicocele. *J. Androl.* 6, 117–126. doi:10.1002/j.1939-4640.1985.tb00826.x

Chakraborty, J., Sinha Hikim, A. P., and Jhunjhunwala, J. (1986). Torsion of the spermatic cord--a long term study of the contralateral testis. *Urol. Res.* 14 (5), 257–260. doi:10.1007/BF00256569

Cho, C. L., Esteves, S. C., and Agarwal, A. (2016). Novel insights into the pathophysiology of varicocele and its association with reactive oxygen species and sperm DNA fragmentation. *Asian J. Androl.* 18 (2), 186–193. doi:10.4103/1008-682X.170441

Danner, C., Frick, J., and Rovan, E. (1982). Testicular function after torsion. *Int. J. Androl.* 5, 276–281. doi:10.1111/j.1365-2605.1982.tb00256.x

Dondero, F., Lenzi, A., Picardo, M. P., Pastor, R., and Valesini, G. (1980). Cell-mediated antisperm immunity in selected forms of male infertility. *Andrologia* 12, 25–29. doi:10.1111/j.1439-0272.1980.tb00572.x

Dubin, L., and Hotchkiss, R. S. (1969). Testis biopsy in subfertile men with varicocele. *Fertil. Steril.* 20 (1), 50–57. doi:10.1016/s0015-0282(16)36904-7

Fang, Y., Su, Y., Xu, J., Hu, Z., Zhao, K., Liu, C., et al. (2021). Varicocele-mediated male infertility: from the perspective of testicular immunity and inflammation. *Front. Immunol.* 12, 729539. doi:10.3389/fimmu.2021.729539

Ferreiro, M. E., Amarilla, M. S., Glienke, L., Méndez, C. S., González, C., Jacobo, P. V., et al. (2019). The inflammatory mediators TNFα and nitric oxide arrest spermatogonia GC-1 cell cycle. *Reprod. Biol.* 19, 329–339. doi:10.1016/j.repbio.2019.11.001

Golomb, J., Vardinon, N., Homonnai, Z. T., Braf, Z., and Yust, I. (1986). Demonstration of antispermatozoal antibodies in varicocele-related infertility with an enzyme-linked immunosorbent assay (ELISA). *Fertil. Steril.* 45 (3), 397–402. doi:10.1016/s0015-0282(16)49224-1

Gualdoni, G. S., Jacobo, P. V., Sobarzo, C. M., Pérez, C. V., Durand, L. A. H., Theas, M. S., et al. (2021). Relevance of angiogenesis in autoimmune testis inflammation. *Mol. Hum. Reprod.* 27 (2), gaaa073. doi:10.1093/molehr/gaaa073

Gürdal, M., Kireççi, S., Huri, E., Karaman, I., and Türkeri, L. (2008). Correlation between duration of varicocele and apoptosis in testicular tissue in an experimental model. *Urology* 72 (4), 933–936. doi:10.1016/j.urology.2008.01.060

Habibi, B., Seifi, B., Mougahi, S. M., Ojaghi, M., and Sadeghipour, H. R. (2015). Increases in interleukin-6 and interferon-gamma levels is progressive in immature rats with varicocele. *Ir. J. Med. Sci.* 184 (2), 531–537. doi:10.1007/s11845-014-1167-3

Hajipour, E., Jalali Mashayekhi, F., Mosayebi, G., Baazm, M., and Zendedel, A. (2018). Resveratrol decreases apoptosis and NLRP3 complex expressions in experimental varicocele rat model. *Iran. J. Basic Med. Sc.* 21 (2), 225–229. doi:10.22038/IJBMS.2018.21943.5625

Hasan, H., Bhushan, S., Fijak, M., and Meinhardt, A. (2022). Mechanism of inflammatory associated impairment of sperm function, spermatogenesis and steroidogenesis. *Front. Endocrinol.* 13, 897029. doi:10.3389/fendo.2022.897029

Jacobsen, F. M., Rudlang, T. M., Fode, M., Østergren, P. B., Sønksen, J., Ohl, D. A., et al. (2020). The impact of testicular torsion on testicular function. *World J. Mens. Health* 38 (3), 298–307. doi:10.5534/wjmh.190037

Jarazo-Dietrich, S., Jacobo, P., Pérez, C. V., Guazzone, V. A., Lustig, L., and Theas, M. S. (2012). Up regulation of nitric oxide synthase-nitric oxide system in the testis of rats undergoing autoimmune orchitis. *Immunobiology* 217, 778–787. doi:10.1016/j.imbio.2012.04.007

Jensen, C. F. S., Østergren, P., Dupree, J. M., Ohl, D. A., Sønksen, J., and Fode, M. (2017). Varicocele and male infertility. *Nat. Rev. Urol.* 14, 523–533. doi:10.1038/nrurol.2017.98

Knudson, G., Ross, L., Stuhldreher, D., Houlihan, D., Bruns, E., and Prins, G. (1994). Prevalence of sperm bound antibodies in infertile men with varicocele: the effect of varicocele ligation on antibody levels and semen response. *J. Urol.* 151 (5), 1260–1262. doi:10.1016/s0022-5347(17)35226-6

Laor, E., Fisch, H., Tennenbaum, S., Sesterhenn, I., Mostofi, K., and Reid, R. E. (1990). Unilateral testicular torsion: abnormal histological findings in the contralateral testis--cause or effect? *Br. J. Urol.* 65 (5), 520–523. doi:10.1111/j.1464-410x.1990.tb14800.x

La Vignera, S., Condorelli, R. A., Morgia, G., Favilla, V., Russo, G. I., Cimino, S., et al. (2015). Different levels of Cd45pos leukocytes in the semen of patients with low testicular volume. *Int. J. Immunopath. Pharmacol.* 28 (1), 85–92. doi:10.1177/0394632015572748

Lee, J. D., Jeng, S. Y., and Lee, T. H. (2006). Increased expression of hypoxia-inducible factor-1alpha in the internal spermatic vein of patients with varicocele. *J. Urol.* 175 (3), 1045–1048. doi:10.1016/S0022-5347(05)00417-9

Lustig, L., Guazzone, V. A., Theas, M. S., Pleuger, C., Jacobo, P., Pérez, C. V., et al. (2020). Pathomechanisms of autoimmune based testicular inflammation. *Front. Immunol.* 11, 583135. doi:10.3389/fimmu.2020.583135

Lustig, L., Guazzone, V. A., and Tung, K. S. K. (2019). "Autoimmune orchitis and autoimmune oophoritis," in *The autoimmune diseases*. Editors N. Rose and I. Mackay 6th edn (London: Elsevier Inc.), 1235–1251. doi:10.1016/B978-0-12-812102-3.00062-2

Lysiak, J. J., Nguyen, Q. A., Kirby, J. L., and Turner, T. T. (2003). Ischemia-reperfusion of the murine testis stimulates the expression of proinflammatory cytokines and activation of c-jun N-terminal kinase in a pathway to E-selectin expression. *Biol. Reprod.* 69 (1), 202–210. doi:10.1095/biolreprod.102.013318

Lysiak, J. J., Turner, S. D., Nguyen, Q. A., Singbarti, K., Ley, K., and Turner, T. T. (2001). Essential role of neutrophils in germ cell-specific apoptosis following ischemia/reperfusion injury of the mouse testis. *Biol. Reprod.* 65, 718–725. doi:10.1095/biolreprod65.3.718

Mastrogiacomo, L., Zanchetta, R., Graziotti, P., Betterle, C., Scrufari, P., and Lembo, A. (1982). Immunological and clinical study of patients after spermatic cord torsion. *Andrologia* 14 (1), 25–30. doi:10.1111/j.1439-0272.1982.tb03091.x

Minutoli, L., Antonuccio, P., Squadrito, P., Bitto, P., Nicotina, P. A., Fazzari, C., et al. (2012). Effects ofpolydeoxyribonucleotide on the histological damage and the altered spermatogenesis induced by testicular ischaemia and reperfusion in rats. *Int. J. Androl.* 35, 133–144. doi:10.1111/j.1365-2605.2011.01194.x

Mirhoseini, M., Talebpour Amiri, F., Karimpour Malekshah, A. A., Rezanejad Gatabi, Z., and Ghaffari, E. (2017). Protective effects of melatonin on testis histology following acute torsion-detorsion in rats. *Int. J. reproductive Biomed.* 15 (3), 141–146. doi:10.29252/ijrm.15.3.141

Mogilner, J. G., Elenberg, Y., Lurie, M., Shiloni, E., Coran, A. G., and Sukhotnik, I. (2006). Effect of dexamethasone on germ cell apoptosis in the contralateral testis after testicular ischemia-reperfusion injury in the rat. *Fertil. Steril.* 85 (1), 1111–1117. doi:10.1016/j.fertnstert.2005.10.021

Mohamed, D. I., Abou-Bakr, D. A., Ezzat, S. F., El-Kareem, H. F. A., Nahas, H. H. A., Saad, H. A., et al. (2021). Vitamin D3 prevents the deleterious effects of testicular torsion on testis by targeting miRNA-145 and ADAM17: *in silico* and *in vivo* study. *Pharm. (Basel, Switz.* 14 (12), 1222. doi:10.3390/ph14121222

Mongioì, L. M., Alamo, A., Calogero, A. E., Compagnone, M., Giacone, F., Cannarella, R., et al. (2020). Evaluation of seminal fluid leukocyte subpopulations in patients with varicocele. *Int. J. Immunopathol. Pharmacol.* 34, 2058738420925719. doi:10.1177/2058738420925719

Moreno, D., Sobarzo, C. M., Lustig, L., Rodríguez Peña, M. G., and Guazzone, V. A. (2019). Effect of ketotifen fumarate on experimental autoimmune orchitis and torsion of the spermatic cord. *Asian J. Androl.* 22 (1), 112–117. doi:10.4103/aja.aja_30_19

Moretti, E., Cosci, I., Spreafico, A., Serchi, T., Cuppone, A. M., and Collodel, G. (2009). Semen characteristics and inflammatory mediators in infertile men with different clinical diagnoses. *Int. J. Androl.* 32 (6), 637–646. doi:10.1111/j.1365-2605.2008.00911.x

Nagler, H. M., and White, R. D. (1982). The effect of testicular torsion on the contralateral testis. *J. Urol.* 128 (6), 1343–1348. doi:10.1016/s0022-5347(17)53504-1

Naughton, C. K., Nangia, A. K., and Agarwal, A. (2001). Pathophysiology of varicoceles in male infertility. *Hum. Reprod. Update* 7 (5), 473–481. doi:10.1093/humupd/7.5.473

Nazari, A., Hassanshahi, G., and Khorramdelazad, H. (2017). Elevated levels of epithelial neutrophil activating peptide-78 (ENA-78) (CXCL5) and Interleukin-1β is correlated with varicocele-caused infertility: a novel finding. *Middle East Fertil. Soc. J.* 22 (4), 333–335. doi:10.1016/j.mefs.2017.06.002

Oh, Y. S., Jo, N. H., Park, J. K., and Gye, M. C. (2016). Changes in inflammatory cytokines accompany deregulation of claudin-11, resulting in inter-sertoli tight junctions in varicocele rat testes. *J. Urol.* 196 (4), 1303–1312. doi:10.1016/j.juro.2016.05.004

Osemlak, P., Miszczuk, K., Jędrzejewski, G., Nachulewicz, P., Beń-Skowronek, I., and Brzozowska, A. (2021). Testicular torsion: its effect on autoimmunisation, pituitary-testis axis and correlation with primary gonadal dysfunction in boys. *Pediatr. Res.* 90 (6), 1193–1200. doi:10.1038/s41390-021-01382-0

Oshinsky, G. S., Rodriguez, M. V., and Mellinger, B. C. (1993). Varicocele-related infertility is not associated with increased sperm-bound antibody. *J. Urol.* 150 (3), 871–873. doi:10.1016/s0022-5347(17)35636-7

Ozbek, E., Turkoz, Y., Gokdeniz, R., Davarci, M., and Ozugurlu, F. (2000). Increased nitric oxide production in the spermatic vein of patients with varicocele. *Eur. Urol.* 37 (2), 172–175. doi:10.1159/000020135

Ozkan, K. U., Küçükaydin, M., Muhtaroğlu, S., and Kontaş, O. (2001). Evaluation of contralateral testicular damage after unilateral testicular torsion by serum inhibin B levels. *J. Pediatr. Surg.* 36 (7), 1050–1053. doi:10.1053/jpsu.2001.24742

Pakyz, R. E., Heindl, R. M., Kallish, M., and Cosentino, M. J. (1990). Spermatic cord torsion: effects of cyclosporine and prednisone on fertility and the contralateral testis in the rat. *J. Androl.* 11, 401–408.

Pan, J., Zhu, Z., Xu, G., Niu, L., Yu, L., Luo, Z., et al. (2018). Expression of claudin-11 in a rat model of varicocele and its effects on the blood-testis barrier. *Mol. Med. Rep.* 18, 5647–5651. doi:10.3892/mmr.2018.9603

Parlaktas, B. S., Atilgan, D., Ozyurt, H., Gencten, Y., Akbas, A., Erdemir, F., et al. (2014). The biochemical effects of ischemia-reperfusion injury in the ipsilateral and contralateral testes of rats and the protective role of melatonin. *Asian J. Androl.* 16 (2), 314–318. doi:10.4103/1008-682X.122202

Pérez, C., Sobarzo, C., Jacobo, P., Jarazo Dietrich, S., Theas, M., Denduchis, B., et al. (2011). Impaired expression and distribution of adherens and gap junction proteins in the seminiferous tubules of rats undergoing autoimmune orchitis. *Int. J. Androl.* 34 (2), e566–e577. doi:10.1111/j.1365-2605.2011.01165.x

Pérez, C. V., Sobarzo, C. M., Jacobo, P. V., Pellizzari, E. H., Cigorraga, S. B., Denduchis, B., et al. (2012). Loss of occludin expression and impairment of blood-testis barrier permeability in rats with autoimmune orchitis: effect of interleukin 6 on Sertoli cell tight junctions. *Biol. Reprod.* 87, 122. doi:10.1095/biolreprod.112.101709

Rodriguez, M. G., Rival, C., Theas, M. S., and Lustig, L. (2006). Immunohistopathology of the contralateral testis of rats undergoing experimental torsion of the spermatic cord. *Asian J. Androl.* 8 (5), 576–583. doi:10.1111/j.1745-7262.2006.00146.x

Sahin, Z., Celik-Ozenci, C., Akkoyunlu, G., Korgun, E. T., Acar, N., Erdogru, T., et al. (2006). Increased expression of interleukin-1alpha and interleukin-1beta is associated with experimental varicocele. *Fertil. Steril.* 85 (1), 1265–1275. doi:10.1016/j.fertnstert.2005.10.025

Shook, T. E., Nyberg, L. M., Collins, B. S., and Mathur, S. (1988). Pathological and immunological effects of surgically induced varicocele in juvenile and adult rats. *AJRIM* 17 (4), 141–144. doi:10.1111/j.1600-0897.1988.tb00218.x

Solis, E. A., Gatti, V. N., Brufman, A. S., Bouvet, B. R., Conforti, C. B., Papparella, C. V., et al. (2001). Immunology and deterioration of seminal parameters in varicocele. *Arch. Españoles Urol.* 54 (8), 797–800.

Terquem, A., and Dadoune, J. P. (1981). Morphological findings in varicocele: an ultrastructural study of 30 bilateral testicular biopsies. *Int. J. Androl.* 4 (5), 515–531. doi:10.1111/j.1365-2605.1981.tb00735.x

Turner, K. A., Rambhatla, A., Schon, S., Agarwal, A., Krawetz, S. A., Dupree, J. M., et al. (2020). Male infertility is a women's health issue—research and clinical evaluation of male infertility is needed. *Cells* 9 (4), 990. doi:10.3390/cells9040990

Turner, T. T., Tung, K. S. K., Tomomasa, H., and Wilson, L. W. (1997). Acute testicular ischemia results in germ cell-specific apoptosis in the rat. *Biol. Reprod.* 57 (6), 1267–1274. doi:10.1095/biolreprod57.6.1267

Vigueras, R. M., Reyes, G., Rojas-Castañeda, J., Rojas, P., and Hernández, R. (2004). Testicular torsion and its effects on the spermatogenic cycle in the contralateral testis of the rat. *contralateral testis rat Laboratory Animals* 38 (3), 313–320. doi:10.1258/002367704323133709

Wang, H., Sun, Y., Wang, L., Xu, C., Yang, Q., Liu, B., et al. (2010). Hypoxia-induced apoptosis in the bilateral testes of rats with left-sided varicocele: a new way to think about the varicocele. *J. Androl.* 31 (3), 299–305. doi:10.2164/jandrol.108.007153

Wang, K., Gao, Y., Wang, C., Liang, M., Liao, Y., and Hu, K. (2022). Role of oxidative stress in varicocele. *Front. Genet.* 23 (13), 850114. doi:10.3389/fgene.2022.850114

Witkin, S. S., and Toth, A. (1983). Relationship between genital tract infections, sperm antibodies in seminal fluid, and infertility. *Fertil. Steril.* 40 (6), 805–808. doi:10.1016/s0015-0282(16)47484-4

Zanchetta, R., Mastrogiacomo, I., Graziotti, P., Foresta, C., and Betterle, C. (1984). Autoantibodies against Leydig cells in patients after spermatic cord torsion. *Clin. Exp. Immunol.* 55 (1), 49–57.

Zeinali, M., Hadian Amree, A., Khorramdelazad, H., Karami, H., and Abedinzadeh, M. (2017). Inflammatory and anti-inflammatory cytokines in the seminal plasma of infertile men suffering from varicocele. *Andrologia* 49 (6), 12685. doi:10.1111/and.12685

Zhu, S. M., Rao, T., Yang, X., Ning, J. Z., Yu, W. M., Ruan, Y., et al. (2017). Autophagy may play an important role in varicocele. *Mol. Med. Rep.* 16 (4), 5471–5479. doi:10.3892/mmr.2017.7253

Frontiers in
Cell and Developmental Biology

Explores the fundamental biological processes of life, covering intracellular and extracellular dynamics.

The world's most cited developmental biology journal, advancing our understanding of the fundamental processes of life. It explores a wide spectrum of cell and developmental biology, covering intracellular and extracellular dynamics.

Discover the latest Research Topics

See more →

Frontiers

Avenue du Tribunal-Fédéral 34
1005 Lausanne, Switzerland
frontiersin.org

Contact us

+41 (0)21 510 17 00
frontiersin.org/about/contact